Vol. 17. No 3, 2015

ISSN 1507-2711
Cena: 25 zł (w tym 5% VAT)

EKSPLOATACJA I NIEZAWODNOŚĆ
MAINTENANCE AND RELIABILITY

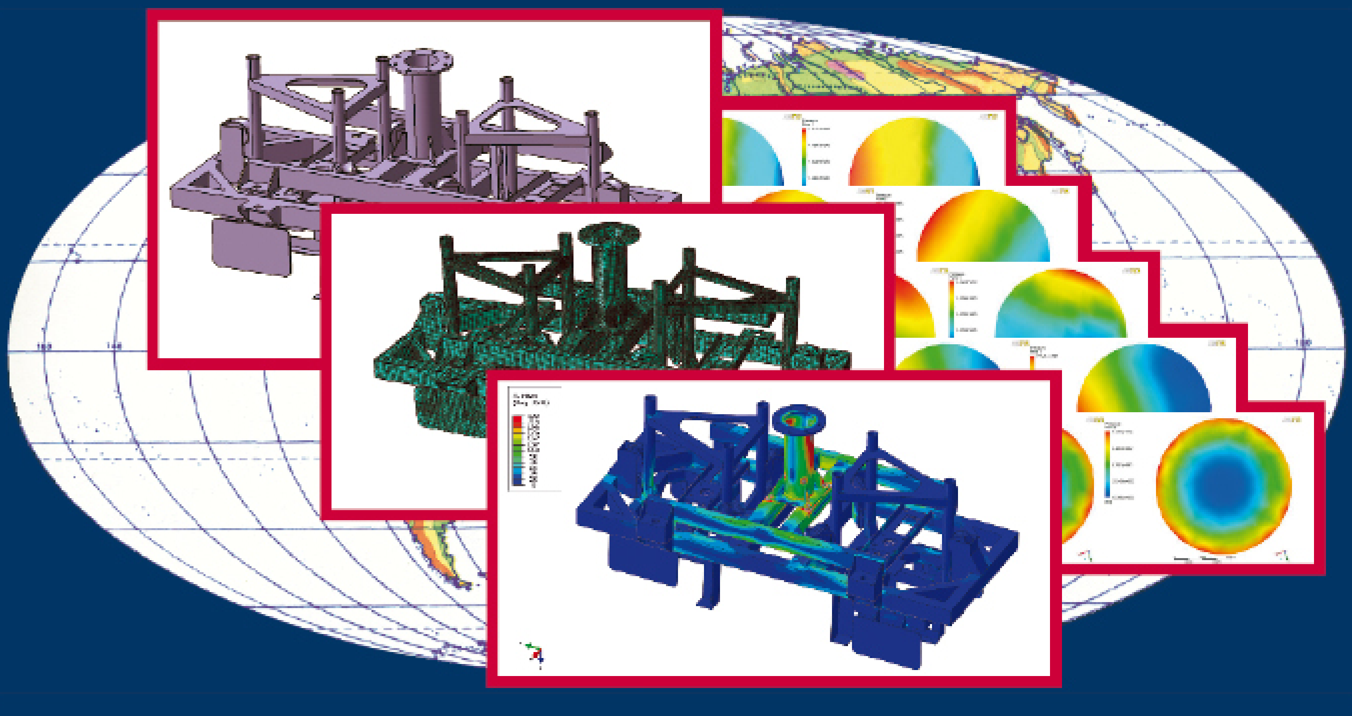

Polskie Naukowo Techniczne Towarzystwo Eksploatacyjne
Warszawa

Polish Maintenance Society
Warsaw

Co-financed by the Minister of Science and Higher Education

The Journal is indexed and abstracted in the Journal Citation Reports (JCR Science Edition), Scopus, Science Citation Index Expanded (SciSearch®) and Index Copernicus International.

The Quarterly appears on the list of journals credited with a high impact factor by the Polish Ministry of Science and Higher Education and is indexed in the Polish Technical Journal Contents database – BAZTECH and the database of the Digital Library Federation.

All the scientific articles have received two positive reviews from independent reviewers.

Our IF is 0.505

Editorial staff:	Dariusz Mazurkiewicz, PhD, DSc (Eng), Associate Professor (Editor-in-Chief, Secretary of the Scientific Board) Tomasz Klepka, PhD, DSc (Eng), Associate Professor (Deputy Editor-in-Chief) Teresa Błachnio-Krolopp, MSc (Eng) (Editorial secretary) Andrzej Koma (Typesetting and text makeup) Krzysztof Olszewski, PhD (Eng) (Webmaster)
Publisher:	Polish Maintenance Society, Warsaw
Scientific patronage:	Polish Academy of Sciences Branch in Lublin
Address for correspondence:	“Eksploatacja i Niezawodność” – Editorial Office ul. Nadbystrzycka 36, 20-618 Lublin, Poland e-mail: office@ein.org.pl http://www.ein.org.pl/
Circulation:	550 copies

Science and Technology

SKRUCH P, DŁUGOSZ M, MITKOWSKI W. **Mathematical methods for verification of microprocessor-based PID controllers for improving their reliability**. Eksploatacja i Niezawodnosc – Maintenance and Reliability 2015; 17 (3): 327–333, http://dx.doi.org/10.17531/ein.2015.3.1.

Proportional-Integral-Derivative (PID) control is the most common control algorithm used in industry. The extensive use of electronics and software has resulted in the situation where the digital PID controller using a microprocessor as well as its software implementation replaces existing pneumatic, mechanical and electromechanical solutions. The reliability of the software system is assured by detection and removal of errors that can lead to failures. The paper presents mathematical methods for verification and testing of microprocessor-based PID controllers that can be used to increase the reliability of the system. The presented methodology explores the concept of testing with a model as an oracle.

VIŠNIAKOV N, KILIKEVIČIUS A, NOVICKIJ J, GRAINYS A, NOVICKIJ V. **Low-cost experimental facility for evaluation of the effect of dynamic mechanical loads on photovoltaic modules**. Eksploatacja i Niezawodnosc – Maintenance and Reliability 2015; 17 (3): 334–337, http://dx.doi.org/10.17531/ein.2015.3.2.

The efficiency of modern photovoltaic systems is strongly reduced when the crystalline structure of the solar cells is being damaged due to extensive mechanical stress caused by climatic factors such as heavy wind or snow. This work is focused on the investigation of the cyclic dynamic mechanical loads required to alter the efficiency of typical solar panels in order to simulate various weather conditions and investigate the reliability of the solar panels when they are subjected to stress. Experimental setup is described in the study. During experiments the solar panels have been treated up to 40 Hz vibrations with the maximum magnitude of the shift of the solar panel in the range of 0.3 mm. Simulation model of the characteristic frequencies during vibrations is also presented in this work. The experimental vibration spectrum has also been determined. The acquired experimental data showed appearance of micro fractures in the crystalline structure of the photovoltaic modules and allowed estimation of the average reliability of a typical modern photovoltaic module in harsh weather conditions. The setup could be successfully applied for express testing of solar panels and investigation of the susceptibility of photovoltaic modules to mechanical stress.

KLARECKI K, RABSZTYN D, HETMANCZYK MP. **Analysis of pulsation of the sliding-vane pump for selected settings of hydrostatic system**. Eksploatacja i Niezawodnosc – Maintenance and Reliability 2015; 17 (3): 338–344, http://dx.doi.org/10.17531/ein.2015.3.3.

Sliding-vane pumps are widely used as sources of the flow in hydrostatic power transmission systems. A noticeable tendency in hydrostatic systems is revealed in the form of minimization of the mass, overall dimensions and at the same time increasing of a power density delivered by pumps. The article presents the preliminary results of the studies related to a pressure pulsation of the hydraulic system equipped with the sliding-vane pump (T7BS type manufactured by Parker & Denison Company). During the studies the pressure pulsation in selected places of pressure line were recorded. A series of measurements were performed for selected settings of the system. The recorded characteristics were analysed in time and frequency domains.

DUAN R, ZHOU H, FAN J. **Diagnosis strategy for complex systems based on reliability analysis and MADM under epistemic uncertainty**. Eksploatacja i Niezawodnosc – Maintenance and Reliability 2015; 17 (3): 345–354, http://dx.doi.org/10.17531/ein.2015.3.4.

Fault tolerant technology has greatly improved the reliability of train-ground wireless communication system (TWCS). However, its high reliability caused the lack of sufficient fault data and epistemic uncertainty, which increased significantly challenges in system diagnosis. A novel diagnosis method for TWCS is proposed to deal with these challenges in this paper, which makes the best of reliability analysis, fuzzy sets theory and MADM. Specifically, it adopts dynamic fault tree to model their dynamic fault modes and evaluates the failure rates of the basic events using fuzzy sets theory and expert elicitation to hand epistemic uncertainty. Furthermore, it calculates some quantitative parameters information provided by reliability analysis using algebraic technique and Bayesian network to overcome some disadvantages of the traditional methods. Diagnostic importance factor, sensitivity index and heuristic information values are considered comprehensively to obtain the optimal diagnostic ranking order of TWCS using an improved TOPSIS. The proposed method takes full advantages of the dynamic fault tree for modelling, fuzzy sets theory for handling uncertainty and MADM for the best fault search scheme, which is especially suitable for fault diagnosis of the complex systems.

SKRUCH P, DŁUGOSZ M, MITKOWSKI W. **Matematyczne metody testowania mikroprocesorowych regulatorów PID umożliwiające zwiększenie ich niezawodności**. Eksploatacja i Niezawodnosc – Maintenance and Reliability 2015; 17 (3): 327–333, http://dx.doi.org/10.17531/ein.2015.3.1.

Regulator PID (regulator proporcjonalno-całkująco-różniczkujący) jest najbardziej rozpowszechnionym i najczęściej stosowanym typem regulatora w przemyśle. Intensywny rozwój elektroniki i informatyki spowodował, że cyfrowe regulatory PID budowane na bazie mikroprocesora z odpowiednim oprogramowaniem zastąpiły dotychczasowe rozwiązania pneumatyczne, mechaniczne i elektromechaniczne. Zagwarantowanie niezawodności układu elektronicznego z oprogramowaniem polega między innymi na wykrywaniu i usuwaniu błędów, które mogą prowadzić do awarii. W pracy przedstawiono matematyczne metody weryfikacji mikroprocesorowych regulatorów PID mające na celu wykrycie błędów w systemie i w konsekwencji zwiększenie jego niezawodności poprzez zmniejszenie prawdopodobieństwa wystąpienia awarii. Metody testowania opierają się na tak zwanym podejściu modelowym, to znaczy, wykorzystują model systemu jako wzorzec zachowania.

VIŠNIAKOV N, KILIKEVIČIUS A, NOVICKIJ J, GRAINYS A, NOVICKIJ V. **Tanie urządzenie doświadczalne do oceny wpływu dynamicznych obciążeń mechanicznych na moduły fotowoltaiczne**. Eksploatacja i Niezawodnosc – Maintenance and Reliability 2015; 17 (3): 334–337, http://dx.doi.org/10.17531/ein.2015.3.2.

Sprawność współczesnych instalacji fotowoltaicznych drastycznie spada, kiedy struktura krystaliczna ogniw słoneczn ych ulega uszkodzeniu z powodu dużych naprężeń mechanicznych powodowanych przez czynniki klimatyczne, takie jak silny wiatr lub śnieg. Niniejsza praca skupia się na badaniu cyklicznych dynamicznych obciążeń mechanicznych niezbędnych do obniżenia sprawności typowych paneli słonecznych w celu symulacji różnych warunków pogodowych oraz badania niezawodności paneli słonecznych poddanych oddziaływaniu czynników zewnętrznych. W publikacji opisano układ doświadczalny. W ramach doświadczeń, panele słoneczne zostały poddane drganiom do 40 Hz przy maksymalnej wielkości przesunięcia panelu słonecznego w zakresie do 0,3 mm. W pracy omówiono także model symulacyjny częstotliwości charakterystycznych w czasie drgań. Określono widmo drgań doświadczalnych. Uzyskane dane doświadczalne wykazały pojawienie się mikropęknięć w strukturze krystalicznej modułów fotowoltaicznych i pozwoliły na oszacowanie średniej niezawodności typowego współczesnego modułu fotowoltaicznego w trudnych warunkach pogodowych. Układ może być z powodzeniem wykorzystywany dla potrzeb doraźnego testowania paneli słonecznych oraz badania podatności modułów fotowoltaicznych na naprężenia mechaniczne.

KLARECKI K, RABSZTYN D, HETMANCZYK MP. **Analiza pulsacji ciśnienia pompy łopatkowej dla wybranych nastaw parametrów układu hydrostatycznego**. Eksploatacja i Niezawodnosc – Maintenance and Reliability 2015; 17 (3): 338–344, http://dx.doi.org/10.17531/ein.2015.3.3.

Pompy łopatkowe należą do często używanych generatorów strugi cieczy roboczej w napędach hydrostatycznych. Zauważalną tendencją w opisywanych układach jest minimalizacja masy oraz wymiarów gabarytowych, przy jednoczesnym zwiększaniu gęstości mocy oferowanej przez pompę. W artykule przedstawiono wyniki wstępnych badań hydraulicznego napędu hydrostatycznego z pompą typu T7BS firmy Parker & Denison. Podczas badań zarejestrowano wartości pulsacji ciśnienia w wybranych miejscach linii tłocznej. Cykl pomiarów przeprowadzono w odniesieniu do wybranych nastaw pracy układu. Uzyskane przebiegi zostały przeanalizowane w dziedzinach czasu oraz częstotliwości.

DUAN R, ZHOU H, FAN J. **Strategia diagnostyki dla systemów złożonych oparta na analizie niezawodności oraz metodach wieloatrybutowego podejmowania decyzji MADM w warunkach niepewności epistemologicznej**. Eksploatacja i Niezawodnosc – Maintenance and Reliability 2015; 17 (3): 345–354, http://dx.doi.org/10.17531/ein.2015.3.4.

Technologia odporna na błędy przyczyniła się do dużej poprawy niezawodności systemów łączności bezprzewodowej pociąg-ziemia (TWCS). Jednakże wysoka niezawodność tych systemów pociąga za sobą brak wystarczających danych o uszkodzeniach oraz niepewność epistemologiczną, której zwiększenie stworzyło liczne wyzwania w zakresie diagnostyki systemów. W niniejszej pracy zaproponowano nowatorską metodę diagnozowania TWCS, która odpowiada na owe wyzwania wykorzystując analizę niezawodności, teorię zbiorów rozmytych oraz metody wieloatrybutowego podejmowania decyzji MADM. W szczególności, zaproponowana metoda wykorzystuje dynamiczne drzewa błędów do modelowania dynamicznych stanów niezdatności oraz pozwala na oszacowanie częstości występowania uszkodzeń dla zdarzeń podstawowych z wykorzystaniem teorii zbiorów rozmytych oraz oceny eksperckiej, rozwiązując w ten sposób problem niepewności epistemologicznej. Ponadto, metoda ta umożliwia obliczenie niektórych parametrów ilościowych na podstawie informacji pochodzących z analizy niezawodności, z zastosowaniem techniki algebraicznej oraz sieci bayesowskich, co pozwala na obejście ograniczeń tradycyjnie stosowanych metod. W artykule przeprowadzono szczegółową analizę czynnika ważności diagnostycznej, wskaźnika czułości oraz wartości informacji heurystycznej w celu określenia optymalnej kolejności działań diagnostycznych dla TWCS z zastosowaniem poprawionej wersji TOPSIS Proponowana metoda w pełni wykorzystuje zalety metody drzewa błędów do modelowania, teorii zbiorów rozmytych – do rozwiązywania problemu niepewności

KAMIŃSKI Z, KULIKOWSKI K. **Determination of the functional and service characteristics of the pneumatic system of an agricultural tractor with mechanical brakes using simulation methods**. Eksploatacja i Niezawodnosc – Maintenance and Reliability 2015; 17 (3): 355–364, http://dx.doi.org/10.17531/ein.2015.3.5.

Agricultural tractors are provided with air braking systems to control and operate braking systems of towed agricultural vehicles. Functional and operational characteristics of the tractor pneumatic system have a significant influence on the synchrony and operate speed of tractor-trailer unit braking system. This paper presents a mathematical model to predict the functional and operational characteristics of tractor pneumatic system by using a digital simulation. Modeling of the energy supplying device (compressor, governor, air reservoir) and modeling of the control device with trailer control valve mechanically connected with the tractor brakes is described. Results of statistical Kolmogorov-Smirnov test used to assess the conformity of experimental and simulated pressure transients during testing the compressor capacity and the response time of control circuit of Pronar 320AM tractor confirmed the computer model developed in Matlab-Simulink. The computer model can be used as a tool to assess the functional and operational characteristics of tractor pneumatic system within the designing process and as a subsystem to analyze transient processes in a pneumatic braking systems of the tractor-trailer units by using simulation methods. Mathematical models of selected components can be also used in modeling other pneumatic braking systems of commercial vehicles.

CHENG ZH, YANG ZY, ZHAO JM, WANG YB, LI ZW. **Preventive maintenance strategy optimizing model under two-dimensional warranty policy**. Eksploatacja i Niezawodnosc – Maintenance and Reliability 2015; 17 (3): 365–373, http://dx.doi.org/10.17531/ein.2015.3.6.

An effective warranty servicing strategy should be made considering both warranty cost and product availability. Based on the two-dimensional free repair warranty, a strategy combining the imperfect preventive maintenance and minimal repair is proposed where the imperfect preventive maintenances are implemented in a special subregion of the warranty and all other failures are repaired minimally. By modeling the warranty cost and product availability, we derive the optimum warranty servicing strategy and corresponding parameters to minimize the cost-effective of unit time. Finally, we provide a numerical illustration and a comparison with some other strategies.

CHODURSKI M, DĘBSKI H, SAMBORSKI S, TETER A. **Numerical strength analysis of the load-bearing frame of a palletizing robot's universal head**. Eksploatacja i Niezawodnosc – Maintenance and Reliability 2015; 17 (3): 374–378, http://dx.doi.org/10.17531/ein.2015.3.7.

The paper deals with numerical strength analysis of the load-bearing structure of an industrial robot's head used for palletization of sacks. The calculations were performed with the Finite Element Method (FEM), enabling reconstruction of the real service conditions in the process of palletization. It was assumed, that the head was adapted to lay two sacks of maximal dimensions 800x500x140mm and a mass of up to 50 kg at a time. The currently exploited palletizing heads are heavy, which essentially increases the costs of the palletization process. The aim of the study was a numerical analysis of the existing head of the palletizing robot, leading to design of a structure having optimized maintenance parameters. The conducted research on decreasing the mass of the palletizing robot's head are important because of the industrial robot's load-bearing capacity, its effectiveness and the costs of the palletization process.

ZAITSEVA E, LEVASHENKO V, KOSTOLNY J. **Application of logical differential calculus and binary decision diagramin importance analysis**. Eksploatacja i Niezawodnosc – Maintenance and Reliability 2015; 17 (3): 379–388, http://dx.doi.org/10.17531/ein.2015.3.8.

System availability evaluation includes different aspects of system behaviour and one of them is the importance analysis. This analysis supposes the estimation of system component influence to system availability. There are different mathematical approaches to the development of this analysis. The structure function based approach is one of them. In this case system is presented in form of structure function that is defined the correlation of system availability and its components states. Structure function enables one to represent mathematically a system of any complexity. But computational complexity of structure function based methods is time consuming for large-scale system. Decision of this problem for the calculation of importance measures can be realized based on application of two mathematical approaches. One of them is Direct Partial Boolean Derivative. New equations for calculating the importance measures are obtained in terms of these derivatives. Other approach is Binary Decision Diagram (BDD), which supports efficient manipulation of Boolean algebra. In this paper new algorithms for calculating of importance measures by Direct

oraz MADM – do wyznaczania najlepszej metody wyszukiwania niezdatności, co jest szczególnie przydatne w przypadku diagnozowania niezdatności systemów złożonych.

KAMIŃSKI Z, KULIKOWSKI K. **Wyznaczanie metodami symulacyjnymi właściwości funkcjonalno-użytkowych pneumatycznej instalacji ciągnika rolniczego z hamulcami mechanicznymi**. Eksploatacja i Niezawodnosc – Maintenance and Reliability 2015; 17 (3): 355–364, http://dx.doi.org/10.17531/ein.2015.3.5.

Ciągniki rolnicze są wyposażone w powietrzne instalacje hamulcowe do sterowania i napędu układów hamulcowych pojazdów ciągnionych. Właściwości funkcjonalno-użytkowe instalacji pneumatycznej ciągnika mają istotny wpływ na synchronię i szybkość działania układu hamulcowego zespołu ciągnik-przyczepa. W niniejszej pracy przedstawiono model matematyczny do prognozowania właściwości funkcjonalno-użytkowych układu pneumatycznego ciągnika metodą symulacji cyfrowej. Opisano modelowanie zespołu zasilającego (sprężarka, regulator, zbiornik powietrza) i modelowanie zespołu sterującego z zaworem sterującym hamulcami przyczepy połączonym mechanicznie z hamulcami ciągnika. Wyniki testu statystycznego Kołmogorowa-Smirnowa oceny zgodności doświadczalnych i symulowanych przebiegów czasowych ciśnienia podczas badania wydatku sprężarki i czasu reakcji obwodu sterującego ciągnika Pronar 320AM potwierdziły adekwatność opracowanego w Matlabie-Simulinku modelu komputerowego. Model komputerowy może być wykorzystany jako narzędzie do oceny właściwości eksploatacyjno-użytkowych instalacji pneumatycznej ciągnika w procesie projektowania oraz jako podsystem do analizy metodami symulacyjnymi procesów przejściowych w pneumatycznych układach hamulcowych zespołów ciągnik-przyczepa. Modele matematyczne wybranych komponentów instalacji mogą być również wykorzystane w modelowaniu innych pneumatycznych układów hamulcowych pojazdów użytkowych.

CHENG ZH, YANG ZY, ZHAO JM, WANG YB, LI ZW. **Model optymalizacji strategii konserwacji zapobiegawczej w warunkach dwuwymiarowej polityki gwarancyjnej**. Eksploatacja i Niezawodnosc – Maintenance and Reliability 2015; 17 (3): 365–373, http://dx.doi.org/10.17531/ein.2015.3.6.

Efektywna strategia obsługi gwarancyjnej powinna uwzględniać zarówno koszty gwarancji jak i dyspozycyjność produktu. W oparciu o pojęcie dwuwymiarowej gwarancji bezpłatnej naprawy, zaproponowano strategię łączącą niepełną konserwację zapobiegawczą z naprawą minimalną, gdzie działania obsługowe w ramach niepełnej konserwacji zapobiegawczej przeprowadza się w ramach specjalnego podobszaru gwarancji, a wszelkie inne uszkodzenia naprawia się w ramach naprawy minimalnej. Modelując koszty naprawy oraz dyspozycyjność produktu, wyprowadzono optymalną strategię obsługi gwarancyjnej oraz odpowiadające jej parametry w celu zminimalizowania kosztów na jednostkę czasu. Na koniec, proponowane rozwiązanie zilustrowano na przykładzie numerycznym oraz porównano z innymi strategiami.

CHODURSKI M, DĘBSKI H, SAMBORSKI S, TETER A. **Numeryczna analiza wytrzymałości ramy nośnej uniwersalnej głowicy robota paletyzującego**. Eksploatacja i Niezawodnosc – Maintenance and Reliability 2015; 17 (3): 374–378, http://dx.doi.org/10.17531/ein.2015.3.7.

W prezentowanej pracy zajęto się numeryczną analizą wytrzymałościową ustroju nośnego głowicy robota przemysłowego, która służy do paletyzacji worków. Obliczenia prowadzono z zastosowaniem metody elementów skończonych, umożliwiającej odwzorowanie rzeczywistych warunków eksploatacyjnych pracy robota w procesie paletyzacji. W obliczeniach przyjęto, że głowica jest przystosowana do układania dwóch worków jednocześnie o maksymalnych wymiarach gabarytowych: 800mm, 500mm, 140mm oraz masie do 50 kg. Stosowane obecnie głowice paletyzujące są ciężkie, co znacznie podnosi koszty procesu paletyzacji. Celem pracy była analiza numeryczna istniejącej głowicy robota paletyzującego, na podstawie której możliwe będzie zaprojektowanie konstrukcji o zoptymalizowanych parametrach eksploatacyjnych. Prowadzone prace nad redukcją masy własnej głowicy robota paletyzującego są istotne ze względu na nośność robota przemysłowego, wydajność oraz koszt procesu paletyzacji.

ZAITSEVA E, LEVASHENKO V, KOSTOLNY J. **Zastosowanie logicznego rachunku różniczkowego oraz binarnego diagramu decyzyjnego w analizie ważności**. Eksploatacja i Niezawodnosc – Maintenance and Reliability 2015; 17 (3): 379–388, http://dx.doi.org/10.17531/ein.2015.3.8.

Ocena gotowości systemu, analiza czułości, miary ważności oraz optymalna konstrukcja to istotne zagadnienia, które stały się obiektem badań z zakresu inżynierii niezawodności. Istnieją różne podejścia matematyczne do owych problemów. Jednym z nich jest podejście oparte na funkcji struktury. Funkcja struktury umożliwia analizę systemów o wszelkim stopniu złożoności. Jednakże, w przypadku sieci o dużej skali, złożoność obliczeniowa metod opartych na funkcji struktury sprawia, że metody te są czasochłonne. W przedstawionej pracy proponujemy wykorzystanie dwóch metod matematycznych analizy ważności. Pierwszą z nich jest bezpośrednia cząstkowa pochodna boole'owska, w kategoriach której opracowano nowe równania do obliczania miar ważności. Drugą jest binarny diagram decyzyjny, który wspiera efektywną manipulację na wyrażeniach algebry Boole'a. W artykule zaproponowano dwa algorytmy służące do obliczania bezpośredniej cząstkowej pochodnej boole'owskiej w oparciu o binarny diagram decyzyjny funkcji struktury. Wyniki eksperymentów wykazują skuteczność nowo opracowanych algorytmów w obliczaniu bezpośredniej cząstkowej pochodnej boole'owskiej oraz miar ważności.

Partial Boolean Derivative based on BDD are proposed. The experimental results of comparison these algorithms with other show the efficiency of new algorithms for calculating Direct Partial Boolean Derivative and importance measures.

GAO W, ZHANG Z, JI H, ZHOU J, LIU Q. **Optimal quasi-periodic preventive maintenance policies for a repairable system with stochastic maintenance interval**. Eksploatacja i Niezawodnosc – Maintenance and Reliability 2015; 17 (3): 389–397, http://dx.doi.org/10.17531/ein.2015.3.9.

The usual preventive maintenance (PM) of a repairable system is done before failure at integer multiples of time T. In some real cases, PM cannot be performed as soon as a planned PM period is reached because of effects of some random factors, while it is usually done within an implemented period, and thus it makes the PM period become a stochastic interval. From this viewpoint, a quasi-periodic imperfect preventive maintenance policy is proposed in this paper, in which a repairable system experiences either a minor failure or catastrophic failure when a failure occurs, and the first (N-1) PM intervals is divided into a planned PM period and an implemented period. In the former, the system may be suffered an unplanned PM for removing a catastrophic failure and performing a PM, whereas in the latter, the system is preventively maintained following an occurrence of a catastrophic failure or a dynamic PM plan, whichever comes first. At the Nth PM interval, the system is replaced either when a catastrophic failure occurs or operational time reaches T, whichever comes first. An optimization of the proposed mode is introduced, the existence and the uniqueness of the optimal solution are presented, and a useful constraint of the implemented period is obtained. Finally, a real case study of PM on Chinese diesel locomotives is examined to illustrate the proposed maintenance policy.

GAO W, ZHANG Z, JI H, ZHOU J, LIU Q. **Optymalna strategia quasi-okresowej konserwacji zapobiegawczej systemu naprawialnego – czas między przeglądami jako wielkość stochastyczna**. Eksploatacja i Niezawodnosc – Maintenance and Reliability 2015; 17 (3): 389–397, http://dx.doi.org/10.17531/ein.2015.3.9.

Zazwyczaj przeglądy okresowe systemu naprawialnego wykonuje się przed wystąpieniem uszkodzenia, w określonych odstępach czasu stanowiących całkowitą wielokrotność czasu T. W warunkach rzeczywistych, jednak, nie zawsze można przeprowadzić przegląd w zaplanowanym terminie ze względu na działanie pewnych losowych czynników, natomiast zazwyczaj przeprowadza się go w dopuszczalnym okresie realizacji, w związku z czym przedział czasu między przeglądami okresowymi staje się wielkością stochastyczną. Biorąc powyższe pod uwagę, w niniejszej pracy zaproponowano strategię quasi-okresowej konserwacji zapobiegawczej, która zakłada, że system naprawialny może ulec albo drobnemu uszkodzeniu albo uszkodzeniu katastroficznemu, a czas, do którego należy wykonać pierwszy przegląd okresowy (N-1) można podzielić na zaplanowany czas przeprowadzenia przeglądu oraz dopuszczalny okres realizacji przeglądu. W pierwszym przypadku, może wystąpić konieczność przeprowadzenia nieplanowanej konserwacji systemu mającej na celu usunięcie uszkodzenia katastroficznego, natomiast w drugim, konserwację przeprowadza się po wystąpieniu uszkodzenia katastroficznego lub zgodnie z dynamicznym harmonogramem przeglądów, zależnie od tego, która z sytuacji zaistnieje wcześniej. W N-tym terminie przeglądu okresowego, dokonuje się wymiany systemu, albo wskutek wystąpienia uszkodzenia katastroficznego albo gdy czas pracy systemu osiągnie wartość T, zależnie od tego, co nastąpi wcześniej. W artykule przedstawiono optymalizację proponowanego trybu działania, wykazano istnienie i jednoznaczność optymalnego rozwiązania oraz wyznaczono przydatne ograniczenie dopuszczalnego okresu realizacji. Na koniec, proponowaną politykę konserwacji zapobiegawczej zilustrowano studium przypadku chińskich lokomotyw spalinowych.

PAWLAK M, KOŚCIELNY JM, WASIEWICZ P. **Method of increasing the reliability and safety of the processes through the use of fault tolerant control systems**. Eksploatacja i Niezawodnosc – Maintenance and Reliability 2015; 17 (3): 398–407, http://dx.doi.org/10.17531/ein.2015.3.10.

The operation idea of fault tolerant control systems, has been presented in the paper. Protection and security layers applied in technical diagnostics associated with safety of control system, have been discussed. The automatic control system of a steam turbine power, has been described as an example of fault tolerant control system. A steam turbine is the main element of energy blocs forming a national energy system. Therefore, the turbine control systems require high reliability. The impact of diagnostics and fault tolerance on the values of reliability and safety coefficients of control systems, have been determined in the paper.

PAWLAK M, KOŚCIELNY JM, WASIEWICZ P. **Metoda podwyższania niezawodności i bezpieczeństwa procesów poprzez stosowanie układów regulacji tolerujących uszkodzenia**. Eksploatacja i Niezawodnosc – Maintenance and Reliability 2015; 17 (3): 398–407, http://dx.doi.org/10.17531/ein.2015.3.10.

Przedstawiono ideę działania układów automatyki tolerujących uszkodzenia. Omówiono warstwy zabezpieczeniowo ochronne stosowane w diagnostyce technicznej, związanej z bezpieczeństwem układów regulacji. Jako przykład układu regulacji tolerującego uszkodzenia torów pomiarowych, opisano układ regulacji mocy turbiny parowej. Turbiny takie stanowią podstawowy element bloków energetycznych, tworzących krajowy system energetyczny. Dlatego też, od układów regulacji turbin wymaga się dużej niezawodności. W pracy określono wpływ diagnostyki i tolerowania uszkodzeń na wartości wskaźników niezawodności i bezpieczeństwa układów automatyki.

SINGH SSK, ABDULLAH S, MOHAMED NAN. **Reliability analysis and prediction for time to failure distribution of an automobile crankshaft**. Eksploatacja i Niezawodnosc – Maintenance and Reliability 2015; 17 (3): 408–415, http://dx.doi.org/10.17531/ein.2015.3.11.

This paper emphasizes on analysing and predicting the reliability of an automobile crankshaft by analysing the time to failure (TTF) through the parametric distribution function. The TTF was modelled to predict the likelihood of failure for crankshaft during its operational condition over a given time interval through the development of the stochastic algorithm. The developed stochastic algorithm has the capability to measure the parametric distribution function and validate the predict the reliability rate, mean time to failure and hazard rate. T, the algorithm has the capability to statistically validate the algorithm to obtain the optimal parametric model to represent the failure of the component against the actual time to failure data from the local automobile industry. Hence, the validated results showed that the three parameter Weibull distribution provided an accurate and efficient foundation in modelling the reliability rate when compared with the actual sampling data. The suggested parametric distribution function can be used to improve the design and the life cycle due to its capability in accelerating and decelerating the mechanism of failure based on time without adjusting the level of stress. Therefore, an understanding of the parametric distribution posed by the reliability and hazard rate onto the component can be used to improve the design and increase the life cycle based on the dependability of the component over a given period of time. The proposed reliability assessment through the developed stochastic algorithm provides an accurate, efficient, fast and cost effective reliability analysis in contrast to costly and lengthy experimental techniques.

SINGH SSK, ABDULLAH S, MOHAMED NAN. **Analiza niezawodności i przewidywanie rozkładu czasu do uszkodzenia wału korbowego pojazdu samochodowego**. Eksploatacja i Niezawodnosc – Maintenance and Reliability 2015; 17 (3): 408–415, http://dx.doi.org/10.17531/ein.2015.3.11.

W prezentowanej pracy przedstawiono metodę analizy oraz predykcji niezawodności wału korbowego pojazdu samochodowego opartą na analizie czasu do uszkodzenia (TTF) z wykorzystaniem funkcji rozkładu parametrycznego. W artykule, stworzono model TTF pozwalający na przewidywanie prawdopodobieństwa uszkodzenia wału korbowego w stanie pracy w danym przedziale czasu za pomocą nowo opracowanego algorytmu stochastycznego. Opracowany algorytm stochastyczny umożliwia mierzenie funkcji rozkładu parametrycznego oraz weryfikację przewidywanego współczynnika niezawodności, średniego czasu do uszkodzenia oraz współczynnika zagrożenia. Algorytm daje możliwość statystycznej weryfikacji modelu w odniesieniu do rzeczywistych danych dotyczących czasu do uszkodzenia pochodzących z lokalnego przemysłu samochodowego. Weryfikacja taka pozwala na otrzymanie optymalnego modelu parametrycznego reprezentującego uszkodzenie części składowej. Zweryfikowane wyniki wykazały, że trójparametrowy rozkład Weibulla stanowi dokładne i wydajne narzędzie do modelowania współczynnika niezawodności w zestawieniu z rzeczywistymi danymi z próby. Proponowaną dystrybuantę parametryczną można wykorzystywać do doskonalenia konstrukcji oraz cyklu życia wału korbowego ponieważ daje ona możliwość przyspieszania i zwalniania mechanizmu uszkodzenia, na podstawie czasu, bez potrzeby regulacji poziomu naprężenia. Zatem, znajomość rozkładu parametrycznego oraz obliczonych na jego podstawie współczynników niezawodności i zagrożenia omawianego elementu mechanizmu korbowego, pozwala na doskonalenie konstrukcji oraz wydłużenie cyklu życia wału korbowego w oparciu o dane dotyczące jego niezawodności w danym okresie czasu. Proponowana metoda oceny niezawodności z wykorzystaniem opracowanego w artykule algorytmu stochastycznego umożliwia dokładną, wydajną, szybką i tanią analizę niezawodności w odróżnieniu od kosztownych i czasochłonnych technik eksperymentalnych.

GODZIMIRSKI J, JANISZEWSKI J, ROŚKOWICZ M, SURMA Z. **Ballistic resistance tests of multi-layer protective panels**. Eksploatacja i Niezawodnosc – Maintenance and Reliability 2015; 17 (3): 416–421, http://dx.doi.org/10.17531/ein.2015.3.12.

Modern light-weight ballistic amours are usually multi-layer structures with low density. The aim of the study was to evaluate the possibility of using multi-layer structures for lightweight armour systems which may be applied as bulletproof ballistic panels of combat helicopters and other lightweight military equipment. The tested multi-layer structures were prepared on the basis of aramid fabrics, thin sheets of 2024-T3 aluminium alloy and Al_2O_3 and SiC ceramics. Additionally, the influence of adhesive connections between the components of the ballistic panels on their protective properties has been assessed. Absorbing energy of a spherical projectile was determined with the use of a laboratory stand consisted of a one-stage helium gas gun and a digital high speed camera. A penetration study on the selected multi-layer panels was also carried out with the use of Parabellum ammunition. It has been shown that the laminated structures composed of thin layers of metal and aramid fabric indicate a lower absorb energy-to-composite basic weight ratio than analogues ratios for metal sheets or fabrics used to produce laminated structures. Similarly, the sandwiches of loose aramid fabrics demonstrate greater ballistic resistance compared to the polymer composites made of such fabrics. There has been also demonstrated the desirability of the use of a ceramic component as a separate layer in which ceramic segments are glued between two layers of a thin metal sheet.

GODZIMIRSKI J, JANISZEWSKI J, ROŚKOWICZ M, SURMA Z. **Badania odporności na przebicie osłon o strukturze wielowarstwowej**. Eksploatacja i Niezawodnosc – Maintenance and Reliability 2015; 17 (3): 416–421, http://dx.doi.org/10.17531/ein.2015.3.12.

Współczesne lekkie osłony balistyczne są zwykle strukturami wielowarstwowymi o małej gęstości. Celem badań była ocena możliwości zastosowania struktur wielowarstwowych na lekkie pancerze, mogące znaleźć zastosowanie jako kuloodporne osłony balistyczne śmigłowców bojowych i innego lekkiego sprzętu wojskowego. Badane materiały przygotowano na bazie tkanin aramidowych, cienkich blach ze stopu aluminium 2024-T3 oraz ceramiki typu Al_2O_3 i SiC. Dodatkowo oceniono wpływ zastosowania połączeń adhezyjnych pomiędzy komponentami osłon balistycznych na ich właściwości ochronne. Określono energię przebijania osłon wykorzystując do tego celu stanowisko zbudowane na bazie działa helowego oraz szybkiej kamery. Wykonano również próby przebicia wytypowanych osłon pociskiem naboju Parabellum. Wykazano, że klejone struktury złożone z cienkich warstw metalowych i tkanin aramidowych charakteryzuje mniejsza odporność na przebicie odniesiona do ich gramatury niż blach metalowych i tkanin, z których były wytwarzane. Również pakiety luźnych tkanin aramidowych cechuje większa odporność na przebicie w porównaniu z kompozytami polimerowymi wytworzonymi z takich tkanin. Wykazano celowość stosowania komponentu ceramicznego w postaci oddzielnego pakietu,w którym płytki ceramiki wklejone są pomiędzy dwie warstwy cienkiej blachy.

KUMBÁR V, VOTAVA J. **Numerical modelling of pressure and velocity rates of flowing engine oils in real pipe**. Eksploatacja i Niezawodnosc – Maintenance and Reliability 2015; 17 (3): 422–426, http://dx.doi.org/10.17531/ein.2015.3.13.

The article deals with the numerical modelling of physical state flowing liquid in a real environment of real technical component (pipe). Specifically it is about to set the pressured and velocity rates along the pipe geometry in a certain places for temperature dependent material (three engine oil with different viscosity class) at three monitored temperatures of flowing medium. The numerical models were created by means finite element method. Observation focused mainly on places behind technical component geometry curvature which are from the point of view of flowing features most interesting.

KUMBÁR V, VOTAVA J. **Numeryczne modelowanie ciśnienia i prędkości przepływu oleju silnikowego przez przewód rurowy w warunkach rzeczywistych**. Eksploatacja i Niezawodnosc – Maintenance and Reliability 2015; 17 (3): 422–426, http://dx.doi.org/10.17531/ein.2015.3.13.

Artykuł dotyczy modelowania numerycznego stanu fizycznego cieczy płynącej w rzeczywistym środowisku rzeczywistego elementu technicznego (przewodu rurowego). W szczególności, celem pracy było określenie ciśnienia i prędkości przepływu materiału, którego właściwości zależą od temperatury, w określonych punktach przewodu rurowego dla trzech monitorowanych temperatur przepływającego czynnika. Do badań użyto trzech typów oleju silnikowego o różnej klasie lepkości. Modele numeryczne tworzono za pomocą metody elementów skończonych. Obserwacje prowadzono głównie w miejscach tuż za zakrzywieniami elementu technicznego, które są najbardziej interesujące z punktu widzenia właściwości przepływu.

MOCEK P, ZAMIAR R, JACHIMCZYK R, GOWARZEWSKI R, ŚWIĄDROWSKI J, GIL I, STAŃCZYK K. **Selected issues of operating 3 MW underground coal gasification installation**. Eksploatacja i Niezawodnosc – Maintenance and Reliability 2015; 17 (3): 427–434, http://dx.doi.org/10.17531/ein.2015.3.14.

Experiences of operating underground coal gasification installation (UCG) are discussed in the article. The gasification experiment was conducted in active Wieczorek coal mine. The assumed maximum gasification capacity of the installation was 600 kg/h of coal, i.e. 3 MW contained in enthalpy of gas. An integrated design process was applied in preparing equipment of the UCG installation. The result was long-lasting tests (over 1400 h) of coal gasification process at near- atmospheric pressure. Gasification was conducted in a 5.4 m thick deposit with a mixture of: air and oxygen, air and CO2, air and water. Data on performance of a semi-industrial scale UCG installation were collected. The aim of the article is to present the process and selected experiences associated with operating the installation. External limitations influencing the gasification method, design of basic nodes and rules of running the process are described. The main problems encountered during the gasification process and UCG gas purification are presented.

MOCEK P, ZAMIAR R, JACHIMCZYK R, GOWARZEWSKI R, ŚWIĄDROWSKI J, GIL I, STAŃCZYK K. **Wybrane zagadnienia eksploatacji instalacji podziemnego zgazowania węgla o mocy termicznej 3 MW**. Eksploatacja i Niezawodnosc – Maintenance and Reliability 2015; 17 (3): 427–434, http://dx.doi.org/10.17531/ein.2015.3.14.

Omówiono doświadczenia z eksploatacji urządzeń podziemnego zgazowania węgla (PZW). Próbę zgazowania przeprowadzono w funkcjonującej Kopalni Węgla Kamiennego "Wieczorek". Projektowana wydajność zgazowania wynosiła 600 kg/h węgla. Przekłada się to na 3 MW mocy termicznej zawartej w entalpii gazu. Przygotowując urządzenia instalacji PZW zastosowano zintegrowany cykl projektowania. Wynikiem było przeprowadzenie długotrwałych (ponad 1400 h) badań procesu zgazowania węgla przy ciśnieniu zbliżonym do atmosferycznego. Zgazowanie prowadzono w złożu o średniej miąższości 5.4 m wykorzystując mieszaninę: powietrza i tlenu, powietrza i CO_2 oraz powietrza i wody. Uzyskano informacje z funkcjonowania w skali półtechnicznej instalacji PZW. Celem publikacji jest przedstawienie procesu i wybranych doświadczeń z funkcjonowania tej instalacji. Opisano ograniczenia zewnętrzne wpływające na sposób rozwiązania technologii zgazowania, konstrukcje podstawowych węzłów i zasady prowadzenia procesu. Wskazane zostały główne problemy występujące w trakcie procesu zgazowania i oczyszczania gazu z PZW.

YANG H, XU G, FAN XN. **A reliability analysis method of cloud theory – Monte Carlo based on performance degradation data**. Eksploatacja i Niezawodnosc – Maintenance and Reliability 2015; 17 (3): 435–442, http://dx.doi.org/10.17531/ein.2015.3.15.

Owing to inadequate degradation data, the randomness and the fuzziness of degradation processes, it is difficult to calculate the reliability of product. By investigating performance reliability using degradation data of performance, the authors proposed a method of analyzing reliability of performance degradation data using Monte Carlo principle and cloud theory. First of all, the performance degradation cloud with the degradation amount and the entropy which denotes the possible discrete degree of the degradation data, is generated by using performance degradation data and a cloud theory forward cloud generator. Then, the minimum membership threshold of cloud droplets and the threshold of product failure were set. Meanwhile, the number of cloud droplets that comply with the minimum membership degree and the failure threshold were counted. Finally, the reliability method of performance degradation data was proposed by using the principle of Monte Carlo and the cloud theory. In this work, the cloud theory was introduced to verify the reliability of the performance degradation of the product. The randomness and the fuzziness in the degradation tests are resolved. In addition, due to the limits of degradation test data, the difficulties in

YANG H, XU G, FAN XN. **Oparta na teorii chmury i modelu Monte Carlo metoda analizy niezawodnościowej danych o obniżeniu charakterystyk**. Eksploatacja i Niezawodnosc – Maintenance and Reliability 2015; 17 (3): 435–442, http://dx.doi.org/10.17531/ein.2015.3.15.

Ze względu na niewystarczające dane o degradacji oraz losowość i rozmycie procesów degradacji, obliczanie niezawodności produktu jest zadaniem trudnym. Chcąc badać niezawodność przy użyciu danych dotyczących obniżenia charakterystyk, autorzy zaproponowali metodę analizy danych o obniżeniu charakterystyk wykorzystującą zasady metody Monte Carlo oraz teorii chmury. Po pierwsze, wykorzystując dane o obniżeniu charakterystyk oraz progresywny generator chmur, wygenerowano chmurę obniżenia charakterystyk zawierającą dane na temat stopnia degradacji oraz stopnia entropii, która określa możliwy dyskretny stopień degradacji danych. Następnie, ustalono minimalny próg przynależności punktów chmury oraz próg uszkodzenia produktu. Policzono liczbę punktów chmury które spełniały warunek minimalnego stopnia przynależności oraz progu uszkodzenia. Wreszcie, zaproponowano metodę analizy niezawodnościowej danych o obniżeniu charakterystyk wykorzystującą zasady modelu Monte Carlo oraz teorii chmury. W pracy przedstawiono teorię chmury, która pozwala na weryfikację niezawodności danych of obniżeniu charakterystyk produktu. Rozwiązano w ten sposób problem losowości i rozmycia występujące w badaniach degradacji. Ponadto, przy użyciu metody Monte Carlo, calculation of the reliability is resolved using the principle of Monte Carlo, the minimum membership of cloud droplets and its minimum degree are therefore guaranteed. This work provides a new method of simulating the reliability of degradation. The feasibility of the method was validated by an example ensuring a high durability of conveyor belt joints is tantamount to guaranteeing their reliable operation and that the results of research conducted so far fail to provide unambiguous solutions to a number of problems that emerge in this case, it is advisable that advanced studies using computer techniques should be conducted within this area.

rozwiązano trudności w obliczaniu niezawodności związane z ograniczeniami danych z badań degradacji, co zagwarantowało minimalną przynależność punktów chmury oraz minimalny stopień uszkodzenia. W prezentowanej pracy przedstawiono nową metodę symulacji niezawodności danych o degradacji. Poprawność przedstawionej metody zweryfikowano na podstawie przykładu. Zapewnienie wysokiej trwałości złączy taśmy przenośnikowej jest równoznaczne z zapewnieniem ich niezawodnej pracy, a ponieważ wyniki prowadzonych dotąd badań nie dostarczają jednoznacznych rozwiązań wielu wyłaniających się w tym przypadku problemów, wskazane jest prowadzenie w tym zakresie zaawansowanych badań z użyciem technik komputerowych.

PŁACZEK M, BUCHACZ A, WRÓBEL A. **Use of piezoelectric foils as tools for structural health monitoring of freight cars during exploitation**. Eksploatacja i Niezawodnosc – Maintenance and Reliability 2015; 17 (3): 443–449, http://dx.doi.org/10.17531/ein.2015.3.16.

Work presents a task of piezoelectric foils application for structural health monitoring of freight cars during their exploitation. Results of laboratory tests conducted on a created in scale laboratory model of the freight car are presented. The possibility of inferred from the dynamic response of the model about the changes in its technical condition was verified. During the first test the model was treated as a half-determined system. In order to excite vibrations a pendulum was used. Measurements were carried out using accelerometers. During the next stage of carried out tests the dynamical response of the model was measured while the object was driving. In order to measure vibrations of the system a Macro Fiber Composite (MFC) piezoelectric foil was used. It was glued on the surface of the model. A series of tests of the model with and without load, as well as with an obstacle on the rail track was carried out. Measured signals were juxtaposed on charts and analysed.

PŁACZEK M, BUCHACZ A, WRÓBEL A. **Użycie Folii piezoelektrycznych jako narzędzi do monitorowania stanu technicznego wagonu towarowego w trakcie eksploatacji**. Eksploatacja i Niezawodnosc – Maintenance and Reliability 2015; 17 (3): 443–449, http://dx.doi.org/10.17531/ein.2015.3.16.

W pracy przedstawiono zagadnienia dotyczące zastosowania folii piezoelektrycznych do monitorowania stanu technicznego wagonów towarowych w trakcie ich eksploatacji. Przedstawiono wyniki badań laboratoryjnych prowadzonych na utworzonym w skali modelu węglarki. Określono możliwość wykrycia zmian stanu technicznego wagonu na podstawie analizy jego odpowiedzi dynamicznej. W pierwszym etapie badań obiekt traktowano jako półokreślony, w celu wymuszenia drgań stosowano wahadło. Pomiar odpowiedzi dynamicznej układu w poszczególnych punktach pomiarowych przeprowadzono z użyciem akcelerometrów. Kolejnym etapem badań był pomiar odpowiedzi dynamicznej modelu w trakcie jazdy. W celu pomiaru drgań konstrukcji nośnej modelu zastosowano przetwornik piezoelektryczny typu Macro Fiber Composite (MFC), który naklejono na powierzchni modelu. Przeprowadzono ciąg badań modelu bez obciążenia oraz z obciążeniem, a także z przeszkodami umieszczonymi na jednej bądź obu szynach. Otrzymane przebiegi zestawiono na wykresach oraz omówiono wyniki badań.

HAO L, ZHENCAI Z. **A copula-based method for reliability sensitivity analysis of structural system with correlated failure modes**. Eksploatacja i Niezawodnosc – Maintenance and Reliability 2015; 17 (3): 450–456, http://dx.doi.org/10.17531/ein.2015.3.17.

Despite many advances in the field of computational reliability analysis, the efficient estimation of the reliability and reliability sensitivity analysis of structural systems with multiple failure modes remains a persistent challenge. The key to deal with the problem lies in the correlation modelling between failure modes. In this paper, the Archimedean copulas are used as an alternative to solve the high-dimensional dependence modeling problem. The probability characteristics of failure modes are described by stochastic perturbation technique, and the reliability index is estimated with the fourth-moment standardization method. Considering that the number of the potential failure modes of the structural systems are relatively large, the probabilistic network evaluation technique is adopted to reduce the computational complexity. The sensitivity analysis is then conducted using the matrix differential technology. The numerical examples show that the applied procedure is able to efficiently consider various failure modes of structural systems in probabilistic assessment and sensitivity analysis.

HAO L, ZHENCAI Z. **Oparta na pojęciu kopuły metoda analizy czułości niezawodnościowej systemu konstrukcyjnego o skorelowanych przyczynach uszkodzeń**. Eksploatacja i Niezawodnosc – Maintenance and Reliability 2015; 17 (3): 450–456, http://dx.doi.org/10.17531/ein.2015.3.17.

Mimo poważnych osiągnięć w dziedzinie komputerowej analizy niezawodności, skuteczna ocena niezawodności i analiza czułości niezawodnościowej systemów konstrukcyjnych o wielu przyczynach uszkodzeń pozostają ciągłym wyzwaniem. Kluczem do rozwiązania problemu jest modelowanie korelacji między przyczynami uszkodzeń. W niniejszym artykule zastosowano kopuły Archimedesa jako alternatywny sposób rozwiązania problemu modelowania zależności wysoko wymiarowych. Charakterystyki prawdopodobieństwa dla przyczyn uszkodzeń opisano przy pomocy metody zaburzeń stochastycznych, zaś wskaźnik niezawodności oszacowano metodą standaryzacji momentu czwartego rzędu. Biorąc pod uwagę, że liczba potencjalnych przyczyn uszkodzeń systemów konstrukcyjnych jest stosunkowo duża, wykorzystano technikę oceny z zastosowaniem sieci probabilistycznych, która pozwala na zmniejszenie złożoności obliczeniowej. Następnie przeprowadzono analizę czułości przy użyciu metody macierzy równań różniczkowych. Przykłady liczbowe pokazują, że zastosowana procedura pozwala na skuteczną ocenę różnych przyczyn uszkodzeń systemów konstrukcyjnych w ramach oceny probabilistycznej oraz analizy czułości.

WOCH M, KURDELSKI M, MATYJEWSKI M. **Reliability at the checkpoints of an aircraft supporting structure**. Eksploatacja i Niezawodnosc – Maintenance and Reliability 2015; 17 (3): 457–462, http://dx.doi.org/10.17531/ein.2015.3.18.

For complex systems, such as the structure of an aircraft, the implementation of prognostic and health management techniques can effectively improve system performance. This paper presents some recent results of research on risk assessment for aircraft structures and intends to show the procedures of reliability calculation for a point of aircraft structure as an object under investigation. In this paper, the ways to determine failure rate and failure probability at the location of interest have been presented based on the example of the PZL-130 TC II ORLIK aircraft structure. The results can be applied to optimize the process of aircraft flight authorization, while ensuring safety during operations.

WOCH M, KURDELSKI M, MATYJEWSKI M. **Niezawodność w punktach struktury nośnej statków powietrznych**. Eksploatacja i Niezawodnosc – Maintenance and Reliability 2015; 17 (3): 457–462, http://dx.doi.org/10.17531/ein.2015.3.18.

W przypadku złożonych systemów, jakim jest struktura samolotu wdrożenie technik prognostycznych oraz zarządzania czasem zdatności do eksploatacji może skutecznie poprawić wydajność systemu. Celem publikacji jest przedstawienie metody oceny niezawodności konstrukcji lotniczych oraz odpowiedniej procedury obliczeń wraz z ostatnimi wynikami badań. W niniejszej pracy określono chwilową intensywność uszkodzeń oraz prawdopodobieństwo awarii w wybranych miejscach struktury samolotu PZL-130 TC II ORLIK. Uzyskane wyniki mogą być zastosowane do optymalizacji procesu dopuszczenia statków powietrznych do lotów, przy jednoczesnym zapewnieniu bezpieczeństwa ich eksploatacji.

KILIKEVIČIENĖ K, SKEIVALAS J, KILIKEVIČIUS A, PEČELIŪNAS R, BUREIKA G. **The analysis of bus air spring condition influence upon the vibration signals at bus frame**. Eksploatacja i Niezawodnosc – Maintenance and Reliability 2015; 17 (3): 463–469, http://dx.doi.org/10.17531/ein.2015.3.19.

The paper analyses the spread of vibration intensity through the bus frame mechanical structure. The research has been completed upon application of the theory of covariance functions. Results of measuring the intensity of vibrations at fixed bus framepoints were recorded on the time scale in the form of data arrays (matrixes). The authors have completed the estimation of covariance functions by measuring the intensity of vibrations between the arrays of digital results and auto-covariance functions of single arrays upon changing the quantization interval on the time scale. The research results enable to define if the solidity of bus frame is disordered and to assess the technical condition of pneumatic suspension considering the vibration of

KILIKEVIČIENĖ K, SKEIVALAS J, KILIKEVIČIUS A, PEČELIŪNAS R, BUREIKA G. **Analiza wpływu stanu technicznego resora pneumatycznego autobusu na sygnały drgań w ramie autobusu**. Eksploatacja i Niezawodnosc – Maintenance and Reliability 2015; 17 (3): 463–469, http://dx.doi.org/10.17531/ein.2015.3.19.

W pracy przeprowadzono analizę rozkładu intensywności drgań w mechanicznej konstrukcji ramy autobusu. Badania prowadzono z zastosowaniem teorii funkcji kowariancji. Wyniki pomiaru intensywności drgań w ustalonych punktach ramy autobusu rejestrowano na skali czasu, w postaci tablic danych (matryc). Funkcje kowariancji obliczano porównując natężenie drgań pomiędzy tablicami wyników cyfrowych, zaś funkcje auto-kowariancji pojedynczych tablic obliczano po zmianie przedziału kwantyzacji w skali czasowej. Wyniki badań pozwalają na określenie, czy zaburzona została stabilność struktury ramy autobusowej oraz umożliwiają ocenę stanu technicznego zawieszenia pneumatycznego na podstawie drgań w określonych punktach ramy. Wyniki te można wykorzystać do frame points. Dangerous zones of bus suspension and reliability level of bus exploitation can be determined by application of these results.

JAŚKOWSKI P. **Methodology for enhancing reliability of predictive project schedules in construction**. Eksploatacja i Niezawodnosc – Maintenance and Reliability 2015; 17 (3): 470–479, http://dx.doi.org/10.17531/ein.2015.3.20.

Construction projects consist in providing new built facilities as well as in maintaining the existing building stock. Reliability engineering in construction encompasses all stages of the structure's life cycle from the earliest concept of the project to decommissioning. The project planning and design stages are aimed at selecting or creating technical and organisational solutions to assure that the built facility meets the sponsor's and the user's requirements; these requirements regulate also the construction process. The result of planning the construction process should be a reliable schedule – immune to disruptive effects of random occurrences, so assuring high probability of the actual processes meeting their predefined deadlines. A practical method of scheduling construction projects should enable the planner to generate schedules resistant to random occurrences, making them reliable so that the users can meet deadlines. The paper presents a proactive methodology for generating construction schedules of enhanced reliability. The methodology covers two fundamental stages. The first stage is a construction duration risk assessment based on a multi-attribute evaluation of operating conditions. The second stage is the allocation of time buffers. An original methodology supporting decisions at each stage is put forward, namely a methodology for evaluating process duration risk level, defining significance of operating conditions, estimating dispersion of process durations, and defining criticality of processes in the schedule. The author proposes a set of measures of schedule robustness to serve as surrogate criteria in the schedule instability cost minimization problem and buffer sizing. The proposed way of allowing for risk and uncertainty in creating reliable schedules is argued to be efficient in protecting the project completion date, as well as stage or even process start dates, against disruptions.

określenia niebezpiecznych stref zawieszenia autobusowego oraz poziomu niezawodności pracy autobusu.

JAŚKOWSKI P. **Metodyka zwiększenia niezawodności predyktywnych harmonogramów realizacji przedsięwzięć budowlanych**. Eksploatacja i Niezawodnosc – Maintenance and Reliability 2015; 17 (3): 470–479, http://dx.doi.org/10.17531/ein.2015.3.20.

Przedsięwzięcia budowlane obejmują swym zakresem procesy związane z wznoszeniem nowych obiektów, jak i utrzymaniem istniejących zasobów. Inżynieria niezawodności w budownictwie obejmuje wszystkie fazy cyklu życia obiektu budowlanego, od przygotowania koncepcyjnego po jego likwidację. Na etapie planowania i projektowania jest dokonywany dobór rozwiązań technicznych i organizacyjnych, które zapewnią spełnienie wymagań stawianych przez inwestora i użytkownika, w tym również w odniesieniu do fazy realizacji obiektu. Rezultatem projektowania przebiegu realizacji przedsięwzięcia powinien być niezawodny harmonogram o wysokim prawdopodobieństwie dotrzymania zaplanowanych terminów i małej wrażliwości na wpływ zjawisk losowych. W artykule zaprezentowano proaktywne podejście metodyczne do projektowania predyktywnych harmonogramów realizacji przedsięwzięć budowlanych, w celu zwiększenia ich niezawodności. Obejmuje ono dwa zasadnicze etapy: ocenę ryzyka czasu realizacji procesów budowlanych w oparciu o wieloatrybutową ocenę warunków realizacyjnych oraz alokację buforów czasu w harmonogramie. Opracowano oryginalną metodykę wspomagającą podejmowanie decyzji na każdym etapie tej procedury, tj. metodykę oceny poziomu ryzyka czasu realizacji procesów, określania istotności warunków realizacyjnych, dyspersji czasu realizacji procesów budowlanych i krytyczności procesów w harmonogramowaniu predyktywnym. Zaproponowano zestaw mierników odporności harmonogramu, stanowiących zastępcze kryteria w problemie minimalizacji kosztu niestabilności i określania wielkości buforów czasu. Proponowane ujęcie uwzględnienia warunków ryzyka w harmonogramach predyktywnych zwiększa ich niezawodność i zapobiega dezaktualizacji terminu końcowego oraz terminów realizacji poszczególnych procesów lub etapów przedsięwzięcia.

Article citation info:
SKRUCH P, DŁUGOSZ M, MITKOWSKI W. Mathematical methods for verification of microprocessor-based PID controllers for improving their reliability. Eksploatacja i Niezawodnosc – Maintenance and Reliability 2015; 17 (3): 327–333, http://dx.doi.org/10.17531/ein.2015.3.1.

Paweł SKRUCH
Marek DŁUGOSZ
Wojciech MITKOWSKI

MATHEMATICAL METHODS FOR VERIFICATION OF MICROPROCESSOR-BASED PID CONTROLLERS FOR IMPROVING THEIR RELIABILITY

MATEMATYCZNE METODY TESTOWANIA MIKROPROCESOROWYCH REGULATORÓW PID UMOŻLIWIAJĄCE ZWIĘKSZENIE ICH NIEZAWODNOŚCI*

Proportional-Integral-Derivative (PID) control is the most common control algorithm used in industry. The extensive use of electronics and software has resulted in the situation where the digital PID controller using a microprocessor as well as its software implementation replaces existing pneumatic, mechanical and electromechanical solutions. The reliability of the software system is assured by detection and removal of errors that can lead to failures. The paper presents mathematical methods for verification and testing of microprocessor-based PID controllers that can be used to increase the reliability of the system. The presented methodology explores the concept of testing with a model as an oracle.

***Keywords**: controller, PID, testing, reliability.*

Regulator PID (regulator proporcjonalno-całkująco-różniczkujący) jest najbardziej rozpowszechnionym i najczęściej stosowanym typem regulatora w przemyśle. Intensywny rozwój elektroniki i informatyki spowodował, że cyfrowe regulatory PID budowane na bazie mikroprocesora z odpowiednim oprogramowaniem zastąpiły dotychczasowe rozwiązania pneumatyczne, mechaniczne i elektromechaniczne. Zagwarantowanie niezawodności układu elektronicznego z oprogramowaniem polega między innymi na wykrywaniu i usuwaniu błędów, które mogą prowadzić do awarii. W pracy przedstawiono matematyczne metody weryfikacji mikroprocesorowych regulatorów PID mające na celu wykrycie błędów w systemie i w konsekwencji zwiększenie jego niezawodności poprzez zmniejszenie prawdopodobieństwa wystąpienia awarii. Metody testowania opierają się na tak zwanym podejściu modelowym, to znaczy, wykorzystują model systemu jako wzorzec zachowania.

***Słowa kluczowe**: regulator, PID, testowanie, niezawodność.*

1. Introduction

Proportional-Integral-Derivative (PID) control is the most common control algorithm used in industry. It has been in use for over a century in various forms: as a purely mechanical device, as a pneumatic device and as an electronic device.

Modern digital PID controller is a system that can be considered as a combination of computer hardware and software designed to perform a dedicated control function. The control is implemented on a custom hardware platform, which is often designed and configured for the particular application. Such systems are called embedded systems [29, 30]. Embedded systems may be observed in common devices employed in everyday living (e.g., coffee machines, washing machines, cell phones) as well as in sophisticated engineering systems (e.g. cars [4, 29], planes, spacecrafts).

PID controllers are also often safety critical systems. Due to the area of application, the PID controller must have high reliability as unexpected failures can be fatal. Ensuring the reliability of embedded software systems based on the detection and removal of errors that can lead to system failure. The process to verify that the system meets the specified requirements is referred to as testing. Testing is also the process of trying to discover every conceivable fault or weakness in a work product [12, 14].

The most common errors that can lead to improper operation of control devices equipped with the software include functional errors in the code, arithmetic errors associated with the use of fixed-point arithmetic, communication and task management errors, lack of robustness to different types of disturbances and work outside the scope of the variability of input signals.

(*) Tekst artykułu w polskiej wersji językowej dostępny w elektronicznym wydaniu kwartalnika na stronie ***www.ein.org.pl***

There are several facts that show clearly possible consequences of poorly tested systems. On February 25, 1991, an Iraqi Scud hit the barracks in Dhahran in Saudi Arabia, killing 28 soldiers from the US Army. This accident was caused by software error in the system's clock [24]. The PATRIOT missile battery has been in operation for 100 hours, by which time the system's internal clock had drifted by one third of a second. For a target moving as fast as Scud, this was equivalent to a position error of 600 meters. Another example is connected with Therac-25 radiation therapy machine that was produced by Atomic Energy of Canada Limited and CGR of France. The machine was involved with at least six known accidents between 1985 and 1987, in which patients were given massive overdoses of radiation, which were in some cases on the order of hundreds of grays [18]. At least five patients died of the overdoses. These accidents were caused by errors in software control application.One of the most infamous computer bugs in history was found during flight 501 that took place on June 4, 1996. This was the first, and unsuccessful, test flight of the European Ariane 5 expendable lunch system. Due to an error in the software design (inadequate protection from integer overflow), the rocket veered off its flight path 37 seconds after launch and was destroyed by its automated self-destruct system [19]. As it was an unmanned flight, there were no victims, but the breakup caused the loss of four Cluster mission spacecraft, resulting in a loss of more than $370 million.

There are two basis classes of software testing: black box testing and white box testing. Black box testing is testing that ignores the internal mechanism of a system or component and focuses solely on the outputs generated in response to selected inputs and execution conditions. White box testing is testing that takes into account the internal mechanism of a system or component.

Black box testing is also called functional testing [2, 3] or specification-based testing. The specification for control systems can be very often presented in the form of models. Test cases should be then generated systematically out of the models [29, 30]. The most popular black box testing techniques include boundary value analysis, equivalence partitioning, decision table testing, state transition testing and use case testing (see e.g. [3, 22]).

Boundary values analysis is a testing technique in which tests are designed to include boundary values of input functions to stimulate the system. The idea comes from the boundary, which is the area where testing is likely to yield defects. Equivalence partitioning is a technique that divides the input data into groups that are expected to exhibit similar behavior, so they can are likely to be processed in the same way. The groups are called equivalence partitions (or classes) and can be also identified for outputs, interval values and parameters. Decision tables are a good way to capture system requirements that contain logical conditions. State transition testing is much used within the embedded software industry and technical automation where the system behavior can be represented using state diagrams. Tests can be also specified from use cases or business scenarios. A use case is a sequence of steps that describe the interactions between an actor (a user of the system) and the system.

White box testing (also called structure-based testing) is based on an identified structure of the software or system. The structure can be considered as the code itself (i.e., statements, decisions or branches), a call tree (a diagram in which modules call other modules), a menu structure, business process or web page structure. Test cases designed with the help of white box testing techniques take into account such input values to cover relevant instruction in the code (instruction testing), decisions (decision testing), conditions, etc.

It should be emphasized that most of the presented techniques and methods are seldom applicable in testing software systems where the dynamics cannot be neglected [20, 27]. The dynamical systems are modeled by difference or differential equations and have usually infinitely many states. There is a need for another approach that will handle continuous aspects of the system (see e.g. [6, 17]). This is because of testing dynamics aspects of such systems requires tests that utilize time continuous input signals and time continuous output signals (even when the system is digitally processed). The process of selecting just a few of the many possible scenarios to be tested is a difficult and challenging task and currently is most often based on qualitative best engineering judgment. Some results [5, 11, 15, 28] developed for hybrid systems can be also applicable to dynamical systems and to fractional-order systems (see e.g. [21]) which recently are of interest to many scientists and engineers.

The paper is organized as follows. In the next section, modeling concepts of the functionality realized by the PID controller are introduced. These concepts are explored further in the next sections and are the base for creating test artifacts such as: test oracle (Section 3), notation of tests (Section 4), implementation of a test comparator (Section 5), test coverage (Section 6) and test generation (Sections 7 and 8). Experimental results are given in Section 9. Conclusions are in Section 10.

2. Mathematical description of the PID controller

An embedded PID controller is a system that can be considered as a combination of computer hardware and software designed to perform a dedicated control function. The PID controller (Fig. 1) works in a closed-loop system and attempts to minimize the error e(t) by adjusting the control input $u(t)$. The error is calculated as the difference between a measured process output $y(t)$ and a desired set point $y_{\mathrm{sp}}(t)$. The control signal is a result of the following calculation

$$u(t) = K\left(e(t) + \frac{1}{T_{\mathrm{i}}}\int_0^t e(\tau)\mathrm{d}\tau + T_d \frac{\mathrm{d}e(t)}{\mathrm{d}t}\right), \tag{1}$$

where K is proportional gain, T_{i} is integral time, T_{d} is derivative time. The control signal is thus a sum of three terms: the P-term (which is proportional to the error), the I-term (which is proportional to the integral of the error), and D-term (which is proportional to the derivative of the error).

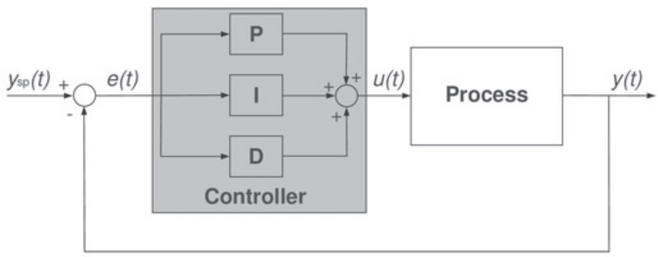

Fig. 1. Block diagram of the closed-loop system with the PID controller

Introduce the notation $w_1(t) = \int_0^t e(\tau)\mathrm{d}\tau$ and $w_2(t) = \dot{w}_1(t)$ the equation (1) can be written as:

$$u(t) = Kw_2(t) + \frac{K}{T_{\mathrm{i}}} w_1(t) + KT_{\mathrm{d}}\dot{w}_2(t), \tag{2}$$

or, equivalently, in matrix notation as:

$$\dot{\boldsymbol{w}}(t) = \boldsymbol{E}\boldsymbol{w}(t) + \boldsymbol{F}u(t), \boldsymbol{w}(0) = \boldsymbol{0}, \tag{3}$$

where $\boldsymbol{w}(t) = \begin{bmatrix} w_1(t) & w_2(t) \end{bmatrix}^{\mathrm{T}} \in W \subset \mathbb{R}^2$

$$\boldsymbol{E} = \begin{bmatrix} 0 & 1 \\ -(T_\mathrm{i}T_\mathrm{d})^{-1} & -T_\mathrm{d}^{-1} \end{bmatrix}, \ \boldsymbol{F} = \begin{bmatrix} 0 \\ (KT_\mathrm{d})^{-1} \end{bmatrix}. \tag{4}$$

The physical and implementation constraints imposed by computer system resources lead to the assumption that the space W is bounded. The assumption means that the space W is contained in a circle of finite radius.

3. Concept of testing with a model as an oracle

The formulas (1) and (3) specify mathematically the system's behavior in clear and unambiguous form. It can be used in computer simulations in an early phase of development to validate the system concept, calibrate parameters and optimize the system performance. In the next phase, the physical system is designed (i.e., hardware and software) that shall meet the specified requirements in the form of the equations (1), (3). Testing process shall be considered as the last phase in the development process that allows verifying that the physical system behavior is identical to that observed during computer simulations. If the tests fail then the system needs to be redesigned. The physical system that is being tested for the correct operation is often referred as system under test (SUT).

The term test oracle describes a source to determine expected results to compare with the actual result of the SUT [1]. The role of such source in the model-based approach is often played by the model (see Fig. 2). The approach stipulates that the same input is applied to both the SUT and to the model. The input signal is physical in case of the SUT (e.g., voltage, current or resistance) and virtual in case of the model; from logical point of view both signals are equivalent. The judgment whether the result of a test is in conformance with the model is delegated to a test comparator. The test comparator is usually a tool that compares the actual output produced by the SUT with the expected output produced by the model.

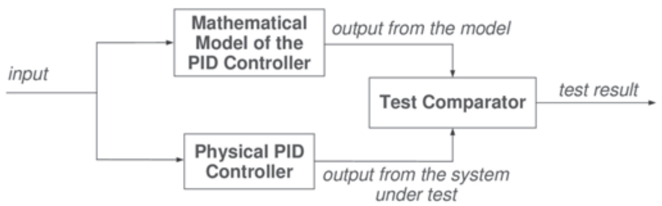

Fig. 2. Concept of testing with a model as an oracle

4. Notation of tests

One of the fundamental tasks of software testing is the creation of test cases. A test case can be considered as a set of inputs, execution preconditions and expected outcomes developed for a particular objective, such as to exercise a particular program path or to verify compliance with a specific requirement [13].

Adapting this definition to the SUT modeling concepts (1), a single test case $\mathrm{T}_{\mathrm{case}}^{(j)}$ can be defined as:

$$\mathrm{T}_{\mathrm{case}}^{(j)} = \left\{T^{(j)}, e^{(j)}(\cdot), u^{(j)}(\cdot)\right\} \tag{5}$$

where j=1,2,…,N, N≥1 is a label to indicate different test cases, $e^{(j)}:[0,T^{(j)}] \to \mathbb{R}$ is an input function, $u^{(j)}:[0,T^{(j)}] \to \mathbb{R}$ is an expected output function, $T^{(j)}$ stands for test execution time. Notation (5) and the model (1) play the key role in the test selection method presented in Section 8.

When the system model is described by the equation (3), then a single test case $\mathrm{T}_{\mathrm{case}}^{(j)}$ can be presented in the form

$$\mathrm{T}_{\mathrm{case}}^{(j)} = \left\{T^{(j)}, u^{(j)}(\cdot), w^{(j)}(\cdot)\right\} \tag{6}$$

where $u^{(j)}:[0,T^{(j)}] \to \mathbb{R}$ is an input function unlike the notation (5) and $\boldsymbol{w}^{(j)}:[0,T^{(j)}] \to \mathbb{R}^2$ is an expected output function. Notation (6) with the model (3) are the base for the test selection method presented in Section 7.

A collection of one or more test cases forms a test suite $\mathrm{T}_{\mathrm{suite}}$, where:

$$\mathrm{T}_{\mathrm{suite}} = \left\{\mathrm{T}_{\mathrm{case}}^{(1)}, \mathrm{T}_{\mathrm{case}}^{(2)}, \ldots, \mathrm{T}_{\mathrm{case}}^{(N)}\right\}. \tag{7}$$

5. Implementation of a test comparator

The test comparator can be considered as a tool that implements a mechanism for determining whether a test passes or fails [14]. In the concept illustrated on Fig. 2, this tool compares the actual output produced by the SUT with the expected output produced by the model (1) or (3).

A possible practical realization of the comparison function for a given test case (5) is presented below:

$$z\left(\mathrm{T}_{\mathrm{case}}^{(j)}\right) = \begin{cases} 0 \text{ if } \forall_{t\in[0,T^{(j)}]} \left|u^{(j)}(t) - u_\mathrm{s}^{(j)}(t)\right| < \varepsilon \left|u^{(j)}(t)\right|, \\ 1 \text{ otherwise}, \end{cases} \tag{8}$$

where z denotes the test result, that is, z=0 when the test passes, z=1 when the test fails, ε>0 is the tolerance range, $u_\mathrm{s}^{(j)}(\cdot)$ stands for the output produced by the SUT.

In the similar way, the comparison function can be defined for notation (6):

$$z\left(\mathrm{T}_{\mathrm{case}}^{(j)}\right) = \begin{cases} 0 \text{ if } \forall_{t\in[0,T^{(j)}]} \| \boldsymbol{w}^{(j)}(t) - \boldsymbol{w}_\mathrm{s}^{(j)}(t) \| < \varepsilon \| \boldsymbol{w}^{(j)}(t) \|, \\ 1 \text{ otherwise}, \end{cases} \tag{9}$$

where $\boldsymbol{w}_\mathrm{s}^{(j)}(\cdot)$ is the output produced by the SUT.

6. Calculation of test coverage

The degree to which a given test suite $\mathrm{T}_{\mathrm{suite}}$ addresses all specified requirements for a given system is determined by a test coverage measure [13]. The most obvious quantification of the system's behavior exercised by the test suite is computed by dividing the number of the system states explored by the test suite by the cardinality of the entire state space. However, the formula has limited usefulness for dynamical systems (and PID controller belongs to this class of systems) because the state space for such systems contains usually infinite number of states.

In following part of this section it is presented a method for calculation of test coverage that was taken from the paper [25].The method described therein has been adapted to the model (3). The test coverage $C_{\boldsymbol{h}}$ ($\mathrm{T}_{\mathrm{suite}}$) of the test suite $\mathrm{T}_{\mathrm{suite}}$ can be defined as follows:

$$C_{\boldsymbol{h}}(\mathrm{T}_{\mathrm{suite}}) = \frac{\left|\bigcup_{j=1}^{j=N} V_h\left(\mathrm{T}_{\mathrm{case}}^{(j)}\right)\right|}{|W_h|} \tag{10}$$

where:

$$W_h = \left\{ \boldsymbol{i} = [i_1, i_2]^{\mathrm{T}} \in \mathbb{Z}^2 : \exists_{\boldsymbol{w} \in W} \boldsymbol{w} \in G_h(\boldsymbol{i}) \right\} \tag{11}$$

is the transformed state space created from the system state space W,

$$G_h(\boldsymbol{i}) = \left\{ \boldsymbol{w} \in \mathbb{R}^2 : \boldsymbol{w} = [w_1, w_2]^{\mathrm{T}}, \frac{w_k}{h_k} = i_k, k = 1,2 \right\}$$

denotes a partition with the size $\boldsymbol{h} = [h_1, h_2]^{\mathrm{T}}, h_1, h_2 > 0$, $\left[\frac{w_k}{h_k} \right]$ is the largest integer greater than $\frac{w_k}{h_k}$,

$$V_{\boldsymbol{h}}\left(\mathrm{T}_{\mathrm{case}}^{(j)}\right) = \left\{ \boldsymbol{i} \in W_{\boldsymbol{h}} : \exists_{t \in [0, T^{(j)}]} \boldsymbol{w}^{(j)} \in G_{\boldsymbol{h}}(\boldsymbol{i}) \right\} \tag{13}$$

is a set of states of the transformed state space covered by the test case $\mathrm{T}_{\mathrm{case}}^{(j)}$. It should be noticed that the sum

$$V_{\boldsymbol{h}}(\mathrm{T}_{\mathrm{suite}}) = \bigcup_{j=1}^{j=N} V_{\boldsymbol{h}}\left(\mathrm{T}_{\mathrm{case}}^{(j)}\right) \tag{14}$$

will contain the information about the states covered by the test suite$\mathrm{T}_{\mathrm{suite}}$.

In the example presented on Fig. 3, bounded two-dimensional internal state space W (the area embraced by the bold solid line) has been transformed to the space

$$W_{\boldsymbol{h}} = \left\{ \boldsymbol{i} = [i_1, i_2]^{\mathrm{T}} \in \mathbb{Z}^2, i_1 = 0, 1, \ldots, 8, i_2 = 0, 1, \ldots, 4 \right\} \backslash \left\{ [0,0]^{\mathrm{T}}, [1,0]^{\mathrm{T}}, [8,0]^{\mathrm{T}}, [0,1]^{\mathrm{T}}, [0,4]^{\mathrm{T}}, [7,5]^{\mathrm{T}}, [8,4]^{\mathrm{T}} \right\}. \tag{15}$$

that consists of 45 elements $G_{\boldsymbol{h}}(\boldsymbol{i}) = [i_1, i_1+1) \times [i_2, i_2+1)$ with the size of 1×1. Fig. 3 contains also system trajectories related to two exampled test cases: $\mathrm{T}_{\mathrm{case}}^{(1)}$ and $\mathrm{T}_{\mathrm{case}}^{(2)}$. 10 grid boxes are visited by the system trajectory belonging to the first test case, 9 – to the second test case. The test suite $\mathrm{T}_{\mathrm{suite}} = \left\{ \mathrm{T}_{\mathrm{case}}^{(1)}, \mathrm{T}_{\mathrm{case}}^{(2)} \right\}$ consisting of these test cases covered in total 17 grid boxes what implies the test coverage at level $C_{\boldsymbol{h}}(\mathrm{T}_{\mathrm{suite}}) = \frac{17}{45} \approx 0.45(45\%)$.

7. A test selection method for conformance testing

In this section, an algorithm for generating test cases is presented. The algorithm uses the modeling concept (3) of the SUT to generate test cases and calculate test coverage according to the method presented in the previous section. It explores transformed state space by using input signals that steer the system from an initial state to a final state. The selection and completeness of test cases is quantified by the coverage metric (10). The main idea of the presented strategy is to check that the functional specification in the form of the equation (3) is correctly implemented, which is variously referred to in the literature as conformance testing [14], correctness testing [16] or functional testing [13].

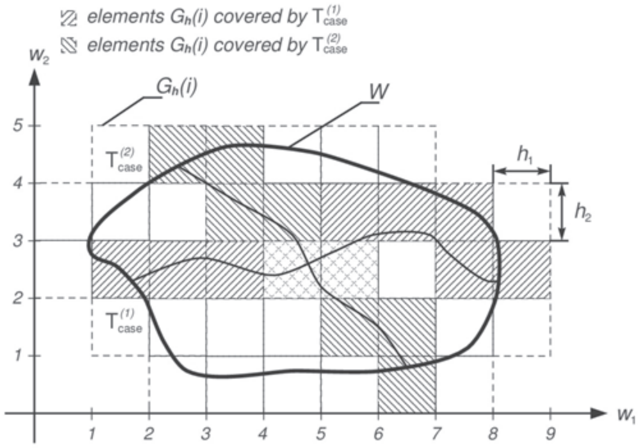

Fig. 3. Illustration of the test coverage for the state space W

Algorithm 1

1°: Set the parameters: $\boldsymbol{h} = [h_1, h_2]^T, h_1, h_2 > 0, \delta \in (0,1], T > 0$

2°: $\mathrm{T}_{\mathrm{suite}} := \varnothing$, $V_h(\mathrm{T}_{\mathrm{suite}}) := \varnothing$, $C_h(\mathrm{T}_{\mathrm{suite}}) := 0$, j:=1

3°: **while** $C_h(\mathrm{T}_{\mathrm{suite}}) < \delta$ do

4°: Find $\boldsymbol{w}_a \in G_h(i_a)$ where $i_a \in W_h \setminus V_h(\mathrm{T}_{\mathrm{suite}})$

5°: Calculate the control function $u(\cdot)$ that steers the system from the zero initial state to the final state $\boldsymbol{w}_a$

6°: Calculate the trajectory $\boldsymbol{w}(t) = \int_0^T e^{(t-\tau)\boldsymbol{E}} \boldsymbol{F} u(\tau) \mathrm{d}\tau$ by solving the equation (3)

7°: $\mathrm{T}_{\mathrm{case}}^{(j)} = \left\{ T^{(j)}, u^{(j)}(\cdot), \boldsymbol{w}^{(j)}(\cdot) \right\}$ where $T^{(j)} \cdot T, u^{(j)}(\cdot) := u(\cdot), \boldsymbol{w}^{(j)}(\cdot) := \boldsymbol{w}(\cdot)$

8°: $\mathrm{T}_{\mathrm{suite}} := \mathrm{T}_{\mathrm{suite}} \cup \mathrm{T}_{\mathrm{case}}^{(j)}$

9°: Calculate $V_h(\mathrm{T}_{\mathrm{suite}})$ and $C_h(\mathrm{T}_{\mathrm{suite}})$

10°: $j := j+1$

11°: **end while**

Remark 1. The size $\mathbf{h}=[h_1, h_2]^{\mathrm{T}}$ of the partition can be chosen according to the formula

$$h_i \frac{\max_{t \geq 0} |w_i(t)|}{10}, i = 1, 2. \tag{16}$$

For safety critical systems there would be recommended to decrease the granulation of the partitions h_i. However, it should be clear that too small granulation significantly increases the number of test cases and overall testing effort.

Remark 2. The system (3) is controllable as the rank of the controllability matrix is equal to the size of the system, that is, rank[$\boldsymbol{E}\ \boldsymbol{EF}$]=2 (see e.g. [20]). This means that there exist generally many different controls which steer the system from the zero initial state to the final state $\boldsymbol{w}_a$ at time T>0. For example, minimum energy control [20] is probably the easiest computable control steering the system to a desired state under the assumption that the constraints posed on the system are not violated.

8. A test selection method for negative testing

In this section, the test selection problem is formulated as an optimization problem. Representative test cases are constructed during optimization procedure using the model (1). The test selection is combined with the test execution and these two activities are conducted at the same time. The main advantage of the approach is focus on error prone situations that leads to drastically reduced number of representative test cases.

The problem is to find a test case $\mathrm{T}_{\text{case}} = \{T, e(\cdot), u(\cdot)\}$ which is a result of the optimization procedure

$$\max_{e \in E_{\text{ad}}} J(e) = \max_{e \in E_{\text{ad}}} \int_0^T \left(u(t) - u_{\text{s}}(t)\right)^2 \mathrm{d}t \tag{17}$$

where E_{ad} stands for the set of admissible error functions. The set E_{ad} can be correlated with physical and implementation constraints imposed by computer system resources.

Algorithm 2

1°: Set the parameters: E_{ad} and T>0

2°: Run the optimization procedurefor the problem (16) to obtain the solution $e^* \in E_{\text{ad}}$

3°: Calculate the control signal $u^*(\cdot)$ using the equation (1) for the error signal $e^*(\cdot)$

4°: $\mathrm{T}_{\text{case}} := \{T, e^*(\cdot), u^*(\cdot)\}$.

9. Experimental results

In order to evaluate the efficiency and usability of the presented algorithms as well as their ability to find faults they were applied to the real system. The faults in the form of incorrect parameters of the PID controller have been deliberately introduced to the system implementation. For better illustration of the results the parameters have been modified by 20% from the correct values. In practice, these faults can be caused by the use of fixed-point arithmetic; they can also result from errors in the identification procedure and can be a direct consequence of programmer error. Introduction of incorrect parameters values to the control system can result in different time to reach the steady state than expected, larger overshoot in the system and in the worst case in instability of the closed-loop system. Good control quality depends strongly on the correct settings what is especially important in optimal control problems [7] applicable, for example, for electric motors [8] and internal combustion engines [26].

Consider the model (1) of the PID controller with the following parameters

$$K = 3.60, \quad T_{\text{i}} = 1.81, \quad T_{\text{d}} = 0.45. \tag{18}$$

Next, the functionality described by the equation (1) has been implemented in software, which runs in a microprocessor on the embedded hardware platform, however with incorrect values of the parameters, that is

$$\tilde{K} = 2.88, \quad \tilde{T}_i = 2.17, \quad \tilde{T}_{\text{d}} = 0.36. \tag{19}$$

The entire system has been tested with the help of the algorithm 1 which has been implemented and executed for the following input parameters: $\boldsymbol{h}=[0.3,0.2]^{\mathrm{T}}$, $\delta=0.7$, $T=20$ [s], $|w_1(t)|\leq 1.5$, $|w_2(t)|\leq 1.0$ (system implementation constraints).The test suite that guarantees the coverage level higher that δ consits of 10 test cases. Elements of the generated test cases of the form of (6) are graphically presented in Figs. 4 and 5. Comparison of the actual trajectory obtained from the SUT with the expected trajectory is shown in Fig. 6. The output from the SUT for the first test case is not within the tolerance range $\varepsilon=0.1$ relative to the expected output, therefore the test case is qualified as *fail*. This proofs existence of the fault in the system.

Consider the following set of admissible error functions:

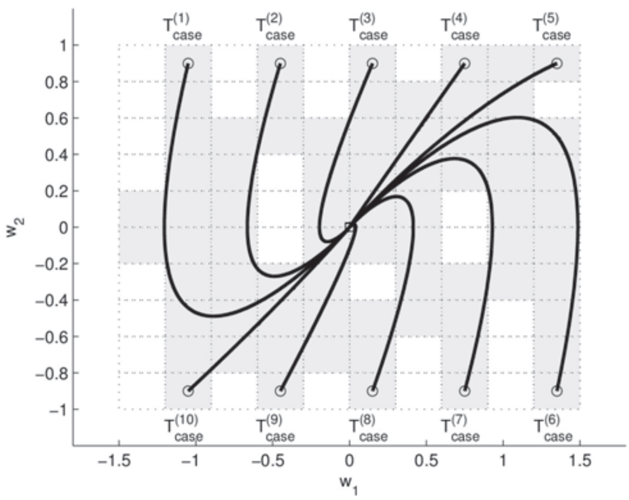

Fig. 4. Trajectories $\boldsymbol{w}^{(j)}$, j=1,2,...,10 and elements (gray rectangles) of the transformed state space W_h covered by the test cases $\mathrm{T}^{(j)}_{\text{case}}$.The model trajectories start in □ and end in ○

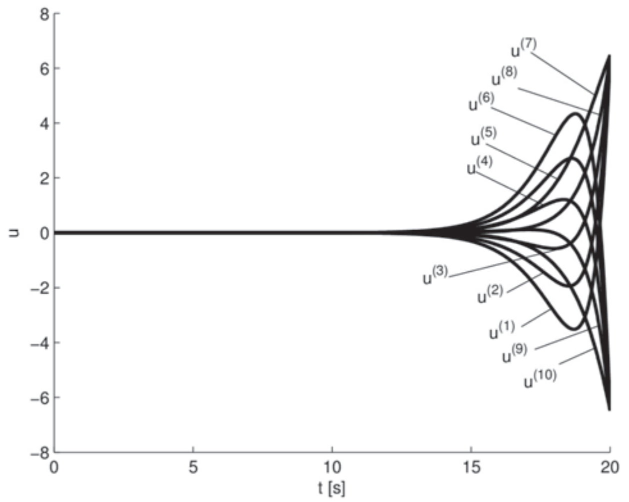

Fig. 5. Input functions for the test cases $\mathrm{T}^{(j)}_{\text{case}}, j = 1,2,\ldots,10$

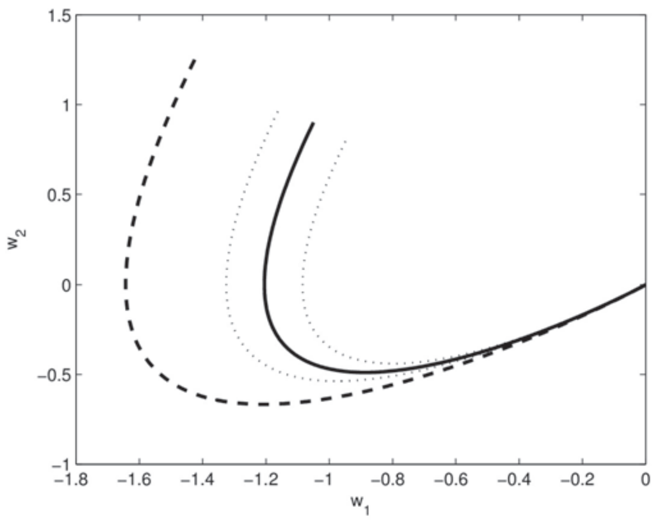

Fig. 6. The comparison of the output function $\boldsymbol{w}_{\text{s}}^{(1)}$ produced by the tested PID system (dotted line) with the expected output function $\boldsymbol{w}^{(1)}$ (solid line) produced by the model. The limits of tolerance of 10% are marked on the drawing by a thin dotted line

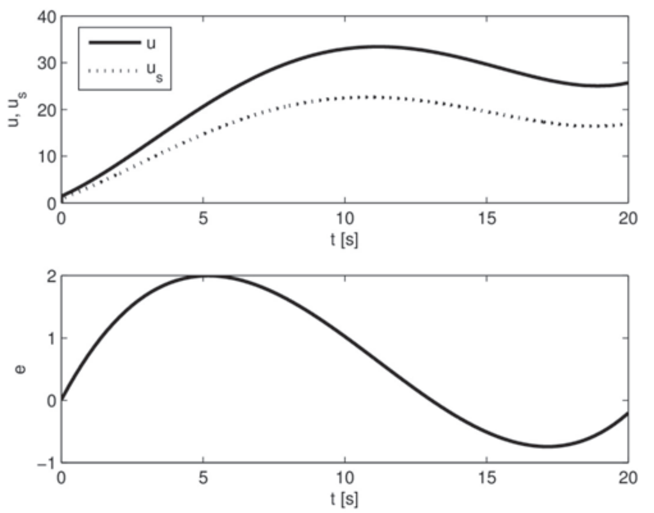

Fig.7. The elements of the test case generated with the help of the algorithm 2

$$E_{\text{ad}} = \left\{ e \in \text{PC}\left(\left[0,T\right],\mathbb{R}\right) : e(t) = \alpha_0 t^3 + \alpha_1 t^2 + \alpha_2 t + \alpha_3, \alpha_i \in \mathbb{R}, \left|e(t)\right| \le 2, i = 0,1,2,3 \right\} \tag{20}$$

that can be used in the optimization procedure (algorithm 2) to find such test cases that maximize the difference (17) between the outputs produced by the tested system and its model within the time T. The implementation of the algorithm with the Nelder-Mead simplex (direct method) [23] leads to the following local optimal solution:

$$e(t)=0.0032t^3-0.1072t^2+0.8534t+0.0089 \,. \tag{21}$$

Elements of the generated test cases of the form of (5) are graphically presented in Fig. 7. The figure includes also for comparison purposes the actual trajectory obtained from the tested system.

The main advantage of the testing method based on the algorithm 2 is a significant reduction of test cases, which the search is done using the optimization procedure. The algorithm focuses on error prone situations. As a result, the time and cost associated with the testing of the system can be significantly reduced. Since the effort put into testing is, according to estimates [2], from 30 up to 90 percentage of the overall effort in the projects, the benefits coming from even a very small reduction of this factor can be very profitable. It should be also noted that the algorithm 2 performs the search for test cases while using the physical system and its mathematical representation. Thus, to start the process of testing both the model and the real system are required for. Moreover, the formulation described in the algorithm 2 takes the form of a functional optimization problem, which may appear difficult to solve as it requires transformation to a value optimization problem.

10. Conclusions

The paper has presented two different methods for testing embedded PID controllers to provide required quality of the system, assure compliance with safety standards and eliminate errors at the stage of system design. Elimination of errors in the early stages of product development can increase system reliability and reduce the risk of failures during the operational phase. All elements of the testing process (i.e., concept of testing, notation of test cases, implementation of a test comparator, test coverage, selection of test cases) have been formulated and described in using the appropriate mathematical notation. The key role in the presented approach plays the mathematical model that represents intended behavior of the designed system. In this way it was possible to develop methods for testing systems where the dynamics plays an important role and where classical testing techniques cannot be applied to.

The presented approach can be easily generalized to other microprocessor-based control systems. Controllers with dynamic compensator [27], electric motor controllers [7, 8], controllers of internal combustion engines, neural networks controllers [9] and fuzzy logic controllers [10] are examples of the systems that can be verified using the algorithms described in this paper.

References

1. Adrion W, Brandstad J, Cherniabsky J. Validation, verification and testing of computer software. Computing Survey 1982; 14(2): 159-192, http://dx.doi.org/10.1145/356876.356879.
2. Beizer B. Software Testing Techniques, 2nd ed. Boston: Van Nostrand Reinhold, 1990.
3. Beizer B. Black-Box Testing: Techniques for Functional Testing of Software and Systems. New York: John Willey & Sons, 1995.
4. Chłopek Z, Biedrzycki J, Lasocki J, Wójcik P. Assessment of the impact of dynamic states of an internal combustion engine on its operational properties. Eksploatacja i Niezawodnosc – Maintenance and Reliability 2015; 17(1): 35-41, http://dx.doi.org/10.17531/ein.2015.1.5.
5. Dang T. Model-based testing of hybrid systems. In: Model-Based Testing for Embedded Systems. Boca Raton: CRC Press 2011; 383-423, http://dx.doi.org/10.1201/b11321-15.
6. Dang T, Nahhal T. Coverage-guided test generation for continuous and hybrid systems. Formal Methods in System Design 2009; 34(2): 183-213, http://dx.doi.org/10.1007/s10703-009-0066-0.
7. Długosz M. Problemy optymalizacyjne układów napędowych robotyki. Przeglad Elektrotechniczny – Electrical Review 2011; 87(9a): 238-242.
8. Długosz M, Lerch T. Komputerowa identyfikacja parametrów silnika prądu stałego. Przeglad Elektrotechniczny – Electrical Review 2010; 85(2): 34-38.
9. Długosz R, Kolasa W, Pedrycz M, Szulc M. Parallel programmable asynchronous neighborhood mechanism for Kohonen SOM implemented in CMOS technology. IEEE Transactions on Neural Networks 2011; 22(12): 2091-2104, http://dx.doi.org/10.1109/TNN.2011.2169809.
10. Długosz R, Pedrycz W. Łukasiewicz fuzzy logic networks and their ultra low power hardware implementation. Neurocomputing 2010; 73(7-9): 1222-1234, http://dx.doi.org/10.1016/j.neucom.2009.11.027.
11. Esposito J. Automated test trajectory for hybrid systems. Proceedings of the 35th Southeastern Symposium on System Theory 2003; 441-444, http://dx.doi.org/10.1109/SSST.2003.1194609.
12. IEEE Std 1012-2004. IEEE standard for software verification and validation, 2004.
13. IEEE Std 61012-1990. IEEE standard glossary of software engineering terminology, 1990.
14. ISTQB International Software Testing Qualification Board. Standard glossary of terms used in software testing, version 2.1, 2010.

15. Julius A, Fainekos G, Anand M, Lee I, Pappas G. Robust test generation and coverage for hybrid systems. Proceedings of the 10th International Conference on Hybrid Systems: Computation and Control (HSCC), Pisa 2007; 329-342, http://dx.doi.org/10.1007/978-3-540-71493-4_27.
16. Kaner C, Faulk J, Nguyen H. Testing Computer Software, 2nd ed. New York: John Willey & Sons, 1995.
17. LaValle S, Kuffner J. Rapidly-exploring random trees: progress and prospects. In: Algorithmic and Computational Robotics: New Directions 2001; 293-308.
18. Leveson N, Turner S. An investigation of the Therac-25 accidents. IEEE Computer 1993; 27(7): 18-41; http://dx.doi.org/10.1109/MC.1993.274940.
19. Lions J. ARIANE 5. Flight 501 failure. Ariane 501 Inquiry Board Report, Paris, 1996.
20. Mitkowski W. Stabilizacja systemów dynamicznych. Warszawa: WNT, 1991.
21. Mitkowski W, Skruch P. Fractional-order models of the supercapacitors in the form of RC lader networks. Bulleting of the Polish Academy of Sciences, Technical Sciences 2013; 61(3): 581-587, http://dx.doi.org/10.2478/bpasts-2013-0059.
22. Myers G. The Art of Software Testing, 2nd ed. New York: John Willey & Sons, 2004.
23. Nelder J, Mead R. A simplex method for function minimization. The Computer Journal 1965; 7(4): 308-313, http://dx.doi.org/10.1093/comjnl/7.4.308.
24. Skeel R. Roundoff error and the Patriot missile. Society for Industrial and Applied Mathematics (SIAM) News 1992; 25(4): 11.
25. Skruch P. A coverage metric to evaluate tests for continuous-time dynamic systems. Central European Journal of Engineering 2011; 1(2): 174-180, http://dx.doi.org/10.2478/s13531-011-0015-8.
26. Skruch P. An educational tool for teaching vehicle electronic system architecture. International Journal of Electrical Engineering Education 2011; 48(2): 174-183, http://dx.doi.org/10.7227/IJEEE.48.2.5.
27. Skruch P: Feedback stabilization of a class of nonlinear second-order systems. Nonlinear Dynamics 2010; 59(4): 681-692, http://dx.doi.org/10.1007/s11071-009-9570-4.
28. Tabuada P. Verification and Control of Hybrid Systems. Dordrech: Springer, 2009, http://dx.doi.org/10.1007/978-1-4419-0224-5.
29. Zander-Nowicka J. Model-based testing of real-time embedded systems in the automotive domain. PhD thesis. Berlin: Fraunhofer IRB Verlag, 2009.
30. Zander J, Schieferdecker I, Mosterman P. (Eds) Model-Based Testing for Embedded Systems. Boca Raton: CRC Press, 2012.

Paweł SKRUCH
Marek DŁUGOSZ
Wojciech MITKOWSKI
Department of Automatics and Biomedical Engineering
AGH University of Science and Technology
Al. A. Mickiewicza 30/B1, 30-059 Kraków, Poland
E-mails: pawel.skruch@agh.edu.pl, mdlugosz@agh.edu.pl,
wojciech.mitkowski@agh.edu.pl

Article citation info:
VIŠNIAKOV N, KILIKEVIČIUS A, NOVICKIJ J, GRAINYS A, NOVICKIJ V. Low-cost experimental facility for evaluation of the effect of dynamic mechanical loads on photovoltaic modules. Eksploatacja i Niezawodnosc – Maintenance and Reliability 2015; 17 (3): 334–337, http://dx.doi.org/10.17531/ein.2015.3.2.

Nikolaj VIŠNIAKOV
Artūras KILIKEVIČIUS
Jurij NOVICKIJ
Audrius GRAINYS
Vitalij NOVICKIJ

LOW-COST EXPERIMENTAL FACILITY FOR EVALUATION OF THE EFFECT OF DYNAMIC MECHANICAL LOADS ON PHOTOVOLTAIC MODULES

TANIE URZĄDZENIE DOŚWIADCZALNE DO OCENY WPŁYWU DYNAMICZNYCH OBCIĄŻEŃ MECHANICZNYCH NA MODUŁY FOTOWOLTAICZNE

The efficiency of modern photovoltaic systems is strongly reduced when the crystalline structure of the solar cells is being damaged due to extensive mechanical stress caused by climatic factors such as heavy wind or snow. This work is focused on the investigation of the cyclic dynamic mechanical loads required to alter the efficiency of typical solar panels in order to simulate various weather conditions and investigate the reliability of the solar panels when they are subjected to stress. Experimental setup is described in the study. During experiments the solar panels have been treated up to 40 Hz vibrations with the maximum magnitude of the shift of the solar panel in the range of 0.3 mm. Simulation model of the characteristic frequencies during vibrations is also presented in this work. The experimental vibration spectrum has also been determined. The acquired experimental data showed appearance of micro fractures in the crystalline structure of the photovoltaic modules and allowed estimation of the average reliability of a typical modern photovoltaic module in harsh weather conditions. The setup could be successfully applied for express testing of solar panels and investigation of the susceptibility of photovoltaic modules to mechanical stress.

Keywords: *solar cells, degradation, measurement of mechanical stress, reliability, climatic stress simulation.*

Sprawność współczesnych instalacji fotowoltaicznych drastycznie spada, kiedy struktura krystaliczna ogniw słonecznych ulega uszkodzeniu z powodu dużych naprężeń mechanicznych powodowanych przez czynniki klimatyczne, takie jak silny wiatr lub śnieg. Niniejsza praca skupia się na badaniu cyklicznych dynamicznych obciążeń mechanicznych niezbędnych do obniżenia sprawności typowych paneli słonecznych w celu symulacji różnych warunków pogodowych oraz badania niezawodności paneli słonecznych poddanych oddziaływaniu czynników zewnętrznych. W publikacji opisano układ doświadczalny. W ramach doświadczeń, panele słoneczne zostały poddane drganiom do 40 Hz przy maksymalnej wielkości przesunięcia panelu słonecznego w zakresie do 0,3 mm. W pracy omówiono także model symulacyjny częstotliwości charakterystycznych w czasie drgań. Określono widmo drgań doświadczalnych. Uzyskane dane doświadczalne wykazały pojawienie się mikropęknięć w strukturze krystalicznej modułów fotowoltaicznych i pozwoliły na oszacowanie średniej niezawodności typowego współczesnego modułu fotowoltaicznego w trudnych warunkach pogodowych. Układ może być z powodzeniem wykorzystywany dla potrzeb doraźnego testowania paneli słonecznych oraz badania podatności modułów fotowoltaicznych na naprężenia mechaniczne.

Słowa kluczowe: *ogniwa słoneczne, degradacja, pomiar naprężenia mechanicznego, niezawodność, symulacja oddziaływania czynników klimatycznych.*

1. Introduction

Renewable energy sources are attracting more and more investors each year, which increases the share of renewable electricity generation [1]. Different dotation programs in the European Union exist to stimulate the popularity of solar and wind power. While many renewable energy sources are large scale implemented by corporations or government due to high cost of installation, solar energy is available for private users and relatively the cost of solar panels is low, which stimulated the mass production and popularity of the technology [2, 10]. However, reliability is a crucial parameter of photovoltaic systems and there are a number of standards covering the maximum allowed performance reductions influenced by stress in harsh weather conditions because dependent on the annual weather conditions the solar panel performance may be significantly reduced. Such weather factors as heavy wind bursts, snow, temperature fluctuations are important in prediction the efficiency of a specific solar module and the durability of the solar system must be taken into account [5, 11]. As a rule during heavy mechanical loads the crystalline structure of the photovoltaic modules is damaged and the micro fractures appear [4], which negatively affect the conversion effectiveness of the energy of light into electricity and stimulates further degradation of the module [9]. In order to minimize such loses in efficiency, enforcements in the frame structure of the photovoltaic system could be made dependent on the specific weather conditions it is being installed in. However, preliminary analysis and simulation of the weather conditions and possible stress are required [8]. Therefore, in order to meet the standards and estimate the degradation ratio the accurate prediction and accumulation of the statistical data of the solar cell performance in harsh weather conditions and under heavy dynamic mechanical loads. The area of research is new and still lacks accurate statistical and experimental data of mechanical stress influence on the appearance of micro cracks in the photovoltaic modules [6, 7]. The standards still do not include mechanical stress information on the photovoltaic modules. Therefore, in this work a computer controlled vibrational stand and an array of 3-axis acceleration evaluating sensors has been applied in order to investigate the influence of dynamic mechanical loads on the crystalline structure of a solar cell and propose a measurement setup for the testing of the solar modules.

2. Theoretical approximation and FEM analysis

The behavior of any subject interacting with dynamic forces can be specified by the dynamic equilibrium equation [12]:

$$[\mathrm{M}]\{\ddot{\mathrm{U}}\}+[\mathrm{S}]\{\dot{\mathrm{U}}\}+[\mathrm{K}]\{\mathrm{U}\}=\{\mathrm{F}\} \tag{1}$$

where [M], [S], [K] are the mass, suppression and stiffness matrices, respectively; {F} is the outer mechanical stress vector; $\{\ddot{\mathrm{U}}\}=\left\{\frac{d^2\mathrm{U}}{d^2t}\right\}$, $\{\dot{\mathrm{U}}\}=\left\{\frac{d\mathrm{U}}{dt}\right\}$, {U} are the accelerations, velocities and displacement, respectively. For the quasi-static process when there is no forced deformation, the equation is further simplified to:

$$[\mathrm{M}]\{\ddot{\mathrm{U}}\}+[\mathrm{K}]\{\mathrm{U}\}=\{0\} \tag{2}$$

The non-zero periodic solutions will take form of:

$$\{\mathrm{U}\}=\left\{\hat{\mathrm{U}}\right\}\cos\omega t \tag{3}$$

After differentiation the equilibrium equation is expressed as:

$$\left([\mathrm{K}]-\omega^2[\mathrm{M}]\right)\left\{\hat{\mathrm{U}}\right\}=\{0\} \tag{4}$$

Any mechanical system could be characterized by the number of natural modes and characteristic frequencies. Any vibration can be evaluated as a superposition of the natural modes in a form of:

$$\{\mathrm{U}(t)\}=\sum_{i=1}^{n}(a_i\cos\omega_i t+b_i\sin\omega_i t)\{\hat{\mathrm{U}}^{(i)}\} \tag{5}$$

where a_i, b_i, n – are the constants based on initial conditions. The solution could estimated analytically.

However, if the geometrical parameters and mechanical conditions of the system are known it is convenient to use the finite element method (FEM) analysis. The differentiation of the model could be performed allowing approximation of the physical processes happening during mechanical stress and the changes in geometrical features of the solid structure under investigation. If the solution is a vector function *f(x)*and the whole model is differentiated into finite elements, for the element *e* the function could be expressed as:

$$\mathrm{f}^e(x)=\mathrm{U}^e\left[\mathrm{E}^e(x)\right] \tag{6}$$

where $\left[\mathrm{E}^e(x)\right]$ is the finite elements matrix, U^e is the vector of element values at boundary conditions.

In order to simulate a more accurate response of the solar panel and determine the possible resonant frequencies a finite element method (FEM) analysis has been performed in SolidWorks software package environment. The parameters selected for simulation are as follows: composite material – Tedlar (PVF), tensile strength 55 MPa, tensile modulus – 2.103 Gpa, mass density –1370 kg/m3, possion ratio – 0.4. The modeling has been performed in 0 – 30 Hz frequency range with vibration amplitude up to 0.3 mm. During simulation four characteristic frequencies and corresponding displacement points have been determined. The simulation data is presented in Fig. 1. As it can be seen in Fig. 1 four resonance frequencies of a typical 2 m x 1.5 m solar panel have been acquired by application of FEM analysis

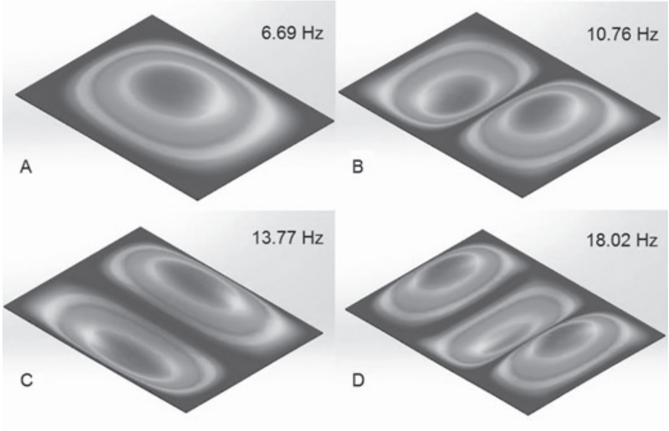

Fig. 1. Finite element method analysis modelling data, where A: characteristic frequency of 6.69 Hz; B: characteristic frequency of 10.76 Hz; C: characteristic frequency of 13.77 Hz; D: characteristic frequency of 18.02 Hz

3. Experimental setup for estimation of mechanical stress

As it was mentioned above in order to simulate the mechanical stress the photovoltaic module might be experiencing in the real weather conditions a vibrational stand has been used. The alteration of the magnitude and the frequency of the vibrations allows to simulate dynamic mechanical stress due to burst of heavy wind the photovoltaic modules may be experiencing. In the experimental setup the solar panel has been attached to the shaker and the arrays of 3-axis acceleration sensors have been applied to the solar panel corners, the back plate, the middle point and the shaker itself. The block diagram of the resultant dynamic mechanical load generating facility is shown in Fig. 2. The position and the quantity of sensors that are shown in the block diagram do not scale with the prototype facility and are shown for schematic purposes. The simultaneous data acquisition, the control of the frequency and the magnitude of the vibrations have been performed and monitored using a computerized setup.

The sensors that have been used in the study are the miniature triaxial piezoelectric accelerometers (“Brüel & Kjær”, 4506). The sensors have been chosen based on the evaluation of the best combination of high sensitivity, low mass and small dimensions. Also low output impedance allowed using long cables. The sensitivity of the device is 100 mV/g. As it was mentioned above both the shaker and the sensors have been connected to the computer, which allowed alteration of the amplitude of vibrations, vibration time, frequency and direction. The photographs of the experimental facility are shown in Fig. 3. The proposed experimental setup is capable of delivering controlled cyclic mechanical loads. The range of shift of the panel plane is 0 – 0.3 mm and the frequency of vibrations could be varied in the range of 0 – 40 Hz. The parameters are sufficient to simulate all possible harsh weather conditions like wind or snow bursts in Europe. Appli-

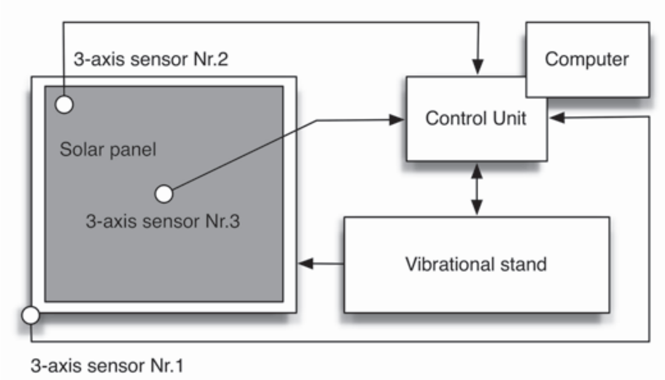

Fig. 2. The block diagram of the dynamic mechanical load generating facility

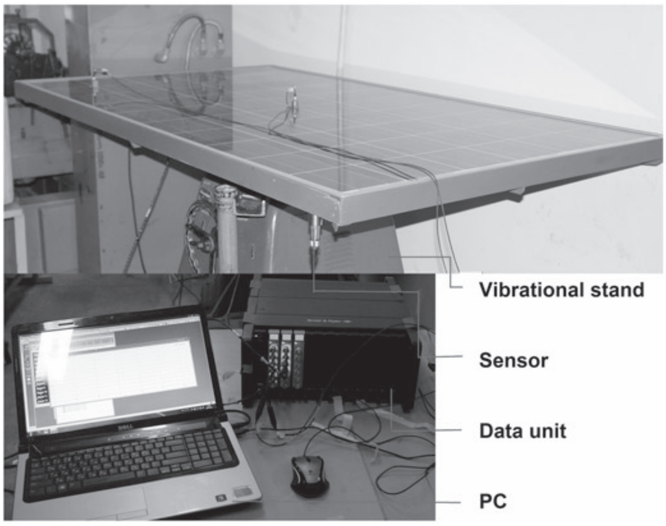

Fig. 3. The photographs of the experimental facility for estimation of mechanical load influence on photovoltaic cells

cation of the proposed setup allows determination of the vibrational resonance frequencies and based on the performed analysis develop reinforcements for the solar panel. It will allow reducing the amount of microcracks appearing in the crystalline structure.

4. Results

During experiments the magnitude and the frequency of the vibrations have been altered in the range of 0 – 0.3 mm and 0 – 40 Hz, respectively. The ranges have been selected in accordance to meet the goal of accurate simulation of real weather conditions when short bursts of heavy wind are possible. The vibration spectrums of the solar panels have been analyzed. A typical resultant response spectrum due to external shockwaves of the 2 m x 1.5 m solar panel is shown in the Fig. 4. An array of 6 acceleration sensors has been used, 3 of which where positioned in the central part of the panel and other 3 closer to corners of the photovoltaic module under investigation. As it can be seen in Fig. 4 during investigation it was determined that there were several characteristic frequencies in the range of 0 – 40 Hz: 7.2 Hz, 10.1 Hz, 13.5 Hz and 17.5 Hz.

The difference between simulation and experimental data was 7.1%, 6.1%, 2% and 2.9%, respectively, which is in acceptable compliance. Based on the acquired data the experiment has been narrowed to the frequency of 17.5 Hz because it was presumed that there was the highest probability of micro fractures in the crystalline structure of photovoltaic cells to occur when the modules are subjected to dynamic mechanical load. The exposure time to the mechanical stress under these conditions has been varied in the range of 0.1 – 3 hours.

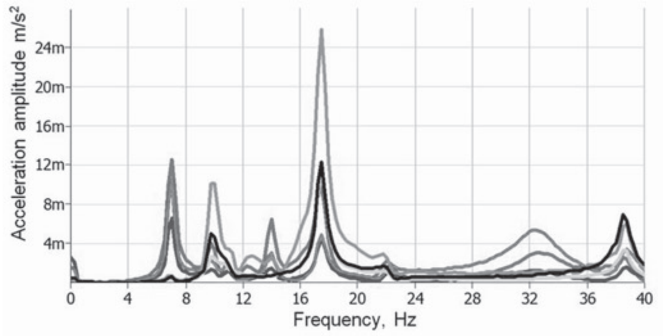

Fig. 4. The resultant response spectrum to shockwaves of the 2 m x 1.5 m photovoltaic module, where: red, green, blue are the responses of the sensors in the central part of the panel; orange, yellow, black are the responses of sensors positioned closer to corners of the photovoltaic module.

Each time after exposure the photovoltaic modules have been checked using electroluminescence technique [3]. The modules have been connected tothe 35 V DC power supply and a constant current have been maintained. The resultant luminescence of silicon has been observed using computerized CCD camera in the infrared region in dark room to remove any influence of light on the experiment. During each experiment the number of resultant micro cracks has been calculated and further exposure to mechanical stress has been carried out. The images of selected clusters of a photovoltaic module after exposure to 0.2 mm vibrations for 30 minutes are shown in Fig. 5.

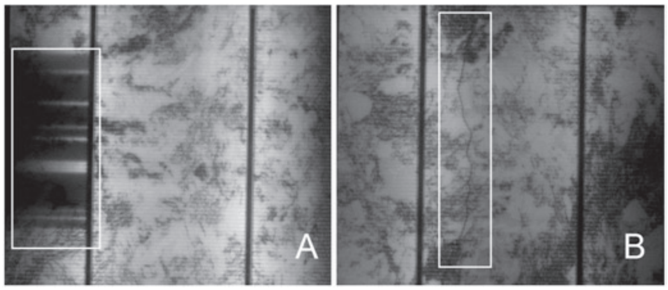

Fig. 5. Images of selected clusters of a photovoltaic module after exposure to 0.2 mm vibrations for 30 minutes, where A: damage of photoreflective layer; B: Microcrack in the crystalline structure

As it can be seen in Fig. 5 after exposure to dynamic mechanical loads defects in the crystalline structure of photovoltaic cells have appeared. In Fig. 5 (A) damage of the photoreflective layer could be observed. This defect is common on solar panels in operation and as a result less light could pass through the layer. In Fig. 5 (B) a microcrack could be observed. Such defects result in the disturbance of the current flow and in the worst-case scenario the whole cluster is not functioning, which negatively affects the output power of the panel.

5. Discussions/Conclusions

A computerized vibrational stand for simulation of the real weather conditions causing dynamic mechanical stress on the photovoltaic cells has been applied to determine the influence of the mechanical stress on the appearance of micro fractures in solar panels. It was determined that there were several resonance frequencies of 7.2 Hz, 10.1 Hz, 13.5 Hz and 17.5 Hz. The FEM simulation was in acceptable compliance with the experimental results. The highest response to shockwaves was observed at the 17.5 Hz frequency, therefore experiments under these conditions have been performed. It has been shown that external mechanical stress results in the damage of the crystalline structure of the photovoltaic cells. The appearance of micro cracks and damage of the photoreflective layer was observed during experiments. It was shown that the low frequency mechanical loads simulating windy weather could cause considerable damage to the photovoltaic cell and therefore reduce the effectiveness of the module. Since the stated working cycle of a photovoltaic cell is assumed to be 15 – 20 years it is crucial to perform express mechanical load tests to ensure decent performance of the system. The proposed setup and analysis method is applicable for the investigation of the dynamic mechanical loads influence on the crystalline structure of the photovoltaic cells.

References

1. Bradford T. Solar Revolution. The Economic Transformation of the Global Energy Industry. Cambridge, MA: The MIT Press 2006.
2. Brandherm B, Baus J, Frey J. Peer Energy Cloud – Civil Marketplace for Trading Renewable Energies. Intelligent Environments (IE), 2012 8th International Conference on. IEEE proceedings 2012; 375–378.
3. Coello J. Introducing Electroluminescence Technique in the Quality Control of Large PV Plants. 26th European Photovoltaic Solar Energy Conference and Exhibition 2011; 3469–3472.
4. Demant M, Rein S, Krisch J, Schoenfelder S, Fischer C, Bartsch S, Preu R. Detection and analysis of micro-cracks in multi-crystalline silicon wafers during solar cell production. 37th Photovoltaic Specialists Conference (PVSC), IEEE 2011; 1641–1646, http://dx.doi.org/10.1109/PVSC.2011.6186271.
5. Goossens D, Kerschaever E. Aeolian dust deposition on photovoltaic solar cells: the effects of wind velocity and airborne dust concentration on cell performance. Solar Energy 1999; 66 (4): 277–289, http://dx.doi.org/10.1016/S0038-092X(99)00028-6.
6. Kajari-Schröder, S., I. Kunze, I., M. Köntges, M. Criticality of cracks in PV modules. Energy Procedia 2012; 27: 658–663, http://dx.doi.org/10.1016/j.egypro.2012.07.125.
7. Köntges M, Kunze I, Kajari-Schröder S, Breitenmoser X, Bjørneklett B. The risk of power loss in crystalline silicon based photovoltaic modules due to micro-cracks. Solar Energy Materials and Solar Cells 2011; 95 (4): 1131–1137, http://dx.doi.org/10.1016/j.solmat.2010.10.034.
8. Petrone G, Spagnuolo G, Teodorescu R, Veerachary M, Vitelli M. Reliability Issues in Photovoltaic Power Processing Systems. Industrial Electronics, IEEE Transactions on 2008; 55 (7): 2569–2580, http://dx.doi.org/10.1109/TIE.2008.924016.
9. Pingel S, Zemen Y, Frank O, Geipel T, Berghold J. Mechanical Stability of Solar Cells within Solar Panels. 24th European Photovoltaic Solar Energy Conference 2009; 3459–3463.
10. Reiche D, Bechberger M. Policy differences in the promotion of renewable energies in the EU member states. Energy Policy 2004; 32 (7): 843–849, http://dx.doi.org/10.1016/S0301-4215(02)00343-9.
11. Skoplaki E, Palyvos J A. On the temperature dependence of photovoltaic module electrical performance: A review of efficiency/power correlations. Solar Energy 2009; 83 (5): 614–624, http://dx.doi.org/10.1016/j.solener.2008.10.008.
12. Vadluga V. Simulation of dynamic deformation and fracture behavior of heterogeneous structures by discrete element method. Summary of doctoral dissertation, Vilnius Gediminas Technical University: technological sciences, mechanical engineering (09T). Vilnius : Technika, 2007.

Nikolaj VIŠNIAKOV
Welding Research and Diagnostics Laboratory, Faculty of Mechanics
Vilnius Gediminas Technical University
J. Basanavičiaus str. 28, Vilnius LT-03224, Lithuania

Artūras KILIKEVIČIUS,
Department of Mechanical Engineering
Vilnius Gediminas Technical University
J. Basanavičiaus str. 28, LT-03224 Vilnius, Lithuania

Jurij NOVICKIJ
Audrius GRAINYS
Vitalij NOVICKIJ
High Magnetic Field Institute, Faculty of Electronics
Vilnius Gediminas Technical University
Naugarduko street 41, Vilnius LT-03327, Lithuania

E-mails: nikolaj.visniakov@vgtu.lt, arturas.kilikevicius@vgtu.lt, jurij.novickij@vgtu.lt, audrius.grainys@vgtu.lt, vitalij.novickij@vgtu.lt

Article citation info:
KLARECKI K, RABSZTYN D, HETMANCZYK MP. Analysis of pulsation of the sliding-vane pump for selected settings of hydrostatic system. Eksploatacja i Niezawodnosc – Maintenance and Reliability 2015; 17 (3): 338–344, http://dx.doi.org/10.17531/ein.2015.3.3.

Klaudiusz KLARECKI
Dominik RABSZTYN
Mariusz Piotr HETMANCZYK

ANALYSIS OF PULSATION OF THE SLIDING-VANE PUMP FOR SELECTED SETTINGS OF HYDROSTATIC SYSTEM

ANALIZA PULSACJI CIŚNIENIA POMPY ŁOPATKOWEJ DLA WYBRANYCH NASTAW PARAMETRÓW UKŁADU HYDROSTATYCZNEGO*

Sliding-vane pumps are widely used as sources of the flow in hydrostatic power transmission systems. A noticeable tendency in hydrostatic systems is revealed in the form of minimization of the mass, overall dimensions and at the same time increasing of a power density delivered by pumps. The article presents the preliminary results of the studies related to a pressure pulsation of the hydraulic system equipped with the sliding-vane pump (T7BS type manufactured by Parker & Denison Company). During the studies the pressure pulsation in selected places of pressure line were recorded. A series of measurements were performed for selected settings of the system. The recorded characteristics were analysed in time and frequency domains.

***Keywords**: vane pump, pressure pulsation, hydrostatic drive.*

Pompy łopatkowe należą do często używanych generatorów strugi cieczy roboczej w napędach hydrostatycznych. Zauważalną tendencją w opisywanych układach jest minimalizacja masy oraz wymiarów gabarytowych, przy jednoczesnym zwiększaniu gęstości mocy oferowanej przez pompę. W artykule przedstawiono wyniki wstępnych badań hydraulicznego napędu hydrostatycznego z pompą typu T7BS firmy Parker & Denison. Podczas badań zarejestrowano wartości pulsacji ciśnienia w wybranych miejscach linii tłocznej. Cykl pomiarów przeprowadzono w odniesieniu do wybranych nastaw pracy układu. Uzyskane przebiegi zostały przeanalizowane w dziedzinach czasu oraz częstotliwości.

***Słowa kluczowe**: pompa łopatkowa, pulsacja ciśnienia, napęd hydrostatyczny.*

1. Introduction

Despite significant progress in the development of hydraulic drive systems, users of the systems fitted with hydrostatic drives [1, 17] still experience a number of displacement pump failures. The process of diagnosing such devices is complicated and requires applying advanced tools [2, 5] or data processing algorithms. Additionally most of these devices are not diagnose susceptible [3, 18], what results from operating conditions [6] and external interferences.

Displacement pump diagnostic methods include vibroacoustic techniques, flow and pressure measurements, temperature control etc. However, each of those methods has its limitations and requires extensive knowledge [20-22].

The most commonly measured parameter of the hydrostatic systems is pressure [4]. Based on the analysis of phenomena relating to displacement pump pressure pulsation, it is possible to determine a number of system operating parameters demonstrating failures [7, 10, 12, 16] or detuning. Vibration due to pressure pulsation is caused by the uneven flow of hydraulic fluid from the pump to the system, which results in the accelerated wear of pump's elements [13, 14], increased emission of noise and reduction in the accuracy of the receivers' positioning. In the experiment presented in this article, the analysis of pressure pulsation in the discharge line was performed on the Parker & Denison T7BS rotary vane pump and the results have been compared with the simulation carried out on the proprietary model.

2. Mathematical and simulation models of the rotary vane pump efficiency

Figure 1 presents the operating diagram of a single acting rotary vane pump. Temporary efficiency [19] of a pump results from the infinitesimal area circled by the vanes of a pump during the phase of crossing the transitory zone between the suction and discharge zones.

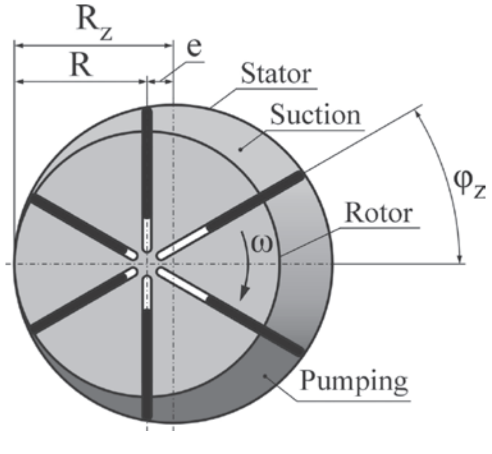

Fig. 1. Operating diagram of a single acting rotary vane pump

(*) Tekst artykułu w polskiej wersji językowej dostępny w elektronicznym wydaniu kwartalnika na stronie ***www.ein.org.pl***

In order to derive the formula to calculate temporary efficiency of the considered pump, the following simplifying assumptions have been adopted:

- outline of the stator track (in the form of a perfect circle),
- transverse dimensions of a pump vane (zero thickness),
- coordinate system – polar coordinate system has been adopted for the analysis (with the pole placed in the axis of the rotor revolution),
- motion of the fluid – raising the fluid while the vanes travel from suction to discharge zone.

In relation to the adopted assumptions, efficiency of the pump has been determined as the capacity between two temporary positions of the vane in the transitory zone:

$$q = \frac{B}{dt}(dA - dA_u) \tag{1}$$

where: B – width of the vane of the considered pump [m],
dA – temporary area circled by the vane while travelling from suction to discharge zone [m^2],
dA_u – temporary area circled by the opposite vane travelling from discharge to suction zone [m^2].

The relation defining the value of temporary area circled by the vane travelling from suction to discharge zoned A, described in the polar coordinate system, takes the following form:

$$dA = 0,5\left(r^2 - R^2\right)d\varphi \rightarrow dA = 0,5\omega\left(r_z^2 - R^2\right)dt \tag{2}$$

where: r_z – temporary radius of the point of contact between the vane and stator track [m],
R – pumprotor radius [m],
ω – rotor angular speed [rad/s].

The relation enabling determination of the area circled by the opposite vane will take the same form as equation 2, with the only difference being other radius of the contact between the vane and track. After inserting equation 2 in the equation 1, the following formula for the pump temporary efficiency has been obtained:

$$q = 0,5B\omega(r_z^2 - r_u^2) \tag{3}$$

where: r_u – radius of the contact of the opposite vane travelling from discharge to suction zone [m].

Temporary radii of the pump vanes' contact may be expressed as:

$$\begin{aligned} & r_z^2 - 2er_z cos\varphi + e^2 - R_z^2 = 0 \\ & r_u^2 - 2er_u \cos\cos\left(\varphi - \pi\right) + e^2 - R_z^2 = 0 \end{aligned} \tag{4}$$

where: e – pump eccentricity [m].

Taking into consideration the conditions determined using formula 3, the equation identifying the values of temporary radii of pump vanes' contact is as follows:

$$q = 0,5B\omega\left[\left(e\cos\phi + \left(e^2(\cos^2\phi - 1) + R_Z^2\right)^{0,5}\right) - \left(e\cos(\phi - \pi) + \left(e^2(\cos^2(\phi - \pi) - 1) + R_Z^2\right)^{0,5}\right)\right] \tag{5}$$

where: φ – temporary angular position of the vane in the transitory zone from suction to discharge.

Having considered that angle φ changes within the range (-π/z÷π/z), where *z* stands for the number of vanes, theoretical flow output of the single acting rotary vane pump with 12 vanes may be presented in the form of the characteristics shown in Fig. 2.

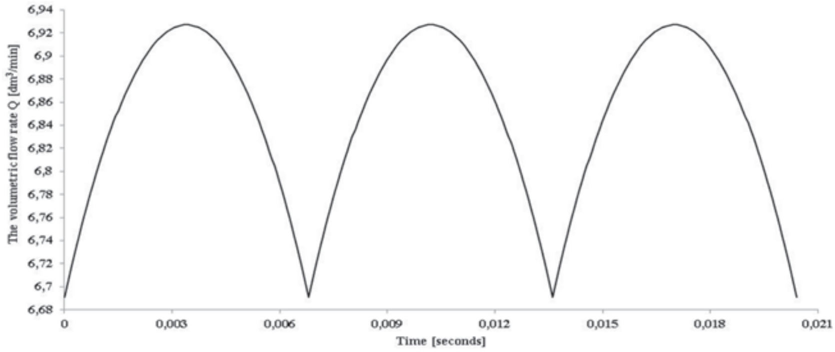

Fig. 2. Diagram of the theoretical temporary pulsation of a rotary vane pump with 12 vanes (vane width 60 mm, stator track diameter 160 mm, eccentricity value 25 mm, rotational speed of the pump shaft n_n=735 rpm)

In case of the considered pump, the irregularity of efficiency, obtained based on the developed mathematical model, was 3,45%.

The acquired simulation characteristics of the flow output of the pump have been implemented in the measurement system model [8, 9, 15], developed in the Matlab-Simulink environment (Fig. 3). The suction line (between the source of stream and maximum valve)has been modeled as the collection of modules consisting of Simscape Hydraulic library function blocks oriented for the purposes of the simulation: hydraulic resistance of the supply bus, capacity of the hydraulic hose and fluid inertia in the hose [11, 23].

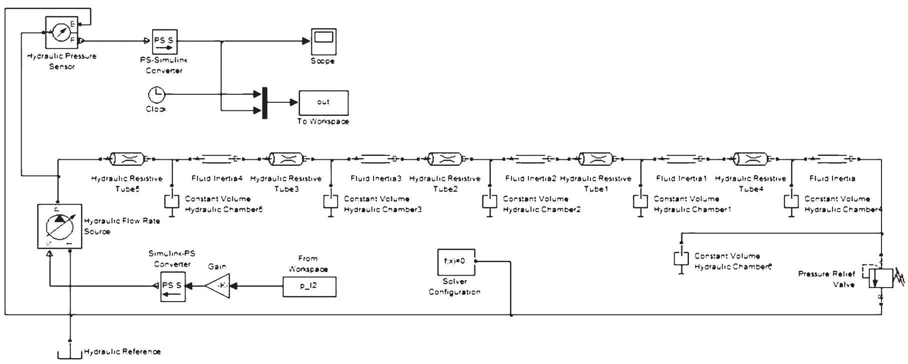

Fig. 3. Measurement system model in the Matlab-Simulink environment

The simulation has been carried out in relation to two selected cases (Fig. 4), with the adopted rotational speed$n_n$of the pump shaft of 735 rpm:

- discharge line with no extra capacity,
- discharge line with extra capacity of the hydraulic fluid.

Values of the pressure pulsation obtained as a result of the simulation and laboratory measurements suggest the proper selection of parameters for the adopted model. The simulation characteristics do not reflect the impact of the maximum valve dynamics on the examined

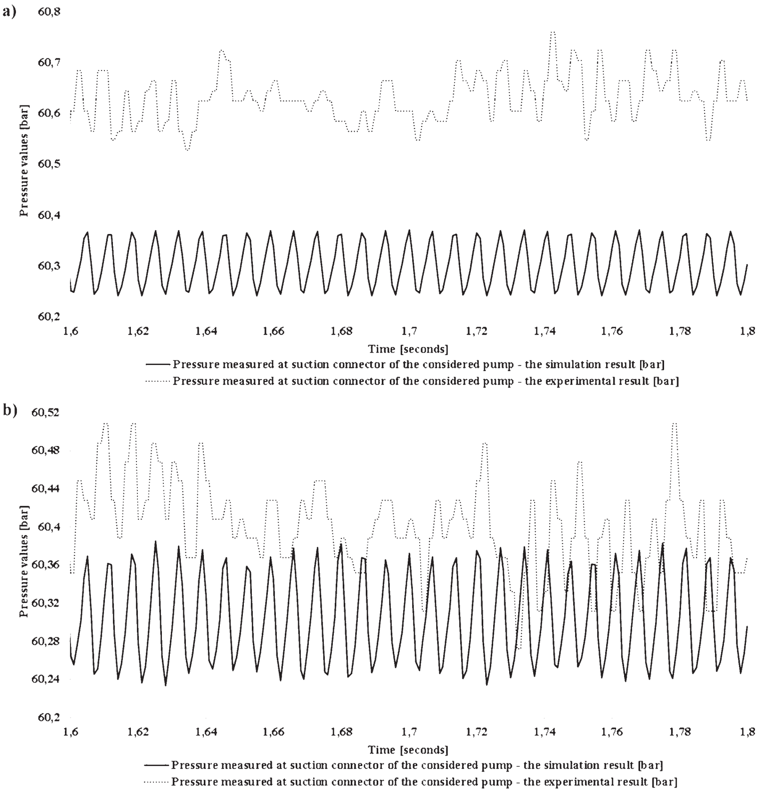

Fig. 4. Characteristics of pressure pulsation obtained as a result of experimental tests and simulation (n_n= 735 rpm, p_s= 60 bar, temperaturets=40°C): a) with no extra capacitance of the discharge line, b) with extra capacitance of the discharge line

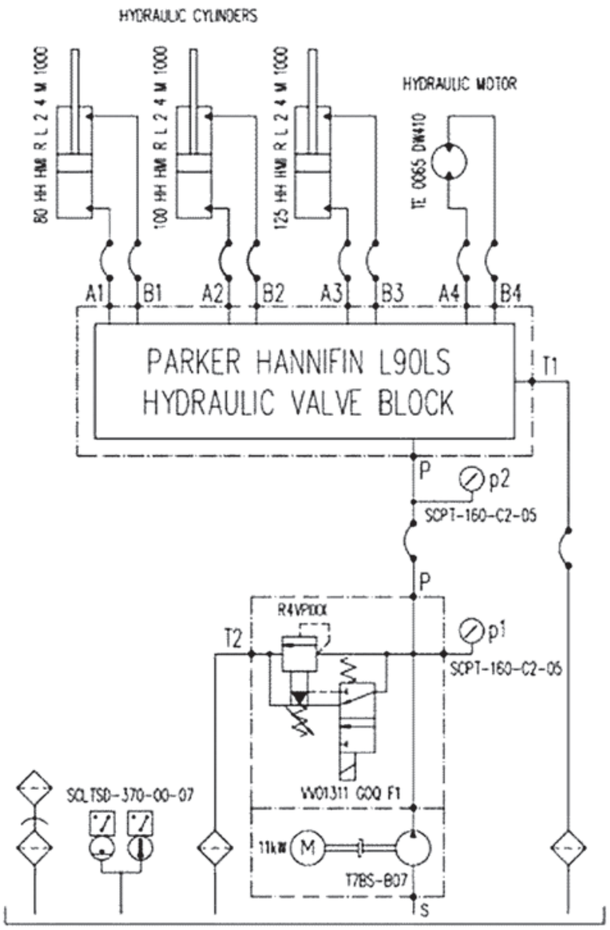

Fig. 5. Schematic diagram of the station used to examine pulsation and vibration of the rotary vane pump

phenomenon, which is the result of the limitations of function block used to model maximum valve.

3. Measuring station and experiment plan

Measuring system (Fig. 5) consists of the double acting rotary vane pump (T7BS B09 3R00 A1M0 manufactured by Parker & Denison) powered by the AC asynchronous motor with frequency converter, L90LS valve block and receivers (hydraulic rotary motor and three hydraulic cylinders).

The pump has been connected with the valve block by means of the elastic discharge pipe of the following parameters: internal diameter d_w=16mm (5/8”), two steel braids (type 2SN), hose length 5m. Pressure sensors SCPT-160-C2-05 have been installed at the pressure flange and before the valve block. Additionally, a flow meter SCFT-060-C2-05has been installed before the valve block. Working fluid temperature was monitored using temperature sensor SCLTSD-370-00-07, installed in the oil tank. Results were monitored and saved using ServiceMaster Plus instrument.

Measurements were taken according to Table 1. Variable parameters included pressure and rotational speed of the pump shaft (regulation of the volumetric flow rate).

Table 1. Parameters of the experiment

Designation ofresearch	Extra capacitance	Speedof the pump shaftn_n [rpm]	Forcing pressure setting p_s [bar]	Oiltemperature t_s [°C]
P1	No	730	60	25
P2	Yes			
P3	No	735	120	
P4	Yes			
P5	No	1441		
P6	Yes			
P7	No	1455	60	
P8	Yes			
P_1	No	730		40
P_2	Yes			
P_3	No	735	120	
P_4	Yes			
P_5	No	1441		
P_6	Yes			
P_7	No	1455	60	
P_8	Yes			

4. Station-based testing

Operating principle of displacement pumps involving periodical changes in the capacity of working areas is the reason of flow output and the pumping pressure fluctuation connected with temporary efficiency. Only screw pumps are free from this defect.

The examined pump T7BS B09 3R00 A1M0 from Parker & Denison is a double acting rotary vane pump with fixed efficiency. Such construction enables relieving the pump shaft from the impact of axial forces coming from the pumping pressure and doubling the efficiency(as compared with the single acting rotary vane pump of the similar size).

As far as pump T7BS is concerned, the rotor is fitted with 12 vanes, and therefore the frequency of vanes travelling from the suction to discharge zone, equal with the frequency of the expected flow output of the pump f_p, is as follows:

$$f_p = \frac{i \cdot n}{60} \quad [Hz] \tag{6}$$

where: i – a number of vanes,
n – rotational speed of the pump shaft [rpm].

Table 2 summarizes the expected values of the pressure peak frequency, resulting from rotation of the pump shaft (f_n) and the subsequent vanes entering the discharge phase (f_p).

Table 2. Expected values of the characteristic frequencies

Designation of study	Extra capacitance	n_n [rpm]	f_n [Hz]	I-stharmonic f_{n_1st} [Hz]	f_p [Hz]	I-stharmonic f_{p_1st} [Hz]
P1	No	730	12,2	24,3	146,0	292,0
P2	Yes	730	12,2	24,3	146,0	292,0
P3	No	735	Hydraulicpower supply overload at setparameters (inability to achieve a pressure of p_s=120 bar)			
P4	Yes	735				
P5	No	1441	24,0	48,0	288,2	576,4
P6	Yes	1441	24,0	48,0	288,2	576,4
P7	No	1455	24,3	48,5	291,0	582,0
P8	Yes	1455	24,3	48,5	291,0	582,0
P_1	No	730	12,2	24,3	146,0	292,0
P_2	Yes	730	12,2	24,3	146,0	292,0
P_3	No	735	Hydraulic power supply overload at setparameters (inability to achieve a pressure of p_s=120 bar)			
P_4	Yes	735				
P_5	No	1441	24,0	48,0	288,2	576,4
P_6	Yes	1441	24,0	48,0	288,2	576,4
P_7	No	1455	24,3	48,5	291,0	582,0
P_8	Yes	1455	24,3	48,5	291,0	582,0

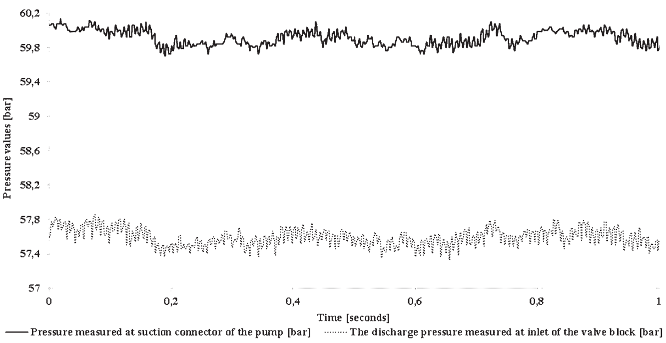

Fig. 6.`Time courses of the pressure values with low rotational speed of the pump with no extra capacitance (experiment P1 – Tab. 1, n_n=735rpm, t_s=25°C, p_s=60 bar)

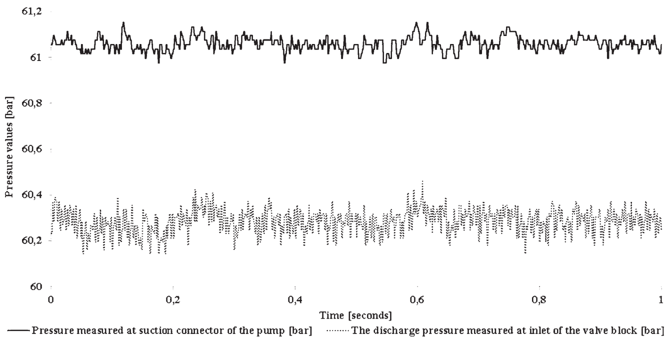

Fig. 7. Time courses of the pressure values with fast rotational speed of the pump with no extra capacitance (experiment P7 – Tab. 1, n_n=1470 rpm, t_s=25°C, p_s=60 bar)

Summary results of measuring pressure on the discharge line of the pump were presented in the time (Table 3) and frequency domains (Table 4).

Besides the pulsation triggered by the pump vanes travelling from suction to discharge zone, in frequency spectrums one can notice (Fig. 10-13) pump shaft rotation frequency and its first harmonic (the reason is eccentricity of the pump shaft in relation to the stator ring track). Juxtaposition of pressure values in the time and frequency domains was presented in Tables 3 and 4.

Furthermore, peak-to-peak value of the pressure measured by the pump is significantly lower than peak-to-peak value of pressure measured by the valve block (L90LS). What's more, in frequency spectrums measured by the valve block, one can observe pressure fluctuations that are almost invisible in the pressure spectrums by the pump.

The reason of the phenomenon connected with the occurrence of additional frequencies is a maximum valve installed in the block L90LS. During measurements, the stream provided by the examined pump to the block L90LS, was flowing through two-stage maximum valve to the discharge pipe line and then to the tank. Operating characteristics of maximum valve, where the main stage poppet operates with variable valve opening, causes self-excited pressure pulsation in case of the valve with not sufficient damping of poppet vibration. In the described case, it is maximum valve that is responsible for the additional pressure pulsation. The sampling frequency of recorded signals amounted to 1000 Hz. At the data processing method the authors adopted 2048 FFT samples analyzed with

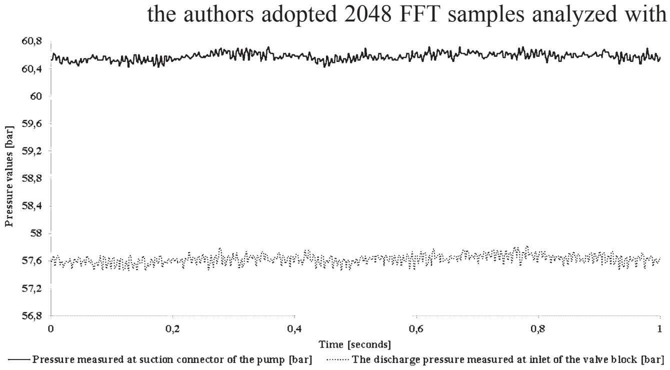

Fig. 8. Time courses of the pressure values with low rotational speed of the pump with no extra capacitance (experiment P_1 – Tab. 1, n_n=735 rpm, t_s=40°C, p_s=60 bar)

a function of the Flat Top window. Frequency spectrums were subjected to averaging in a domain of the four groups of samples. Due

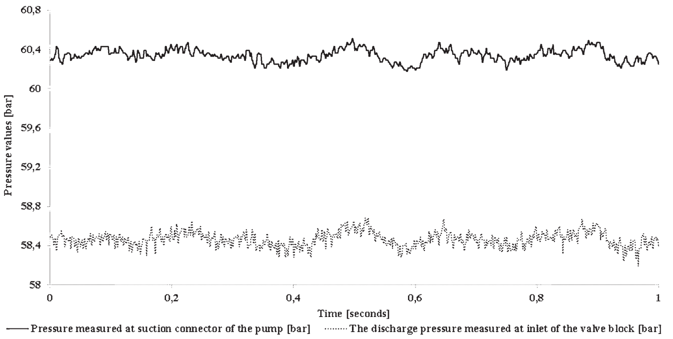

Fig. 9. Time courses of the pressure values with fast rotational speed of the pump with no extra capacitance (experiment P_7 – Tab. 1, n_n=1470 rpm, t_s=40°C, p_s=60 bar)

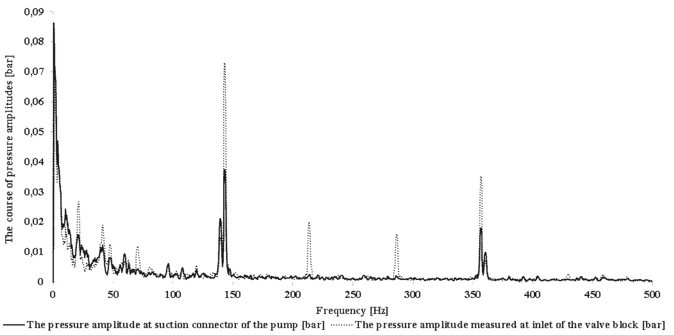

Fig. 10. Frequency spectrums of pressure frequencies with low rotational speed of the pump with no extra capacitance (experiment P1 – Tab. 1, n_n=735 rpm, t_s=25°C, p_s=60 bar)

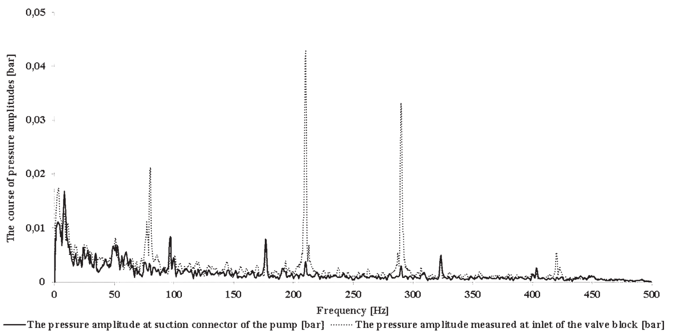

Fig. 11. Frequency spectrums of pressure frequencies with fast rotational speed of the pump with no extra capacitance (experiment P7 – Tab. 1, n_n=1470 rpm, t_s=25°C, p_s=60 bar)

to limitations of the measurement device recording the first harmonic responsible for entering successive blades in the discharge phase f_p at high speeds was not possible (Table 4).

As can be observed, a factor that has strong influence on pressure pulsation amplitudes resulting from eccentricity (frequencyf_n) is temperature, and at the same time hydraulic fluid viscosity. Pulsation amplitude resulting from the fact of vanes entering discharge zone is much lower. Additionally, it may be noticed (Table 4) that low frequency of pressure pulsation f_n (circa 12 Hz) is damped by the hose connecting the pump with valve block.

Amplitudes of pressure pulsation resulting from the fact of vanes entering discharge zone (f_p) are several times lower;one may, however, notice their reinforcement by the discharge line.

In case of higher rotational speed of the pump shaft, one may observe strengthening of pressure pulsation at the discharge line between the pump and valve block not only in case of frequencyf_p, but also frequencyf_n (here equal to circa 24 Hz). In the extreme case, 4

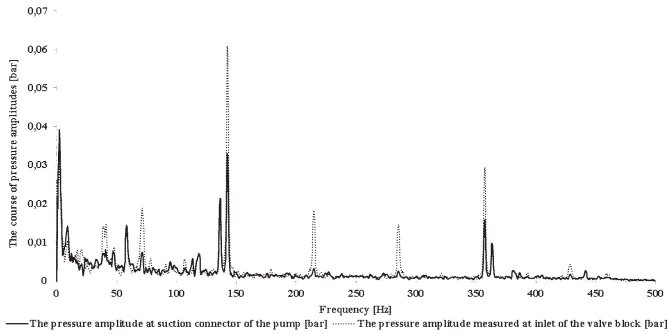

Fig. 12. Frequency spectrums of pressure frequencies with low rotational speed of the pump with no extra capacitance (experiment P_1 – Tab. 1, n_n=735 rpm, t_s=40°C, p_s=60 bar)

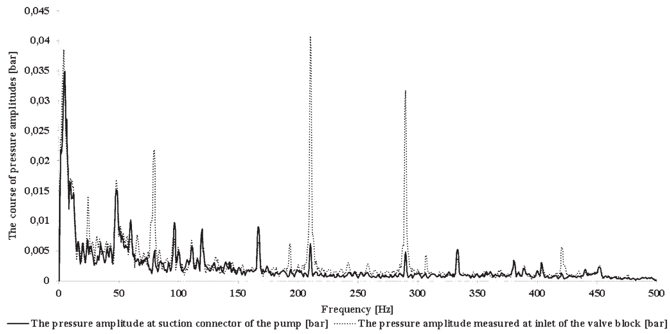

Fig. 13. Frequency spectrums of pressure frequencies with low rotational speed of the pump with no extra capacitance (experiment P_7 – Tab. 1, n_n=1470 rpm, t_s=40°C, p_s=60 bar)

times stronger pressure pulsation of 24 Hz and 12 times stronger pressure pulsation of 290 Hz.

The impact of discharge pressure on the pulsation amplitude at the pressure flange of the pump (pressure p_1) is not dominating. Nevertheless, it may be observed that the amplitude of pressure pulsation in relation to the frequency of pump shaft rotation $f_n$increases with increase of discharge pressure. It may be a sign of the increase of pump shaft eccentricity, which should not happen taking into consideration its design (double acting pump is fitted with the shaft relieved from the radial forces coming from the discharge pressure).

The obtained results of experimental tests were compared with the respective simulation results (Fig. 4 and Table 5).

Despite discrepancies between the obtained values it should be stated that model tests of the impact of pump pulsation on the measurements of discharge pressure are close to the actual measurements to such extent that it is possible to use them for the process of designing new hydraulic systems. Another stage in the development of a mathematical model will be the process of tuning parameters, in order to develop the diagnostic model based on the pump equations.

5. Conclusions

The acquired results are to a large extent compatible with expectations. Due to small irregularities in the efficiency of rotary vane pump (theoretically lower by 3,5%),the observed pressure pulsation is characterized by low peak-to-peak values, in the worst case not exceeding 0,73bar (p_s=120 bar, n_n=1441 rpm, t_s=40°C). Spectrum analysis indicates the necessity of paying attention to the relationship between the amplitude of pressure pulsation with the rotation frequency of a pump shaft dependent on the fluid viscosity and discharge pressure.

In case of pressure pulsation, resulting from the periodicity of pump operation, one should focus on the impact of discharge line on the values of its amplitude at the receiver. It results from the strong

Table 3. Comparison of pressure pulsation values in time domain

Designation ofstudy	Pressure at thepump outlet p_1 [bar]			Pressureat the inlet of valve block p_2 [bar]		
	p_{1_MAX}	p_{1_MIN}	p_{1_PTP}	p_{2_MAX}	p_{2_MIN}	p_{2_PTP}
P1	60,14	59,70	0,43	57,859	57,33	0,52
P2	59,96	59,55	0,41	57,615	57,14	0,47
P3	Hydraulicpower supplyoverload at setparameters (inability toachieve apressureof p_s=120 bar)					
P4						
P5	119,94	119,64	0,32	115,92	115,23	0,69
P6	119,88	119,66	0,22	115,64	115,2	0,44
P7	61,15	60,98	0,18	60,46	60,14	0,32
P8	61,23	61,06	0,18	60,41	60,11	0,3
P_1	60,72	60,43	0,3	57,82	57,46	0,37
P_2	60,56	60,25	0,31	57,61	57,23	0,39
P_3	Hydraulicpower supplyoverload at setparameters (inability toachieve apressureof p_s=120 bar)					
P_4						
P_5	120,19	119,76	0,436	114,75	114,03	0,73
P_6	120,49	120,19	0,296	114,93	114,47	0,46
P_7	60,51	60,18	0,332	58,68	58,19	0,49
P_8	60,58	60,37	0,216	58,74	58,41	0,33

Table 4. Comparison of pressure pulsation values in frequency domain

Designation ofstudy	Pressure peaks p_1 of the characteristic frequencies [bar]				Pressure peaks p_2 of the characteristic frequencies [bar]			
	f_n	f_{n_1st}	f_p	f_{p_1st}	f_n	f_{n_1st}	f_p	f_{p_1st}
P1	0,0195	0,0111	0,0028	0,0010	0,0110	0,0081	0,0058	0,0010
P2	0,0182	0,0052	0,0021	0,0012	0,0151	0,0070	0,0045	0,0011
P3	Hydraulicpower supplyoverload at setparameters (inability toachieve apressureof p_s=120 bar)							
P4								
P5	0,0090	0,0121	0,0016	-	0,0199	0,0073	0,0138	-
P6	0,0086	0,0120	0,0010	-	0,0364	0,0062	0,0072	-
P7	0,0064	0,0059	0,0016	-	0,0061	0,0054	0,0198	-
P8	0,0051	0,0057	0,0017	-	0,0067	0,0041	0,0185	-
P_1	0,0069	0,0055	0,0016	0,0010	0,0070	0,0032	0,0037	0,0012
P_2	0,0055	0,0094	0,0019	0,0010	0,0054	0,0075	0,0037	0,0018
P_3	Hydraulicpower supplyoverload at setparameters (inability toachieve apressureof p_s=120 bar)							
P_4								
P_5	0,0054	0,0185	0,0016	-	0,0096	0,0110	0,0059	-
P_6	0,0130	0,0172	0,0012	-	0,0323	0,0122	0,0053	-
P_7	0,0068	0,0151	0,0017	-	0,0141	0,0165	0,0083	-
P_8	0,0067	0,0167	0,0018	-	0,0066	0,0154	0,0082	-

Table 5. Comparison of the results of simulation and experimental tests

Designation ofstudy	Extra capacitance	Averagepressure$p_{average}$ [bar]	Peak to peak pressure p_{1_PTP} [bar]	Results source
P_1	No	60,63	0,23	Experiment
m_P_1	No	60,30	0,123	Simulation
P_2	Yes	60,40	0,24	Experiment
m_P_2	Yes	60,30	0,152	Simulation

reinforcement of pressure pulsation with higher frequencies by the discharge line.

Further research shall also focus on the way of setting the discharge pressure aiming at the reduction of the potential external interferences. The simplest method would be using the adjustable throttle valve in order to set the discharge pressure.

Acknowledgement

The presented studies were conducted with usage of the equipment in the Hydrostatic Drives Laboratory belonging to the EMT Systems Ltd.

References

1. Bosch Rexroth AG. Hydraulik. Grundlagen und Komponenten. Lohr a. Main 2003 (in German).
2. Buchacz A, Płaczek M. Damping of Mechanical Vibrations Using Piezoelements, Including Influence of Connection Layer's Properties on the Dynamic Characteristic. Solid State Phenomena 2009; 147-149: 869-875, http://dx.doi.org/10.4028/www.scientific.net/SSP.147-149.869.
3. Chalamowski M. Diagnostic susceptibility of Hydraulic Systems. Scientific Papers of the Maritime University in Szczecin 2004; 73 (1): 117-127.
4. da Costa Bortoni E., Almeida R. A., Viana A. N. C. Optimization of parallel variable-speed-driven centrifugal pumps operation. Energy Efficiency 2008; 1 (3): 167-173, http://dx.doi.org/10.1007/s12053-008-9010-1.
5. Dymarek A, Dzitkowski T. Active reduction of identified machine drive system vibrations in the form of multi-stage gear units. Mechanika 2014; 20 (2): 183-189.
6. Gendarz P. Bildung von geordneten Konstruktionsfamilien unter Anwendung von Ähnlichkeitsgesetzen. Forschung im Ingenieurwesen 2013; 3-4 (77): 105-115, http://dx.doi.org/10.1007/s10010-013-0167-1.
7. Gidziński T. Damage caused by errors in exploitation of vane pumps. Hydraulic and Pneumatic 2006; 1: 5-8.
8. Klarecki K., Hetmanczyk M.P., Rabsztyn D. Influence of the selected settings of the controller on the behavior of the hydraulic servo drive. Mechatronics - Ideas for Industrial Application. Advances in Intelligent Systems and Computing 2015; 317: 91-100, http://dx.doi.org/10.1007/978-3-319-10990-9_9.
9. Klarecki K., Hetmanczyk M.P., Rabsztyn D. The influence of volumetric performance settings of a multi-piston pump on parameters of forced vibrations. Vibroengineering Procedia 2014; 3: 76-81.
10. Kudźma Z. Damping pressure and noise pulsation in transient and established conditions in hydraulic systems. Publishing House of Wroclaw University 2012.
11. Kudźma Z. Dynamic properties of hydraulic hoses. Hydraulic and Pneumatic 2005; 6: 14-17.
12. Kudźma Z., Palczak E., Rutanski J., Stosiak M. Selected problems in exploitation of machines with hydrostatic drive. Mining Machines 2009; 4: 3-8.
13. Kunz A., Gellrich R., Beckmann G., Broszeit E. Theoretical and practical aspects of the wear of vane pumps Part A. Adaptation of a model for predictive wear calculation. Wear 1995; 181-183 (2): 862-867.
14. Kunz A., Gellrich R., Beckmann G., Broszeit E. Theoretical and practical aspects of the wear of vane pumps Part B. Analysis of wear behaviour in the vickers vane pump test. Wear 1995; 181-183 (2), 868-875, http://dx.doi.org/10.1016/0043-1648(94)07087-3.
15. Lisowski E., Panek M. CFD modeling method of vanes working in the vane pump. Eksploatacja i Niezawodnosc - Maintenance and Reliability 2004; 2: 36-41.
16. Mucchi E., Agazzi A., D'Elia G, Dalpiaz G. On the wear and lubrication regime in variable displacement vane pumps. Wear 2013; 306, (1-2): 36-46, http://dx.doi.org/10.1016/j.wear.2013.06.025.
17. Osiecki A. Hydrostatic drives. Warsaw: WNT, 2014.
18. Roskowicz M., Jastrzębski G. Evaluation of the possibility of diagnosing aircrafts hydraulic systems. WAT Bulletin 2009; 4 (LVIII): 335-349.
19. Stryczek S. Hydrostatic drive. Warsaw: WNT, 1995 (in Polish).
20. Wszolek G., Czop P., Skrobol A., Slawik D. A nonlinear, data-driven model applied in the design process of disc-spring valve systems used in hydraulic dampers. SIMULATION Transactions of the Society for Modeling and Simulation International 2013; 89 (3): 419-431, http://dx.doi.org/10.1177/0037549712441976.
21. Wszolek G., Czop P., Slawik D. Development of an Optimization Method for Minimizing Vibrations of a Hydraulic Damper. SIMULATION Transactions of the Society for Modeling and Simulation International 2013; 89 (9): 1073-1086, http://dx.doi.org/10.1177/0037549713486012.
22. Yuan J., Yuan S. Prediction of performance for dissimilar centrifugal pumps coupled in series or in parallel. Drainage and Irrigation Machinery 2004; 22 (6): 1-4.
23. Zarzycki Z. Modeling of the hydraulic dynamic properties of closed conduits. Comparison of models with distributed parameters with lumped parameters models. Journal of Theoretical and Applied Mechanics 1989; 27(4): 625-634.

Klaudiusz KLARECKI
Dominik RABSZTYN
Mariusz Piotr HETMANCZYK
Faculty of Mechanical Engineering, The Silesian University of Technology
Institute of Engineering Processes Automation and Integrated Manufacturing Systems
ul. Konarskiego 18A, 44-100 Gliwice, Poland
E-mail: klaudiusz.klarecki@polsl.pl, dominik.rabsztyn@polsl.pl, mariusz.hetmanczyk@polsl.pl

Article citation info:
DUAN R, ZHOU H, FAN J. Diagnosis strategy for complex systems based on reliability analysis and MADM under epistemic uncertainty. Eksploatacja i Niezawodnosc – Maintenance and Reliability 2015; 17 (3): 345–354, http://dx.doi.org/10.17531/ein.2015.3.4.

Rongxing DUAN
Huilin ZHOU
Jinghui FAN

DIAGNOSIS STRATEGY FOR COMPLEX SYSTEMS BASED ON RELIABILITY ANALYSIS AND MADM UNDER EPISTEMIC UNCERTAINTY

STRATEGIA DIAGNOSTYKI DLA SYSTEMÓW ZŁOŻONYCH OPARTA NA ANALIZIE NIEZAWODNOŚCI ORAZ METODACH WIELOATRYBUTOWEGO PODEJMOWANIA DECYZJI MADM W WARUNKACH NIEPEWNOŚCI EPISTEMOLOGICZNEJ

Fault tolerant technology has greatly improved the reliability of train-ground wireless communication system (TWCS). However, its high reliability caused the lack of sufficient fault data and epistemic uncertainty, which increased significantly challenges in system diagnosis. A novel diagnosis method for TWCS is proposed to deal with these challenges in this paper, which makes the best of reliability analysis, fuzzy sets theory and MADM. Specifically, it adopts dynamic fault tree to model their dynamic fault modes and evaluates the failure rates of the basic events using fuzzy sets theory and expert elicitation to hand epistemic uncertainty. Furthermore, it calculates some quantitative parameters information provided by reliability analysis using algebraic technique and Bayesian network to overcome some disadvantages of the traditional methods. Diagnostic importance factor, sensitivity index and heuristic information values are considered comprehensively to obtain the optimal diagnostic ranking order of TWCS using an improved TOPSIS. The proposed method takes full advantages of the dynamic fault tree for modelling, fuzzy sets theory for handling uncertainty and MADM for the best fault search scheme, which is especially suitable for fault diagnosis of the complex systems.

Keywords: *Train-ground wireless communication system, Reliability analysis, MADM, Epistemic uncertainty, TOPSIS.*

Technologia odporna na błędy przyczyniła się do dużej poprawy niezawodności systemów łączności bezprzewodowej pociąg-ziemia (TWCS). Jednakże wysoka niezawodność tych systemów pociąga za sobą brak wystarczających danych o uszkodzeniach oraz niepewność epistemologiczną, której zwiększenie stworzyło liczne wyzwania w zakresie diagnostyki systemów. W niniejszej pracy zaproponowano nowatorską metodę diagnozowania TWCS, która odpowiada na owe wyzwania wykorzystując analizę niezawodności, teorię zbiorów rozmytych oraz metody wieloatrybutowego podejmowania decyzji MADM. W szczególności, zaproponowana metoda wykorzystuje dynamiczne drzewa błędów do modelowania dynamicznych stanów niezdatności oraz pozwala na oszacowanie częstości występowania uszkodzeń dla zdarzeń podstawowych z wykorzystaniem teorii zbiorów rozmytych oraz oceny eksperckiej, rozwiązując w ten sposób problem niepewności epistemologicznej. Ponadto, metoda ta umożliwia obliczenie niektórych parametrów ilościowych na podstawie informacji pochodzących z analizy niezawodności, z zastosowaniem techniki algebraicznej oraz sieci bayesowskich, co pozwala na obejście ograniczeń tradycyjnie stosowanych metod. W artykule przeprowadzono szczegółową analizę czynnika ważności diagnostycznej, wskaźnika czułości oraz wartości informacji heurystycznej w celu określenia optymalnej kolejności działań diagnostycznych dla TWCS z zastosowaniem poprawionej wersji TOPSIS Proponowana metoda w pełni wykorzystuje zalety metody drzewa błędów do modelowania, teorii zbiorów rozmytych – do rozwiązywania problemu niepewności oraz MADM – do wyznaczania najlepszej metody wyszukiwania niezdatności, co jest szczególnie przydatne w przypadku diagnozowania niezdatności systemów złożonych.

Słowa kluczowe: *system łączności bezprzewodowej pociąg-ziemia, analiza niezawodności, MADM, niepewność epistemologiczna, TOPSIS.*

1. Introduction

Train-ground wireless communication system (TWCS) is a safety-critical subsystem of urban rail transit and its reliability has a direct effect on the stability and safety of the train operation system. For fast technology innovation, the performance of TWCS has been greatly improved with the wide application of high dependability safeguard techniques on one hand, but on the other hand, its complexity of technology and structure increasing significantly raise challenges in system maintenance and diagnosis. These challenges are shown as follows. (1) Lack of sufficient fault samples. Fault samples integrity has a significant influence on the system diagnostic performance. However, it is extremely difficult to obtain mass fault samples which need many case studies in practice due to some reasons. One reason is imprecise knowledge in an early stage of the new product design. The other factor is the changes of the environmental conditions which may cause that the historical fault data cannot represent the future failure behaviours. (2) Failure dependency of components. TWCS adopts many redundancy units and fault tolerance techniques to improve its reliability. So the behaviours of components in the system and their interactions, such as failure priority, sequentially dependent failures, functional dependent failures, and dynamic redundancy management, should be taken into account. (3) Uncertainty of diagnostic test cost for components. Usually, different components have different diagnostic test cost and it is very difficult to estimate a precise diagnostic test cost due to the lack of sufficient data, especially for the new components. Aiming at these challenges, many efficient diagnostic methods have been proposed. Assaf et al. proposed a reliability-based approach to determine the diagnosis order of components using diagnostic importance factor (DIF), which uses the dynamic fault tree to model the failure dependency of components and can, to some extent alleviate fault data acquisition bottleneck [1, 19]. However, the solution for dynamic fault tree was based on Markov Chains (MC) model- which is ineffective in handing larger dynamic fault tree and modelling power capabilities. For this purpose, Duan et al. proposed a hybrid diagnosis method using dynamic fault tree and discrete-time Bayesian network (DTBN) [17]. Dynamic logic gates were converted to DTBN and the reliability results were calculated by a standard Bayesian Network (BN) inference algorithm. However, it is an approximate solution for dynamic fault tree and requires huge memory resources to obtain the query variables probability accurately. Furthermore, these diagnostic methods, which are usually assumed that the failure rates of the components are considered as crisp values describing their reliability characteristics, have been found to be inadequate to deal with the challenge (1) mentioned above. Therefore, fuzzy sets theory has been introduced as a useful tool to handle challenges (1) and (3). The fuzzy fault tree analysis model employs fuzzy sets and possibility theory, and deals with ambiguous, qualitatively incomplete and inaccurate information [8, 12-13]. However, these approaches use the static fault tree to model the system fault behaviours and cannot cope with the challenge (2). So fuzzy dynamic fault tree (FDFT) analysis has been introduced [7, 22], which takes into account not only the combination of failure events but also the order in which they occur. Nonetheless, the solution for FDFT is still MC based approach, which has the infamous state space explosion problem. To overcome these difficulties and limitations, Duan et al. proposed a new diagnosis method using fuzzy sets and dynamic fault tree, which use fuzzy sets to evaluate the failure rates of the basic events and uses a dynamic fault tree model to capture the dynamic failure mechanisms [18]. But the solution for the dynamic fault tree is still based on DTBN and cannot avoid the aforementioned problems. Assaf et al. firstly introduced the cost diagnostic importance factor (CDIF) to incorporate the diagnostic test cost into the diagnosis process in order to optimize the fault diagnosis [2]. They assumed the test cost of the components was crisp value, which was highly impracticable and almost impossible to apply. So it cannot deal with the challenge (3). In addition, all the diagnosis algorithms are based on minimal cut sets and DIF or CDIF, which are in essence single attribute decision making, and usually cause minimal cut sets with a smaller DIF to be diagnosed first, thereby influencing the diagnosis result.

Motivated by the problems mentioned above, this paper presents a novel diagnosis strategy for TWCS based on fuzzy sets, dynamic fault tree and MADM shown in Figure 1. It pays particular attention to meeting above three challenges. We adopt expert elicitation and fuzzy sets theory to deal with insufficient fault data and handle the uncertainty problem by treating diagnostic test cost as fuzzy numbers. Furthermore, we use a dynamic fault tree model to capture the dynamic behaviours of the TWCS failure mechanisms and calculate some quantitative parameters information provided by reliability analysis using BN and algebraic technique in order to avoid the aforementioned problems. In addition, components' DIF, sensitivity index (SI) and heuristic information values (HIV) are considered comprehensively to design a novel diagnosis strategy which can locate the fault with the objective of fast and low-cost diagnosis.

The aim of this project is to present the scientific decision for the fault diagnosis of TWCS and offer a new idea for fault diagnosis in complex systems. The rest sections of this paper are organized as follows: Section 2 provides a brief introduction on TWCS and its dynamic fault tree model. Estimation of failure rates for the basic events is described in Section 3. Section 4 presents a novel dynamic fault tree solution which uses BN and algebraic technique. Section 5 presents a new diagnosis algorithm which makes use of the components' DIF, SI and HIV using MADM solution. The outcomes of the research and future research recommendations are presented in the final section.

Fig. 1. Diagnosis framework for TWCS

2. Dynamic fault tree of TWCS

Credible wireless communication technology is one of the development directions of communication based train control because it can meet the demands of real-time large amount of information transmission of train-ground. TWCS based on orthogonal frequency division multiplexing adopts some redundancy techniques to ensure higher reliability and is widely applied in the train control system, which transmits real-time data between train and ground. TWCS mainly includes train-ground communication access devices and train-ground communication transmission system. Train-ground communication access devices are responsible for information acquisition, information composition, information decomposition, information encoding, information decoding, and information transmission security mechanism. This can guarantee a safe, reliable and real-time information transmission. Specifically, train-ground communication access devices include decentralized radio control unit (DRCU) and mobile radio control unit (MRCU). DRCU, situated in the decentralized control center, offers the interfaces between the decentralized control system and the traction power supply system and controls the information transmission of the decentralized train-ground communication devices. In addition, it also performs the most challenging tasks such as information acquisition, composition, decomposition, encoding and decoding among the decentralized control system, the vehicle control system, localization system and the traction power supply system. MRCU, located on the opposite ends of the train, not only offers the interfaces between the vehicle control system and the localization system, but also implements information processing among the vehicle control system, the localization system, the decentralized control system and the traction power supply system. Train-ground communication transmission system includes ground radio transceiver equipment, mobile radio transceiver equipment and wireless communication channel. It is its responsibility for the reliable, transparent data transmission between train and ground devices.

TWCS is a typically complex system and adopts redundancy techniques to ensure higher reliability. For example, the hardware redundancy technique is employed in the design of DRCU and MRCU. High coupling degree together with complicated logic relationships exists between these modules. So the dynamic behaviours of components in these modules and their interactions, such as failure priority, sequentially dependent failures, functional dependent failures, and dynamic redundancy management, should be taken into consideration. Obviously, traditional static fault tree is unsuitable to model these dynamic fault behaviours. Therefore, we use the dynamic fault tree model to capture the dynamic behaviours of system failure mechanisms such as

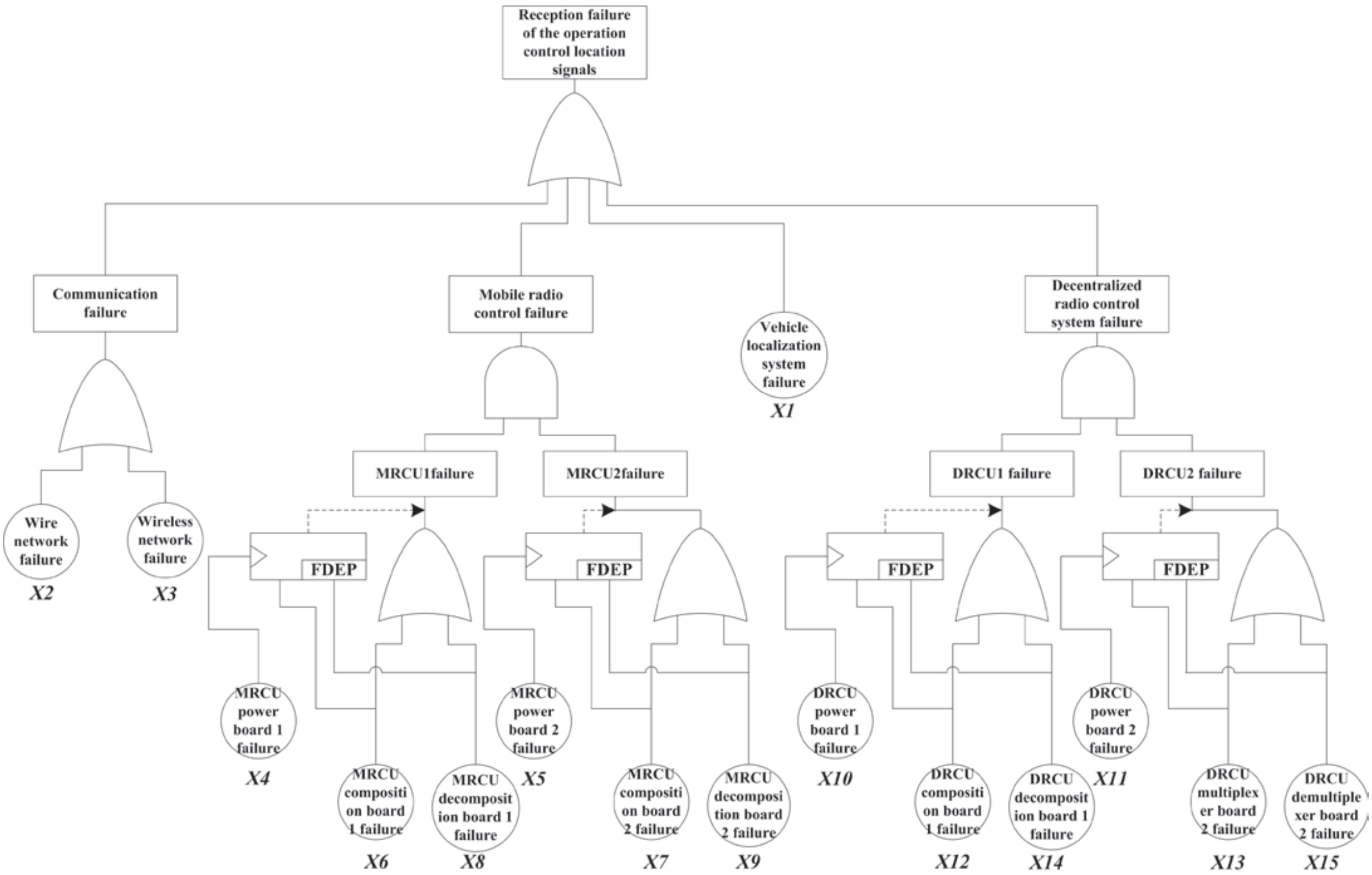

Fig. 2. Dynamic fault tree of TWCS

sequence-dependent events, spares and dynamic redundancy management, and priorities of failure events. Taken reception failure of the operation control location signals as the top event, the dynamic fault tree of TWCS is shown in Figure 2.

3. Estimation of failure rates for TWCS

In order to calculate some reliability parameters for diagnosis, failure rates of the basic events must be known. However, fault tolerant technology has greatly improved the system reliability and its high reliability caused the lack of sufficient fault data and epistemic uncertainty. For this reason, it is very difficult to estimate precisely the failure rates of the basic events, especially for the new equipment. In this study, the expert elicitation through several interviews and questionnaires and fuzzy sets theory are used to estimate the failure rates of the basic events through qualitative data processing. An overall architecture of the estimation of failure rates for TWCS is shown in Figure 3.

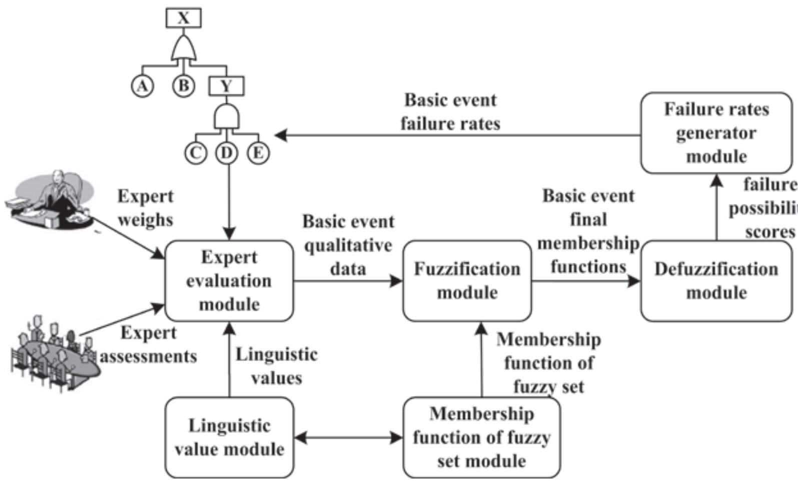

Fig. 3. Structure of the estimation of failure rates for TWCS

3.1. Experts evaluation

Experts are people who are familiar with the system and understand the system working environment and the system operation. Therefore, experts can be selected from different fields, such as the design, installation, maintenance, operation and management of the system, to judge the failure rates of the basic events. They are more comfortable justifying event failure likelihood using qualitative natural languages based on their experiences and knowledge about the system, which capture uncertainties rather than by expressing judgments in a quantitative manner. The granularity of the set of linguistic values commonly used in engineering system safety is from four to seven terms. In this paper, the component failure rate is defined by seven linguistic values, i.e. very high, high, reasonably high, moderate, reasonably low, low and very low.

3.2. Fuzzification module

Experts evaluation expressed in terms of qualitative natural languages should be converted into the operational format of fuzzy numbers, for example, trapezoidal fuzzy numbers. This function can be implemented by fuzzification module. The objective of fuzzification module is to quantify the basic event qualitative data into their corresponding quantitative data in the form of membership function of fuzzy numbers. In addition, each predefined linguistic value has a corresponding mathematical representation and the shapes of the membership functions to mathematically represent linguistic variables in engineering systems are illustrated in Figure 4. To eliminate bias coming from an expert, six experts are asked to justify how likely a basic event will fail in the system under investigation. Therefore, it is necessary to combine or aggregate these opinions into a single one. There are many approaches to aggregate fuzzy numbers. An appealing approach is the linear opinion pool [6]:

$$M_i = \sum_{j=1}^{n} \omega_j A_{ij}, \quad i = 1, 2, 3, ..., m \tag{1}$$

where m is the number of basic events; A_{ij} is the linguistic expression of a basic event i given by expert j; n is the number of the experts; ω_{ij} is a weighting factor of the expert j and M_i represents combined fuzzy number of the basic event i.

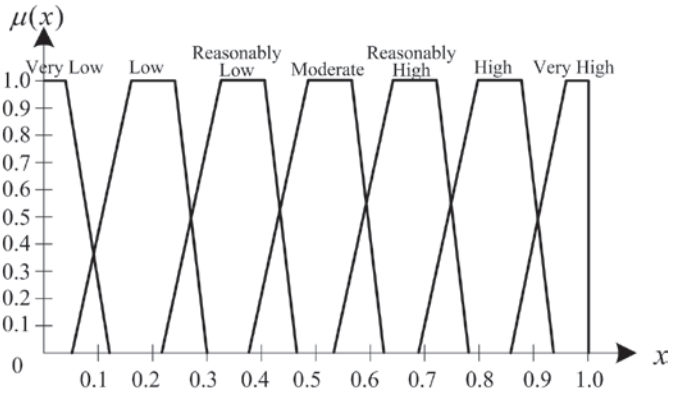

Fig. 4. Fuzzy numbers used for representing linguistic value

Usually, an α-cut addition followed by the arithmetic averaging operation is used for aggregating more membership functions of fuzzy numbers of different types. The membership function of the total fuzzy numbers from n experts' opinion can be computed as follows:

$$f(z) = \max_{z = x_1 + x_2 +, ..., + x_n} \left[\omega_1 f_1(x) \wedge \omega_2 f_2(x) \wedge ... \wedge \omega_n f_n(x)) \right] \tag{2}$$

where $f_n(x)$ is the membership function of a fuzzy number from expert n and $f(z)$ is the membership function of the total fuzzy numbers.

3.3. Calculating fuzzy fault rates of the basic events

Apparently, the final quantitative data taken from the fuzzification module are still in the form of fuzzy numbers and cannot be used for fault tree analysis because they are not crisp values. So, fuzzy number must be converted to a crisp score, named as fuzzy possibility score (FPS) which represents the most possibility that an expert believes occurring of a basic event. This step is usually called defuzzification. There are several defuzzification techniques. It is very important to choose a suitable defuzzification technique for a specific application. We use an area defuzzification technique to realize this algorithm, which has lowest relative errors and the closest match with the real data [16]. If (a, b, c, d; 1) is a trapezoidal fuzzy number, then its area defuzzification technique is as follows:

$$FPS = \frac{(a + 2b - 2c - d)((2a + 2b)^2 + (c + d)(-3a + 2c - d) - 2c(3b + d) - 4ab)}{18(a + b - c - d)^2} \tag{3}$$

The event fuzzy possibility score is then converted into the corresponding fuzzy failure rate, which is similar to the failure rate. Based on the logarithmic function proposed by Onisawa [14], which utilizes the concept of error possibility and likely fault rate, the fuzzy failure rate can be obtained by the following equation (4). Table 1 shows the fuzzy failure rates of the basic events for TWCS.

$$FFR = \begin{cases} \dfrac{1}{10^{\left[\frac{1-FPS}{FPS}\right]^{\frac{1}{3}} \times 2.301}}, & FPS \neq 0 \\ 0, & FPS = 0 \end{cases} \tag{4}$$

Table 1. Basic events' FPS and FFR

Basic events	Fuzzy numbers	FPS	FFR
X1	[0.1602, 0.2093, 0.2381, 0.3001]	0.0749	4.8e-6
X2	[0.1654, 0.2113, 0.2550, 0.3601]	0.0806	6.6e-6
X3	[0.2589, 0.2905, 0.5835, 0.6001]	0.1355	5.4e-5
X4,X5	[0.2501, 0.2662, 0.4261, 0.4601]	0.1269	4.2e-5
X6,X7	[0.2701, 0.3298, 0.5902, 0.6501]	0.1463	7.2e-5
X8,X9	[0.1604, 0.2003, 0.2498, 0.3528]	0.0791	6.1e-6
X10,X11	[0.2381, 0.2472, 0.4201, 0.4591]	0.1209	3.5e-5
X12,X13	[0.2688, 0.3201, 0.5799, 0.6241]	0.1439	6.8e-5
X14,X15	[0.2583, 0.3001, 0.4998, 0.5941]	0.1367	5.6e-5

4. Calculating reliability parameters using BN and algebraic technique

After the dynamic fault tree is constructed and all basic events have their corresponding failure rates with the exponential distribution function, reliability results of TWCS can be calculated by solving the dynamic fault tree. Traditional solution for dynamic fault tree is based on MC model [11], which has the infamous state space explosion problem and cannot solve a larger dynamic fault tree. Therefore, DTBN was proposed to solve the dynamic fault tree in [3-4]. Dynamic logic gates are converted to DTBN and the reliability results are calculated using a standard BN inference algorithm. However, this is an approximate solution and requires huge memory resources to obtain the probability distribution accurately. In addition, as the number of intervals increases, the accuracy and execution time increases greatly. An innovative algorithm has been introduced to reduce the dimension of conditional probability tables by an order of magnitude [9]. However, this method cannot perform posterior probability updating. In the following section, we present an improved method to calculate the reliability parameters using BN and algebraic technique to overcome the disadvantages mentioned above.

4.1. Mapping static fault tree into BN

There is a clear correspondence between static fault tree and BN. The fault tree can be seen as a particular deterministic case of the BN. Conceptually it is straightforward to map a fault tree into a BN: one only needs to "re-draw" the nodes and connect them while correctly enumerating reliabilities. Figure 5 shows the conversion of an OR and an AND gate into equivalent nodes in a BN. Parent nodes A and B

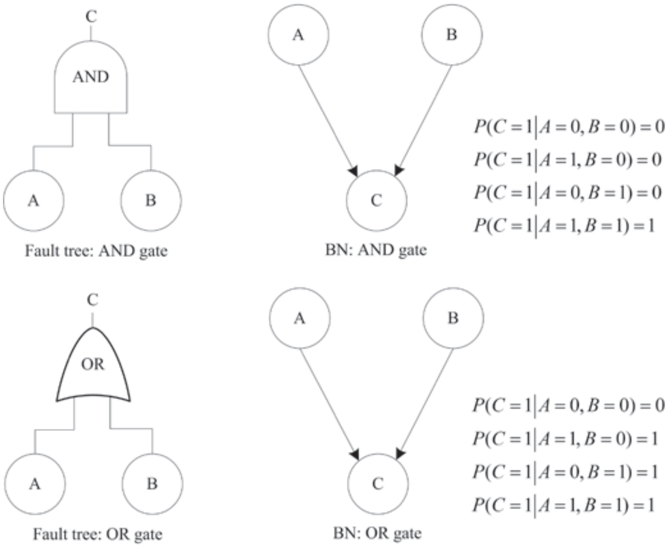

Fig. 5 The Equivalent BN of OR and AND Gate

are assigned prior probabilities, which coincident with the probability values assigned to the corresponding basic nodes in the fault tree, and child node C is assigned its conditional probability table (CPT). Since the OR and AND gates represent deterministic causal relationships, all the entries of the corresponding CPT are either 0 or 1. The detailed algorithm of converting a fault tree into a BN was proposed in [3, 15].

4.2. Fault Probability of a Module with Sequence Dependence

Let us consider an event sequence composed of n events, $e_1, e_2, \cdots, e_n$ including several spare events. An event in the sequence is denoted by e_j^i, which means that the event that failed in the j-th order of the sequence is designated a spare of an event that failed in the i-th order. e_j^0 denotes an event that was originally in active mode. e_j^i ($i > 0, i < j$) has a dormancy factor $0 \le \alpha_j \le 1$. The sequence probability of $< e_1^{i1}, e_2^{i2}, \cdots, e_n^{in} >$ can be calculated using the n–tuple integration as:

$$\begin{aligned} & Pr(< e_1^{i1}, e_2^{i2}, \cdots, e_n^{in} >)(t) \\ & = \int_0^t \int_0^{x_n} \cdots \int_0^{x_2} \prod_{e_j^0 \in S_a} f_j(x_j) \prod_{e_j^i \in S_{ss}} f_{j\alpha}(x_j) \\ & \times \prod_{e_j^i \in S_{sa}} \overline{F}_{j\alpha}(x_i) f_j(x_j - x_i) dx_1 dx_2 \cdots dx_n \end{aligned} \tag{5}$$

where x_j indicates the occurrence time of e_j^i, $f_j(x)$ is the probability distribution function of e_j^i and $\overline{F}_{j\alpha}(x)$ is the survival function of e_j^i in standby mode. S_a is a set of events that were originally in active mode and S_{sa} (S_{ss}) is a set of spare events that fail in active (standby) mode [20].

When the failure time of e_j^i in active mode follows an exponential distribution with λ_j, the sequence probability is:

$$\begin{aligned} & Pr(< e_1^{i1}, e_2^{i2}, \cdots, e_n^{in} >)(t) \\ & = \prod_{e_j^i \in S_{ss}} \alpha_j L^{-1} \left\{ \frac{1}{s} \prod_{i=1}^{n} \left(\frac{\lambda_i}{s + a_i} \right) \right\} \end{aligned} \tag{6}$$

where $a_i = \sum_{k=i}^{n} \lambda_k - \sum_{\substack{k=i \\ e_k^j \in S_{ss}}}^{n} (1-\alpha_k)\lambda_k - \sum_{\substack{k=i \\ e_k^j \in S_{sa}}}^{n} (1-\alpha_j)\lambda_j, for \ a_i > 0$

and L^{-1} is the inverse Laplace transform operator.

If every a_i in the above equation is distinct from the other, the sequence probability is:

$$\begin{aligned} & Pr(< e_1^{i1}, e_2^{i2}, \cdots, e_n^{in} >)(t) \\ & = \prod_{e_j^i \in S_{ss}} \alpha_j \prod_{i=1}^{n} \lambda_i \sum_{k=0}^{n} \frac{e^{-a_k t}}{\prod_{j=0, j \ne k}^{n} (a_j - a_k)} \end{aligned} \tag{7}$$

where $a_0 = 0$.

4.3. Mapping dynamic fault tree into BN

Dynamic fault tree extends traditional fault tree by defining special gates to capture the components' sequential and functional dependencies. Currently there are six types of dynamic gates defined: the functional dependency gate (FDEP), the cold, hot, and warm spare gates (CSP, HSP, WSP), the priority AND gate (PAND), the sequence enforcing gate (SEQ). Here, we briefly discuss the FDEP and the WSP gates as they will be later used in our examples.

(1) WSP Gate

The WSP gate has one primary input and one or more alternate inputs. The primary input is initially powered on and the alternate inputs are in standby mode. When the primary fails, it is replaced by an alternate input, and in turn, when this alternate input fails, it is replaced by the next available alternate input, and so on and so forth. In standby mode, the component failure rate is reduced by a factor α called the dormancy factor. α is a number between 0 and 1. A cold spare has a dormancy factor $\alpha=0$; and a hot spare has a dormancy factor $\alpha=1$. The WSP gate output is true when the primary and all the alternate inputs fail. Figure 6 shows the WSP gate and its equivalent BN. Table 2 shows the CPT of the node A. Supposing that A and S follow the same exponential distribution with λ; Here, $p_1(t)$ and $p_2(t)$ in this table can be derived as:

$$p_1(t) = P(A=1|S=0) = \frac{P(S=0, A=1)}{P(S=0)} = 1 - e^{-\lambda_A \alpha t} \tag{8}$$

$$\begin{aligned} p_2(t) &= P(A=1|S=1) = \frac{P(S=1, A=1)}{P(S=1)} \\ &= \frac{P(< P, A^S >)(t) + P(< A, S >)(t)}{F_S(t)} \end{aligned} \tag{9}$$

$P(< P, A^S >)(t)$ and $P(< A, S >)(t)$ are sequence probabilities calculated by equation (10):

$$\begin{aligned} & P(< P, A^S >)(t) + P(< A, S >)(t) \\ & = 1 - e^{-\lambda t} + \frac{e^{-(\lambda + \lambda\alpha)t} - e^{-\lambda t}}{\alpha} \end{aligned} \tag{10}$$

The output of node WSP is an AND gate whose CPT is shown in Figure 5.

Table 2. The CPT of the node A

	S=0	S=1
A=0	$1-p_1(t)$	$1-p_2(t)$
A=1	$p_1(t)$	$p_2(t)$

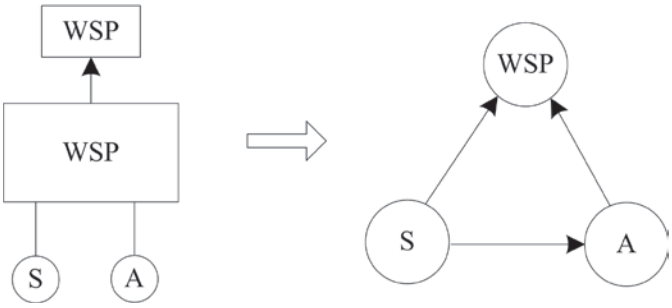

Fig. 6. WSP and its equivalent BN

(2) FDEP Gate

FDEP is used to model situations where one component's correct operation is dependent upon the correct operation of some other component. It has a single trigger input, which could be another basic event or the output of another gate, a non-dependent output reflecting the status of the trigger, and one or more dependent basic events. Figure 7 shows FDEP gate and its equivalent BN. Table 3 shows the CPT of the node A. Here, $p_3(t)$ in this table can be derived as:

$$p_3(t) = P(A=1|T=0) = 1 - e^{-\lambda_A t} \tag{11}$$

The CPT of output node FDEP is shown in Table 4.

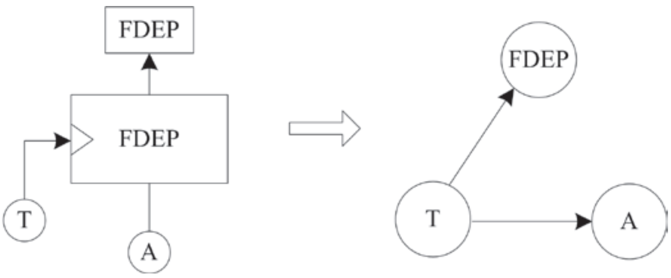

Fig. 7. FDEP and its equivalent BN

Table 3. The CPT of the node A

	T=0	T=1
A=0	$1-p_3(t)$	0
A=1	$p_3(t)$	1

Table 4. The CPT of the node FDEP

	T=0	T=1
$FDEP$=0	1	0
$FDEP$=1	0	1

4.4. Calculating reliability parameters

According to the dynamic fault tree shown in Figure 2 and the basic failure data shown in Table 1, we can map the dynamic fault tree into an equivalent BN using the proposed method. Its equivalent BN is given in Figure 8. Once the structure of a BN is known and all the probability tables are filled, it is straight forward to calculate the reliability parameters of TWCS using the inference algorithm. These reliability parameters mainly include system reliability, DIF and SI.

(1) System reliability

Assume the mission time of TWCS is 1000 hours. We can calculate the system unreliability using the following equation:

$$P(S)=P(S=state1)=0.1036 \tag{12}$$

(2) DIF

DIF is defined conceptually as the probability that an event has occurred given the top event has also occurred. DIF is the corner stone of reliability based diagnosis methodology. This quantitative measure allows us to discriminate between components by their importance from a diagnostic point of view. Components with larger DIF are checked first. This assures a reduced number of system checks while fixing the system:

$$DIF_i = P(i|S) \tag{13}$$

where i is a component in system S.

Suppose the system has failed at the mission time 1000 hours, we enter the evidence that TWCS has failed i.e. $P(S=state1)=1$ and calculate DIF using the jointree algorithm.

(3) SI

Sensitivity analysis allows the designer to quantify the importance of each of the system's components and the impact the improvement of component reliability will have on the overall system reliability. Here we show how one can perform sensitivity through the usage of SI [10]. SI of the i^{th} basic event is defined as:

$$\begin{aligned} \alpha_{SI,i} &= \frac{\gamma_i}{\gamma_{\max}} \qquad i=1,2,\cdots,m \\ \gamma_i &= 1-\frac{P(S|\bar{i})}{P(S)} \\ \gamma_{\max} &= \max\{\gamma_1,\gamma_2,\cdots\gamma_m\} \end{aligned} \tag{14}$$

where $P(S)$ is the probability of the top event failure; $P(S|\bar{i})$ is the probability that the top event has occurred given the basic event i has not occurred.

5. Diagnosis strategy based on MADM

MADM models try to answer the question of 'what is the best alternative?' given a set of selection attributes and a set of alternatives. Generally there are three independent steps in MADM models to obtain the ranking of alternatives [23]: (1) Determine the relevant attribute and alternatives. (2) Attach numerical measures to the relative importance of the attribute and to the impacts of the alternatives on these attribute. (3) Calculation procedures to determine a ranking score of each alternative. Technique for Order Preference by Similarity to Ideal Solution (TOPSIS) is one of the known classical methods to solve MADM problem, developed by Hwang and Yoon [5]. It bases on the concept that the chosen alternative should have the shortest

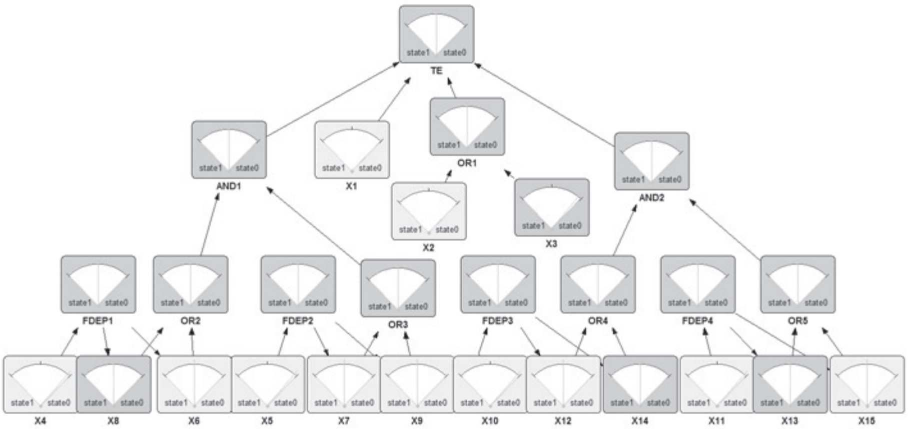

Fig. 8. The equivalent BN of TWCS

distance from the positive ideal solution (PIS) and the farthest from the negative ideal solution (NIS). In the process of TOPSIS, the performance ratings and the weights of the attributes are usually given as crisp values. Under many conditions, crisp data are not sufficient to model real-life situations. Since human opinions are often vague and cannot estimate his performance with an exact numerical value. A more realistic approach may be to use linguistic assessments instead of numerical values, that is, to suppose that the ratings of the attributes are assessed by means of linguistic variables. In this paper, we treat the optimal diagnostic sequence problem as a MADM problem and propose an improved TOPSIS to solve the MADM problem.

5.1. Constructing diagnostic decision table for TWCS

DIF enables us to discriminate between components by their importance from a diagnostic point of view. SI allows the designer to quantify the importance of each of the system's components and the impact the improvement of component reliability will have on the overall system reliability. So we treat DIF and SI as attribute $v1$ and $v2$ respectively. Owing to the different complexity of components their test costs are different. A balance should be taken into account between the DIF and test costs. Therefore, we introduce a new measure of importance called HIV, which allows us to optimize the cost of diagnosis. This measure is simply the DIF per unit cost. HIV appears in the following equation (15):

$$HIV_i = DIF_i / T_i \tag{15}$$

where DIF_i is the DIF of the component i; T_i is the test cost of the component i.

Test costs of the components are usually very difficult to express as crisp values because of uncertainty. So we introduce fuzzy linguistic expression to assess the test costs of components. Table 5 and 6 show the evaluation standards of the test costs and components' test costs for TWCS, respectively. HIV has an important effect on the diagnostic sequence and is treated as attribute $v3$. Table 7 shows the diagnostic decision table for TWCS.

Table 5. Evaluation standards of the test costs

Linguistic expression for test costs	Fuzzy numbers
Very High	(0.7, 0.9, 1)
High	(0.5, 0.7, 0.9)
Moderate	(0.3, 0.5, 0.7)
Low	(0.1, 0.3, 0.5)
Very Low	(0.1, 0.2, 0.3)

5.2. Normalizing diagnostic decision table

Different attributes usually have different values and dimensions, which are not always directly comparable, so we should normalize the diagnostic decision table [21]. For the quantitative data, we normalize them with the following equation:

$$b_{ij} = \frac{a_{ij}}{\sqrt{\sum_{i=1}^{n} a_{ij}^2}}, 1 \le i \le 15, 1 \le j \le 3 \tag{16}$$

where a_{ij} is the j^{th} attribute value of the i^{th} component.

For the fuzzy numbers, we normalize them with the following equation:

$$b_{ij}^l = \frac{a_{ij}^l}{\sqrt{\sum_{i=1}^{n} \left\| \tilde{a}_{ij} \right\|^2}}, b_{ij}^m = \frac{a_{ij}^m}{\sqrt{\sum_{i=1}^{n} \left\| \tilde{a}_{ij} \right\|^2}}, b_{ij}^r = \frac{a_{ij}^r}{\sqrt{\sum_{i=1}^{n} \left\| \tilde{a}_{ij} \right\|^2}} \tag{17}$$

Table 6. Components' test costs for TWCS

Components	test costs
X1	High
X2	Moderate
X3	Very High
X4,X5	Very Low
X6,X7	Low
X8,X9	Low
X10,X11	Very Low
X12,X13	Low
X14,X15	Low

Table 7. The diagnostic decision table for TWCS

Components	DIF	SI	HIV
X1	0.0048	0.0083	{0.0096,0.0069,0.0054}
X2	0.0637	0.1210	{0.2123,0.1274,0.0910}
X3	0.5050	1.0000	{0.7214,0.5611,0.5050}
X4	0.0906	0.1090	{0.9060,0.4530,0.3020}
X5	0.0906	0.1090	{0.9060,0.4530,0.3020}
X6	0.2390	0.3110	{2.3900,0.7967,0.4780}
X7	0.2390	0.3110	{2.3900,0.7967,0.4780}
X8	0.2170	0.2790	{2.1700,0.7233,0.4340}
X9	0.2170	0.2790	{2.1700,0.7233,0.4340}
X10	0.0727	0.0843	{0.7270,0.3635,0.2423}
X11	0.0727	0.0843	{0.7270,0.3635,0.2423}
X12	0.2070	0.2570	{2.0700,0.6900,0.4140}
X13	0.2070	0.2570	{2.0700,0.6900,0.4140}
X14	0.1850	0.2260	{1.8500,0.6167,0.3700}
X15	0.1850	0.2260	{1.8500,0.6167,0.3700}

where $\tilde{a}_{ij} = \left\{a_{ij}^l, a_{ij}^m, a_{ij}^r\right\}, \tilde{b}_{ij} = \left\{b_{ij}^l, b_{ij}^m, b_{ij}^r\right\}$; $\left\|\tilde{a}_{ij}\right\|$ is the module of the triangular fuzzy number $\tilde{a}_{ij}$:

$$\left\|\tilde{a}_{ij}\right\| = \sqrt{\frac{1}{3}\left[\left(a_{ij}^l\right)^2 + \left(a_{ij}^m\right)^2 + \left(a_{ij}^r\right)^2\right]} \tag{18}$$

We can obtain the normalized diagnostic decision table shown in Table 8 for TWCS using equation (16) ~ (18). Considering the same importance of each attribute, we can construct the weighted normalized diagnostic decision table shown in Table 9.

5.3. Determining the optimal diagnosis sequence

Attributes can be divided into two groups: beneficial attributes where higher values are preferable and non-beneficial attributes where lower value is preferable. There are three attributes in diagnostic decision table and they belong to the beneficial attributes. When the attributer a_{ij} is a beneficial attribute, the positive and negative ideal solutions are calculated as:

$$\tilde{X}_j^+ = \left\{\tilde{r}_1^+, \tilde{r}_2^+, \cdots, \tilde{r}_k^+\right\} = \left\{\max_i r_{ij}^l, \max_i r_{ij}^m, \max_i r_{ij}^r\right\} \tag{19}$$

$$\tilde{X}_j^- = \left\{\tilde{r}_1^-, \tilde{r}_2^-, \cdots, \tilde{r}_k^-\right\} = \left\{\min_i r_{ij}^l, \min_i r_{ij}^m, \min_i r_{ij}^r\right\} \tag{20}$$

where $\tilde{r}_j^+$ is the maximal value of the j^{th} attribute and $\tilde{r}_j^-$ is the minimal value of the j^{th} attribute

When the attributer a_{ij} is a non-beneficial attribute, the positive and negative ideal solutions are calculated as:

$$\tilde{X}_j^+ = \left\{\min_i r_{ij}^l, \min_i r_{ij}^m, \min_i r_{ij}^r\right\} \tag{21}$$

$$\tilde{X}_j^- = \left\{\max_i r_{ij}^l, \max_i r_{ij}^m, \max_i r_{ij}^r\right\} \tag{22}$$

The distance of each alternative from $\tilde{X}_j^+$ and $\tilde{X}_j^-$ can be currently calculated as:

$$D_i^+ = \sqrt{\sum_{j=1}^{k}\left|\tilde{r}_{ij} - \tilde{r}_j^+\right|^2} \tag{23}$$

$$D_i^- = \sqrt{\sum_{j=1}^{k}\left|\tilde{r}_{ij} - \tilde{r}_j^-\right|^2} \tag{24}$$

A closeness coefficient is defined to determine the ranking order of all alternatives once the D_i^+ and D_i^+ of each alternative has been calculated. The closeness coefficient of each alternative is calculated as:

$$C_i = D_i^- \Big/ \left(D_i^+ + D_i^-\right) \tag{25}$$

Table 10 shows the distance of each alternative from the positive and negative ideal solutions together with the corresponding closeness coefficient. Obviously, an alternative comes closer to the PIS and farther from NIS as C_i approaches to 1. Therefore, we can determine the ranking order of all alternatives and choose the best one from among a set of feasible alternatives. According to Table 10, we can obtain the optimal diagnostic ranking order of TWCS: X3, X6(X7), X8(X9), X12(X13), X14(X15), X4(X5), X10(X11), X2, X1, which considers the DIF, SI and HIV comprehensively.

Table 8. The normalized diagnostic decision table

Components	DIF	SI	HIV
X1	0.0060	0.0065	{0.0024,0.0017,0.0014}
X2	0.0791	0.0946	{0.0539,0.0323,0.0231}
X3	0.6270	0.7818	{0.1831,0.1424,0.1282}
X4	0.1125	0.0852	{0.2300,0.1150,0.0767}
X5	0.1125	0.0852	{0.2300,0.1150,0.0767}
X6	0.2967	0.2431	{0.6066,0.2022,0.1213}
X7	0.2967	0.2431	{0.6066,0.2022,0.1213}
X8	0.2694	0.2181	{0.5508,0.1836,0.1102}
X9	0.2694	0.2181	{0.5508,0.1836,0.1102}
X10	0.0903	0.0659	{0.1845,0.0923,0.0615}
X11	0.0903	0.0659	{0.1845,0.0923,0.0615}
X12	0.2570	0.2009	{0.5254,0.1751,0.1051}
X13	0.2570	0.2009	{0.5254,0.1751,0.1051}
X14	0.2297	0.1767	{0.4696,0.1565,0.0939}
X15	0.2297	0.1767	{0.4696,0.1565,0.0939}

Table 9. The weighted normalized diagnostic decision table

Components	DIF	SI	HIV
X1	0.0020	0.0022	{0.0008,0.0006,0.0005}
X2	0.0264	0.0315	{0.0180,0.0108,0.0077}
X3	0.2090	0.2606	{0.0610,0.0475,0.0427}
X4	0.0375	0.0284	{0.0767,0.0383,0.0256}
X5	0.0375	0.0284	{0.0767,0.0383,0.0256}
X6	0.0989	0.0810	{0.2022,0.0674,0.0404}
X7	0.0989	0.0810	{0.2022,0.0674,0.0404}
X8	0.0898	0.0727	{0.1836,0.0612,0.0367}
X9	0.0898	0.0727	{0.1836,0.0612,0.0367}
X10	0.0301	0.0220	{0.0615,0.0308,0.0205}
X11	0.0301	0.0220	{0.0615,0.0308,0.0205}
X12	0.0857	0.0670	{0.1751,0.0584,0.0350}
X13	0.0857	0.0670	{0.1751,0.0584,0.0350}
X14	0.0766	0.0589	{0.1565,0.0522,0.0313}
X15	0.0766	0.0589	{0.1565,0.0522,0.0313}

6. Conclusion

In this paper, we have discussed the use of dynamic fault tree, fuzzy sets theory and MADM to diagnose the complex systems fault. Specifically, it has emphasized three important issues that arise in engineering diagnostic applications, namely the challenges of insufficient fault data, uncertainty and failure dependency of components. In terms of the challenge of insufficient fault data and uncertainty, we

Table 10. The corresponding closeness coefficient of components

Components	D+	D-	C
X1	0.3539	0.0000	0.0000
X2	0.3140	0.0401	0.0032
X3	0.0823	0.3349	0.8027
X4	0.2983	0.0675	0.1845
X5	0.2983	0.0675	0.1845
X6	0.2106	0.1765	0.4559
X7	0.2106	0.1765	0.4559
X8	0.2228	0.1596	0.4174
X9	0.2228	0.1596	0.4174
X10	0.3101	0.0534	0.1468
X11	0.3101	0.0534	0.1468
X12	0.2302	0.1511	0.3963
X13	0.2302	0.1511	0.3963
X14	0.2430	0.1344	0.3561
X15	0.2430	0.1344	0.3561

adopt expert elicitation and fuzzy sets theory to evaluate the failure rates of the basic events for TWCS; In terms of the challenge of failure dependency, we use a dynamic fault tree to model the dynamic behaviours of system failure mechanisms. Furthermore, we calculate some reliability parameters used for fault diagnosis using BN and algebraic technique in order to avoid the aforementioned disadvantages. In addition, we treat the optimal diagnostic sequence problem as a MADM problem, propose an improved TOPSIS to solve the MADM problem and obtain the optimal diagnostic ranking order of TWCS. The proposed method makes full use of the dynamic fault tree for modelling, fuzzy sets theory for handling uncertainty and MADM for the best fault search scheme, which is especially suitable for fault diagnosis of the complex systems.

In the future work, we will focus on how to determine the attributes weights and take full advantage of the previous fault diagnosis results to dynamically update the diagnostic decision table, thereby optimizing the diagnosis efficiency.

Acknowledgement

This work was supported by the National Natural Science Foundation of China (71461021), the Natural Science Foundation of Jiangxi Province (20142BAB207022), the Science and Technology Foundation of Department of Education in Jiangxi Province (GJJ14166) and the Postdoctoral Science Foundation of Jiangxi Province (2014KY36).

References

1. Assaf T, Dugan, J.B. Design for diagnosis using a diagnostic evaluation measure. IEEE Instrumentation and Measurement Magazine 2006; (4):37-43, http://dx.doi.org/10.1109/MIM.2006.1664040.
2. Assaf, T., Dugan, J.B., Diagnosis based on reliability analysis using monitors and sensors. Reliability Engineering & System Safety 2008; 93(4): 509-521, http://dx.doi.org/10.1016/j.ress.2006.10.024.
3. Bobbio A., Portinale L., Minichino M. Improving the analysis of dependable systems by mapping fault trees into Bayesian networks. Reliability Engineering and System Safety 2001; 71(3): 249-260; http://dx.doi.org/10.1016/S0951-8320(00)00077-6.
4. Boudali H. Dugan J.B. A discrete-time Bayesian network reliability modelling and analysis framework. Reliability Engineering and System Safety 2005; 87(3): 337-349, http://dx.doi.org/10.1016/j.ress.2004.06.004.
5. Hwang C.L., Yoon K. Multiple Attributes Decision Making Methods and Applications. Berlin, Heidelberg: Springer, 1981, http://dx.doi.org/10.1007/978-3-642-48318-9.
6. Huang, D, Chen, T and Wang, M.J.J. A fuzzy set approach for event tree analysis. Fuzzy Sets and Systems 2001; 118(1):153-165, http://dx.doi.org/10.1016/S0165-0114(98)00288-7.
7. Huang HongZhong, Li Yanfeng, Sun Jian, Yang Yuanjian. Fuzzy Dynamic Fault Tree Analysis for the Solar Array Drive Assembly. Journal of Mechanical Engineering 2013; 49 (19): 70-76, http://dx.doi.org/10.3901/JME.2013.19.070.
8. Jafarian E, Rezvani M. A. Application of fuzzy fault tree analysis for evaluation of railway safety risks. Proceedings of the Institution of Mechanical Engineers, Part F: Journal of Rail and Rapid Transit 2012; 226: 14-25, http://dx.doi.org/10.1177/0954409711403678.
9. Khakzad N, Khan F, Amyotte P. Risk-based design of process systems using discrete-time Bayesian networks. Reliability Engineering and System Safety 2013; 109: 5-17, http://dx.doi.org/10.1016/j.ress.2012.07.009.
10. Lu Ying, Li Qiming, and Zhou Zhipeng. Safety risk prediction of subway operation based on fuzzy Bayesian network. Journal of Southeast University (Natural science edition) 2010; 40(5): 1110-1114.
11. Meshkat L, Dugan J B and Andrews JD. Dependability analysis of systems with on-demand and active failure modes using dynamic fault trees. IEEE Transactions on Reliability 2002; 51(2): 240-251, http://dx.doi.org/10.1109/TR.2002.1011531.
12. Manjit Verma, Amit Kumar. Fuzzy fault tree approach for analysing the fuzzy reliability of a gas power plant. International Journal of Reliability and Safety 2012; 6(4): 354-370, http://dx.doi.org/10.1504/IJRS.2012.049598.
13. Mhalla A, Collart Dutilleul S, Craye E. Estimation of failure probability of milk manufacturing unit by fuzzy fault tree analysis, Journal of Intelligent and Fuzzy Systems 2014; 26(2): 741-750.
14. Onisawa T. An approach to human reliability in man-machine systems using error possibility. Fuzzy Sets and System 1988; 27(2): 87-103, http://dx.doi.org/10.1016/0165-0114(88)90140-6.
15. Przytula K.W., Milford R. An efficient framework for the conversion of fault trees to diagnostic Bayesian network models. In Proceedings of IEEE Aerospace Conference 2006: 1-14, http://dx.doi.org/10.1109/AERO.2006.1656103.
16. Purba J H, Lu J, Zhang G, et al. A fuzzy reliability assessment of basic events of fault trees through qualitative data processing. Fuzzy Sets and Systems 2014; 243: 50-69, http://dx.doi.org/10.1016/j.fss.2013.06.009.

17. Rongxing Duan, Guochun Wan, Decun Dong. Intelligent Fault Diagnosis Method Based on Dynamic Fault Tree Analysis. Journal of Computational Information Systems 2010; 6(3): 949-957.
18. Rongxing Duan, Huilin Zhou, Diagnosis strategy for micro-computer controlled straight electro-pneumatic braking system using fuzzy set and dynamic fault tree. Eksploatacja i Niezawodnosc - Maintenance and Reliability 2014; 16 (2): 217–223.
19. Shaoxu, Ni, Yufang, Zhang, Xiaofeng Liang. Intelligent Fault Diagnosis Method Based on Fault Tree. Journal of Shanghai Jiaotong University 2008; 42(8):1372-1386.
20. Tetsushi Y and Yanagi S. Dynamic fault tree analysis using bayesian networks and sequence probabilities. IEICE Transactions on Fundamentals of Electronics, Communications and Computer Sciences 2013; 96(5): 953-962.
21. Yao C., Chen D., Feng Z. Dynamic Group Decision-making Fault Diagnosis Method Based on Bayesian Network and TOPSIS. China Mechanical Engineering 2013; 24 (16): 2235-2241.
22. Y.F. Li, H.Z. Huang, Y. Liu, N.C. Xiao, H.Q. Li. A new fault tree analysis method: fuzzy dynamic fault tree analysis. Eksploatacja i Niezawodnosc – Maintenance and Reliability 2012; 14 (3): 208-214.
23. Yusuf Tansel İç. An experimental design approach using TOPSIS method for the selection of computer-integrated manufacturing technologies. Robotics and Computer-Integrated Manufacturing 2012; 28(2): 245-256, http://dx.doi.org/10.1016/j.rcim.2011.09.005.

Rongxing DUAN
Huilin ZHOU
Jinghui FAN
School of Information Engineering
Nanchang University
Xuefu Rd., 999 Jiangxi, China
E-mail: duanrongxing@ncu.edu.cn,
zhouhuilin@ncu.edu.cn, Jinghuifan@ncu.edu.cn

Article citation info:
KAMIŃSKI Z, KULIKOWSKI K. Determination of the functional and service characteristics of the pneumatic system of an agricultural tractor with mechanical brakes using simulation methods. Eksploatacja i Niezawodnosc – Maintenance and Reliability 2015; 17 (3): 355–364, http://dx.doi.org/10.17531/ein.2015.3.5.

Zbigniew KAMIŃSKI
Krzysztof KULIKOWSKI

DETERMINATION OF THE FUNCTIONAL AND SERVICE CHARACTERISTICS OF THE PNEUMATIC SYSTEM OF AN AGRICULTURAL TRACTOR WITH MECHANICAL BRAKES USING SIMULATION METHODS

WYZNACZANIE METODAMI SYMULACYJNYMI WŁAŚCIWOŚCI FUNKCJONALNO-UŻYTKOWYCH PNEUMATYCZNEJ INSTALACJI CIĄGNIKA ROLNICZEGO Z HAMULCAMI MECHANICZNYMI*

Agricultural tractors are provided with air braking systems to control and operate braking systems of towed agricultural vehicles. Functional and operational characteristics of the tractor pneumatic system have a significant influence on the synchrony and operate speed of tractor-trailer unit braking system. This paper presents a mathematical model to predict the functional and operational characteristics of tractor pneumatic system by using a digital simulation. Modeling of the energy supplying device (compressor, governor, air reservoir) and modeling of the control device with trailer control valve mechanically connected with the tractor brakes is described. Results of statistical Kolmogorov-Smirnov test used to assess the conformity of experimental and simulated pressure transients during testing the compressor capacity and the response time of control circuit of Pronar 320AM tractor confirmed the computer model developed in Matlab-Simulink. The computer model can be used as a tool to assess the functional and operational characteristics of tractor pneumatic system within the designing process and as a subsystem to analyze transient processes in a pneumatic braking systems of the tractor-trailer units by using simulation methods. Mathematical models of selected components can be also used in modeling other pneumatic braking systems of commercial vehicles.

Keywords: *farm tractor, pneumatics, braking system, energy-supplying device, trailer control valve, modeling, simulation.*

Ciągniki rolnicze są wyposażone w powietrzne instalacje hamulcowe do sterowania i napędu układów hamulcowych pojazdów ciągnionych. Właściwości funkcjonalno-użytkowe instalacji pneumatycznej ciągnika mają istotny wpływ na synchronię i szybkość działania układu hamulcowego zespołu ciągnik-przyczepa. W niniejszej pracy przedstawiono model matematyczny do prognozowania właściwości funkcjonalno-użytkowych układu pneumatycznego ciągnika metodą symulacji cyfrowej. Opisano modelowanie zespołu zasilającego (sprężarka, regulator, zbiornik powietrza) i modelowanie zespołu sterującego z zaworem sterującym hamulcami przyczepy połączonym mechanicznie z hamulcami ciągnika. Wyniki testu statystycznego Kołmogorowa-Smirnowa oceny zgodności doświadczalnych i symulowanych przebiegów czasowych ciśnienia podczas badania wydatku sprężarki i czasu reakcji obwodu sterującego ciągnika Pronar 320AM potwierdziły adekwatność opracowanego w Matlabie-Simulinku modelu komputerowego. Model komputerowy może być wykorzystany jako narzędzie do oceny właściwości eksploatacyjno-użytkowych instalacji pneumatycznej ciągnika w procesie projektowania oraz jako podsystem do analizy metodami symulacyjnymi procesów przejściowych w pneumatycznych układach hamulcowych zespołów ciągnik-przyczepa. Modele matematyczne wybranych komponentów instalacji mogą być również wykorzystane w modelowaniu innych pneumatycznych układów hamulcowych pojazdów użytkowych.

Słowa kluczowe: *ciągnik rolniczy, pneumatyka, układ hamulcowy, zespół zasilający, zawór sterujący hamulcami przyczepy, modelowanie, symulacja.*

1. Introduction

In agricultural tractors, a variety of friction braking mechanisms are used, including band brakes, drum brakes, and dry or wet multi-disc brakes [5]. To transfer the energy needed to run the service brakes of a tractor, a mechanical, hydraulic or an air drive is used. Selection of the drive type and the energy source depends on the design and weight of the tractor. In low- and medium-power tractors, manually operated hydraulic brake systems are used, which are relatively inexpensive and simple. Because of their cost, mechanically actuated brakes are still attractive in low-power tractors.

Agricultural tractors with mechanical or hydraulic brakes are equipped with a pneumatic system designed to run the air braking systems of towed trailers and agricultural machines. So called combined systems are currently used [32], which have the capability to operate with the single- and dual-line braking systems of towed vehicles.

A typical combined pneumatic system of a farm tractor consists of two major parts: an energy supply unit and a control device. The function of the energy supply unit is to compress and purify air and to maintain the adequate pressure in the tractor and trailer reservoirs in order to ensure the required trailer braking performance. The role of the control device is to provide the follow-up control of the single- or dual-line braking system of a towed vehicle in a manner that enables the synchronous braking of the both vehicles. Control devices differ mainly in the type of the trailer brake control valve, which can be actuated either mechanically, hydraulically or pneumatically, de-

(*) Tekst artykułu w polskiej wersji językowej dostępny w elektronicznym wydaniu kwartalnika na stronie ***www.ein.org.pl***

pending on the tractor brakes [32]. A schematic diagram of a tractor's pneumatic system with a mechanically actuated brake valve is shown in Figure 1.

Because of the road safety, agricultural vehicles braking systems must meet several specific requirements [8, 9] for braking performance, high operation speed during rapid braking (the response time should not exceed 0.6 s) and the compatibility of the tractor and towed vehicle braking systems [27] (the synchrony of operation of individual circuits). Research by Scarlett [28] reveals that 90% tested trailers failed to achieve the legally required braking efficiency level. The incompatibility of the tractor and trailer brake systems resulting in jack-knifing or skidding during braking was the cause of approximately 9.7% of the fatalities in the UK in the period 1999-2004 [7].

The functional and service characteristics of brake systems, including dynamic characteristics that determine the speed and synchrony of action, may be predicted already at an early stage of design using digital simulation methods. This requires the development of mathematical and computer models for individual devices of the braking system. In the process of modelling, the pneumatic elements are substituted with idealized elements in the form of lumped volumes and resistances [18, 20]. Due to the discrete nature and complexity of braking systems, even components with parameters distributed in a continuous manner, such as pneumatic lines, are substituted with models of lumped parameters in mathematical modelling [14]. Discretization in space yields a system of ordinary differential equations, which can be solved using specialized software designed for simulation of complex engineering systems, including object-oriented software [34]. The advantage of model-based design is the increased the speed and efficiency of testing new solutions, the possibility of comparing them against the established requirements, and the earlier detection of any errors resulting from malfunctioning or incorrect design assumptions, as compared to the construction of physical prototypes.

The main difficulty in modelling the agricultural tractor pneumatic system is the lack of appropriate models for basic components in the literature, including air compressors and brake valves. Mathematical models for estimating the compressor performance and the thermodynamic behaviour of compressors under different working conditions [2, 10, 30] are too complex for modelling of the dynamics of multi-circuit pneumatic and hydraulic braking systems. In turn, most of the models known from the literature concerns the typical brake valves used in the air braking systems of commercial vehicles [11, 23, 29] and trailers [12, 13, 15, 21, 24].

In this paper, the functional and structural mathematical model of the pneumatic system of a small-power agricultural tractor is presented. Modelling of the trailer brake control valve serving for controlling dual-line trailer brake systems in conjunction with mechanical foot brakes of tractors is described in detail. The mathematical and computer model of this valve considers a number of phenomena, such as heat exchange, the inertia of movable elements, and friction, which are generally omitted already at the stage of physical creation or at the stage of running the computer model for digital simulation [11, 23, 29]. Whereas, in the case of modelling the energy supply unit described in [16], the most important final model equations are only given. A computer program implemented in Matlab-Simulink was used to estimate selected functional and service characteristics, including the assessment of supply unit compressor performance and the control device response time in accordance to the requirements for brake systems. The simulation results were compared with the results of experimental tests carried out under the same conditions. The developed model can be used in the process of designing a tractor's braking system at the stage of dynamic calculations. It can also be utilized as a subsystem in the simulation of transient processes in the pneumatic braking system of a tractor-trailer unit.

2. Experimental setup for testing the tractor pneumatic braking system

A simplified schematic diagram of the normal-pressure combined pneumatic braking system of a Pronar 320AM agricultural tractor [26] equipped with a mechanical brakes drive is shown in Figure 1. The energy supply unit includes filter 1, air compressor 2, unload valve (governor) 3, and compressed air reservoir 4. In high-pressure systems with a compressor discharge pressure of up to 18 bar, a pressure limiting valve (pressure reducer) is additionally installed downstream the air reservoir. Compressed air is also fed through a 4-way cross fitting to the control device, which includes proportional brake valve 11 and inverse brake valve brake 7. Trailer control valve 11 is connected, via mechanism 12, with the tractor brake pedal. The driver's foot pressure on the treadle, transferred to valve 11 by a linkage system, causes the opening of the valve and a pressure increase in the line with coupling head 10 controlling the dual-line trailer braking system. The trailer braking system supply line is connected to coupling head 9. For controlling the single-line trailer braking system, inversion valve 7 is used, which, on the increase of pressure in control port 4, causes a pressure drop in the supply and control line with coupling head 8.

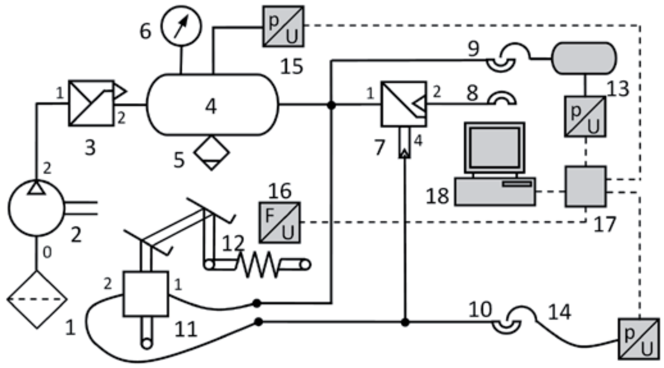

Fig. 1. Schematic diagram of the normal-pressure combined single- and dual-line air braking system of a Pronar MTZ 320AM farm tractor with the experimental setup for testing the control line response time: 1 – filter, 2 – 601.23.944 compressor by FOS Polmo Łódź , 3 – 51 10 018 unloader valve by Visteon, 4 – 10 dm³ air reservoir, 5 – drain valve, 6 – single pressure gauge, 7 – inversion trailer control valve, 8 – "single-line" coupling head (black), 9 – "supply" coupling head (red), 10 – "brake" coupling head (yellow), 11 – 41 13 014 trailer brake control valve by Visteon (the primary section used), 12 – valve applying mechanism, 13 – 0,385 dm³ air vessel, 14 – 2.5 m-long 13 mm-internal diameter pipe, 15 – pressure transducer, 16 – pedal force transducer, 17 – input/output adapter, 18 – computer with a measuring card

In Figure 1, the experimental setup, in the version for testing the response time of the tractor dual-line pneumatic system control device, is distinguished by the grey background. Changes in the force on the brake pedal and in pressure in selected locations of the pneumatic system are recorded by a measuring system consisting of voltage transducers 15 and 16, adapter 17, and a Senga MC1212 measuring card (12 bit resolution) mounted on computer 18 for data collection during tests being run. Tensometric brake pedal force sensor 16, type CL 23, with an industrial amplifier, type CL10D, manufactured by ZEPWN (with a measuring range of 0÷1 kN; an output signal range of 0÷10 V; and an accuracy class of 0.1%) is used for measuring the force on the brake pedal. The pressure is measured with industrial pressure transducer 10, type Danfoss MBS 32 (with a pressure range of 0÷10 bar; an output range of 0÷10 V; and an accuracy class of 0.3%). The transducers are voltage supplied from input/output adapter 17. Output voltage signals from the force-pressure transducers are acquired from input/output adapter 17 using the measuring card and then directly converted into force and pressure data with the use of integrated software installed on the computer. The maximum rpm of engine are measured with digital tachometer DMT-21 (with a measuring range: 0 – 9999 rpm, an accuracy class of 0.2). Sample runs of registered changes of force and pressure during measuring a response time in steering unit of Pronar 320AM tractor are shown in Figure 5 and 6.

3. Modelling of the mechanically actuated trailer brake control valve

In the control circuit of the Pronar 320AM tractor's pneumatic system, the primary section of the Visteon 41 13 014 main foot brake valve [31] was used as trailer control valve 11 (Figure 1). This valve, normally used in dual-circuit air brake systems, is coupled with a linkage system operated by the treadle in the cabin. A schematic diagram of the structure of the valve, for the modelling purposes reduced to a single circuit, is given in Figure 2.

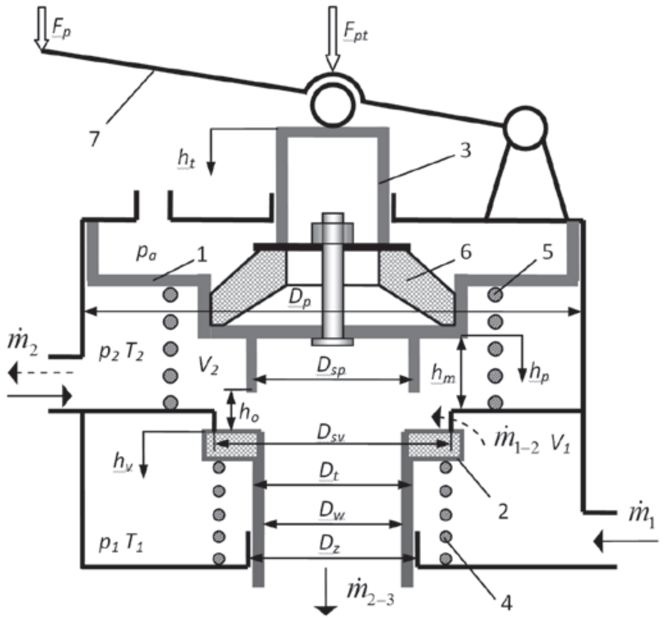

Fig. 2. A mechanically actuated trailer brake control valve: 1 – control piston, 2 – inlet head, 3 – tappet, 4 – head spring, 5 – piston return spring, 6 – rubber spring, 7 – actuating linkage

The air mass flux $\dot{m}_1$ flows into a fixed-volume inlet chamber V_1 from the supply circuit. During braking, control piston 1, moving downward by the action of force F_p on the brake pedal, transferred via linkage 7 to tappet 3, opens inlet head 2. Compressed air from the inlet chamber flows into a variable-capacity outlet chamber V_2 as a mass flux $\dot{m}_{1-2}$. The flux $\dot{m}_2$ flowing from the outlet chamber V_2 is routed to the control circuit of the trailer braking system, resulting in activation of the trailer brakes. During the brake release caused by the decrease in the brake pedal force, the pressure in the chamber V_2, in combination with the force of spring 5, raises piston 1 again. By the action of return spring 4, poppet valve 2 closes (cutting off the inlet chamber from the outlet chamber), and the passage between the seat in piston 1 and head 2 opens. The outlet chamber V_2 is vented. The compressed air from the control line returns to the outlet chamber as the mass flux $\dot{m}_2$ (flow reversal), and then flows out to the atmosphere as the mass flux $\dot{m}_{2-3}$. The venting of the outlet chamber and the control line causes a drop in the trailer brake force.

When creating the current mathematical model of the trailer control valve, a number of simplifying assumptions were made [15], including the following:

- Compressed air was regarded as a thermodynamically ideal gas (i.e. obeying the Clapeyron law), while being viscous and compressible.
- The valve adjusting element, irrespective of its design, was regarded as a local resistance (nozzle), whose effective flow field (conductance) depended on the head lift.
- The airflow through the adjusting element was considered one-dimensional and adiabatic.
- The air properties were assumed to be uniform both in the individual valve chambers and in the entire cross-section of flow through the local resistance.
- In the valve opening phase, the force interaction between the head and the control piston was omitted, which means that both elements moved together as a single mass (one equation of motion).
- The air leakage in the valve chambers were neglected.
- The influence of the housing on the control piston in its end position was neglected; stopping of the piston was accomplished via the acceleration control logic (hard stopping).
- The heat exchange between the system's air and the environment took place by natural convection at a constant wall temperature which was equal to ambient temperature.

In accordance with the law of conservation of matter, the masse changes in the inlet chamber of volume V_1 (Figure 2) and the outlet chamber of volume V_2 are described by the equations:

$$\frac{dm_{V1}}{dt} = \dot{m}_1 - \dot{m}_{1-2} \tag{1}$$

$$\frac{dm_{V2}}{dt} = \dot{m}_{1-2} \mp \dot{m}_2 - \dot{m}_{2-3} \tag{2}$$

where: $\dot{m}_i$ – the mass flux (kg/s) flowing into (the sign +) or from (the sign –) a given chamber; the respective flux subscripts conform to the convention on denoting the braking valve chamber ports (the small numerals at the valve ports in Figure 2).

For the description of the air mass flux flow through the local pneumatic resistances, the Saint-Venant–Wantzel relationship [3] in the following generalized form was used:

$$\dot{m} = (\mu A_m)\frac{p_m}{\sqrt{RT_m}}\psi_{max}\psi(\sigma) \tag{3}$$

where: (μA_m) – conductance, i.e. the product of the discharge coefficient μ and the flow cross-section area A_m [m^2], p_m – pressure [Pa] upstream of the resistance, T_m – the air temperature [K] upstream of the resistance, R – gas constant for air, being equal to 288 [J/(kgK)], Ψ_{max} – maximum value of the Saint-Venant – Wantzel function for the critical pressure ratio σ^* (product of the pressures upstream and downstream of the resistance), which is given by:

$$\psi_{max} = \psi(\sigma^*) = \sqrt{\kappa\left(\frac{2}{\kappa+1}\right)^{\frac{\kappa+1}{\kappa-1}}} = 0.68473 \tag{4}$$

where : κ – adiabatic exponent, for air being equal to κ=1.4.
Instead of the dimensionless two-range Saint – Venant flow function $\Psi(\sigma)$ as given by:

$$\Psi(\sigma)=\begin{cases}1 & \text{for} \quad \sigma \le \sigma^* \\ \dfrac{1}{\Psi_{\max}}\sqrt{\dfrac{2\kappa}{\kappa-1}\left(\sigma^{\frac{2}{\kappa}}-\sigma^{\frac{\kappa+1}{\kappa}}\right)} & \text{for} \quad \sigma^* < \sigma \le 1\end{cases}$$

a single-range hyperbolic function [20, 22] was used, as being more convenient for numerical computation and yet sufficiently accurate:

$$\psi(\sigma)=b\frac{1-\sigma}{b-\sigma} \tag{5}$$

A constant parameter value of b=1.13, which is typical of the pneumatic elements used in the braking systems of vehicles, was assumed.

Using equation (3), the equations of mass fluxes flowing through the braking valve are obtained as:

$$\dot{m}_{1-2}=\mu_{12}A_{12}\frac{p_1}{\sqrt{RT_1}}\psi_{\max}\psi\left(\frac{p_2}{p_1}\right) \tag{6}$$

$$\dot{m}_{2-3}=\mu_{23}A_{23}\frac{p_2}{\sqrt{RT_2}}\psi_{\max}\psi\left(\frac{p_a}{p_2}\right) \tag{7}$$

The flow cross-section areas A_{12} (during braking) and A_{23} (during releasing) are dependent on the piston travel h_p and the distance h_v of head 2 from the valve seat and are given by:

$$A_{12}=\begin{cases}0 & \text{if} \quad h_v \le h_{vo} \\ \pi D_{sv}\left(h_v-h_{vo}\right) & \text{if} \quad h_{vo} < h_v \le h_{vm} \\ \dfrac{\pi\left(D_{svw}^2-D_{spz}^2\right)}{4} & \text{if} \quad h_v > h_{vm}\end{cases} \tag{8}$$

$$A_{23}=\begin{cases}0 & \text{if} \quad h_p \ge h_o-h_{po} \\ \pi D_{sp}\left(h_o-h_{po}-h_p\right) & \text{if} \quad h_{pm} \le h_p < h_o-h_{po} \\ \dfrac{\pi D_w^2}{4} & \text{if} \quad h_p < h_{pm}\end{cases} \tag{9}$$

where: D_{sv}, D_{svw} – stationary seat average diameter [m] and inner diameter [m], respectively; D_{spz} – moveable seat outer diameter [m] (in the piston); h_{vo}, h_{vm} – head 2 position [m] corresponding to the beginning of opening (allowing for plate seal deformation) and position [m] corresponding to attaining the maximum flow field value, respectively; D_{sp} – the average diameter [m] of the moveable seat, D_p, D_w – the outer diameter [m] and the inner diameter [m] respectively of the head sleeve, h_{po}, h_{pm} – piston position [mm] corresponding to the beginning of opening the passage to the atmosphere (allowing for plate seal deformation) and position [mm] in which the flow field attains the maximum value, respectively.

The following relationship exist between the displacement h_p of control piston 1and the displacement h_v of head 2:

$$h_v=\begin{cases}0 & h_p \le h_o \\ h_p-h_o & h_p > h_o\end{cases} \tag{10}$$

where: h_o – the maximum distance (clearance) [m] between head 2 and piston 1 in the upper extreme position.

The mechanical components of a brake valve can be considered as a dynamical system with two degrees of freedom. The equation of motion of tappet 3 and its associated elements being under the action of external forces, has the following form:

$$m_t\frac{d^2h_t}{dt^2}=F_{pt}-F_{st}+F_{ft} \tag{11}$$

where: m_t – the reduced mass [kg] of all drive elements from the brake pedal to the tappet; h_t – tappet displacement [m]; F_{st} – the action force [N] of rubber spring 6; F_{ft} – total friction force [N]; F_{pt} – force [N] applied to the tappet coming from the brake pedal force F_p, as calculated from the formula:

$$F_{pt}=F_p i_p \eta_p \tag{12}$$

where: i_p, η_p – the force ratio and efficiency ratio of the mechanical between the treadle and the tappet, respectively.

The positioning force F_{st} of rubber spring 6 depends on its deformation $\delta=h_t$-h_p, and can be described by the third-degree equation:

$$F_{st}=c_1\delta+c_2\delta^2+c_3\delta^3 \tag{13}$$

where: c_1, c_2, c_3 – coefficients determined from the approximation of the experimental curve $F_{st}(\delta)$.

A more complex relationship for F_{st} can be found in study [29]. Taking into account the preload spring force adjustment in the model, the initial condition $h_t(0)=h_{t0}\neq 0$ is taken, while the preload force may not lead to a loss of contact between piston 1 and the valve housing: $h_p(0)\approx 0$.

It is assumed that the total friction force has a constant component being dependent on the poppet speed:

$$F_{ft}=-\text{sgn}\left(\frac{dh_t}{dt}\right)\cdot\left(F_{ct}+k_{vt}\frac{dh_t}{dt}\right) \tag{14}$$

where: F_{ct} – fixed value friction force [N]; k_{vt} – viscous friction coefficient [Ns/m].

The equation of motion of control piston 1 (without the housing action force) has the following form:

$$m_z\frac{d^2h_p}{dt^2}=F_{p2a}+F_{st}+F_{sp}+F_v+F_{fp} \tag{15}$$

where: m_z – reduced mass [kg] of the elements moving together with piston 1; F_{p2a} – pressure force [N] acting on the piston; F_{st} – rubber spring 6 action force [N]; F_{sp} – piston return spring 5 force [N]; F_{fp} – force [N] of piston 1 friction against the housing; F_v – force [N] of head 2 pressure on piston 1.

The reduced mass of the elements moving together with the piston is:

$$m_z=\begin{cases}m_p+m_{sp}/4 & h_p \le h_o \\ m_p+m_v+\left(m_{sp}+m_{sv}\right)/4 & h_p > h_o\end{cases} \tag{16}$$

where: m_p – mass [kg] of control piston 1; m_v – mass [kg] of head 2 with the sleeve guide; m_{sv} – mass [kg] of spring 4 clamping head 2; m_{sp} – mass [kg] of return spring 5.

The force of pressure acting on the pistons is:

$$F_{p2a} = \frac{\pi D_p^2}{4} p_a - \frac{\pi D_{sp}^2}{4} p_a - \frac{\pi\left(D_p^2 - D_{sp}^2\right)}{4} p_2 = -\frac{\pi\left(D_p^2 - D_{sp}^2\right)}{4}\left(p_2 - p_a\right) \tag{17}$$

The force of return spring 5 pressure on piston 1 is calculated from the relationship:

$$F_{sp} = -\left(F_{spo} + c_p h_p\right) \tag{18}$$

where: F_{spo} – spring 5 preset force [N] for h_p=0 [N]; c_p – stiffness (N/m) of spring 5 [N/m].

When determining the relationship for the force F_v of head pressure on the piston, it was assumed that the poppet valve had an unladen design ($D_{sp} \approx D_z$), thus the relationship is:

$$F_v = \begin{cases} 0 & h_p \le h_o \\ -\left[F_{svo} + c_v\left(h_p - h_o\right)\right] - \left(p_1 - p_2\right)\dfrac{\pi\left(D_{sv}^2 - D_{sp}^2\right)}{4} - \operatorname{sgn}\left(\dfrac{dh_p}{dt}\right)\left[F_{cv} + k_{vv}\left(\dfrac{dh_p}{dt}\right)\right] & h_p > h_o \end{cases} \tag{19}$$

where: D_z – head sleeve guide diameter [m]; F_{cv} – head guide kinematic friction force [N]; k_v – viscous friction coefficient [Ns/m].

The force of static and kinetic friction of piston 1 against the housing is described using the Karnopp model [1] according to:

$$F_{fp}\left(\frac{dh_p}{dt}, F_e\right) = -\begin{cases} \operatorname{sgn}\left(F_e\right)\cdot \min\left(F_{sp}, \left|F_e\right|\right) & \text{while } \left|\dfrac{dh_p}{dt}\right| < \Delta v \\ \operatorname{sgn}\left(\dfrac{dh_p}{dt}\right)\cdot\left[F_{cp} + k_v\cdot\left(\left|\dfrac{dh_p}{dt}\right| - \Delta v\right)\right] & \text{while } \left|\dfrac{dh_p}{dt}\right| \ge \Delta v \end{cases} \tag{20}$$

The total static friction force F_{sp} and kinetic friction force F_{cp} of piston 1, as well as the kinetic friction force F_{cv} of the guide of head 2, are described by the relationships:

$$\begin{gathered} F_{sp} = \pi D_p\left(f_s + k_s\left|p_2 - p_a\right|\right) \\ F_{cp} = \pi D_p\left(f_c + k_c\left|p_2 - p_a\right|\right) \\ F_{cv} = \pi D_z\left(f_c + k_c\left|p_1 - p_a\right|\right) \end{gathered} \tag{21}$$

where: f_s, f_c – static friction force [N/m] and kinetic friction force [N/m], respectively, per unit piston perimeter, independent of the differential pressure across the piston; k_s, k_c – proportionality factors [m].

Based on the energy conservation law for open systems [3], excluding the kinetic and potential energies, equations for the change in the internal energy of air in the control volumes V_1 and V_2 of the chamber are obtained in the following form:

$$\frac{dU_1}{dt} = \dot{Q}_1 + \dot{H}_1 - \dot{H}_{1-2} \tag{22}$$

$$\frac{dU_2}{dt} = \dot{Q}_2 + \dot{W}_2 + \dot{H}_{1-2} \mp \dot{H}_2 - \dot{H}_{2-3} \tag{23}$$

where: U_i – internal energy [J] of air in the i-th chamber; $\dot{H}_i$ – enthalpy of the fluxes [W] flowing to or from a particular chamber; $\dot{W}_i$ – rate of external work done by air in the *i*-th chamber [W]; $\dot{Q}_i$ – heat flux [W] exchanged between the *i*-th chamber air and the environment:

$$\begin{aligned} &U_i = m_{Vi}\cdot c_v T_i \qquad \dot{H}_i = \dot{m}_i c_p T_{mi} \\ &\dot{W}_i = -p_i\cdot\dot{V}_i \qquad \dot{Q}_i = \alpha_i\cdot A_w\left(T_w - T_i\right) \end{aligned} \tag{24}$$

where: c_v, c_p – specific heat capacity of the gas at a constant volume and pressure: c_v=717 J/(kgK), c_p=1005 J/(kgK); T_i – temperature [K] of the *i*-th chamber air; m_{Vi} – mass of the *i*-th chamber air [kg]; T_{mi} – flux temperature [K] (for the flux flowing out from the chamber, $T_{mi} = T_i$); T_w – valve housing wall temperature [K] equal to ambient temperature; α_i – heat transfer coefficient [W/(m^{2}K)] of the *i*-th chamber; A_i – internal surface area [m^2] of the *i*-th chamber, being dependent on the piston displacement, similarly as the volume V_i [m^3].

After differentiation of the internal energy:

$$\frac{dU_i}{dt} = c_v\left(\frac{dm_{Vi}}{dt}T_i + m_{Vi}\frac{dT_i}{dt}\right) \tag{25}$$

and using the equation of state of an ideal gas in the chamber V_i (as formulated in a differential form):

$$p_i\frac{dV_i}{dt} + V_i\frac{dp_i}{dt} = R\left(\frac{dm_{Vi}}{dt}T_i + m_{Vi}\frac{dT_i}{dt}\right) \tag{26}$$

the following has been obtained:

$$\frac{dU_i}{dt} = \frac{c_v}{R}\left(p_i\frac{dV_i}{dt} + V_i\frac{dp_i}{dt}\right) \tag{27}$$

Using the relationship $R/c_v = \kappa - 1$ and combining equations (22), (23) and (27) leads to the following differential equations for air pressure variation in the brake chamber V_1 and the valve chamber V_2:

$$\frac{dp_1}{dt} = \frac{1}{V_1}\left(\kappa - 1\right)\left(\dot{Q}_1 + \dot{H}_1 - \dot{H}_{1-2}\right) \tag{28}$$

$$\frac{dp_2}{dt} = \frac{1}{V_2}\left[\left(\kappa - 1\right)\left(\dot{Q}_2 + \dot{H}_{1-2} \mp \dot{H}_2 - \dot{H}_{2-3}\right) - \kappa\cdot p_2\frac{dV_2}{dt}\right] \tag{29}$$

Substituting equations (1) and (2) in equation (26) and calculating the air mass from the ideal gas equation $m_{Vi}=(p_iV_i)/RT_i$, and after making necessary transformations, the following differential equations for air temperature variation in particular brake chambers are obtained:

$$\frac{dT_1}{dt} = \frac{T_1}{p_1 V_1}\left[V_1\frac{dp}{dt} - RT_1\left(\dot{m}_1 - \dot{m}_{1-2}\right)\right] \tag{30}$$

$$\frac{dT_2}{dt} = \frac{T_2}{p_2 V_2}\left[p_2\frac{dV_2}{dt} + V_2\frac{dp_2}{dt} - RT_2\left(\dot{m}_{1-2} \mp \dot{m}_2 - \dot{m}_{2-3}\right)\right] \tag{31}$$

4. Modelling the energy supply unit

A simplified computational diagram of the energy supply unit of a tractor's pneumatic system is presented in Figure 3. The desired air pressure p_t in reservoir 5 is maintained by unloader valve 3 (governor).

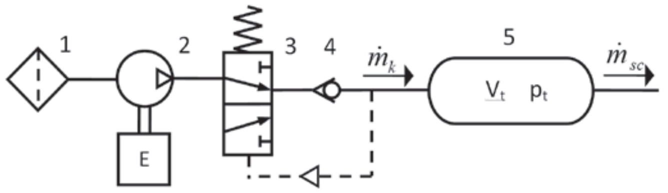

Fig. 3. Computational diagram of an agricultural tractor's pneumatic system energy supply unit: 1 – filter, 2 – compressor, 3 – unloader valve (governor), 4 – check valve, 5 – air reservoir

The increase in pressure up to a maximum preset value p_{max} makes unload valve 3 switch over, and the air from compressor 2 is forced to the atmosphere (the idle run of the compressor). The pressure drop in the system to the preset minimum value p_{min} causes the switching over of the unload valve again and re-charging of the system by compressor. This type of unload valve action can be described by the function of a bi-stable relay with a hysteresis loop of the width equal to $p_{max} - p_{min}$:

$$f_{rel}(p_t) = \begin{cases} \left.\begin{matrix} 1 \text{ if } p_t < p_{\max} \\ 0 \text{ if } p_t \geq p_{\max} \end{matrix}\right\} \text{if } \dfrac{dp_t}{dt} \geq 0 \\ \left.\begin{matrix} 0 \text{ if } p_t \geq p_{\min} \\ 1 \text{ if } p_t < p_{\min} \end{matrix}\right\} \text{if } \dfrac{dp_t}{dt} < 0 \end{cases} \tag{32}$$

Assuming that the compressor discharge pressure is equal to the reservoir pressure p_t (a short length and a small capacity of the pipe connecting the compressor with the reservoir), the mass flux $\dot{m}_k$ [kg/s] of air discharged by the compressor can be described as follows [16]:

$$\dot{m}_k(n_k, p_t) = f_{rel} \cdot \eta_v \cdot V_s \cdot i_c \frac{n_k}{60} \rho_a = f_{rel} \cdot \eta_v \frac{\pi \cdot D_c^2}{4 \cdot 60} \cdot S \cdot i_c \cdot n_k \cdot \rho_a \tag{33}$$

where: η_v – volumetric efficiency, V_s – displacement volume [m^3], D_c – cylinder diameter [m], S – piston stroke [m], i_c – number of cylinders, n_k – compressor shaft speed [rpm], ρ_a – air density [kg/m^3] under ambient conditions.

The value of volumetric efficiency η_v as dependent on the compressor shaft speed n_k and discharge pressure (reservoir pressure p_t) was determined by the non-linear regression method based on the compressor suction capacity curve:

$$\varsigma_v = A_1 + A_2 n_k + A_3 n_k^2 + A_4 p_t + A_5 p_t^2 \tag{34}$$

where: p_t – discharge pressure [kPa]; $A_1 \div A_5$ – regression coefficients. For the FOS Polmo 601.23. 924 compressor model (Polmo, 2011): A_1= 0.809863; A_2=0.321974·10^{-4}; A_3=-1.19758·10^{-8}; A_4=-7.07972·10^{-4}; A_5=3.1248·10^{-7} (R^2=99.39%, MAPE=1.02%).

Changes in reservoir air pressure and temperature are described by the following equations [16]:

$$\frac{dp_t}{dt} = \frac{1}{V_t}\left[(\kappa - 1)\left(\dot{Q} + \dot{H}_k - \dot{H}_{sc}\right)\right] \tag{35}$$

$$\dot{Q} = \alpha_t A_t (T_w - T_t) \qquad \dot{H}_i = \dot{m}_i c_p T_i$$

$$\frac{dT_t}{dt} = \frac{T_t}{p_t V_t}\left[V_t \frac{dp_z}{dt} - RT_t(\dot{m}_k - \dot{m}_{sc})\right] \tag{36}$$

where: $\dot{m}_{sc}$ – mass flux [kg/s] entering the supply and control circuits; $\dot{H}_k$ – enthalpy flux [W] from the compressor; $\dot{H}_{sc}$ – enthalpy flux [W] from the reservoir; $\dot{Q}$ – heat flux [W]; α_t – heat transfer coefficient [W/(m^{2}K)]; A_t – heat transfer area [m^2]; T_w – reservoir wall temperature [K]; T_t – reservoir air temperature [K] as estimated from the polytropic equation:

$$T_k = T_a \left(\frac{p_t}{p_a}\right)^{\frac{n-1}{n}} \tag{37}$$

where: n – polytropic exponent, n=1.25÷1.4 [4]; p_a, T_a – ambient pressure [Pa] and temperature [K], respectively.

5. Examples of experimental and simulation studies

The important functional and service characteristics of agricultural vehicles are checked within certification tests, product qualification tests or periodical inspections. The proposal for a programme of agricultural tractor approval testing in respect of braking, presented in study [17], includes the performance testing of the service and parking brake systems [6] and air brake system checking, including:

- the unload valve operating range,
- coupling head pressure values,
- air system leakage,
- the capacity of reservoirs,
- air compressor capacity, and
- the control device response time.

The research methodology was developed in accordance with the requirements of the Regulation [9] being prepared by the WGAT (Working Group on Agricultural Tractors) for agricultural and forestry vehicles and the 13 ECE Regulation [8] applicable to road vehicles.

The possibilities of using simulation methods for predicting the functional and service characteristics during the model-based design of tractor air brake systems is shown on the example of testing the capacity of the air compressor and the response time of the control device of a Pronar 320AM tractor. The computer models for all of the tractor pneumatic system components were created as *S-function* graphic subsystems stored in the Matlab program's *m-files*, derived from described algorithms and procedures [14, 16].

The obtained experimental and simulation results were used to validate the tractor pneumatic system computer model by using statistical methods. The validation included checking the significance of the differences between the time curves of empirical and simulation pressures in the pneumatic system using the nonparametric Kolmogorov-Smirnov (K-S) test. To eliminate the influence of the integration step-size on the test results, the time interval corresponding to the transitional process was divided into 100 equal parts, thus creating a time vector for which the vectors of the interpolated values of experimental and simulated pressures were calculated using Matlab's standard function *interp1* [33]. Then, using Matlab's standard function *kstest2* [19], the parameter h and the two-sample Kolmogorov-Smirnov test statistics *ks2* were calculated to compare the distributions of values in the two experimental and simulation pressure data vectors. The null hypothesis is rejected (h = 1) at the significance level p, if:

$$ks2 > ks(p)\sqrt{\frac{n_1 + n_2}{n_1 \cdot n_2}} \tag{38}$$

where: n_1, n_2 – number of samples being compared, $ks(p)$ – critical value of the Kolmogorov-Smirnov test; for $ks(0.05)=1.36$ and $n_1=n_2=101$, condition (39) is satisfied if $ks2>0.1923$.
The modelling performance was also assessed using the coefficient of determination R^2 and the mean absolute percentage error (MAPE), defined as [35]:

$$R^2 = 100\left(1 - \frac{\sum_{i=1}^{n}(p_{mi} - p_i)^2}{\sum_{i=1}^{n}(p_i - \overline{p})^2}\right) \tag{39}$$

$$MAPE = \frac{100}{n}\sum_{i=1}^{n}\left|\frac{p_{mi} - p_i}{p_i}\right| \tag{40}$$

where: n – number of values in each of the sets, p_i – measured values of the feature tested, p_{mi} – corresponding values determined from the model, $\overline{p}$ – average measured pressure value.

5.1. Testing of compressor capacity

The experimental and simulation tests of compressor capacity during the operation of the tractor pneumatic system consisted in the recording of pressure variations during compressed air charging of an additional reservoir supplied through the towing vehicle's feed circuit. The time to fill the reservoir representing the capacity of the towed vehicle's air brake system was measured from the moment of starting a hot engine until reaching the prescribed pressure at the maximum engine speed. The additional reservoir volume was calculated from the relationship:

$$V = 20\frac{M_t}{p_{\max}} \tag{41}$$

where: M_t – the permissible maximum load [t] per all axles of the towed vehicle or semi-trailer, p_{max} – maximum regulated pressure value [bar].

For the Pronar 320AM tractor designed for towing trailers of a mass of M_t=3.5 t, a volume variation range of V = 8.75 ÷ 11.1 dm^3 is obtained, which depends on the adopted pressure p_{max} (8 bar in the dual-line braking system or 6.3 bar in the single-line braking system).

Example results of the simulation (solid lines) and experimental (dashed lines) tests of the Pronar 320AM tractor during filling the reservoir with a volume of V=10.42 dm^3 at an engine speed of about 3000 rpm is shown in Figure 4.

The agreement between the experimental p_{ve} and simulated p_v reservoir pressure transients was confirmed by the results of the Kolmogorov-Smirnov test (h=0, $ks2$=0.0198<0.1923). The adequacy of

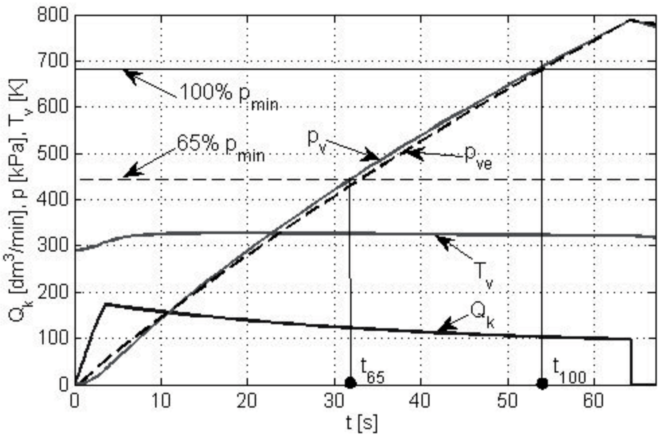

Fig. 4. Results of the simulation test of operation of the Pronar 320AM tractor's pneumatic system energy supply unit, carried out to check the compressor capacity: Q_k – compressor capacity rate, p_v; T_v – reservoir air pressure and temperature; p_{ve} – experimental pressure (R^2=99.83%, MAPE=2.47%, K-S test results: h=0, ks2=0.0198)

the computer model was also confirmed by the obtained values of the statistical indicators R^2=99.83% and MAPE=2.47%.

Then, based on the time variation of reservoir pressure, the time t_{65} required for the pressure to rise from zero to 65% of the minimum preset value (p_{min}=6.83 bar) and the time t_{100} needed for reaching 100% of the minimum preset value were determined. The time values of t_{65}=33.023 s and t_{100}=54.104 s obtained from experimental tests and of t_{65}=31.898 s and t_{100}=53.519 s obtained from the simulation tests (with a relative terror of 3.38% and 1.08%, respectively) are significantly shorter than the maximum values, i.e. 360 and 540 s respectively, allowable for tractors designed for towing vehicles. The results of the experimental and simulation studies have confirmed the correctness of selection of the compressor for the tractor energy supply unit.

5.2. Testing of the response time

The response time of the tractor's dual-line pneumatic system control circuit was determined based on the changes in the brake pedal force and pressure measured at the end of a 2.5 m-long 13 mm-internal diameter line of (an imitation of the trailer control line) connected to the brake coupling (Figure 1). At the beginning of each test, the energy supply unit pressure was equal to the pressure at which the governor restores the feed to the system (the minimum preset value p_{min}). For this test, a pressure vessel with a capacity of 0,385 ± 0,005 dm^3 was connected to the supply coupling. The volume of this vessel corresponds to the internal volume of a 2.5 m-long 13 mm-internal diameter pipe at a pressure of 6.5 bar.

A computer model of the tractor pneumatic system, developed within the Matlab-Simulink program for the study of the transition processes in the control device (corresponding to the diagram in Figure 1), is shown in Figure 5.

The actual input signal in the form of the brake pedal force F_p and the actual response signal of the system, including the variations of pressure p_{te} in the reservoir 4 (Figure 1), pressure p_{se} in vessel 13 and pressure p_{ce} at the end of line 14 connected to brake coupling head 10, were input to the computer model in the form of *FromFile*-type source blocs. Examples of simulation (solid lines) and experimental (dashed lines) results obtained during testing of the response time of the Pronar 320AM tractor pneumatic system control circuit are shown in Figures 5 and 6.

The consistence between the experimental p_{ce} and simulated p_c pressure transients was confirmed by the results of the Kolmogorov-

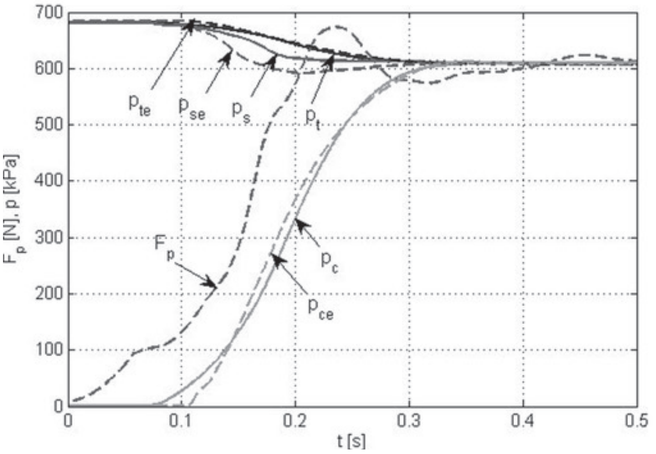

Fig. 5. Results of the experimental and simulation tests of the Pronar MTZ 320 AM tractor control circuit: p_t, p_s, p_c – simulated pressure in the air reservoir, in the vessel connected to the supply coupling head, and at the end of the control line, respectively; p_{te}, p_{se}, p_{ce} – experimental pressure at the same places, F_p – force measured on the brake pedal (R^2=99.24%, MAPE=16.43%, K-S test results: h=0, ks2=0.0990, 101 points)

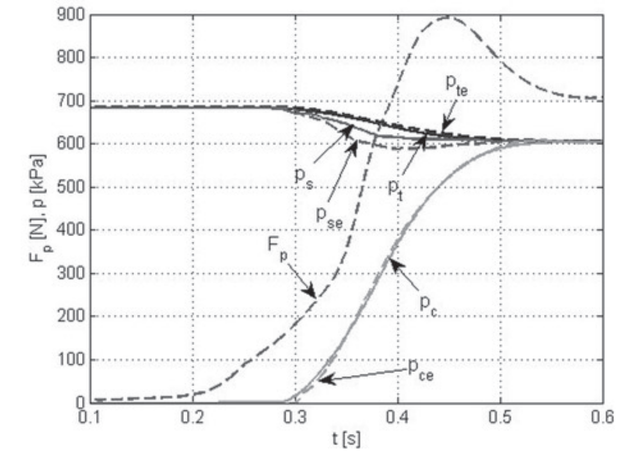

Fig. 6. Results of the experimental and simulation tests of the Pronar MTZ 320 AM tractor control circuit: p_t, p_s, p_c – simulated pressure in the air reservoir, in the vessel connected to the supply coupling head, and at the end of the control line, respectively; p_{te}, p_{se}, p_{ce} – experimental pressure at the same places, F_p –force measured on the brake pedal (R^2=99.84%, MAPE=7.21%, K-S test results: h=0, ks2=0.0396, 101 points)

Smirnov test and by the values of the R^2 and *MAPE* indicators (the results are provided in the captions to the figures).

Then, based on the recorded experimental variations of force F_p and pressure p_{ce}, the response time t_r, i.e. the time for reaching 10% and 75% of the asymptotic pressure value, was determined as a function of the brake pedal actuation time t_f, starting from the shortest possible actuation times and then gradually increasing them up to a time of about 0.4 seconds.

After determining the linear regression equations of response times t_{10} and t_{75} as a function of the time t_f of pedal brake force variations (Figure 7) by least squares method, the response time for rapid braking corresponding to an actuation time of t_f=0.2 was calculated. The results of calculation of the pneumatic system control device response time, as obtained from the experimental tests, are summarized in Table 1.

For the determination of the response time by the digital simulation method, the computer model shown in Figure 5 was used after inputting the brake pedal force F_p standard signal, i.e. the one ramping from 0 to a maximum of 600 N for a duration of 0.2 s. The simulation

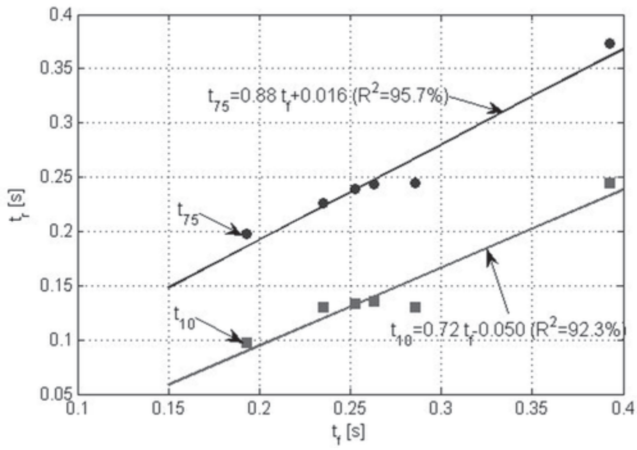

Fig. 7. Relation between the response time t_r (t_{10} and t_{75}) and the actuation time t_f (experimental results)

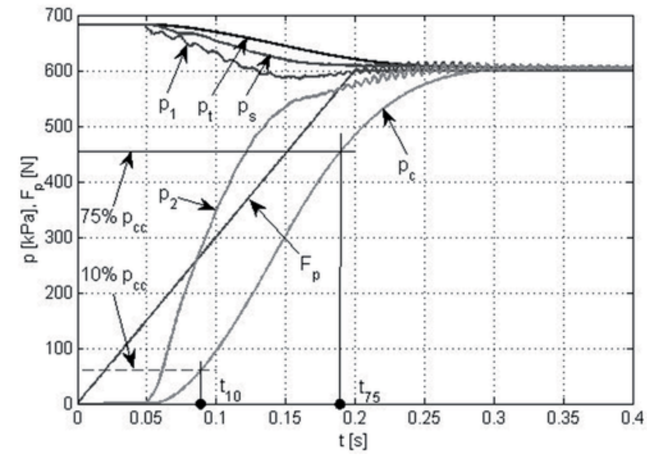

Fig. 8. The results of simulation test of reaction time t_r for the standard course of force F_p

results are shown in Figure 8. The values of the response times t_{10} and t_{75}, as determined based on the pressure p_c variation, are given in Table 1.

It follows from the experimental and simulation studies that the obtained response time values are significantly lower than the permissible values t_{10}=0.2 and t_{75}=0.4s, which indicates the correct choice of the elements shaping the dynamic characteristics of the tractor pneumatic system. The determined relative error of the response time does not exceed 5%, indicating a satisfactory accuracy of the computer model for the modelling purpose.

Table 1. Response time [s] of the control circuit for 10% and 75% of the asymptotic pressure

	Requirements	Experiment	Simulation	Relative error
t_{10}	≤0.2	0.094	0.0893	5.00%
t_{75}	≤0.4	0.192	0.1896	1.25%

6. Conclusions

The developed computer model can be used to predict, by simulation methods, selected functional and service characteristics in the design of the pneumatic system of small- power agricultural tractors equipped with mechanical brakes. The computer model can also serve as a subsystem for the study of transient processes in the multi-circuit pneumatic braking system of a tractor-trailer unit with the aim of shaping the desired dynamic properties, including the speed and synchrony of action (brake compatibility).

The obtained values of the statistical indicators R^2, *MAPE*, as well as the results of the Kolmogorov-Smirnov test assessing the consistence between the experimental and simulation pressure transients during testing of the compressor capacity and control circuit response time have confirmed the adequacy of the Pronar 320AM tractor pneumatic system computer model implemented in Matlab-Simulink. The studies have also shown the correctness of selection of the compressor capacity and the high speed of operation of the control device in terms of the requirements imposed.

The mathematical model of the supply unit and the trailer control valve can be used for modelling other commercial vehicle pneumatic braking systems. Based on the described trailer control valve model equations, mathematical and computer models for other braking valves of similar construction can be created, while considering heat transfer, the inertial forces of valve moving parts, and static and kinetic friction forces.

This research was sponsored by Rector's project no. S/WM/2/2013.

References

1. Armstrong-Helouvry B., Dupont P., Canudas de Wit C. A survey of models analysis tools and compensation methods for the control of machines with friction. Automatica 1994; 30(7): 1083–1138, http://dx.doi.org/10.1016/0005-1098(94)90209-7.
3. Beater P. Pneumatic Drives. System Design, Modeling and Control, Berlin, Heidelberg, Springer-Verlag, 2007.
4. Bloch H.P. A Practical Guide to Compressor Technology. John Wiley & Sons, Hoboken, New Jersey, 2006, http://dx.doi.org/10.1002/0471929786.
5. Breuer B.J., Bill K. H. Brake Technology Handbook (R-375). SAE International, Warrendale. 2008.
6. Czaban J., Kamiński Z. Performance testing of agriculture tractor braking systems. Archiwum Motoryzacji 2010; (1): 15-25.
7. Dodd M., Bartlett R., Knight I. Provision of information and services on the subject of the performance requirements, testing methods and limit values for braking systems of agricultural and forestry tractors, their trailers and interchangeable towed machinery – final report. TRL Unpublished Project Report, Wokingham, UK, 2007, No. UPR/VE/064/07,
8. ECE Regulation No. 13. Uniform provisions concerning the approval of vehicles of categories M, N and O with regard to braking. UN Economic Commission for Europe, Geneva, Switzerland, 2001.
9. EEC (2008) Draft Regulation of the European Parliament and the Council on the braking systems of agricultural or forestry tractors, their trailers and interchangeable towed machinery, amending Directive 2003/37/EC, Council Directive 89/173/EEC and repealing Council Directive 76/432/EEC. (17.11.2008) http://circa.europa.eu/Public/irc/enterprise/automotive/library?l=/agricultural_tractors/meeting_november_2008/99rev16_v171108pdf/_EN_1.0_&a=d
10. Govindan N., Jayaraman V., Venkatasamy S.R., Ramasamy M. Mathematical modeling and simulation of reed valve reciprocating air compressor. Thermal Science 2009; 13(3): 47-58, http://dx.doi.org/10.2298/TSCI0903047G.
11. He L., Wang X., Zhang Y., Wu J., Chen L. Modeling and Simulation Vehicle Air Brake System. Proceedings 8th Modelica Conference. Dresden, Germany, 2011; March 20-22: 430-435. (https://modelica.org/events/modelica2011/Proceedings/pages/papers/17_3_ID_144_a_fv.pdf).
12. Kamiński Z. Dynamic calculations of pneumatic relay valve. Acta Mechanica et Automatica 2009; 3(1): 62-64.
13. Kamiński Z. Mathematical modeling of pneumatic relay valve. Hydraulika i Pneumatyka 2009; 5: 22-25.
14. Kamiński Z. Mathematical Modeling of Pneumatic Pipes in a Simulation of Heterogeneous Engineering Systems. ASME Journal of Fluids Engineering 2011; 133(12): 1-8, http://dx.doi.org/10.1115/1.4005261.
15. Kamiński Z. Mathematical Modelling of the Pneumatic Relay Emergency Valve for Dual-line Agricultural Trailer Braking Systems. Proceedings of the Institution of Mechanical Engineers, Part D: Journal of Automobile Engineering 2012; 226(5): 603-612. (http://pid.sagepub.com/content/early/2011/10/11/0954407011423133: 1-9).
16. Kamiński Z. Modelling of the energy supply equipment of the air braking system of a farm tractor. The Archives of Automotive Engineering 2011; 3: 33-39.
17. Kamiński Z., Czaban J. Proposition of exploration program of braking systems of agriculture tractors. MOTROL 2006; 8: 92-100.
18. Kulesza Z., Siemieniako F. Modeling the air brake system equipped with brake and relay valves. Scientific Journals Maritime University of Szczecin 2010; 24(96): 5-11.
19. Martinez W.L., Martinez A.R. Computational Statistics Handbook with MATLAB, 2th edition, Boca Raton, FL: Chapman & Hall/CRC, 2008.
20. Metljuk N.F., Avtushko V.P. Dinamika Pnevmaticheskikh Privodov Avtomobilej. Mashinostroenie, Moskva, 1980.
21. Miatluk M., Czaban J. An Analysis of Transient Processes in Pneumatic Brake System with Automatic Regulator of Brake Forces of Automotive Vehicles. Commission of Motorization and Power Industry in Agriculture 2006; 6: 85-93.
22. Miatluk M., Kamiński Z., Czaban J. Characteristic Features of the Airflow of Pneumatic Elements of Agricultural Vehicles. Commission of Motorization and Power Industry in Agriculture 2003; 3: 174-181.
23. Natarajan S.V., Subramanian S.C., Darbha S., Rajagopal K.R. A model of the relay valve used in an air brake system. Nonlinear Analysis: Hybrid Systems 2007; 1(3): 430-442, http://dx.doi.org/10.1016/j.nahs.2006.11.003.
24. Nėmeth H., Ailer P., Hangos K.M. Unified model simplification procedure applied to a single protection valve. Control Engineering Practice 2005; 13(3): 315-326, http://dx.doi.org/10.1016/j.conengprac.2004.03.013.
25. Polmo (2011) Fabryka Osprzętu Samochodowego Polmo" Łódź S.A. Single cylinder compressors. 2011, http://www.polmo-lodz.com.pl/katalog/.
26. Pronar. Tractors. Pronar 320AM. http://www.pronar.pl/ciagniki/___pronar_320am__.html.
27. Radlinski R.W., Flick, M.A. Tractor and trailer brake system compatibility. SAE Transactions, 1986; paper no. 861942.
28. Scarlett A. In-service assessment of agricultural trailer and trailed appliance braking system condition and performance. The Agricultural Trailer Braking Study. 2009; RR697 Research Report, (http://www.hse.gov.uk/research/rrpdf/rr697.pdf).

29. Subramanian S.C., Darbha S., Rajagopal K.R. Modelling the pneumatic subsystem of a S-cam air brake system. Trans. of the ASME, J. Dynamic Systems, Measurement and Control 2004; 126(1): 36-46, http://dx.doi.org/10.1115/1.1666893.
30. Venkatesan J., Nagarajan G., Seeniraj R.V., Kumar S. Mathematical modeling of water cooled automotive air compressor. International Journal of Engineering and Technology 2009; 1(1): 50-56, http://dx.doi.org/10.7763/IJET.2009.V1.9.
31. Visteon. Foot brake valve. http://www.demont.com.pl/katalog/4113-1i2.pdf
32. Wabco Air-braking system. Agriculture and forestry vehicles. Edition 8 (Version 2/02.2010(en)). www.wabco-auto.com.
33. Yang W.Y., Cao, W., Chung, T. S., Morris J. Applied Numerical Methods Using MATLAB. John Wiley & Sons, Inc., Hoboken, New Jersey, 2005, http://dx.doi.org/10.1002/0471705195.
34. Zhang H., Wu J., Zhang Y., Chen L. Objected oriented modelling and simulation of pneumatic brake system with ABS. IEEE Intelligent Vehicle Symposium, Xi'an, Shaanxi, China, 2009; June 3-5: 780-785.
35. Zurada J., Levitan A., Guan J. A Comparison of Regression and Artificial Intelligence Methods in a Mass Appraisal Context, Journal of Real Estate Research 2011; 33(3): 349-387.

Zbigniew KAMIŃSKI
Krzysztof KULIKOWSKI
Department of Machine Construction and Exploitation
Faculty of Mechanical Engineering
Białystok University of Technology
ul. Wiejska nr 45C, 15-351 Białystok, Poland
E-mails: z.kaminski@pb.edu.pl, k.kulikowski@doktoranci.pb.edu.pl

Article citation info:
CHENG ZH, YANG ZY, ZHAO JM, WANG YB, LI ZW. Preventive maintenance strategy optimizing model under two-dimensional warranty policy. Eksploatacja i Niezawodnosc – Maintenance and Reliability 2015; 17 (3): 365–373, http://dx.doi.org/10.17531/ein.2015.3.6.

Zhong Hua CHENG
Zhi Yuan YANG
Jian Min ZHAO
Ya Bin WANG
Zhi Wei LI

PREVENTIVE MAINTENANCE STRATEGY OPTIMIZING MODEL UNDER TWO-DIMENSIONAL WARRANTY POLICY

MODEL OPTYMALIZACJI STRATEGII KONSERWACJI ZAPOBIEGAWCZEJ W WARUNKACH DWUWYMIAROWEJ POLITYKI GWARANCYJNEJ

An effective warranty servicing strategy should be made considering both warranty cost and product availability. Based on the two-dimensional free repair warranty, a strategy combining the imperfect preventive maintenance and minimal repair is proposed where the imperfect preventive maintenances are implemented in a special subregion of the warranty and all other failures are repaired minimally. By modeling the warranty cost and product availability, we derive the optimum warranty servicing strategy and corresponding parameters to minimize the cost-effective of unit time. Finally, we provide a numerical illustration and a comparison with some other strategies.

Keywords: *two-dimensional warranty, imperfect preventive maintenance, availability.*

Efektywna strategia obsługi gwarancyjnej powinna uwzględniać zarówno koszty gwarancji jak i dyspozycyjność produktu. W oparciu o pojęcie dwuwymiarowej gwarancji bezpłatnej naprawy, zaproponowano strategię łączącą niepełną konserwację zapobiegawczą z naprawą minimalną, gdzie działania obsługowe w ramach niepełnej konserwacji zapobiegawczej przeprowadza się w ramach specjalnego podobszaru gwarancji, a wszelkie inne uszkodzenia naprawia się w ramach naprawy minimalnej. Modelując koszty naprawy oraz dyspozycyjność produktu, wyprowadzono optymalną strategię obsługi gwarancyjnej oraz odpowiadające jej parametry w celu zminimalizowania kosztów na jednostkę czasu. Na koniec, proponowane rozwiązanie zilustrowano na przykładzie numerycznym oraz porównano z innymi strategiami.

Słowa kluczowe: *gwarancja dwuwymiarowa, niepełna konserwacja zapobiegawcza, dyspozycyjność.*

1. Introduction

A warranty servicing strategy has significant impact on manufacturer's warranty cost and the product availability. As requirement of consumers for the quality of products is increasing, product availability will obviously affect consumer satisfaction and the reputation of manufacturer and then the product sales, so reasonable warranty strategy should be made considering both warranty cost and product availability to meet the interests of both sides.

Preventive maintenance could reduce the product failure rate so that reduce the warranty cost and improve availability effectively. With the updating of warranty policy, warranty cost model under the preventive maintenance is developed in many studies. Chun [2] introduced the periodic preventive maintenance in prior time when he studied product warranty. This model is generalized by Jack and Dagpunar [7], where the product can be repaired "as good as new" after preventive maintenance, and preventive maintenance period is variable. Yeh and Lo [12] extends the model with making the preventive maintenance degree reach some specific level to minimize the warranty cost. The study [4] derives an optimal preventive warranty strategy to minimize the product's long term expected cost by balancing the saving and added cost by preventive maintenance during warranty period, and obtains the optimal preventive maintenance period and puts forward effective algorithm. The above studies introduce preventive maintenance into the one-dimensional warranty policy and are aimed at getting the lowest warranty cost without considering the product availability. In addition, preventive maintenance is not always effectively, as the new product just begins to operate, unreasonable preventive maintenance often leads to a high warranty cost and low availability since the failure rate is relatively low at the beginning of exploitation.

A summary of the different warranty policies is given in [1]. They can be divided into one-dimensional and two-dimensional policies broadly. For the study of optimizing models under two-dimensional warranty, Iskandar and Murthy [6] proposed a repair-replacement strategy with two subregions to optimize the warranty cost, where minimal repair and replacement strategy is adopted in different subregions. In [5], the strategy in [6] is improved to a new repair-replacement strategy with three subregions, where the first failure in the middle subregion Ω_2 will be handled by replacement, and the remaining failures are all repaired minimally. The strategy in [5] is improved to an imperfect repair strategy by Yun and Kang [13], where the first repair in the middle subregion is imperfect, and all remaining repairs are minimal, and then, this strategy is generalized to an n-subregion strategy by Varnosafaderani and Chukova [10, 11], where the first repair in each intermediate subregions (Ω_2-Ω_{n-1}) are imperfect, and other failures are repaired minimally. The above studies mentioned are aimed at optimizing the warranty cost without considering the preventive maintenance and product availability, but the availability, like warranty cost, is also an important factor to influence the warranty strategy because it is related to consumer satisfaction, especially for some specific customer as army.

In view of the above analysis, this paper introduces the minimal-imperfect preventive maintenance combination strategy considering a product with a two-dimensional free repair warranty and presents a mathematical optimization model to derive the optimal preventive maintenance strategy in the warranty period with respect to the warranty cost and product availability.

2. Warranty servicing strategy

The product is sold with a two-dimensional free repair warranty. As mentioned in earlier research, the two-dimensional warranty is characterized by a region Ω in a two-dimensional plane and the repair is free to consumer in this region [6].

In this paper, the case where warranty region Ω is a rectangle with the age limit K and usage limit L is studied, and the warranty expires when either limit is exceeded. The minimal – imperfect preventive maintenance combination strategy is introduced to deal with the failure in warranty region. The warranty servicing strategy is implemented as follows.

Firstly, as in [6], the warranty region Ω [(0, K)×(0, L)] is divided into two disjoint subregions Ω_1 and Ω_2, as shown in Fig. 1. The shapes of the subregions are governed by a rate parameter r ($r \geq 0$), such that

$$r1 = \frac{L1}{K1}, \quad r2 = \frac{L}{K}.$$

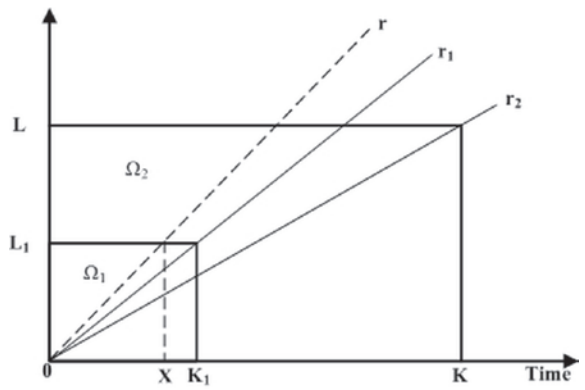

Fig. 1. Subregions of the warranty region

Then, given the subregions Ω_1 and Ω_2, the minimal - imperfect preventive maintenance combination strategy is as follows:

(a) all repairs in Ω1 are minimal with cost Cf and duration T_f.
(b) The first imperfect preventive maintenance is taken at the time point the warranty over the subregion Ω_1 expires, and periodic preventive maintenance (PM) is implemented in Ω_2 with cost C_p, duration T_p and period T, and the remaining failures are rectified by minimal maintenance.

The warranty policy introduced above is of certain practical significance. In the subregion Ω_1, the failure rate is relatively low since the product just begins to operate, so minimal repair is effective. PM strategy is adopted in Ω_2 since the failure rate rises with the increase of the product's age/usage, and the proper PM action can reduce the shutdown loss and maintenance cost caused by failure. In practice, having a combination of the minimal repair and PM often leads to lower warranty servicing cost and higher product availability.

3. Modeling product failure and imperfect maintenance

Two different approaches have been used to model the product failure process for the analysis of two-dimensional warranty policies. They are one-dimensional and two-dimensional approaches, and the detailed description has been introduced in related literature [8]. In this study, the failure process under two dimensions is modeled using the one-dimensional approach.

In the one–dimensional approach, product usage is considered as a function of the age of the product. Assuming that the relationship is linear with a nonnegative coefficient R, such that

$$U(t) = RT(t),$$

where $U(t)$ and $T(t)$ are the usage and age of the product at time t, and the usage rate R is a nonnegative random variable with a known distribution function $G(r)$. When no product failure occurs before t or all the failures are repaired, then $T(t)$ = t. However, if the product is not repairable and the failure product must be replaced by a new one, then $T(t) < t$. For details, see [6].

Product failures are modeled by a stochastic process with an intensity function dependent on age and usage of the product. Given a usage rate r, the intensity function will have a single variable t since the usage can be conveyed by age, such that

$$\lambda(t|r) = \varphi(T(t), U(t)).$$

With the simplest being a polynomial of order one [6], the following conditional intensity function form is given by:

$$\lambda(t|r) = \theta 0 + \theta 1 r + \theta 2 T(t) + \theta 3 U(t), \tag{1}$$

and a polynomial of order two is given in [5], as follows:

$$\lambda(t|r) = \theta 0 + \theta 1 r + \theta 2 T(t)^2 + \theta 3 T(t) U(t), \tag{2}$$

with the parameters $\theta_i > 0$.

To model the imperfect preventive maintenance effect on the failure rate of the product, a modification of the "virtual age" model proposed in [3] is introduced, where the effect of an imperfect maintenance is expressed by a reduction of the system virtual age, that is, after preventive maintenance, the failure rate decreases to a former level as the age of the product reduces, and the corresponding former age is the "virtual age" (or effective age).

Given the minimal - imperfect preventive maintenance combination strategy, we introduce the improvement factor α, and the virtual age reduction depends on α. Based on the model in [3], the failure rate of the product is defined by its virtual age (or effective age), and when an imperfect maintenance is performed on the product, its virtual age will be reduced. Assume that the j-th preventive maintenance interval is Δj, and after the j-th imperfect preventive maintenance with improvement factor α_j, the virtual age reduces by $\alpha_j T(\Delta j)$. So the virtual age after the j-th preventive maintenance can be given by:

$$vj(t) = T(t) - \sum_{i=1}^{j} \alpha i T(\Delta i). \tag{3}$$

Since the product in this study is repairable and all failures are repaired minimally, then $T(t) = t$, and the eq.(3) can be transformed to:

$$vj(t) = t - \sum_{i=1}^{j} \alpha i \Delta i, \tag{4}$$

so the conditional intensity function after the j-th preventive maintenance becomes:

$$\lambda_j\left(t|r\right)=\lambda\left(v_j(t)|r\right)=\lambda\left(t-\alpha_1X-\sum_{i=2}^{j}\alpha_iT|r\right)\quad with\sum_{i=2}^{1}\alpha_iT=0\ ,\ (5)$$

where $\lambda(\bullet|r)$ is the initial intensity function of the process and X is the time point that the warranty over the subregion Ω_1 will expire (see Fig.1). $\alpha_i\in[0,1]$ represents the degree of a repair (improvement factors), which is the level of the applied effort to improve the state of product. Based on the model, $\alpha = 0$ means that the preventive maintenance is minimal and PM action has no significant effect on the state of the product. Besides, $\alpha = 1$ means that the repair is perfect and the state of product is restored to ''as good as new'' state. The conditional intensity function of the process after an imperfect maintenance is between the conditional intensities after a minimal repair and a perfect repair.

4. Two-dimensional warranty cost and availability models

Let $EC^{\Omega}\left(\varpi\right)$ and $EA^{\Omega}\left(\varpi\right)$ denote the expected warranty cost and availability over the warranty region Ω respectively, where ϖ represents the parameters of the minimal – imperfect preventive maintenance combination strategy and is given by $\varpi=\left(K_1,T,r_1\right)$. We assume that $K_1+T_p<K$. Each whole preventive warranty cost is denoted by C_p, which includes the preventive warranty expected cost and the loss of shutdown. Analogously, each whole failure warranty cost is denoted by C_f . Consider the following two cases: (a) $r_1\le r_2$; (b) $r_1>r_2$. See Fig.2.

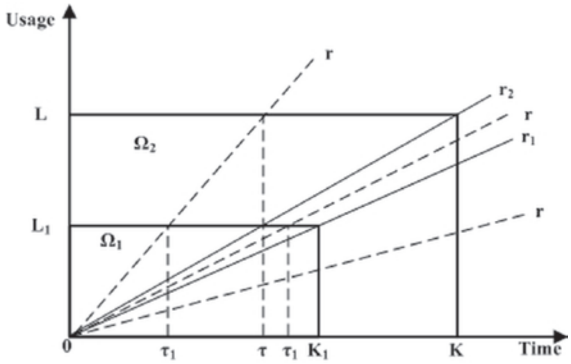

(a) $r_1\le r_2$

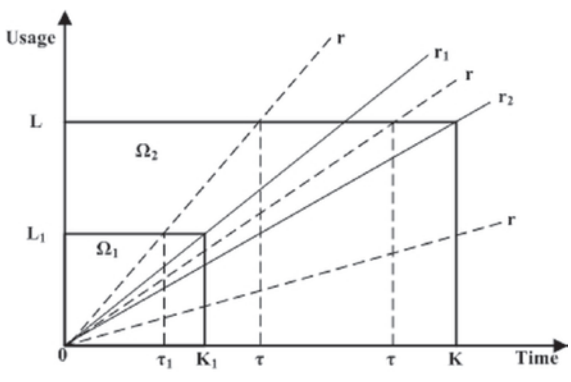

(b) $r_1>r_2$

Fig. 2. analysis for case (a) and (b)

4.1. Case (a): $r_1\le r_2$

For this case, the warranty region is divided according r_1 and r_2, and considering the value of usage rate $R=r$, the following three subcases are discussed:

$$\text{(a.1)}\ r\le r_1\ ;\ \text{(a.2)}\ r_1<r\le r_2\ ;\ \text{(a.3)}\ r_2<r\ .$$

We denote the expected warranty costs and availability, conditional on $R=r$, for the three subcases by $EC_r^1\left(\varpi\right)$, $EC_r^2\left(\varpi\right)$, $EC_r^3\left(\varpi\right)$ and $EA_r^1\left(\varpi\right)$, $EA_r^2\left(\varpi\right)$, $EA_r^3\left(\varpi\right)$, respectively.

4.1.1. Case (a.1): $r\le r_1$

Cost model: In this case, the warranty over the subregions Ω_1 and Ω_2 will expire at time points K_1 and K, respectively (see Fig.2). Then the expected warranty cost can be given as follows:

$$EC_r^1\left(\varpi\right)=C_fEN\left(K_1|r\right)+nC_p+\sum_{i=1}^{n-1}EC_{fi}\left(T\right)+EC_{fn}\left(K_1,K\right),\quad(6)$$

where $EN\left(K_1|r\right)$ represents failure quantities in the subregion Ω_1. n is the number of imperfect preventive maintenance in the subregion Ω_2. $EC_{fi}\left(T\right)$ is the expected cost of minimal repairs in the i-th periodic preventive maintenance interval. $EC_{fn}\left(K_1,K\right)$ is the expected cost of minimal repairs between $K_1+T_p+\left(n-1\right)\left(T+T_p\right)$ and K.

Since failures over [0, K_1] are repaired minimally and no preventive maintenance is implemented, the expected number of minimal repairs in the subregion Ω_1 is equal to:

$$EN\left(K_1|r\right)=\int_0^{K_1}\lambda\left(t|r\right)dt\ .\quad(7)$$

In general, the duration of a repair is minute relative to preventive maintenance period, so we can neglect the influence and use the eq.(7) to derive approximately expected the number of failure [9].

Periodic imperfect preventive maintenance will be implemented in the subregion Ω_2. Given the period of preventive maintenance T and maintenance duration T_p, n is expressed by:

$$n=n\left(K_1,K|r\right)=int\left[\left(K-K_1-T_p\right)/\left(T+T_p\right)+1\right].\quad(8)$$

The warranty over the subregion Ω_1 will expire at time K_1, so the the conditional intensity function after the j-th imperfect maintenance (the j-th preventive maintenance interval) becomes:

$$\lambda_j\left(t|r\right)=\lambda\left(t-\alpha_1K_1-\sum_{i=2}^{j}\alpha_iT|r\right).\quad(9)$$

Then, in the i-th periodic preventive maintenance interval, failures are rectified by minimal repairs. Then, the numbers of minimal repairs is given by:

$$EN_r\left(i\right)=\int_{K_1+(i-1)T+iT_p}^{K_1+i(T+T_p)}\lambda_i\left(t|r\right)dt\ .\quad(10)$$

So the total expected cost of the minimal repairs in the n preventive maintenance intervals can be given as follows:

$$\sum_{i=1}^{n-1} ECfi(T) = \sum_{i=1}^{n-1} ENr(i)Cf \ . \tag{11}$$

In the same way, the failure number of the product between $K1 + Tp + (n-1)(T + Tp)$ and K is expressed as:

$$ENr(n) = \int_{K1+(n-1)T+nTp}^{K} \lambda n(t|r)dt \ . \tag{12}$$

So the expected warranty cost of the product of the time between $K1 + Tp + (n-1)(T + Tp)$ to K is given as:

$$ECfn(K1, K) = ENr(n)Cf \ . \tag{13}$$

Then, the expected warranty cost can be obtained by inserting eq.(7)-(13) into (6):

$$EC_r^1(\varpi) = Cf\int_0^{K1} \lambda(t|r)dt + int\left[(K - K1 - Tp)/(T + Tp) + 1\right]Cp + \sum_{i=1}^{n-1} \int_{K1+(i-1)T+iTp}^{K1+i(T+Tp)} \lambda i(t|r)dtCf + \int_{K1+(n-1)T+nTp}^{K} \lambda n(t|r)dtCf \ . \tag{14}$$

Availability model: In this case, since the warranty will cease at time K, expected availability in the warranty region can be expressed as follows:

$$EA_r^1(\varpi) = \frac{K - ED_r^1(\varpi)}{K}, \tag{15}$$

where $ED_r^1(\varpi)$ is the expected shutdown time in the warranty region and has the similar expression with $EC_r^1(\varpi)$ by T_p and T_f replace C_p and C_f. So $ED_r^1(\varpi)$ is given by:

$$ED_r^1(\varpi) = TfEN(K1|r) + nTp + \sum_{i=1}^{n-1} ETfi(T) + ETfn(K1, K) \ . \tag{16}$$

Similarly, $ETfi(T)$ is the expected shutdown time of minimal repairs in the i-th periodic preventive maintenance interval, and $ETfn(K1, K)$ is the expected shutdown time of minimal repairs between $K1 + Tp + (n-1)(T + Tp)$ and K. The expressions as follows:

$$\sum_{i=1}^{n-1} ETfi(T) = \sum_{i=1}^{n-1} ENr(i)Tf \ , \tag{17}$$

$$ETfn(K1, K) = ENr(n)Tf \ . \tag{18}$$

The remaining parameters are the same as in eq.(6). Then, the function of expected availability can be given as follows:

$$EA_r^1(\varpi) = 1 - \frac{1}{K}\left[\begin{array}{l} Tf\int_0^{K1} \lambda(t|r)dt + int\left[(K - K1 - Tp)/(T + Tp) + 1\right]Tp \\ + \sum_{i=1}^{n-1} \int_{K1+(i-1)T+iTp}^{K1+i(T+Tp)} \lambda i(t|r)dtTf + \int_{K1+(n-1)T+nTp}^{K} \lambda n(t|r)dtTf \end{array}\right]. \tag{19}$$

To facilitate subsequent calculation, the expected cost in the warranty region can be viewed as a function of the decision variables ($K1$, T) and the warranty time limit K, denote:

$$EC_r^1(\varpi) \overset{def}{=} \phi(K1, K, T). \tag{20}$$

Similarly, the expected availability in warranty region is denoted by:

$$EA_r^1(\varpi) \overset{def}{=} \xi(K1, K, T) \ . \tag{21}$$

4.1.2. Case (a.2): $r1 < r \le r2$

In this case, due to exceeding the usage limit L1, the warranty over the subregions Ω_1 and Ω_2 will expire at time points $\tau 1$ and K respectively (see Fig.2). With $\tau 1 = L1/r$. Then the expected warranty cost for this case becomes:

$$\begin{aligned} EC_r^2(\varpi) &= \phi(\tau 1, K, T) \\ &= CfEN(\tau 1|r) + nCp + \sum_{i=1}^{n-1} ECfi(T) + ECfn(\tau 1, K), \end{aligned} \tag{22}$$

where the time limit K_1 in eq.(6) is replaced by $\tau 1$.

Similarly, the expected availability in the warranty region becomes:

$$\begin{aligned} EA_r^2(\varpi) &= \xi(\tau 1, K, T) \\ &= \left\{K - \left[TfEN(\tau 1|r) + nTp + \sum_{i=1}^{n-1} ETfi(T) + ETfn(\tau 1, K)\right]\right\} \Big/ K \ . \end{aligned} \tag{23}$$

4.1.3. Case (a.3): $r2 < r$

In this case, due to exceeding the usage limit L_1 and L, the warranty over the subregions Ω_1 and Ω_2 will expire at time points $\tau 1$ and τ , respectively (see Fig.2). With:

$$\tau 1 = \frac{L1}{r}, \ \tau = \frac{L}{r},$$

then the expected warranty cost for this case becomes:

$$\begin{aligned} EC_r^3(\varpi) &= \phi(\tau 1, \tau, T) \\ &= CfEN(\tau 1|r) + nCp + \sum_{i=1}^{n-1} ECfi(T) + ECfn(\tau 1, \tau), \end{aligned} \tag{24}$$

where the time limit K_1 and K in eq.(6) is replaced by $\tau 1$ and τ , respectively.

Similarly, the expected availability in the warranty region becomes:

$$EA_r^3(\varpi)=\xi(\tau 1,\tau,T)$$
$$=\left\{\tau-\left[TfEN(\tau 1|r)+nTp+\sum_{i=1}^{n-1}ETfi(T)+ETfn(\tau 1,\tau)\right]\right\}\Big/\tau \quad (25)$$

In the end, we remove the conditioning on $R=r$, where R has distribution function $G(r)$, to get the expected warranty cost for case (a), given by:

$$EC^{\Omega}(\varpi)=\int_0^{r1}EC_r^1(\varpi)dG(r)+\int_{r1}^{r2}EC_r^2(\varpi)dG(r)+\int_{r2}^{\infty}EC_r^3(\varpi)dG(r). \quad (26)$$

Similarly, the expected availability in the warranty region is given by:

$$EA^{\Omega}(\varpi)=\int_0^{r1}EA_r^1(\varpi)dG(r)+\int_{r1}^{r2}EA_r^2(\varpi)dG(r)+\int_{r2}^{\infty}EA_r^3(\varpi)dG(r). \quad (27)$$

4.2. Case1 (b): $r1>r2$

For this case, similar to case (a), the following three subcases are considered:

(b.1) $r\le r2$; (b.2) $r2<r\le r1$; (b.3) $r1<r$.

We use the same denotation setting with case (a) to model the expected warranty cost and availability under case (b).

Using eq.(17), the expected warranty cost under the three subcases are given by:

$$EC_r^1(\varpi)=\phi(K1,K,T),$$

$$EC_r^2(\varpi)=\phi(K1,\tau,T),$$

$$EC_r^3(\varpi)=\phi(\tau 1,\tau,T).$$

The expected availability under the three subcases are given by:

$$EA_r^1(\varpi)=\xi(K1,K,T),$$

$$EA_r^2(\varpi)=\xi(K1,\tau,T),$$

$$EA_r^3(\varpi)=\xi(\tau 1,\tau,T).$$

Note that subcases (1) and (3) for case (b) are the same as that for case (a), and the only difference is for subcase (2) since the warranty ceases at distinct time. See Fig. (2).

On removing the conditioning, we have the expected warranty cost given by:

$$EC^{\Omega}(\varpi)=\int_0^{r2}EC_r^1(\varpi)dG(r)+\int_{r2}^{r1}EC_r^2(\varpi)dG(r)+\int_{r1}^{\infty}EC_r^3(\varpi)dG(r), \quad (28)$$

accordingly, the expected availability is given by:

$$EA^{\Omega}(\varpi)=\int_0^{r2}EA_r^1(\varpi)dG(r)+\int_{r2}^{r1}EA_r^2(\varpi)dG(r)+\int_{r1}^{\infty}EA_r^3(\varpi)dG(r). \quad (29)$$

5. Deriving optimum warranty servicing strategy

Scientific warranty servicing strategy demands to control warranty cost and guarantee availability simultaneously. To derive the optimum warranty servicing strategy, the optimizing model is given as follows:

$$\begin{cases} min \quad EC^{\Omega}(\varpi) \\ s.t. \quad EA^{\Omega}(\varpi)\ge A_0 \\ 0<K_1<K;\ 0<T<K-K_1 \end{cases} \quad (30)$$

where the decision variable $\varpi=(K_1,T,r_1)$. The optimizing model is to minimize the warranty cost on the premise of ensuring the expected availability greater than A_0, which can derive optimum warranty servicing strategy for both manufacturer and consumer. As the model is difficult to calculate, a grid search in specific regions is performed to obtain the optimum results.

In general, when the (K_1,r_1) is fixed, the expected warranty cost $EC^{\Omega}(\varpi)$ will increase first and then decrease with the growth of the preventive maintenance interval T, and the expected availability $EA^{\Omega}(\varpi)$ has the opposite trend. Based on the optimizing model proposed above, the following three cases are considered (see Fig.3):

case (1): $T_u<T_c$, then $T^*=T_u$,

case (2): $T_l\le T_c\le T_u$, then $T^*=T_c$,

case (3): $T_c<T_l$, then $T^*=T_l$,

where T_l and T_u represent the lower and upper limits of PM interval T under $EA^{\Omega}(\varpi)\ge A_0$, respectively, and T_c is the PM interval to minimize the expected warranty cost without constrains, T^* is the optimal solution of the optimizing model under fixed (K_1,r_1). Similarly, the values of T^* can be obtained under different (K_1,r_1), and then, the optimum warranty servicing strategy $\varpi^*=(K_1^*,T^*,r_1^*)$ and the corresponding $EC^{\Omega}(\varpi^*)$ and $EA^{\Omega}(\varpi)^*$ can be derived by comparative analysis. The analytic procedure is analogous for other curve forms.

To obtain more integrated information about the optimum warranty servicing strategy, unit cost-effective of the product is introduced as follows:

$$EV^{\Omega}(\varpi)=EC^{\Omega}(\varpi)\big/E\tau\ EA^{\Omega}(\varpi), \quad (31)$$

where $E\tau$ is the expected warranty period, and it is given by:

$$E\tau=KG(r_2)+\int_{r_2}^{\infty}L/rdG(r). \quad (32)$$

The unit cost-effective of the product with optimum warranty servicing strategy can be derived using eq.(31), combining with the optimizing solutions, which can provide scientific information for both manufacturer and consumer.

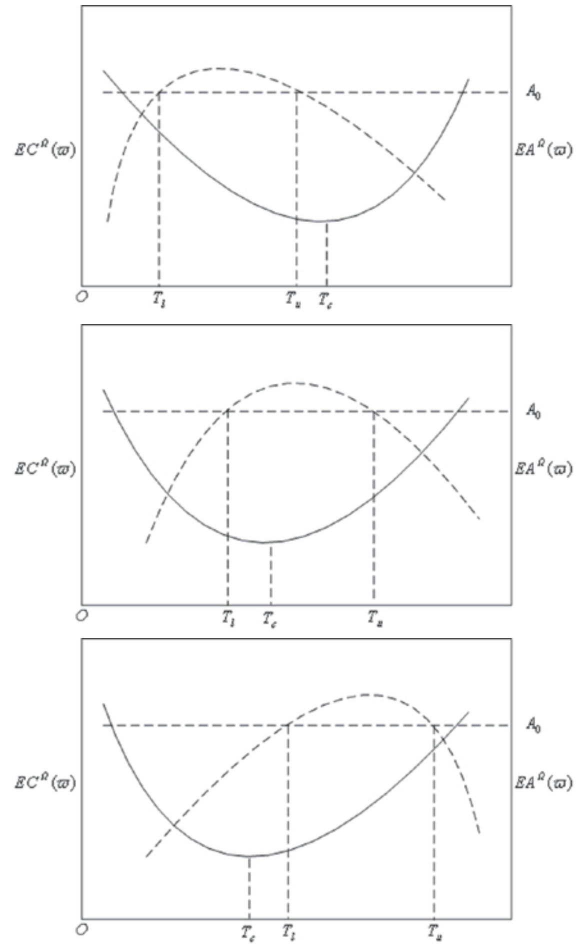

Fig. 3. Optimal T under different cases

6. An example

Considering an automobile component sold with a free-repair warranty policy, we will pay attention to the warranty cost from the manufacturer perspective and the availability from the consumer perspective. Assume K=3 (3 years) and L=3 (30000 *km*), so r_2=L/K=1. And the acceptable lower limit of availability is $A_0 = 0.92$.

For the convenience of calculation, let improvement factors $\alpha_i = \alpha$, that is each PM actions corresponding the same improvement factor. Commonly, the PMs duration T_p is less than the minimal repair duration T_f, and $C_p \le C_f$. The C_f and T_f are assumed to be constant with the value 1 and 0.02 respectively; then, C_p and T_p are assumed to be the function of improvement factor α, as follows:

$$C_p = C_0 + C\alpha^{\beta}, \text{ and } T_p = \alpha T_f = 0.02\alpha .$$

The expression shows the cost of preventive maintenance will increase exponentially with the growth of improvement factor. In this instance, let $C_0 = 0.1$, $C = 1$ and $\beta = 3$.

In this example, as in [5], we consider the form for the initial conditional failure intensity given by eq.(2), as follows:

$$\begin{aligned}\lambda\left(t|r\right) &= \theta_0 + \theta_1 r + \theta_2 T\left(t\right) + \theta_3 U\left(t\right) \\ &= 0.1 + 0.2r + \left(0.7 + 0.7r\right)t^2 \quad .\end{aligned}$$

The distribution of usage rate can be estimated using the real data. In this study, the following two distributions are considered:

Normal: R ~ N [1, 0.46],
Excessive: R ~ N [2, 0.86].

To see the impact of different usage rate distribution forms on the warranty servicing strategy, a uniform distribution is given to make a comparison:

R ~ uniform [0.2, 1.8] with E(R) =1, D(R) =0.46.

For different values of α and for each of the three usage categories, a grid search is performed to find the optimal decision variables denoted by $\varpi^* = \left(K_1^*, T^*, r_1^*\right)$ using the optimizing model in section 5. The variable K_1 and T are increasing in steps of 0.1 over the interval [0, 3] and [0.1, 3], respectively. For convenience, the value of rate parameter r_1 is increasing in steps of 0.2 starting 0.2, and the remaining cases can be calculation in the same way.

Using the mathematical model and optimization procedure proposed above, the optimal values of $EC^{\Omega}(\varpi)$ and $EA^{\Omega}(\varpi)^*$ can be obtained for the three usage categories. Fig.4 shows the values of expected warranty cost and availability with normal usage, as r_1 = 1 and $\alpha = 0.6$.

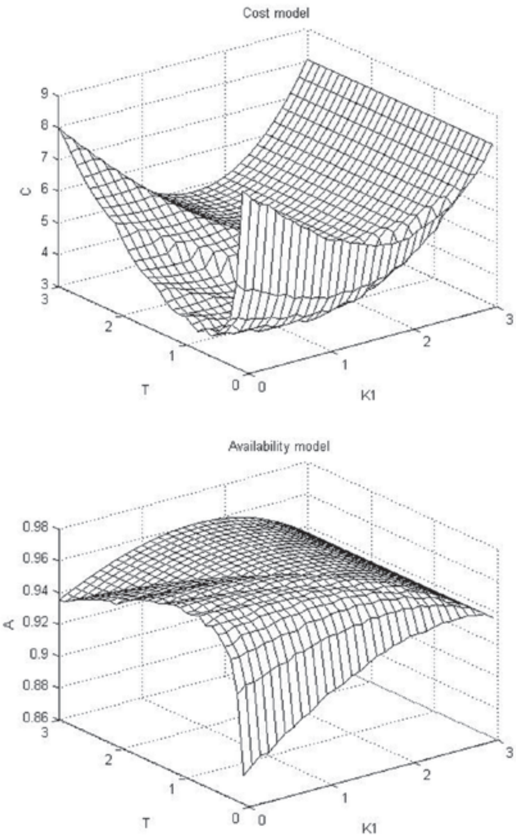

Fig. 4. Grid patterns of cost and availability functions

Let $K_1 = 0.6$, the warranty cost and availability trends can be derived by dimension reduction analysis to Fig.4, as shown in Fig.5. Obviously, it matches case (2) proposed in section 5, so $T^* = T_c$.

Similarly, we can derive the corresponding optimal results with different r_1 and α under different usage categories, and the summary of these results is shown in Table 1 – Table 4.

Firstly, the two usage categories under normal distribution are considered and the results are presented in Table 1–Table 3.

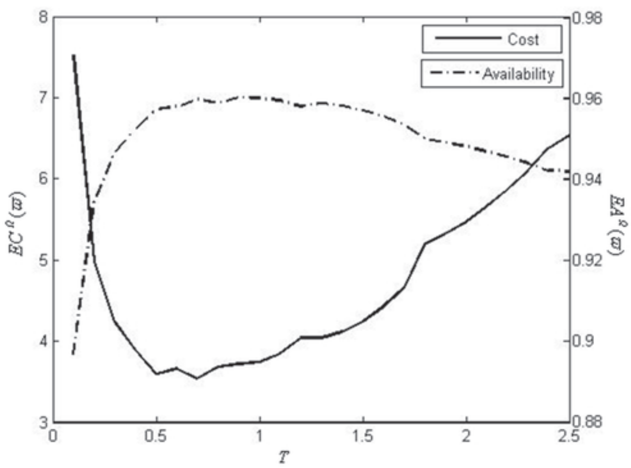

Fig. 5. The warranty cost and availability trends

In Table 1, the minimum cost-effective of unit time $EV^{\Omega}\left(\varpi^*\right)$ under different improvement factors is given in column 4, and the correspondingly optimal expected warranty cost $EC^{\Omega}(\varpi^*)$ and availability $EA^{\Omega}(\varpi)^*$ are given in columns 2–3. Columns 5–6 present the minimum warranty cost $EC_{0,T}$ and maximum availability $EA_{0,T}$ when K_1=0, that is, the periodic PMs are implemented during the whole warranty period. The last two columns present the minimum warranty cost EC_{MR} and maximum availability EA_{MR} without PM actions in warranty region. The notations in Table 2 are the same as in Table 1.

Optimal warranty servicing strategy and corresponding cost and availability in each row are printed in boldface in Table 1–Table 3. The following results can be obtained by analyzing these tables:

For each of the two usage categories, The warranty cost $EC^{\Omega}\left(\varpi^*\right)$ is always less than $EC_{0,T}$ and EC_{MR}, and the availability $EA^{\Omega}\left(\varpi^*\right)$ always higher than $EA_{0,T}$ and EA_{MR} under different α values, which leads to a relatively lower unit efficient cost under the warranty servicing strategy introduced in section 2. For example, for the excessive usage category, when $\alpha = 0.7$, the warranty cost under the combination strategy can be reduced by 55.1% and 7.4% compared adopting the minimal repair or periodic preventive maintenance alone, respectively, and the corresponding availability has an increase of 3.4% and 0.2%.

The values of unit efficient cost are decreasing firstly and then increasing with the rise of improvement factor. The optimal value is obtained when $\alpha = 0.5$ for normal usage and $\alpha = 0.7$ for excessive usage, which indicates that it is worthy to perform a better degree of imperfect preventive maintenance with high usage rates.

Table 1 Optimization results for the normal usage rate under different α

α	$EC^{\Omega}\left(\varpi^*\right)$	$EA^{\Omega}\left(\varpi^*\right)$	$EV^{\Omega}\left(\varpi^*\right)$	$EC_{0,T}$	$EA_{0,T}$	EC_{MR}	EA_{MR}
0.1	6.7394	0.9383	2.9172	6.7573	0.9364	8.0017	0.9347
0.2	5.6044	0.9406	2.4200	5.6375	0.9368		
0.3	4.3174	0.9487	1.8483	4.3352	0.9441		
0.4	3.8647	0.9549	1.6438	3.9238	0.9506		
0.5	3.5530	0.9604	1.5025	3.6726	0.9594		
0.6	3.5844	0.9606	1.5155	3.6285	0.9598		
0.7	3.5852	0.9608	1.5155	3.6815	0.9602		
0.8	3.6323	0.9611	1.5350	3.7327	0.9606		
0.9	3.7662	0.9612	1.5914	3.8216	0.9609		

Table 2. Optimization results for the excessive usage rate under different α

α	$EC^{\Omega}\left(\varpi^*\right)$	$EA^{\Omega}\left(\varpi^*\right)$	$EV^{\Omega}\left(\varpi^*\right)$	$EC_{0,T}$	$EA_{0,T}$	EC_{MR}	EA_{MR}
0.1	2.6446	0.9302	2.2312	2.6589	0.9298	3.7121	0.9286
0.2	2.2884	0.9310	1.9346	2.3106	0.9309		
0.3	2.0496	0.9397	1.7072	2.0725	0.9395		
0.4	1.8773	0.9472	1.5569	1.9204	0.9470		
0.5	1.7712	0.9535	1.4610	1.8181	0.9533		
0.6	1.6850	0.9586	1.3846	1.8097	0.9585		
0.7	1.6647	0.9603	1.3691	1.7971	0.9587		
0.8	1.7078	0.9601	1.4006	1.8539	0.9587		
0.9	1.8120	0.9596	1.4868	1.9854	0.9584		

Table 3. Optimal warranty servicing strategy for the two usage categories under normal distribution

Usage category	α	K_1^*	L_1^*	T^*	r_1^*	$EV^{\Omega}(\varpi^*)$
Normal	0.1	0.7	0.70	0.2	1.0	2.9172
	0.2	0.8	0.80	0.2	1.0	2.4200
	0.3	0.7	0.70	0.3	1.0	1.8483
	0.4	0.9	0.90	0.5	1.0	1.6438
	0.5	1.0	1.00	0.5	1.0	1.5025
	0.6	0.9	0.90	0.7	1.0	1.5155
	0.7	1.2	1.20	0.6	1.0	1.5155
	0.8	1.1	1.10	0.7	1.0	1.5350
	0.9	1.3	1.30	0.7	1.0	1.5914
Excessive	0.1	1.5	0.60	0.3	0.4	2.2312
	0.2	1.6	0.64	0.2	0.4	1.9346
	0.3	1.1	0.66	0.3	0.6	1.7072
	0.4	1.3	0.78	0.4	0.6	1.5569
	0.5	1.6	0.96	0.5	0.6	1.4610
	0.6	1.5	0.90	0.6	0.6	1.3846
	0.7	1.2	0.96	0.6	0.8	1.3691
	0.8	0.8	0.80	0.6	1.0	1.4006
	0.9	1.2	1.20	0.6	1.0	1.4868

Table 4. Optimal warranty servicing strategy for different usage rate distributions

Distribution forms	α	K_1^*	T^*	r_1^*	$EV^{\Omega}(\varpi^*)$
Normal distribution	0.1	0.7	0.2	1.0	2.9172
	0.2	0.8	0.2	1.0	2.4200
	0.3	0.7	0.3	1.0	1.8483
	0.4	0.9	0.5	1.0	1.6438
	0.5	1.0	0.5	1.0	1.5025
	0.6	0.9	0.7	1.0	1.5155
	0.7	1.2	0.6	1.0	1.5155
	0.8	1.1	0.7	1.0	1.5350
	0.9	1.3	0.7	1.0	1.5914
Uniform distribution	0.1	0.7	0.2	1.0	2.9802
	0.2	0.7	0.2	1.0	2.4739
	0.3	0.8	0.3	1.0	2.0782
	0.4	0.7	0.4	1.0	1.7656
	0.5	0.7	0.5	1.0	1.5429
	0.6	0.8	0.6	1.0	1.3930
	0.7	0.9	0.7	1.0	1.2689
	0.8	0.9	0.7	1.0	1.2848
	0.9	1.0	1.0	1.0	1.3054

The optimal parameters related to warranty servicing strategy are given in Table 3, which include the usage limit and age limit of Ω_1 and preventive maintenance period T. It can be seen from the table that:

In most cases, the r_1^* under normal usage is greater than under excessive usage, that is to say, the shape of the minimal repair region Ω_1 is relatively flat and with a lower usage limit under excessive usage for a fixed α . It can be also noticed that the usage limit of region Ω_1 has a growth trend when the improvement factors increase. The optimal warranty servicing strategies are printed in boldface.

Table 4 shows the optimal warranty servicing strategy and the value of unit efficient cost under normal distribution (R ~ N [1, 0.46]) and uniform distribution (R ~ uniform [0.2, 1.8]). As presented in this table, although the expectation and variation of the two distributions are identical, there are obvious differences in the optimal results, so it is important to confirm reasonable distribution according to reality before making warranty servicing strategy.

Table 1 – Table 4 include the balance of the needs and interests between the manufacture and the consumer under different imperfect PM improvement factor, the corresponding calculation results as warranty cost, the availability and unit efficient cost, which can provide scientific reference for selecting the reasonable warranty servicing strategy to balance the benefit of manufacturer and consumer.

In addition, for the convenience of implement or maintenance capacity constraints reasons, the PM's period T or improvement factor α may be a limited value in reality, then we can also derive the optimum warranty servicing strategy using the mathematical model proposed in this paper (as shown in Fig. 4).

7. Conclusions

In this paper, a strategy combining the imperfect preventive maintenance and minimal repair is proposed under the free repair warranty policy, then warranty cost and availability models are built, and optimum warranty servicing strategies are identified with respect to both warranty cost and product availability. We provide a numerical illustration to show the optimization method and accurate calculation results under different strategies and make a comparison, which can offer a reference to select the optimum warranty servicing strategy benefiting both manufacturer and consumer.

The result of this paper can be extended in several ways. One possible extension is to consider the preventive maintenance under pro-rata warranty policy since the PMs can improve the product availability and benefit to consumer. Another option for generalization is to develop the functional relationship between the product availability and sales, and then, make the optimum warranty servicing strategy.

Acknowledgement

The research work is supported by the National Natural Science Foundation of China with contract number 70971135.

References

1. Blischke W R, Murthy D N P. Warranty cost analysis. New York: CRC Press, 1994.
2. Hun Y H. Optimal number of periodic preventive maintenance operations under warranty. Reliability Engineering and System Safety 1992; 37(3): 223-225, http://dx.doi.org/10.1016/0951-8320(92)90127-7.
3. Doyen L, Gaudoin O. Classes of imperfect repair models based on reduction of failure intensity or virtual age. Reliability Engineering and System Safety 2004; 84(1): 45-56, http://dx.doi.org/10.1016/S0951-8320(03)00173-X.
4. Guo J, Fei H. An optimal preventive maintenance policy for product sold with warranty. Journal of Mathematics 2009; 29(4): 546-550.
5. Iskandar B P, Murthy D N P, Jack N. A new repair–replace strategy for items sold with a two-dimensional warranty, Computers and Operations Research 2005; 32 (3): 669-682, http://dx.doi.org/10.1016/j.cor.2003.08.011.
6. Iskandar B P, Murthy D N P. Repair-replace strategies for two-dimensional warranty policies. Mathematical and Computer Modelling 2003; 38: 1233-1241, http://dx.doi.org/10.1016/S0895-7177(03)90125-7.
7. Jack N, Dagpunar J S. An optimal imperfect maintenance policy over a warranty period. Microelectronics and Reliability 1994; 34(3): 529-534, http://dx.doi.org/10.1016/0026-2714(94)90091-4.
8. Murthy D N P, Iskandar B P, Wilson R J. Two-dimensional failure free warranties: Two-dimensional point process models. Operations Research 1995; 43: 356-366, http://dx.doi.org/10.1287/opre.43.2.356.
9. Tsai Y, Wang K, Tsai L. A study of availability-centered preventive maintenance for multi-component systems. Reliability Engineering and System Safety 2004; 84(3): 261-270, http://dx.doi.org/10.1016/j.ress.2003.11.011.
10. Varnosafaderani S, Chukova S. An imperfect repair strategy for two-dimensional warranty. Journal of the Operational Research Society, 2012; 63(6): 846-859,http://dx.doi.org/10.1057/jors.2011.66.
11. Varnosafaderani S, Chukova S. A two-dimensional warranty servicing strategy based on reduction in product failure intensity. Computers and Mathematics with Applications 2012; 63: 201-213, http://dx.doi.org/10.1016/j.camwa.2011.11.011.
12. Yeh R H, Lo H C. Optimal preventive maintenance warranty policy for repairable products. European Journal of Operational Research 2001; 134(1): 59-69, http://dx.doi.org/10.1016/S0377-2217(00)00238-1.
13. Yun W Y, Kang K M. Imperfect repair policies under two-dimensional warranty. Proceedings of the Institution of Mechanical Engineers 2007; 221(4): 239-247, http://dx.doi.org/10.1243/1748006XJRR55.

Zhonghua CHENG
Zhiyuan YANG
Jianmin ZHAO
Yabin WANG
Zhiwei LI
Department of Management Engineering
Mechanical Engineering College
Shijiazhuang, Hebei, 050003, P.R. China
E-mail: zszs197466@163.com, yzy_sjz90@126.com, jm_zhao@hotmail.com, wangyabin123@163.com, arhqs@126.com

Article citation info:
CHODURSKI M, DĘBSKI H, SAMBORSKI S, TETER A. Numerical strength analysis of the load-bearing frame of a palletizing robot's universal head. Eksploatacja i Niezawodnosc – Maintenance and Reliability 2015; 17 (3): 374–378, http://dx.doi.org/10.17531/ein.2015.3.7.

Marek CHODURSKI
Hubert DĘBSKI
Sylwester SAMBORSKI
Andrzej TETER

NUMERICAL STRENGTH ANALYSIS OF THE LOAD-BEARING FRAME OF A PALLETIZING ROBOT'S UNIVERSAL HEAD

NUMERYCZNA ANALIZA WYTRZYMAŁOŚCI RAMY NOŚNEJ UNIWERSALNEJ GŁOWICY ROBOTA PALETYZUJĄCEGO*

The paper deals with numerical strength analysis of the load-bearing structure of an industrial robot's head used for palletization of sacks. The calculations were performed with the Finite Element Method (FEM), enabling reconstruction of the real service conditions in the process of palletization. It was assumed, that the head was adapted to lay two sacks of maximal dimensions 800x500x140mm and a mass of up to 50 kg at a time. The currently exploited palletizing heads are heavy, which essentially increases the costs of the palletization process. The aim of the study was a numerical analysis of the existing head of the palletizing robot, leading to design of a structure having optimized maintenance parameters. The conducted research on decreasing the mass of the palletizing robot's head are important because of the industrial robot's load-bearing capacity, its effectiveness and the costs of the palletization process.

***Keywords**: FEM, palletization, robot's head, load-bearing frame, modelling, grasper.*

W prezentowanej pracy zajęto się numeryczną analizą wytrzymałościową ustroju nośnego głowicy robota przemysłowego, która służy do paletyzacji worków. Obliczenia prowadzono z zastosowaniem metody elementów skończonych, umożliwiającej odwzorowanie rzeczywistych warunków eksploatacyjnych pracy robota w procesie paletyzacji. W obliczeniach przyjęto, że głowica jest przystosowana do układania dwóch worków jednocześnie o maksymalnych wymiarach gabarytowych: 800mm, 500mm, 140mm oraz masie do 50 kg. Stosowane obecnie głowice paletyzujące są ciężkie, co znacznie podnosi koszty procesu paletyzacji. Celem pracy była analiza numeryczna istniejącej głowicy robota paletyzującego, na podstawie której możliwe będzie zaprojektowanie konstrukcji o zoptymalizowanych parametrach eksploatacyjnych. Prowadzone prace nad redukcją masy własnej głowicy robota paletyzującego są istotne ze względu na nośność robota przemysłowego, wydajność oraz koszt procesu paletyzacji.

***Słowa kluczowe**: MES, paletyzacja, głowica robota, rama nośna, modelowanie, chwytak.*

1. Introduction

The advancing process of packaging and palletizing automation [1-6] caused a big demand of universal and lightweight graspers of the industrial robot's heads, being able to carry and lay down ladings on transportation pallets. Among main tasks of the graspers one can distinguish catching a manipulated object, holding it during moving and proper releasing at the place of destination. The grasper is a tool adapted to the robot's arm and is a separate assembly of interacting elements [7]. The proper catching of the object depends among others on its shape, mass, center of mass location, surface quality in the very place of grasping, prehensile possibilities of the grasper and the misalignment of the ready to move object with respect to the pick-up point.

The second phase of the grasper service is holding the object during manipulation. Within the service range at that phase the motion induced accelerations occur. Their values have essential effect on the burden of the analysed object's load-bearing elements. The last stage of service is a process of the detail release at the destination location, which starts with reaching the end position and precise stopping. If the detail's release takes place with no obstacles (the anti-collision systems does not react) the robot retreats in order to move back from the manipulated object.

The object of research was a palletizing robot's head exploited in the process of sacks packaging. The analyzed device was an expanded multifunctional grasper equipped with fully automated control - the Wikpol's palletizing head given in Fig. 1.

The considered head consisted of several key-elements: the attachment terminal, the load-bearing frame, the movable frame, the grasper's fork, as well as the bottom and the side holdfast. The grasper can be included in the group of forceful-shaped ones. The sacks transported by the head are raised with the fork being a system of jaws closing at the sacks in the bottom. During transportation the sacks lay on the fork and are simultaneously held with the side holdfast in horizontal direction and with the top holdfast in vertical direction. From the point of view of the prehensive endings' degrees of freedom the presented head can be included in the vise-like graspers family, because of the horizontal movement of the fork. The movable elements of the head are moved with standardized pneumatic actuators. The head's frame is attached directly to the robot having a total lading capacity of 250 kg. The palletizing head in its current design has its own

(*) Tekst artykułu w polskiej wersji językowej dostępny w elektronicznym wydaniu kwartalnika na stronie ***www.ein.org.pl***

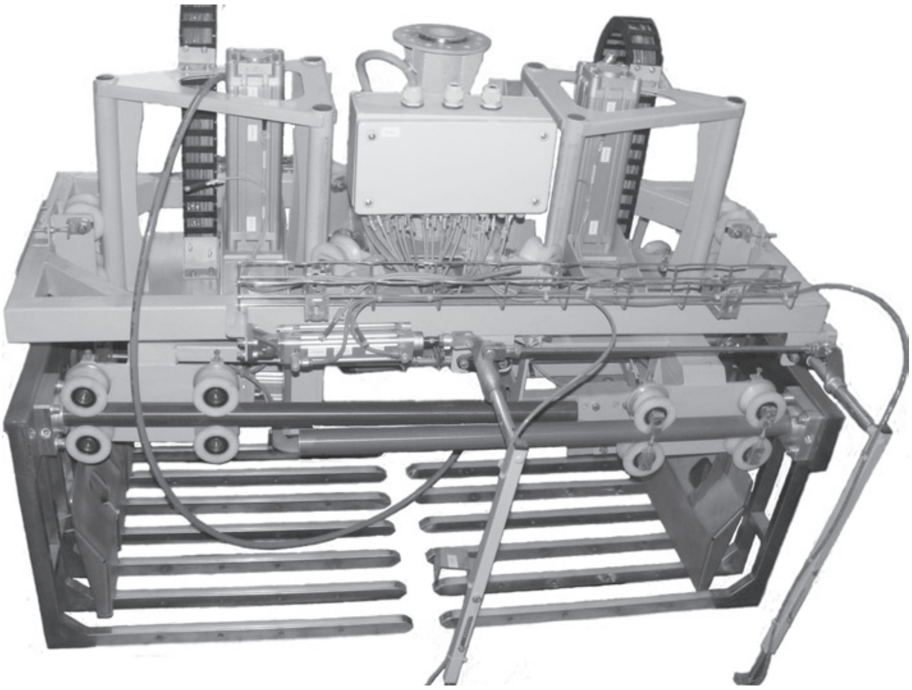

Fig. 1. Palletizing head produced by the „Wikpol" company

mass of 200 kg, which allows it to carry - together with the dedicated manipulator - two sacks of 25 kg mass.

The aim of the conducted research was to design a lightweight load-bearing frame having high stiffness and thus able to carry simultaneously two sacks of 50 kg mass each. The project of the new head was a modification of the existing construction through elimination of the low effort elements responsible for significant mass increase of the object. To achieve this the heavy elements, i.e. the attachment terminal and the load-bearing frame were subjected to a detailed strength analysis [8-10]. The whole modelling process, as well as a detailed numerical strength calculations were performed with the Finite Element Method (FEM) in the ABAQUS® commercial software environment [11-12].

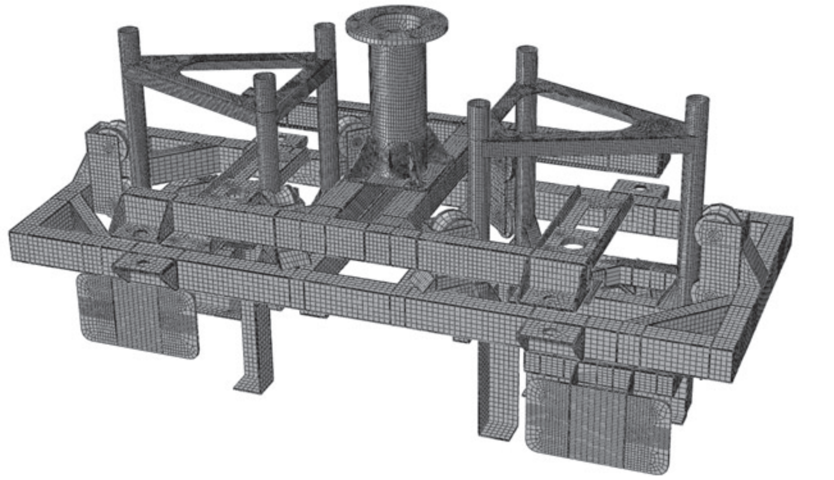

Fig. 3. Discrete model of the palletizing head's frame with boundary conditions and applied load

2. Research object and scope

The object of research were the load-bearing elements of the Wikpol's palletizing head, without the control system components and the structural details unimportant from the strength point of view. The geometric model of the analysed object (Fig. 2) was developed in the form of an assembly based on the device technical documentation with the use of the CATIA V5 CAD software. The elaborated model of the load-bearing frame of the palletizing head reflected the device configuration corresponding to service conditions occurring during transportation of lading. It applies first of all to the relative configuration of the movable frames and the load-bearing frame, as well as to setting the lading's and the fork's center of mass in the conditions of service.

The developed geometrical model of the palletizing head was a basis for discrete model enabling execution of numerical calculations with the Finite Element Method. The process of geometrical model's discretization was conducted with the C3D8R eight- noded solid elements of reduced integration and having three translational degrees of freedom at each node [13-18]. The applied finite elements were of first order. For the purpose of providing the compatibility between the overall mass of the palletizing head and its elaborated discrete model it was necessary to take into consideration the mass of rejected elements (excluded from the geometrical model) giving 58.2 kg in total. The above mentioned elements were included in the model as point masses assigned to the respective regions of the frame at appropriate locations. The elaborated discrete model of the palletizing head taking into account the reciprocal contact interactions among respective parts of the model and providing their appropriate cooperation is shown in Fig. 3.

The model of the accepted boundary conditions assumed that the connection of the palletizing head with the robot's bunch was encastered. Having this in target all the translational degrees of freedom of the nodes at the head's attachment surface were restrained. It was assumed, that the head was loaded with no ex-

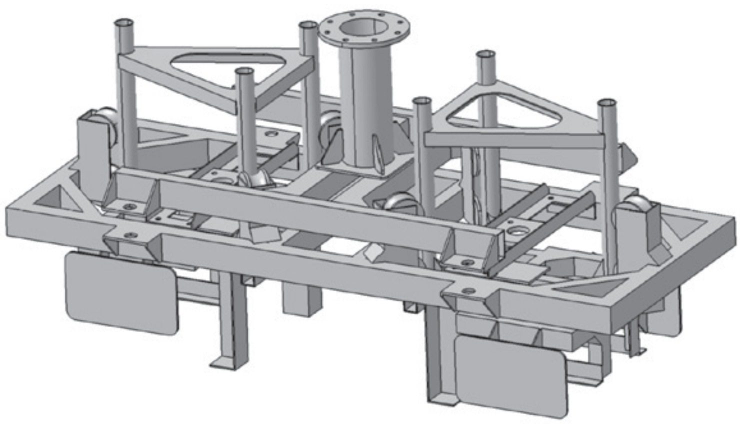

Fig. 2. Geometrical model of the load-bearing frame of the palletizing head

ternal forces except the carried lading's weight and the device's own mass. For lack of a model of the fork, on which the sacks lay directly during transportation, in the analysis a sum of the fork and the sack masses was accepted and their common center of mass was determined with appropriate CATIA V5 software functions. The calculations considering a loading case, in which the head transported a lading composed of two sacks with the total mass of 100 kg were performed. In the calculations the weight of the tested object itself was allowed for, whereas the load simulating manipulating moves of the robot were included through introduction of acceleration of 40 m/s^2 acting in horizontal direction [19-20], which corresponded with maximal value of retard obtained during an emergency stop of the robot.

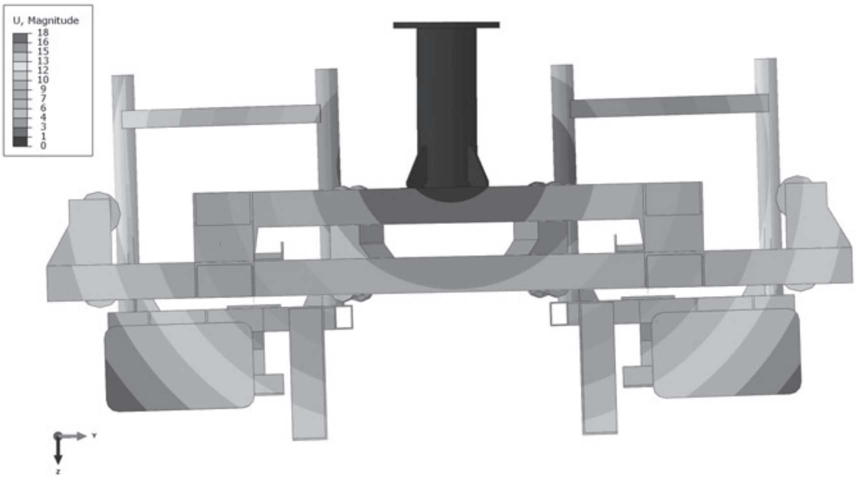

Fig. 5. Nodal displacements of the numerical model

In the numerical calculations the linear elastic material model was accepted as during the head's exploitation no permanent deformations took place. All the load-bearing elements of the frame were assumed to be made of steel with the following mechanical characteristics: Young modulus E= 210 GPa, Poisson ratio ν=0.3 and mass density ρ = 7860 kg/m^3. The yield stress essential in the effort assessment of the head frame's load-bearing elements was R_e=235 MPa. It was additionally assumed, that in the model large displacements could occur, making the problem geometrically nonlinear. In the performed calculations the incremental-iterative Newton-Raphson method was used [17-18].

3. Numerical results

The performed calculations enabled determination of the Huber-Mises-Hencky equivalent stress distributions [13-15] in the load-bearing elements of the head, as well as determination of the head's displacements in case of the emergency robot stopping. The equivalent stress results are given in Fig. 4, whereas the nodal displacements – in Fig. 5. The obtained general level of the equivalent stress in the elements of the head did not exceed σ≈235MPa, whereas the observed local cumulations of the stress near the head pipe's stiffening ribs indicated substantial exceeding of the yield stress in these regions. The scale of the displayed stress contours was limited to 235 MPa in order to gain a more emphasized picture of the stress contour. Maximal nodal displacement in the model occurred place at the movable frame's boundaries and reached 18 mm.

Typical behaviour of the examined load-bearing structure observed in the model was an occurrence of high stress in the attachment terminal, at simultaneous very low stress in the load-bearing frame.

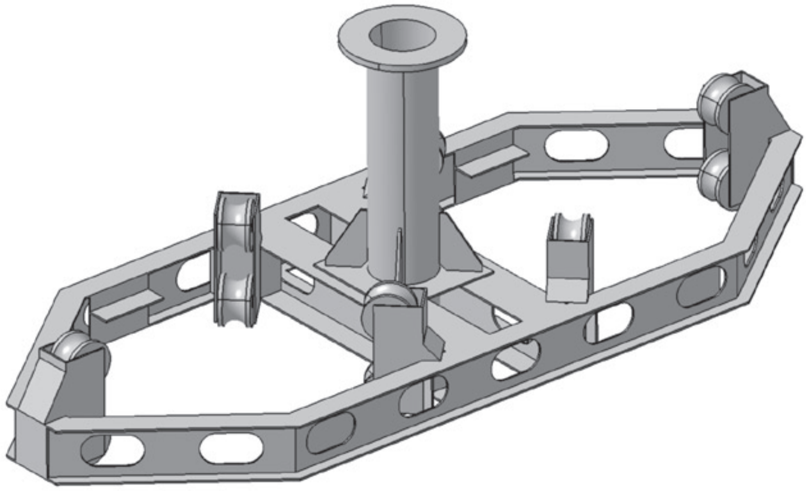

Fig. 6. Geometrical model of the modified load-bearing frame

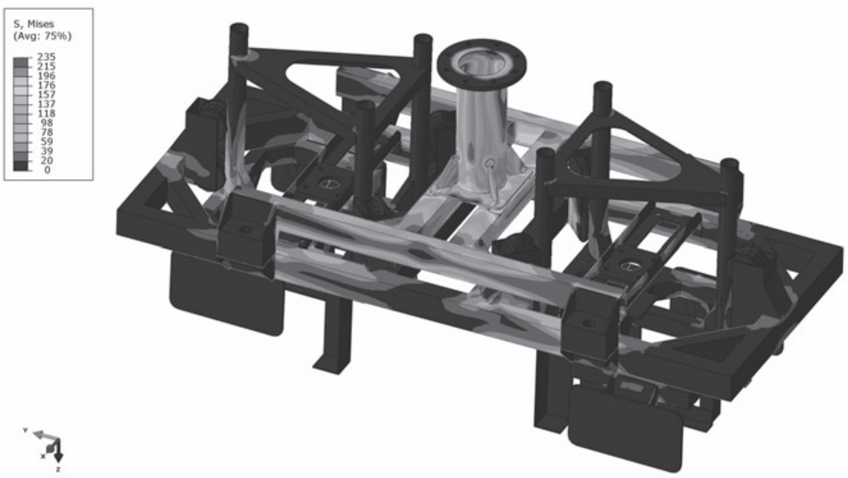

Fig. 4. The Huber-Mises-Hencky equivalent stress contour

As the terminal is responsible only for the grasper connection to the robot's bunch, it was neglected in the model. Instead, the connecting functionality was assigned to the load-bearing frame. Elimination of the attachment terminal model was made in practice by elongation of the pipe fixing it to the robot's bunch in order to join it with the load-bearing frame without changing the distance between the frame and the bunch. Moreover, the evidently low effort level of the closed-section profiles constituting the load-bearing frame was the reason to make an attempt to replace them with open-section profiles having a form of I-beams. In the I-beams' webs holes were made that shouldn't weaken these elements' strength, whereas they would result in mass reduction. In the proposed structural design a steel with higher (compared

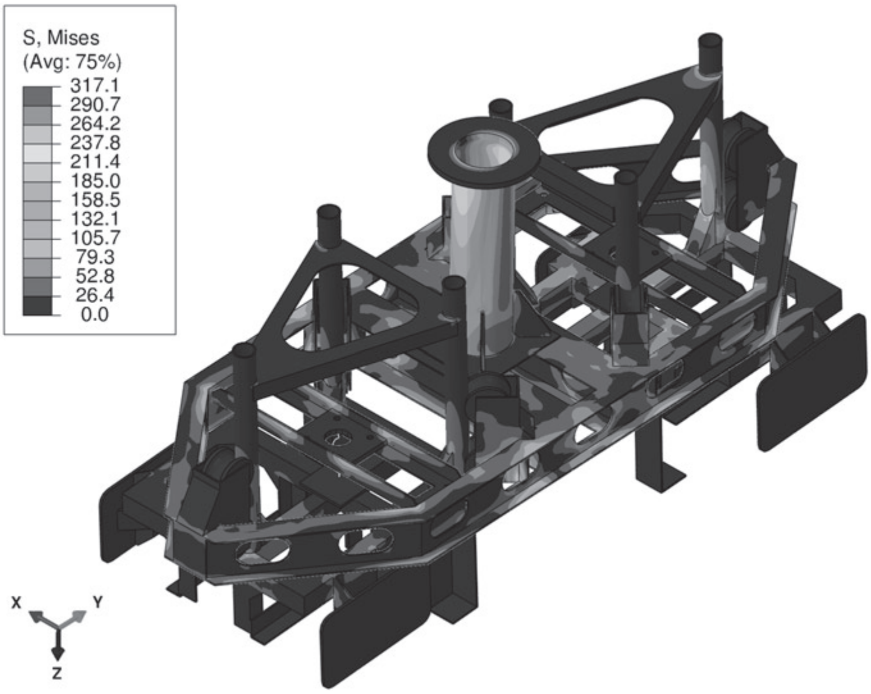

Fig. 7. The equivalent H-M-H stress field in the modified load-bearing frame

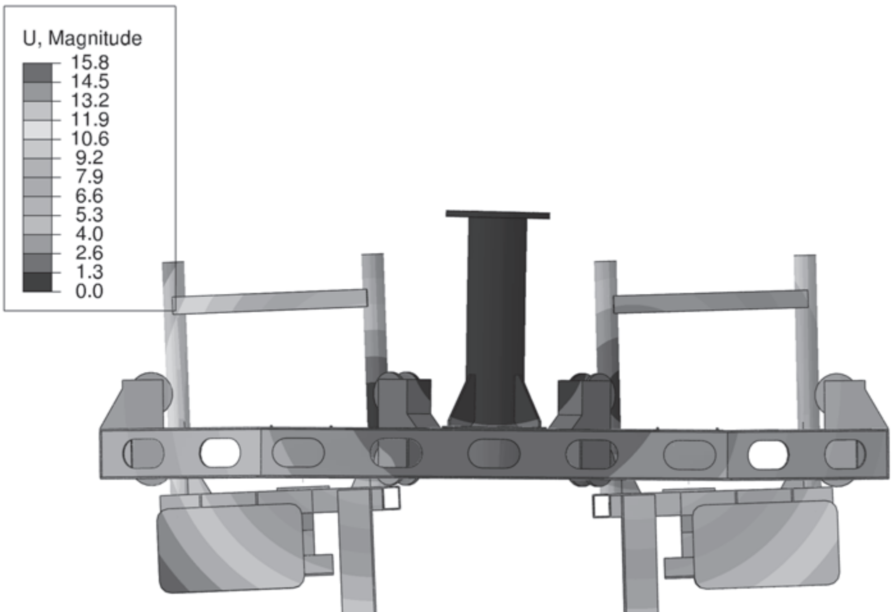

Fig. 8. Nodal displacements of the modified load-bearing frame

to the previous construction) yield strength equal R_e=350 MPa was accepted. In Fig. 6 the modified load-bearing frame is shown, which allows to reduce the palletizing head's mass by ca. 11 kg and simultaneously simplifies the whole head's design essentially.

The process of discretization of the geometrical model, as well as the parameters' identification of the numerical analysis of the modified head frame was performed identically, as in the case of the frame model before modifications.

The performed calculations proved essential improvement of the degree of effort in the particular load-bearing elements of the head's frame. In the considered case the equivalent stress level according to the H-M-H hypothesis in the load-bearing frame overcame the accepted yield stress of the material R_e=350 MPa and in parallel a definitely more uniform effort in all the load-bearing elements of the structure was attained. It is well visible, that the holes made in the frame did not cause additional stress concentration (even though their size was large) and - advantageously - they essentially reduced the load-bearing frame's mass. The maximal stress values occurred in the internal roll set of the movable frame and equaled σ=317 MPa. Such a value does not jeopardize the device's safe service but is an indication to consider modification of that element as well.

Analysis of the nodal displacements (Fig. 8) justifies a statement that maximal displacements were 15.8 mm. This means that changing the structural design of the load-bearing frame decreased the maximal value of nodal displacements in comparison with the original model. The load-bearing frame's re-design gave significant advantage in the form of the head's mass reduction. The performed numerical analysis allowed elimination of the outer frame of the head, in which the effort of the load-bearing elements was very low. The proposed design reached the assumed aims and essentially simplified the whole device's construction.

4. Conclusions

The way of the FEM-based modelling of the load-bearing structures presented in the current paper enabled conducting analysis of deformation and effort of the load-bearing elements subjected to a complex external loading. This is extremely significant in case of searching for new structural design, when at the stage of designing complicated machines and mechanisms too many unknown parameters occur. Recognition of the stress field in the load-bearing elements of the structure is thus a question of primary importance, allowing an assessment of the accepted structural design. Numerical analyses enable also optimization of the model parameters in order to choose the best solution from the point of view of ability to carry the defined service loads. The performed analysis enabled an assessment of the proposed structural design, being a basis for introducing the necessary modifications of the construction details in order to obtain the optimal solution in this sense.

The FEM numerical calculations of the load-bearing frame of the palletizing robot' head proved, that its load-bearing capacity could be significantly increased at simultaneous reduction of its own mass. In the presented case the computed equivalent stress contours showed that many load-bearing elements of the head exhibited a very low effort. The modification of the load-bearing frame allowed essential reduction of the elements' mass – 27.5% with respect to the basic variant, keeping the stiffness and the functionality of the structure. It is fairly important from the maintenance point of view, because it enables a significant increase in the effectiveness of the device through increasing the palletization possibilities of higher lading weight. The developed 3D solid model simulated the service conditions of all the elements very well and enabled subsequent modifications of not only the load-bearing frame, but also of the whole device, i.e. the universal head of the palletizing robot. The performed study enabled an assessment of the proposed structural design and as such was a basis for introduction of the necessary particular modifications in order to obtain the optimal design within that scope. The presented modelling procedure is universal and can be applied to different-type robot heads.

Acknowledgement

The research was supported by the statutory resources allowed to the Department of Applied Mechanics, Lublin University of Technology as "The Grant for Young Researchers" No. 30/MN/2014.

References

1. Abaqus 6.13 analysis user's manual, Dassault Systèmes, 2013.
2. Abdou G., Lee E.: Physical model for robotics palletization. Computers in Industry 1991;16(3):255–266, http://dx.doi.org/10.1016/0166-3615(91)90063-F.
3. Balasubramanian R.: The pallet loading problem: A survey. International Journal of Production Economics, 1992;28(2):217–225, http://dx.doi.org/10.1016/0925-5273(92)90034-5.
4. Belforte G., Deboli R., Gay P., Piccarolo P., Ricauda Aimonino D.: Robot Design and Testing for Greenhouse Applications. Biosystems Engineering 2006;95(3):309–321, http://dx.doi.org/10.1016/j.biosystemseng.2006.07.004.
5. Ehab Ellobody, Ran Feng and Ben Young: Finite Element Analysis and Design of Metal Structures. Butterworth-Heinemann, Waltham, USA, 2014.
6. Ferdynus M.: An energy absorber in the form of a thin-walled column with square cross-section and dimples. Eksploatacja i Niezawodnosc – Maintenance and Reliability 2013;3(15):253-258.
7. Friedel Hartmann Casimir Katz: Structural Analysis with Finite Elements. Springer-Verlag Berlin Heidelberg 2007.
8. Guo-Qiang Li and Jin-Jun Li: Advanced: Analysis and Design of Steel Frames. John Wiley & Sons Ltd, The Atrium, Southern Gate, Chichester, West Sussex, England, 2007.
9. Guo-Qiang Li, Jin-Jun Li: Advanced Analysis and Design of Steel Frames. John Wiley & Sons Ltd, The Atrium, Southern Gate, Chichester, 2007, http://dx.doi.org/10.1002/9780470319949.
10. Hernan M.: An introduction to Automated Palletizing. Anderson Technical Services, Ohio 2000.
11. Kathryn A. Dowsland, William B. Dowsland: Invited review. Packing problems. European Journal of Operational Research 1992;56(1):2–14, http://dx.doi.org/10.1016/0377-2217(92)90288-K.
12. Khennane A.: Introduction to Finite Element Analysis Using MATLAB® and Abaqus. Taylor & Francis Group, LLC, Boca Raton, 2013, http://dx.doi.org/10.1201/b15042.
13. Morecki A.: Podstawy robotyki. Teoria i elementy manipulatorów i robotów (in Polish). WNT, Warsaw 1999.
14. Nestor E. and Nava R. (eds): Advanced Mechanics in Robotic Systems. Springer-Verlag London Limited 2011.
15. Olszewski M.: Manipulatory i roboty przemysłowe (in Polish). WNT, Warsaw 1985.
16. Peter Marti: Theory of structures. Fundamentals framed structures, plates and shells. Wilhelm Ernst & Sohn, Verlag für Architektur und technische Wissenschaften GmbH & Co. KG, Berlin, Germany, 2013, http://dx.doi.org/10.1002/9783433602638.
17. Rakowski G., Kacprzyk Z.: Metoda elementów skończonych w mechanice konstrukcji (in Polish). Warsaw University of Technology Press, Warsaw 2005.
18. Rusiński E., Czmochowski J., Smolnicki T.: Zaawansowana metoda elementów skończonych w konstrukcjach nośnych (in Polish). Wroclaw University of Technology Press, Wroclaw 2000.
19. Yaohua He, Yong Wu, Robert de Souza: A global search framework for practical three-dimensional packing with variable carton orientations. Computers & Operations Research 2012;39:2395–2414, http://dx.doi.org/10.1016/j.cor.2011.12.007.
20. Yu-Qiu Long, Song Cen and Zhi-Fei Long: Advanced Finite Element Method in Structural Engineering. Springer-Verlag GmbH Berlin Heidelberg, 2009, http://dx.doi.org/10.1007/978-3-642-00316-5.

Marek CHODURSKI
Department of Applied Mechanics, Lublin University of Technology
Nadbystrzycka 36, 20–618 Lublin, Poland

Hubert DĘBSKI
Department of Machine Design and Mechatronics, Lublin University of Technology
Nadbystrzycka 36, 20-618 Lublin, Poland

Sylwester SAMBORSKI
Andrzej TETER
Department of Applied Mechanics, Lublin University of Technology
Nadbystrzycka 36, 20–618 Lublin, Poland

E-mail: chodurski@wp.pl, h.debski@pollub.pl, s.samborski@pollub.pl, a.teter@pollub.pl

Article citation info:
ZAITSEVA E, LEVASHENKO V, KOSTOLNY J. Application of logical differential calculus and binary decision diagramin importance analysis. Eksploatacja i Niezawodnosc – Maintenance and Reliability 2015; 17 (3): 379–388, http://dx.doi.org/10.17531/ein.2015.3.8.

Elena ZAITSEVA
Vitaly LEVASHENKO
Jozef KOSTOLNY

APPLICATION OF LOGICAL DIFFERENTIAL CALCULUS AND BINARY DECISION DIAGRAMIN IMPORTANCE ANALYSIS

ZASTOSOWANIE LOGICZNEGO RACHUNKU RÓŻNICZKOWEGO ORAZ BINARNEGO DIAGRAMU DECYZYJNEGO W ANALIZIE WAŻNOŚCI

System availability evaluation includes different aspects of system behaviour and one of them is the importance analysis. This analysis supposes the estimation of system component influence to system availability. There are different mathematical approaches to the development of this analysis. The structure function based approach is one of them. In this case system is presented in form of structure function that is defined the correlation of system availability and its components states. Structure function enables one to represent mathematically a system of any complexity. But computational complexity of structure function based methods is time consuming for large-scale system. Decision of this problem for the calculation of importance measures can be realized based on application of two mathematical approaches. One of them is Direct Partial Boolean Derivative. New equations for calculating the importance measures are obtained in terms of these derivatives. Other approach is Binary Decision Diagram (BDD), which supports efficient manipulation of Boolean algebra. In this paper new algorithms for calculating of importance measures by Direct Partial Boolean Derivative based on BDD are proposed. The experimental results of comparison these algorithms with other show the efficiency of new algorithms for calculating Direct Partial Boolean Derivative and importance measures.

Keywords: *decision diagram, importance analysis, logical differential calculus, reliability engineering.*

Ocena gotowości systemu, analiza czułości, miary ważności oraz optymalna konstrukcja to istotne zagadnienia, które stały się obiektem badań z zakresu inżynierii niezawodności. Istnieją różne podejścia matematyczne do owych problemów. Jednym z nich jest podejście oparte na funkcji struktury. Funkcja struktury umożliwia analizę systemów o wszelkim stopniu złożoności. Jednakże, w przypadku sieci o dużej skali, złożoność obliczeniowa metod opartych na funkcji struktury sprawia, że metody te są czasochłonne. W przedstawionej pracy proponujemy wykorzystanie dwóch metod matematycznych analizy ważności. Pierwszą z nich jest bezpośrednia cząstkowa pochodna boole'owska, w kategoriach której opracowano nowe równania do obliczania miar ważności. Drugą jest binarny diagram decyzyjny, który wspiera efektywną manipulację na wyrażeniach algebry Boole'a. W artykule zaproponowano dwa algorytmy służące do obliczania bezpośredniej cząstkowej pochodnej boole'owskiej w oparciu o binarny diagram decyzyjny funkcji struktury. Wyniki eksperymentów wykazują skuteczność nowo opracowanych algorytmów w obliczaniu bezpośredniej cząstkowej pochodnej boole'owskiej oraz miar ważności.

Słowa kluczowe: *diagram decyzyjny, analiza ważności, logiczny rachunek różniczkowy, inżynieria niezawodności.*

1. Introduction

A mathematical representation and description or creation of mathematical model of the initial object is an important step in reliability/availability analysis. There are some types of such mathematical models in reliability engineering. As a rule the mathematical model type is conditioned by mathematical method that is used for system availability or reliability estimates. One of mathematical model is the structure function of a system that is defined by one-to-one mapping of system state and states of the system components. The structure function can be interpreted as Boolean function if the initial system has two possible states as functioning and failure only and the system analysed in the stationary state [4, 32]. Therefore mathematical methods of Boolean algebra can be used for the structure function analysis and as result for estimation of system availability. There are a lot of algorithms for the calculation of special indices and measures in reliability engineering based on Boolean algebra methods. Some of them are *Importance Measures* (IMs).

IMs were introduced by Birnbaum in [6]. These measures express the contribution of a component state to system reliability/availability. At the present time there are different types of IMS that allows investigating different aspects of the influence of appointed component state change to behaviour of system reliability or availability. Every system component has a measure of its importance to the system functioning and failure according to values of IMs, that are calculated for every component. IMs have been widely used for identifying a system's weakness and supporting system improvement activities from design perspective. With the importance values of all components, proper actions can be taken on the weakest component to improve system availability at minimal cost or effort.

Detailed analysis and comparison of IMs are presented, for example, in papers[8, 13, 19, 25]. Different mathematical approaches are used and developed for calculating IMs, some of which are Boolean methods [3, 8, 5], Markov model [12], minimal cuts/paths set methods [11, 19], and Logical Differential Calculus [35]. In this paper, we develop a method for computing IMs based on Logical Differential Calculus with the application of *Binary Decision Diagram* (BDD).

Logical Differential Calculus is a mathematical approach that permits to investigate changes in Boolean function depending on changes of its variables values [1, 33]. Therefore, this tool can be used to evaluate the influence of every system component state change on the system performance level [24, 32, 37]. In this paper the Direct Partial Boolean Derivatives are used for the development of algorithms for the estimation of system availability. However, the Logical Differential Calculus methods and Direct Partial Boolean Derivatives in particular are characterized by high computational complexity that increases depending on the number of system components. In Boolean algebra there are some tools to decide this problem and one of them is BDD. A BDD is one of the more effective methods for the representation of a Boolean function of large dimensions[1].

A BDD is used not only in Boolean algebra. A BDD is widely and efficiently used in reliability analysis[14, 15, 16, 28]. Methods for transformation of a Fault Tree to the ordered BDD (OBDD) are proposed in papers [17, 28]. These methods permit to substantiate the correct application of OBDD in reliability analysis. The development of these methods and OBDD use for other problems in reliability analysis has been proposed in a lot of papers. For example, new algorithm for the manipulation of series and parallel systems based on BDD are investigated in [31]. The paper authors [18, 21, 22, 23] consider the OBDD application for reliability analysis of dynamic, phased-mission and networking systems.

The computation of IMs by BDD is considered in papers [8] and[14]. Authors of paper [14] investigated IMs definitions in terms of OBDD. In papers [14] and [22] similar algorithms for the calculation of IM as Birnbaum Importance are proposed based on equal interpretation of this measure definition/equation. The Birnbaum Importance is calculated directly using the OBDD. But these algorithms can be used for the OBDD only.

The combination of two mathematical tools for IMs computation. In this paper we develop the results that have been considered in [31, 37] for BDD. The strong evidence of Logical Differential Calculus application in importance analysis is considered in [37] and new equations for computation of the IMs as Structural Importance, Birnbaum Importance and Criticality Importance in the terms of Logical Differential Calculus have been are proposed in the paper [37]. In this paper we use these equations for the development a new BDD-based approach. We compare of IMs values calculated by the new algorithms and classical definition of IMs (these definition are in [3] for Structural Importance and in [6, 12] for Birnbaum Importance). New algorithms allow obtaining the IMs values that are equal with the IMs values computed by the definitions in [3, 6, 12]. Therefore the principal step of the new approach for the calculation of IM presented in this paper is the application of Logical Differential Calculus, in particular Direct Partial Boolean Derivatives that have been considered in [1, 33, 37]. Two algorithms for the calculation of Direct Partial Boolean Derivatives are proposed in this paper and compared with alternative algorithms.

The remainder of the work is organized as follows. Section 2 introduces concepts of the system structure function, Logical Differential Calculus and BDD. In Section 3 the calculation of IMs by Logical Differential Calculus is described. In this section the definitions of IMs in terms of Logical Differential Calculus are considered. Two algorithms for the IMs quantification based on BDD are considered in this section too. These algorithms are founded on two mathematical tools: Logical Differential Calculus and BDD. A benchmark study is presented to illustrate the proposed algorithms.

2. Mathematical background

2.1. The system structure function

Consider the mathematical model of the system of n components. The component state is denoted asx_i ($i = 1, \dots, n$). The value $x_i = 1$ corresponds to the operable state of the i-th component, and $x_i = 0$, to its failure.Every system component is characterized by probabilities of its states. Theprobability of i-th component failure is:

$$q_i = \Pr\{x_i = 0\}. \tag{1}$$

Then, the probability of operability of the i-th component is defined as:

$$p_i = \Pr\{x_i = 1\}. \tag{2}$$

Consider the system in stationary state. The system availability in stationary state is represented mathematically by the structure function[4, 27]:

$$\phi\,(x) = \phi(x_1, \dots, x_n):\quad \{0, 1\}^n \rightarrow \{0, 1\}, \tag{3}$$

where the vector $x = (x_1, \dots, x_n)$ is the vector of the system components states.

Note, the structure function (3) can be interpreted as Boolean function. As a rule, a coherent system is investigated in reliability engineering. Such system will be considered in this paper. The structure function of a coherent system has the following assumptions [6]:

(a) The system and its components have two states: up (working) and down (failed);
(b) All system components are relevant to the system;
(c) The system structure function is monotone non-decreasing: $\phi(x_1, \dots, 1, \dots, x_n) \neq \phi(x_1, \dots, 0, \dots, x_n)$;
(d) The failure and repair rate of the components are constant;
(e) Repaired components are as good as new.

Principal indices and measures of the system can be calculated based on the structure function. The one of them is the system unavailability that is the probability of the system failure[27]:

$$U = \Pr\{\phi(x) = 0\} \tag{4}$$

and the system availability that is probability of the system functioning state:

$$A = \Pr\{\phi(x) = 1\}. \tag{5}$$

The system unavailability and availability correlate by the equation:

$$U + A = 1$$

The system unavailability (4) and availability (5) are calculated based on every system component state x_i probabilities (1) and (2).For example, the structure function of the system in Fig.1 of 4 components is defined as:

$$\phi\,(x) = \mathrm{AND}(x_1, \mathrm{OR}(x_2, \mathrm{AND}(x_3, x_4))) = x_1 \wedge (x_2 \wedge (x_3 \wedge x_4)). \tag{6}$$

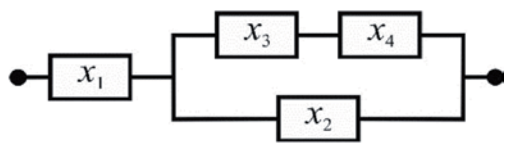

Fig. 1. The series-parallel system example

The system availability is calculated according to (5) taking into account the truth table of the structure function or its canonical DNF:

$$\phi(x) = x_1\overline{x}_2x_3x_4 \vee x_1x_2\overline{x}_3\overline{x}_4 \vee x_1x_2\overline{x}_3x_4 \vee x_1x_2x_3\overline{x}_4 \vee x_1x_2x_3x_4$$

and the system availability is calculated according to (5):

$$A = p_1q_2p_3p_4 + p_1p_2q_3q_4 + p_1p_2q_3p_4 + p_1p_2p_3q_4 + p_1p_2p_3p_4 = p_1p_3p_4 + p_1p_2 - p_1p_2p_3p_4. \quad (7)$$

The system unavailability (4) and availability (5) are important measures, but these measures don't allow to investigate all aspect of the system availability. Therefore other measures must be defined that permit to estimate of the system behavior in point of view of reliability analysis. It can be, for example, IMs or other indices. The use of these measures and indices are caused the development of special methods and algorithms for these estimations. There are different mathematical approaches that are used for development and calculation of reliability indices and measures. And one of them are based on Boolean algebra, because the structure function (3) can be interpreted as a Boolean function. Two mathematical tools will be used in this paper: BDD and Logical Differential Calculus.

A BDD is a graphical form of a Boolean function [1] that is efficiency for the representation and analysis of a Boolean function of large dimension. The second tool is the Logical Differential Calculus [2, 10, 33]. Mathematical methods of Logical Differential Calculus permit to investigate the influence of a variable value change to the Boolean function value. In papers[24, 32, 37] some methods and algorithms of applying Logical Differential Calculus in reliability engineering are considered. In this case the system availability agrees with a Boolean function value and the i-th component state is interpreted as the i-th variable value. Consider these tools below.

2.2. Logical Differential Calculus in Reliability Analysis

The application of Logical Differential Calculus in reliability analysis has been considered in [24, 32, 37]. Authors of these papers use Boolean Derivative (Boolean Difference).In this paper we propose to use other derivative that allows analysis of the influence of variable value change to a function value in more detail. It is Direct Partial Boolean Derivative.

Definition 1. The Direct Partial Boolean Derivative of the function $\phi(\boldsymbol{x})$ with respect to variable x_i reflects the fact of changing the function from j to $\overline{j}$ when the value of variable x_i changes from s to $\overline{s}$ [34]:

$$\partial\varphi(j \to \overline{j})/\partial x_i(s \to \overline{s}) = \begin{cases} 1, \text{ if } \varphi(s_i, \boldsymbol{x}) = j \text{ and } \varphi(\overline{s}_i, \boldsymbol{x}) = \overline{j} \\ 0, \text{ other} \end{cases} \quad (8)$$

where $\phi(s_i, x) = \phi(x_1,\dots, x_{i-1}, s, x_{i+1},\dots, x_n)$,$s, j \in \{0, 1\}$; $=1-j$, $=1-s$; and $\equiv$ is the symbol of equivalence operation.

Direct Partial Boolean Derivatives allows mathematical representationof a system fault that is caused by the i-th system component failure by derivatives $\partial\varphi(1 \to 0)/\partial x_i(1 \to 0)$ and $\partial\varphi(1 \to 0)/\partial x_i(0 \to 1)$. Derivatives $\partial\varphi(0 \to 1)/\partial x_i(0 \to 1)$ and $\partial\varphi(0 \to 1)/\partial x_i(1 \to 0)$ describe the system renewal if the i-th component repaired

Direct Partial Boolean Derivative of a coherent system has the following properties for monotone function [29, 37]:

$$\partial\varphi(1 \to 0)/\partial x_i(0 \to 1) = \partial\varphi(0 \to 1)/\partial x_i(1 \to 0) = 0, \quad (9)$$

$$\partial\varphi(0 \to 1)/\partial x_i(0 \to 1) = \overline{\partial\varphi(1 \to 0)/\partial x_i(1 \to 0)}\,. \quad (10)$$

Because the structure function of a coherent system $\phi(\boldsymbol{x})$ is monotone (assumption c) we will investigate the derivatives of a system fault $\partial\varphi(1 \to 0)/\partial x_i(1 \to 0)$ and renewal $\partial\varphi(0 \to 1)/\partial x_i(0 \to 1)$. Therefore the denotation will be used for these derivatives below:

$$\partial\phi(\boldsymbol{x})/\partial x_i = \partial\varphi(0 \to 1)/\partial x_i(0 \to 1) = \overline{\partial\varphi(1 \to 0)/\partial x_i(1 \to 0)}$$

and the Direct Partial Boolean Derivative $\partial\phi(\boldsymbol{x})/\partial x_i$is calculated as[34, 37]:

$$\partial\varphi(\boldsymbol{x})/\partial x_i = \varphi(1_i, \boldsymbol{x}) \wedge \overline{\varphi(0_i, \boldsymbol{x})}\,. \quad (11)$$

Direct Partial Boolean Derivative (11) permits us to determine the boundary states of a system for which the change of the i-th component state cause the change of the system availability. Nonzero values of the derivatives indicate the system states (the vector of system components states) for which the i-th component fault causes the system failure (Fig. 2).

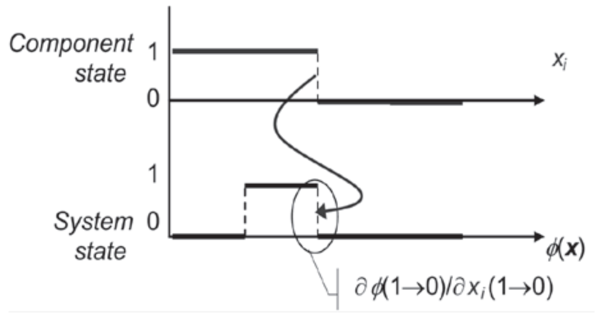

Fig. 2. The interpretation of Direct Partial Boolean Derivative

For example, consider the system in Fig.1 with the structure function (6). The structure function truth table of this system and Direct Partial Boolean Derivatives with respect to variable x_i (i =1, 2, 3, 4) are shown in Table 1. Note, the symbol "*" in this table marks the state vectors for which derivatives don't exist. The nonzero values of derivatives indicate the boundary states of the system. These states are defined by the vector states:

- for the first component $\boldsymbol{x}$= (<u>1↔0</u>, 0, 1, 1), $\boldsymbol{x}$ = (<u>1↔0</u>, 1, 0, 0), $\boldsymbol{x}$ = (<u>1↔0</u>, 1, 0, 1), $\boldsymbol{x}$ = (<u>1↔0</u>, 1, 1, 0), $\boldsymbol{x}$ = (<u>1↔0</u>, 1, 1, 1);
- for the second component $\boldsymbol{x}$ = (1, <u>1↔0</u>, 0, 0), $\boldsymbol{x}$ = (1, <u>1↔0</u>, 0, 1), $\boldsymbol{x}$ = (1, <u>1↔0</u>, 1, 0);
- for the third component$\boldsymbol{x}$ = (1, 0, <u>1↔0</u>, 1);
- for the third component $\boldsymbol{x}$ = (1, 0, 1, <u>1↔0</u>).

Direct Partial Boolean Derivative with respect to the first variable x_1 has 5 nonzero values that indicate boundary states. In this case, astate change of the first component influences the system availability. Vector state $\boldsymbol{x}$= (<u>1↔0</u>, 0, 1, 1)indicates that the first component failure causes the system failure if the second component isn't functioning and the third and forth components are working. Vector states$\boldsymbol{x}$ = (<u>1↔0</u>, 1, 0, 0),$\boldsymbol{x}$ = (<u>1↔0</u>, 1, 0, 1), $\boldsymbol{x}$ = (<u>1↔0</u>, 1, 1, 0), $\boldsymbol{x}$ = (<u>1↔0</u>, 1, 1, 1) define the system failure for any states of the third and the forth components if the second component is functioning. Other derivatives in Table 1 have similar meanings.

The algorithms for calculating Direct Partial Boolean Derivatives have been considered in numerous papers. Trivial algorithm has been considered by Akers in [2]. This result has been developed by Bochmann, Posthoff and Steinbach [7, 26]. In paper [30] a parallel version of these algorithms has been proposed. The calculation of Boolean Derivative (Boolean Difference) based on the BDD has been investigated in [24]. However, this algorithm cannot be used for Direct

Table 1. The structure function and Direct Boolean Derivatives of the series-parallel system (Fig. 1)

$x_1\ x_2\ x_3 x_4$	$\phi(\boldsymbol{x})$	$\partial\phi(\boldsymbol{x})/\partial x_1$	$\partial\phi(\boldsymbol{x})/\partial x_2$	$\partial\phi(\boldsymbol{x})/\partial x_3$	$\partial\phi(\boldsymbol{x})/\partial x_4$
0 0 0 0	0	*	*	*	*
0 0 0 1	0	*	*	*	0
0 0 1 0	0	*	*	0	*
0 0 1 1	0	*	*	0	0
0 1 0 0	0	*	0	*	*
0 1 0 1	0	*	0	*	0
0 1 1 0	0	*	0	0	*
0 1 1 1	0	*	0	0	0
1 0 0 0	0	0	*	*	*
1 0 0 1	0	0	*	*	0
1 0 1 0	0	0	*	0	*
1 0 1 1	1	1	*	1	1
1 1 0 0	1	1	1	*	*
1 1 0 1	1	1	1	*	0
1 1 1 0	1	1	1	0	*
1 1 1 1	1	1	0	0	0

Partial Boolean Derivatives calculation. Therefore the algorithm for the calculation of Direct Partial Boolean Derivatives based on BDD isn't developed.

2.3. Binary Decision Diagram

Consider some background of BDD before the development of algorithm for the calculation of Direct Partial Boolean Derivatives based on BDD.

BDD is a widely used tool for reliability analysis. Some methods for reliability analysis based on this tool are discussed in papers [14, 15, 16]. BDD is based on a disjoint decomposition of Boolean function called the Shannon expansion [14]. This expansion for the structure function (3) can be defined as:

$$\varphi(\boldsymbol{x}) = x_i \wedge \varphi(1_i, \boldsymbol{x}) \vee \bar{x}_i \wedge \varphi(0_i, \boldsymbol{x}) \,. \tag{12}$$

In order to express Shannon decomposition concisely, the if-then-else (*ite*) format[9] is defined as:

$$\phi(\boldsymbol{x}) = ite(x_i{=}0,\ \phi(0_i, \boldsymbol{x}),\ \phi(1_i,\ \boldsymbol{x})). \tag{13}$$

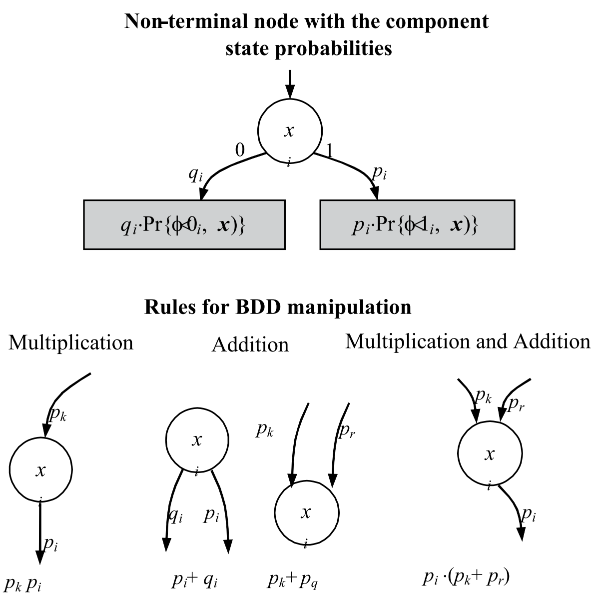

Fig. 3. Interpretation of component state and basic computational rules in BDD

BDD of system

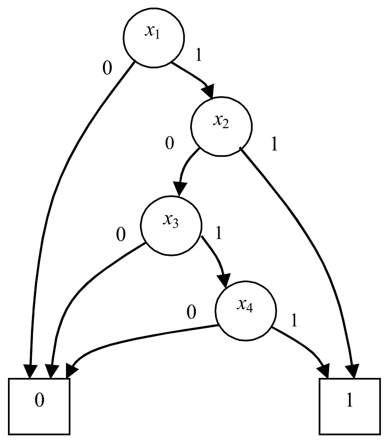

The pseudo-code of the BDD

```
(x) = ite(x1, 0, L)
  L = ite(x2, M, 1)
  M = ite(x3, 0, N)
  N = ite(x4, 0, 1)

or

(x) = ite(x1,0,ite(x2,ite(x3,0,
                  ite(x4,0,1)),1))
```

Fig. 4. Graphical and software implementation of the BDD of system

A BDD is a directed acyclic graph of a Boolean function representation [9]. For structure function (3), this graph has two terminal nodes, labelled 0 and 1. Each non-terminal node is labelled with a structure function variable x_i and has two outgoing edges. The left edge is labelled "0" and represents the fail state of system component. The other outgoing edge is labelled "1" and represents the operational state of a system component.

Terminal nodes of the BDD correspond to the system state. Non-terminal node outgoing edges are interpreted as component states. The probabilistic interpretation of the system assumes that every edge from the node to which the variable x_i is assigned with the label s_i is marked by the i-th component state probability p_i or q_i (Fig. 3). The node in this diagram assigned with the i-th variable x_i, and the outgoing edges corresponding to $\phi(1_i, \boldsymbol{x})$ and $\phi(0_i, \boldsymbol{x})$that correspond to the Shannon decomposition (12). This equation in arithmetic form is the following:

$$\varphi(\boldsymbol{x}) = x_i \cdot \varphi(1_i, \boldsymbol{x}) + \bar{x}_i \cdot \varphi(0_i, \boldsymbol{x}) - \left(x_i \cdot \varphi(1_i, \boldsymbol{x})\right) \cdot \left(\bar{x}_i \cdot \varphi(0_i, \boldsymbol{x})\right) = x_i \cdot \varphi(1_i, \boldsymbol{x}) + \bar{x}_i \cdot \varphi(0_i, \boldsymbol{x})$$

Node probability is calculated using the equation [14]:

$$\begin{aligned}\Pr\{\varphi(\boldsymbol{x})\} &= \Pr\left\{x_i \cdot \varphi(1_i, \boldsymbol{x})\right\} + \Pr\left\{\bar{x}_i \cdot \varphi(0_i, \boldsymbol{x})\right\} = \\ &= p_i \cdot \Pr\left\{\varphi(1_i, \boldsymbol{x})\right\} + q_i \cdot \Pr\left\{\varphi(0_i, \boldsymbol{x})\right\}\end{aligned} \,. \tag{14}$$

Note that the paths from the root to the terminal node in a BDD are mutually disjoint. Therefore the system availability can be calculated based on (12) and (14) for the system that is represented in form of the BDD:

$$A = \Pr\{\varphi(\boldsymbol{x}) = 1\} = p_i \cdot \Pr\left\{\varphi(1_i, \boldsymbol{x}) = 1\right\} + q_i \cdot \Pr\left\{\varphi(0_i, \boldsymbol{x}) = 1\right\} \tag{15}$$

and conforms with the probability of the sum of paths from the root node to the terminal node "1". Rules for this calculation are presented in Fig. 3. The system unavailability is calculated similarly but paths from the root node to the terminal node labelled “0” are analysed in this case.

For example, consider a system 2-out-of-3 with structure function (6). The system is defined by the BDD (Fig.4). The calculation of the system availability and unavailability is implemented based on two sub-diagrams. Every diagram is the sum of paths from the BDD top to one of the terminal nodes (Fig.5).

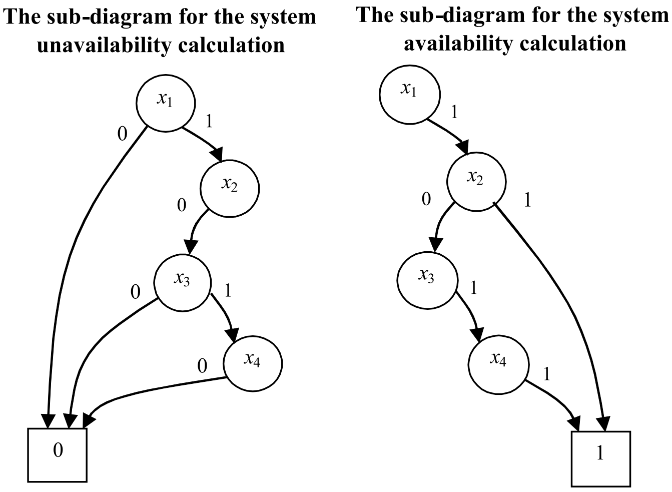

Fig. 5. Sub-diagrams for the system availability and unavailability calculation

According to the sub-diagrams in Fig.5 the system availability and unavailability are calculated as:

$$A = p_1(p_2 + q_2p_3p_4) = p_1p_2 + p_1p_3p_4\text{-}p_1p_2p_3p_4 \quad (16)$$

$$U = q_1 + p_1q_2(q_3 + p_3q_4). \quad (17)$$

The system availability (16) is equal to the system availability (7) that was defined according to typical rules. Therefore, BDD can be used for the calculation of the system’s availability and unavailability.

3. Importance Analysis

System’s unavailability (4) and availability (5) are widely used measures in reliability engineering, but these measures do not enable the analysis of a change of the system availability depending on a change of the component states. There are measures for estimating the influence of component states’ changes on system availability called IMs. Importance analysis allows the estimation of influence of every system component breakdown to the system failure. This paper provides new algorithms for importance analysis based on Direct Partial Boolean Derivative and BDD of structure function.

3.1. Importance Measures

Consider some of IMs and calculation algorithms based on on Direct Partial Boolean Derivative.

Structural Importance (SI). The SI is one of the simplest measures in importance analysis and this measure focuses on the topological aspects of a system. According to the definition in papers [3] this measure determines the proportion of working states of a system in which the working of the *i*-th component makes the difference between system failure and operation:

$$SI_i = \frac{\rho_i}{2^{n-1}} \quad (18)$$

where ρ_i is the number of system states when the change in component state results in system failure.

Table 2. SI and MSI indices for the system in Fig. 1

i	ρ_i	$\rho_{i=1}$	SI_i	MSI_i
1	5	5	0.625	1.000
2	3	4	0.250	0.750
3	1	2	0.125	0.500
4	1	2	0.125	0.500

The number ρ_i in [3] is defined by special analysis of values of the structure function, but according to the definition 1 this number can be calculated as the number of nonzero values of the Direct Partial Boolean Derivatives (11) $\partial\phi(\boldsymbol{x})/\partial x_i$.

There is one more definition of SI [37]. It is *Modified Structural Importance* (MSI) that represents the influence of the *i*-th system component failure to system failure:

$$MSI_i = \frac{\rho_i}{\rho_{i=1}} \quad (19)$$

where $\rho_{i=1}$ is the number of system states for which $\phi(1_i,\boldsymbol{x}) = 1$ (it is defined by the structure function (3)).

The values of SI (18) and MSI (19) are presented in Table 2. According to this Table the first system component has maximal influence to the system availability in terms of the system’s topology. The values of the MSI indices show that the first component is dominant in terms of system topology because only this component’sfault causes the system’s failure. The breakdown of the third or the forth component has minimal influence to the system failure according values of SI and MSI (Table 2).

Birnbaum Importance (BI). The BI is one of basic IMs and this measure is defined as the probability that the system is sensitive to inoperative state of the *i*-th system component[19]:

$$BI_i = \Pr\{\varphi(0_i,\boldsymbol{x}) = 0\} - \Pr\{\varphi(1_i,\boldsymbol{x}) = 0\}\ .$$

In paper[37] new equation for the BI calculation has been proposed based on Direct Partial Boolean Derivatives:

$$BI_i = \Pr\{\partial\varphi(x)/\partial x_i = 1\}\ . \quad (20)$$

According to [37] this equation is proofed as:

$$\begin{aligned} I_B(x_i) &= \Pr\left\{\left(\varphi(1_i,\boldsymbol{x}) \wedge \overline{\varphi(0_i,\boldsymbol{x})}\right) = 1\right\} = \Pr\{\varphi(1_i,\boldsymbol{x}) = 1\}\cdot\Pr\left\{\overline{\varphi(0_i,\boldsymbol{x})} = 1\right\} = \\ &= \Pr\{1-\varphi(1_i,\boldsymbol{x}) = 0\}\cdot\Pr\left\{1-\overline{\varphi(0_i,\boldsymbol{x})} = 0\right\} = \Pr\{1-\varphi(1_i,\boldsymbol{x}) = 0\}\cdot\Pr\{1-(1-\varphi(0_i,\boldsymbol{x}) = 0)\} = \\ &= \Pr\{\varphi(0_i,\boldsymbol{x}) = 0\} - \Pr\{\varphi(1_i,\boldsymbol{x}) = 0\}\cdot\Pr\{\varphi(0_i,\boldsymbol{x}) = 0\} \end{aligned}$$

and for a coherent system with a monotonically structure function [29]:

$$\begin{aligned} I_B(x_i) &= \Pr\{\varphi(0_i,\boldsymbol{x}) = 0\} - \Pr\{\varphi(1_i,\boldsymbol{x}) = 0\}\cdot\Pr\{\varphi(0_i,\boldsymbol{x}) = 0\} = \\ &= \Pr\{\varphi(0_i,\boldsymbol{x}) = 0\} - \Pr\{\varphi(1_i,\boldsymbol{x}) = 0 \wedge \varphi(0_i,\boldsymbol{x}) = 0\} = \Pr\{\varphi(0_i,\boldsymbol{x}) = 0\} - \Pr\{\varphi(1_i,\boldsymbol{x}) = 0\}. \end{aligned}$$

For example, the structure function of the system (Table 1) has 5 nonzero values for the derivatives $\partial\phi(\boldsymbol{x})/\partial x_1$, so the first component BI is calculated as:

$$IB_1 = \Pr\{\partial\phi(\boldsymbol{x})/\partial x_1 = 1\} = q_2p_3p_4 + p_2q_3q_4 + p_2q_3p_4 + p_2p_3q_4 + p_2p_3p_4,$$

and for other components:

$$IB_2 = \Pr\{\partial\phi(\boldsymbol{x})/\partial x_2 = 1\} = p_1q_3q_4 + p_1q_3p_4 + p_1p_3q_4.$$

$$IB_3 = \Pr\{\partial\phi(\boldsymbol{x})/\partial x_3 = 1\} = p_1q_2p_4$$

$$IB_4 = \Pr\{\partial\phi(\boldsymbol{x})/\partial x_4 = 1\} = p_1q_2p_3.$$

Therefore SI, MSI and BI indices can be calculated based on Direct Partial Boolean Derivatives.

Criticality Importance (CI). BI (20) describes the influence of a failure of the i-th system component on the system's availability, but doesn't take into account the probability of this component's failure. CI adjusts it and is defined as the probability that the i-th system component is relevant to the system's failure if it has failed [19]:

$$CI_i = BI_i \cdot \frac{q_i}{U}. \tag{21}$$

where BI_i is the i-th system component BI measure (20); q_i is probability of the i-th system failure (1) and U is the system's unavailability (4).

Dynamic Reliability Indices (DRI). DRI have been considered in paper [36]. DRIs allow the estimation of a component relevant to system failure. There are two groups of DRI: *Component Dynamic Reliability Indices* (CDRI) and *Dynamic Integrated Reliability Indices* (DIRI).

CDRI indicates the influence of the i-th component'sfault on the system's failure and is similar to the definition of modified SI, but CDRI includestwo probabilities: (*a*) the probability of the system's failure caused by the i-th component's inoperation and (*b*) the probability of a component failure:

$$CDRI_i = MSI_i \cdot q_i. \tag{22}$$

where $MSI_i$is defined by (19); $q_i$is probability of a component failure (1).

DIRI is the probability of system failure that is caused by one of the system components in-operation (one of n):

$$IDIRI = \sum_{i=1}^{n} ICDRI_i \prod_{\substack{q=1\\q\neq i}}^{n} (1 - ICDRI_q). \tag{23}$$

Therefore SI, MSI, BI, CI, CDRI and DIRI indices can be calculated based on Direct Partial Boolean Derivatives and the development of the algorithm for computation of these derivatives is important step in importance analysis based on quantification estimation of IMs.

3.2. Direct Partial Boolean Derivative Calculation based on BDD

One of possible BDD-basedmethod for calculatingIMs has been presented in [14]. The authors of the paper [14] proposed to define components states by the structure function BDD for computation of IM according to typical equation of IMs. Logical Differential Calculus has been used for calculation of some IMs in [35]. However, the proposed algorithms don't account for specific of the system with two states (available and unavailable).

We develop two algorithms for calculating Direct Partial Boolean Derivative (11) based on BDD of the structure function. These algorithms have identical basic principle: it is construction of the "*tree of paths*" by analyzing the paths from the root to the sink node of the BDD that agrees with conditions:

$$\varphi(0_i, \boldsymbol{x}) = 0 \quad \text{and} \quad \varphi(1_i, \boldsymbol{x}) = 1 \tag{24}$$

Therefore the tree of paths for condition $\phi(0_i, \boldsymbol{x}) = 0$ unites all paths from the root to the sink node 0 that include out coming edges of the non-sink node x_i labelled 0. The tree of paths for the condition $\phi(1_i, \boldsymbol{x}) = 1$ is constructed similarly.

For example, consider the construction of the tree of paths for the series-parallel system by the BDD (Fig. 4). Form the tree of paths of the derivative $\partial\phi(\boldsymbol{x})/\partial x_2$ for the condition $\phi(0_2, \boldsymbol{x}) = 0$ (Fig. 6). The variable, on which the derivative is calculated, isn't included in the

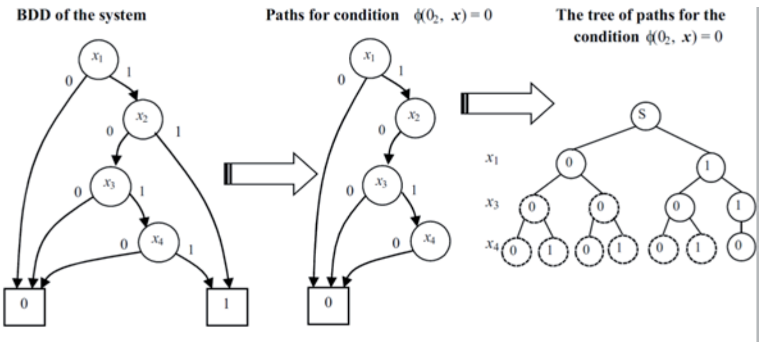

Fig. 6. The tree of paths for condition of the BDD in Fig.4

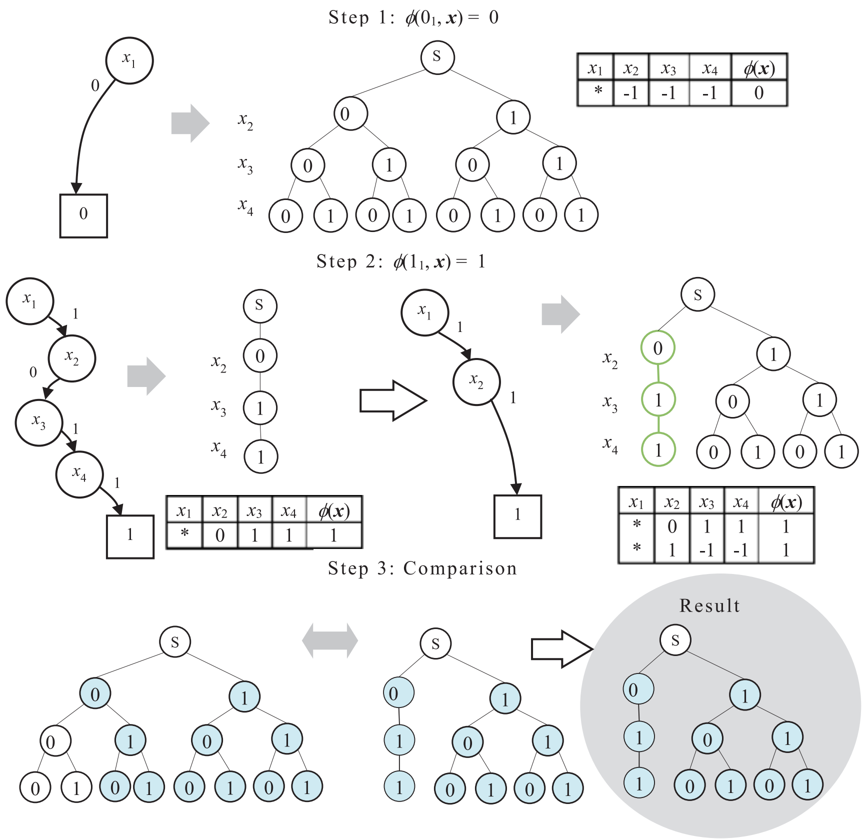

Fig. 7. Example of the Algorithm 1

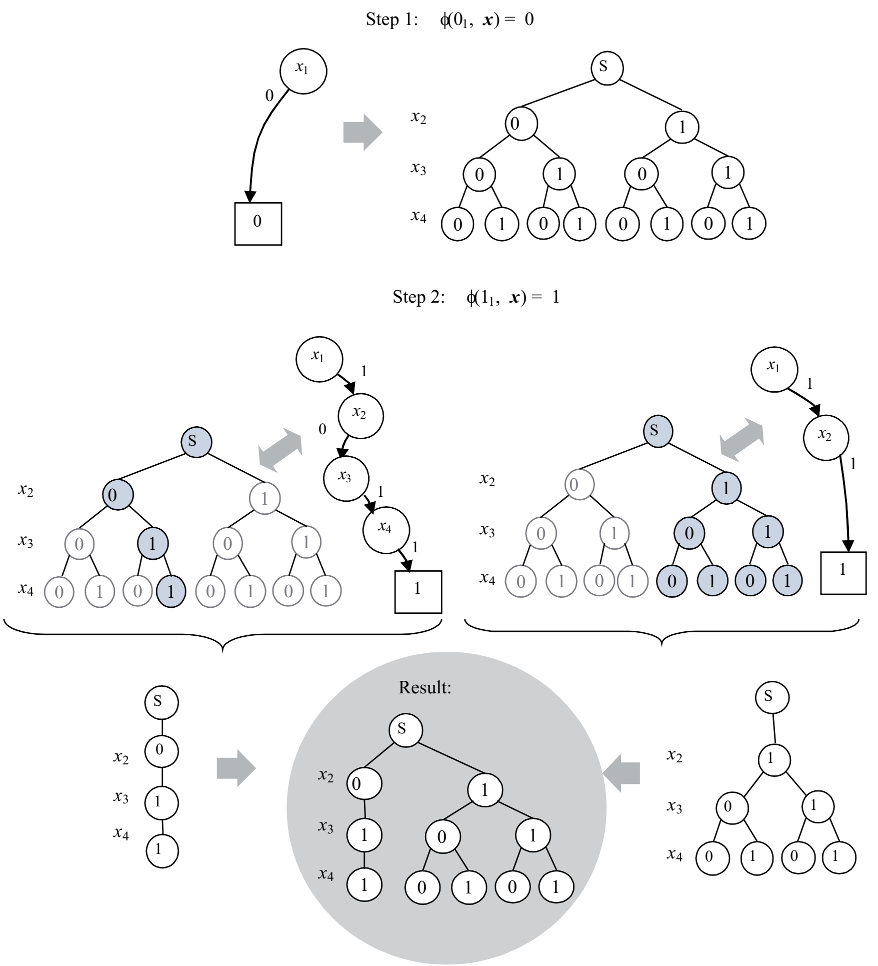

Fig. 8. Example of the Algorithm 2

tree of paths and conforms to the root labelled "S". It is the second variable x_2 in this example. Two paths are analysed for the specified condition (Fig. 6). The first (left) path has value of the first variable as 0 (x_1 = 0) and doesn't include the variablesx_3 and x_4. Therefore these variables(x_3 and x_4) can have any value (these values are indicated in the tree of paths by dotted line). The second path has variable x_1 = 1 and variable $x_3$with two values. In case of x_3= 0 the variable x_4 can have any value because it is absent in this path. But the variable x_4= 0 if x_3= 1. Therefore the tree of paths in Fig. 6 locates all paths for the condition ϕ $(0_2, \boldsymbol{x}) = 0$.

Two algorithms are developed for the Direct Partial Boolean Derivative (11) calculation by the BDD based on the use of the trees of paths.

The *Algorithm 1* has three steps. The tree of paths for the condition $\phi(0_i, \boldsymbol{x}) = 0$ is formed at the *first step*. The tree of paths for the condition $\phi(1_i, \boldsymbol{x}) = 1$ is constructed at the *second step*. The *third step* of the algorithm compares these two trees. The general part of these trees is a decision that is corresponded to non-zero values of the Direct Boolean Derivative (11).

For example, Fig. 7 illustrates the calculation of the Direct Partial Boolean Derivative $\partial\phi(\boldsymbol{x})/\partial x_1$ based on the Algorithm 1 for BDD of the structure function (6) of the series-parallel system in Fig.1 with the structure function (6). The BDD of this function is presented in Fig.4. The *first step* of the algorithm is forming the tree of paths for condition $\phi(0_1, x) = 0$. This tree building is shown in detail for the second variable $\phi(0_2, x)$ = 0above (Fig. 6). The tree for condition $\phi(0_1, x) = 0$ includes all possible values of variables x_2, x_3 and x_4, because the sub-diagram for this condition doesn't include nodes of these variables. The *second step* of the algorithm permits to obtain the tree of paths for condition $\phi(1_1, x) = 1$. This tree includes all paths from the out-coming edge labelled 1 of the first variable x_1 to the sink node 1 of the BDD. The *third step* of the algorithm is comparing two trees that satisfy condition $\phi(0_1, x) = 0$ and $\phi(1_1, x) = 1$ accordingly. The final tree of paths (the algorithm result) includes paths that are equal for two trees. Therefore, the final tree includes 5 paths that are conformed with non-zero values of the derivative $\partial\phi(\boldsymbol{x})/\partial x_1$:$\boldsymbol{x}$= ($\underline{1\leftrightarrow 0}$, 0, 1, 1), $\boldsymbol{x}$ = ($\underline{1\leftrightarrow 0}$, 1, 0, 0), $\boldsymbol{x}$ = ($\underline{1\leftrightarrow 0}$, 1, 0, 1), $\boldsymbol{x}$ = ($\underline{1\leftrightarrow 0}$, 1, 1, 0), $\boldsymbol{x}$ = ($\underline{1\leftrightarrow 0}$, 1, 1, 1).

Algorithm 1 and Algorithm 2 are tested based on the sets of benchmarks LGSynth91 with the tool ABC (A System for Sequential Synthesis and Verification developed by Berkeley Verification and Synthesis Research Center) [20]. This benchmark has the PLA – EXPRESSO format and Table 3 summarizes the selected benchmarks, specifying the number of input variables, the number of output functions, the number of product terms appearing in the benchmark and their analysis for BDDs construction.

Table 3. Benchmark characteristics and analysis for BDD

Benchmark	Input	Output	Product terms	Number of non-terminal nodes in the BDD	Number of variables of the structure function
5xp1	7	10	75	5	14
alu4	14	8	1028	11	163
apex1	45	45	206	9	15
apex3	54	50	280	9	46
apex4	9	19	438	10	136
b12	15	9	431	5	8
bw	5	28	87	6	20
clip	9	5	167	10	68
con1	7	2	9	7	13
cps	24	109	654	19	105
duke2	22	29	87	8	41
e64	65	65	65	10	10
ex1010	10	10	1024	11	459
ex4	128	28	620	10	76
ex5	8	63	256	8	8
inc	7	9	34	7	15
misex1	8	7	32	7	12
misex2	25	18	29	13	13
misex3	14	14	1848	15	1640
misex3c	14	14	305	9	103
pdc	16	40	2810	15	21
rd53	5	3	32	6	15
rd73	7	3	141	8	70
rd84	8	4	256	9	130
sao2	10	4	58	11	76
seq	41	35	1459	13	18
squar5	5	8	32	6	6
Z5xp1	7	10	128	8	8

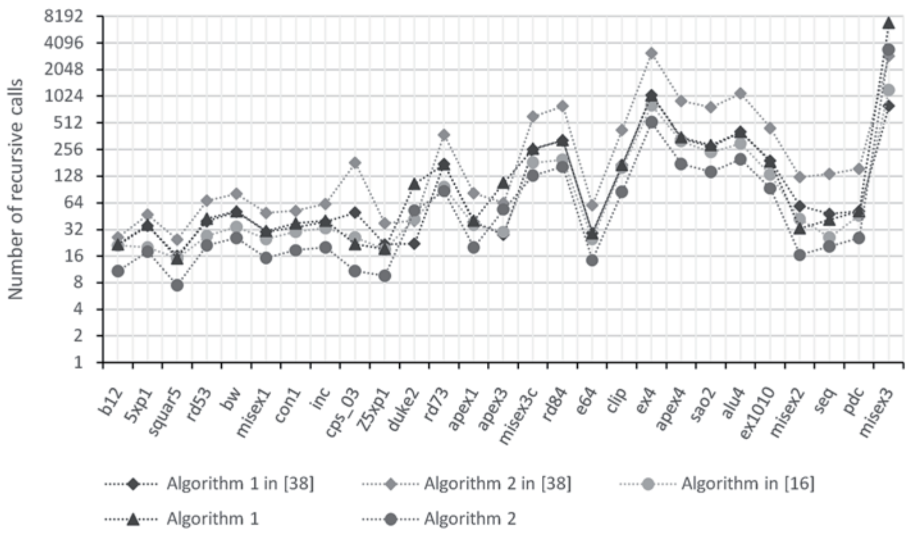

Fig. 9. Comparison of algorithms computational complexity by number of recursive calls

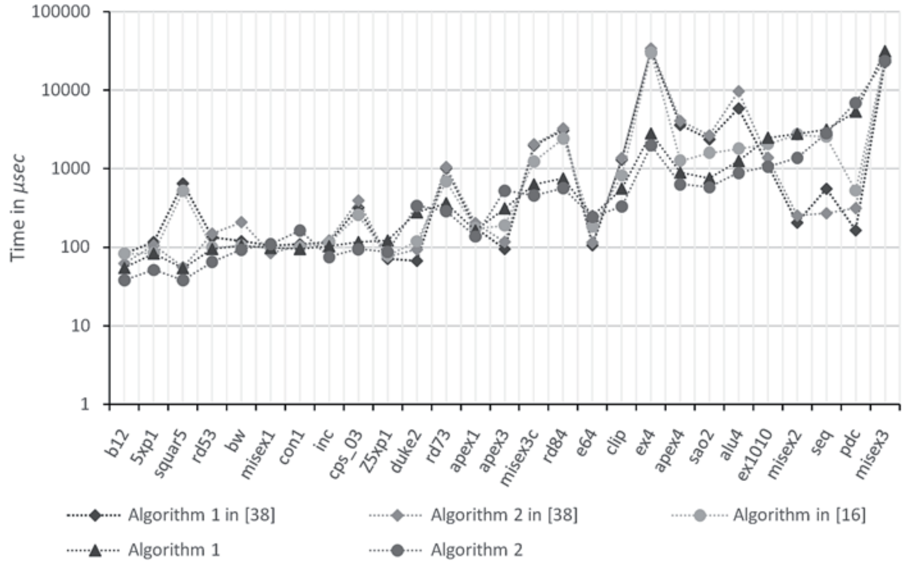

Fig. 10. Comparison of algorithms computational complexity by computational time (in µsec)calls

Table 4. The calculation of indexes SI, SIM, BI, CI, CDRI for benchmark rd84

x_i	q_i	p_i	SI_i [3]	BI_i [6]	CI_i [12]	New algorithm		
						SI_i	BI_i	CI_i
1	0.3	0.47	0.0078125	0.122472	0.0401868	0.0078125	0.122472	0.0401868
2	0.1	0.9	0.0078125	0.095256	0.0104188	0.0078125	0.095256	0.0104188
3	0.4	0.6	0.0078125	0.142884	0.0625129	0.0078125	0.142884	0.0625129
4	0.5	0.5	0.0078125	0.171461	0.0937693	0.0078125	0.171461	0.0937693
5	0.1	0.9	0.0078125	0.095256	0.0104188	0.0078125	0.095256	0.0104188
6	0.3	0.7	0.0078125	0.122472	0.0401868	0.0078125	0.122472	0.0401868
7	0.2	0.8	0.0078125	0.107163	0.0234423	0.0078125	0.107163	0.0234423
8	0.1	0.9	0.0078125	0.095256	0.0104188	0.0078125	0.095256	0.0104188

These benchmarks are used for the comparison, control and examination of two algorithms. In addition these algorithms have been compared with the similar algorithm that has been proposed in [16] and with algorithm proposed in [38]. Experiments permit the computational complexity of the proposed algorithms to be estimated. Computational complexities such as the number of recursive calls of algorithms are shown in Fig. 9 and the t`ime for computation of non-zero values of Direct Partial Boolean Derivatives is presented in Fig. 10.

The analysis of the data in Fig.9 and Fig.10 shows that the two proposed algorithms have similar characteristics but Algorithm 2 has lesser computational complexity, which is well seen in the chart on Fig. 9. Characteristics of the algorithms in [16] and [38] are worse in comparison of proposed algorithms. Therefore, the Algorithm 2 can be used for the calculation of non-zero values of Direct Partial Boolean Derivatives for the structure function preferable. The non-zero values of Direct Partial Boolean Derivatives permit to calculate IMs (18) – (23). It is important that these equations are agree with well know definitions of IMs. Therefore IMs values calculated by the proposed Algorithm 1and Algorithm 2 based on the definitions (18) – (23) are equal IMs values computed by the definition from [3, 6, 12].

For example, consider the benchmark rd84 (Table 3). In the Table 4 SI, BI and CI values are shown that are calculated by new algorithm (Algorithm 2) and traditional algorithm. This Table consists of two parts. The first of them include IMs values that are calculated based on the definitions in papers [3, 6, 12]. IMs values computed by new algorithms are described in the second part of this Table. Note IMs values are equal for two proposed algorithms (Algorithm 1 and Algorithm 2). Therefore IMs values for two different approaches are equal, because new algorithms realize equations for IMs calculation (18), (19) and (21) – (23) that have the mathematical substantiation of the correlation with IMs definitions in [3], [6], [12].

4. Conclusions and Future Work

This work presented an efficient approach to analyze the reliability and importance analysis. This approach can be summarized in following characteristics. First characteristic of proposed approach is possibility of calculating IMs using mathematical apparatus Direct Partial Boolean Derivatives, which is based on new equations for IMs (18) – (23).The background of this approach is the computation of non-zero values of derivatives that are used in these equations of IMs. Next aspect is based on development of new algorithms for calculation of Direct Partial Boolean Derivatives based on BDD, which allows analysis of the function of large dimensions. The last important point of presented work is the introduction an experimental analysis based on BDD algorithms, which are highly efficientlyboth in computational time and storage demand for importance analysis and they also make it possible for us to study practical and large systems. Research based on this approach as sensitivity analysis, importance measures, and optimal design issues of large systems will become more important in the future. Algorithms proposed in this work can be generalized for the non-coherent system. In this case the calculation of IMs will be based on the analysis of two Direct Partial Boolean Derivatives $\partial\varphi(0\to1)/\partial x_i(0\to1)$ and $\partial\varphi(0\to1)/\partial x_i(1\to0)$

. Proposed algorithms can be modified for the integration to IMs [13, 19], which could allow investigating of influence of some system components to reliability or availability of system. These measures will be defined based on the Direct Partial Boolean Derivative with respect to variable vector [36]. All these generalization (for non-coherent system and integrated IMs) can be implemented based on non-important modification of Direct Partial Logic Derivatives. The derivative with respect to variable vector will be exploited for the integrated IMs calculation.

Acknowledgement

This work was partially supported by grant of Scientific Grant Agency of the Ministry of Education of Slovak Republic (Vega 1/0498/14).

References

1. Akers SB. Binary Decision Diagrams. IEEE Transaction on Computers 1978; 27: 509–16, http://dx.doi.org/10.1109/TC.1978.1675141.
2. Akers SB. On a Theory of Boolean Functions. Journal of the Society for Industrial and Applied Mathematics 1959; 7: 487–98, http://dx.doi.org/10.1137/0107041.
3. Armstrong MJ. Reliability-importance and dual failure-mode components. IEEE Transaction on Reliability 1997; 46: 212–21, http://dx.doi.org/10.1109/24.589949.
4. Barlow RE, Proschan F. Importance of system components and fault tree events. Stochastic Processes and their Applications 1975; 3: 153–73, http://dx.doi.org/10.1016/0304-4149(75)90013-7.
5. Beeson S, Andrews JD. Importance measures for noncoherent-system analysis. IEEE Transactions on Reliability 2003; 52: 301–10, http://dx.doi.org/10.1109/TR.2003.816397.
6. Birnbaum ZW. On importance of difference components in a multi-component system. Multi-Variant Anal 2 1969: 581–92.
7. Bochmann D, Posthoff C. Binäre dynamische Systeme. Berlin: Akademie-Verlag; 1981.
8. Borgonovo E. The reliability importance of components and prime implicants in coherent and non-coherent systems including total-order interactions. European Journal of Operational Research 2010; 204: 485–95, http://dx.doi.org/10.1016/j.ejor.2009.10.021.
9. Bryant RE. Graph-Based Algorithms for Boolean Function Manipulation. IEEE Transactions on Computers 1986; C-35: 677–91, http://dx.doi.org/10.1109/TC.1986.1676819.
10. Davio M., J.-P. Deschamps, A. Thayse, Discrete and switching functions. St. Saphorin, Switzerland: Georgi Pub. Co.; New York: McGraw-Hill International Book Co; 1978.
11. Duflot N, Bérenguer C, Dieulle L, Vasseur D. A min cut-set-wise truncation procedure for importance measures computation in probabilistic safety assessment. Reliability Engineering & System Safety 2009; 94: 1827–37, http://dx.doi.org/10.1016/j.ress.2009.05.015.
13. Gao X, Cui L, Li J. Analysis for joint importance of components in a coherent system. European Journal of Operational Research 2007; 182: 282–99, http://dx.doi.org/10.1016/j.ejor.2006.07.022.
14. Chang Y-R, Amari S V, Kuo S-Y. Computing system failure frequencies and reliability importance measures using OBDD. IEEE Transaction on Computers 2004; 53: 54–68, http://dx.doi.org/10.1109/TC.2004.1255790.
15. Chang Y-RY, Huang CY, Kuo S. Performance assessment and reliability analysis of dependable and distributed computing systems based on BDD and recursive merge. Applied Mathematics and Computation 2010; 217: 403–13, http://dx.doi.org/10.1016/j.amc.2010.05.075.
16. Changqian W, Chenghua W. A Method for Logic Circuit Test Generation Based on Boolean Partial Derivative and BDD. 2009 WRI World Congress on Computer Science and Information Engineering 2009; 3: 499–504, http://dx.doi.org/10.1109/CSIE.2009.44.
17. Jung WS, Han SH, Ha J. A fast BDD algorithm for large coherent fault trees analysis. Reliability Engineering & System Safety 2003; 83 (3): 369-374, http://dx.doi.org/10.1016/j.ress.2003.10.009
18. Kim Bjorkman, Solving dynamic flowgraph methodology models using binary decision diagrams, Reliability Engineering & System Safety, 2013; 111: 206-216, http://dx.doi.org/10.1016/j.ress.2012.11.009.
19. Kuo W, Zhu X. Importance Measures in Reliability, Risk, and Optimization. Chichester, UK: John Wiley & Sons, Ltd; 2012, http://dx.doi.org/10.1002/9781118314593.
20. Laboratory CB and EA. The Benchmark Archives at CBL 2013.
21. Liudong Xing, Akhilesh Shrestha, Yuanshun Dai, Exact combinatorial reliability analysis of dynamic systems with sequence-dependent failures, Reliability Engineering & System Safety 2011; 96 (10): 1375-1385, http://dx.doi.org/10.1016/j.ress.2011.05.007.
22. Liudong Xing, An Efficient Binary-Decision-Diagram-Based Approach for Network Reliability and Sensitivity Analysis, IEEE Transactions on System, Man and Cybernetics – Part A: System and Humans 2008; 38(1).
23. Liudong Xing, Gregory Levitin, BDD-based reliability evaluation of phased-mission systems with internal/external common-cause Reliability Engineering & System Safety 2013; 112:145-153, http://dx.doi.org/10.1016/j.ress.2012.12.003.
24. Moret BME, Thomason MG. Boolean Difference Techniques for Time-Sequence and Common-Cause Analysis of Fault-Trees. IEEE Transaction on Reliability 1984; R-33: 399–405, http://dx.doi.org/10.1109/TR.1984.5221879.
25. Nokland TE, Aven T. On selection of importance measures in risk and reliability analysis. International Journal of Performability Engineering 2013; 9: 133–47.
26. Posthoff C, Steinbach B. Logic Functions and Equations. Binary Models for Computer Science 2004, http://dx.doi.org/10.1007/978-1-4020-2938-7.
27. Rausand M, Hyland A, editors. System Reliability Theory. Hoboken, NJ, USA: John Wiley & Sons, Inc.; 1994, http://dx.doi.org/10.1002/9780470316900.
28. Rauzy A. Mathematical foundations of minimal cut sets. IEEE Transactions on Reliability 2001; 50: 389–96, http://dx.doi.org/10.1109/24.983400.
29. Ryabinin, IA. and Parfenov, YuM., Determination of "Weight" and "Importance" of Individual Elements at Reliability Estimation of a Complex System. Energetics Transport 1978, 6: 22–32.
30. Shmerko V, Lyshevski S, Yanushkevich S. Computer Arithmetics for Nanoelectronics. CRC Press 2009, http://dx.doi.org/10.1201/b15950.

31. Shumin Li, Shubin Si, Hongyan Dui, Zhiqiang Cai, Shudong Sun, A novel decision diagrams extension method, Reliability Engineering & System Safety 2014; 126: 107-115, http://dx.doi.org/10.1016/j.ress.2014.01.017.
32. Schneeweiss WG. A short Boolean derivation of mean failure frequency for any (also non-coherent) system. Reliability Engineering & System Safety 2009; 94: 1363–7, http://dx.doi.org/10.1016/j.ress.2008.12.001.
33. Talansev A. Analysis and synthesis of some electrical circuits by means of special logical operators. Automation and Remote Control 1959; 20; 898–907.
34. Tucker JH, Tapia MA, Bennett AW. Boolean Integral Calculus for Digital Systems. IEEE Transactions on Computers 1985; C-34; 78–81, http://dx.doi.org/10.1109/TC.1985.1676517.
35. Zaitseva E, Levashenko V. Multiple-Valued Logic mathematical approaches for multi-state system reliability analysis. Journal of Applied Logic 2013; 11: 350-362, http://dx.doi.org/10.1016/j.jal.2013.05.005.
36. Zaitseva E. Importance Analysis of a Multi-State System Based on Multiple-Valued Logic Methods. Recent Advances in System Reliability - Signatures, Multi-State System, Statistical Inference - Springer 2012; 113–34.
37. Zaitseva E., Levashenko V. Importance analysis by logical differential calculus. Automation and Remote Control - Springer 2013; 74: 171–82, http://dx.doi.org/10.1134/S000511791302001X.
38. Zaitseva E., Levashenko V., Kostolny J. Multi-State System Importance Analysis based on Direct Partial Logic Derivative. International Conference on Quality, Reliability, Risk, Maintenance and Safety Engineering 2012; 1514 – 1519, http://dx.doi.org/10.1109/ICQR2MSE.2012.6246513.

Elena ZAITSEVA
Vitaly LEVASHENKO
Jozef KOSTOLNY
Department of Informatics
University of Zilina, Faculty of Management Science and Informatics
Univerzitna 8215/1, 010 26 Zilina, Slovakia.
E-mail: elena.zaitseva@fri.uniza.sk, jozef.kostolny@fri.uniza.sk

Article citation info:
GAO W, ZHANG Z, JI H, ZHOU J, LIU Q. Optimal quasi-periodic preventive maintenance policies for a repairable system with stochastic maintenance interval. Eksploatacja i Niezawodnosc – Maintenance and Reliability 2015; 17 (3): 389–397, http://dx.doi.org/10.17531/ein.2015.3.9.

Wenke GAO
Zhisheng ZHANG
Hong JI
Yifan ZHOU
Qi LIU

OPTIMAL QUASI-PERIODIC PREVENTIVE MAINTENANCE POLICIES FOR A REPAIRABLE SYSTEM WITH STOCHASTIC MAINTENANCE INTERVAL

OPTYMALNA STRATEGIA QUASI-OKRESOWEJ KONSERWACJI ZAPOBIEGAWCZEJ SYSTEMU NAPRAWIALNEGO – CZAS MIĘDZY PRZEGLĄDAMI JAKO WIELKOŚĆ STOCHASTYCZNA

The usual preventive maintenance (PM) of a repairable system is done before failure at integer multiples of time T. In some real cases, PM cannot be performed as soon as a planned PM period is reached because of effects of some random factors, while it is usually done within an implemented period, and thus it makes the PM period become a stochastic interval. From this viewpoint, a quasi-periodic imperfect preventive maintenance policy is proposed in this paper, in which a repairable system experiences either a minor failure or catastrophic failure when a failure occurs, and the first (N-1) PM intervals is divided into a planned PM period and an implemented period. In the former, the system may be suffered an unplanned PM for removing a catastrophic failure and performing a PM, whereas in the latter, the system is preventively maintained following an occurrence of a catastrophic failure or a dynamic PM plan, whichever comes first. At the Nth PM interval, the system is replaced either when a catastrophic failure occurs or operational time reaches T, whichever comes first. An optimization of the proposed mode is introduced, the existence and the uniqueness of the optimal solution are presented, and a useful constraint of the implemented period is obtained. Finally, a real case study of PM on Chinese diesel locomotives is examined to illustrate the proposed maintenance policy.

Keywords: *maintenance; quasi-periodic imperfect preventive maintenance policy; implemented period; stochastic preventive maintenance interval.*

Zazwyczaj przeglądy okresowe systemu naprawialnego wykonuje się przed wystąpieniem uszkodzenia, w określonych odstępach czasu stanowiących całkowitą wielokrotność czasu T. W warunkach rzeczywistych, jednak, nie zawsze można przeprowadzić przegląd w zaplanowanym terminie ze względu na działanie pewnych losowych czynników, natomiast zazwyczaj przeprowadza się go w dopuszczalnym okresie realizacji, w związku z czym przedział czasu między przeglądami okresowymi staje się wielkością stochastyczną. Biorąc powyższe pod uwagę, w niniejszej pracy zaproponowano strategię quasi-okresowej konserwacji zapobiegawczej, która zakłada, że system naprawialny może ulec albo drobnemu uszkodzeniu albo uszkodzeniu katastroficznemu, a czas, do którego należy wykonać pierwszy przegląd okresowy (N-1) można podzielić na zaplanowany czas przeprowadzenia przeglądu oraz dopuszczalny okres realizacji przeglądu. W pierwszym przypadku, może wystąpić konieczność przeprowadzenia nieplanowanej konserwacji systemu mającej na celu usunięcie uszkodzenia katastroficznego, natomiast w drugim, konserwację przeprowadza się po wystąpieniu uszkodzenia katastroficznego lub zgodnie z dynamicznym harmonogramem przeglądów, zależnie od tego, która z sytuacji zaistnieje wcześniej. W N-tym terminie przeglądu okresowego, dokonuje się wymiany systemu, albo wskutek wystąpienia uszkodzenia katastroficznego albo gdy czas pracy systemu osiągnie wartość T, zależnie od tego, co nastąpi wcześniej. W artykule przedstawiono optymalizację proponowanego trybu działania, wykazano istnienie i jednoznaczność optymalnego rozwiązania oraz wyznaczono przydatne ograniczenie dopuszczalnego okresu realizacji. Na koniec, proponowaną politykę konserwacji zapobiegawczej zilustrowano studium przypadku chińskich lokomotyw spalinowych.

Słowa kluczowe: *konserwacja; strategia quasi-okresowej niepełnej konserwacji zapobiegawczej; dopuszczalny okres realizacji przeglądu; czas między przeglądami jako wielkość stochastyczna.*

1. Introduction

Maintenance systems are responsible for keeping equipment and assets fit, safe to operate and suitably configured to perform their tasks, and thus maintenance has a major impact on delivery, quality and cost. The choice of a maintenance policy is an important step in the planning of maintenance activities. Preventive maintenance (PM) is one of some major maintenance policies, and it is important in complex systems because it can reduce downtime and breakdown risk. Nonetheless, it is inescapable for almost all users that a PM plan may be influenced regularly by some random factors, such as operational condition, production task, tasks of repairmen, processing time of a job, roundtrip cycle of the transport equipment, and catastrophic failures of the system, etc, which may result in an advancing or postponing to the PM plan at random, and thus users generally adjust the PM actions to be implemented within an allowable time period whose length is determined by engineers' experience. Consequently, PM periods become a stochastic value but not a fixed value in reality. Herein, the allowable time period is termed as the implemented period of PM activity. For example, the PM period in some Chinese locomotives is 23000km~30000 km [3, 16], and it is 12~18 months in some Japanese planes [4]. i.e. the planned PM period of Chinese diesel locomotives is 23000km, and the length of the implemented period is 7000km and PM actions are executed randomly within [23000 30000] km. It is similar to Japanese planes. This PM policy is termed as quasi-periodic PM policy in this paper. It is a reasonable and popular approach because users can flexibly arrange the PM action according to their actual requirements in a short term. The selection of the implemented period's length is often considered according to some various factors. Under this situation, a PM action thus can be regarded as a random event that is limited in the implemented period, and the actual PM interval of the system is likely to be longer than the planned period. Therefore, it is necessary to optimize and discuss the quasi-periodic PM policy of a repairable system. Meanwhile, a question should be considered that how the length of the implemented period influences the maintenance cost, which may be more useful for users to make a PM decision.

Most of the current research assumed that the usual PM of a repairable system is done before failure at integer multiples of a fixed period[6, 9, 14]. Some of them considered the influence of some random factors on preventive replacement. Sheu et al,[13] considered a generalized age-replacement policy with age dependent minimal repair and a random lead-time. Castro and Sanjuan [1] analyzed a maintenance policy for a repairable system with delay repairs. In that paper, if the system fails in $[0, T^*)$ then it is repaired, whereas if it fails in (T^*, T) the repair is not performed, and the system is replaced when the non-repairable failures reached N over (T^*, T). Xu et al, [15] discussed an age-dependent replacement policy, in which the interarrival lifetimes of components are characterized as random fuzzy variables. Chen [5] considered an age replacement policy for a system, which continuously works for multiple jobs with random working times, and can undergo minimal repairs upon failures. The planned replacement is postponed at the first completion of the working time or when a job incurs some damage to the system within a planned time T. Nakawaga [6] introduced several random replacement policy including age replacement, periodic replacement and block replacement policy. It is clear that these papers only considered the effect of system's internal factors on the PR policy. Few of them considered the other model with stochastic PM period. Nakagawa et al,[8] presented two random inspection policies, where a system is checked at periodic or successive times and also at every completion of working times. Gao et al,[3] introduced a case study on the sequential PM of combined governors in diesel locomotives, in which a sequential PM activity is performed within an allowable period whose length is determined by the engineer's experience, while the number of the PM is given which may lighten the complexity of the model. Chang[2] proposed several preventive maintenance policies for an operating system that works for jobs at random times and is imperfectly maintained upon failure. In these researches, PM action is only changed by a single factor, e.g. working cycle of a job, while it should be simultaneously affected by some external and internal factors. Therefore, an optimization problem for the periodic PM policy considering various effects of random factors is more reasonable and interesting.

In this paper, a quasi-periodic PM policy for repairable system with stochastic PM interval is introduced, which is different with the general periodic PM policy because the determination of the PM policy simultaneously considers some external and internal random factors, and the PM period is a limited random value rather than a fixed value. In this policy, the first $(N-1)$ PM intervals are divided into a planned PM period and an implemented period. Suppose that the failure of the system either is a minor or is a catastrophic failure with stochastic probability, and the PM plan would be changed by some random factors, and thus actual PM activities are randomly performed considering the dynamic PM plan and the occurrence of the catastrophic failure of the system. The main characteristic of this model is that catastrophic failures of the system and dynamic PM plan are competing to cause a PM action with different PM cost. Then, an optimization of the proposed model policy is introduced, and the existence and uniqueness of the optimal solution are clearly presented as well. In addition, a constraint of the implemented period is obtained, which may be a most useful conclusion for a real situation.

The rest of the paper is arranged as follows: The model and its assumption are introduced in section 2; model formulation and maintenance optimization are presented and explored in section 3; some special cases are analyzed in section 4; a real case study is examined in section 5; and a brief summary is given in the last section.

For ease of reference, some notations are stated as follows:

a_i	adjustment factor in hazard rate function after the $(i-1)th$ PM $(1=a_1\le a_2\le, \ldots, \le a_N)$
$A_i(t)$	s-expected total minor repair cost occurred over $(0, t)$ between the $(i-1)th$ and the ith PM
C	mean cost rate of the system
C_e	extra cost caused by a catastrophic failure
$C_{p,i}$	cost of the ith PM
C_r	cost of a replacement
C_m	cost of a minimal repair
$F_{p,i}(y)$	cumulative distribution function of minor failures occurred in the ith PM interval
$F_{q,i}(y)$	cumulative distribution function of catastrophic failures occurred in the ith PM interval
$h_i(t)$	hazard rate function at time t of the system subject to $(i-1)$ PM, i=1,2, …, N
N	threshold of PM number
$NHPP$	non-homogeneous Poisson process
p_i	the probability of a failure is a minor failure when the system fails in the ith PM interval
q_i	the probability of a failure is a catastrophic failure when the system fails in the ith PM interval
R	total maintenance cost over a renewal cycle
T	length of a planned periodic PM interval
W	length of an impended period of PM activities
Y	length of a renewal interval
$Y_{s,i}$	occurring time of a catastrophic failure occurred in the ith PM
Y_{sc}	dynamic PM schedule over $[T\ T+W]$
Z	random variable

2. Model and its assumptions

In the proposed quasi-periodic imperfect PM policy, a scheduled PM plan and a dynamic PM plan are presented. The scheduled PM plan is a long-term planning and is predetermined without considering the provisional effects of some random factors. According to the scheduled plan, the system is preventively maintained at kT (k=1,2,… ,N-1), and replaced at NT. Nevertheless, the dynamic PM plan is a short-term planning considering effect of some provisional external factors. The first (N-1) PM interval is divided into a planned PM period and an implemented period. The length of the planned PM period is made by the scheduled PM plan and it is a fixed value with length T, while the length W of the implemented period is given by engineers' experience in which the dynamic PM plan is randomly distributed. Minor repairs, PMs and a replacement activity are considered jointly in the maintenance policy. A replacement cycle is defined as the time interval between the installation of the system and the first replacement or between two consecutive replacements. Under this framework, the replacement cycle constitutes a regenerative process. The following context is about the introduction of the maintenance process and model assumptions.

Without loss generality, assume that lifetime distribution of the system follows a general distribution $F(t)$ with finite mean value $\mu<+\infty$ and a probability density function $f(t)$. The hazard rate function $h(t)=f(t)/\bar{F}(t)$ is a continuous, positive and $h(t)\to+\infty$ as $t\to+\infty$, which is $a_i h(t)$ just before the ith PM and becomes $h_{i+1}(t)=a_{i+1}h(t)$ (i=1,2,…,N-1) right after the ith PM, here a_i is adjustment factor in hazard rate function after the $(i-1)$ *th* PM ($1=a_1\le a_2\le\ldots\le a_N$) [11] and $t\in[0,T+W]$. The system experiences one of the two types failure: minor failure and catastrophic failure. A failure either is a minor failure with probability p_i or is a catastrophic failure with probability q_i ($q_i=1-p_i$, i is the PM cycle), where $0\le q_i\le 1$ and q_i is non-decrease in i. The system is replaced when the PM number reaches the threshold N. After a replacement, it can be restored to "as good as new" state, and the operational procedure is repeated.

According to the PM in real cases, such as PM for locomotives, the planned PM period for the locomotive is T, while it may be adjusted in $[T-w_1, T+w_2]$ by engineers considering transport task or a transport cycle, etc., where w_1 and w_2 are constant and we set $w_1+w_2=W$. i.e. the actual PM schedule may be ahead of the planned PM schedule or delayed in a certain range. For ease of research, herein assume that the scheduled operational time period with a length T and the implemented period with a length W. Consequently, the actual PM schedule randomly distributed within $[T, T+W]$. Certainly, an occurrence of a catastrophic of the system bring an unplanned PM in $(0, T)$ is possible, which is also considered in this model and explained in the following maintenance process.

The maintenance process is shown in Fig.1, where the planned PM actions intend to be implemented at kT (k=1,2,…,N-1, it is replaced when $k=N$), whereas the actual PM actions are executed at the time t_1, t_2,…, t_N for the effects of some random factors mention above. Subplot (a) shows that the first ith PM actions is performed at t_i following the dynamic PM plan, and the system is preventively maintained for a occurrence of the catastrophic failure at t_{i+1} (marked as $Y_{s,i+1}$). In this PM activity, removing of the catastrophic failure and the execution of the (i+1) PM to the system is jointly performed, and thus the PM cost is different with the first ith PM. Subplot (b) and (c) display the two cases of the replacement at the Nth PM interval. The former shows that the replacement is caused by a catastrophic failure at t_N (marked as $Y_{s,N}$), where $t_N-t_{N-1}<T$; the latter exhibits that the replacement is executed at t_N for the operational time reached T, the replacement cost is also different with the former.

Although there are some random factors affecting the PM activities, they may be forecasted in the relative short implemented period in practice. Thus the system can be arranged to be preventively maintained during the implemented period. According to this fact, we assume that the dynamic PM plan in the implement period following the uniform distribution with a probability density function $1/W$. The dynamic PM schedules are marked as Y_{sc} in each implemented period in Fig. 1, where $Y_{sc}\in(0,W)$.

Finally, four model assumptions are given following above maintenance process:

1) All failures can be instantly detected and repaired.
2) A minor repair C_m is unrelated to the occurred failures and the severed time of the system. The cost of PM $C_{p,i}$ (i denotes the *ith* PM, i=1,2,…,N-1) is not relevant to the severed times of the system, but it relates to the number of PM and it is a constant sequence increasing in i. A catastrophic failure causes an additional cost C_e. The cost of a planned replacement is a constant C_r, and it is C_e+C_r for an unplanned replacement ($C_e+C_{p,i}<C_r$, $C_r>C_m$).
3) The system can be arranged to be completely preventively maintained in each implemented period.
4) All minor repair, PM and replacement time are negligible.

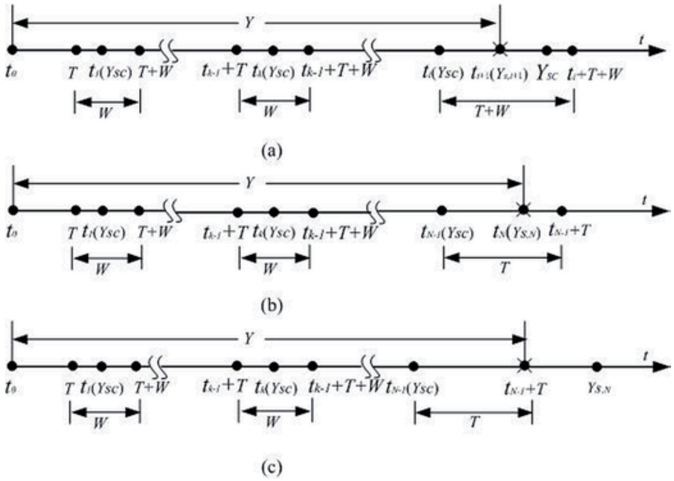

Fig. 1. Maintenance process plot

3. Modeling and optimization

According the above description of the maintenance process and model assumptions, modeling and optimization of the proposed quasi-periodic imperfect PM policy are presented in detail in this section.

3.1. Modeling

In terms of the model assumptions given in section 2, if no PM or replacement action is performed, the cumulative distribution function of minor failures between the (i-1)th and ith (i=1,2,…,N) PM can be written as:

$$F_{p,i}(t)=1-\exp\left(-\int_0^t p_i h_i(y)\mathrm{d}y\right)$$

Similarly, the cumulative distribution function of catastrophic failures between the $(i-1)$th and ith (i=1,2,…,N) PM can be given by:

$$F_{q,i}(t)=1-\exp\left(-\int_0^t q_i h_i(y)\mathrm{d}y\right)$$

In order to describe the maintenance cost, a NHPP $\{N_i(t), t\ge 0\}$ become with intensity $h_i(t)$ and successive arrival time $X_{i,j}$ (i=1,2,… ,N) is considered. During each PM interval, a failure occurred at time $X_{i,j}$ ($X_{i,j}\in(t_i,t_{i+1})$) either is a minor failure with probability p_i or is a catastrophic failure with probability q_i. Let $S_{i,j}$ is 1 or 0, it is 1 if a failure is a minor failure, otherwise, it is 0. Let $V_i(t)=\sum_{j=1}^{N_i(t)}S_{i,j}$ count the minor failure occurred in $(0,t)$ which is a s-independent NHPP with intensity $p_ih_i(t)$, and $N_i(t)-V_i(t)$ count the catastrophic failures occurred in $(0,t)$ which also is a s-independent NHPP with intensity $q_ih_i(t)$. Then, according to the Lemma 1 of the reference [12], if $\{V_i(t), t>0\}$ be a NHPP with intensity $p_i(t)h_i(t)$ and $E[V(t_i)]=\int_0^t p_ih_i(t)\mathrm{d}t$, and a cost C_m of a minor repair is occurred at the successive arrival time $X_{i,j}$, then the s-expected total minor repair cost occurred over (0, t] between the (i-1)th and the ith PM can be expressed as below:

$$A_i(t) = C_m \int_0^t p_i h_i(u)\mathrm{d}u \tag{1}$$

According to the introduction of maintenance process and model assumptions, there are six cases that may cause a PM or replacement in a renewal cycle, and thus the renewal cycle Y of the system can be denoted as follows, where Ys_i, Y_{sc}, which are presented as the definition in notations.

$$Y = \sum_{i=1}^{N-1} \begin{matrix} \{ I_{Y_{(s_i)}<T}(Y_{s_i}) \\ + I_{T<Y_{(s_i)}<T+Y_{(sc)}<T+W}(Y_{s_i}) \\ + I_{T+Y_{(sc)}<Y_{(s_i)}<T+W}(T+Y_{sc}) \\ + I_{T+Y_{(sc)}<T+W<Y_{(s_i)}}(T+Y_{sc}) \} \end{matrix} + I_{Y_{(s_N)}\in(0,T)}(Y_{s_N}) + I_{Y_{(s_N)}>T}(T) \tag{2}$$

where $I_B(Z)$ is an indicator function of the set B, i.e.,

$$I_B(Z) = \begin{cases} 1, & if\ Z \in B \\ 0, & otherwise \end{cases}$$

Similarly, the total maintenance cost of the renewal cycle is denoted as R, which can be described as below:

$$R = \sum_{i=1}^{N-1} \begin{matrix} \{ I_{Y_{(s_i)}<T,Y_{(sc)}<W}[A_i(Y_{s_i}) + C_{p,i} + C_e] \\ + I_{T<Y_{(s_i)}<T+Y_{(sc)}<T+W}[A_i(Y_{s_i}) + C_{p,i} + C_e] \\ + I_{T+Y_{(sc)}<Y_{(s_i)}<T+W}[A_i(T+Y_{sc}) + C_{p,i}] \\ + I_{T+Y_{(sc)}<T+W<Y_{(s_i)}}[A_i(T+Y_{sc}) + C_{p,i}] \} \end{matrix} \tag{3}$$
$$+ I_{Y_{(s_N)}<T}[A_i(Y_{s_N}) + C_e + C_R] + I_{T<Y_{(s_N)}}[A_i(T) + C_R]$$

where $I_B(Z)$ is the same as above, other variables are defined as notations. The s-expected cost per unite time is stated as follows using the renewal reward theorem

$$C(T) = \lim_{t\to+\infty} C(t)/t = E[R]/E[Y] \tag{4}$$

where $E[R]$ and $E[Y]$ respectively denote the s-expected total maintenance cost and the s-expected renewal cycle, and thus they need to be computed firstly. $E[Y]$ can be given by:

$$E[Y] = \sum_{i=1}^{N-1} \begin{matrix} \{ \int_0^T y f_{q,i}(y)dy + \frac{1}{W}(\int_0^W \int_T^{T+u} y f_{q,i}(y)dydu \\ + \int_T^{T+W} \int_0^{y-T} (T+u) f_{q,i}(y)\mathrm{d}u\mathrm{d}y \\ + \int_{T+W}^{+\infty} \int_0^W (T+u) f_{q,i}(y)\mathrm{d}u\mathrm{d}y) \} \end{matrix} + \int_0^T \bar{F}_{q,N}(y)\mathrm{d}y$$

which, upon simplification, is equal to:

$$E[Y] = \frac{1}{W}\sum_{i=1}^{N-1} \{ \int_0^W \int_0^{T+u} \bar{F}_{q,i}(y)\mathrm{d}y\mathrm{d}u \} + \int_0^T \bar{F}_{q,N}(y)\mathrm{d}y$$

Similarly, the s-excepted total cost of the renewal cycle can be stated as below:

$$E[R] = \frac{1}{W}\sum_{i=1}^{N-1} \begin{matrix} \{ \int_0^T \int_0^W [A_i(y) + C_{p,i} + C_e] f_{q,i}(y)\mathrm{d}u\mathrm{d}y + \int_0^W \int_T^{T+u} [A_i(y) + C_{p,i} + C_e] f_{q,i}(y)\mathrm{d}y\mathrm{d}u \\ + \int_0^W \int_{T+u}^{T+W} [A_i(T+u) + C_{p,i}] f_{q,i}(y)\mathrm{d}y\mathrm{d}u + \int_0^W \int_{T+W}^{+\infty} [A_i(T+u) + C_{p,i}] f_{q,i}(y)\mathrm{d}y\mathrm{d}u \} \end{matrix}$$
$$+ \int_0^T (A_N(y) + C_e) f_{q,N}(y)\mathrm{d}y + A_N(T)\bar{F}_{q,N}(T) + C_R$$

Let $M(T,N)$ denote the items that are relative to the minor repair cost C_m, and $J(T,N)$ denote the items that are relative to the extra cost C_e. They can be respectively interpreted as below:

$$M(T,N) = \frac{1}{C_m}\{ \frac{1}{W}\sum_{i=1}^{N-1} \begin{matrix} \{ \int_0^T \int_0^W A_i(y) f_{q,i}(y)\mathrm{d}u\mathrm{d}y + \int_0^W \int_T^{T+u} A_i(y) f_{q,i}(y)\mathrm{d}y\mathrm{d}u \\ + \int_0^W \int_{T+u}^{T+W} A_i(T+u) f_{q,i}(y)\mathrm{d}y\mathrm{d}u + \int_0^W \int_{T+W}^{+\infty} A_i(T+u) f_{q,i}(y)\mathrm{d}y\mathrm{d}u \} \end{matrix}$$
$$+ \int_0^T A_N(y) f_{q,N}(y)\mathrm{d}y + A_N(T)\bar{F}_{q,N}(T) \}$$

$$J(T,N) = \frac{1}{W}\sum_{i=1}^{N-1} \{ \int_0^{T+W} F_{q,i}(y)\mathrm{d}y + \int_T^{T+W} F_{q,i}(y)\mathrm{d}y \} + F_{q,N}(T)$$

which can simplified into:

$$M(T,N) = \frac{1}{W}\sum_{i=1}^{N-1} \{ \frac{p_i}{q_i} \int_T^{T+W} F_{q,i}(y)\mathrm{d}y \} + \frac{p_N}{q_N} F_{q,N}(T)$$

$$J(T,N) = \frac{1}{W}\sum_{i=1}^{N-1} \int_T^{T+\mathrm{W}} F_{q,i}(y)\mathrm{d}y + F_{q,N}(T)$$

Further, the s-excepted total cost is rewritten as:

$$E[R] = \sum_{i=1}^{N-1} C_{p,i} + C_R + C_m M(T,N) + C_e J(T,N) \tag{5}$$

Then, the s-expected cost per unite time can be given by Eq.(6).

$$C(T,N) = \frac{\mathrm{E}[R]}{E[Y]} = \frac{\sum_{i=1}^{N-1} C_{p,i} + C_m M(T,N) + C_e J(T,N) + C_R}{\frac{1}{W}\sum_{i=1}^{N-1} \{ \int_T^{T+W} \int_0^u \bar{F}_{q,i}(y)\mathrm{d}y\mathrm{d}u \} + \int_0^T \bar{F}_{q,N}(y)\mathrm{d}y} \tag{6}$$

In the following parts, an optimal N^* and optimal T^* need to be find which together minimize $C(T,N)$ in the infinite-horizon case.

3.2. Optimal value of T*

The focus of this subsection is to find the optimal value T^* that can minimize the function $C(T;N)$ given in Eq.(6). Firstly, differentiating $C(N,T)$ in Eq.(6) with respect to T and setting $dC/dT = 0$ yields:

$$C(T^*;N) = \frac{C_m M'(T^*,N) + C_e J'(T^*,N)}{E[Y]'}$$
$$= \frac{\sum_{i=1}^{N-1} (C_m \frac{p_i}{q_i} + C_e) \int_{T^*}^{T^*+W} f_{q,i}(u)\mathrm{d}u + W(C_m \frac{p_N}{q_N} + C_e) f_{q,N}(T^*)}{\sum_{i=1}^{N-1} \int_{T^*}^{T^*+W} \bar{F}_{q,i}(u)\mathrm{d}u + W\bar{F}_{q,N}(T^*)} \tag{7}$$

Then, submitting Eq.(6) into Eq.(7) implies Eq.(8)

$$\sum_{i=1}^{N-1} C_{p,i} + C_R = E[Y]\frac{C_m M'(T,N) + C_e J'(T,N)}{E[Y]'} - C_m M(T,N) - C_e J(T,N)$$
$$= \frac{\{\sum_{i=1}^{N-1}(C_m \frac{p_i}{q_i} + C_e)\int_T^{T+W} f_{q,i}(u)\mathrm{d}u + (C_m \frac{p_N}{q_N} + C_e)Wf_{q,N}(T)\}\{\frac{1}{W}\sum_{i=1}^{N-1}\int_T^{T+W}\int_0^u \bar{F}_{q,i}(y)\mathrm{d}y\mathrm{d}u + W\int_0^T \bar{F}_{q,N}(y)\mathrm{d}y\}}{\sum_{i=1}^{N-1}\int_T^{T+W}\bar{F}_{q,i}(u)\mathrm{d}u + W\bar{F}_{q,N}(T)} \tag{8}$$
$$-\{\frac{1}{W}\sum_{i=1}^{N-1}(C_m \frac{p_i}{q_i} + C_e)\int_T^{T+W} F_{q,i}(y)\mathrm{d}y + (C_m \frac{p_N}{q_N} + C_e)F_{q,N}(T)\}$$

The solution of Eq.(8) is optimal T^* if it is existent. To prove its (i.e., T^*, $\min(C(N;T))=C(T^*;N)$) existent and uniqueness under certain conditions, the effect of W in Eq.(8) needs to be determined firstly. To this end, set the right hand side (*rhs*) of Eq.(8) to be $\phi(T;N)$.

$$\phi(T;N) = \frac{\{\sum_{i=1}^{N-1}(C_m \frac{p_i}{q_i} + C_e)\int_T^{T+W} f_{q,i}(u)\mathrm{d}u + (C_m \frac{p_N}{q_N} + C_e)Wf_{q,N}(T)\}}{\sum_{i=1}^{N-1}\int_T^{T+W}\bar{F}_{q,i}(u)\mathrm{d}u + W\bar{F}_{q,N}(T)}\{\frac{1}{W}\sum_{i=1}^{N-1}\int_T^{T+W}\int_0^u \bar{F}_{q,i}(y)\mathrm{d}y\mathrm{d}u + W\int_0^T \bar{F}_{q,N}(y)\mathrm{d}y\} \tag{9}$$
$$-\{\frac{1}{W}\sum_{i=1}^{N-1}(C_m \frac{p_i}{q_i} + C_e)\int_T^{T+W} F_{q,i}(y)\mathrm{d}y + (C_m \frac{p_N}{q_N} + C_e)WF_{q,N}(T)\}$$

Further, let

$$\varepsilon(T;N) = \frac{\{\sum_{i=1}^{N-1}(C_m \frac{p_i}{q_i} + C_e)\int_T^{T+W} f_{q,i}(u)\mathrm{d}u + (C_m \frac{p_N}{q_N} + C_e)Wf_{q,N}(T)\}}{\sum_{i=1}^{N-1}\int_T^{T+W}\bar{F}_{q,i}(u)\mathrm{d}u + W\bar{F}_{q,N}(T)}$$

and

$$\vartheta = \lim_{T\to+\infty}\frac{\sum_{i=1}^{N-1} C_{p,i} + C_m M(T,N) + C_e J(T,N) + C_R}{\frac{1}{W}\sum_{i=1}^{N-1}\{\int_T^{T+W}\int_0^u \bar{F}_{q,i}(y)\mathrm{d}y\mathrm{d}u\} + \int_0^T \bar{F}_{q,N}(y)\mathrm{d}y}$$

According to actual case, generally $T>W$, and thus let $T=W$ in Eq.(9). Then we have $\phi(W;N)$ as the function with regard to W:

$$\phi(W;N) = \phi(T;N)|_{T=W} \tag{10}$$

Finally, setting the left hand side (*lhs*) of Eq.(8) to be $\phi(w_{P,N};N)$ yields Eq.(11), where $w_{P,N}>0$ is a solution to Eq.(11).

$$\sum_{i=1}^{N-1} C_{p,i} + C_R = \phi(w_P;N) \tag{11}$$

The proof of the solution to Eq.(11) is existent and unique using the following theorem 1.

Theorem 1 Assume that $h(t)$ is an increasing or "bathtub" type function, and $h(t)\to+\infty$ as $t\to+\infty$, and $a_i h(t) < a_{i+1}h(t)$, then the solution of $w_P>0$ to Eq.(11) is existent and unique if $\varepsilon(+\infty;N) > \vartheta$.

The proof of the theorem is shown in appendix *A*.

Furthermore, in terms of Theorem 1 and the following theorem, the solution to Eq.(8) is existent and unique as well.

Theorem 2 Assume that $h(t)$ is an increasing or "bathtub" type function, $h(t)\to+\infty$ as $t\to+\infty$, and $a_i h(t) < a_{i+1}h(t)$, then the solution of $T>W$ to Eq.(8) is existent and unique if $\varepsilon(+\infty;N) > \vartheta$ and the given $W\in(0, w_P]$.

The proof of this theorem is similar as the theorem 1.

According to above theorem, w_P is the constraint of experience value W. Till then, for a system, C_m, p_i and $h(t)$ are known, and under an identical maintenance condition, a_i is also known. Thus, the optimal solution $T\geq W$ is existent if $W\leq w_P$, otherwise, the experience value W is too large for the case.

3.3. Optimal value of N^*

According, the following in−equation holds for the optimal value of N if $N>1$:

$$C(T,N+1) \geq C(T,N) \tag{12}$$

$$\text{and } C(T,N-1) \geq C(T,N) \tag{13}$$

According to $C(T,N+1)\geq C(T,N)$ and $C(T,N-1)\geq C(T,N)$, in-equations $S(T,N)\geq C_R$ and $S(T,N-1) < C_R$ can be obtained respectively, where:

$$S(T,N) = \frac{C_{p,N-1} + C_m(M(T,N+1) - M(T,N)) + C_e(J(T,N+1) - J(T,N))}{\frac{1}{W}\int_T^{T+W}\int_0^u \bar{F}_{q,N}(y)\mathrm{d}y\mathrm{d}u + \int_0^T(\bar{F}_{q,N+1}(y) - \bar{F}_{q,N}(y))\mathrm{d}y}$$
$$\{\frac{1}{W}\sum_{i=1}^{N-1}\{\int_T^{T+W}\int_0^u \bar{F}_{q,i}(y)\mathrm{d}y\mathrm{d}u\} + \int_0^T \bar{F}_{q,N}(y)\mathrm{d}y\} - \{\sum_{i=1}^{N-1} C_{p,i} + C_m M(T,N) + C_e J(T,N)\} \tag{14}$$

$S(T,N)$ keeps increasing in N for all $T>0$, as can be observed in the following:

$$S(T,N)-S(T,N-1)=\{\frac{C_{p,N}+C_m(M(T,N+1)-M(T,N))+C_e(J(T,N+1)-J(T,N))}{\int_0^W\int_T^{T+u}\bar{F}_{q,N}(y)\mathrm{d}y\mathrm{d}u+\int_0^T(\bar{F}_{q,N+1}(y)-\bar{F}_{q,N}(y))\mathrm{d}y}$$
$$-\frac{C_{p,N-1}+C_m(M(T,N)-M(T,N-1))+C_e(J(T,N)-J(T,N-1))}{\int_0^W\int_T^{T+u}\bar{F}_{q,N-1}(y)\mathrm{d}y\mathrm{d}u+\int_0^T(\bar{F}_{q,N}(y)-\bar{F}_{q,N-1}(y))\mathrm{d}y}\}$$
$$[\sum_{i=1}^{N-1}\{\int_0^W\int_0^{T+u}\bar{F}_{q,i}(y)\mathrm{d}y\mathrm{d}u\}+W\int_0^T\bar{F}_{q,N}(y)\mathrm{d}y]>0 \tag{15}$$

It is thus verified that an unique N can be determined by $S(T,N)\geq C_R$ and $S(T,N-1)<C_R$ and an unique N^* does exist for minimizing the mean cost per unit time $C(T,N)$.

4. Special cases

This section displays some especial cases of the proposed model.

Case 1 $W=0$ and $p_i=1$, $C_{p,i}=C_p$

This model is the periodic imperfect PM policy [7], in which the system is preventively maintained at kT ($k=1,2,\ldots,N-1$) and is replaced at NT, and failures are removed by minor repair. Following is the mean cost rate function.

$$C(T;N)=\frac{\mathrm{E}[R]}{E[Y]}=\frac{(N-1)C_p+C_m\sum_{i=1}^{N}\int_0^T h_i(y)\mathrm{d}y+C_R}{NT} \tag{16}$$

Case 2 $W=0$ and $p_i\neq1$

This model is the periodic imperfect PM policy, in which the system is planned to be preventively maintained at kT ($k=1,2,\ldots,N-1$) and is replaced at NT. The system experiences one of the two types failure: minor failure and catastrophic failure. Minors are removed by minor repair, whereas catastrophic failures are recited by a unplanned PM with cost $C_e+C_{p,i}$ (or C_e+C_r, $k=N$).

$$C(T;N)=\frac{\mathrm{E}[R]}{E[Y]}=\frac{\sum_{i=1}^{N-1}C_{p,i}+\sum_{i=1}^{N}(C_\mathrm{e}+\frac{p_i}{q_i}C_m)F_{q,i}(T)+C_R}{\sum_{i=1}^{N}\int_0^T\bar{F}_{q,i}(y)\mathrm{d}y} \tag{17}$$

According to the mean cost rate of the special case 2 is given as Eq.(17). The optimal T^* of the periodic PM policy can be obtained from Eq.(18), and the optimal N^* can be attained from the in-equation (19) under the Matlab2010.

$$C_R+\sum_{i=1}^{N-1}C_{p,i}=\frac{\sum_{i=1}^{N}\int_0^T\bar{F}_{q,i}(y)\mathrm{d}y}{\sum_{i=1}^{N}\bar{F}_{q,i}(T)}\sum_{i=1}^{N}(C_\mathrm{e}+\frac{p_i}{q_i}C_m)f_{q,i}(T)-\sum_{i=1}^{N}(C_\mathrm{e}+\frac{p_i}{q_i}C_m)F_{q,i}(T) \tag{18}$$

$$L(N-1;T)\leq C_r\leq L(N;T) \tag{19}$$

Where:

$$L(N;T)=\frac{C_{p,N}+(C_\mathrm{e}+\frac{p_{N+1}}{q_N}C_m)F_{q,N}(T)}{\int_0^T\bar{F}_{q,N+1}(y)\mathrm{d}y}\sum_{i=1}^{N}\int_0^T\bar{F}_{q,i}(y)\mathrm{d}y-\{\sum_{i=1}^{N-1}C_{p,i}+\sum_{i=1}^{N}(C_\mathrm{e}+\frac{p_i}{q_i}C_m)F_{q,i}(T)\}$$

Case 3 $W\neq0$ and $p_i=1$

This model is a quasi-periodic imperfect PM policy, in which the system is replaced after (N-1) PM actions, and each PM plan is randomly distributed in $(T,T+W]$ with probability density $1/W$, and failures are removed by minor repair. The mean cost rate function is stated as follows:

$$C(T;N)=\frac{\mathrm{E}[R]}{E[Y]}=\frac{WC_R+\sum_{i=1}^{N-1}(WC_{p,i}+C_m\int_T^{T+W}\int_0^u h_i(y)\mathrm{d}y\mathrm{d}u)+C_mW\int_0^T h_i(y)\mathrm{d}y}{NT+(N-1)0.5W} \tag{20}$$

5. Real cases study

In this section, the procedures and features of the proposed model and some sensitive analysis on model parameters are illustrated using a real case study on one type of Chinese diesel locomotive. Diesel locomotives are intensively used in most Chinese railway enterprises, and their maintenance becomes a hot issue in daily operating. Periodic PM is widely used for the convenience of scheduling, and an overhaul is performed after 4~6 PMs in current [16]. Meanwhile, the PM plan usually includes a scheduled PM plan and a dynamic PM plan, and actual PM action is dynamic and stochastic in maintenance period for the influence of production trust, tasks of repairmen, condition of the whole locomotive, etc. The planned PM period T of some Chinese diesel locomotives is 23000 km, and the implemented period W is 7000 km, and thus PM actions are executed randomly within [23000 30000]. Therefore, PM of diesel locomotives satisfies the characteristic of the proposed dynamic quasi-periodic PM, and thus their maintenance is used as a real case study to illustrate the proposed PM policy.

5.1. Maintenance optimization

Herein, we assume that the maintenance cost modeling satisfies the following assumptions:

1) The dynamic PM plan is randomly distributed following the uniform distribution with a probability density function $1/W$ within $[T^*\ T^*+W]$.
2) The overhaul is the same as replacement and can restore the system to "as good as new".
3) p_i and a_i are the sequence of i:

$$p_i=\gamma^{i^\theta}-\gamma^{(i+1)^\theta}+\gamma$$

$$a_i=0.85+0.15i$$

4) Other assumptions are the same as the quasi-periodic PM policy in part 2.

Other parameters are shown as following Table 1.

The reliability model of the diesel locomotive in summer is obtained from maintenance recorders [16], and its hazard rate function is given as bellows:

$$h(t)=\frac{f(t)}{\bar{F}(t)}=2.49\times10^{-5}(t/35199)^{-0.1246}+1.73\times10^{-4}(t/34289)^{4.9318}$$

Table 1. Parameters

Items	Value	Remarks	Items	Value	Remarks
C_r	10000￥	Assume	W	7000km	A current maintenance regulation of one type Chinese diesel locomotives
C_e	6000￥	Assume	γ	0.85	Assume
C_m	5000￥	Assume	θ	0.75	Assume
$C_{p,i}$	2000￥	Assume			

It can be found that $h(t)$ is a "bathtub" type function, which is discussed above. Then, for convenience of getting the solution, an algorithm following the analysis is given, which can be used to compute numerically the optimal number N^*, and the optimal period T^*.

Algorithm

Step1 Input parameters γ , θ , C_m, C_e, $C_{p,i}$, C_r, a_i, W and set N=1.

Step2 Substitute N into Eq.(11), we can obtain W_P. If $W \le w_p$, then go to the next step.

Otherwise, the solution is inexistence and the algorithm ends.

Step3 Substitute N into Eq.(8), and T' is obtained, and go to the next step.

Step4 Substitute the obtained T' into $S(T',N)$, attained N'. If $N'=N$, go to the step6.

Otherwise, go to the next step.

Step5 Set $N=N+1$, go to the step2.

Step6 Give outputs of the optimal $T^*=T'$ and $N^*=N'$, and the algorithm ends.

Under the Matlab 2010b, the optimal N^*=5, T^*=21420km, the $C(T^*,N^*)$=0.38826￥/km and w_P=16450km are obtained. i.e. for Chinese diesel locomotives in summer in the area, the optimal solution is existent and unique if the implemented period $W \le 16450$, and dynamic PM activities are performed stochastically in time period [21420, 28420]. The three-dimension of (N,t,C) is shown as Fig.2, from which the existence of C_{min} can be found directly.

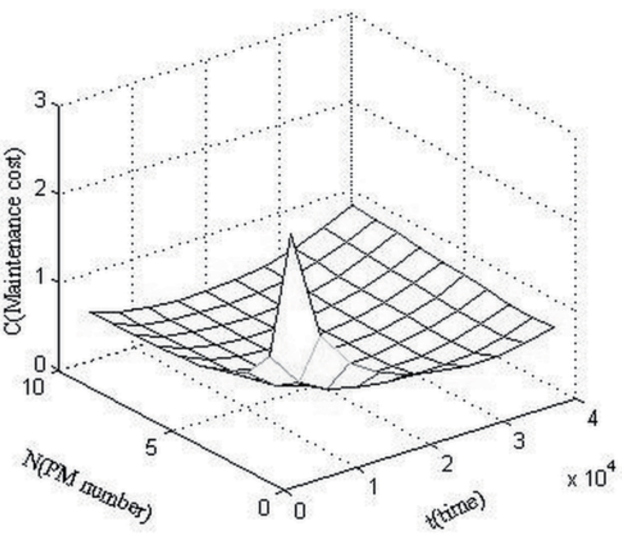

Fig. 2. Three-dimension plot of (N,t,C)

5.2. Discussion

a) Effect analysis of *W*

According to the proposed PM policy, W is the only and critical parameter that can be determined by users, and thus it is necessary to analysis its influence on the optimal result. Subplot (*a*) of Fig.3 shows the trend of long running cost rate with the increase of W. It can be found directly that the growth of W can increase the long running cost rate. Subplot (*b*) of Fig.3 exhibits the probable operating time zone of the system with the increase of W. It illustrates that the increase of W can cause a decrease of T and enlarge probable operating time zone. A long W may be convenient for repairman, but maybe discommodity for production. Therefore, the choice of W should be decreased as soon as possible under the condition of meeting the requirements of practice.

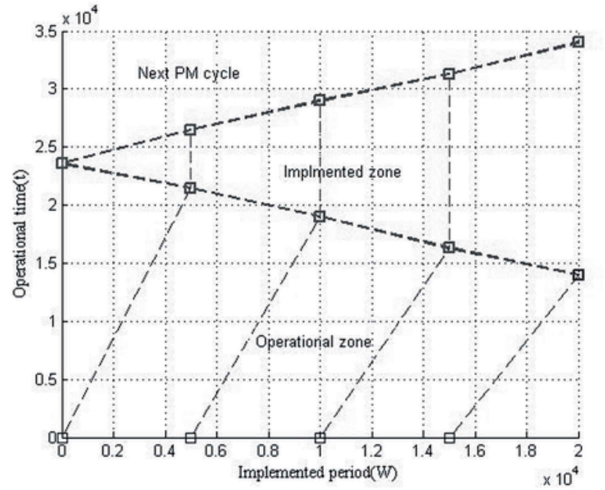

(a) Plot on W-C_{min}

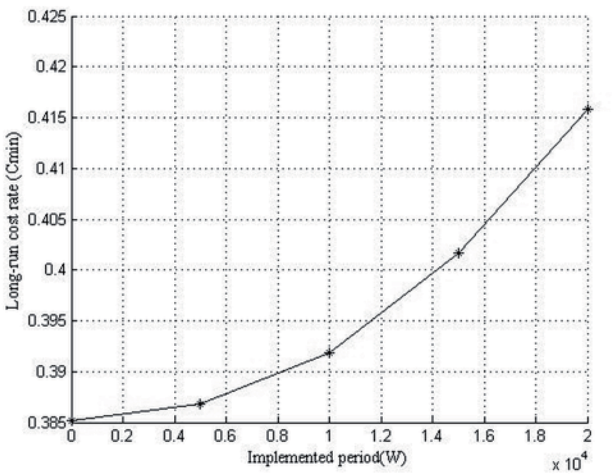

(b) Plot on W-t

Fig. 3. Optimal results with different W

b) Necessity analysis of the proposed policy

In reality, PM actions always stochastically performed in each implemented period $[T_0,T_0+W]$ if ignore the randomness of PM, where T_0 is the optimal PM cycle when W=0. It can be seen from Fig.4 that the actual maintenance cost rate is greater than the policy without considering the implemented period (W=0). Assume that the time of perform PM action is T_s ($T_s \in [T_0,T_0+W]$), the actual maintenance cost rate is $C(T_s)$ that stochastically distribute within [max($C(T_s)$), min($C(T_s)$)].

Fig. 4 shows probable cost rate with different maintenance policy, illustrated with the following two cases.

Case 1: The PM cycle T_0 is determined by the usual PM policy (W=0), while the actual PM is performed within [T_0-w_1,T_0+w_2], where W=w_1+w_2=7000. It can be found that the actual cost rate stochastically distributes within [0.388, 0.402] and the mean value is nearly 0.396, while the computed cost rate is 0.385. That is to say, the computed cost rate is not the truth, and the waste must be occurred. Meanwhile, we can also found that the actual maintenance cost rate is increasing with the increase of W (e.g. W=8000).

Case 2: The PM cycle is determined by the proposed PM policy with W=7000, where the mean cost rate is 0.388<0.396. The save part is greater than the gap of the general PM and the general sequential PM policy. This result illustrates the necessity of the proposed PM policy.

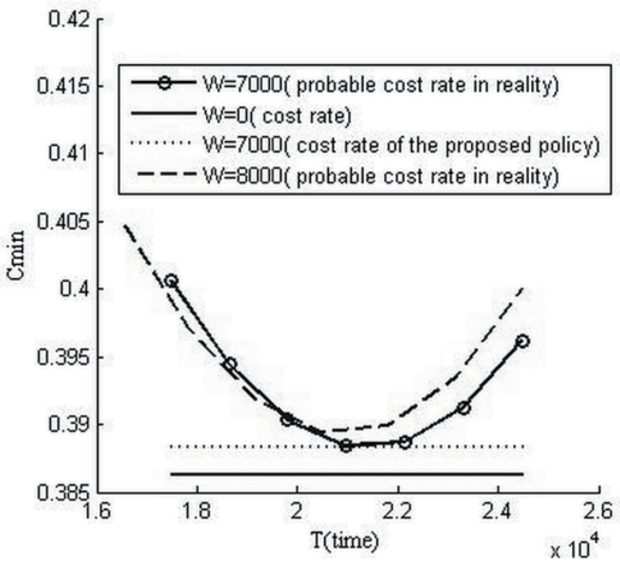

Fig. 4. Probable cost rate with different maintenance policy

6. Results

In this paper, a quasi-periodic imperfect PM policy for repairable system with stochastic maintenance interval was proposed. Expected long-run cost per unit time for the operating system was determined. The optimal PM number N^* and optimal implemented period [T^*, T^*+W] for PM actions were also derived, their existence and uniqueness being well demonstrated as well. The constraint of the experience value W was also obtained in theory. Some special cases of the proposed model were discussed in brief, and a real case study on Chinese diesel locomotives was provided for verification. From the case study, effects of W on optimal results and necessity of the proposed PM policy were discussed. In addition, it was found from the compare that the PM cost rate exist a great gap between considering and not considering the randomness of PM actions in PM policy making. It should be paid close attention in practice that the cost rate is increasing with the increase of W, and the length of W should be small as far as possible under satisfying the needs of practice. The obtained results can be extended to further studies on the sequential PM with stochastic maintenance interval. We are currently working on some of these topics.

Acknowledgements

The authors are grateful for valuable suggestions of Guanjun Wang, an associate professor of the Department of Mathematics, Southeast University of China. The research work is also supported jointly by the Natural Science Foundation of China (51275090 and 71201025), and the opening topic fund of Jiangsu key laboratory of large engineering equipment detection and control (JSKLEDC201404).

Appendix

Theorem 1: Assume that $h(t)$ is an increasing or "bathtub" type function, and $h(t)\to+\infty$ as $t\to+\infty$, and $a_i h(t)< a_{i+1}h(t)$, then the solution of w_P >0 to Eq.(11) is existent and unique.

Proof:

1) If $h(t)$ is an increasing function and $h(t)\to+\infty$ as $t\to+\infty$, and $a_i h(t)< a_{i+1}h(t)$. $\phi(W)$ and $\varepsilon(W)$ are increasing in W since $h(t)$ is strictly increasing in t. $\lim_{W\to 0}\phi(W)=0$, and $\vartheta\approx constant$, and $\lim_{W\to+\infty}\phi(W)=+\infty$ and $\varepsilon(+\infty)>\vartheta$.

   Then, $0<C_r<\phi(+\infty)$.The solution of w_P >0 to Eq.(11) is existent and unique.
   The proof of the theorem can refer [10] in detail.

2) If $h(t)$ is a "bathtub" type function and $h(t)\to+\infty$ as $t\to+\infty$, and $a_i h(t)< a_{i+1}h(t)$.
   Then, there is a t_0 which makes $h'(t)$=0 since $h(t)$ is a "bathtub" type function in t.
   Further, $h(t)$ is decreasing within (0,t_0) and increasing within [t_0,+ ∞).
   $\varepsilon(W)$ is decreasing if $h(t)$ is decreasing with t, then,

$$\lim_{W\to 0}\phi(W)=2\bar{F}_q(W)\bar{F}_q(2W)(h(2W)-h(W))<0$$

   Similarly, ε(W) is increasing if h(t) is increasing with t. Then,

$$\lim_{W\to+\infty}\phi(W)=+\infty$$

   Thus, $\phi(W)$ is also a "bathtub" type function with W, and $\lim_{W\to 0}\phi(W)<0$. Then, $\varphi(0)<C_r<\varphi(+\infty)$.

   Therefore, the solution of w_P >0 to Eq.(11) is existent and unique.

References

1. Castro I. T. and E. L. Sanjuan. An optimal maintenance policy for repairable systems with delayed repairs. Operations Research Letters 2008; 36(5): 561-564, http://dx.doi.org/10.1016/j.orl.2008.05.007.
2. Chang C. C. Optimum preventive maintenance policies for systems subject to random working times, replacement, and minimal repair. Computers & Industrial Engineering 2014; 67: 185-194, http://dx.doi.org/10.1016/j.cie.2013.11.011.
3. GAO W., et al. Optimal Combinatorial Replacement Policy under a Given Maintenance Interval for the Combined Governor in Diesel Locomotives. Eksploatacja i Niezawodnosc - Maintenance and Reliability 2013; 15(2): 89-98.
4. KODO I. and N. TOSHIO. Optimal operation censoring policy of aircraft. 2012 Asia-Pacific International Symposium on Advanced Reliability and Maintenance Modeling. 2012. 184-191.

5. Mingchih C. Optimal random replacement models with continuously processing jobs. Applied Stochastic Models in Business and Industry 2013; 29: 118–126, http://dx.doi.org/10.1002/asmb.952.
6. Nakagawa T. Maintenance theory of reliability. London: Springer, 2005.
7. NAKAGAWA T. PERIODIC AND SEQUENTIAL PREVENTIVE MAINTENANCE POLICIES. Journal of Applied Probability 1986; 23(2): 536-542, http://dx.doi.org/10.2307/3214197.
8. Nakagawa T., et al. A summary of periodic and random inspection policies. Reliability Engineering & System Safety 2010; 95(8): 906-911, http://dx.doi.org/10.1016/j.ress.2010.03.012.
9. Sarkar A., et al. Survey of maintenance policies for the Last 50 Years. International Journal of Software Engineering & Applications (IJSEA) 2011; 12(3): 130-148, http://dx.doi.org/10.5121/ijsea.2011.2310.
10. Sheu S.-H. and C.-C. Chang. An Extended Periodic Imperfect Preventive Maintenance Model With Age-Dependent Failure Type. IEEE TRANSACTIONS ON RELIABILITY 2009; 58(2): 397-405, http://dx.doi.org/10.1109/TR.2009.2020103.
11. SHEU S.-H., et al. An Extended Sequential Imperfect Preventive Maintenance Model with Improvement Factors. Communications in Statistics—Theory and Methods 2012; 41(7): 1269-1283, http://dx.doi.org/10.1080/03610926.2010.542852.
12. Sheu S.-H. and J.-P. Jhang. A generalized group maintenance policy. European Journal of Operational Research 1996; 96: 232-247, http://dx.doi.org/10.1016/S0377-2217(96)00073-2.
13. Sheu S.-H., et al. Extended optimal replacement model with random minimal repair costs. European Journal of Operational Research 1995; 85: 636-649, http://dx.doi.org/10.1016/0377-2217(93)E0364-4.
14. Wu S. Preventive Maintenance Models:A Review. London: Springer, 2011.
15. Xu S., et al., Random fuzzy age-dependent replacement policy, in Fuzzy Systems and Knowledge Discovery, Pt 1, Proceedings, L. Wang and Y. Jin, Editors. 2005. 336-339.
16. Zhang Z., et al. Reliability Modeling and Maintenance Optimization of the Diesel System in Locomotives. Eksploatacja i Niezawodnosc – Maintenance and Reliability 2012; 14(4): 302-311.

Wenke GAO
School of Energy and Power Engineering
Lanzhou University of Technology
Lanzhou 730050, China
School of Mechanical Engineering
Southeast University
Nanjing 211189, China

Zhisheng ZHANG
School of Mechanical Engineering
Southeast University
Nanjing, China, 211189

Hong JI
School of Energy and Power Engineering
Lanzhou University of Technology
Lanzhou 730050, China

Yifan ZHOU
School of Mechanical Engineering
Southeast University
Nanjing, China, 211189

Qi LIU
School of Mechanical Science and Engineering
Jilin University
Changchun, China, 130025

E-mail: gaowk_best@163.com

Article citation info:
PAWLAK M, KOŚCIELNY JM, WASIEWICZ P. Method of increasing the reliability and safety of the processes through the use of fault tolerant control systems. Eksploatacja i Niezawodnosc – Maintenance and Reliability 2015; 17 (3): 398–407, http://dx.doi.org/10.17531/ein.2015.3.10.

Mariusz PAWLAK
Jan Maciej KOŚCIELNY
Piotr WASIEWICZ

METHOD OF INCREASING THE RELIABILITY AND SAFETY OF THE PROCESSES THROUGH THE USE OF FAULT TOLERANT CONTROL SYSTEMS

METODA PODWYŻSZANIA NIEZAWODNOŚCI I BEZPIECZEŃSTWA PROCESÓW POPRZEZ STOSOWANIE UKŁADÓW REGULACJI TOLERUJĄCYCH USZKODZENIA*

The operation idea of fault tolerant control systems, has been presented in the paper. Protection and security layers applied in technical diagnostics associated with safety of control system, have been discussed. The automatic control system of a steam turbine power, has been described as an example of fault tolerant control system. A steam turbine is the main element of energy blocs forming a national energy system. Therefore, the turbine control systems require high reliability. The impact of diagnostics and fault tolerance on the values of reliability and safety coefficients of control systems, have been determined in the paper.

Keywords: *control system, functional safety, protection and security layers, diagnostics, fault tolerance, redundancy, reconfiguration, reliability and safety coefficients, energetic block, steam turbine.*

Przedstawiono ideę działania układów automatyki tolerujących uszkodzenia. Omówiono warstwy zabezpieczeniowo ochronne stosowane w diagnostyce technicznej, związanej z bezpieczeństwem układów regulacji. Jako przykład układu regulacji tolerującego uszkodzenia torów pomiarowych, opisano układ regulacji mocy turbiny parowej. Turbiny takie stanowią podstawowy element bloków energetycznych, tworzących krajowy system energetyczny. Dlatego też, od układów regulacji turbin wymaga się dużej niezawodności. W pracy określono wpływ diagnostyki i tolerowania uszkodzeń na wartości wskaźników niezawodności i bezpieczeństwa układów automatyki.

Słowa kluczowe: *bezpieczeństwo, diagnostyka, układ regulacji, tolerowanie uszkodzeń, redundancja, rekonfiguracja, turbina parowa, blok energetyczny, wskaźniki niezawodności.*

1. Introduction

The control system faults are one of the main causes of breakdowns in industrial processes. According to presented by ABB data, 36% of all problems are caused by failures of control system components, including faults of sensors and actuators primarily. These devices are installed on the process installation, which creates for them difficult and variable operating conditions. Control units, installed in the control rooms, are damaged relatively rare. If we consider damages caused by control systems exclusively, then not more than 10% of them are caused by faults of control units. The others are the consequences of faults of sensors and actuators. In contrast, paradoxically different redundant solutions are developed and are commercially available primarily for any kind of controllers and computer networks.

Examples of serious industrial accidents caused by damage to the measuring equipment are:

- Damage in the fuel storage Buncefield, on 11 December 2005. A fault of the level sensor caused overflow of the fuel tank and ignition. Next, a series of explosions and fire of aviation fuel occurred. It was the largest fire in Europe. There were 40 injuries and substantial material damage (£ 5bn) [1].
- Damage in Texas City, USA, on 23 March 2005, in the largest oil refinery BP International. During a start-up procedure of the separator plant at the Isomerization Department, producing high octane unleaded gasoline additives, level sensors have failed. It caused the level overflow in the distillation column, resulting in a rapid evaporation, a pressure increase, a raffinate ejections, and consequently explosion and fire. 15 people were killed and 170 were injured. Separator plant and evaporation of hydrocarbons plant were destroyed [2].

The need to ensure an adequate level of security, i.e. reducing the risk to an acceptable level, was the cause of the development of international standards of functional safety. Functional safety related to all activities in the life cycle of the E/E/PE control systems (containing the electrical/ electronic/ programmable electronic components), constitutes an important aspect of functional safety. Various standards have been developed, e.g. in the area of general principles of functional safety - IEC 61508 [11,20,21], in the field of industrial processes - EN 61511, in the scope of machines - EN 62061 [12] and in the scope of nuclear energy - IEC 61513.

The most important is the new version of IEC 61508 standard [21]. It was adopted as a European standard EN 61508, and next as a national standard PN-EN 61508 [33]. IEC 61511 standard is currently being updated and will be published with a delay as a European standard (EN) and national (EN). It contains a number of additions and refers more broadly to the current IEC 61508 standard, mainly of its parts 5, 6 and 7. New versions of these standards broadly include theoretical issues (numerous citation of recognized publications) and the requirements for mathematical models in terms of verification and validation of the proposed solutions [21].

(*) Tekst artykułu w polskiej wersji językowej dostępny w elektronicznym wydaniu kwartalnika na stronie ***www.ein.org.pl***

The concept of Fault Tolerant Control Systems (FTCS), has been discussed in the paper. According to the authors, these systems could provide a new protection layer within the meaning of the standards associated with the functional safety. Mainly faults of sensors and actuators are taken into account in FTC systems, which leads to a significant value increase of the reliability and safety coefficients of the control systems and thus of the whole process. An exemplary control system of the condensing turbine tolerating sensor faults, has been presented in the paper [29-32, 41]. The influence of diagnosis and fault tolerance on values of the reliability and safety coefficients, has been also discussed.

2. Protection layers

The purpose of safety-related control systems is to reduce the risk, and thus to decrease the frequency of occurrence of dangerous events or to reduce the effects of such events.The applied security systems have a layered structure as shown in Fig.1.

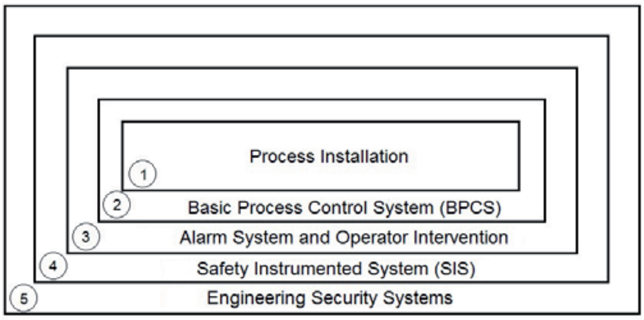

Fig. 1. The protection layers.

The first layer represents the process installation, which should be resistant to internal and external disturbances (security actions and technological blockades). The second layer is represented by a basic process control system (BPCS). It can be Distributed Control System (DCS), which integrates a control and monitoring tasks or system consisting of Supervisory Control and Data Acquisition (SCADA) and PLC/PAC (Programmable Logic Controller/Programmable Automation Controller). The third layer is a separate alarm system and operator's intervention. SIS (Safety Instrumented System) constitutes the fourth layer. The aim of these four mentioned above layers is to prevent the occurrence of failures. The fifth layer engineering security systems, such as the safety valves, curtains, protective barriers, housing, etc., which aim is to reduce the effects of damage occurred. Even higher layers realize internal and external procedures, and technical measures, whose aim is to minimize human and material losses.

Commonly used SIS systems implement the safety automatic algorithms and the activation of blockades, whose task is to achieve the proper process operation. Signals generated by SIS systems, for instance, cut off supply or raw materials, block actuators in a safe position, run the shut-off valves, set a safe operating status of engines, pumps, ventilators, etc. Usually, SIS actions are associated with shut-off a part of the process installation or even the whole process, which leads to economic losses.

Therefore, in the lower layers (1, 2 and 3), it is advisable to use solutions that can guarantee the elimination of hazards in the early stages of their development. Methods of reducing the risk, which do not caused the process shut-off, are:

1. Robust construction of process installation thanks to solid design and high quality building and exploitation; passive solutions are used, which do not require any control as well as any operator's intervention to avoid the dangerous situations,
2. Hardware and software redundancy of the control system elements,
3. Separate alarm-advisory systems,
4. Appropriately designed process visualization,
5. Training of operators, especially with use of process simulators, based on which the various emergency scenarios can be applied,
6. On-line diagnosis systems of the process and automation field devices,
7. Fault tolerant control systems (FTCS).

The first four solutions are commonly known and used. While the others are recently developed intensively [13,21,28]. The last three of the methods listed above are not covered sufficiently in safety standards.

3. Idea of fault tolerant control systems

The fault tolerant control algorithms are currently one of the most important directions of research and development in the field of automation. They were discussed, among others, in monographs [3, 8, 9, 13, 18, 25, 28, 36]. The first works on the FTC focused on the aerospace industry. Nowadays, however, in addition to applications in aircrafts, FTC systems are designed for industrial processes more frequently [14-16, 39, 38-41].

Integration of FTCS with diagnostic systems represent a new, additional layer for safety and protection of controlled processes. Block diagram of the automation system with a layer of the on-line diagnosis and fault tolerant control and security system SIS is shown in Fig. 2. The presented solution constitutes a modern concept of risk reduction while ensuring minimum of the economic losses caused by failures.

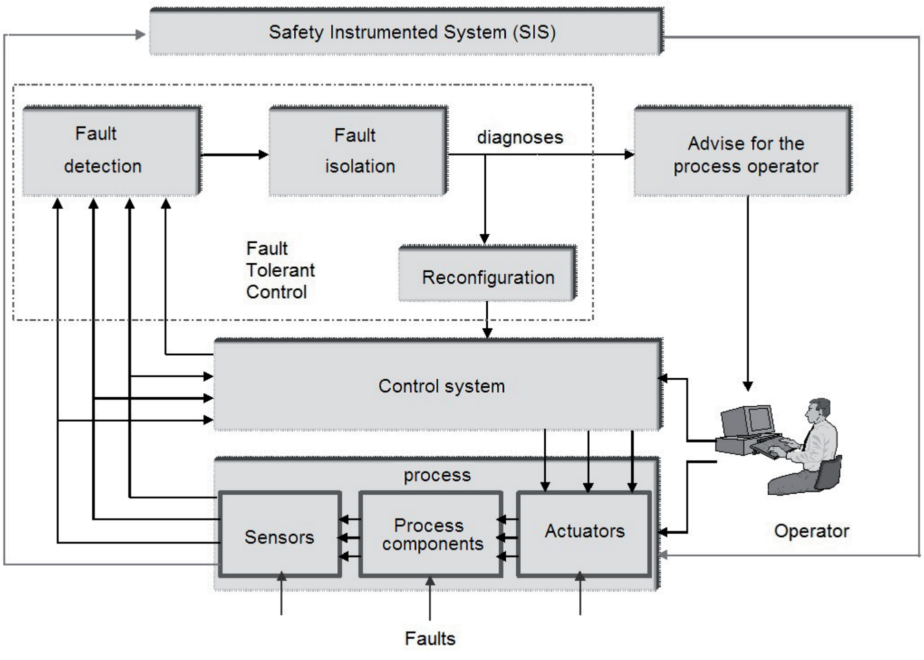

Fig. 2. Diagram of control system, on-line diagnosis and process security

The idea of development of active FTC systems lies in the implementation of on-line diagnostics and real-time reconfiguration of the hardware or software structure system in the cases when faults occur. Therefore, these systems have a variable structure, as given in Fig.3.

A very important aspect of any of the FTC system is a realization method of fault detection and fault isolation. The solution adopted should provide an early detection of faults as well as such their distinguishability, which will allow to take a decision about the necessary reconfiguration of the system. Methods of diagnosis of industrial processes are discussed in monographs [5, 7, 17 ,18, 22, 23, 27, 35, 42] and in many review articles, including works [4,6,14,19,23,24,26].

The concept of fault tolerant control systems is consistent with the structure of a dynamic redundancy of the type "1 oo 2". The main difference lies in the fact that:

- Instead of a hardware redundancy, the analytical (information) redundancy (i.e. software redundancy) is used in FTC systems,
- In control systems, a dynamic redundancy is mostly used for controllers, while in FTCS the sensor and actuator are taken into account especially,
- Different diagnostic methods are used:
  - to diagnosis of the controller faults - methods of computer system diagnosis,
  - to diagnosis of the sensor and actuator faults - methods of process diagnosis,
- Dynamic redundancy is introduced by system manufacturers (the designer can apply it or resign from it), while providing fault tolerance becomes the task of the designers.

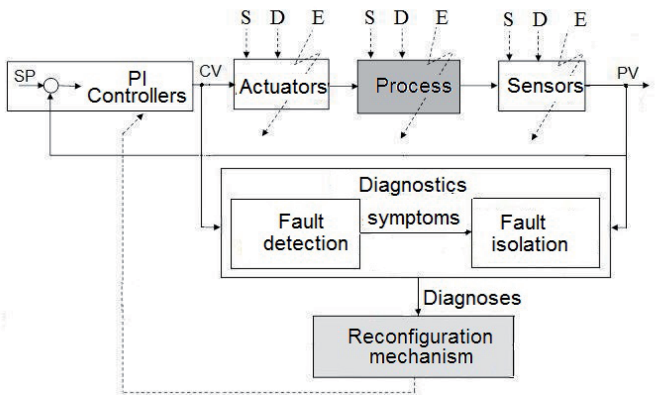

Fig. 3. The diagram of fault tolerant control systems (SP – SetPoints, CV – Control Variables, PV – Process Variables, E – Faults, D – Disturbances, S –Noises)

In complex control systems, even in the absence of hardware redundancy, are usually a possibilities to reconfigure the automation system to avoid or to reduce the negative impact of the sensor faults on the process functioning [6,16,30,31,37,41]. The virtual sensors are most commonly used to reproduce signals from damaged sensors. They calculate the signal value based on the partial process models, using the other measurement signals. It is also possible to substitute dynamically the value of signals from the damaged sensors by the equivalent signals.

It is much more difficult to build control systems tolerating the faults of actuators. In the case of multi-dimensional systems, having many control signals, the inability to access to one of them, can in some cases be realized by the access to the other control signals. For example, a single engine failure in an aircraft may be compensated by appropriate access to the other control signals (steering the stabilizers on the aircraft wings, power dosing of the other engines). In contrast to simple automation systems, it is necessary to use redundant actuators.

Development of FTC system requires for each possible fault, the design of a set of operation algorithms, enabling a proper system operation during the existence of each particular fault. It is also necessary to design the set of procedures for a bumpless switch to the redundant control for each of the faults. However, the condition for such changes is a quick detection and precise isolation of faults.

Research in the field of FTC systems is focused on advanced control systems, while more than 90% of all applications are associated with PID controllers. This is the reason of delay of the current state of technology in relation to the progress in research. The current control systems, enable design of FTC systems to a limited extent only. They are not equipped with adequate diagnostic and reconfiguration software. Nowadays, FTCS applications are related to research and pilot deployments.

An example of the control system of the condensing turbine, which tolerates the sensor faults, is described in chapter 4 [25-28, 41].

4. The example of the condensing turbine control system, tolerating faults of sensors

4.1. The control system structure

The task of a condensing turbine is to obtain the maximum electrical power from the generator working in an integrated set of boiler-turbine-generator making up the energy block. The national electricity grid consists of many such energy blocks. Some of them have a high power. This makes the failure of a single block may violate the security of the entire system. Therefore, much attention is given to increasing the reliability of the control systems in the individual energy blocks, and thus the entire national power system [15,40].

The proper work of a condensing turbine is ensured by the control system shown in Fig. 4. The system has two different functional structures [30, 31, 41], used independently and designed for control the:

- rotary speed of the turbine, during the start-up of energy block,
- turbine power control with varying loads, during the normal operation of the energy block.

In the first case, the controlled variable is the rotary speed of turbine, measured in a mode of static redundancy type "2 oo 3". While the setpoint value is determined in accordance with the programmed gradient of growth of rotary speed, taking into account the critical speed bandwidth. The purpose of this system is to achieve synchronous rotation of the turbine, allowing the inclusion of the block to work in the national electricity grid (so called synchronization).

In the second case, the controlled variable is the active power (P) of energy block. While the setpoint value is determined based on the following signals [29,41]:

1. Base setpoint of power (P_B), signal introduced from the operator interface,
2. System setpoint of power (Y1), signal transmitted from ARCM system (automatic control of frequency and power of electro-energy system) [15,29], so called secondary control of electro-energy system,
3. BPP (actual operating point), signal introduced by the operator of electro-energy system,
4. Correction signal related to the pressure of fresh steam (pT), generated by POM (steam power limiter),
5. Correction signal related to the absolute vapor pressure in the condenser (pS), generated by PrOM (vapor power limiter),
6. Signal of the primary control related to the frequency of the electro-energy system. The energy block implementing this type of system control, varies the power depending on the voltage frequency changes in the power network.

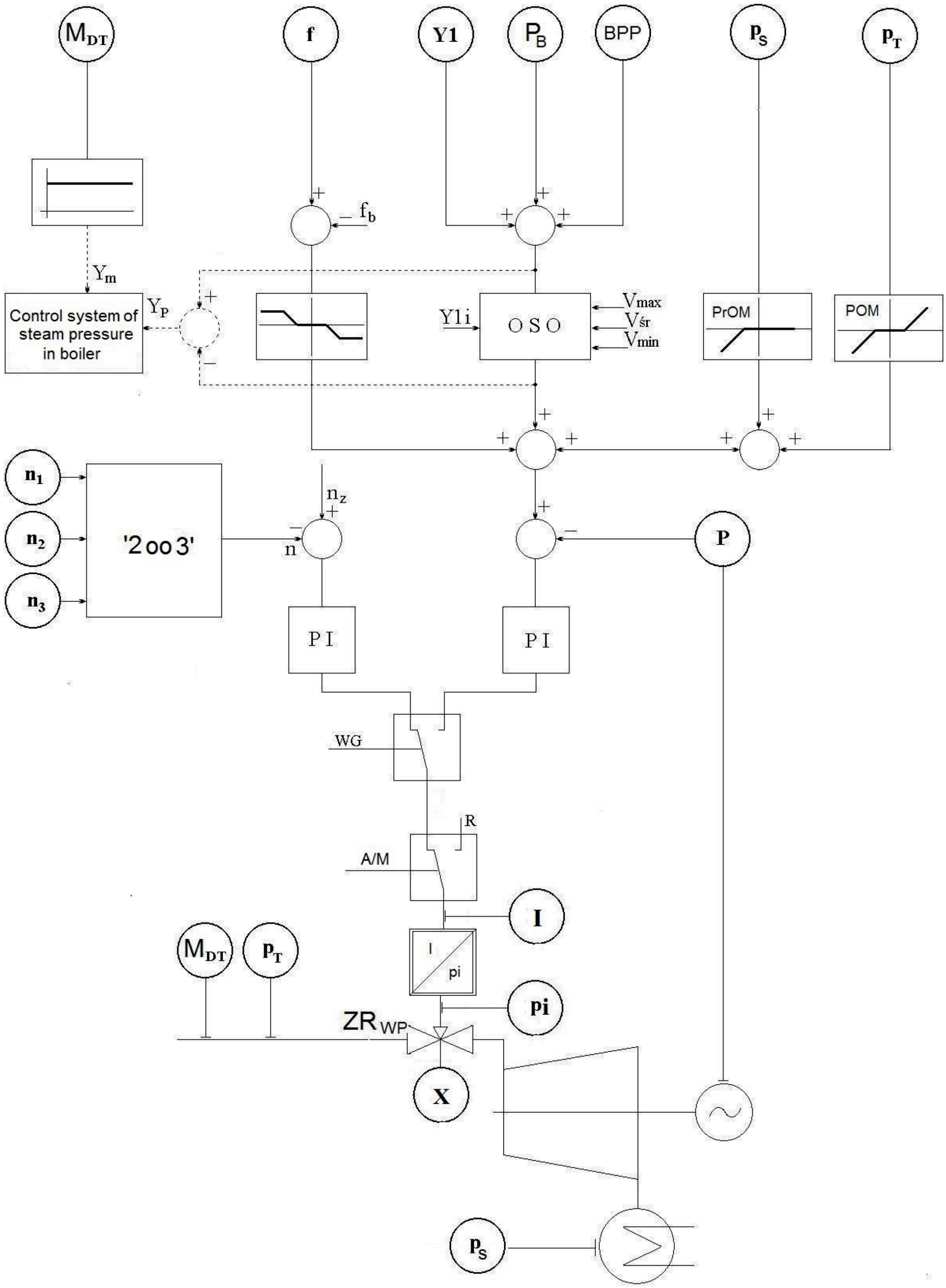

Fig. 4. The block diagram of the control system of a condensing turbine (to improve the clarity of illustration, certain symbols are twice)

Setpoint values defined in pp. 1-3 are introduced as one of three speeds (V_{min}, V_{avg}, V_{max}), formed by OSO (loading speed limiter).

PI controller is used in both cases. It generates a current control signal (I), which is transmitted through the operator console A/M (auto/manual) to the electrohydraulic transducer, which controls the complex set of high-pressure hydraulic valves (ZR_{WP}). Switch-over of the system structure is made by the binary signal WG transmitted from switch of the turbine generator WG.

The list of signals used to control and protection of the condensing turbine, has been shown in Table 1. The signals 10, 11 and 12 are measured for diagnostic reasons exclusively.

Table 1. List of signals used in the control system of the condensing turbine.

No.	Analog signal	Symbol	Units
1	active power of generator	P	MW
2	pressure of fresh steam	p_T	MPa
3	absolute vapor pressure in condenser (vacuum)	p_S	kPa (%)
4	mass flow of steam	M_{DT}	t/h
5	base setpoint of power	P_B	MW
6	system setpoint of power	Y1	MW
7	actual operating point	BPP	MW
8	frequency of electric current	f	Hz
9	rotational speed of turbine	n	1/min
10	control signal, current signal	I	mA
11	oil pressure pulse	p_i	MPa
12	opening degree of control valves	X	%

4.2. Fault Detection and Fault Isolation

There are two phases distinguish during a process diagnosis (Fig. 3): fault detection (FD) and fault isolation (FI). For FD purposes, the method based on relationships between values of process variables, is used in the considered example. On the basis of these relationships, the partial process models are designed, which constitute an information redundancy. The goal is to find models with possible simple structures which satisfactorily meet established requirements. The search for simple structures arises from the need to minimize the calculation time of model output. Adopted relationships should also take into account the dynamics of the value changes of the model parameters. Taking into account the above aspects, the following relations were distinguished for the modeling purposes:

$$\hat{P}_t = f(M_{DT_{t-1}}, P_{t-1}) \tag{1}$$

$$\hat{M}_{DT_t} = f(X_{t-1}, M_{DT_{t-1}}) \tag{2}$$

$$\hat{p}_i = f(I) \tag{3}$$

$$\hat{I} = f(P, p_T) \tag{4}$$

Symbols used in the formulas (1, 2, 3, 4), have been defined in Table 1.

One way to design models for diagnostic purposes is to use the idea of neural fuzzy systems, Takagi-Sugeno-Kang (NFS-TSK). This mathematical apparatus can be used for reliability analysis [10] or modeling for the purpose of analytical redundancy [10, 38].

Neural fuzzy systems are a combination of fuzzy modeling and the structure of artificial neural networks. The construction of NFS model begins with choosing the input and output variables. When creating a fuzzy neural model, expert knowledge is used to determine the number of fuzzy sets for each input and distribution of these fuzzy sets. The value ranges of the model inputs are determined on the basis of measured process data archived by the SCADA or DCS. The number of fuzzy sets determines unambiguously the number of rules. The type of membership function (trapezoidal, triangular, Gaussian) should also be specified. Finally, the model weights are calculated according to the selected neural network learning algorithm. The designed model should provide sufficient modeling accuracy for diagnostic purposes.

There are known algorithms of model identification, with the use of genetic optimization, in which the selection of TSK model structure and parameters is fully automatically implemented [38].

NFS model created in accordance with the formula (1), is shown in Fig. 5. On the other hand, Fig. 6 presents the trends of the following variables: M_{DT} - the mass flow of the steam, P - the active power of the generator, P^ - output from the model represented by the formula (1) with specified input signals, r1- residuum of the model, understood as the difference r1=P-P^. The residuum chart confirms that model sufficiently reflects reality for diagnostic purposes.

The presented relationships were also tested in terms of their sensitivity to detect of sensor faults. The sensor faults

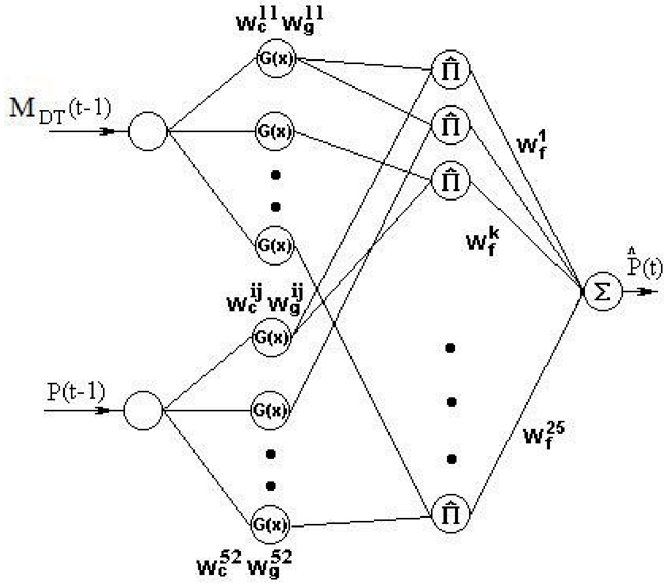

Fig. 5. The structure of the neural fuzzy model created in accordance with formula (1)

can be classified into two basic types: catastrophic faults and parametric faults. The catastrophic faults cause a sudden change of the residuum value. Such a change implies the need to make immediate appropriate safety action. In contrast, the parametric faults are associated with the aging of the components. They are manifested in the form of accumulation of the residuum value. Measures of these changes are mean or variance of the residuum value. On the basis of these parameters a decisions about the need to change the operation manner of the control system may be undertaken.

In order to verify the sensitivity of the model to detect disturbances in the measurement circuit of the active power of the generator, a special fault was simulated. The fault consisting in setting a fixed value of the signal, at a certain moment, for a certain time. Simulation effects of this disturbance, are shown in Fig. 7. The trends demonstrate that the residuum is sensitive to the simulated fault of the active power sensor. The average values of residuals in the sliding window, are used for detecting of faults of measuring circuits. This constitutes the simplest way of filtration.

The next step in the diagnostic process is the isolation of the damaged measuring circuit. There are many methods of fault isolation. One of the ways is to present relationship: faults-symptoms in the shape of a binary diagnostic matrix. The elements of the matrix take

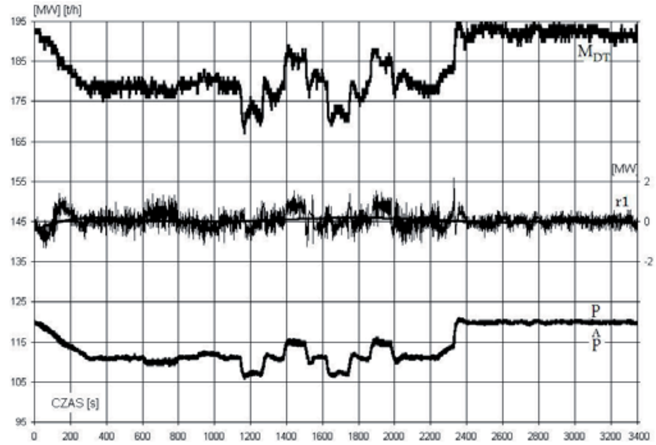

Fig. 6. The modeling results for the data not covered by a training data set. Model was created on basis of formula (1)

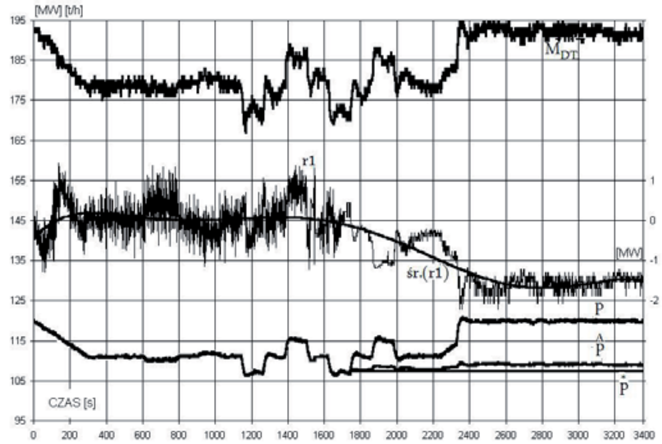

Fig. 7. Simulation of a disturbance in the measurement circuit of the active power (P). Symbols used: P - active power generator, P^ - calculated output of the model based on formula (1), P - fault simulation of the power measurement circuit, MDT- steam mass flow, r1 - model residuum*

a value of 0 or 1, wherein a value of 1 indicates that the residuum is sensitive to a given fault. The fault occurrence causes that the residuum deviates from zero. The exceeding of the defined threshold, is interpreted as a symptom occurrence.

During the design process, one should identify the sensitivity of all the residuals for each fault. The binary diagnostic matrix prepared for the analyzed control system is shown in Table 2.

Table 2. The binary diagnostic matrix.

	M_{DT}	P	p_T	p_i	I
$r_1 = P - \hat{P}$	1	1	0	0	0
$r_2 = M_{DT} - \hat{M}_{DT}$	1	0	0	0	0
$r_3 = p_i - \hat{p}_i$	0	0	0	1	1
$r_4 = I - \hat{I}$	0	1	1	0	1

Detection of sensor fault must result in the reconfiguration of the control system structure or changing the control algorithm. The condensing turbine control system plays a very responsible role in the national power system, therefore immobilizing of the turbine due to fault of the measuring circuits of process variables is not allowed [31, 32].

4.3. Reconfiguration after the occurrence of faults

When starting to design the control system tolerating faults of measuring circuits, it is to specify a set of possible states of the operation (F) of the system, in the case of particular faults:

$$F = \{f_m : m = 1,2...,M\} \tag{5}$$

Brief description of the possible change of the system operation when occur the faults defined in Table. 1, has been presented in Table 3.

Table 3. System reconfiguration after the occurrence of possible faults of measuring circuits

State	Fault of measuring circuit	Possible change of operation when fault occur
F1	Active power (P) produced by generator	Use of virtual power sensor or switching to manual control of turbine valves from operator console.
F2	Pressure of fresh steam (p_T)	Disconnection of the primary control. Blockade of intervention power (blockade of Y1i signal). Turning off the steam power limiter (POM). Setting the minimum speed in the loading speed limiter (OSO).
F3	Absolute vapor pressure in condenser (vacuum) (p_S)	Turning off the vacuum power limiter (PrOM). Blockade of intervention power (blockade of Y1i signal).
F4	Mass flow of steam (M_{DT})	Disconnection of the signal Y_m coupling of the boiler control system with the turbine control system.
F5	System setpoint of power (ARCM-Y1)	Disconnection of the signal Y1from the secondary control (system power setpoint).
F6	Actual operating point (BPP)	Changing the setpoint from BPP on P_B - the base setpoint of power (on the operator panel).
F7	Frequency of the electric current (f)	Use of turbine rotary speed instead of a current frequency.
F8	The rotational speed of the turbine (n)	Rejection of measurements from a faulty sensor and work with the other two.
F9	Measurement of the control signal (I)	Reconfiguration of diagnostic system which supports the control system.
	The oil pressure pulse (p_i)	
	The opening degree of control valves (X)	

One of the most important signals introduced to the control system for the purpose of control and safety, is the steam pressure p_T. In control systems with a leading turbine, checking the steam pressure is intended to protect the energetic block against the unacceptable power fluctuations. The power generated by the energetic block should be adapted to the current possibilities of water, air and fuel supply installations. Therefore, in case of fault detection of the steam pressure measuring circuit, one should change the operation manner of the control system so that the fault does not have a negative impact on the whole energetic block. For this purpose, it is necessary to reconfigure the system, consisting of the following actions:

1) Disconnection of the primary control system, because it is relatively fast and can have a negative impact on the operation of the energetic block, in the absence of appropriate value of the steam pressure,
2) Blockade of the binary signal Y1i of the intervention power,
3) Turning off the steam power limiter (POM). The characteristics of the output of this programming block is depending on the measured value of the steam pressure. Incorrectly measured pressure value may send false signals to the power setpoint for the whole energetic block,
4) Setting of minimum speed V_{min} [MW/min] in OSO (loading speed limiter).

With the above assumptions, the block can operate to a limited extent, even with the remote signals, as shown in Fig.8. Additional protective signals Y_m and Y_p, coupling the power control system with a control steam pressure in the boiler, which ensure to get the adequate power in the system with the leading turbine. In this kind of systems the turbine power control plays in the energetic block the primary role. In contrast, the boiler steam pressure control is subordinated. One should stress, however a general rule, that it is better to switch off the remote setpoint source, than defending the remote control mode at all costs. This could result in disconnection of the energetic block from the national electro-energy system.

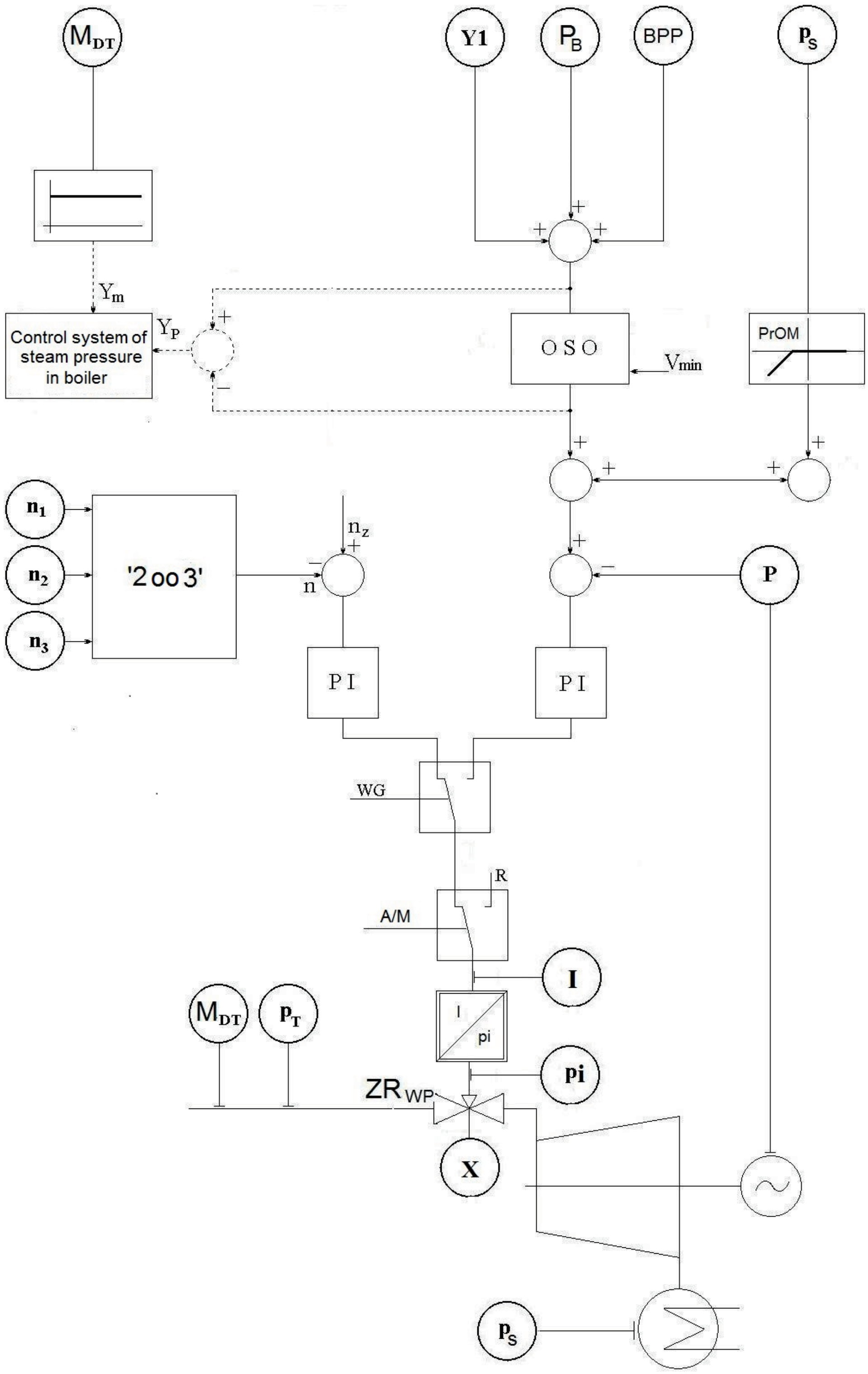

Fig. 8. Block diagram of the turbine control system shown in Fig. 3, after the reconfiguration made after fault detection of the measuring circuit pT

5. Influence of diagnostics and fault tolerance on the coefficients of system reliability and system safety

A positive influence of fault tolerance and diagnosis carried out in real time on the reliability and security of the system can be demonstrated by analyzing the coefficients characterizing these properties. Definition of the fully operational system state and the faulty system states (e.g. F1-F9 states shown in Table 3), is given in Fig. 9. The characteristic time intervals have the following meaning:

- Mean time to failure (*MTTF*) - T_λ ,
- Mean time to repair (*MTTR*), i.e. the average time interval from the failure occurring till the repair of a faulty device - T_μ ,
- Mean time between failures (*MTBF*), i.e. $MTBF = MTTF + MTTR$,
- Mean time of diagnosis - T_D
- Mean time of renewal, i.e. replacing the defective device to the efficient one together with the restoration of the system after repair/replacement - T_N .

In case of the repairable systems, such as FTCS, the system availability coefficient, is widely used as the reliability indicator [44]. It is defined by the formula:

$$A = \frac{T_\lambda}{T_\lambda + T_\mu} \tag{6}$$

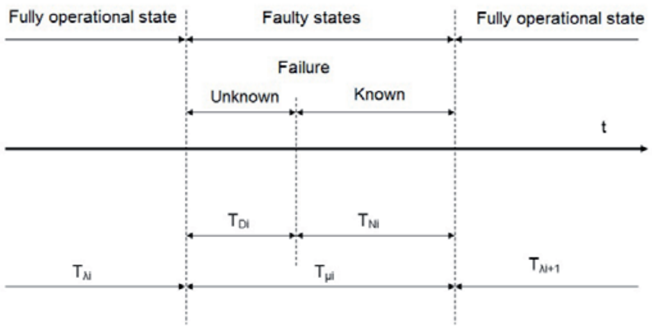

Fig. 9. Definition of the fully operational system state and the faulty system states.

Mean time to repair is the sum of mean time of diagnosis and mean time of renewal:

$$T_\mu = T_D + T_N \tag{7}$$

Shortening the time of diagnosis reduces repair time and thus raises the value of the availability coefficient of the system (6). In practice, the time of diagnosis is close to zero: $T_D \approx 0$. However, in the event of failures, which are tolerated by the control systems, the time of automatically realized reconfiguration is reduced to zero .

The intensity of failures is an inverse of mean time to failure:

$$\lambda = \frac{1}{T_\lambda} \tag{8}$$

The following types of failures are distinguished in the standard of functional safety PN-EN61508 [33]:

- dangerous, detectable,
- dangerous, undetectable,
- safety (do not cause the danger), detectable,
- safety (do not cause the danger), undetectable.

The total intensity (probability) of occurrence of failures λ is the sum of the intensity of dangerous failures detectable λ_{DD}, dangerous undetectable λ_{DU}, safety detectable λ_{SD} and safety undetectable λ_{SU}.

$$\lambda = \lambda_{DD} + \lambda_{DU} + \lambda_{SD} + \lambda_{SU} \tag{9}$$

Safety Integrity Level (SIL), defined in the standard PN-EN61508 [33], depends on:

- the average probability of lack of fulfillment the safety function (PFD_{SYS}) – for security systems operating on a call or
- the average probability of dangerous failure per hour (PFH_{SYS}) - for security systems operating continuously.

The values of these probabilities depend on diagnostic coverage *DC*, among others.

Diagnostic coverage *DC* is a relative reduction of the probability of dangerous hardware failures resulting from the performing of the on-line diagnostic tests (according to PN-EN 61508 [33]):

$$DC = \frac{\lambda_{DD}}{\lambda_{DD} + \lambda_{DU}} \tag{10}$$

The formula (10) indicates that the performance of on-line diagnostic tests of all dangerous failures, gives the possibility to increase the diagnostic coverage factor *DC* to 1. This reduces the risk, in other words decreases the probabilities PFD_{SYS} or PFH_{SYS}.

Another indicator illustrating the effect of diagnosis is the Safety Failure Fraction (SFF):

$$SFF = \frac{\lambda_{SD} + \lambda_{SU} + \lambda_{DD}}{\lambda_{SD} + \lambda_{SU} + \lambda_{DD} + \lambda_{DU}} = \frac{\lambda - \lambda_{DU}}{\lambda} \tag{11}$$

This factor is essential for SIL verification of the E/E/PE systems carried out on the basis of data related to the tolerability of hardware failures. The more failures are detectable, the value of this ratio increases, and with full detectability it reaches a value of 1.

In the definitions of *DC* and *SFF* specified in the standard, there are distinguished failures both detectable and undetected using on-line diagnostic tests. However, it looks like a mistake resulting from imprecise terminology. In fact, the condition for effective protective action is a precise failure isolation. Therefore, there is a need not only for detectability, but also distinguishability of each failure in the isolation phase.

The basic structure of the considered turbine control system (Fig. 10) is helpful in determination of the probability of dangerous failure (*PFH*).

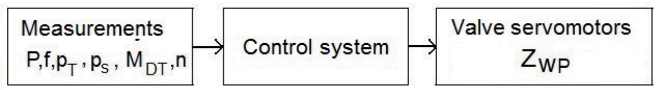

Fig. 10. The basic structure of the considered turbine control system.

Probability PFH_{SYS} of the entire system is defined by formula (12):

$$PFH_{SYS} = PFH_{Measurements} + PFH_{Control\ system} + PFH_{Valve\ servomotors} \tag{12}$$

In view of the fact that all the fault tolerance of measuring devices, $PFH_{Measurements}$ probability is zero and thus the value of the indicator *PFH* of the entire system decreases.

The considered example shows that the implementation of fault tolerant control systems contributes significantly to improving the safety and reliability of control systems and controlled processes.

6. Summary

The integration of diagnostic software with control software is necessary to the implementation of fault tolerant control systems. Two solutions are possible. The first is based on integration of control software executed in PLC controllers with on-line diagnostic system implemented in a master computer. This diagnostic system receives necessary data from PLC controllers. Such a system is AMandD, designed in Institute of Automatic Control and Robotics at Warsaw University of Technology [23]. Information about faults transmitted from the diagnostic system to the controller initiates the necessary reconfiguration of control systems. AMandD system is still being developed under the name DiaSter, in cooperation with Rzeszow University of Technology, Silesian University of Technology and University of Zielona Gora [17, 38].

Such solution with a separate diagnostic system can cause too large delays in support of protective actions. A better solution is to implement necessary diagnostic software in PLC controllers. It should be an integral part of process control software. Speed of response to fault occurring in this case is much higher. The diagnostic methods should be used to ensure rapid detection of faults. They include methods based on models of objects. Such a solution has been implemented in the condensing turbine control system, in one of the national energetic blocks [29-32, 41].

It can be expected that in the nearest future, the rapid development of control systems equipped with software for process diagnosis and fault tolerance will take place. Also the number of industrial applications will grow in this field. Of course, such systems before deploying them to the industry, require full verification and validation of hardware and software, in accordance with the requirements of the relevant functional safety standards (PN-EN 61508 i PN-EN 61511 lub PN-EN 62061), in the overall functional safety management in the life cycle [20, 21]. A certain barrier for industrial applications is lack of sufficient number of appropriate specialists. However, now in many technical universities these issues are included in the curricula and young engineers will be prepared to implement innovative control systems.

References

1. http://www.sache.org/beacon/files/2009/09/pl/read/2009-09-Beacon-Polish%20-s.pdf
2. http://archiwum.ciop.pl/18388.html
3. Blanke M, Kinnaert M, Lunze J, Staroswiecki M. Diagnosis and Fault-Tolerant Control. Berlin Springer-Verlag, 2004.
4. Calado J M F, Korbicz J, Patan K, Patton R J, Sáda Costa J M G. Soft computing approaches to fault diagnosis for dynamic systems. European Journal of Control 2001; 7(2–3): 248–286, http://dx.doi.org/10.3166/ejc.7.248-286.
5. Chiang L H, Russell E L, Braatz R D. Fault Detection and Diagnosis in Industrial Systems. London: Springer, 2001, http://dx.doi.org/10.1007/978-1-4471-0347-9.
6. Frank P M. Fault diagnosis in dynamic systems using analytical and knowledge-based redundancy. Automatica 1990; 26: 459-474, http://dx.doi.org/10.1016/0005-1098(90)90018-D.
7. Gertler J. Fault Detection and Diagnosis in Engineering Systems, New York - Basel - Hong Kong: Marcel Dekker. Inc., 1998.
8. Hajiyev C, Caliskan F. Fault Diagnosis and Reconfiguration in Flight Control Systems. London: Kluwer Academic Publishers, 2003, http://dx.doi.org/10.1007/978-1-4419-9166-9.
9. Héctor B, Fabián G. Reconfigurable Distributed Control. London: Springer, 2005.
10. Huang H Z. Structural reliability analysis using fuzzy sets theory. Eksploatacja i Niezawodnosc – Maintenance and Reliability 2012; 14(4): 284–294.
11. IEC 61508 (2010). Functional safety of electrical/electronic/programmable electronic safety – related systems. Parts 1-7. International Electrotechnical Commission (IEC), Geneva.
12. IEC 62061 (2005). Safety of machinery – Functional safety of safety-related electrical/electronic and programmable electronic control systems (E/E/PE). International Electrotechnical Commission (IEC), Geneva.
13. Isermann I. Fault-Diagnosis Systems: An Introduction from Fault Detection to Fault Tolerance. Berlin: Springer, 2005.
14. Isermann R, Ballé P. Trends in the application of model-based fault detection and diagnosis of technical process. Control Engineering Practice 1997; 5(5): 709-719, http://dx.doi.org/10.1016/S0967-0661(97)00053-1.
15. Jormakka H, Koponen P, Pentikainen H, Bartoszewicz-Burczy H. On managing physical and cyber threats to energy systems identification and countermeasure requirements. Eksploatacja i Niezawodnosc – Maintenance and Reliability 2010; 3: 27-33.
16. Kamal E, Aitouche A, Ghorbani R, Bayart M. Fuzzy Scheduler Fault-Tolerant Control for Wind Energy Conversion Systems. Control Systems Technology, IEEE Transactions 2014; 1(22):119 – 131, http://dx.doi.org/10.1109/TCST.2013.2246162.
17. Korbicz J, Kościelny J M. Modeling, Diagnostics and Process Control. Implementation in the DiaSter System. Springer, 2010.
18. Korbicz J, Kościelny J M, Kowalczuk Z, Cholewa W, et al. Fault Diagnosis: Models, artificial intelligence methods, applications. Berlin: Springer, 2004, http://dx.doi.org/10.1007/978-3-642-18615-8.
19. Korbicz J. Robust fault detection using analytical and soft computing methods. Bulletin of the Polish Academy Sciences. Technical Sciences 2006, 54(1):75-88.
20. Kosmowski K. Layer of protection analysis in the context of functional safety management. 10th Conference Diagnostics of Processes and Systems. Zamość: 2011; 1:371-378
21. Kosmowski K, Śliwiński M. Od lipca 2015 r. zmiany w normie PN EN 61511. IV Forum Bezpieczeństwa Funkcjonalnego, Urząd Dozoru Technicznego, Ożarów Mazowiecki, 26-27 lutego 2015.
22. Kościelny J M. Diagnostyka zautomatyzowanych procesów przemysłowych –Diagnosis of automated industrial processes. Akademicka Oficyna Wydawnicza Exit – Academic Publishing House Exit, Warsaw, 2001.
23. Kościelny J M, Syfert M, Wnuk P. Advanced monitoring and diagnostic system 'AMandD'. 6th IFAC Symposium on Fault Detection, Supervision and Safety of Technical Processes. SAFEPROCESS'06, Beijing, P.R. China, August 29-September 1 2006, 635-640, http://dx.doi.org/10.1016/B978-008044485-7/50107-X.
24. Leonhardt S, Ayoubi M. Methods of fault diagnosis. Control Engineering Practice 1997; 5(5): 683-692, http://dx.doi.org/10.1016/S0967-0661(97)00050-6.
25. Mahmoud M, Jiang J, Zhang Y M. Active Fault Tolerant Control Systems. Stochastic Analysis and Synthesis. Lecture Notes in Control and Information Sciences. Berlin: Springer, 2003.
26. Patton R J, Lopez-Toribio C J, Uppal F J. Artificial intelligence approaches to fault diagnosis for dynamic systems. International Journal of Applied Mathematics and Computer Science 1999; 9(3): 471-518.
27. Patton R J, Frank P, Clark R. Issues of fault diagnosis for dynamic systems. Berlin: Springer, 2000, http://dx.doi.org/10.1007/978-1-4471-3644-6.
28. Patton R, Montander S. Active fault tolerant control for nonlinear systems with simultaneous actuator and sensor faults. International Journal of Control, Automation and Systems 2013; 6(11): 1149-1161.
29. Pawlak M, Karczewski J. New Structure of Governor Electrohydraulic Power which meets the Requirements of the Implemented LFC-System. ActaEnergetica 2014; 1(18): 126-135.
30. Pawlak M, Karczewski J. Struktura UAR turbiny kondensacyjnej biorącej udział w regulacji systemu elektroenergetycznego – Structure of control system of condensation turbine taking part in control of electroenergy system. VII Konferencja Problemy Badawcze Energetyki

Cieplnej – VII Conference on Thermal Energy Research Issues. Warsaw, 2005.
31. Pawlak M. Zmodernizowany układ regulacji elektrohydraulicznej turbiny zaprojektowany w OTC Lodz – Modernized electro-hydraulic control system of turbine designed in Thermal Technology Branch ITC" in Lodz. Energetyka – Energetics, 2011; 22: 70-73.
32. Pawlak M. Zwiększenie niezawodności bloku energetycznego współspalającego biomasę - Reliability increase of energy block using biomass. Cieplne Maszyny Przepływowe – Turbomachinery, 2010; 138: 37-43.
33. PN-EN 61508 (2010). Bezpieczeństwo funkcjonalne elektrycznych/ elektronicznych/ programowalnych elektronicznych systemów związanych z bezpieczeństwem. Części 1-7. Polski Komitet Normalizacyjny.
34. PN-EN 61511 (2009). Bezpieczeństwo funkcjonalne. Przyrządowe systemy bezpieczeństwa do sektora przemysłu procesowego. Części 1-3. Polski Komitet Normalizacyjny.
35. Simani S, Fantuzzi C, Patton R J. Model-based Fault Diagnosis in Dynamic Systems using Identification Techniques. New York: Springer, 2003, http://dx.doi.org/10.1007/978-1-4471-3829-7.
36. Steffen T. Control Reconfiguration of Dynamic Systems: Linear Approaches and Structural Tests, Lecture Notes in Control and Information Sciences. Berlin: Springer, 2005.
37. Stoican F, Olaru S, Seron M, Doná J. Fault tolerant control scheme based on sensor–actuation channel switching and dwell time. International Journal of Robust and Nonlinear Control 2014; 4(24): 775–792, http://dx.doi.org/10.1002/rnc.2907.
38. Syfert M, Wnuk P, Kościelny J M. DiaSter - Intelligent system for diagnostics and automatic control support of industrial processes. JAMRIS - Journal of Automation, Mobile Robotics & Intelligent Systems 2011; 4: 41-46.
39. Tao G, Chen S, Joshi S M, Tang X. Adaptive Control of Systems with Actuator Failures. Berlin: Springer, 2004, http://dx.doi.org/10.1007/978-1-4471-3758-0.
40. Trybus L. Systemy sterowania w energetyce. Control systems in energetics. XV Krajowa Konferencja Automatyki. XV Domestic Conference of Automatics. Warsaw: 2005; 1:29-40.
41. Wasiewicz P, Pawlak M. Development of fault tolerant control system for condensation power turbine. 6th IFAC Symposium on Fault Detection Supervision and Safety of Technical Processes. SAFEPROCESS'06, Beijing, P.R. China, August 29-September 1 2006, 523-528, http://dx.doi.org/10.1016/B978-008044485-7/50082-8.
42. Witczak M. Fault Diagnosis and Fault-Tolerant Control Strategies for Non-Linear Systems. Berlin: Springer-Verlag, 2014, http://dx.doi.org/10.1007/978-3-319-03014-2.
43. Wnuk P. The use of evolutionary optimization in fuzzy TSK model identification. 6th IFAC Symposium on Fault Detection, Supervision and Safety of Technical Processes. SAFEPROCESS'06, Beijing, P.R. China, August 29-September 1 2006, 414-419, http://dx.doi.org/10.1016/B978-008044485-7/50070-1.
44. Zamojski W. Niezawodność i eksploatacja systemów. System reliability and maintenance. Wrocław: Oficyna Wydawnicza Politechniki Wrocławskiej, Wroclaw University of Technology Publishing House, 1981.

Mariusz PAWLAK
Jan Maciej KOŚCIELNY
Piotr WASIEWICZ
Institute of Automatic Control and Robotics
Warsaw University of Technology,
sw. Andrzeja Boboli 8, 02-525 Warsaw, Poland
E-mail: m.pawlak@mchtr.pw.edu.pl, jmk@mchtr.pw.edu.pl,
p.wasiewicz@mchtr.pw.edu.pl

Article citation info:
SINGH SSK, ABDULLAH S, MOHAMED NAN. Reliability analysis and prediction for time to failure distribution of an automobile crankshaft. Eksploatacja i Niezawodnosc – Maintenance and Reliability 2015; 17 (3): 408–415, http://dx.doi.org/10.17531/ein.2015.3.11.

Salvinder Singh Karam SINGH
Shahrum ABDULLAH
Nik Abdullah Nik MOHAMED

RELIABILITY ANALYSIS AND PREDICTION FOR TIME TO FAILURE DISTRIBUTION OF AN AUTOMOBILE CRANKSHAFT

ANALIZA NIEZAWODNOŚCI I PRZEWIDYWANIE ROZKŁADU CZASU DO USZKODZENIA WAŁU KORBOWEGO POJAZDU SAMOCHODOWEGO

This paper emphasizes on analysing and predicting the reliability of an automobile crankshaft by analysing the time to failure (TTF) through the parametric distribution function. The TTF was modelled to predict the likelihood of failure for crankshaft during its operational condition over a given time interval through the development of the stochastic algorithm. The developed stochastic algorithm has the capability to measure the parametric distribution function and validate the predict the reliability rate, mean time to failure and hazard rate. T, the algorithm has the capability to statistically validate the algorithm to obtain the optimal parametric model to represent the failure of the component against the actual time to failure data from the local automobile industry. Hence, the validated results showed that the three parameter Weibull distribution provided an accurate and efficient foundation in modelling the reliability rate when compared with the actual sampling data. The suggested parametric distribution function can be used to improve the design and the life cycle due to its capability in accelerating and decelerating the mechanism of failure based on time without adjusting the level of stress. Therefore, an understanding of the parametric distribution posed by the reliability and hazard rate onto the component can be used to improve the design and increase the life cycle based on the dependability of the component over a given period of time. The proposed reliability assessment through the developed stochastic algorithm provides an accurate, efficient, fast and cost effective reliability analysis in contrast to costly and lengthy experimental techniques.

Keywords: *reliability; time to failure; monotonic function, hazard rate.*

W prezentowanej pracy przedstawiono metodę analizy oraz predykcji niezawodności wału korbowego pojazdu samochodowego opartą na analizie czasu do uszkodzenia (TTF) z wykorzystaniem funkcji rozkładu parametrycznego. W artykule, stworzono model TTF pozwalający na przewidywanie prawdopodobieństwa uszkodzenia wału korbowego w stanie pracy w danym przedziale czasu za pomocą nowo opracowanego algorytmu stochastycznego. Opracowany algorytm stochastyczny umożliwia mierzenie funkcji rozkładu parametrycznego oraz weryfikację przewidywanego współczynnika niezawodności, średniego czasu do uszkodzenia oraz współczynnika zagrożenia. Algorytm daje możliwość statystycznej weryfikacji modelu w odniesieniu do rzeczywistych danych dotyczących czasu do uszkodzenia pochodzących z lokalnego przemysłu samochodowego. Weryfikacja taka pozwala na otrzymanie optymalnego modelu parametrycznego reprezentującego uszkodzenie części składowej. Zweryfikowane wyniki wykazały, że trójparametrowy rozkład Weibulla stanowi dokładne i wydajne narzędzie do modelowania współczynnika niezawodności w zestawieniu z rzeczywistymi danymi z próby. Proponowaną dystrybuantę parametryczną można wykorzystywać do doskonalenia konstrukcji oraz cyklu życia wału korbowego ponieważ daje ona możliwość przyspieszania i zwalniania mechanizmu uszkodzenia, na podstawie czasu, bez potrzeby regulacji poziomu naprężenia. Zatem, znajomość rozkładu parametrycznego oraz obliczonych na jego podstawie współczynników niezawodności i zagrożenia omawianego elementu mechanizmu korbowego, pozwala na doskonalenie konstrukcji oraz wydłużenie cyklu życia wału korbowego w oparciu o dane dotyczące jego niezawodności w danym okresie czasu. Proponowana metoda oceny niezawodności z wykorzystaniem opracowanego w artykule algorytmu stochastycznego umożliwia dokładną, wydajną, szybką i tanią analizę niezawodności w odróżnieniu od kosztownych i czasochłonnych technik eksperymentalnych.

Słowa kluczowe: *niezawodność; czas do uszkodzenia; funkcja monotoniczna, wskaźnik zagrożenia.*

1. Introduction

Failure of mechanical components such as the crankshaft is a constant key issue in managing the life cycle and risk analysis in the automobile industry. Generally, there are two methods used in determining the appropriate model in determining the time to failure for the automobile crankshaft which were (1). Understanding of the physical nature of failure through the experimental analysis, (2). By analysing and predicting the reliability based physical nature of failure through a stochastic process. It is known that the crankshaft is designed to last a lifetime with a significant safety limit [2-3, 5] but its failure is still unavoidable due the variation of loading sequence during its operating condition. Therefore, the consequences of failure of the crankshaft over its operating period would cause a more severe failure towards the engine block and the other connecting subcomponents [6, 22]. It has been shown in the literature [9-12, 14, 33] through their experimental analysis and simulation, the mean time to failure would be random due to high cycle and low stress of bending and torsion loads. Therefore, the component has to meet strict criteria, to ensure its reliability characteristics.

Nevertheless, there is a possibility of unavoidable component failure, which over time results from fluctuating service loading [8,15]. Not only does a component approaching fatigue failure threaten the correct functioning of the entire system, it causes other components to operate at suboptimal levels. Earlier experimental studies discussing the model of uncertainty have concluded that crack growth behaviour and the overall fatigue life are a result of variability and uncertainty in the load spectrum [1, 4, 17]. The importance of predicting fatigue failure is therefore unequivocal, and data from real-time monitoring can provide an accurate assessment of the durability of a component or structure, so performance can be maintained and the equipment lifetime is maximised [25-27]. Hence, stochastic modelling method will provide a new perspective in contrast to the conventional deterministic models. The prior model evolves in the direction of more computational mathematical methods based on the Markov process, rather than lengthier Karhunen–Loeve, Weiner integral, and Rayleigh techniques [23, 33-34].

Therefore, the modelling of the stochastic process using the suggested Markov chain provides an alternative method is assessing time to failure for a given structure or component. This is because the Markov chain is a probabilistic method that has the ability to synthetically generate and calculate an accurate relationship between experimental and simulation data based on the failure state conditions [10]. Likewise, the probability relates to the physical condition of components the reliability of random fatigue crack growth under variable amplitude loading can model the effects of the loading sequence and correlate this to the effects on the structure. Therefore, the failure of most components is relative towards the function performed by that component or the system over a given period of time where this was used to quantify the time to failure in terms of reliability [35,36]. This is because the Weibull distribution has the capability to increase or decrease the failure time without changing the level of stress through the various properties of the shape, scale and location parameter that was further characterized mathematically into 2 modes: (1). Non-monotonic failure - observing the bath tub curve, (2). Monotonic failure; in predicting the failure rate [21, 28].

The reliability lifecycle assessment of an automobile crankshaft is studied in this paper by modelling the stochastic algorithm based on the time to failure distribution. This is much needed by the local automobile industry because at the present time, the automotive industry uses dynamic phenomena to predict fatigue failure under service loading that leads to conservative designs and higher costs in manufacture and maintenance. This stochastic algorithm modelling evolves around the mathematical tool to quantifying variable loading over a given period of time by synthetically generating time to failure data that is near similar based on actual max–min. This stochastic algorithm uses the probabilistic approach which consists of measures that define a sample space based on a time function, assigned to each outcome. Likewise, the importance of modelling the stochastic algorithm is to bridge the gap between the stochastic process and the experimental method by characterizing reliability lifecycle assessment through the parametric distribution models under random mixed mode loading. Thus, the stochastic algorithm is developed in order to assess the reliability rate, mean time to failure and hazard rate through the parametric distribution to model. More poignantly, the significant difference between the both the stochastic algorithm and experimental model is validated through the statistical process in determining the optimal reliability and hazard rate based on the parametric distributions.

2. Methodology

2.1. Development of framework

Reliability is an important tool in lifetime prediction for all mechanical components especially in the automobile industry. The reliability lifetime prediction for the crankshaft must be approached at the fundamental level by understanding the physics and mechanism of failure that would occurs on the crankshaft over a given period. Therefore it is important to identify the physics and mechanism of failure before beginning the reliability modelling (Fig. 1).

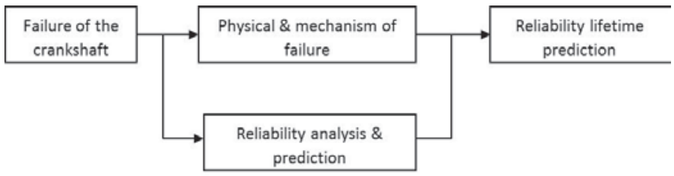

Fig. 1. Reliability lifetime prediction process flow for the crankshaft

The reliability time to failure assessment (Fig. 2) illustrates the operational loading condition of the crankshaft through a combination of the bending and torsional stresses, where in general the combination of the stresses will lead towards the failure of the crankshaft over a given period of time. Since the fatigue failure is considered to be stochastic in nature, therefore it is justified to model the failure of the component based on random loading over a given period of time. Various studies in the literature [16, 32] have mentioned that the time to failure for the component would be between 30 hours to 700 hours depending on the severity of the operating condition.

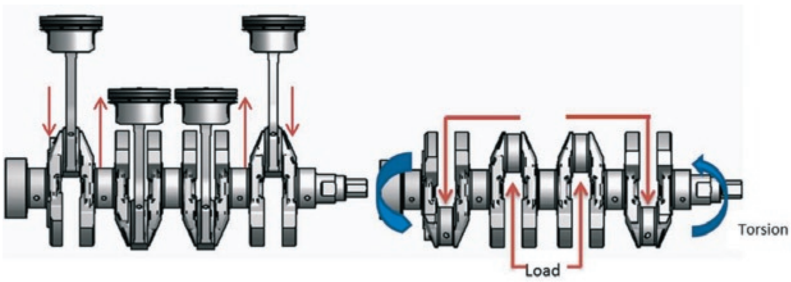

Fig. 2. Operational loading of the automobile crankshaft under bending and torsional stresses

Hence, the Discrete Markov Chain is used to computationally model the failure probability criterion through the characterization of failure states over a given period of time. Likewise, the development of the schematic stochastic algorithm provides a computational accurate and efficient prediction based on the time to failure [7, 13] when compared with the practical operating condition of the crankshaft. The development of the algorithm based on the framework provides the reliability assessment especially when there are constrains due to cost and lengthy duration of experimental setups. The TTF parametric distribution of Weibull, Lognormal and Gaussian is developed to determine the optimal model in reliability prediction for the crankshaft based on the physics and mechanism of failure (Fig. 3).

The flowchart (Fig. 3) explains:

1. Characterize the failure model of the crankshaft through the stochastic process based on the mechanism of failure.
2. Simulate the time to failure through the Markov Chain model to obtain near identical data as the sampling data.
3. Derive the TTF parametric distribution of Weibull, Lognormal and Gaussian distribution model to determine the reliability, failure rate and mean time to failure.
4. Statistically evaluate the reliability rate, failure rate and mean time to failure with obtained automobile sampling data.
5. Propose an appropriate TTF parametric distribution model as an optimal model in reliability analysis and prediction for the crankshaft.

In this paper, the TTF prediction and updating framework is presented in application to the problem of reliability assessment of the automobile crankshaft. This suggested method uses the Markov

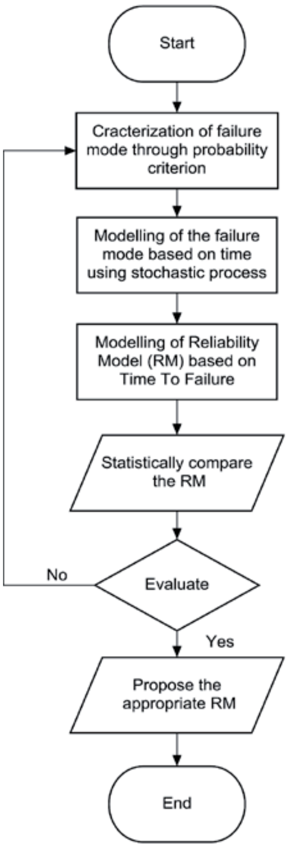

process which is a modification of the previously developed Bayesian framework for fatigue damage prediction[11]. The stochastic process is applied in two levels: first, to generate synthetical data that mirrors the actual time to failure data using the failure probabilitic criterion through the Markov process; second, to assess the reliability of the component based on each of the parameteric distribution class within a set of the synthetically generated data. Consequently, this model provides the advantage of being able to quantify the optimal parametric distribution associated with (1) model parameters and (2) model choice for the reliability assessment, in response to the actual loading condition in modeling in predicting fatigue failure. Finally the TTF models is validated with the existing industrial data obtained from the local automobile industry to determine the optimal parametric distribution model to be used for the reliability assessment of the crankshaft. The conceptual scheme (Fig. 4) of the proposed stochastic model framework for reliability assessment of time to failure based on the parametric distribution is illustrated.

Fig. 3. Structure of the proposed TTF stochastic failure algorithm model.

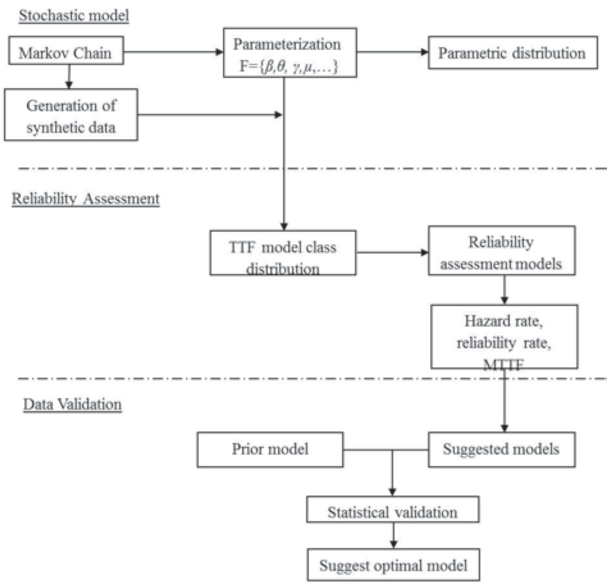

Fig. 4. Stochastic framework for TTF reliability assessment

2.2. Modelling of time to failure through the Markov Chain model

The characterization of failure is modelled as a state transition probability based on the mechanism of failure using the Markov Chain process. The Markov Chain has the capability in providing information for the future state, where the future state is independent of the past state given that present state is known [7]:

$$P_r[X_k = j|X_{k-1} = i, X_{k-2} = i_1, ..., X_0 = i_k] = P[X_k = j|X_{k-1} = i_k] = p_{ij} \tag{1}$$

The time to failure for the crankshaft is modelled as a two state Markov Chain two-state condition (Fig. 5) based on the actual loading condition is represented in the state condition. Likewise consider the states as follows: B: bending and T: torsion where in the Markov model, each occurrence between states is characterized by an occurrence rate and is modeled as a recurrent state condition. The recurrent tells us that the chain will keep on changing over a given period of time until failure and it is observed that the transitions from B to T and T to B may have consequences but both form one unique cluster, i.e., the instrinct state of failure for the component.

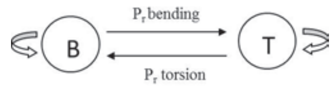

Fig. 5. Markov failure model (occurrence rate from state bending to torsion and vice versa).

Based on the experimental time to failure recorded from previous studies as mentioned earlier provided the physics and mechanism of failure for the crankshaft where from the preceding state condition (Fig. 4), the following Markov Chain model is numerically modelled to represent the state transition of failure over the given period of time.

$$\begin{aligned}
&P_r[X_t = B|X_{t-1} = T_1, X_{t-2} = T_1, ..., X_0 = B_t]P[X_{t-1} = T_1, X_{t-2} = T_2, ..., X_0 = B_t] \\
&= P_r[X_t = B|X_{t-1} = T_1]P_r[X_{t-1} = T_1, X_{t-2} = T_2, ..., X_0 = B_t] \\
&= P_r[X_t = B|X_{t-1} = T_1]P_r[X_{t-1} = T_1|X_{t-2} = T_2, ..., X_0 = T_t]P_r[X_{t-2} = T_2, ..., X_0 = B_t] \\
&= P_r[X_t = B|X_{t-1} = T_1]P_r[X_{t-1} = T_1|X_{t-2} = T_2]P_r[X_{t-2} = T_2..., X_0 = B_0] \\
&= P_r[X_{t-1} = T|X_0 = B] = P_r[X_{n+1} = T|X_n = B]
\end{aligned} \tag{2}$$

where $X_t, t = 0, 1, 2, ...$ The Markov Chain model from the preceding equations creates the ability to generate a new sequence of numerically random yet near similar sampling data that will be further used in determining the reliability of the crankshaft over a given period of time [24].

Hence, the developed Markov Chain model looks at the probabilistic criterion for bending and torsion loading based on the modelled state condition under the mixed mode loading criteria, even though it has been mentioned that the torsional load can be neglected because this load is considered less than ten percent of the bending load [Fonte]. Hence, based on the perception, probability matrix (P^n) is modelled in terms of the probabilistic matrices to model the probabilistic condition though various sets of probabilistic condition to illustrate as the probability of going from P_B to P_T.

$$P^n = \begin{pmatrix} P_{11} & P_{12} \\ P_{21} & P_{22} \end{pmatrix}^t \tag{3}$$

Due to this effect, the probability matrix (P^n), in the form of the time (T) was used to analyze the time condition each time the chain visited the individual state condition. Therefore, the stochastic process, in the form of the time vector, (T) was used to analyze the loading condition each time the chain visited the individual state condition:

$$L = \begin{pmatrix} L_{max} \\ L_{min} \end{pmatrix} \tag{4}$$

Furthermore, the time taken for torsion loading to start its effect is when the crankshaft is in the operating condition due to forces acting in the direction of the axial rotation but it must be supported by the bending loading conditions and this is modelled in terms of the probability matrix (μ). The purpose of using this matrix is to provide a weightage on the failure criterion besides eliminating confusing for the initial condition of the failure of the component.

$$\mu = \begin{pmatrix} \mu_{11} & \mu_{1b} \end{pmatrix} \tag{5}$$

Finally, the discrete Markov Chain is expressed in the generalized scalar terms, by providing a direct time-based approach for determining the TTF for the transition from one state to another. This generalized term is used in for the reliability assessment in in reliability assessment for the fatigue failure [7, 18].

$$E(X) = \mu.P^n.[L] \tag{6}$$

2.3. Fundamental formulation for reliability

TTF for an automobile crankshaft under loading condition would occur randomly over a given period of time [29,30] and is modelled through the three parameter Weibull, Lognormal and Gaussian TTF parametric distribution function:

Weibull:

$$f(t:\theta,\beta,\gamma) = \frac{\beta}{\theta}(\frac{t-\gamma}{\theta})exp[-(\frac{t-\gamma}{\theta})^\beta] \tag{7}$$

where θ = scale parameter, β = shape parameter and γ = location parameter.

Lognormal:

$$f(t:\mu,\sigma) = \frac{1}{\sigma t\sqrt{2\pi}}exp - \frac{1}{2}\frac{(\ln t-\mu)^2}{\sigma^2} \tag{8}$$

Gaussian:

$$f(t:\mu,\sigma) = \frac{1}{\sigma\sqrt{2\pi}}exp - \frac{1}{2}(\frac{t-\mu}{\sigma})^2 \tag{9}$$

where μ = mean, σ = standard deviation.

The cumulative density function, reliability function and hazard rate function can be derived using (7), (8) and (9) for the TTF parametric distribution of Weibull, Lognormal and Gaussian.
Cumulative density function:

$$F(t) = \int_0^t f(t)dt \tag{10}$$

Reliability function:

$$R(t) = 1 - F(t) \tag{11}$$

Hazard rate function:

$$\lambda(t) = \frac{f(t)}{R(t)} \tag{12}$$

The failure rate distribution function for the TTF parametric distribution is derived based on its operating time:

Weibull:

$$F(t:\beta,\theta,\gamma) = -\frac{1}{(exp\frac{t-\gamma}{\theta})^\beta} + 1 \tag{13}$$

Lognormal:

$$F(t:\mu,\sigma) = \frac{1}{2}[1 + erf[\frac{ln(t)-\mu}{\sqrt{2}\sigma}]]; \tag{14}$$

Normal:

$$F(t:\mu,\sigma) = \frac{1}{2}[1 + erf[\frac{x-\mu}{\sqrt{(2\sigma^2)}}]] \tag{15}$$

The TTF parametric distribution of Weibull, Lognormal and Gaussian is derived to determine reliability function of the crankshaft:

Weibull:

$$R(t:\beta,\theta,\gamma) = \frac{1}{(exp\frac{t-\gamma}{\theta})^\beta} \tag{16}$$

Lognormal:

$$R(t:\mu,\sigma) = 1 - erf[\frac{ln(t)-\mu}{\sqrt{2}\sigma}] \tag{17}$$

Normal:

$$R(t:\mu,\sigma) = 1 - erf[\frac{x-\mu}{\sqrt{(2\sigma^2)}}] \tag{18}$$

The behaviour of failure in terms of decreasing failure rate; constant failure rate; increasing failure rate hazard is obtained mathematically through (12) for the TTF parametric distribution of Weibull, Lognormal and Gaussian:

Weibull:

$$\lambda(t:\beta,\theta,\gamma) = (\frac{\beta}{\theta})(\frac{t-\gamma}{\theta})^{\beta-1} \tag{19}$$

Lognormal:

$$\lambda(t:\mu,\sigma) = \frac{\frac{1}{2}[1+erf[\frac{ln(t)-\mu}{\sqrt{2}\sigma}]]}{1-erf[\frac{ln(t)-\mu}{\sqrt{2}\sigma}]} \tag{20}$$

Normal:

$$\lambda(t:\mu,\sigma) = \frac{\frac{1}{2}[1+erf[\frac{x-\mu}{\sqrt{(2\sigma^2)}}]]}{1-erf[\frac{x-\mu}{\sqrt{(2\sigma^2)}}]} \tag{21}$$

Based on the failure rate distribution function, a statistical regression analysis is performed to determine the estimated values for shape and scale parameter

$$F(t:\beta,\theta,\gamma) = 1 = exp[-(\frac{t-\gamma}{\theta})^\beta] \tag{22}$$

using the Weibull transformation, the following is obtained:

$$y = \beta(ln(t) - ln(\theta)) \tag{23}$$

where:

$$x = ln(t) \text{ and } y = ln[\frac{1}{ln[1-F(t)]}] \tag{24}$$

with the value of β would represent the gradient of the slope and the intercepting axis is ln(θ) and is used on *WPP*.

3. Results and Discussion

3.1. Markov Chain simulation model

The TTF was generated computationally and compared with the maximum and minimum of the expected time to failure as shown in Table 1. The first order discrete Markov Chain was convenient in modelling the sequence of maximum and minimum TTF for the extreme conditions based on the various RPM series. Hence, it is observed that the differences between the synthetically generated data using discrete Markov Chain and the automobile data were approximately between 2% to 9%. It shows that the Markov Chain displayed properties of generating new but random sequence data for the sequences of maximum and minimum load conditions that were almost similar to the field data. Likewise, it is observed that the range of data generated (Fig. 6) is within the given range limit of the failure time. This indicated that there will be no outliers in the TTF prediction of the component under the sequence of bending and torsional loads. Hence, making the reliability assessment a little less tedious because of the TTF falling with the specific control limit.

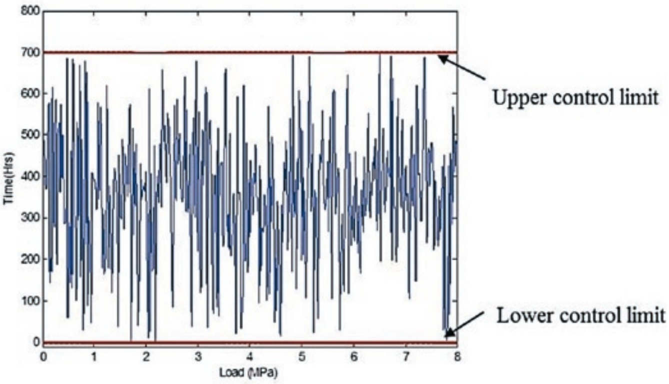

Fig. 6. Observation of the generated data within the upper and lower time limits.

Table 1. Synthetically generated data based on the actual min-max using Markov process

Rotation per minute (RPM)	Data generated from the Markov Chain	
	Minimum (Hours)	Maximum (Hours)
1000	0.12	699.43
1500	0.09	697.38
2000	0.065	698.38
2500	0.068	695.25
3000	0.057	699.17
683500	0.098	697.12
4000	0.067	696.02
4500	0.013	693.29
5000	0.05	695.87
5500	0.028	699.58
6000	0.041	685.82
6500	0.021	694.63

These sequences of maximum and minimum time are frequently used to model the failure rate and reliability using the parametric distribution through the parameterization properties such as the mean, standard deviation, shape and scale parameters. The effects of the parameterization properties is to accelerate and decelerate the failure of the component without adjust the stress levels of the component [29]. Therefore, this justifies the use of the of proposed algorithm in reliability assessment based on the characteristics of the various parametric distribution. Hence, the degree of error of the chosen model are evaluated individually to validate the accuracy of the synthetically generated data [10].

3.2. Reliability analysis and prediction

The shape parameter is evaluated on the *WPP* through the Weibull transformation of the numerical data set ($t_1, t_2, t_3, \ldots, t_n$) generated from the Markov Chain to describe the properties for failure of the crankshaft during its lifetime (Fig. 7). This is an important aspect where the *WPP* is used in estimating the probability of failure occurrence over a given period of time.

The shape parameter is evaluated to be greater than 2.0 with an estimated scale parameter of 220 hours. This indicates that the failure properties would gradually increase with minimal risk of early failure as shown in Table 2 with the understanding that the crankshaft is designed to withstand a lifetime.

The probability density function and cumulative density function provides a mathematical model for evaluating and predicting the failure of the crankshaft due to random bending and torsional stresses over a given period of time. TTF parametric distribution of Weibull, Lognormal and Gaussian is plotted (Fig. 8 and Fig. 9) to statistically determine the mean square error for each of the distribution with the sampling data obtained from the automobile industry. Although the Gaussian distribution is one of the most prominent distributions in statistics that is derived as the probability distribution of the sum of random variables but it is rarely used in modelling the failure distribution because it is defined within a range of the range (−¥,¥) though by the defined positive support. Likewise, the Gaussian distribution belongs to the exponential family, i.e. Weibull and lognormal distribution; that are the exponential family that is analytically tractable. Previous studies [29, 31] even suggested that in terms of reliability assessment, the Gaussian distribution can also be applied to representing failure time. However, in the automobile industry, the Gaussian distribution has never assumed to be normally distributed as the failure would occur randomly under extreme loading condition [19-20]. Hence, by modelling the would provide an optimal model in determining the most appropriate parametric distribution to represent the TTF for the crankshaft under this operational condition.

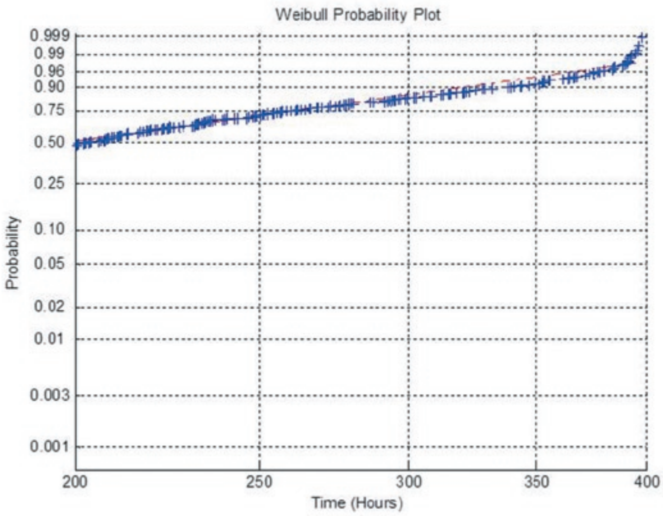

Fig. 7. Plot of three parameter Weibull for the crankshaft

Table 2. Theoretical properties of shape parameter

Shape Parameter	Properties
0 < β < 1	Decreasing failure rate
β = 1	Exponential distribution
0 < β < 1	Increasing failure rate, concave
β = 1	Rayleigh distribution
β > 2	Increasing failure rate, convex
3≤ β ≤ 4	Increasing failure rate, approaches normal distribution; symmetrical

In prediction of desired reliability life it is very important to understand the physics and failure mechanism of the crankshaft for better improvement. The contributing factor for failure mechanism of the crankshaft is due of the bending and torsional stresses with the fluctuation of loads during the operational time period [1, 2, 3, 5, 6, 32]. The optimal desired reliability life prediction (Fig. 10) based on the

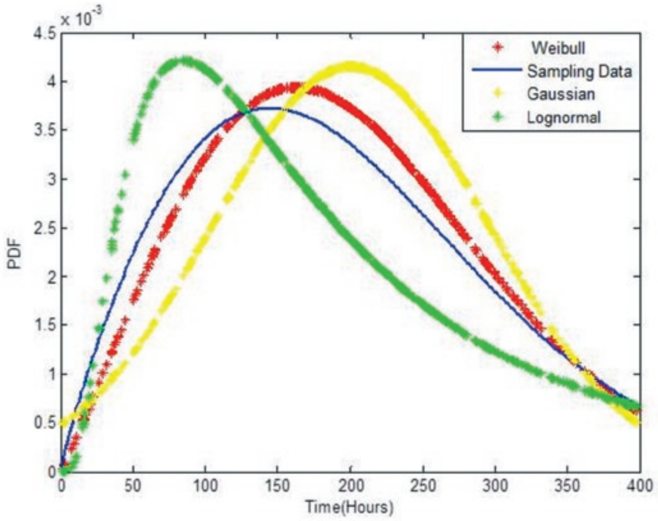

Fig. 8. Probability density function comparison between TTF parametric distribution and sampling data

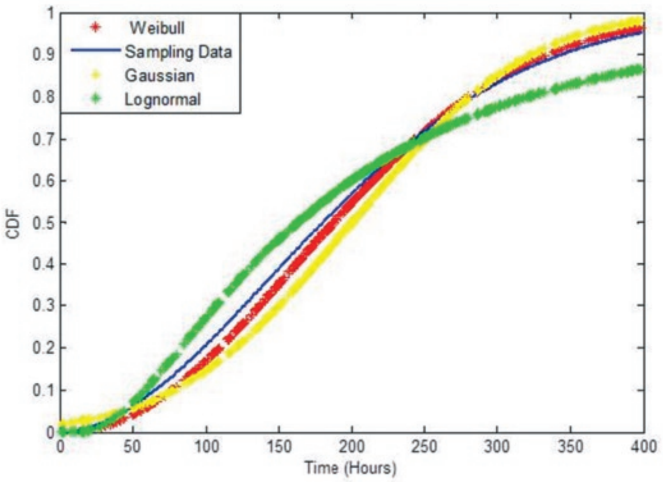

Fig. 9. Cumulative density function comparison between TTF parametric distribution and sampling data.

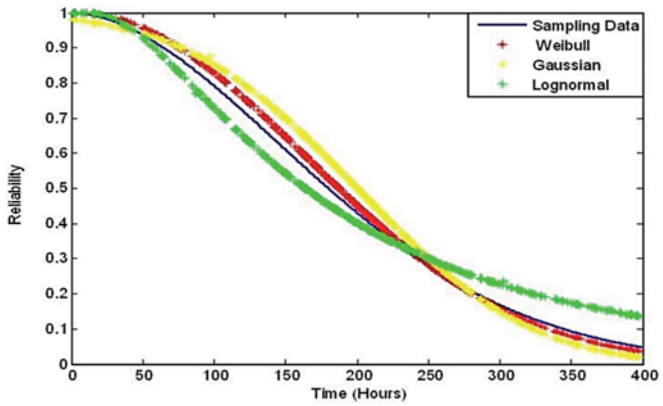

Fig. 10. Comparison of desired reliability life between TTF parametric distribution and sampling data

mechanism of failure using the Markov Chain process using on the TTF parametric distribution as derived earlier. It is shown that the desired reliability life will reduce gradually over time with a physical interpretation of gradual wear out and deterioration due bending and torsional stress acting onto the crankshaft over a given period of time.

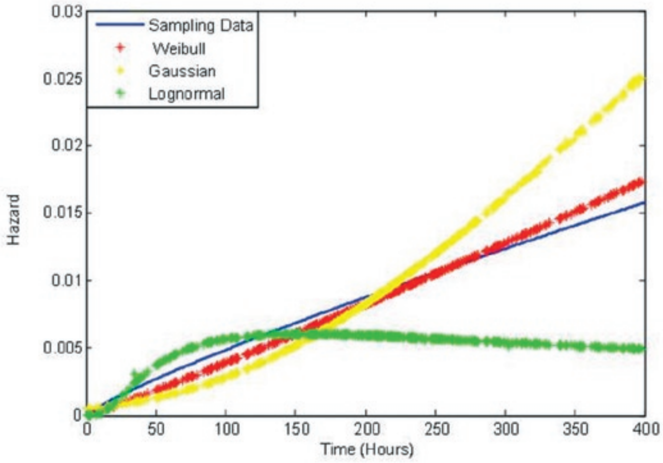

Fig. 11. Hazard rate comparison between TTF parametric distribution and sampling data

The failure rate (Fig. 11) displayed an exponential increment due to high cycle and low bending and torsional stress throughout the entire operational time period of the crankshaft. It was observed that Weibull showed minimal differences and near similarity towards the sampling data due to shape parameter, where shape parameter provides an important role in characterising the failure process model of the crankshaft under mixed mode loading when compared towards the automobile sampling data.

3.3. Evaluation of TTF characterisation fitting for optimal reliability prediction

Based from graphically comparison shown earlier, the accuracy of each distribution was tested using the statistical RMSE technique in determining the optimal model to represent the reliability for the crankshaft. Then the degree of error effect among the parametric data and the three statistical distributions is evaluated. Hence, among three kinds of statistical distributions, the Weibull three-parameter has best fitting effect with minimal percentage of error in comparison with the Gaussian and lognormal distribution as shown in Table 3. Therefore, three-parameter Weibull distribution is recommended for crankshaft TTF data fitting with the intension to verify and distinguish which TTF parametric distribution will provide as a fundamental predictive result in analysing and predicting the reliability for an automobile crankshaft based on the actual sampling data.

$$RMSE = \sqrt{\frac{1}{n}\sum_{i=1}^{n}(\hat{Y}_i - Y_i)^2} \qquad (21)$$

In the preceding equation, $\hat{Y}_i$ is the sampling data obtained from the automobile industry and Y_i is the numerical data set obtained from the Markov Chain model.

The statistical moment from numerical data set obtained from the Markov Chain model is compared towards the sampling data from the automobile industry as shown in Table 4. It is observed that the MTTF for the three parameter Weibull occurs earlier compared to the sampling data indicating a better failure prediction compared to the other TTF distributions. The advantage of an earlier MTTF prediction is essential for preventive maintenance for burn-in period to increase the life cycle reliability and reduce the failure rate of the crankshaft. In practice, the MTTF is taken into account especially during the designing phase in order to avoid any over estimation of the safety factor. Besides that, the MTTF provides essential failure estimation that assist the development of the maintenance schedule.

Table 3. RMSE comparison of three parameter Weibull, Gaussian and Lognormal functions towards the sampling data

Distribution	Three parameter Weibull		Gaussian		Lognormal	
	MSE	RMSE	MSE	RMSE	MSE	RMSE
PDF	$7.03x10^{-8}$	0.00027	$3.30\ x10^{-7}$	0.00057	$8.96\ x10^{-8}$	0.00029
CDF	0.0062	0.079	0.0092	0.096	0.00917	0.096
Reliability function	0.0043	0.065	0.0095	0.097	0.069	0.26
Hazard rate function	$6.16\ x10^{-7}$	0.00079	$6.01\ x10^{-6}$	0.0025	$7.53\ x10^{-6}$	0.0027

Table 4. Statistical moment comparison between sampling data and simulation.

Statistical Analysis	Sampling Data	Simulation		
		Gaussian	Lognormal	Three parameter Weibull
MTTF (Hours)	200	201.2	225.3	199.1
Median (Hours)	200	202.7	162.4	181.3
Standard Deviation (Hours)	115.9	96.1	96.2	117.4
Variance (Hours)	13443.5	9236.2	9246.9	13782.8

4. Conclusion

This study investigated an optimal model to represent the TTF parametric distribution by developing the stochastic algorithm using the Markov Chain to predict the reliability of the crankshaft. The main purpose is to bridge the gap between the experimental and simulation analysis as throughout decades of investigation, numerous fatigue models have been proposed and a large amount of data has been derived from expensive experimental programs. The proposed algorithms models the fatigue failure under random TTF is to overcome the shortcomings of laboratory testing, because even under assumed ideal laboratory testing, fatigue tests showed a considerable amount of scatter under stochastic dynamic service loads. Hence, through the developed algorithm using the Markov process, the characterization of the parametric distribution functions had been modelled through the generation of synthetic data. Likewise, the statistical validation of the algorithm illustrated that the synthetically generated data from the Markovian process suggested that the three parameter Weibull distribution model provides an optimal reliability assessment with RMSE and MSE ranging 5 to 9% when compared towards the actual automobile sampling data.

Besides that, the physical failure properties is seen through the Weibull transformation method, where the shape parameter was the calculated to be greater than 2.0 to indicate that the failure of the crankshaft would occur gradually with low risk of early failure. Furthermore, the proposed algorithms showed that the three parameter Weibull distribution provides an optimal model in predicting the reliability, mean time to failure and hazard rate for an automobile crankshaft through the time dependent failure analysis. Thus, the three parameter Weibull distribution using the Markov Chain model of generating data is an accurate and efficient method for reliability lifecycle assessment when compare with the automobile sampling data in this case study.

Acknowledgement

The authors would like to thank the Ministry of Education for funding this study under the HLP Grant No. HLP-KPT.B.600-2/3-781226085655 and also a token of appreciation to the National Automobile Industry for providing the necessary information pertaining to the success of this study.

References

1. Aid A, Amrouche A, Bachir Bouiadjra B, Benguediab M, Mesmacque G. 2011. Fatigue life prediction under variable loading based on a new damage model. Materials and Design 2011; 23: 183-191, http://dx.doi.org/10.1016/j.matdes.2010.06.010.
2. Alfares M A, Falah A H, Elkholy A H. Failure analysis of a vehicle engine crankshaft. Journal of Failure Analysis and Prevention 2007; 7(1): 12-17, http://dx.doi.org/10.1007/s11668-006-9006-0.
3. Asi O. Failure analysis of a crankshaft made from ductile cast iron. Engineering Failure Analysis 2005; 13(8): 1260-1267, http://dx.doi.org/10.1016/j.engfailanal.2005.11.005.
4. Atzori B, Berto F, Lazzarin P & Quaresimin M. A stress invariant based criterion to estimate fatigue damage under multiaxial loading. International Journal of Fatigue 2006; 28: 485-493, http://dx.doi.org/10.1016/j.ijfatigue.2005.05.010.
5. Bahumik S K, Rangaraju R, Venkataswamy M A, Baskaran T A, Parameswara M A. Fatigue fracture of crankshaft of an aircraft engine. Engineering Failure Analysis 2002; 9(3): 255-263, http://dx.doi.org/10.1016/S1350-6307(01)00022-X.
6. Becarra J A, Jimenez F J, Torrez M, Sanchez D T, Carvajal E. Failure analysis of reciprocating compressor crankshafts. Engineering Failure Analysis 2011; 18(2): 735-746, http://dx.doi.org/10.1016/j.engfailanal.2010.12.004.
7. Bocchini P, Saydam D, Franggopol D M. Efficient, accurate and simple Markov Chain Model for the life cycle analysis of bridge groups. Structural Safety 2013; 40: 51-64, http://dx.doi.org/10.1016/j.strusafe.2012.09.004.
8. Bue L F, Stefano A D, Giagonia C. Misfire detection system based on the measure of crankshaft angular velocity. Springer, 2007.
9. Changli C, Chengjie Z, Deping W. Analysis of an unusual crankshaft failure. Engineering Failure Analysis 2005; 12(3): 465-473, http://dx.doi.org/10.1016/j.engfailanal.2004.01.006.
10. Chen X, Yu X, Hu R, Li J. Statistical distribution of crankshaft fatigue: Experiment and modelling. Engineering Failure Analysis 2014; 4: 210-220, http://dx.doi.org/10.1016/j.engfailanal.2014.04.015.
11. Chiachío M, Chiachío J, Rus G, Beck J L. Predicting fatigue damage in composites: A Bayesian framework. Structural Safety 2014; 51: 57-68, http://dx.doi.org/10.1016/j.strusafe.2014.06.002.
12. Czarnigowski J, Drozdziel P, Kordos Paweł. Characteristic rotational speed ranges of a crankshaft during combustion engine operation at car maintenance. Eksploatacja i Niezawodnosc – Maintenance and Reliability 2002; 2(14): 55-62.
13. Distefano S, Peliafito A. Reliability and availability of dependent dynamic system with DRBD's. Reliability Engineering and System Safety 2009; 94(9): 1381-1393, http://dx.doi.org/10.1016/j.ress.2009.02.004.

14. Drozdziel P, Krzywonos L. The estimation of the reliability of the first daily diesel engine start-up during its operation in the vehicle. Eksploatacja i Niezawodnosc – Maintenance and Reliability 2009; 1(41): 4-10.
15. Druschitz P A, Warrick R J, Grimley P R, Towalski R C, Killion D L, Marlow R. Influence of crankshaft materila and design on NVH characteristics of a Modern, Aluminum Block, V-6 Engine. SAE Technical Paper Series 1999-01-1225.
16. Fonte M, Li B, Reis L, Freitas M. Crankshaft failure analysis of a motor vehicle. Engineering Failure Analysis 2013; 35: 147-152, http://dx.doi.org/10.1016/j.engfailanal.2013.01.016.
17. Gagg C R, Lewis, R P. In-service fatigue failure of engineered products and structures – Case study review. Engineering Failure Analysis 2009; 16: 1775–1793, http://dx.doi.org/10.1016/j.engfailanal.2008.08.008.
18. Gaver D P, Jacobs P A. Reliability growth by failure mode removal. Reliability Engineering and System Safety 2014;130: 27-32, http://dx.doi.org/10.1016/j.ress.2014.04.012.
19. Jean M B, Cecile M. Damage tolerance and reliability assessment under random Markovian loads. Procedia IUTAM 2013; (6): 123-131.
20. Johannesson P. On rainflow cycles and the distribution of the number of interval crossings by a Markov chain, Probabilistic Engineering Mechanics 2002;17: 123-130, http://dx.doi.org/10.1016/S0266-8920(01)00033-9.
21. Jiang R, Murthy D N P. A study of Weibull Shape Parameter: Properties and Significance. Reliability Engineering and System Safety 2012; 96(12): 1619-1626, http://dx.doi.org/10.1016/j.ress.2011.09.003.
22. Jung D H, Kim H K, Pyoun Y S, Gafurov A, Choi G C, Ahn J M. Reliability prediction of the fatigue life of a crankshaft. Journal of Mechanical Science and Technology 2009; 23: 1071-1074, http://dx.doi.org/10.1007/s12206-009-0343-2.
23. Kihl D P, Sarkani S, Beach J E. Stochastic fatigue damage accumulation under broadband loadings. International Journal of Fatigue 1995; 17(5): 321-329, http://dx.doi.org/10.1016/0142-1123(95)00015-L.
24. Ling Y, Shantz C, Mahadevan S, Sankararaman S. Stochastic prediction of fatigue loading using real-time monitoring data International Journal of Fatigue 2011; 33(7): 868-879, http://dx.doi.org/10.1016/j.ijfatigue.2011.01.015.
25. Liu Y, Mahadevan S. Stochastic fatigue damage modeling under variable amplitude loading. International Journal of Fatigue 2007;29:1149-1161, http://dx.doi.org/10.1016/j.ijfatigue.2006.09.009.
26. Lu Z, Liu Y. Experimental investigation of random loading sequence effect on fatigue crack growth. Materials and Design 2011; 32: 4773–4785, http://dx.doi.org/10.1016/j.matdes.2011.06.034.
27. Nechval K N, Nechval N A, Berzins G, Purgailis M. Probabilistic assessment of the fatigue reliability. Eksploatacja i Niezawodnosc – Maintenance and Reliability 2007; 3(35): 3-6.
28. Neetu S, Kanchan, J Suresh K S. The Beta Generalized Weibull distribution: Properties and application. Reliability Engineering and System Safety 2012; 102: 5-15, http://dx.doi.org/10.1016/j.ress.2012.02.003.
29. Newby M. Accelerated failure time models for reliability data analysis Reliability Engineering and System Safety 1988;20(3): 187-197, http://dx.doi.org/10.1016/0951-8320(88)90114-7.
30. Okamura H, Dohi T, Osaki S. Software reliability growth models with normal failure time distribution. Reliability Engineering and System Safety 2013; 116: 135-141, http://dx.doi.org/10.1016/j.ress.2012.02.002.
31. Pandey R K. Failure of diesel engine crankshaft Engineering Failure Analysis 2003; 10(2): 165-175, http://dx.doi.org/10.1016/S1350-6307(02)00053-5.
32. Ray A, Targilara S. A nonlinear stochastic model of fatigue crack dynamics. Probabilistic Engineering Mechanics 1997;12(1): 33-40, http://dx.doi.org/10.1016/S0266-8920(96)00012-4.
33. Shen H, Lin J, Mu E. Probabilistic model on stochastic fatigue damage. International Journal of Fatigue 2000;22: 569–572, http://dx.doi.org/10.1016/S0142-1123(00)00030-X.
34. Sugier J, Anders G J. Modelling and evaluation of deterioration process with maintenance activities. Eksploatacja i Niezawodnosc – Maintenance and Reliability 2013; 15(4): 305-311.
35. Xiuyun P, Zaizai Y. Estimation and application for a new extended Weibull distribution. Reliability Engineering and System Safety 2014; 121: 34-42, http://dx.doi.org/10.1016/j.ress.2013.07.007.
36. Zhang T, Dwight R. Choosing an optimal model for failure data analysis by graphical approach. Reliability Engineering and System Safety 2013; 115: 111-23, http://dx.doi.org/10.1016/j.ress.2013.02.004.

Salvinder Singh Karam SINGH
Shahrum ABDULLAH
Department of Mechanical and Material Engineering
Faculty of Engineering and Built Environment
Universiti Kebangsaan Malaysia
43600 UKM
Bangi Selangor Malaysia

Nik Abdullah Nik MOHAMED
Department of Mechanical Engineering
Universiti Malaysia Pahang,
Pekan 26600 Pahang Malaysia

E-mail: salvinder@gmail.com, shahrum@eng.ukm.my, nikabdullah@ump.edu.my

Article citation info:
GODZIMIRSKI J, JANISZEWSKI J, ROŚKOWICZ M, SURMA Z. Ballistic resistance tests of multi-layer protective panels. Eksploatacja i Niezawodnosc – Maintenance and Reliability 2015; 17 (3): 416–421, http://dx.doi.org/10.17531/ein.2015.3.12.

Jan GODZIMIRSKI
Jacek JANISZEWSKI
Marek ROŚKOWICZ
Zbigniew SURMA

BALLISTIC RESISTANCE TESTS OF MULTI-LAYER PROTECTIVE PANELS

BADANIA ODPORNOŚCI NA PRZEBICIE OSŁON O STRUKTURZE WIELOWARSTWOWEJ*

Modern light-weight ballistic amours are usually multi-layer structures with low density. The aim of the study was to evaluate the possibility of using multi-layer structures for lightweight armour systems which may be applied as bulletproof ballistic panels of combat helicopters and other lightweight military equipment. The tested multi-layer structures were prepared on the basis of aramid fabrics, thin sheets of 2024-T3 aluminium alloy and Al_2O_3 *and SiC ceramics. Additionally, the influence of adhesive connections between the components of the ballistic panels on their protective properties has been assessed. Absorbing energy of a spherical projectile was determined with the use of a laboratory stand consisted of a one-stage helium gas gun and a digital high speed camera. A penetration study on the selected multi-layer panels was also carried out with the use of Parabellum ammunition. It has been shown that the laminated structures composed of thin layers of metal and aramid fabric indicate a lower absorb energy-to-composite basic weight ratio than analogues ratios for metal sheets or fabrics used to produce laminated structures. Similarly, the sandwiches of loose aramid fabrics demonstrate greater ballistic resistance compared to the polymer composites made of such fabrics. There has been also demonstrated the desirability of the use of a ceramic component as a separate layer in which ceramic segments are glued between two layers of a thin metal sheet.*

Keywords: *ballistic tests, terminal ballistics, multi-layer armour, penetration resistance.*

Współczesne lekkie osłony balistyczne są zwykle strukturami wielowarstwowymi o małej gęstości. Celem badań była ocena możliwości zastosowania struktur wielowarstwowych na lekkie pancerze, mogące znaleźć zastosowanie jako kuloodporne osłony balistyczne śmigłowców bojowych i innego lekkiego sprzętu wojskowego. Badane materiały przygotowano na bazie tkanin aramidowych, cienkich blach ze stopu aluminium 2024-T3 oraz ceramiki typu Al_2O_3 *i SiC. Dodatkowo oceniono wpływ zastosowania połączeń adhezyjnych pomiędzy komponentami osłon balistycznych na ich właściwości ochronne. Określono energię przebijania osłon wykorzystując do tego celu stanowisko zbudowane na bazie działa helowego oraz szybkiej kamery. Wykonano również próby przebicia wytypowanych osłon pociskiem naboju Parabellum. Wykazano, że klejone struktury złożone z cienkich warstw metalowych i tkanin aramidowych charakteryzuje mniejsza odporność na przebicie odniesiona do ich gramatury niż blach metalowych i tkanin, z których były wytwarzane. Również pakiety luźnych tkanin aramidowych cechuje większa odporność na przebicie w porównaniu z kompozytami polimerowymi wytworzonymi z takich tkanin. Wykazano celowość stosowania komponentu ceramicznego w postaci oddzielnego pakietu,w którym płytki ceramiki wklejone są pomiędzy dwie warstwy cienkiej blachy.*

Słowa kluczowe: *badania balistyczne, balistyka końcowa, pancerze wielowarstwowe, odporność na przebicie.*

1. Introduction

Multi-layer armour systems are used increasingly for many military and civil applications, for instance, in lightweight ships, vehicles, airplane protection or body armours [10, 18, 23]. In the past, the armours were typically monolithic and made of high-strength steel plates. However, over the recent few decades, there has been observed a tendency to apply armours providing maximum ballistic protection at minimum weight. Among many original concepts of ballistic protection systems, there should be distinguished multilayer lightweight armours that seems to be the most perspective ones [10, 14, 18, 23]. These armour systems consist of a number of layers performing a specific role in destroying a projectile and absorbing the impact energy. In general, there can be distinguished hard and soft layers. First of them are made mostly of high-strength light alloy or ceramic and are responsible for the "wear" of the projectile and dissipation of the projectile kinetic energy during the penetration process. The second type of layers called "soft" or "low mechanical impedance" act as a shock absorber and a medium which captures fragments resulting from destruction of both the projectile and the hard armour layer.

A modern lightweight armour is a system of several or even more than ten layers of different materials, combined or separated, forming a so-called "multi-layered composite structure". The type of the layers materials used and their thickness and a structure system determine the protective properties of a given armour. The simplest structure configuration of a modern light-weight armour consists of three layers, i.e., a front ceramic layer placed directly on a soft layer supported by the light alloy or a fibre composite layer (support layer).

The ceramic layers are usually made of aluminium oxide (Al_2O_3), silicon carbide (SiC) and boron carbide (B_4C) [10, 18, 21]. As materials applied for light-weight armours, there were also tested silicon nitride (Si_3N_4), titanium diboride (TiB_2), aluminum nitride (AlN), sialon (SiAlON), glasses [4, 10, 18] and ceramic composites reinforced with metal or intermetallic phases [7]. For technological reasons, ce-

(*) Tekst artykułu w polskiej wersji językowej dostępny w elektronicznym wydaniu kwartalnika na stronie ***www.ein.org.pl***

ramic armour layers are made of segments fastened to the support. As a support layer - in the case of modern light-weight armours – high strength elastomers (e.g. rubber, synthetic elastomers, polyurea [8, 20]) or the metal foam [6] are usually applied. These materials create a transition layer between ceramic segments and the base layer which can be an integral part of the panel armour or a structural component (primary armour) of the protected object. Thus, this layer is usually made of aluminium alloys, titanium alloys or a composite reinforced with glass, carbon or aramid fibres.

Literature emphasizes also the role of an adhesive bonding in shaping the protective properties of a multi-layer armour [1, 11]. For example, in work [1] it was found that a two-layer armour (aluminium oxide/aluminium) had optimum thickness of the adhesive layer (0.3 mm) for which the ballistic effectiveness of the armour is the highest. Presently, the adhesives based on epoxy resins or cyanoacrylate adhesives are used the most commonly to bond individual layers of an armour.

Development of a multi-layer armour structure is a very complex task. The attempt to solve it is based on the results of experimental studies [16, 19], numerical modelling [3, 17] or analytical considerations [22]. Numerical modelling is particularly helpful in optimizing a structure of the multi-layer armour. In literature, there can be found numerous applications of numerical modelling in the study of the multilayer structures behaviour. For this purpose, an artificial neural networks technology [13, 15] has been also used recently. It is a comparative technology in comparison with numerical modelling since it shortens the time of a problem solution. The prediction of a multi-layer armour behaviour based on the numerical analysis, however, requires the calibration of numerical models based on the experimental results. For this purpose, the ballistic tests are performed under experimental conditions as similar as possible to the model one. This type of ballistic tests is carried out with the use of a sphere as a projectile because, compared to the standard small arms ammunition, any additional effects of increasing complexity of the perforation phenomenon (e.g. rotation of the gyro-stabilized projectile, bullet precession, etc.) are avoided [5, 2, 9, 12]. Experimental studies are therefore essential despite they are expensive and time consuming. Moreover, they allow an objective assessment of the solution or concept validity at the stage of preliminary tests.

Owing to the fact that presently the subject matter of multi-layer light-weight armours is particurarly studied extensively by many research laboratories around the world, there was made an attempt to examine own solutions of multi-layer armours. This work constitutes the first stage of the undertaken works aimed to, firstly, provide the experimental data for calibration of the numerical models and, secondly, the experimental evaluation of protective properties of the developed multi-layer structures which can be utilized as bulletproof panels of combat helicopters and other light-weight military equipment. Additionally, the aim of this study was to assess an influence of adhesive connections on protective properties of the developed ballistic structures.

2. Research object and methodology

Taking into considerations the requirement of low density of the investigated multi-layer armours it was decided to produce them using AW 2024-T3 aluminium alloy (EN AW-AlCu4Mg1i – solution treated and artificially aged) and four different aramid fabrics with various structure and basic weight. Moreover, hexagonal segments of Al_2O_3 aluminum oxide or SiC as well as stainless steel in the form of a thin sheet with thickness of 0.2 mm were also was applied. Two types of AW 2024-T3 aluminum alloy sheet with thickness of 0.3 mm and 3 mm, and four aramid fabrics dented by Microflex, CT 709, T750 and XPS10 were used. The ceramic layer consisted of the segments in the shape of a straight regular hexagonal prism (inscribed circle diameter – 20.2 mm, thickness – 4.2 mm). The laminated structures were manufactured with the use of epoxy adhesive Epidian 57 with the hardener Z1. The application of epoxy adhesive, instead of a saturant, resulted from the fact that the used aramid fabrics are not practically possible to be impregnated and typical saturants used to impregnate the fabrics are characterized by worse adhesion to metals as compared with adhesives.

Before being glued, the sheets surface were prepared through abrasion with the use of an abrasive cloth (50 grit size) attached to a sponge and washing with petroleum cleaner. There were also made attempts of sandblasting of the sheets surfaces, however it was abandoned because of plastic sheets deformations and, consequently, the problems with gluing them on the whole surface. The adhesive layers in the joints of the specimens were pre-cured at room temperature using surface pressures of 0.05 MPa for 24 hours and subsequently for 6 hrs at 60 °C. As a result, the raw plates with the dimensions of 150 × 250 mm were obtained and afterwards, with the use of an abrasive water jet technology, they were cut into the plates in the shape and with the dimensions shown in Fig. 1.

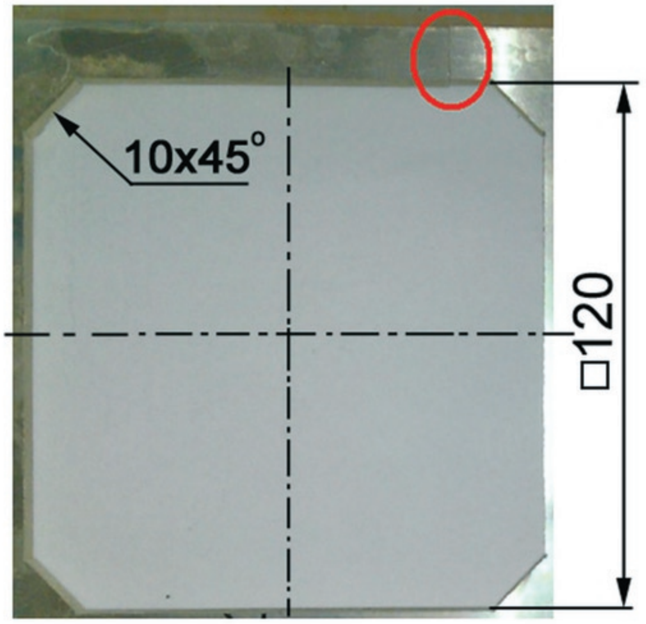

Fig. 1. A multi-layer plate after cutting out with the use of an abrasive water jet technology (red circle indicates the starting point of cutting)

The cut-out specimens of the multi-layer armours were mounted into a steel frame (Fig. 2b) which was then positioned in the vice opposite the muzzle of the helium gas gun (Fig. 2a). The ballistic resistance of the panels was tested by shooting at the specimens with the spherical steel projectiles of an 8 mm diameter placed into Teflon sabots (Fig. 3). During the shooting at the light-weight armours specimens, the ball trajectory was recorded with the use of a digital high speed camera (Phantom v12). The camera observation area was selected as to include both the space in front of and behind the armour (Fig. 4). Owing to such a recording configuration, it was possible to obtain the experimental data based on which the projectile velocity before the impact into the target and after its perforation was able to calculated. As a measure of ballistic resistance, there was accepted the value of the energy absorbed by the armour during its perforation, in short called as the absorbing energy (E_{abs}) – a difference of kinetic energies of the projectile before and after the perforation of the armour specimen.

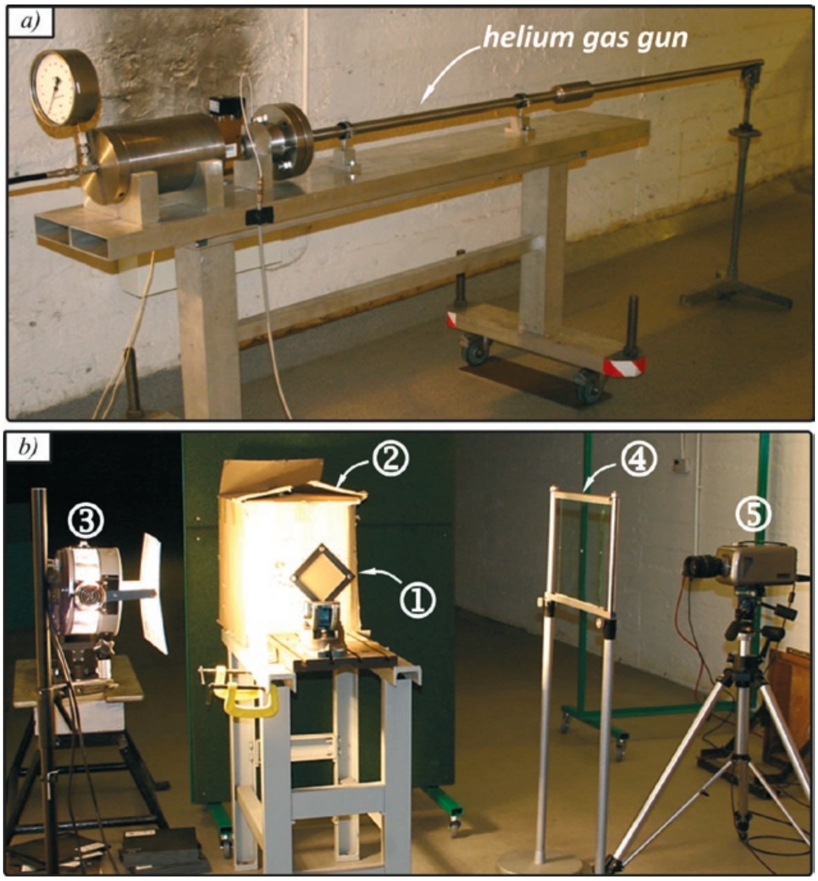

Fig. 2. The experimental stand for testing ballistic perforation resistance: (a) view of the light gas launching system and (b) fastening arrangement for armour specimen and an optical recording system; 1 - armour specimen, 2 - projectile recovery chamber, 3 - lighting system, 4 - protective screen, 5 - high speed camera

Fig. 3. Steel spherical projectiles with a diameter of 8 mm and Teflon sabots

3. Tests results

The first stage of the ballistic tests aimed at comparing the ballistic resistance of three configurations of the protective panels made of AW 2024-T3 alloy, i.e. the sheet with thickness of 3 mm, a package of 3 mm thickness formed from ten metal sheets with thickness of 0.3 mm and packages consisting of two and three metal sheets with thickness of 3 mm each. The purpose of the experiment was to assess if the sheets packages are characterized with higher ballistic resistance compared with the uniform plates, and whether the absorbing energy depends linearly on the protective panel thickness. The energy was calculated from equation (1).

$$E_{abs} = \frac{m(V_1^2 - V_2^2)}{2} \tag{1}$$

where: E_{abs} – absorbing energy, m – ball mass, V_1 – ball velocity before the impact, V_2 – residual velocity

The research results are shown in Table 1.

The absorbing energy-to-the package thickness ratio of the tested specimens was similar regardless of its construction. The difference between absorb energy of the metal sheet and the package of ten metal sheets with the same thickness was equal to 2.5%. With the increase of thickness of the package, the absorbing energy-to-the unit thickness ratio decreased slightly (about 8%, compared with a 3 mm sheet and a three-sheet package of the same thickness of 3 mm each).

The second stage of the dynamic tests involved research of aramid-epoxy composites consisting of layers of different aramid fabrics bonded with Epidian 57/Z1 adhesive. Additionally, the armour panel obtained by gluing 7 XPS102 fabrics were tested. As a result, the specimens of armour composed of the same number of layers as previously prepared aramid-epoxy laminate (L XPS102) were obtained. The research results are shown in Table 2.

The absorbing energy in the ballistic test relative to the basic weight of the tested laminates proved to be comparable to absorbing energy of AW 2024-T3 aluminum alloy sheet. Considering the four tested fabrics, XPS102 fabric is characterized with the best protective properties. The absorbing energy of the loose XPS102 fabric (stitching on the specimen edge) was almost two times higher than the puncture energy of the laminate made of this fabric.

The next stage concerned the FML type composites consisting of alternately arranged layers of thin metal sheets (8 layers) and aramid fabric (7 layers) adhesive bonded using Epidian 57/Z1 adhesive. All the fabrics were adhesive bonded to the AW 2024-T3 alloy sheets, and additionally the XPS102 fabric bonded to the stainless steel sheets. The results are presented in Table 3.

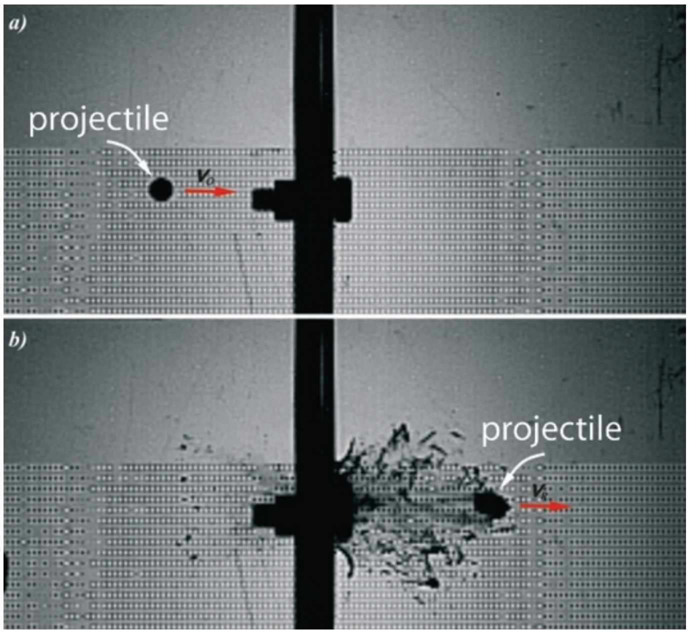

Fig. 4. The observation area of a high-speed camera: view of a spherical projectile and an armour specimen before (a) and after (b) impact

The absorbing energy relative to the basic weight of the tested composites proved to be slightly lower than the absorbing energy of laminates and AW-2024-T3 metal alloy. Therefore, it was decided to reinforce the above-mentioned FML composites with a 4.2 mm ce-

Table 1. Ballistic resistance of aluminium alloy sheets (AW 2024-T3)

Material	Thickness [mm]	Density [g/cm^3]	Absorbing energy [J]	Energy/ Thickness [J/mm]	Basic weight [kg/m^2]	Energy/ Basic weight [J/kg/m^2]
AW 2024-T3	3	2.7	142.39	47.46	8.1	17.57
	2x3	2.7	271.48	45.25	16.2	16.76
	3x3	2.7	393.15	43.68	24.3	16.18
	10x0.3	2.7	146.12	48.71	8.1	18.04

Table 2. The ballistic resistance of laminates (L) and the loose fabric aramid layers (7W)

Material	Thickness [mm]	Density [g/cm^3]	The absorbing energy [J]	Energy/ Thickness [J/mm]	Basic weight [kg/m^2]	Energy/ Basic weight [J/kg/m^2]
L CT709	1.75	1.2	failed recording		2.1	?
L XPS102	3.9	1.18	80.49	20.64	4.6	17.49
L Microflex	2.15	1.23	39.94	18.58	2.64	15.11
L T750	4.1	1.05	72.71	17.73	4.3	16.89
XPS102-7W	3.2	1.18	118.18	36.93	3.78	31.30

Table 3. Ballistic resistance of composites FML prepared on based AW 2024-T3 alloy or steel sheets (S) and aramid fabrics

Material	Thickness [mm]	Density [g/cm^3]	The absorbing energy [J]	Energy/ Thickness [J/mm]	Basic weight [kg/m^2]	Energy/ Basic weight [J/kg/m^2]
K CT709	4.1	2.03	100.37	24.48	8.32	12.06
K XPS102	6.35	1.69	159.33	26.67	10.73	15.78
K Microflex	4.65	1.91	112.32	24.15	8.89	12.64
K T750	6.79	1.69	182,17	26.83	11.48	15.88
K XPS102S	4.85	2.23	159.99	32.99	10.82	14.79
K XPS102S	4.85	2.23	162.52	33.51	10.82	15.03

Table 4. FML types composites based on 2024-T3 alloy and aramid fabrics with Si_2C type ceramic

Material	Basic weight with ceramic [g/cm^2]	Thickness with ceramic [mm]	Density [g/cm^3]	Velocity [m/s]	The absorbing energy [J]	Energy/ Thickness [J/mm]	Energy/ Basic weight [J/kg/m^2]
KC CT709	22.80	8.75	2.61	655	>448	>51	> 19.54
KC XPS102	24.55	11	2.23	657	>451	>41	> 18.39
KC Microflex	23.36	9.3	2.51	Parabellum lead projectile		> 52.7	>20.98
KC T750	25.96	11.44	2.27	Parabellum lead projectile		> 42.8	>18.88

ramic layer (silicon carbide – SiC). The bonded layer of SiC covered with one additional layer of carbon fabric saturated with Epidian 57/Z1 adhesive. In the case of ceramic – aramid – metal panels, shooting tests with the use of a steel ball and a helium gas gun proved no perforation of two of the tested specimens (Tab. 4). Therefore, for comparative purposes, two remaining specimens were tested for ballistic resistance using Parabellum pistol bullets (kinetic energy of a Parabellum bullet is equal to 450 J, which is comparable with the energy of the steel ball shooting from the helium propellant system). The aim of such the proceedings was the need to find out whether, based on the test results obtained using a helium gas gun, it is possible to conclude on ballistic resistance of the tested panels with use of live ammunition. As expected, Parabellum bullets did not penetrate the tested composites panels (Fig. 5, Fig. 6).

The last stage of the tests concerned the aramid fabrics covered with one layer of ceramic segments. In the first case, there were considered seven layers of CT709 fabric stitched together and covered with one layer of Al_2O_3 ceramic adhesive bonded between two metal sheets of AW 2024-T3 alloy with thickness of 0.3 mm. In the second case, a polymer composite based on seven layers of T750 fabric and L285 resin with a SiC ceramic layer bonded was made. The ballistic resistance of such prepared protective panels was tested with Parabellum bullets.

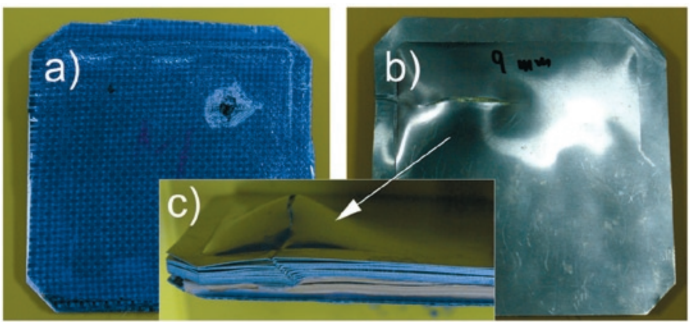

Fig. 5. View of KC Microflex specimen after shooting test using Parabellum projectile: a – view from the ceramic side, b – deformation and fracture of the last metal layer, c – delamination of the specimen

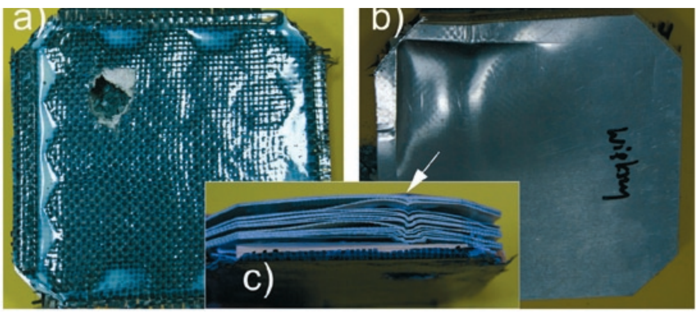

Fig. 6. View of KC T750 specimen after shooting test using Parabellum bullet: a – view from the ceramic side, b – deformation of the last metal layer, c – delamination of the specimen

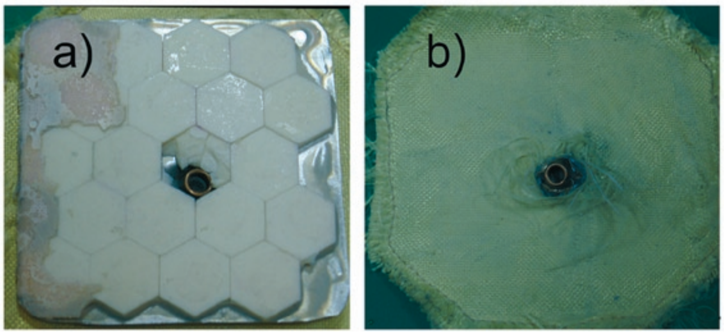

Fig. 7. View of a specimen consisting of 7 CT709 fabric layers stitched together and one layer of Al2O3 ceramic after the shooting test using Parabellum bullet: a – view of destruction of the ceramic, b – view of the fabric with the arrested bullet

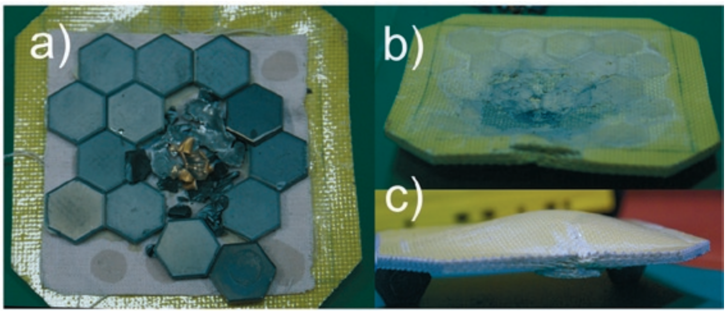

Fig. 8. View of a specimen made of composite based on T750 fabric – with a bonded SiC ceramic layer after the shooting test using Parabellum bullet: a – view from the ceramic side, b – view of the composite with traces of the detached ceramic, c – permanent deformation of the composite

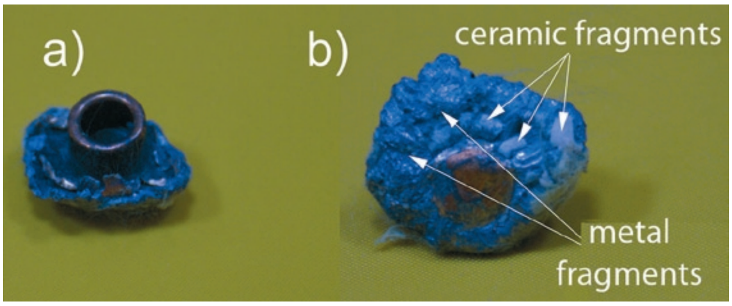

Fig. 9. Parabellum bullet after perforation of the ceramic layer which was stuck between two thin sheets of aluminum alloy: a) general view, b) view of the deformed bullet with a visible piece of metal and ceramic

In both cases, the bullet did not perforate the test specimens (Fig. 7, Fig. 8). Ceramic segments bonded with the use of Epidian 57 adhesive to the composite made of T750 fabric seperated from plastically deformed material (Fig. 8). In the case of the ceramic segments stuck between two layers of aluminum alloy thin sheets, only one ceramic segment was destroyed. The other segments glued to the metal sheet still provided protection. (Fig. 7). Furthermore, it was observed that the head portion of the deformed bullet (Fig. 9) was expanded by fragments of a ceramic and metal layer which integrated with a jacketed and lead bullet core.

4. Evaluation of test results

While constructing light armours of aircrafts, a quotient of the absorbing energy-to-basic weight ratio should be assumed as the main parameter allowing the comparison of their quality. Comparing the values of this parameter, it can be concluded that the armour panel made of 2024-T3 aluminum alloy and the tested aramid fabrics are characterized by comparable antiballistic properties. The reasearch also shows that loose packages of thin layers indicate higher ballistic resistance compared with monolithic structures - in the case of metal layers, an increase was observed at the level of only 8%, however, in the case of XPS102 fabrics it was two-fold. Further studies should check whether stitching the fabrics could have an influence on the significant increase of ballistic resistance and whether the arrangement of seams can affect the ballistic properties of the aramid fabric packages.

The worse ballistic resistance of the monolithic structures compared with the structures composed of loose thin layers shows that the adhesive bonding of them is not an appropriate solution,what has been proven in the research of FML composites. Their ballistic resistance measured with an absorbing energy-to-basic weight ratio proved to be less than the ballistic resistance of laminates and metal sheets. FML materials are characterized by high fatigue life resulted from slow propagation of the cracks suppressed by delamination of the adhesive bondings. During the destruction of FML specimens, local delamination occurred, however it did not affect their ballistic resistance.

The studies have confirmed the usefulness of applying an outer rigid ceramic layer to deformation of the bullets and dissipitating the kinetic energy. None of the specimens witha ceramic layer was perforated neither by the steel ball or Parabellum bullet. Due to the small dimensions of ceramic segments,they should be joined into larger segments. A reasonable solution to obtain larger segments is adhesive bonding the plates to fabrics, metal sheets or other materials. Due to the efficiency of the armour, it is important that a single projectile destroys a relatively small surface of the ceramic layer. The test has shown that in the case of one-sided bonding of the ceramic segments, the impact with the projectile crushes one plate and causes separation of several neighboring segments at the same time. Adhesive sticking ofthe ceramic segments between two thin sheets of aluminum alloy forms a sandwich structure with increased bending stiffness, which results in reduction of the ceramic layer destruction to a single segment.

5. Conclusions

The results of the tests on light-weight ballistic panels presented in the article allow formulation of the following conclusions:

1. The selected adhesive bonding structures consisting of thin metal layers and aramid fabrics layers indicate lower ballistic resistant related to their weight than metal sheets and fabrics which they were produced
2. The packages of loose aramid fabrics indicate higher ballistic resistance compared to the polymer composites made of the same fabric.
3. The ceramic layers significantly increase ballistic resistance of protection panels and their usage in such armours seems fully justified.
4. Adhesive bonding of the ceramic segments between two thin sheets of aluminum alloy and not bonding them directly with aramid fabrics prevents from damage of the ceramic segments adjacent to the area of the direct impact of the projectile.

References

1. Arias A, López-Puente J, Navarro C, Zaera R. The effect of the thickness of the adhesive layer on the ballistic limit of ceramic/metal armours. An experimental and numerical study. International Journal of Impact Engineering 2005; 32: 321-336, http://dx.doi.org/10.1016/j.ijimpeng.2005.07.014.
2. Atiq S, Boccaccini A R, Boccaccini D N, Dlouhy I, Kaya C. Fracture behaviour of mullitefibre reinforced-mullitematrix composites under quasi-static and ballistic impact loading. Composites Science and Technology 2005; 65: 325-333, http://dx.doi.org/10.1016/j.compscitech.2004.08.002.
3. Bansal S, Krishnan K, Rajan S D, Sockalingam S. Numerical simulation of ceramic composite armor subjected to ballistic impact. Composites: Part B 2010; 41: 583-593, http://dx.doi.org/10.1016/j.compositesb.2010.10.001.
4. Bell W C, Grujicic M, Pandurangan B. Design and material selection guidelines and strategies for transparent armor systems. Materials and Design 2012; 34: 808-819, http://dx.doi.org/10.1016/j.matdes.2011.07.007.
5. Bogetti T A, Cheeseman B A. Ballistic impact into fabric and compliant composite laminates. Composite Structures 2003; 61: 161-173, http://dx.doi.org/10.1016/S0263-8223(03)00029-1.
6. Bogetti T A, Fink B K, Gama B A, et al. Aluminium foam integral armor: a new dimension in armor design. Composite Structures 2001; 52: 381-395, http://dx.doi.org/10.1016/S0263-8223(01)00029-0.
7. Bojar Z, Dolata-Groszc A, Formanek B, Jóźwiak S, Szczucka-Lasota B. Intermetallic alloys with oxide particles and technological concept for high loaded materials. Journal of Materials Processing Technology - J MATER PROCESS TECHNOL 2005; 162:46-51.
8. Cheesemanb B A, Grujicic M, Hea T, Pandurangana B, Randow C L, Yenb C F. Computational investigation of impact energy absorption capability of polyuria coatings via deformation-induced glass transition. Materials Science and Engineering A 2010; 527: 7741-7751, http://dx.doi.org/10.1016/j.msea.2010.08.042.
9. Ching T W, Tan V B C. Computational simulation of fabric armour subjected to ballistic impacts. International Journal of Impact Engineering 2006; 32: 1737-1751, http://dx.doi.org/10.1016/j.ijimpeng.2005.05.006.
10. Dekel E, Rosenberg Z. Terminal Ballistics. Springer-Verlag. Berlin Heidelberg 2012.
11. D'entremont B, Grujicic M, Pandurangan B. The role of adhesive in the ballistic/structural performance of ceramic/polymer-matrix composite hybrid armor. Materials and Design 2012; 41: 380-393, http://dx.doi.org/10.1016/j.matdes.2012.05.023.
12. Deshpande V S, Fleck N A, Karthikeyan K, Russell B P, Wadley H N G. The effect of shear strength on the ballistic response of laminated composite plates. European Journal of Mechanics A/Solids 2013; 42: 35-53, http://dx.doi.org/10.1016/j.euromechsol.2013.04.002.
13. Ekici B, Hartomacioglu S, Kilic N. Determination of penetration depth at high velocity impact using finite element method and artificial neural network tools. Defence Technology 2015: 1-13 (in press).
14. Falzon B G, Iannucci L, Yong M. Efficient modelling and optimisation of hybrid multilayered plates subject to ballistic impact, International Journal of Impact Engineering 2010; 37: 605-624, http://dx.doi.org/10.1016/j.ijimpeng.2009.07.004.
15. Fernández-Fdz D, Zaera R. A new tool based on artificial neural networks for the design of lightweight ceramic-metal armour against high-velocity impact of solids. International Journal of Solids and Structures 2008, 45: 6369-6383, http://dx.doi.org/10.1016/j.ijsolstr.2008.08.009.
16. Fragiadakis D, Gamache R M, Roland C M. Elastomer - steel laminate armor, Composite Structures 2010; 92: 1059-1064, http://dx.doi.org/10.1016/j.compstruct.2009.09.057.
17. Hall I W, Tasdemirci A. Development of novel multilayer materials for impact applications: A combined numerical and experimental approach, Materials and Design 2009; 30: 1533-1541, http://dx.doi.org/10.1016/j.matdes.2008.07.054.
18. Hazell P J. Ceramic Armour: Design and Defeat Mechanisms. Argos Press. Canberra 2006.
19. Javadpour G, Shokrieh M. Penetration analysis of a projectile in ceramic composite armor. Compos. Struct 2008; 82 (2): 269-276, http://dx.doi.org/10.1016/j.compstruct.2007.01.023.
20. Mendis P, Mohotti D, Ngo T, Raman S N. Polyurea coated composite aluminium plates subjected to high velocity projectile impact. Materials and Design 2013; 52: 1-16, http://dx.doi.org/10.1016/j.matdes.2013.05.060.
21. Płonka B, Senderski J, Wiśniewski A, Witkowski Z. Wielowarstwowe metalowo-ceramiczne pasywne pancerze dla helikopterów i pojazdów specjalnych. Problemy Techniki Uzbrojenia 2011; 40: 57-64.
22. Sánchez-Gálvez V, Zaera R. Analytical modelling of normal and oblique ballistic impact on ceramic/metal lightweight armours. Int. J. Impact Eng. 1998; 21 (3): 133-148, http://dx.doi.org/10.1016/S0734-743X(97)00035-3.
23. Wiśniewski A. Pancerze - budowa, projektowanie i badanie. Wydawnictwa Naukowo-Techniczne. Warszawa 2001.

Jan GODZIMIRSKI
Jacek JANISZEWSKI
Marek ROŚKOWICZ
Zbigniew SURMA
Military University of Technology
Faculty of Mechatronics and Aviation
ul. Sylwestra Kaliskiego 2, 00-908 Warsaw, Poland
E-mail: jan.godzimirski@wat.edu.pl, jacek.janiszewski@wat.edu.pl, marek.roskowicz@wat.edu.pl, zbigniew.surma@wat.edu.pl

Article citation info:
KUMBÁR V, VOTAVA J. Numerical modelling of pressure and velocity rates of flowing engine oils in real pipe. Eksploatacja i Niezawodnosc – Maintenance and Reliability 2015; 17 (3): 422–426, http://dx.doi.org/10.17531/ein.2015.3.13.

Vojtěch KUMBÁR
Jiří VOTAVA

NUMERICAL MODELLING OF PRESSURE AND VELOCITY RATES OF FLOWING ENGINE OILS IN REAL PIPE

NUMERYCZNE MODELOWANIE CIŚNIENIA I PRĘDKOŚCI PRZEPŁYWU OLEJU SILNIKOWEGO PRZEZ PRZEWÓD RUROWY W WARUNKACH RZECZYWISTYCH

The article deals with the numerical modelling of physical state flowing liquid in a real environment of real technical component (pipe). Specifically it is about to set the pressured and velocity rates along the pipe geometry in a certain places for temperature dependent material (three engine oil with different viscosity class) at three monitored temperatures of flowing medium. The numerical models were created by means finite element method. Observation focused mainly on places behind technical component geometry curvature which are from the point of view of flowing features most interesting.

***Keywords*:** *numerical modelling, flow, engine oil, temperature, viscosity, density, FEM.*

Artykuł dotyczy modelowania numerycznego stanu fizycznego cieczy płynącej w rzeczywistym środowisku rzeczywistego elementu technicznego (przewodu rurowego). W szczególności, celem pracy było określenie ciśnienia i prędkości przepływu materiału, którego właściwości zależą od temperatury, w określonych punktach przewodu rurowego dla trzech monitorowanych temperatur przepływającego czynnika. Do badań użyto trzech typów oleju silnikowego o różnej klasie lepkości. Modele numeryczne tworzono za pomocą metody elementów skończonych. Obserwacje prowadzono głównie w miejscach tuż za zakrzywieniami elementu technicznego, które są najbardziej interesujące z punktu widzenia właściwości przepływu.

Słowa kluczowe*: modelowanie numeryczne, przepływ, olej silnikowy, temperatura, lepkość, gęstość, MES.*

1. Introduction

The great amount of plants, engineers and researches now deal with how to save production costs in the production of certain products. The situation in engineering is same. Lowering material quantity for production can save considerable amount. But there is an issue how to save the material and keep the same quality goods or else production goods safety at the same time. The experimental costs can exceed savings themselves. In this case the numerical modelling can be very well proved [1] and [15].

If the input has a good quality, [13] confirm that result can be very precise in case of using suitably chosen modelled methods. These obtained models can help to engineers to propose such parts which are not uselessly excessive but at the same time they should be safe in accordance to requested standards [14]. Ideal part shapes can be simulated as well both from the statistical view and dynamical view – elasticity, firmness, hydrodynamics, aerodynamics, thermodynamics etc. [10].

According to publication [5] the numerical modelling of many physical phenomenon is closely connected to simulation of certain form of velocity by mathematical means. The liquid velocity is related to solutions of various problems which are given by physical simulation.

Mathematical model consists in equations definition which describes processes above. In view of the fact that there are plane two-dimensional processes, axially symmetrical or three-dimensional and timely dependent, there are described by partial differential system equations which must be solved by numerical methods. Their use is subjected to broaden knowledge from field of flowing, turbulence, numerical methods, and computer technology. Commercial programme systems can be used to solve flowing. User’s task is to assemble correct calculating model which includes some mathematical, psychical and technical principles. It is necessary to find for such a model all input data in valid standards, carry out solution at terminal, and correctly interprets results for next use and also to carry out effective inspection in all phases of all input and output data. User has to categorize all information on geometrical data (two-dimensional or three-dimensional data, topology), external power data and physical data (information about flowing medium and its physical features). User´s necessary task is to have knowledge of hydro-mechanics, thermos-mechanics and other science by problem intricacy[2].

In this study is described the numerical modelling of physical state flowing engine oil in a real pipe by means finite element method. Specifically it is about to set the pressured and velocity rates along the pipe geometry. The theoretical idea is that the variation in viscosity and density of liquid causes significant changes in pressure drop and flow density [6] and [7].

2. Material and Methods

Engine oil feeding tube for turbo-blower was real technical component in this contribution. This pipe is used intractor engines. Its shape, dimensions and monitored spots beyond geometry curvature are displayed in the Fig. 1.

Quality input data were necessary to obtain for numerical modelling. According to temperature dependent flowing liquid, engine oils with viscosity class 5W-30, 10W-40 and 15W-40 were chosen. At this engine oil temperature dependence of density and dynamical viscosity dependence was measured. The measured values of dynamical viscosity and density are displayed in Table 1.

Temperature dependence of dynamical viscosity was measured by rotary viscometer Anton Paar DV-3P with temperature sensor Pt100. The standardized spindle R3 was used which is most suitable for measuring liquid with similar viscosity. Temperature range of

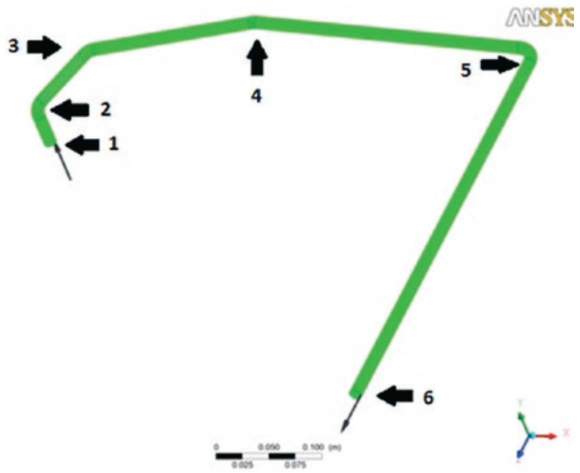

Fig.1. Real technical component (pipe)

measuring was chosen between –10°C and 100°C, similarly stated by [8] and [9].

Temperature dependence of specific weight (density) was measured by digital hydrometer Densito PX30 with API range for measuring of oil products. Temperature range was chosen between −10°C and 70°C.

The numerical modelling was done in programme FLUENT, because this program is optimal for finite element method and for Navier-Stokes differential equations solving.

Table 1. Values of dynamic viscosity and density of engine oils at various temperatures

Temperature (°C)	Density (kg.m^{-3})			Dynamic viscosity (mPa.s)		
	5W-30	10W-40	15W-40	5W-30	10W-40	15W-40
–10	859	867	881	1433	2415	5298
0	856	863	878	828	1108	2667
10	852	862	876	374	607	739
20	848	860	873	227	306	412
30	845	856	870	144	180	225
40	838	854	867	89	115	144
50	835	852	862	67	85	98
60	834	848	858	57	70	74
70	833	846	854	49	59	63
80				42	53	56
90				40	47	52
100				38	45	50

Continuous functions from measured data of dynamical viscosity and density were necessary to create for needs of numerical modelling [6]. Similar work process can be observed at[12].

The exponential function was most suitable function for using of results interpose by general form[11]:

$$\eta = a \exp(bt) \tag{1}$$

Where η is a dynamic viscosity; t is temperature; a, b are coefficients. Values of thesecoefficients are shown in Table 2. R^2 is coefficient of determination.

Table 2. Values of coefficients for Eq. (1)

Viscosity class of engine oil	a (mPa.s)	b (1/°C)	R^2
5W-30	790.6	–0.05976	0.9936
10W-40	1186	–0.06996	0.9955
15W-40	2379	–0.08122	0.9924

The linear function was chosen as the most suitable function using for results interpose of measured density values [7]:

$$\rho = ct + d \tag{2}$$

where ρ is density; t is temperature; c, d are coefficients. Values of these coefficients are shown in Table 3. R^2 is coefficient of determination.

Table 3. Values of coefficients for Eq. (2)

Viscosity class of engine oil	c (1/°C)	d (mPa.s)	R^2
5W-30	–0.3869	855.5	0.9841
10W-40	–0.2571	864.2	0.9866
15W-40	–0.3226	878.7	0.9848

There is a process in the Fig. 2 showing exponential functions interposed measured values of dynamical viscosity. In the Fig. 3 there is a displayed process of linear functions interposed measured density values.

3. Results and Discussion

Modelling of pressured profiles, mass flow and velocity of engine oil streaming with viscosity class 5W-30, 10W-40 and 15W-40 in certain places along geometry of technical component was made by Finite Element Method. There were used general continuity equation, see Eq. (3), and Navier-Stokes equations, see Eq. (4), [5]:

$$\frac{\partial u}{\partial x} + \frac{\partial v}{\partial y} + \frac{\partial w}{\partial z} = 0 \tag{3}$$

$$\begin{aligned}
&\frac{\partial u}{\partial t} + \frac{\partial(uu)}{\partial x} + \frac{\partial(uv)}{\partial y} + \frac{\partial(uw)}{\partial z} = -\frac{1}{\rho}\frac{\partial p}{\partial x} + \nu\left(\frac{\partial^2 u}{\partial x^2} + \frac{\partial^2 u}{\partial y^2} + \frac{\partial^2 u}{\partial z^2}\right) + f_x \\
&\frac{\partial v}{\partial t} + \frac{\partial(vu)}{\partial x} + \frac{\partial(vv)}{\partial y} + \frac{\partial(vw)}{\partial z} = -\frac{1}{\rho}\frac{\partial p}{\partial y} + \nu\left(\frac{\partial^2 v}{\partial x^2} + \frac{\partial^2 v}{\partial y^2} + \frac{\partial^2 v}{\partial z^2}\right) + f_y \\
&\frac{\partial w}{\partial t} + \frac{\partial(wu)}{\partial x} + \frac{\partial(wv)}{\partial y} + \frac{\partial(ww)}{\partial z} = -\frac{1}{\rho}\frac{\partial p}{\partial z} + \nu\left(\frac{\partial^2 w}{\partial x^2} + \frac{\partial^2 w}{\partial y^2} + \frac{\partial^2 w}{\partial z^2}\right) + f_z
\end{aligned} \tag{4}$$

where u, v, w are velocity components; p is pressure; ρ is density; ν is kinematic viscosity; $f_{x,y,z}$ denotes external forces (gravity, centrifugal). Other exact equations are shown in publication [5].

Average pressure values, weight flowing and velocity of engine oil streaming at medium temperature 0°C, 20°C and 70°C are presented in Table 4, gradually for all six chosen cross-sections.

From calculated data the plummet of pressure can be observed during temperature increase of engine oil flowing as well as increasing of velocity flowing which is related to increase of liquid weight flowing.For illustration were chosen only figures of engine oil with viscosity class 15W-40.

In the Fig. 4 there are velocity streamlines in cross-sections 1–6 at liquid temperature of 0°C. In the Fig. 5 there are velocity vectors in cross-sections 1–6 at liquid temperature of 20°C. In the Fig. 6 there are pressures in cross-sections 1–6 at liquid temperature of 70°C.

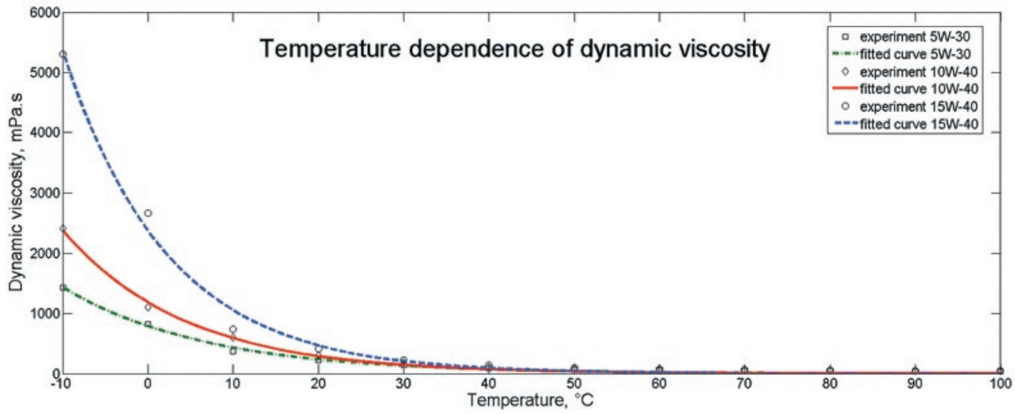

Fig. 2. Temperature dependences dynamic viscosity of engine oils and fitting by exponential function

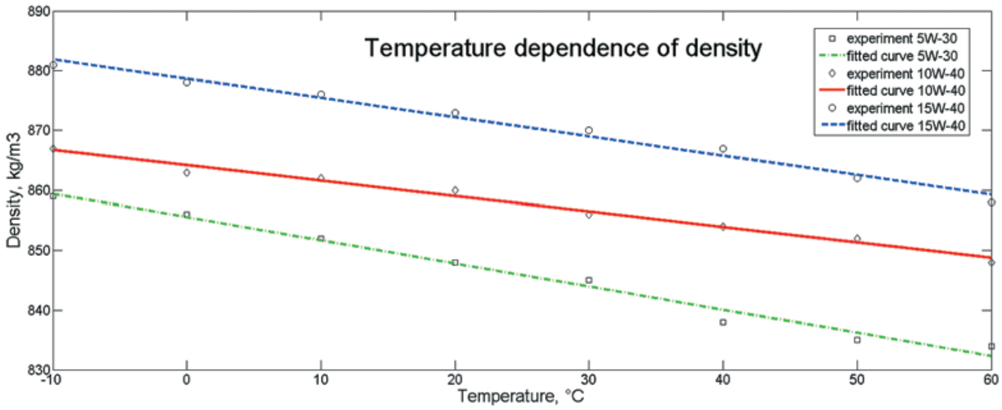

Fig. 3. Temperature dependencesdensity of engine oils density and fitting by linear function

Table 4. Values of pressure, mass flow and velocity of engine streaming for specific temperatures

		Pressure (kPa)			Mass flow (g.s^{-1})			Velocity (m.s^{-1})		
Temp. (°C)	Cross-section	5W-30	10W-40	15W-40	5W-30	10W-40	15W-40	5W-30	10W-40	15W-40
0	1	500.0	499.8	499.8	17.62	14.61	11.30	15.81	13.12	10.02
	2	472.4	468.0	465.6	18.01	15.07	11.55	15.92	13.21	10.04
	3	431.2	419.5	418.7	17.65	14.69	11.34	15.86	13.17	10.04
	4	342.9	317.6	327.2	17.51	14.55	11.26	15.81	13.14	10.04
	5	194.1	176.6	184.8	17.49	14.58	11.22	15.82	13.14	10.04
	6	0.002	0.002	0.001	17.53	14.61	11.29	15.82	13.14	10.04
20	1	499.9	499.9	499.9	17.85	16.37	16.59	16.55	14.73	14.68
	2	421.8	471.4	470.7	17.97	16.78	16.98	16.60	14.86	14.81
	3	360.9	428.0	428.0	17.88	16.55	16.76	16.54	14.79	14.74
	4	279.9	336.7	337.8	17.84	16.41	16.62	16.52	14.74	14.69
	5	119.1	191.4	192.8	17.83	16.36	16.56	16.53	14.75	14.70
	6	0.001	0.005	0.005	17.85	16.40	16.61	16.52	14.74	14.69
70	1	499.9	499.9	499.9	19.12	18.92	18.18	17.04	16.62	16.02
	2	467.9	468.2	469.5	19.66	19.48	18.70	17.47	16.99	16.28
	3	432.6	433.2	434.4	18.81	18.78	18.34	17.16	16.74	16.12
	4	347.6	348.5	351.2	19.10	18.97	18.36	17.08	16.66	16.04
	5	202.7	203.1	204.0	18.62	18.57	18.09	17.30	16.85	16.16
	6	0.013	0.012	0.012	19.39	19.25	18.54	17.05	16.64	16.03

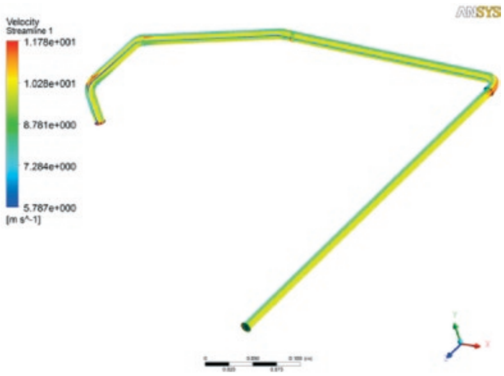

Fig. 4. Velocity streamline in chosen places at oil temperature of 0°C

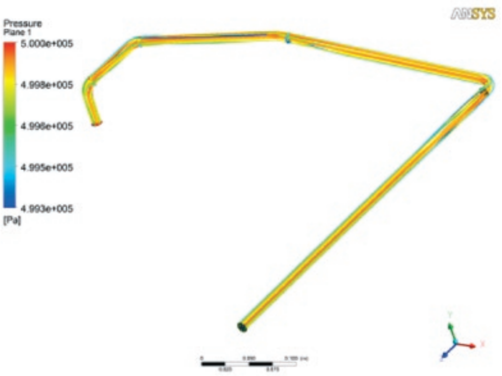

Fig. 5. Velocity vectors in chosen places at oil temperature of 20°C

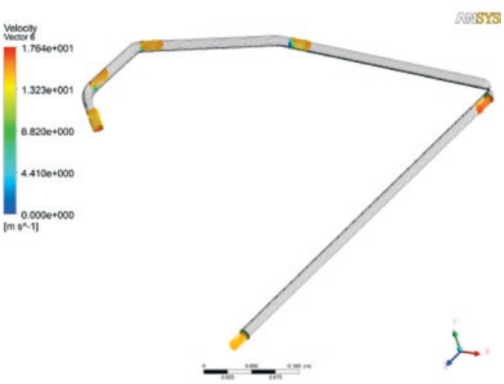

Fig. 6. Pressures in chosen places at oil temperature of 70°C

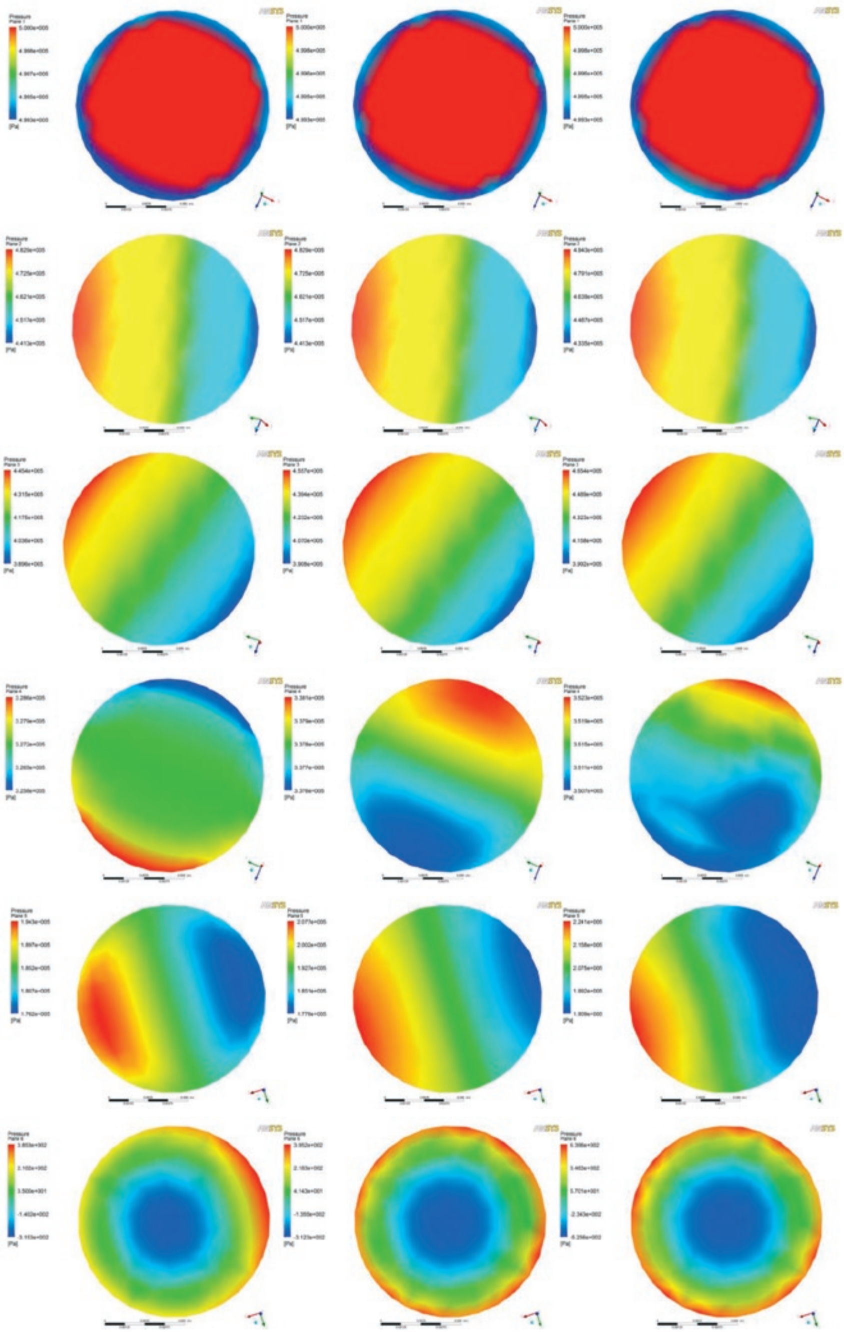

Fig. 7. Pressure decomposition in plane of sections 1–6 at oil temperature of 0°C, 20°C and 70°C

In the Fig. 7 there is a graphical representation of pressure decomposition in chosen cross-sections 1–6, at liquid temperature 0°C, 20°C and 70°C. During creation of numerical models of pressure decomposition in cross-sections was chosen the smoothest displaying system as in [3] and [4].

In several cross-sections are not any significant differences of pressure at the different temperatures. Only cross-section 4 shows some differences of pressure whole temperatures. It may be caused by high velocity of engine oil, which is lead to turbulent flow.

4. Conclusion

Numerical modelling of physical states of streaming liquid in real environment of technical component was made in this article. As a liquid was used engine oil and real technical component was engine oil feed pipe to turbo-blower. This feed pipe is used in tractor engines.

Firstly, the temperature dependence of dynamical viscosity and density of engine oils with viscosity class 5W-30, 10W-40 and 15W-40 was measured by using method of modern measuring devices. These data were interposed suitably chosen regression curved lines – exponential function (viscosity) and linear function (density) – to reach dependence connection which is necessary for numerical modelling.

Also, by using programme there were created numerical models of average values of weight flowing, velocity streaming and decomposition of pressure liquid in six chosen cross sections. These cross-sections were suitably chosen – input, output and geometry curving of feed pipe. Numerical modelling was made at temperatures of 0°C, 20°C, and 70 °C.

The results of average pressure values, weight flowing and velocity of engine oil streaming at three different temperatures show increasing velocity of flowing liquid with increase of temperature and decrease of dynamical viscosity. That is why the weight flowing values of flowing liquid increased.

During numerical modelling creation of pressure decomposition in cross-sections was chosen smoothest displaying system, therefore all colour highlighted pressure values are very precise.

The theoretical idea is that the variation in viscosity and density of liquid causes significant changes in pressure drop and flow density was partially confirmed. With increasing temperature the viscosity and density of engine oil decreased, which was caused higher values of flow velocity and mass flow. This also applies vice versa. Temperature dependence, respectively viscous and density dependence on the pressure drop was not shown.

The results of these experiments can be used for design engineers to predict physical states of engine oil flowing (or similar viscous liquids) in pipe of similar diameter and geometry. The pressure and velocity results are able to predict, which material and what thickness must be used to produce real pipes.

Acknowledgment

The research has been supported by the project TP 6/2015, financed by Internal Grand Agency AF MENDELU.

References

1. Barata J. Modelling of biofuel droplets dispersion and evaporation, Renewable Energy 2008; 33(4): 769-779, http://dx.doi.org/10.1016/j.renene.2007.04.019.
2. Buchar J, Adamík V, Rolc S. Numerical simulation of the explosive tube fixing, Journal de physique IV 2006; 134: 353-358, http://dx.doi.org/10.1051/jp4:2006134054.
3. Faccini JLH, De Sampaio PAB, Su J. Numerical modelling of stratified gas-liquid flow in inclined circular pipes. International Conference on Nuclear Engineering 2009; 5: 691-696, http://dx.doi.org/10.1115/ICONE17-75986.
4. Jafari M, Mansoori Z, Saffar Avval M, Ahmadi G, Ebadi A. Modeling and numerical investigation of erosion rate for turbulent two-phase gas-solid flow in horizontal pipes. Powder Technology 2014; 267: 362-370, http://dx.doi.org/10.1016/j.powtec.2014.08.004.
5. Kozubková M. Flow modelling of fluids, Ostrava: VŠB TU, 2008. (in Czech)
6. Kumbár V, Dostál P. Temperature dependence density and kinematic viscosity of petrol, bioethanol and their blends, Pakistan Journal of Agricultural Sciences 2014; 51(1): 175–179.
7. Kumbár V, Votava J. Differences in engine oil degradation in spark-ignition and compression-ignition engine, Eksploatacja i Niezawodnosc – Maintenance and Reliability 2014; 16(4): 622-628.
8. Kumbár V, Votava J. Excessive additive effect on engine oil viscosity, Acta Universitatis Agriculturae et Silviculturae Mendelianae Brunensis 2014; 62(5): 1015-1020, http://dx.doi.org/10.11118/actaun201462051015.
9. Maggi CP. Advantages of Kinematic Viscosity Measurement in Used Oil Analysis. Practicing Oil Analysis Magazine 2006; 5: 38–52.
10. Mang T, Dresel W. Lubricants and Lubrication, Weinheim: Wiley-vch, 2001.
11. Šedivý P. Temperature dependence of physical quantities, Hradec Králové: KFO press, 2012. (in Czech)
12. Severa L, Havlíček M, Kumbár V. Temperature dependent kinematic viscosity of different types of engine oil, Acta Universitatis Agriculturae et Silviculturae Mendelianae Brunensis 2009; 57(4): 95–102, http://dx.doi.org/10.11118/actaun200957040095.
13. Stevar MSP, Vorobev A. Shapes and dynamics of miscible liquid/liquid interfaces in horizontal capillary tubes, Journal of Colloid and Interface Science 2012; 38(3): 184–197, http://dx.doi.org/10.1016/j.jcis.2012.06.053.
14. Troyer D. Understanding absolute and kinematic viscosity, Practicing Oil Analysis 2002; 1: 15-19.
15. Yamamoto S, Nagaoka M, Ueda R, Wakisaka Y, Noda S. Numerical simulation of diesel combustion with a high exhaust gas recirculation rate, International Journal of Engine Research 2002; 11(1): 17-27, http://dx.doi.org/10.1243/14680874JER05309.

Vojtěch KUMBÁR
Jiří VOTAVA
Department of Engineering and Automobile Transport
Mendel University in Brno
Zemědělská 1/1665, 61300 Brno, Czech Republic
E-mail: vojtech.kumbar@mendelu.cz, jiri.votava@mendelu.cz

Article citation info:
MOCEK P, ZAMIAR R, JACHIMCZYK R, GOWARZEWSKI R, ŚWIĄDROWSKI J, GIL I, STAŃCZYK K. Selected issues of operating 3 MW underground coal gasification installation. Eksploatacja i Niezawodnosc – Maintenance and Reliability 2015; 17 (3): 427–434, http://dx.doi.org/10.17531/ein.2015.3.14.

Piotr MOCEK
Radosław ZAMIAR
Robert JACHIMCZYK
Ryszard GOWARZEWSKI
Jerzy ŚWIĄDROWSKI
Iwona GIL
Krzysztof STAŃCZYK

SELECTED ISSUES OF OPERATING 3 MW UNDERGROUND COAL GASIFICATION INSTALLATION

WYBRANE ZAGADNIENIA EKSPLOATACJI INSTALACJI PODZIEMNEGO ZGAZOWANIA WĘGLA O MOCY TERMICZNEJ 3 MW*

Experiences of operating underground coal gasification installation (UCG) are discussed in the article. The gasification experiment was conducted in active Wieczorek coal mine. The assumed maximum gasification capacity of the installation was 600 kg/h of coal, i.e. 3 MW contained in enthalpy of gas. An integrated design process was applied in preparing equipment of the UCG installation. The result was long-lasting tests (over 1400 h) of coal gasification process at near- atmospheric pressure. Gasification was conducted in a 5.4 m thick deposit with a mixture of: air and oxygen, air and CO_2, air and water. Data on performance of a semi-industrial scale UCG installation were collected. The aim of the article is to present the process and selected experiences associated with operating the installation. External limitations influencing the gasification method, design of basic nodes and rules of running the process are described. The main problems encountered during the gasification process and UCG gas purification are presented.

Keywords: *underground coal gasification, pilot installation, controlling process.*

Omówiono doświadczenia z eksploatacji urządzeń podziemnego zgazowania węgla (PZW). Próbę zgazowania przeprowadzono w funkcjonującej Kopalni Węgla Kamiennego "Wieczorek". Projektowana wydajność zgazowania wynosiła 600 kg/h węgla. Przekłada się to na 3 MW mocy termicznej zawartej w entalpii gazu. Przygotowując urządzenia instalacji PZW zastosowano zintegrowany cykl projektowania. Wynikiem było przeprowadzenie długotrwałych (ponad 1400 h) badań procesu zgazowania węgla przy ciśnieniu zbliżonym do atmosferycznego. Zgazowanie prowadzono w złożu o średniej miąższości 5.4 m wykorzystując mieszaninę: powietrza i tlenu, powietrza i CO_2 oraz powietrza i wody. Uzyskano informacje z funkcjonowania w skali półtechnicznej instalacji PZW. Celem publikacji jest przedstawienie procesu i wybranych doświadczeń z funkcjonowania tej instalacji. Opisano ograniczenia zewnętrzne wpływające na sposób rozwiązania technologii zgazowania, konstrukcje podstawowych węzłów i zasady prowadzenia procesu. Wskazane zostały główne problemy występujące w trakcie procesu zgazowania i oczyszczania gazu z PZW.

Słowa kluczowe: *podziemne zgazowanie węgla, instalacja pilotowa, sterowanie procesem.*

1. Introduction

The idea of underground coal gasification (UCG) is to supply gas reagent directly into the gasification area located in a coal seam [4, 7, 20]. The products of chemical conversion processes occurring there are: process gas, water, condensates containing hydrocarbons (tar substances), unreacted char, and thermally processed mineral substance of coal. Mixture containing H_2, CO, CO_2, N_2, H_2S, CH_4, C2+, and water steam is exhausted from the georeactor. Solids (coke breeze from decomposing coal and thermal transformations of hydrocarbons, dust) also get into the gas pipeline. Some of the mineral matter of coal, biochar and condensates remain underground. UCG gas contains impurities, hence, depending on its application, it should be dedusted and desulfurized. Then its components should be condensed and undergo further conversion processes [8, 13, 27]. The operation depends on the requirements which process gas shall meet [1, 8, 18, 19, 25].

Underground coal gasification installation differs greatly in its function from conventional gasification equipment. Industrial surface gasification installations, fed with coal, biomass or mixtures of waste; do not differ so much in their parameters, particularly availability, from typical equipment of energy sector and chemical industry [17, 21, 24]. Its elements are relatively less durable, especially the ones which are exposed to aggressive components of process gas. Surface gasification systems, where hot gas is fed into atmospheric pressure combustion chamber, do not have long sections connecting the gasification reactor with the furnace. As a result, the amount of condensing tar components is reduced. Integrated gasification combined cycle installations (IGCC), i.e. high pressure gasification installations, are not so easily available. It is so because of technologically demanding parameters of work from a reactor through a dust separator to a combustion turbine [6, 11, 12, 23]. It also means relatively more often check-ups of the turbine and its system.

(*) Tekst artykułu w polskiej wersji językowej dostępny w elektronicznym wydaniu kwartalnika na stronie ***www.ein.org.pl***

Underground coal gasification installations, unlike other gasification systems, do not require building a conversion reactor. The process of injecting gasification agents, followed by exhausting and purifying the products, requires certain equipment. Its characteristic elements are: long sections of substrate and process gas pipelines, differentiated thermodynamic parameters in the georeactor, safety requirements, and technical and operational limitations [13, 14, 15].

The factor which determines technicalities is the followed UCG technology. Gasification conducted in coal seams with mining operations or seams of high risk of UCG gas outflow [26, 29], requires maintaining near-atmospheric pressure in the gasification area. The produced gas has relatively low density. In its content dominate components for which equilibrium conditions of chemical conversion are characteristic for low pressure (CO, H2). Such UCG gas should be exhausted with large-diameter pipelines.

Integrated methods of coal gasification and "in situ" process gas conversion, such as CRIP method [22], to obtain high content of CH_4 and CO_2 in process products, enable maintaining pressure near hydrostatic pressure at the gasification depth in the reactor and a significant part of the gas transmission installation. Processes conducted at higher than hydrostatic pressure are limited by a risk of uncontrollable leak of gas and increased risk of polluting ground water with condensing components. High pressure installations require different solutions concerning both supply of substrates and exhausting products, purifying them and stabilizing UCG process [23]. High-pressure methods are more efficient at converting coal within a seam. They offer possibility of applying larger streams of water in gasification agent. In the case of the process much stricter technical regime is required **[**2**].**

Within the framework of project financed by the National Centre for Research and Development titled: "Development of coal gasification technology for highly efficient production of fuels and energy", an original pilot installation of underground coal gasification with air, air enriched with oxygen, and air mixed with water or CO_2 was realised. Its aim was trial exploitation of a coal seam with underground gasification method at a semi-industrial scale. Comparing with hitherto research in Poland, an increase in the scale of the project was significant. The tests were to obtain process data as well as balance and economic data which would enable designing a pilot – industrial scale installation. It was also important to acquire practical knowledge of running the process in conditions hitherto untested in Poland. Within the framework of conducted technical works and tests the following elements were prepared:

- new concept of purifying UCG gas,
- own method of controlling the installation,
- method of transmitting gas in long sections of a high-temperature and thermally compensated, insulated pipeline. As a result, significant part of condensation occurs on the surface.

The designed installation is particularly unique taking into consideration the fact it was designed to meet safety requirements of an active mine. It required devising right methods of gasification and monitoring workings around the georeactor.

The aim of the article is to present experiences of operating UCG installation at semi-industrial scale. The process was conducted in an active and operating coal mine, with low-pressure method. The external limitations which influence the way the installation was designed, design of basic nodes and rules of conducting the process are described. Main problems occurring when the installation was operating are described as they are important for further development of the method to produce energy.

2. Assumptions of gasification process

Underground gasification was conducted in Wieczorek coal mine of Katowicki Holding Węglowy (KHW) S.A. The process was conducted in coal seam no. 501, at the depth of 464 m related to the

Table 1. Main parameters of gasification process and purification system, markings as in Figures 2-6

Parameter, Unit	Value
Seam thickness H, m	5.4
Conditions of seam deposition u	[3]
Planned maximum gasification capacity, kg/h	600
Obtained maximum capacity, kg/h	830
Average capacity during exploitation, kg/h	174
Max stream of gasification air from D1, D1R, m^3_n/h	1400
Max stream of UCG gas, m^3_n/h	1800
Amount of other gasification agents	acc. to Fig. 1
Assumed length of test (ignition, process, extinguishing), day	~90
Main elements of controlling installation:	Method:
Pressure in installation	- through stabilizing negative pressure behind georeactor in three control – measurement points selected by the operator (PID).
Temperature in installation	- through setting threshold value of air stream or through content of oxidant in gasification agent
Temperature at given cooling stages	- (PI) for HE01 regulation of the input value through capacity of a gas/air heat exchanger, other ones (HE11,HE21, HE22, HE23) calibrated through initial setting of the flow of water.
Performance of scrubber SV	- periodical, stream of water adjusted with manually operated valves
Temperature of water in cooling system HE11,HE21,HE22,HE23	- filling the system, 3-position control.
Regulation of reverse adsorbers	- setting reverse, exchange of sorbent basing on data from the system monitoring gas composition.
Amount of gas agents supplied into georeactor	- setting the valve for gases supplied from tanks of N_2,O_2, CO_2, setting inverter for gases supplied with blowers D1,D1R. In case of emergency for D1, D1R throttle/release PID control
Minimal acceptable temperature of process gas in the underground part (sump), °C	70
Range of calorific value of raw gas, MJ/m^3_n	3.2-:-4.7

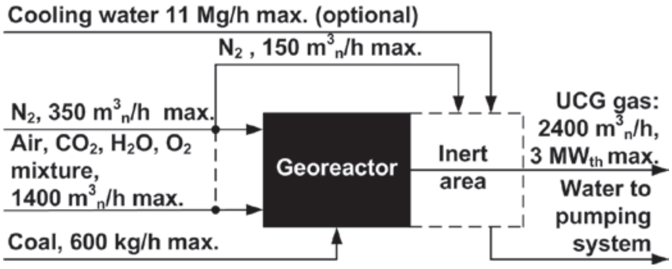

Fig. 1. Balance assumptions of underground gasification

ground surface elevation. The method of locating a georeactor in the rock mass was described in [10], while in [13] and [14] there are details concerning UCG installation design before modifications. Main assumptions of UCG are contained in Table 1. In Figure 1, which is a simplified balance diagram of the georeactor, there are assumed substance streams. Spatial configuration of the georeactor is presented in Figure 2. DN150 pipeline transported a gasification agent. DN100 pipeline served as a spare pipeline and back-up supply of inert gas into the georeactor and exhaust of excess liquid products from the cavity. DN300 pipeline exhausted process products from the georeactor.

3. Conducting the process

The rules which govern coal mines in Poland are described in documents required by the legal regulations [16]. Supervising authorities voiced no formal objections concerning the procedures of controlling the installation and assumptions associated with its safety during the tests. The gasification process was directly controlled from a control room in the surface section of the installation. Multipoint measurements of air composition and monitoring it in the workings surrounding the gasified coal seam was realized with Zefir mine system [5]. Communication between mine monitoring system and the UCG supervising system enabled taking decisions in operator mode.

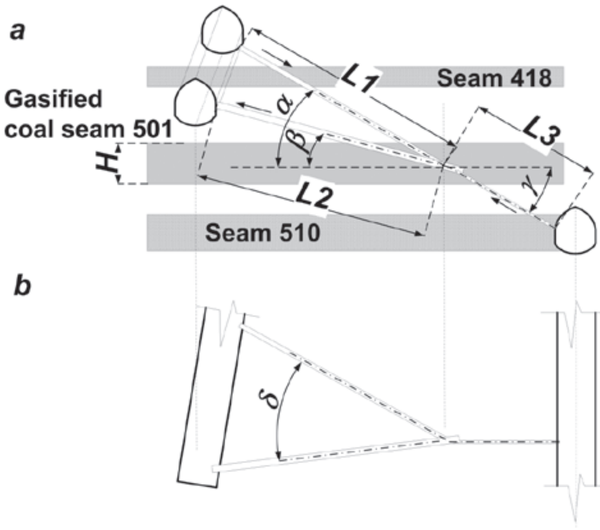

Fig. 2. Spatial configuration of georeactor: a. side view. b. top view

4. Limitations considered during design and construction stages

Limitations, apart from the ones resulting from assumptions of running the process, (Table 1.) were as follows:

- approximately 42 m of the process gas pipeline under water,
- the pipeline in the vicinity of coal seams [3]. It was associated with the risk of heating and, as a consequence, igniting the coal seam. That is why temperature of the pipeline should not exceed 40 ºC,
- maximum acceptable concentration of carbon oxide in the underground part could not exceed 26 ppm vol.,
- mining operations in the vicinity of the installation,
- pumps exhausting condensate could not be used in the underground part,
- underground part of the UCG installation was to be maintenance-free.

The above mentioned limiting parameters were determined mainly by operating in conditions of the coal mine. To protect coal seams in the vicinity of the pipeline against heat the whole length of DN300 pipeline was insulated. It prevented part of tar compounds and water from condensing. It enabled exhausting condensate to the surface part of the installation to a place dedicated for the purpose. The effect of using insulation was an increase in thermal stresses in the process gas production pipeline. Expansion joints were used to reduce the thermal stress. Distribution of temperature in DN300 pipeline during the experiment was determined basing on analytical methods [15].

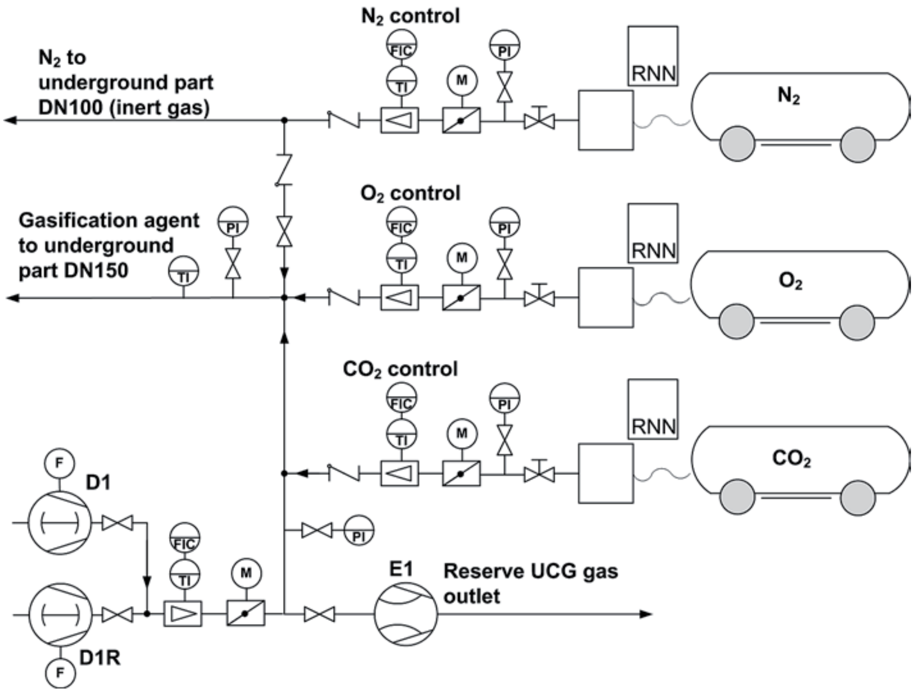

Fig. 3. Diagram of installation dosing gasification agents

5. Description of gasification process

The process part of the gasification installation worked under SCADA system, which was based on ASKOM software [28]. The measurement control system of gasification process and gas purification was based on data from 68 sensors located in crucial points of the installation. Figure 3 presents feeding gasification agents located in the surface section. In figures measurement points of main elements are presented too.

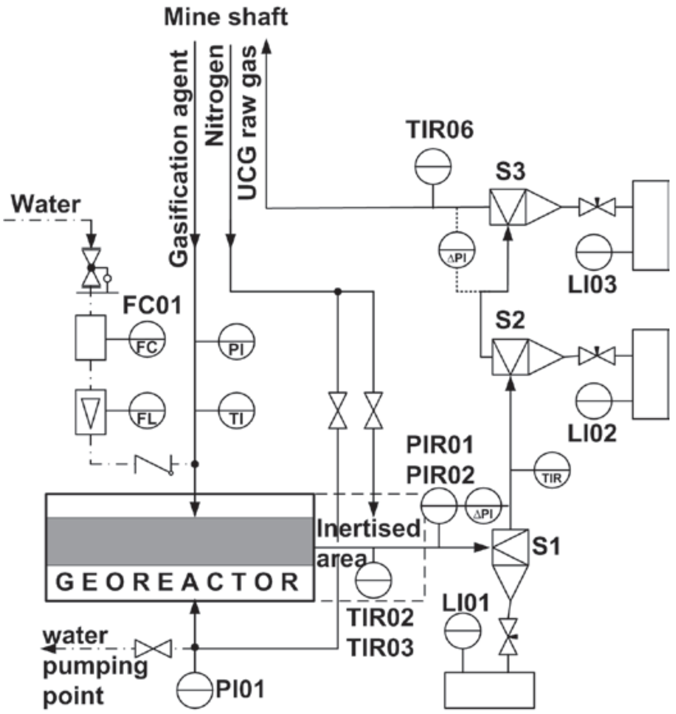

Fig. 4. Underground section of gasification installation. — gas, — · — · water

Nitrogen was injected with DN100 pipeline into the cavity, and into a section of a research gallery behind a stopping. It was possible to connect the pipeline with DN150 gasification agent pipeline, where oxygen was mixed with air from oil-free blowers D1/D1R. The streams of substrates were controlled: with valves – for oxygen, carbon dioxide, nitrogen and air; and with an inverter for air. Ejector E1 played a role of a pressure regulator in the underground installation if the gas production pipeline was cut-off (blocking, caving in the cavity). Then it was possible to exhaust gas and lower the pressure. The ejector was fed with nitrogen, or air, depending on the potential explosion hazard, which was marked basing on chromatographic measurements of UCG gas composition. Part of nitrogen was also used to blow sections of purification system and to feed blowers of a dust monitor (the elements are not marked in the figures).

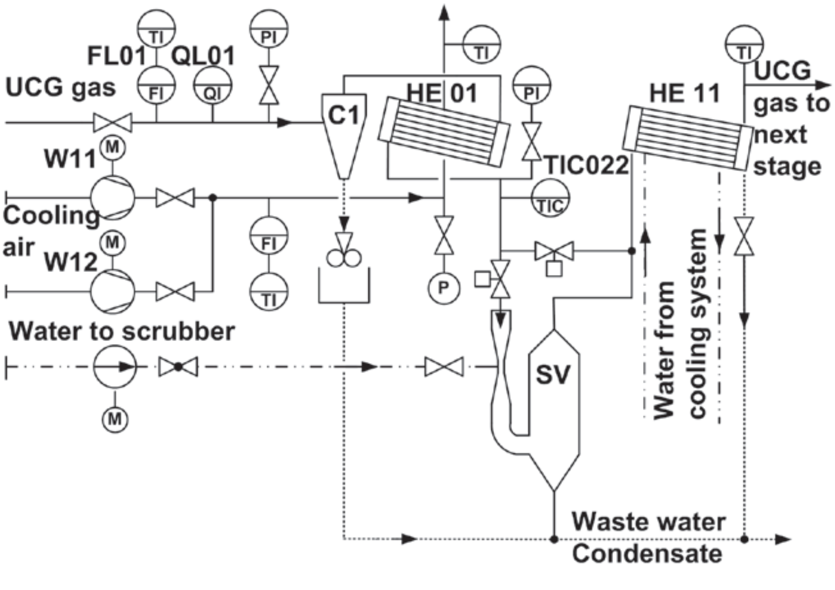

Fig. 5. First stage of gas purification system: cyclone C1, initial cooler HE01, scrubber SV, main cooler HE11.— gas, - - - - condensate, dust, — · — · water

The process diagram of underground part of the installation is presented in Figure 4, where the crucial parameters applied in the controlling process are presented: pressure before (PI01) and behind the georeactor (PIR01, PIR02) and temperature of raw gas (TIR02, TIR03). Sensors PIR02 TIR03 were kept in reserve. The level of condensate in expansion tanks of separators S1, S2, S3 was observed with level gauges LI01, LI02, LI03. In separators S1 and S3 decreases in pressure were also measured. Measurements of the decrease enabled checking if the elements of installation are not blocked.

In Figure 4 there are dust and condensate separators S1, S3, S4. While building the installation one of the separators was scrapped (marked as S2), leaving the old markings (S1, S3, S4). A system of feeding process water, which is controlled with FC01 based on measurements of the stream of water, is shown as well. The stream of water feeding the georeactor was measured with flow meter FRC01. Water went into DN150 raw gas pipeline directly before the inlet feeding substrates into the coal seam. UCG gas pipeline together with separators was located in workings which formed part of the existing underground infrastructure and the mine shaft.

Once having left the underground section raw gas was purified. The first stage of the purification system is presented in Figure 5.

Process gas was dedusted in cyclone C-1, then it was initially cooled in heat exchanger HE01 with air fed with fans W11 or W12. Capacity of the fans was controlled with an inverter PI. The value controlled during initial cooling of the gas was its temperature measured with sensor TIC022 behind heat exchanger HE01. Then the gas went through scrubber Venturi SV and the main tar separator HE11. Condenser HE11 and other heat exchangers except HE01 were cooled with treated water.

Coolant was regenerated in a fan cooler. Water circulation systems are not described in the article. At the final stage of gas purification (Fig. 6) water cooled HE21, HE22, HE23 and a gasodynamic, centrifugal tar separator were used. Condensate was collected in a heated collector. Then it was pumped into pallet tanks (IBC). Condensate was exhausted with membrane pumps PM1 and PM2. Gas was purified of acidic compounds in activated carbon adsorbers F01/ F02. Adsorbent regeneration in adsorbers was conducted reversely with air supplied with fan W-13 heated to a given temperature with heater N1. Purified gas was taken through hydraulic back-pressure valve to the flare, where it was combusted.

Monitoring the workings around the georeactor is not the subject of the article. The issue was arranged with Zefir system of the mine, which was supplemented with additional sensors of concentrations of: hydrogen, carbon and methane; and temperature sensors and anemometric flow meters for ventilating air.

6. Experiences of installation performance

Pressure within the installation was distributed in a specific way. Before the georeactor there was slightly high pressure, behind it there was negative pressure. Increase in volumetric flow of gas caused by contraction and conversion of coal within the deposit and an increase in temperature led to an increase in resistance of flow. When the difference in pressure between a measuring point in the georeactor and the surrounding workings measured with sensor PI01 exceeded 2000 Pa there was a risk that gases would infiltrate into the surrounding of the georeactor through the geological structure (workings and ventilation system). The observation was a result of measurements of concentration of hydrogen and carbon oxide in monitoring wells drilled around the gasification zone. Risk of gas outflow into ventilation

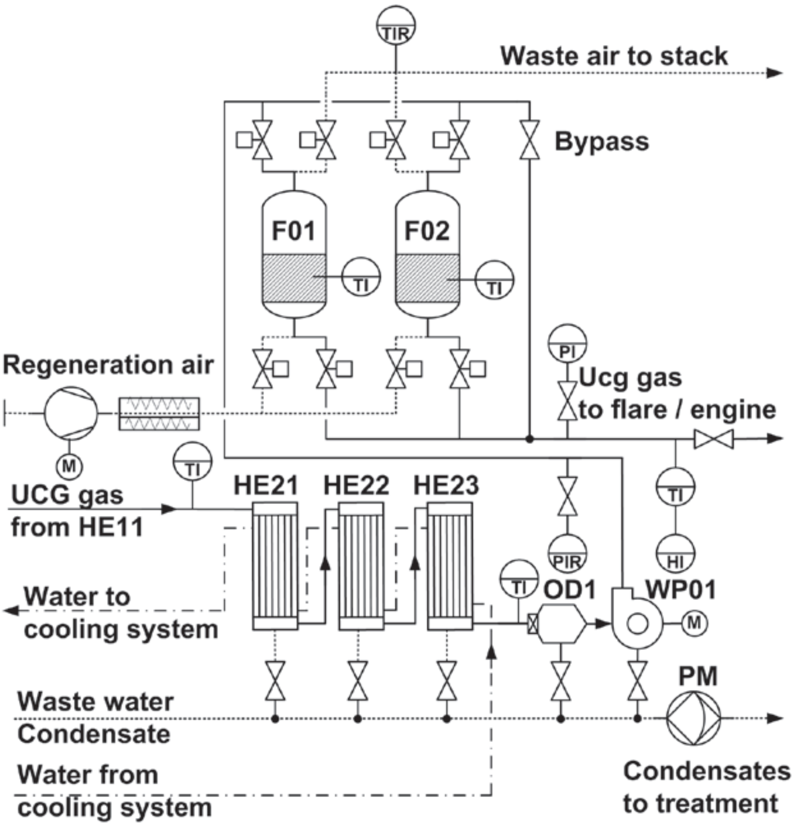

Fig. 6. Third stage of gas purification system. — gas, - - - - condensate, air, dust, —·— water

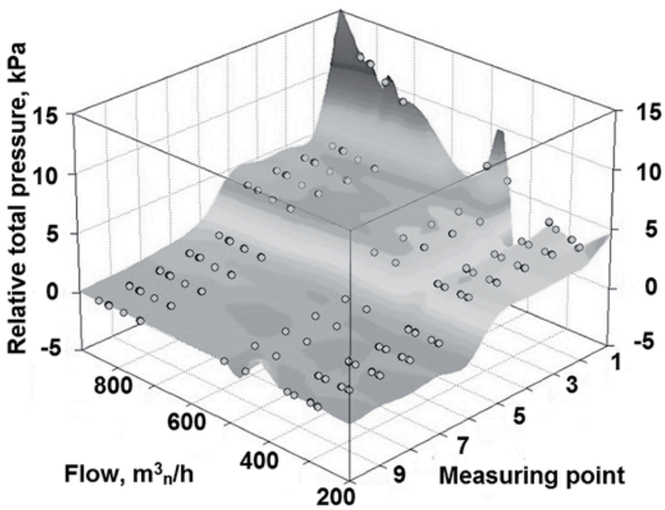

Fig. 7. Flow characteristics of the installation "cold performance". Markings of measuring points: 1. Behind blower D1; 2. Before georeactor; 3. Behind georeactor; 4. Behind separator S1; 5. Behind separator S3; 6. Before cyclone C1; 7. Behind HE01; 8. Behind HE11; 9. Behind cooling system; 10. Before flare

air made it necessary to control negative pressure within the georeactor not to exceed the value of negative pressure in the gasification products exhaust pipeline. High pressure measured before georeactor was maintained at the level of approximately 1500 Pa. Negative pressure behind the georeactor was a function of assumed gasification capacity and an analysis of gas composition conducted in the research gallery. Flow characteristics of the installation changed in time, which resulted from changing volume of the cavity and, to some extent, from condensates, dust and soot, depositing in the pipeline. Initial "cold performance" characteristics of the whole installation, determined before ignition, is presented in Figure 7.

It was determined with WP01 off through regulating capacity of the air stream from blower D1 with an inverter. The test was conducted with gas flowing outside the reverse system of adsorbers (bypass in Figure 6).

6.1. Surface section - feeding gasification agents

Controlling streams of gas substrates during the experiments worked properly. Problems were associated with stabilizing pressure and a stream of nitrogen supplied to inertise a research gallery. It was an effect of the fact that assembly of regulators in the nitrogen path was not considered. It was a consequence of initial assumptions that the research gallery (Figure 2) would be flooded. During initial tests, due to excessive seepage of water and risk of flooding wells of the georeactor, the method of securing the georeactor against leakages was changed. Instead of flooding it was decided to build a sand stopping in the gallery. Inert atmosphere in the research gallery was maintained by supplying a stream of nitrogen of approximately 35-50 kg/h N_2.

During the experiment the process gas production pipeline got blocked and ejector E1 was used to release process gases. Jet pump Huragan 80, installed in DN100 pipeline inlet, was used to produce appropriate negative pressure in the installation. Depending on the explosion hazard it was supplied with nitrogen or compressed air from mine ventilation network.

6.2. Underground part

In the underground part circuit breakers, some of the underground sensors and UCG installation control system were regularly checked as it is required by mining regulations. During such a check-up personnel did not receive continuous measurement signals for up to two hours the experiment. At the time the installation was manually controlled. Sudden events like caving, which alter flow characteristics, posed a threat to stability of the installation working.

As there were not any pumps for the condensate in separators S1, S2, S3 it was necessary to maintain acceptable temperature of gas in DN300 pipeline (no lower than 70°C) in the sump. Its aim was to prevent excessive condensing and blocking the pipeline. Failing to maintain minimal acceptable values of temperature of gas in the sump caused excessive tar condensation. The phenomenon was caused mainly by an increase in the amount of water flowing into the shaft (e.g. rainfall, leakage in backfill installation).

Another important issue was also drift of pressure meters. As a result the meters had to be checked and calibrated, i.e. the personnel had to inspect the pipeline. Due to the safety rules assumed at the very beginning of the experiment such actions were impossible.

Dosing water for the process was much more difficult because of impurities in water in pipelines. Water in the fire suppression system was taken from a backfill water settling pond. It contained a lot of sand, which resulted in unreliability of the dosing system.

6.3. Surface part of process gases purification

Figure 8 presents a photograph of the installation seen from the side of the gas flare. Process gas purification was based on gradual condensation. It required maintaining the right temperature of raw gas exhausted from the shaft and at given cooling stages. The main controlled parameters were decreases in temperature at given stages of cooling and the stream of gas of water feeding the scrubber.

Gas condensation system worked throughout the whole experiment. The desulfurization process of raw gas in a scrubber was periodically examined. During the tests approximately 90±20 g water-tar condensate per 1 m^3_n of UCG gas was exhausted. Purification efficiency was approximately 85 – 92 % for all fractions, depending on the tested configuration of the equipment and the stream of water injected into membrane heat exchangers and scrubber SV. The effect of applying significant negative pressure on process gas in DN300 pipeline before fan WP01, which was done to protect the underground section of the installation, was a difficulty in pumping water–tar condensate. Chemical compounds in the pumped liquid lowered durability of membranes in the applied condensate pumps. It was necessary to replace membrane pumps with more reliable equipment, of higher capacity and better suited to deal with water-tar mixtures.

During the experiment there were also problems with too low temperature of gas at the inlet of the surface module of purification system which led to condensation in points not prepared for it. The problems were solved through periodical increases in the temperature in the heat exchangers over their standard operational temperature.

Fig. 8. Flare and part of UCG gas purification system

7. Stability of the process

Controlling the UCG process was very stable. The selected measurement ranges in sensors coupled with the control system and applying automatic control of the main parameters worked fine. Increasing volume of the cavity was a factor which stabilised functioning of the installation. That is why given responses to changes in set values and disturbances occurred, as the process progressed, with longer and longer delay.

The most significant disturbance to the process was condensation, which occurred as a result of too low temperature in the sump. There were two main causes of condensation. The first one was the georeactor working at too low parameters. It was a result of the scope of works during the experiment and limitations concerning maximum temperature of UCG gas at the georeactor outlet (550°C, whereas, the

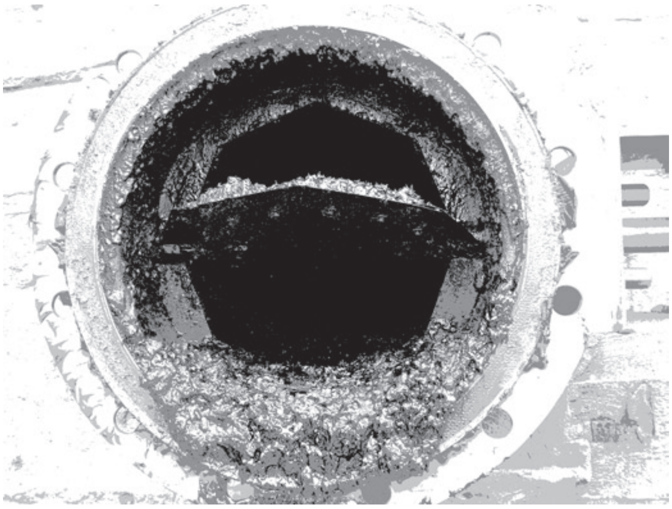

Fig. 9. View of a butterfly valve seat in DN300 raw gas pipeline

maximum computational temperature of long-lasting exploitation was 750°C) imposed by District Mining Office. The other cause was water flowing into the sump of the shaft. The water came from rainfall, leakages in backfill installation and other workings. The flow of water cooled the surface of the insulated pipeline. In practice the first signs of reduced flow in the pipelines were usually observed between 20 and 40 hours before the event. Excessive condensing was avoided through maintaining proper distribution of temperature of gas in the installation and observing decreases in pressure of UCG gas flowing in different sections of the installation.

Figure 9 shows the seat of a butterfly valve installed in DN300 pipeline at the inlet of raw gas into purification system. As it can be seen in the photo significant amount of condensate and dust deposited on protrusions near the valve seat. Near the valve in a smooth pipeline the process did not occur, hence, it is important to insulate heat leakage bridges (flanges, points of mounting support, compensators) properly. In this given case flanges of the pipeline and the valve were such bridges.

Figure 10 presents the changes in temperature in main elements of the installation after initiating gasification process. The initial rapid increase in temperature is an effect of using ignition material and

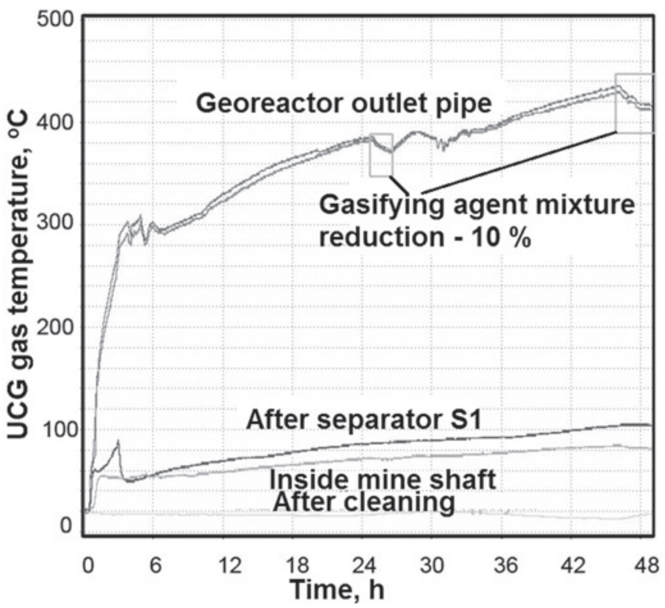

Fig. 10. Distribution of temperature in gasification process in its initial phase for different points of gasification installation

significant amount of volatile matter formed in the first stage of the process.

8. Summary

1. Applying original, integrated design and measurements enabled obtaining a technologically efficient method of producing energy in UCG process.
2. The assumed method of stabilizing low-pressure within the volume of georeactor enabled operating safely in the underground part of installation. Ordinary mining operations were conducted in its vicinity throughout the experiment, and concentrations of toxic components (i.e.: CH_4, CO i H_2) did not exceed the threshold limit values.
3. Insulating the production pipeline reduced the amount of substances condensing inside the raw gas pipeline and transferred most of condensation into the surface part of the installation.
4. Efficiency of purifying gas of condensing substances was (except H2O) on average 86 % with the scrubber off, and 92 % with the scrubber on.
5. Procedures of operating underground gasification plant were prepared basing on the operational and exploitation data. The procedures can be treated as a standard if the type of industrial processes are implemented.
6. Trace concentration of O_2 in process gas while the georeactor was working means the installation is sufficiently leak tight.
7. Tests conducted in laboratory reactors and minimal model installations do not enable obtaining information concerning exploitation and durability of the installation, thermal issues in industrial conditions and events typical for industrial processes. It is necessary to conduct further research into prolonged gasification in mining operations conditions.

This paper is a part of the ongoing Research Task "Development of coal gasification technology for highly efficient production of fuels and energy" funded by the National Centre for Research and Development under the Strategic Programme for Research and Development entitled: 'Advanced energy generation technologies'.

References

1. Advanced materials modelling and lifting technologies for gas turbine components operating in coal gasification plant. Cleaner Coal Technology Programme Project Profile 287, DTI, Alstom 2001.
2. Bell D A, Towler B F, Fan M. Coal gasification and its applications. New York: Elsevier 2011.
3. Chećko J. Analiza warunków geologiczno - górniczych i hydrogeologicznych w.rejonie projektowanego georeaktora zlokalizowanego w KWK "Wieczorek" (Analysis of geological, mining and hydrogeological conditions in the area of planned georeactor in Wieczorek coal mine). Przegląd Górniczy 2; 2013: 37-45.
4. Couch G. Underground coal gasification. London, United Kingdom: IEA Clean coal Centre. 2009. Report No. CCC 151.
5. Dec B, Gajoch A. System dyspozytorski ZEFIR - struktura programu (Zefir dispatching system). Mechanizacja i Automatyzacja Górnictwa. 2000, 4-5, 108-118.
6. Doctor R D, Molburg J C, Thimmapuram P R. KRW oxygen-blown gasification combined cycle. carbon dioxide recovery, transport and disposal, Raport NETL 1996, http://dx.doi.org/10.2172/373835.
7. Howard J B, ed. Elliot M A. Chemistry of coal utilization. Vol. II. New York: Willey and Sons 1981.
8. Karcz A. Koksownictwo (Coke engineering). P. II. Kraków: Wyd. Akademii Górniczo – Hutniczej, 1991.
9. Kowalski J. Wytwarzanie gazu do syntezy (Producing gas for syntheses). Warszawa: PWT, 1954.
10. Krause E, Lasek S. Wpływ uwarunkowań górniczo - geologicznych oraz wentylacyjnych na projektowaną lokalizację georeaktora oraz bezpieczeństwo procesowe podziemnego zgazowania węgla w czynnej kopalni (Influence of geological, mining and ventilation conditions on planned location of georeactor and safety of underground coal gasification in active coal mine). Przegląd Górniczy, 2013; 2: 46-54.
11. Matuszewski M, Rutkowski R, Schoff R, Comparison of Pratt and Whitney Rocketdyne IGCC and commercial IGCC performance, Raport NETL 2006 r.
12. Maurstad O. An overview of coal based integrated gasification combined cycle (IGCC) Technology. MIT Publication no.: MIT LFEE 2005-002 WP. 2005.
13. Mocek P, Gil I, Świądrowski J. Instalacja procesowa dla hybrydowej technologii podziemnego zgazowania węgla (Process installation for hybrid technology of underground coal gasification). Przemysł Chemiczny 2014; 1: 66-69.
14. Mocek P, Gil I, Wodołażski A. Wybrane zagadnienia projektowania instalacji oczyszczania produktów podziemnego zgazowania węgla (Selected problems of designing installation to purify underground coal gasification products). Przegląd Górniczy 2013; 2: 99-107.
15. Mocek P, Gil I. Przesył gazu z podziemnego zgazowania węgla (Underground coal gasification gas transmission). Przegląd Górniczy 2013; 2: 107-115.
16. Prawo geologiczne i górnicze. Ustawa z dnia 9 czerwca 2011 r. Dziennik Ustaw 2011 nr 163 poz. 981.
17. Rezaiyan J, Cheremisinoff N P, Gasification technologies. A primer for engineers and scientists. Boca Raton: Taylor & Francis Group, 2005.
18. Spath P L, Dayton D C. Preliminary Screening — Technical and Economic Assessment of Synthesis Gas to Fuels and Chemicals with Emphasis on the Potential for Biomass-Derived Syngas. Raport NREL/TP-510-34929, 2003.
19. Specification for Fuel Gases for Combustion in Heavy-Duty Gas turbines. Raport GE power Systems Gas Turbine; GEI41040G, 2002.
21. Stańczyk K, Howaniec N, Smoliński A, Świądrowski K, Kapusta K, Wiatowiski M. Gasification of lignite and hard coal with air and oxygen enriched coal in a pilot scale ex situ reactor for underground gasification. Fuel 2011; 5: 1953-1962, http://dx.doi.org/10.1016/j.fuel.2010.12.007.
22. Steinbrecht D, Wolff H J, Matzmohr R, Nassour R, Didk H. Investigations of low calorific landfill gases by a small scale fluidised bubbling bed combustion plant. Global NEST Journal 2007; 9: 42-50.
23. Swan Hills Synfuels. Swan Hills In-situ coal gasification technology development final outcomes report. Alberta Innovates - Energy and Environment Solutions Report 2012.
24. Tampa Electric Polk power station integrated gasification combined cycle project. Raport NETL nr.: DE-FC-21-91MC27363: 2002 r.

25. Tomeczek J. Zgazowanie Węgla (Coal Gasification). Gliwice: Wyd. Politechniki Śląskiej, 1994.
26. Vulfovich K E. Producton of synthetic hydrocarbons for coal through its underground gasification. International Journal of Mining Science and Technology 2013; 23: 279-285, http://dx.doi.org/10.1016/j.ijmst.2013.04.006.
27. Wiatowski M, Stańczyk K, ŚwiądrowskiJ, Kapusta K, Cybulski K, Krause E, Grabowski J, Rogut J, Howaniec N, Smoliński A. Semi-technical underground coal gasification (UCG) using the shaft method in Experimental Mine "Barbara". Fuel 2012; 99: 170-179, http://dx.doi.org/10.1016/j.fuel.2012.04.017.
28. Woolcock J, Brown R. A Review of Cleaning Technologies for Biomass-Derived Syngas. Biomass and Bioenergy 2013; 52: 54-84, http://dx.doi.org/10.1016/j.biombioe.2013.02.036.
29. www.asix.com.pl
30. Yang L, Zhang X, Liu S, Yu L, Zhang W. Field test of large-scale hydrogen manufacturing from underground coal gasification (UCG). International Journal of Hydrogen Energy 2008; 33: 1275-1285, http://dx.doi.org/10.1016/j.ijhydene.2007.12.055.

Piotr MOCEK
Department of Energy Saving And Air Protection
Central Mining Institute
Plac Gwarków 1, 40-166 Katowice, Poland

Radosław ZAMIAR
INTROL 4 TECH Sp. z o.o.
16 Lipca 14, 41-506 Chorzów Batory, Poland

Robert JACHIMCZYK
P.W. „SEMAKO" Sp. z o.o.
Wiejska 40, 44-153 Łany Wielkie k/ Gliwic, Poland

Ryszard GOWARZEWSKI
Katowicki Holding Węglowy
Wieczorek Coal Mine, Poland

Jerzy ŚWIĄDROWSKI
Iwona GIL
Krzysztof STAŃCZYK
Department of Energy Saving And Air Protection
Central Mining Institute
Plac Gwarków 1, 40-166 Katowice, Poland

Email: pmocek@gig.eu, rzamiar@i4t.com.pl, rjachimczyk@semako.pl, rgowarzewski@khw.pl, jswiadrowski@gig.eu, igil@gig.eu, kstanczyk@gig.eu

Article citation info:
YANG H, XU G, FAN XN. A reliability analysis method of cloud theory – Monte Carlo based on performance degradation data. Eksploatacja i Niezawodnosc – Maintenance and Reliability 2015; 17 (3): 435–442, http://dx.doi.org/10.17531/ein.2015.3.15.

Heng YANG
Gening XU
Xiaoning FAN

A RELIABILITY ANALYSIS METHOD OF CLOUD THEORY – MONTE CARLO BASED ON PERFORMANCE DEGRADATION DATA

OPARTA NA TEORII CHMURY I MODELU MONTE CARLO METODA ANALIZY NIEZAWODNOŚCIOWEJ DANYCH O OBNIŻENIU CHARAKTERYSTYK

Owing to inadequate degradation data, the randomness and the fuzziness of degradation processes, it is difficult to calculate the reliability of product. By investigating performance reliability using degradation data of performance, the authors proposed a method of analyzing reliability of performance degradation data using Monte Carlo principle and cloud theory. First of all, the performance degradation cloud with the degradation amount and the entropy which denotes the possible discrete degree of the degradation data, is generated by using performance degradation data and a cloud theory forward cloud generator. Then, the minimum membership threshold of cloud droplets and the threshold of product failure were set. Meanwhile, the number of cloud droplets that comply with the minimum membership degree and the failure threshold were counted. Finally, the reliability method of performance degradation data was proposed by using the principle of Monte Carlo and the cloud theory. In this work, the cloud theory was introduced to verify the reliability of the performance degradation of the product. The randomness and the fuzziness in the degradation tests are resolved. In addition, due to the limits of degradation test data, the difficulties in calculation of the reliability is resolved using the principle of Monte Carlo, the minimum membership of cloud droplets and its minimum degree are therefore guaranteed. This work provides a new method of simulating the reliability of degradation. The feasibility of the method was validated by an example ensuring a high durability of conveyor belt joints is tantamount to guaranteeing their reliable operation and that the results of research conducted so far fail to provide unambiguous solutions to a number of problems that emerge in this case, it is advisable that advanced studies using computer techniques should be conducted within this area.

***Keywords**: performance degradation; Cloud theory; Monte Carlo Method; Randomness; Fuzziness.*

Ze względu na niewystarczające dane o degradacji oraz losowość i rozmycie procesów degradacji, obliczanie niezawodności produktu jest zadaniem trudnym. Chcąc badać niezawodność przy użyciu danych dotyczących obniżenia charakterystyk, autorzy zaproponowali metodę analizy danych o obniżeniu charakterystyk wykorzystującą zasady metody Monte Carlo oraz teorii chmury. Po pierwsze, wykorzystując dane o obniżeniu charakterystyk oraz progresywny generator chmur, wygenerowano chmurę obniżenia charakterystyk zawierającą dane na temat stopnia degradacji oraz stopnia entropii, która określa możliwy dyskretny stopień degradacji danych. Następnie, ustalono minimalny próg przynależności punktów chmury oraz próg uszkodzenia produktu. Policzono liczbę punktów chmury które spełniały warunek minimalnego stopnia przynależności oraz progu uszkodzenia. Wreszcie, zaproponowano metodę analizy niezawodnościowej danych o obniżeniu charakterystyk wykorzystującą zasady modelu Monte Carlo oraz teorii chmury. W pracy przedstawiono teorię chmury, która pozwala na weryfikację niezawodności danych of obniżeniu charakterystyk produktu. Rozwiązano w ten sposób problem losowości i rozmycia występujące w badaniach degradacji. Ponadto, przy użyciu metody Monte Carlo, rozwiązano trudności w obliczaniu niezawodności związane z ograniczeniami danych z badań degradacji, co zagwarantowało minimalną przynależność punktów chmury oraz minimalny stopień uszkodzenia. W prezentowanej pracy przedstawiono nową metodę symulacji niezawodności danych o degradacji. Poprawność przedstawionej metody zweryfikowano na podstawie przykładu. Zapewnienie wysokiej trwałości złączy taśmy przenośnikowej jest równoznaczne z zapewnieniem ich niezawodnej pracy, a ponieważ wyniki prowadzonych dotąd badań nie dostarczają jednoznacznych rozwiązań wielu wyłaniających się w tym przypadku problemów, wskazane jest prowadzenie w tym zakresie zaawansowanych badań z użyciem technik komputerowych.

***Słowa kluczowe**: obniżenie charakterystyk, teoria chmury, metoda Monte Carlo, losowość, rozmycie.*

1. Introduction

The failure of products mainly results from the combined action of its own factors and external conditions [3]. The failure forms can be divided into two types: the basic properties of the product before failure is intact, as in a moment, suddenly all functions are lost; this kind of failure is called sudden failure [36]. For example, when using mechanical products, failure occurs due to the load which is greater than allowable value applied; In contrast with the sudden failure, the other kind is degradation failure whose main performance becomes slowly worse with the increase of time and frequency. When the performance is lower than the lowest limit [37], the product loses its function. Before the products' failure, the degradation failure type undergoes a process changing quantitatively and then qualitatively, it is the main failure form of most of products in the process of normal use and is also the main reason for the shortening of service life. There are many reasons for the performance degradation of the products, and different products have different mechanisms of the degradation. For example, Wang XD, Yi Z and Shen ZC carried out radiation experiments for white paint (S781) in a simulated space environment, to test the spectral reflectance and the rule of the solar absorptance degradation, and found that Zinc vacancy is the main reason of the optical degradation of S781 white paint [24]. The failure of steel tube is caused by too deep or too many pits on the surface. To study the failure mechanism of the depth and density growth of steel tube surface pit with time and pressure, a new model of steel tube was put forward by M. Nuhi under different temperature and different environment pressure aiming [11]. The research on the mechanism of degradation products is to study the concern question using the degradation law. Among which, degradation rule of the products was widely used to study the reliability of the products. For example, in view of two parameters related situation for the product in the degradation process and based on gamma process product in literature [15], a variety of performance characteristics of the degraded reliability model was proposed using binary Birnbaum-Saunders and its edge distribution. In literature [21], the degradation process for gamma random process and the strong laser device reliability were analyzed by using the method of simulation. Based on single chip ceramic dental implants in autoclave with radiation environment and the steam fatigue aging environment test in literature [1], ceramic surface of porous implants rule and its reliability of the mechanical performance degradation were studied. A more comprehensive reliability model for correlation failure in failure mode of long life product under real-time copulas was established using the degradation data of products in literature [22]. In order to more effectively diagnose the malfunction position of rolling bearing, the different performances of degradation degree of bearing, and the method of finding the position of the bearing fault and the intelligent classification of fault type features, the EMD bearing fault diagnosis methods were put forward based on collection optimization in literature [25]. The residual life prediction method for thermal aging of the reliability of casting austenitic stainless steel pipe used in light water reactor was studied in literature [19] under high temperature working conditions.

However, for some high value and long life products, small sample is the main obstacle for researching the reliability of the products concerning degradation method and reliability using the degradation data [20]. Aiming at this problem, domestic and foreign scholars have done a lot of works. A degradation test was performed for six main parameters of pricing function module of the smart meter using the method of accelerated degradation in the literature [33]. The degradation path of billing module of smart meters and the failure probability were measured by fitting the degradation data and using the extrapolation degradation path under different times. The metal covering current leakage and hydrophobic on the surface of lightning rod was measured with the increase of time by soaking the lightning rod in salt water at 90°C and performance degradation and time relations as well as the reliability of the over time was obtained in the literature [2]. As accelerated degradation tests carried out for products in the lab fail to achieve the use of real environment, the integrated field-use and laboratory accelerated degradation test information was put forward in the literature [26] for Bayesian method of reliability assessment and markov chain Monte Carlo method. Considering the difficult problems of data extraction by sequential degradation product in complex dynamic failure mode, the implementation of the product, and the reliability and prediction in the long-term level, the reliability of the product degradation and state level predicted by the complex neurons were proposed using feed forward neural network of multilayer in literature [13]. Accelerated degradation tests were conducted in literatures [35] and [38] to study the reliability evaluation for the performance degradation of metallized film capacitor and the problems of metallized film pulse capacitor. Owing to various reasons, such as human and environmental, degradation process is associated with uncertain information. It was assumed in literature [9] that the randomness of performance degradation path and the performance reliability of the cumulative distribution function curve of plunger pump were obtained by using an efficient Monte Carlo simulation method. As ambiguity exists in the process of degradation problems, the reliability methods for assessing the performance degradation were proposed based on fuzzy C – average clustering, and the degradation of fatigue life of 6307 rolling bearing was evaluated in literature [14]. Product reliability was calculated by the degradation process of products and the threshold was considered with blind number type in literature [28] respectively. The reliability of the degradation data of products was discussed in literature [29] under the condition of degradation threshold for fuzzy numbers.

Most of the above mentioned literatures assume that the degradation obeys a certain distribution; then the distribution evaluate, calculate and predict the reliability of the product or life by fitting the degradation curve. This approach can be implemented by a small number of data reliability for the whole life prediction of the products. But in actual application, for some products, we merely need to pay attention to the reliability of some key degradation time points. The key degradation time points need to be set in advance, otherwise it is difficult to observe the degradation value accurately [10]. While little care is needed for the rest of the points, even some long life products, which can get products by carrying out accelerated degradation tests for the whole life of the data in reliability assessment for the life of the products. For example, some of the key time points just need to be known before the product reaches the period of validity or effective and to verify whether the product's reliability conforms to the requirements. If not, the reliability of the product has to be improved. In the reliability test for degradation of some high value products, due to the limitation of experimental factors such as cost, little degradation experiment data were obtained only for small batch. Therefore, apart from the specimen quality was contained in the degradation of the test data and test conditions are caused by randomness, the ambiguity is caused by factors such as test operator as well. For these problems, scholars at home and abroad studied the randomness and fuzziness problems in the process of performance degradation using Poisson process – Normal [16], Monte Carlo simulation [9], neural network [4], fuzzy C – average [14], logistic regression [34], hidden Markov model [12] methods, respectively. However, in general, all the existing methods in the process of the degradation are still in exploration. In the paper, cloud theory is introduced in the degradation process of products in a certain amount of degradation time, by using numbers of cloud droplets in cloud theory generated and screening to meet the requirements of minimum membership of cloud droplets. It ensures that cloud droplets participate in the operation relating the degradation of membership degree, by using the Monte Carlo reliability principle to finally focus on the reliability of moment.

2. Cloud Theory

Cloud theory was put forward by Chinese scholar Li DY. The core of Cloud theory is cloud droplets, which not only show the characteristics of probability distribution of random theory, but also have the concept of membership degree in fuzzy comprehensive. The theory realizes the common description of two kinds of uncertainty problems. Since been proposed, cloud theory has already been widely used in computer simulation, reliability evaluation, etc. For example, because it is difficult to quantitatively evaluate the reliability of combat aircrafts, the theory of cloud implements the quantitative reliability evaluation of battle classification by translating the qualitative data into quantitative data [27]. Based on cloud theory, the cloud droplets containing the distribution function of the random process are the membership function of fuzzy theory, which was be studied in the literature [17] as well. For complex system in the assessment, there are abundant uncertainty information and requirements for multiple hierarchy comprehensive evaluation, combining with the cloud theory and the theory of information fusion system performance evaluation methods which were proposed in literature [18]. With comprehension of the integrated reliability of road network combining cloud theory, radar map and road network, an integrated reliability evaluation was proposed in literature [7] based on cloud theory and radar map. For cloud computing problem of information security and reliability, a new reverse algorithm for cloud depth was proposed, and the algorithm has been applied to the trust of online trading decisions in literature [8]. Aimed at the uncertainty in the spatial load forecasting model of distribution network, knowledge based on cloud model was put forward according to a new spatial load forecasting model of distribution network. Meanwhile, this model implements quantitative and qualitative mappings to each other in literature [32].

2.1. Definition of Cloud

U is a precise value of domain in quantitative theory. C is the qualitative concept on the U . If quantitative values $x \in U$ and U are a random qualitative concept of C implementation about x , uncertainty $u(x)$ of C , $x \in [0,1]$ is a steady tendency of random numbers. That is:

$$u : U \to [0,1], \forall x \in U \quad x \to u(x)$$

$u : U \to [0,1]$, x in the theory of domain U called cloud, the distribution of each x is a cloud droplets.

2.2. Characteristics of Cloud [6]

(1) The domain U of cloud theory can be one-dimensional and multi-dimensional as well.
(2) The random implementation and membership degree of randomness and fuzziness of relevance are related to the distribution of probability theory and fuzzy setting membership function.
(3) Any map of x to the interval [0, 1] is a one-to-many transformation; the uncertainty of x in C is a probability distribution, instead of a fixed value.
(4) Cloud is composed of cloud droplets. There is no order among cloud droplets. A cloud droplet is an implementation of qualitative concept in quantity. The more cloud droplets, the more the overall characteristics of the qualitative concept can reflect.
(5) Both the appearing probability and the uncertainty of cloud droplets are large, so the cloud droplets contribute more to the concept.

2.3. Positive Generator and the Process of Cloud

There are three kinds of cloud generators, including Positive generator, adverse generator and conditions generator [23]. Positive generator generates random point and its corresponding membership degree using the data of the expectation, variance and dispersion degree of data as the basic input parameters. It is the commonly used method for generating random points, as shown in Fig. 1.

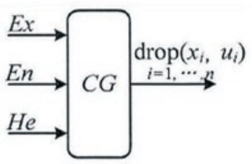

Fig. 1. Positive Cloud generator

2.4. The formation of performance degradation of cloud droplets

Assuming that a certain degradation test that has m test samples with rule-type performance degradation test, at given time points in the number of n ($t_1 < t_2 < \cdots t_n$), respectively. The same method is used to measure the degradation of data samples, the measured Degradation data as follows:

$$\begin{array}{l} x_{11}, x_{12}, \cdots x_{1n} \\ x_{21}, x_{22}, \cdots x_{2n} \\ \cdots \\ x_{m1}, x_{m2}, \cdots x_{mn} \end{array}$$

For the *i*-th amount of degradation products x_{it_j} at the time for t_j point, by using the cloud droplets as the generator, the i −th product in the t_j moment is generated based on the amount of cloud droplets of degradation x_{it_j} . Steps are as follows:

(1) With the i th product at t_j moment in degradation x_{it_j} as the expectation Ex_{it_j} of the occurrence of cloud droplets, all of the degradation values of the specimens at t_j moment determine the discrete degree amount of degradation products in t_j time and the entropy En_{it_j} of i th product in t_j moment of cloud droplets generator. At the same time, at the degree of quantitatively estimated discrete, the hyper entropy of cloud droplets generator is determined.

(2) Expectations for En_{it_j} , $He^2_{it_j}$ for the variance of a normal random number En'_{kit_j} are produced [23].

(3) Expectations for Ex_{it_j} , $En'^2_{kit_j}$ for the variance of a normal random number x_{kit_j} are produced. Random number x_{kit_j} corresponding to the membership degree was calculated as follows:

$$u_{kit_j} = e^{-\frac{\left(x_{kit_j} - Ex_{it_j}\right)^2}{2En'^2_{kit_j}}} \tag{1}$$

(4) With membership degree u_{kit_j} and normal random number x_{kit_j} , a cloud droplet was formed as drop (x_{kit_j} , u_{kit_j});

(5) According to the preset number, step (2) to step (4) were repeated to meet the required number of cloud droplets, as shown in Fig. 2.

As the normal random number was generated in normal distribution in step (2) and (3), literature [5] showed that the normal distribution was effective and correct.

According to the method, the specimen degradation experiment was carried out using the key time point cloud amount of degradation, as shown in Fig. 3.

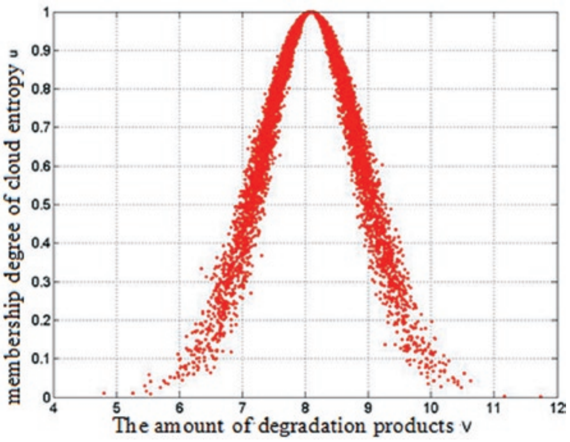

Fig. 2. Degradation cloud generated by one degradation point

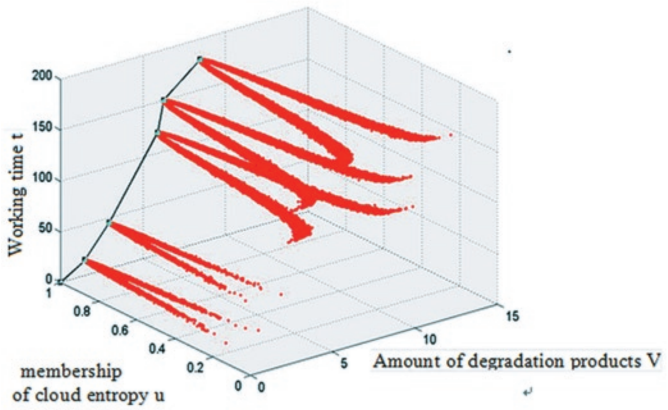

Fig. 3. Degradation Cloud generated by the amount of degeneration of a degraded sample at five key time points

3. Monte Carlo method based degraded reliability of cloud

3.1. Monte Carlo Method

Monte Carlo method, as a probability simulation method, is also known as random sampling techniques or test method. At the same level, it is a stochastic simulation method. It is a random sampling method based on the theory of probability, stochastic process and mathematical statistics. It is in accordance with the rules of sampling, which generates a large number of random Numbers. The generated random Numbers and part of the test data were used for studying quantities, and the distribution of data is therefore obtained. The limited experiment data in scientific research commonly lead to a low reliability. The random Numbers produced by Monte Carlo method provide supplementary for the test data, and expand the samples analysis. The small sample is solved by the numerical calculation of the randomness of problem. The results of credibility research increase. Practice shows that by using Monte Carlo method, the required accuracy can be satisfied in the generation of a sufficient number of random Numbers.

In reliability, because the probability of the appearance of an event can be solved using Monte Carlo method, this kind of event probability is obtained by using the method of sampling. The small sample data reliability is one of the main problems, so Monte Carlo method has been widely used in the reliability problems, which is agreed by scholars. The basic idea of Monte Carlo method for solving product reliability is to set a large number of random Numbers of events and boundaries, and the number of random number more than threshold value and the total number of random Numbers using Monte Carlo method in accordance with the rules produced. Then, the probability of events, which is the ratio of the number of random number more than threshold value to the total number of random Numbers, can be obtained [31].

3.2. Cloud - Reliability Calculation Method of Monte Carlo Method Based on the Theory of Performance Degradation Data

In the process of degradation test, especially in the less degradation experiments, due to various causes of the uncertainty of degradation test data, reliability calculation shows big error by calculating the degradation data of the products under the condition of limited data collection and performance degradation. Monte Carlo method solves the randomness problem of the products in the process of the performance degradation caused by the limited data. But in the actual degradation test, especially in condition with limited degradation test data, because of factors such as the understanding of the limitations, the degradation data owned by the division has the characteristics of ambiguity, which is based on the research on the reliability and the randomness of the product performance degradation. The randomness and fuzziness is more serious. In order to solve the coexistence of randomness and fuzziness in the process of data degradation, the cloud droplets, which present the characteristics of randomness and fuzziness, in the theory of cloud is adopted based on Monte Carlo method. With the expected degradation x_{it_j} in t_j time quantity for i-th product, performance degradation of cloud model is generated in t_j moment, and the minimum membership threshold of the cloud droplets of products is set, as shown in Fig. 4. Meanwhile, the product failure threshold is set, as displayed in Fig. 5. The number of the i-th product cloud droplets which satisfy the requirement of minimum membership at time t_j are counted, then The number of The i-th product cloud droplets which satisfy the requirement of minimum membership and exceed the degradation threshold at time t_j are counted. Eq. (2) shows the calculation of reliability of products meeting certain membership requirements of performance degradation with i in t_j time.

$$R_i\left(t_j\right)=1-\frac{\sum_{k=1}^{M} C_{t_j}\left(drop_i\left(\left(x_{kit_j},\mu_{kit_j}\right)\middle|\left(\mu_{kit_j}>\mu_g,x_{kit_j}>TH\right)\right)\right)}{\sum_{k=1}^{M} C_{t_j}\left(drop_i\left(\left(x_{kit_j},x_{kit_j}\right)\middle|\left(x_{kit_j}>\mu_g\right)\right)\right)} \quad (2)$$

where:

x_{kit_j} is the k -th random number caused by the amount of degradation in the first degradation test at time t_j .

μ_k is the membership of the k –th random number x_{kit_j} caused by the amount of degradation in the first degradation test at time t_j .

μ_g is the minimum membership of the random number

TH is the failure threshold of product performance degradation

$drop_i\left(\left(x_{kit_j},\mu_{kit_j}\right)\middle|\left(\mu_{kit_j}>\mu_g,x_{kit_j}>TH\right)\right)$ is the cloud droplets meeting the membership degree, which is greater than the minimum membership degree. It is larger than the failure threshold of performance degradation of random number;

M is the total number of random number;

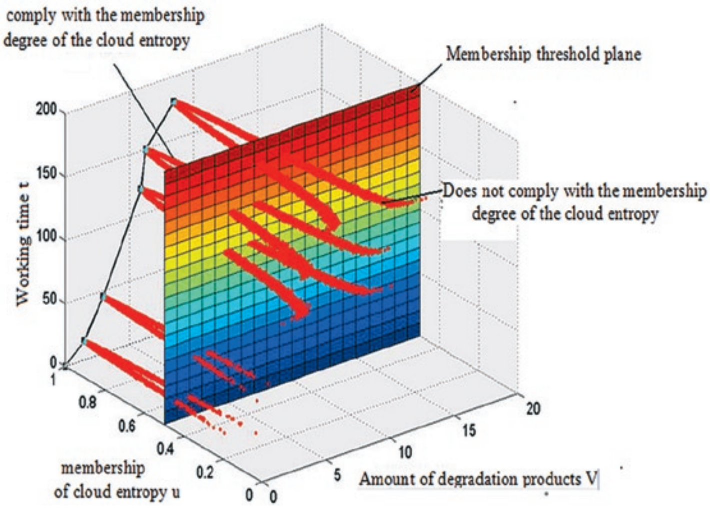

Fig. 4. Sketch map of setting the minimum threshold of degradation cloud

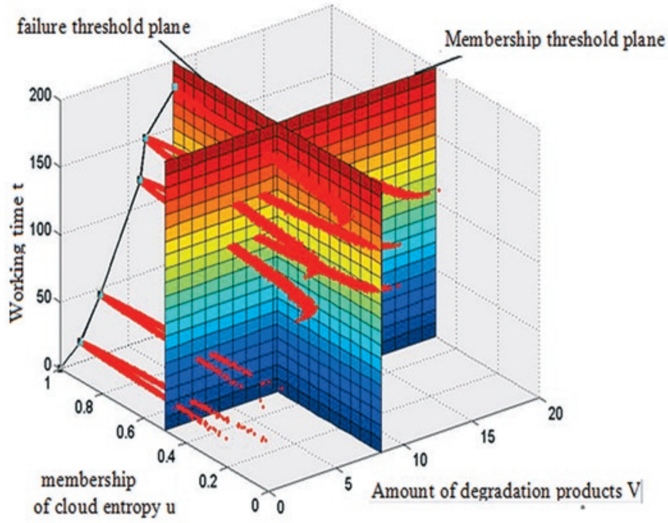

Fig. 5. Sketch map of setting the minimum threshold and membership threshold of degradation cloud

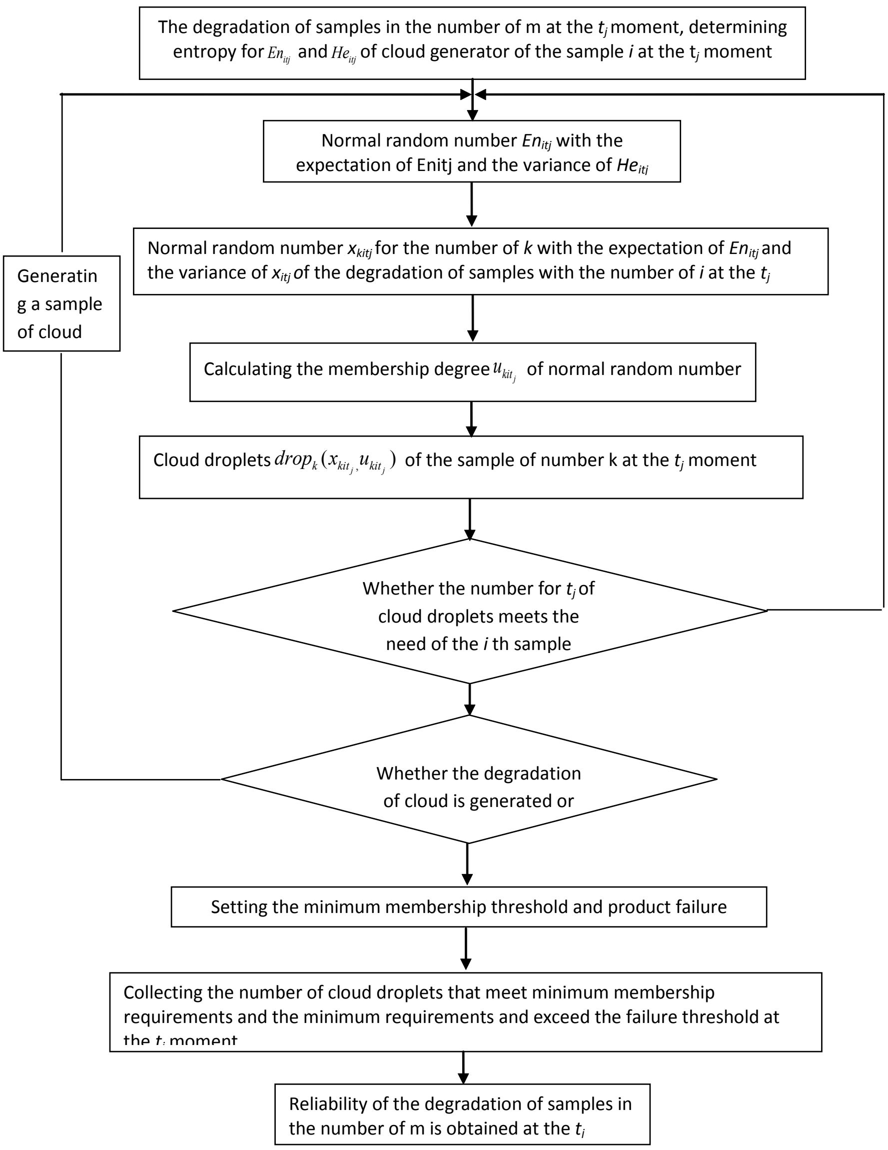

Fig. 6. Reliability calculation flowchart of degradation simples in the number of m at

$\sum C_{t_j}(\bullet)$ is the number of cloud droplets which meet the requirements.

The above method for calculating the credible degree at a crucial moment by using Monte Carlo method and the cloud theory sets a degradation process of the degradation sample as an example. The method for calculating the reliability of the degradation test samples in the number of m is similar to the above one, as illustrated in the Fig. 6.

4. Example

The reliability of the degradation of the example was analyzed in literature [33] and by Yang and Xue in literature [30] based on stochastic process method. This paper also used the data in literature [30] as an example, which demonstrates the process of the calculation method.

The data for product degradation test are shown in Table 1. The quantity degradation with time is illustrated in Fig.7. The sample quantity in the tests is 7, the measuring frequency is 5, and each point is measured for 15 h, 45 h, 120 h, 150 h and 180 h.

Degradation cloud droplets were established using the performance degradation of each product during the expected observation time, as demonstrated in Fig. 8. Fig. 9 indicates that the minimum membership threshold of cloud droplets is 0.5, and the product failure threshold is 8.5.

Based on the degradation values generated by above seven samples of cloud droplets, the reliabilities of the products in the five key points of events are calculated according to the Eq. (2), and the results are demonstrated in Table 2.

5. Conclusion

As the reliability of the key point in time is calculated based on the product degradation data and the small amount of data in the process

Table 1. Measured degradation data

Time t /h	V_1	V_2	V_3	V_4	V_5	V_6	V_7
0	0	0	0	0	0	0	0
15	1.472	1.839	1.472	1.839	1.839	1.839	2.575
45	2.943	4.047	3.311	2.943	3.311	2.943	3.679
120	5.886	6.990	5.886	4.415	5.518	5.886	5.886
150	6.254	8.093	6.622	5.150	6.254	6.990	7.726
180	8.461	9.933	8.093	6.622	7.726	8.461	10.301
Note：V_i (i=1，2，3…，7) is the ith sample.							

Table 2. Reliabilities calculated at each key point

time	15	45	120	150	180
reliability	1	1	1	0.9620	0.5175

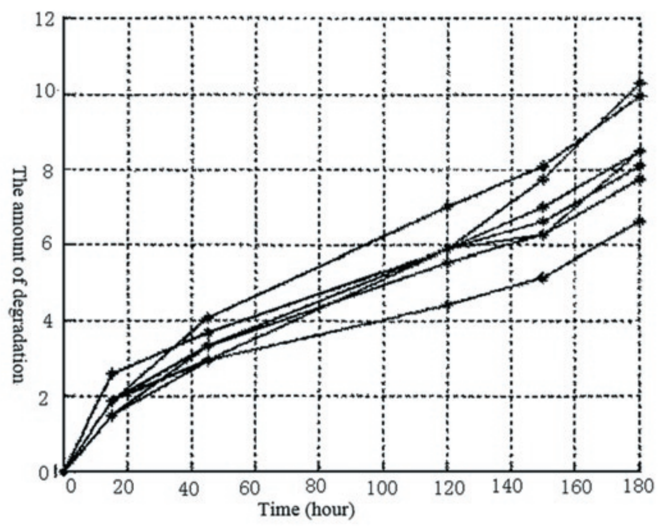

Fig. 7. the variation of the degradation of the seven samples with time

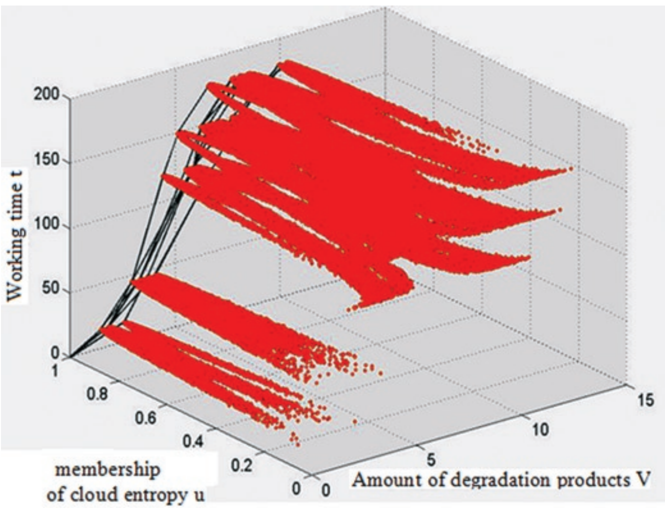

Fig. 8. Degradation cloud generated by the degradation amount of seven samples

of the degradation products and the degradation experiment shows randomness and fuzziness, the cloud theory was introduced into the calculation of the reliability of the performance degradation data. By using the theory of cloud, a large number of random and membership degree of cloud droplets were generated, cloud droplets meeting the requirements of minimum membership were selected and the failure threshold was set. The reliability of some time points was calculated using Monte Carlo method.

Based on the proposed method, the

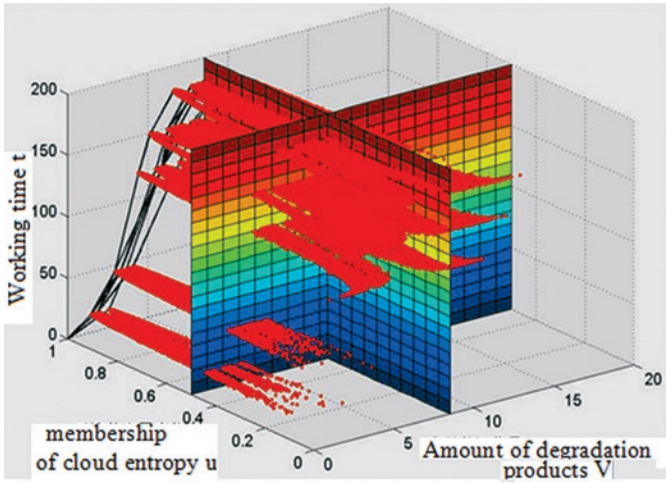

Fig. 9. Degradation cloud of setting minimum threshold and membership threshold

product reliability was 0.5175 at 180 h. The reliability of 0.5489 was calculated merely considering the randomness in the process of degradation in literature [37]. By analyzing the data in Table 1, the average degradation data at 180 h reached 8.514, which was higher than that of the threshold (8.5). So, the method put forward in this paper is superior to that in literature [37].

Acknowledgement

This research was supported by the National Natural Science Foundation of China (Grant No.51275329) and the National"12th Five-year" Science and Technology support plan (Grant No. 2011BAK06B05) and Natural Science Foundation of Shanxi province(Grant No.2015011059).

References

1. Clarisse Sanon. Low temperature degradation and reliability of one-piece ceramic oral implants with a porous surface. Dental materials 2013; 29: 389-397, http://dx.doi.org/10.1016/j.dental.2013.01.007.
2. Daiana Antonio Da Silva, Eduardo Coelho Marques Da Costa, Jorge Luiz De Franco. Reliability of directly-molded polymer surge arresters: Degradation by immersion test versus electrical performance. Electrical Power and Energy Systems 2013; 53: 488-498, http://dx.doi.org/10.1016/j.ijepes.2013.05.023.
3. He L, Yin C, Ping W, Yuan R, Huang HZ. Reliability and risk assessment of aircraft electric systems. Eksploatacja i Niezawodnosc - Maintenance and Reliability 2014; 16 (4): 497-506.
4. Huang RQ, Xi LF. Residual life predictions for ball bearings based on self-organizing map and back propagation neural network methods. Mechanical Systems and Signal Processing 2007; 21: 193-207, http://dx.doi.org/10.1016/j.ymssp.2005.11.008.
5. Li DY, Liu CY. Study on the universality of the normal cloud model. Engineering Science 2004; 6(8): 28-34.
6. Li DY, Meng HJ, Shi XM. Membership clouds and membership cloud generators. Computers Research and Development 1995; 32(6): 16-21.
7. Li XJ, Liu LJ, Liu LZ. Evaluation of road network comprehensive reliability based on cloud theory and radar graph model. Application Research of Computer 2013; 30(10): 3007-3010.
8. Lv SJ, Zhang YS, Lou YH. Research of trusted technology based on cloud model. Application Research of Computer 2013; 30(8): 2523-2526.
9. Ma JM, Zhan XY. Performance reliability analysis of a Piston Pump affected by random degradation. Journal of Mechanical Engineering 2010; 46(14): 189-193, http://dx.doi.org/10.3901/JME.2010.14.189.
10. Min HH, Jeng SL, Shen PS. Assessing device reliability based on scheduled discrete degradation measurements. Probabilistic Engineering Mechanics 2009; 24: 151-158, http://dx.doi.org/10.1016/j.probengmech.2008.04.003.
11. M Nuhi, T Abu Seer, A Mal Tamimi. Reliability analysis for degradation effects of pitting corrosion in carbon steel pipes. Procedia Engineering 2011; 10: 1930-1935, http://dx.doi.org/10.1016/j.proeng.2011.04.320.
12. Ocak H, Loparo K A, Discenzo F M. Online tracking of bearing wear using wavelet packet decomposition and probabilistic modeling:A method for bearing prognostics. Journal of Sound and Vibration 2007; 302:951-961, http://dx.doi.org/10.1016/j.jsv.2007.01.001.
13. Olga Ink, Enrico Zio, Ulrich Weidmann. Predicting component reliability and level of degradation with complex-valued neural networks. Reliability Engineering and System Safety 2014; 121:198-206, http://dx.doi.org/10.1016/j.ress.2013.08.004.
14. Pan YN, Chen J, Li XL. Fuzzy c-means based equipment degradation assessment. Journal of Shanghai Jiaotong University 2009; 43(11): 1794-1797.
15. Pan ZQ, Narayanaswamy Balakrishnan. Reliability modeling of degradation of products with multiple performance characteristics based on gamma processes. Reliability Engineering and System Safety 2011; 96: 949-957, http://dx.doi.org/10.1016/j.ress.2011.03.014.
16. Qiang ZY, Feng J, Liu Q, Zhou JL. Reliability analysis based on performance degradation model of compound Poisson-Normal process. Systems Engineering and Electronics 2006; 28(11): 1775-1778.
17. Qin Y, Ju XG, Lu Q. A new reliability evaluation method based on cloud theory and stochastic process. Information and Control 2012; 41(4): 454-458.
18. Qin Y, Lu Q, Huang ST. A method of system performance evaluation based on the cloud theory and the information fusion theory. Computer Engineering and science 2012; 34(2): 181-185.
19. Ren SH, Xue F, Yv WW. Reliability residual-life prediction method for thermal aging based on performance degradation. Nuclear Power Engineering 2013; 34(5): 96-99.
20. Siljak H, Subasi A. Fourier spectrum related properties of vibration signals in accelerated motor aging applicable for age determination. Eksploatacja i Niezawodnosc - Maintenance and Reliability 2014; 16 (4): 616-621.
21. Sun ZQ, Zhao JY. Gamma process of degradation failure reliability analysis. Journal of Naval Aeronautical Engineering Institute 2010; 25(5): 581-584.
22. Tang JY, He P, Liang HQ. Comprehensive reliability assessment of long life products with correlated multiple failure modes. Journal of Mechanical Engineering 2013; 49(12): 176-182, http://dx.doi.org/10.3901/JME.2013.12.176.
23. Tan QN. The reliability modeling, analysis and comprehensive evaluation method of complex systems. PhD Thesis, Beijing: Beijing Jiaotong University, 2013.
24. Wang XD, Yi Z, Shen ZC. Proton radiation damage in ZnO-pigmented white paints and optical degradation mechanisms. Journal of Materials Engineering 2013; 3(5): 1-5.
25. Wang YJ, Jiang YC, Kang SQ. Diagnosis method of fault location and performance degradation degree of rolling bearing based on optimal ensemble EMD. Journal of Scientific Instrument 2013; 34(8): 1834-1840.
26. Wang Z, Pan R, Li XY, Jiang TM. A Bayesian reliability evaluation method with integrated accelerated degradation testing and field information. Reliability Engineering and System Safety 2013; 112:38-47, http://dx.doi.org/10.1016/j.ress.2012.09.015.
27. Wu L, Zhang ZM, Meng XC. Application of cloud theory in reliability assessment of combat aircraft. Computer Simulation 2005; 22(7): 235-236.
28. Yang H, Xu GN. Reliability Analysis on the data of performance degradation based on the blind number theory. Journal of Mechanical Strength 2013; 35(6): 777-782.
29. Yang H, Xu GN. Reliability analysis on the data of Performance degradation based on the fuzzy threshold. Journal of Construction Machinery 2013; 11(4): 19-23.
30. Yang K, Xue J. Continuous states reliability analysis. Proc. Annual Reliability and Maintainability Symposium, Philadelphia, PA, USA, 13-16 January 1997: 175-176.
31. Yang WM, Sheng YX. Digital simulation of system reliability. Beijing: the Press of Beihang University, 1990.
32. Yang XM, Yuan JS, Wang JF. A new spatial forecasting method for distribution network based on cloud theory. Proceedings of the CSEE 2006; 26(6): 30-36.

33. Yang Z, Chen YX, Li YF, Kang R. Smart electricity meter reliability prediction based on accelerated degradation testing and modeling. Electrical Power and Energy Systems 2014; 56: 209-219, http://dx.doi.org/10.1016/j.ijepes.2013.11.023.
34. Yan JH, Lee J. Degradation assessment and fault modes classification using logistic regression. Journal of Manufacturing Science and Engineering Transactions of the ASME 2005; 127: 912-914, http://dx.doi.org/10.1115/1.1962019.
35. Zhao JY, Liu F. Reliability assessment from accelerated performance degradation tests. Journal of Harbin Institute of Technology 2008; 40(10): 1669-1671.
36. Zhao JY, Liu F, Sun Q. Reliability analysis of Metallized-film pulse capacitor under competing failure modes. Systems Engineering-Theory&Practice 2006; 26(1): 60-64.
37. Zhao JY. Study on reliability modeling and applications based on performance degradation. PhD Thesis, Changsha: China National University of Defense Technology, 2005.
38. Zhao JY, Sun Q, Zhou JL. Metallized film pulse capacitor based on the accelerated degradation data reliability analysis. Strong Laser and Particle Beams 2006; 18(9): 1495-1498.

Heng YANG
Gening XU
Xiaoning FAN
College of Mechanical Engineering
Taiyuan University of science and Technology
Waliu Road, No 66
Wanbolin District, Taiyuan, Shanxi Province, China
E-mail: yh-235@163.com , xugening@sina.com, fannyfxn@163.com

Article citation info:
PŁACZEK M, BUCHACZ A, WRÓBEL A. Use of piezoelectric foils as tools for structural health monitoring of freight cars during exploitation. Eksploatacja i Niezawodnosc – Maintenance and Reliability 2015; 17 (3): 443–449, http://dx.doi.org/10.17531/ein.2015.3.16.

Marek PŁACZEK
Andrzej BUCHACZ
Andrzej WRÓBEL

USE OF PIEZOELECTRIC FOILS AS TOOLS FOR STRUCTURAL HEALTH MONITORING OF FREIGHT CARS DURING EXPLOITATION

UŻYCIE FOLII PIEZOELEKTRYCZNYCH JAKO NARZĘDZI DO MONITOROWANIA STANU TECHNICZNEGO WAGONU TOWAROWEGO W TRAKCIE EKSPLOATACJI*

Work presents a task of piezoelectric foils application for structural health monitoring of freight cars during their exploitation. Results of laboratory tests conducted on a created in scale laboratory model of the freight car are presented. The possibility of inferred from the dynamic response of the model about the changes in its technical condition was verified. During the first test the model was treated as a half-determined system. In order to excite vibrations a pendulum was used. Measurements were carried out using accelerometers. During the next stage of carried out tests the dynamical response of the model was measured while the object was driving. In order to measure vibrations of the system a Macro Fiber Composite (MFC) piezoelectric foil was used. It was glued on the surface of the model. A series of tests of the model with and without load, as well as with an obstacle on the rail track was carried out. Measured signals were juxtaposed on charts and analysed.

***Keywords**: piezoelectric foils, structural health monitoring, non-destructive testing, freight cars.*

W pracy przedstawiono zagadnienia dotyczące zastosowania folii piezoelektrycznych do monitorowania stanu technicznego wagonów towarowych w trakcie ich eksploatacji. Przedstawiono wyniki badań laboratoryjnych prowadzonych na utworzonym w skali modelu węglarki. Określono możliwość wykrycia zmian stanu technicznego wagonu na podstawie analizy jego odpowiedzi dynamicznej. W pierwszym etapie badań obiekt traktowano jako półokreślony, w celu wymuszenia drgań stosowano wahadło. Pomiar odpowiedzi dynamicznej układu w poszczególnych punktach pomiarowych przeprowadzono z użyciem akcelerometrów. Kolejnym etapem badań był pomiar odpowiedzi dynamicznej modelu w trakcie jazdy. W celu pomiaru drgań konstrukcji nośnej modelu zastosowano przetwornik piezoelektryczny typu Macro Fiber Composite (MFC), który naklejono na powierzchni modelu. Przeprowadzono ciąg badań modelu bez obciążenia oraz z obciążeniem, a także z przeszkodami umieszczonymi na jednej bądź obu szynach. Otrzymane przebiegi zestawiono na wykresach oraz omówiono wyniki badań.

***Słowa kluczowe**: folie piezoelektryczne, monitorowanie stanu technicznego, badania nieniszczące, wagony towarowe.*

1. Introduction

Rail transport is a very important part of the modern economy, one of the components determining its dynamic development. It is therefore important to conduct research and taking action aimed at the development and refinement of this branch of industry. Such actions directly translate into an increase in its effectiveness, safety, reduction of burden on the environment and society. Nowadays numerous studies are conducted, aimed at introducing new technologies and solutions, both in terms of railway infrastructure and logistics management systems, as well as in traction vehicles themselves [1, 2, 4, 11, 14-17, 20, 22, 29, 32]. Introduction of modern technology helps eliminate or reduce nuisance problems associated with the implementation of any kind of transport or the operation of the used technical means [18, 19].

This paper contains a report on the part of works conducted in the research and development project entitled “Analytical and experimental studies and determination of the structural features of components and assemblies in innovative structure of repaired wagons”. This project is realized within the Program of Applied Research by Institute of Engineering Processes Automation and Integrated Manufacturing Systems of Silesian University of Technology together with consortium partners: company DB Schenker and Germaz. The main objective of the project is to develop a technology of modernization of freight wagons for the transport of coal and aggregates, through the use of innovative materials and technologies to repair this type of wagons during periodic repairs. Actions which have been undertaken within the project are to improve the operating conditions considered types of wagons by increasing their resistance to corrosion and freezes transported cargo to the shell of the body in the winter conditions, and thus an easier unloading. An additional objective is also verification of strength of modernized carriages and an estimation of the possibility of reducing their weight, while maintaining or increasing the permissible load. One of elements of the project is also to develop a system for diagnosing the technical condition of the modernized shell of wagon body during operation. For this purpose the use of non-destructive testing methods of technical state of constructions will be used, including methods that use the analysis of dynamic response of the object. Therefore research is conducted which examines the possibility of use of the foils with piezoelectric properties as sensors used in the system of vibration measurement of tested items. These research efforts are a continuation of previous work related to the analysis of possibilities to use of composite materials as a part of the wagons boxes shell [1, 2]. The authors in their works also take is-

(*) Tekst artykułu w polskiej wersji językowej dostępny w elektronicznym wydaniu kwartalnika na stronie ***www.ein.org.pl***

sues related to the analysis and synthesis of vibrating mechanical and mechatronic systems including those in which the classical or non-classical piezoelectric transducers are used as actuators or vibration dampers [3, 5, 7-9, 26, 27, 31]. In the Gliwice Research Centre they are also conducted extensive research in the field of analysis and synthesis of mechanical systems and mechatronics [6, 12, 13, 21, 33].

2. Measuring and testing the dynamic response of railway infrastructure

Issues related to the study of the dynamic response of both railway rolling stock and railway infrastructure are the subject undertaken by a number of research centres. Dynamic loads generated during the passage of railway trains are deleterious to the infrastructure, such as bridges or buildings located near tracks, as well as people staying in them. There is however the possibility of their use in systems for condition monitoring of infrastructure components [10, 14, 16, 25, 30]. Due to the dynamic loads generated by moving with higher and higher speed of trains, in the face of aging and worn out infrastructure, these issues are now becoming extremely important. In recent years it can be noticed that significantly increase interest in this subject, as well as the increase in the number of performed acceptance tests of objects under dynamic loading [28]. This is the result of activities related to the implementation of the program of modernization of railway lines in Poland and the introduction of high-speed rail, so passenger transport at speeds above 200 km/h. These issues are discussed among others in the works [14, 16, 25, 28], regarding the dynamic impact of high-speed trains on railway bridges and viaducts, as well as acceptance testing of such facilities under dynamic loading test. Also important are issues of protection of building against vibration generated by the ground and underground rail communication as well as protection and minimize the impact of vibrations on both the passengers and persons in the buildings surrounding the railway line [30].

The aim of these authors' research is to determine the possibility of identifying the technical state of the modernized freight wagon based on continuous measurement of the dynamic response during operation. The idea is to create a system integrated with elements of the modernized wagon body shell and for generating alarm signals that will be able to be read periodically by the service, or sent directly after the occurrence, using a wireless system. As sensors piezoelectric transducers in the form of films will be used. They will be integrated with elements of the modernized wagon shell.

Also in the paper [29] the principles and operation of a system for monitoring loads or state truss railway bridges are presented. Piezoelectric transducers are used as sensors. In this case, the system is based on an analysis of the signals generated by the piezoelectric transducers mounted on railroad tracks before entering the bridge and on the truss bridge elements. The wireless transmission of measured signals to a data center is possible. The system is thus characterized by low cost of installation and lack of significant restrictions on the traffic of railway rolling stock during installation and operation. The amplified and filtered measuring signal can be interpreted in order to identify the load, so weighing the passing train and monitoring the technical condition of the truss bridge. According to the authors, research work aims to create an integrated system for monitoring the technical condition of structures and detect of overloaded rail depots. The theoretical assumptions of the authors are supported by the presentation of the results of measurements on a waveform signals recorded by piezoelectric sensors when the train is passing and the reference signal level to the mass of the wagon, determined by a static weight. The values obtained allow clear identification of the type of wagon after previous calibration of the measurement system.

The results of the simulation and modelling of the impact of static and dynamic load on strength of the railway platform, used in railroad transport systems while horizontal handling are presented in paper [10]. The process for modelling and analysis of wagon chassis platform using finite element method is presented. Model verification based on static analysis and comparing its results with the results of the experiment on a real object was presented. Next, the modal analysis was carried out as well as the results of a simulation of moving of the loaded frame over an obstacle with a height of 5 mm were presented. The response of the structure in the form of vertical displacement changes of the central model node in a half of the length of the wagon and the accompanying stress changes reduced was calculated.

The measurement of the dynamic response of the ground floor of the building located in the vicinity of the Warsaw subway tunnel it became the foundation of the system of monitoring, whereby it is possible to identify trains that generate excessive vibration due to the deformation of worn wheel [30]. The authors present a comparison of horizontal vibration acceleration waveforms on ground floor of the building during the passage of two trains of the same type with different values of radial run out wheels. It has been shown that in the case of rolling stock with deformed wheels is possible dozen times increase in the level of generated vibrations. It has been proven so that there is a possibility to inference about technical condition railway rolling stock based on the analysis of dynamic response of infrastructure forced by its passing. The authors of this study adopted the assumption that such a system can be successfully integrated with the modernized freight wagon and allow monitoring of its technical condition during operation. Attempt to estimate the forces acting on the wheel sets of rail vehicles based on the measured dynamic response is also shown in paper [23]. Using a developed model of wagon and a finite element method, forces acting on the object of study as a result of deformation of the railway track were determined.

3. The object of research, its model and the test stand

The object of research is the four axial freight wagon of ordinary type Eaos 1415-A3 production BREC Belgium. The considered freight wagon after periodic refurbishment and its model created using CAx-class program are presented in Fig. 1. CAD model was created on the basis of documentation provided by the consortium member – company DB Schenker, which includes eleven construction drawings and technical documentation, technical conditions execution of repairs and acceptance after repair, air brake calculations, the program and report on the operational tests. Missing data for the object in question was obtained during the inspection and measurement of real objects and consultation with technical staff responsible for carrying out repairs and technical tests.

During the consultations it was established that the typical problems during the operation of a freight wagon of this type are:

- corrosion of car body shell and the floor,
- freezes of transported cargo to the shell boxes in winter conditions,
- mechanical damage shell boxes, damaged during use improper methods of unloading (of the wagon is designed for unloading with the use of tippers).

Verification of the correctness of the CAD model of the freight wagon was made by comparing the actual mass of the object and the model after assigning material properties. The resulting inaccuracy is 5.34% and it is the result of not taken into account the braking system in the model. Developed CAD model was then used to carry out a series of analysis with use of the class of CAx software such as modal analysis, strength analysis or setting a speed limit while passing wagon loaded or deprived of cargo along the arc of a specified radius of curvature.

In order to conduct research on the dynamic response analysis of freight wagon on extortion and estimate the possibility of inference on its basis of the technical condition of the object the laboratory stand that is shown in Fig. 2 was created. The simplified model of the supera)

b)

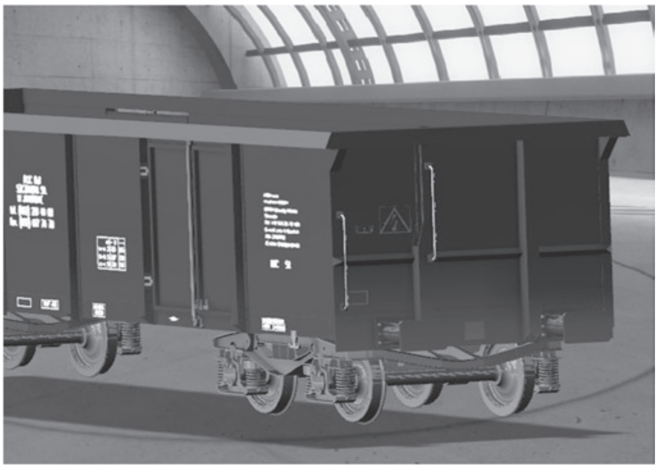

Fig. 1. The freight car type EAOS 1415-A3 (a) and its CAD model (b)

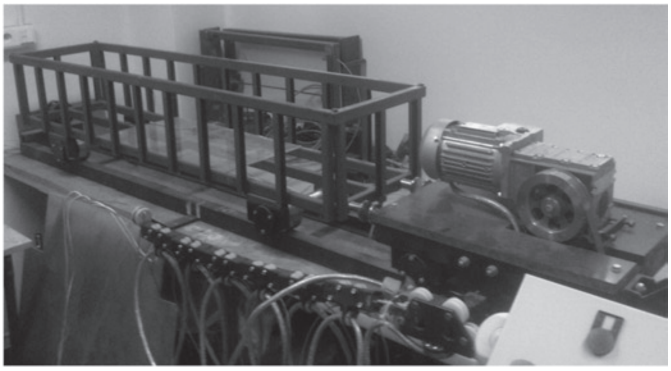

Fig. 2. The laboratory stand for testing the dynamic response of freight car model

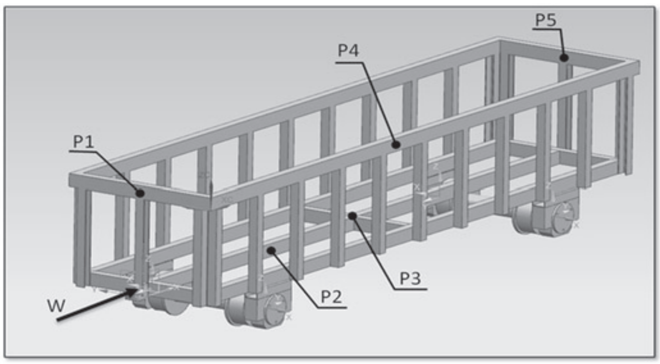

Fig. 3. The CAD model of the laboratory stand with marked positions of the measuring points

structure of the wagon in a scale as well as the model of the track on which the freight car is moving through using the electrically powered locomotive were built up.

The CAD model of the laboratory stand was created and after modal analysis measuring points in which accelerometers and piezoelectric films will be attached were selected. Fig. 3 shows the locations of the measuring points on the model of the superstructure of a freight wagon.

During the measurement of the dynamic response of the system using accelerometers tested wagon model was suspended to separate it from the track. In order to induce vibrations a pendulum was applied. The laboratory stand is shown in Fig. 4. The PCB 352C68 accelerometer and measuring amplifier HBM MGCplus with measurement card AP18i and software CatmanEasy were used [34]. The measurements were repeated five times for each of the measuring points.

Fig. 4. Model of the freight car (the half-determined system) together with the pendulum

During testing of the dynamic response in motion in the role of sensor a piezoelectric MFC film was used. Fig. 5 shows the MFC piezoelectric transducer glued on the surface of the freight wagon model. Macro Fiber Composite piezoelectric transducers are made of rectangular ceramic bars sandwiched between adhesive layers, the electrodes and the polyamide film. They are supplied as ready-to-use transducers that can be glued on the surface of elements or embedded in the composite structure. The transmitters are durable, efficient and resistant to damage. They can be successfully used as actuators or mechanical vibration dampers and sensors [24, 35].

Fig. 5. The MFC transducer type M8514-P1 glued on the tested model

The NI-9215 measurement card was used for data acquisition. It is produced by National Instruments. Its range is ±10 V with 16 bit resolution measurement and sampling frequency of each of the four channels is 100ks/s. The card was installed in the measuring unit NI cDAQ-9191 that enables wireless transmission of measurement data in enclosed areas within 30 meters, while in the open air for a distance of 100 meters. The measuring system was fed with gel battery. This configuration of measurement channel made it possible to carry out the measurements of freight wagon model in motion of the track way. Data acquisition and development were made in LabVIEW.

4. Results

In the first stage of work studies of the dynamic response of a freight wagon model were conducted by using a pendulum. Measurements were performed using the accelerometer successively in five measuring points of the model marked in Fig. 3. The research was carried out without a load wagon, as well as with 20 kg of cargo load. The aim of such actions was to determine the possibility of inference on the state of the object based on the measured responses to extortion and identification of measurement points where such inference is possible. Fig. 6 and 7 show the obtained waveforms of the dynamic response in the case of the selected measuring points.

At the measuring point P3 a change of the measured signal after load of model can be clearly seen. The maximum value of the acceleration measured without load exceeded 20 m·s^{-2}, and after the load has dropped to about 5 m·s^{-2}. The time necessary to completely suppress of the excited the vibration decreased from 0.55 s to 0.2 s. At this measuring point the vibration were measured in the vertical direction and thus perpendicular to the direction of the force.

a)

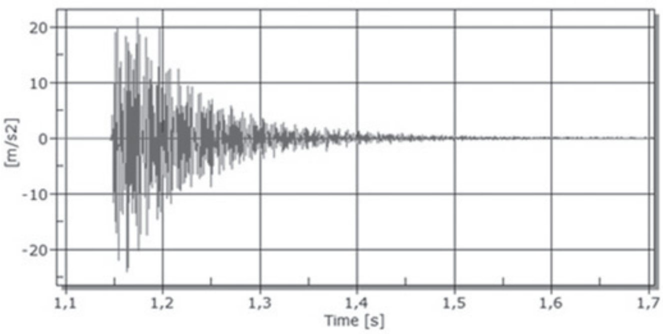

b)

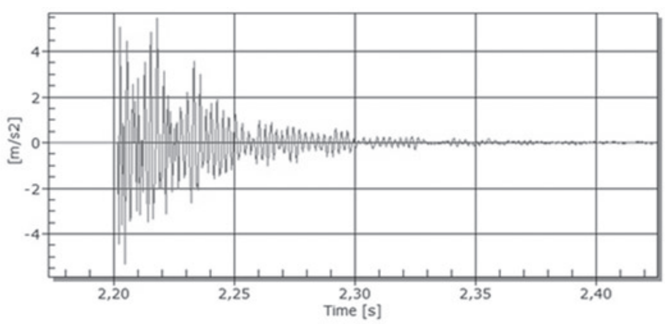

Fig. 6. The course of the system response to extortion at the measurement point P3 without load (a) and with load (b)

At the measuring point P5 there was no clear change in the registered system response to extortion. The maximum amplitude of vibration acceleration in both cases reached more than 50 m·s^{-2} and the time of suppress the vibration decreased from 0.5 seconds to 0.4 seconds. For the measurement point P5 vibration parameters of the system were measured in the direction of the force.

Table 1 shows the results of measurements carried out for all measuring points. Change of the measured waveform of the signal after load the wagon are clearly visible in the case of the points at

a)

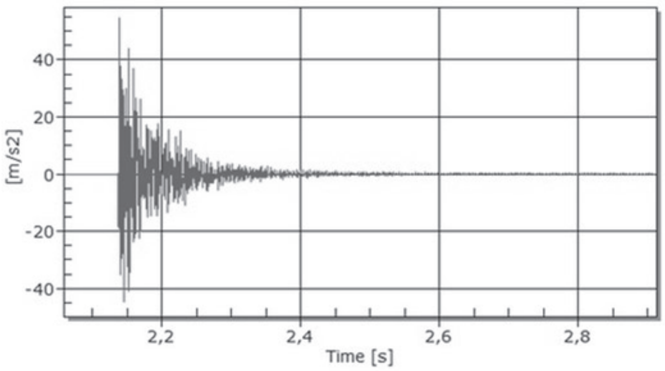

b)

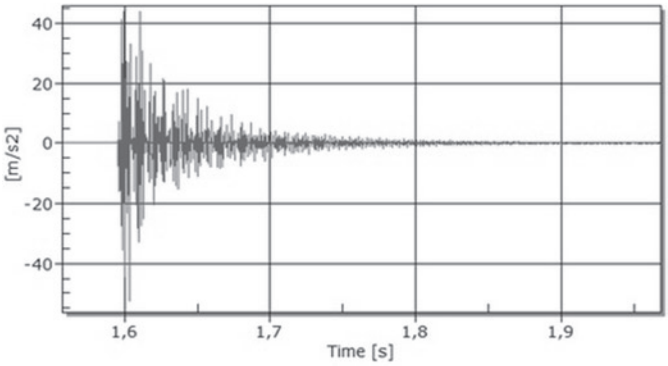

Fig. 7. The course of the system response to extortion at the measurement point P5

Table 1. Comparison of the results of vibration measurements

Measuring point	Without load		With load	
	a [m/s^2]	t [s]	a [m/s^2]	t [s]
P1	40	0,55	40	0,35
P2	14	1	8	0,4
P3	23	0,55	6	0,2
P4	25	0,8	15	0,4
P5	55	0,5	50	0,4

which measurements were carried out in the direction perpendicular to the force (points P2, P3 and P4). In other cases, there were no major changes in recorded waveforms.

During the further research the model of freight car was moving through the track way with a set speed and registration of its dynamic response was done using a MFC piezoelectric film glued in place of the measurement point P2. Electrical voltage signals generated by the piezoelectric film as a result of its deformation due to vibrations in the system were recorded. In order to allow the free movement of the model the wireless transmission of measurement data was used. Measurements were made for the model with load of 20 kg and without load. Each of the runs was repeated ten times in order to verify reproducibility of results.

Fig. 8 shows the electric voltage waveforms generated by the MFC-type piezoelectric film during the test of wagon model without and with load when there was not any obstacle on the track way.

A significant change in the recorded voltage signal during tests of the freight car model with the load can be observed. The electric voltage generated by the piezoelectric film has an asymmetrical waveform. There is also visible increase in the maximum values of generated electric voltage.

a)

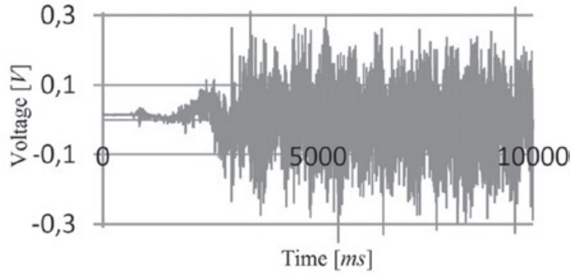

b)

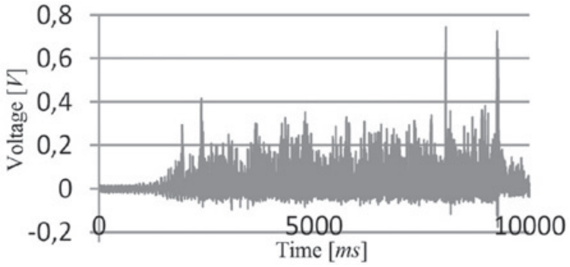

Fig. 8. The waveform generated by the MFC transducer during the movement of the model without load (a) and with load (b), without obstacle on the rail

In further tests an obstacle was placed on a rail way. It had the form of a steel element glued to one or both rails with diameter 25 mm and a thickness of 2 mm. In the case of mounting obstacles on both tracks, they were placed at the same distance from the beginning of the track. In order to verify the reproducibility of measurements they were conducted ten times in situations where an obstacle was mounted on the left rail, right rail or on both of the rails. The recorded voltage signal waveforms generated by the MFC piezoelectric foil glued on the freight wagon model in place of the measuring point P2 are presented in Fig. 9 to 11. Waveforms were recorded wirelessly using NI measurement module cDAQ-9191 and NI 9215 measurement card.

a)

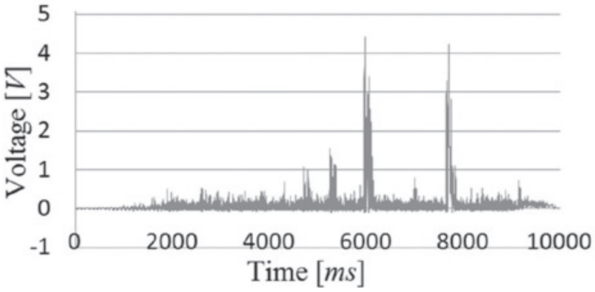

b)

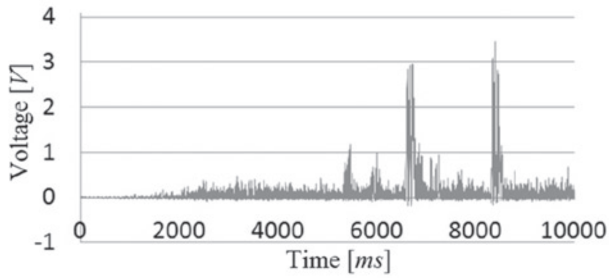

Fig. 9. The waveform generated by the MFC transducer during the movement of the model without load (a) and with load (b), with an obstacle on the left rail

When analysing the received waveforms from tests with the obstacle mounted on the left rail, in both cases (with and without load) it can be seen a significant increase in the voltage generated by the piezoelectric transducer during overcoming obstacles by both wagon axes. It can also to notice increase in electric voltage generated at

a)

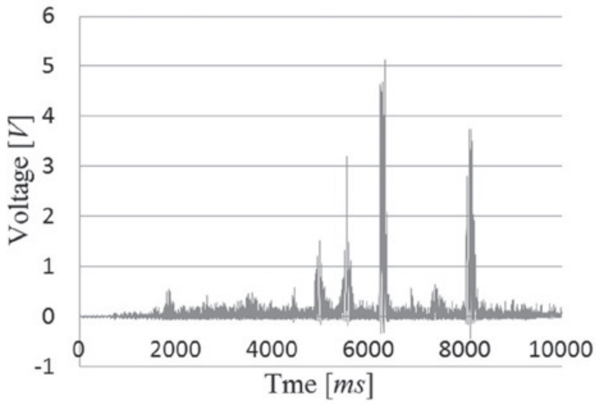

b)

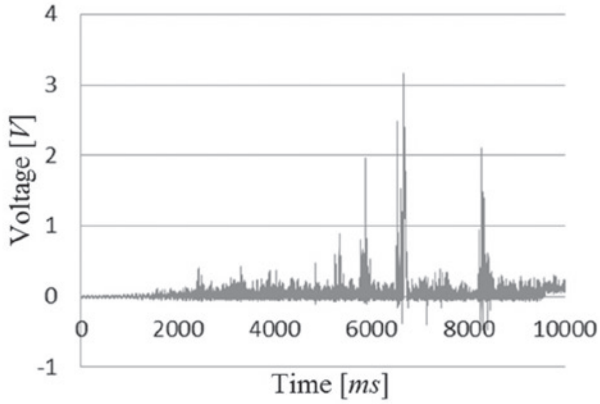

Fig. 10. The waveform generated by the MFC transducer during the movement of the model without load (a) and with load (b), with an obstacle on the right rail

a)

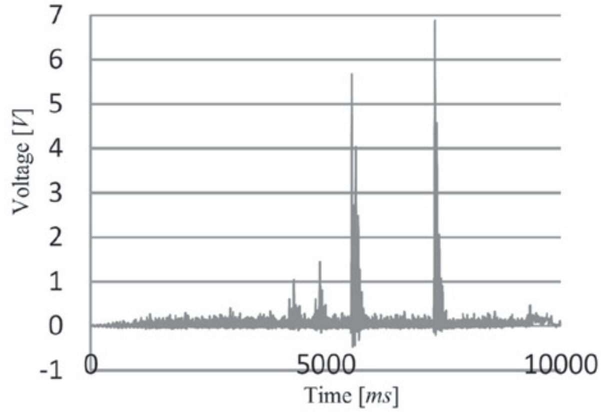

b)

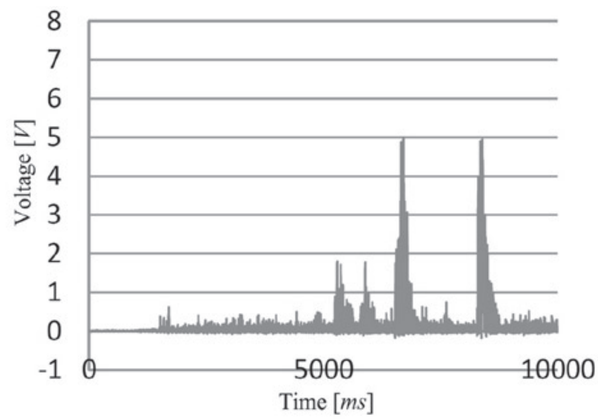

Fig. 11. The waveform generated by the MFC transducer during the movement of the model without load (a) and with load (b), with an obstacle on the both rails

the time of overcoming obstacles by trolley drive system. The peaks of voltage in this case do not have high value and can be interpreted ambiguously by the level of signal generated throughout the test. In the case of model with load slight decrease in the maximum values of generated electric voltage can be observed.

After placing obstacles on the right rail there was an increase in the value of the voltage generated by the piezoelectric film during the test. In this case, the obstacle is positioned on the same side of model that the piezoelectric transducer is glued. The signals generated by the piezoelectric film can be clearly interpreted. During the tests with load also the decrease in maximum values of recorded signal relative to the tests without load can be observed.

The last stage of the research was test with obstacles placed on both rails. Registered waveforms of electrical voltage generated by the piezoelectric transducer are given in Fig. 11.

In the case of the distribution obstacles on both rails of the track a considerable increase in the maximum values of generated signals can be observed. Unambiguous interpretation of signals generated by the piezoelectric transducer, both during transit of freight car model and the trolley through the obstacles is possible. At the same time, as in earlier measurements, there was a decrease of maximal values of the signal in tests with the load relative to the model unloaded.

5. Conclusions

The paper presents a report on the examinations of dynamic response to the excitation of a freight wagon type 1415-A3. The model of the wagon was studied in conditions of isolation from the rail tracks and while driving. Measurements were made using accelerometers and MFC piezoelectric transducers. The system was excited to oscillate by the pendulum in the case of half-determined system or through the obstacles placed on the track way. The possibility to infer about the state of the object on the basis of received signals was studied. Work is an introduction to the establishment of a system of non-destructive techniques for inspect freight wagons during their exploitation. Operation of the system will be based on the analysis of the dynamic response of the object measured using piezoelectric transducers glued to the selected points on object. The aim of the work was to verify the possibility of infer about the state of the object by measuring its response to the dynamic excitation and the possibility of its separation from the noise, which is the result of his work in normal operating conditions. It was shown that, as in the case of a measurement vibration forced by trains movement in which the sensors are mounted on elements of the railway infrastructure or surrounding buildings [29, 30], it is possible to verify the condition of the object based on the signals generated by respectively disposed piezoelectric sensors.

Measuring points on the created freight wagon model were selected in the study and a series of tests was conducted. It was proved that when accelerometers are used to measure the dynamic response of the system, changes are clearly visible only in the case of measuring the parameters of vibration in a direction other than the direction of excitation. Such a measurement would be impossible in the case of a real object that is excited to vibrations by forces acting during its normal operation. In this case, it may be an effective solution to use of piezoelectric foil glued on the surface of selected elements of the object, which in the proposed system will function as sensors. Preliminary studies conducted on the created laboratory stand proved the effectiveness of the proposed method. The electric voltage signal generated by the piezoelectric film glued on the surface of objects can be analysed and interpreted in order to infer for his condition. The decrease in the voltage generated by the piezoelectric transducers after model loading was observed during all tests. It is a result of its greater stiffness. It is also possible to uniquely identify signals generated in the course of passing over an obstacle, both the model of freight wagon as well as the trolley drive.

Tests on real objects – freight cars type 1415-A3 will be carried out as a part of further work. On the basis of modal analysis carried out for the created CAD model of the considered freight wagon measuring points in which piezoelectric films should be glued will be selected.

Acknowledgements

The work was carried out under the project number PBS2/A6/17/2013 agreement implemented under the Applied Research Program, funded by the National Centre for Research and Development.

References

1. Baier A. et al: Experimental synthesis and analysis of geometric and structural properties of chosen elements of railway wagons, Silesian University of Technology Publishing House, 2012, Gliwice.
2. Baier A, Zolkiewski S.: Initial research of epoxy and polyester warp laminates testing on abrasive wear used in car sheathing, Eksploatacja i Niezawodnosc - Maintenance and Reliability 2013; 15 (1): 37-43.
3. Białas K.: Mechanical and electrical elements in reduction of vibrations. Journal of Vibroengineering 2012; 14(1): 123-128.
4. Bruni S., Vinolas J., Berg M., Polach O., Stichel S.: Modelling of suspension components in a rail vehicle dynamics context. Vehicle System Dynamics 2011; 49 (7): 1021-1072, http://dx.doi.org/10.1080/00423114.2011.586430.
5. Buchacz A., Płaczek M.: The analysis of a composite beam with piezoelectric actuator based on the approximate method. Journal of Vibroengineering 2012; 14 (1): 111-116.
6. Buchacz A., Galeziowski D.: Synthesis as a designing of mechatronic vibrating mixed systems. Journal of Vibroengineering 2012; 14 (2): 553-559.
7. Buchacz A., Płaczek M., Wróbel A.: Control of characteristics of mechatronic systems using piezoelectric materials. Journal of Theoretical and Applied Mechanics 2013; 51: 225-234.
8. Buchacz A., Płaczek M., Wróbel A.: Modelling and analysis of systems with cylindrical piezoelectric transducers. Mechanika, 2014; 20(1): 87-91, http://dx.doi.org/10.5755/j01.mech.20.1.6597.
9. Buchacz A, Płaczek M, Wróbel A.: Modelling of passive vibration damping using piezoelectric transducers - the mathematical model. Eksploatacja i Niezawodnosc - Maintenance and Reliability 2014; 16 (2): 301-306.
11. Connolly D. P., Kouroussis G., Giannopoulos A., Verlinden O., Woodward. K., Forde M. C.: Assessment of railway vibrations using an efficient scoping model. Soil Dynamics and Earthquake Engineering 2014; 58: 37-47, http://dx.doi.org/10.1016/j.soildyn.2013.12.003.
12. Dymarek A., Dzitkowski T.: Modelling and synthesis of discrete - continuous subsystems of machines with damping. Journal of Materials Processing Technology 2005; 164-165: 1317-1326, http://dx.doi.org/10.1016/j.jmatprotec.2005.02.190.
13. Dymarek A., Dzitkowski T.: Searching for the values of damping elements with required frequency spectrum. Acta Mechanica et Automatica 2010; 4: 19-22.
14. Grebowski K., Zielińska M.: Modelowanie oddziaływań dynamicznych pociągu typu Pendolino na konstrukcje zabytkowych mostów

kolejowych w Polsce. Przegląd Budowlany 2015; 1: 27-32.
15. Hecht M.: Wear and energy-saving freight bogie designs with rubber primary springs: principles and experiences. Proceedings of the Institution of Mechanical Engineers Part F: Journal of Rail and Rapid Transit 2009; 223 (2): 105-110, http://dx.doi.org/10.1243/09544097JRRT227.
16. Herwig A., Bruhwiler E.: In-situ dynamic behaviour of a railway bridge girder under fatigue causing traffic loading. Proceedings of the 11th International Conference on Applications of Statistics and Probability in Civil Engineering, ICASP11, Zurich, Switzerland, 1-4 August 2011: 389-395, http://dx.doi.org/10.1201/b11332-58.
17. Iacob-Mare C., Manescu T. S.: Study of the freight wagon body through the method of finite elements. Metalurgia 2013; 65 (7): 13.
18. Jamroziak K., Kosobudzki M.: Determining the torsional natural frequency of underframe of off-road vehicle with use of the procedure of operational modal analysis. Journal of Vibroengineering, 2012; 14 (2): 472-476.
19. Jamroziak K., Kosobudzki M., Ptak J.: Assessment of the comfort of passenger transport in special purpose vehicles. Eksploatacja i Niezawodnosc - Maintenance and Reliability 2013,15 (1): 25-30.
20. Jönsson P. A., Stichel S., Persson I.: New simulation model for freight wagons with UIC link suspension, Vehicle System Dynamics 2008; 46: 695-704, http://dx.doi.org/10.1080/00423110802036976.
21. Klarecki K., Hetmańczyk M., Rabsztyn D.: Influence of the selected settings of the controller on the behavior of the hydraulic servo drive. Mechatronics - Ideas for Industrial Application. Advances in Intelligent Systems and Computing 2015; 317: 91-100, http://dx.doi.org/10.1007/978-3-319-10990-9_9.
22. Kovalev R., Lysikov N., Mikheev G. et al: Freight car models and their computer-aided dynamic analysis. Multibody System Dynamics 2009; 22 (4): 399-423, http://dx.doi.org/10.1007/s11044-009-9170-6.
23. Mehrpouya M., Ahmadian H.: Estimation of applied forces on railway vehicle wheelsets from measured vehicle responses. International Journal of Vehicle Structures and Systems 2009; 1(4): 104-110, http://dx.doi.org/10.4273/ijvss.1.4.08.
24. Okabe Y., Nakayama F.: Damage Detection in CFRP Laminates by Ultrasonic Wave Propagation Using MFC Actuator and FBG Sensor. Transactions of Space Technology Japan 2009; 7 (26): 7-12, http://dx.doi.org/10.2322/tstj.7.Pc_7.
25. Oleszak P., Cieśla J., Szaniec W.: Badanie skutków oddziaływań bocznych na wiadukcie kolejowym leżącym na łuku. Budownictwo i Architektura 2013; 12(2): 47-54.
26. Płaczek M.: Dynamic characteristics of a piezoelectric transducer with structural damping, Solid State Phenomena, Mechatronic Systems and Materials IV 2013; 198: 633-638.
27. Płaczek M.: Modelling and investigation of a piezo composite actuator application, Int. J. Materials and Product Technology 2015; 50 (3/4): 244-258, http://dx.doi.org/10.1504/IJMPT.2015.068532.
28. Salamak M., Łaziński P., Pradelok S., Bętkowski P.: Badania odbiorcze mostów kolejowych pod próbnym obciążeniem dynamicznym - wymagania i praktyka. Projektowanie, budowa i utrzymanie infrastruktury w transporcie szynowym. INFRASZYN 2014, Zakopane, 9-11 kwietnia 2014: 218-227.
29. Sekuła K., Kołakowski P., Świercz A.: System monitorowania obciążeń oraz stanu technicznego kratownicowych mostów w kolejnictwie. Monitorowanie Stanu Technicznego Konstrukcji i Ocena Jej Żywotności, Seminarium MONIT, Warszawa, 19 listopada 2010: 1-4.
30. Stypuła K.: Wybrane problemy ochrony zabudowy powierzchniowej przed drganiami generowanymi przez komunikację podziemną. Górnictwo i Geoinżynieria 2009; 3(1): 351- 362.
31. Wróbel A.: Kelvin Voigt's model of single piezoelectric plate. Journal of Vibroengineering 2012; 14 (2): 534-537.
32. Wróbel A., Płaczek M., Buchacz A., Majzner M.: Study of mechanical properties and computer simulation of composite materials reinforced by metal, Int. J. Materials and Product Technology 2015; 50 (3/4): 259-275, http://dx.doi.org/10.1504/IJMPT.2015.068533.
33. Zolkiewski, S.: Damped Vibrations Problem Of Beams Fixed On The Rotational Disk. International Journal of Bifurcation and Chaos 2011; 21 (1): 3033-3041, http://dx.doi.org/10.1142/S0218127411030337.
34. http://www.hbm.com/
35. http://www.smart-material.com/

Marek PŁACZEK
Andrzej BUCHACZ
Andrzej WRÓBEL
Institute of Engineering Processes Automation
and Integrated Manufacturing Systems
Faculty of Mechanical Engineering
Silesian University of Technology
ul. Konarskiego 18A, 44-100 Gliwice, Poland
E-mail: marek.placzek@polsl.pl, andrzej.buchacz@polsl.pl,
andrzej.wrobel@polsl.pl

Article citation info:
HAO L, ZHENCAI Z. A copula-based method for reliability sensitivity analysis of structural system with correlated failure modes. Eksploatacja i Niezawodnosc – Maintenance and Reliability 2015; 17 (3): 450–456, http://dx.doi.org/10.17531/ein.2015.3.17.

Lu HAO
Zhu ZHENCAI

A COPULA-BASED METHOD FOR RELIABILITY SENSITIVITY ANALYSIS OF STRUCTURAL SYSTEM WITH CORRELATED FAILURE MODES

OPARTA NA POJĘCIU KOPUŁY METODA ANALIZY CZUŁOŚCI NIEZAWODNOŚCIOWEJ SYSTEMU KONSTRUKCYJNEGO O SKORELOWANYCH PRZYCZYNACH USZKODZEŃ

Despite many advances in the field of computational reliability analysis, the efficient estimation of the reliability and reliability sensitivity analysis of structural systems with multiple failure modes remains a persistent challenge. The key to deal with the problem lies in the correlation modelling between failure modes. In this paper, the Archimedean copulas are used as an alternative to solve the high-dimensional dependence modeling problem. The probability characteristics of failure modes are described by stochastic perturbation technique, and the reliability index is estimated with the fourth-moment standardization method. Considering that the number of the potential failure modes of the structural systems are relatively large, the probabilistic network evaluation technique is adopted to reduce the computational complexity. The sensitivity analysis is then conducted using the matrix differential technology. The numerical examples show that the applied procedure is able to efficiently consider various failure modes of structural systems in probabilistic assessment and sensitivity analysis.

Keywords: *reliability; reliability sensitivity; correlation analysis; copula.*

Mimo poważnych osiągnięć w dziedzinie komputerowej analizy niezawodności, skutecznaocena niezawodności i analiza czułości niezawodnościowej systemów konstrukcyjnych o wielu przyczynach uszkodzeń pozostają ciągłym wyzwaniem. Kluczem do rozwiązania problemu jest modelowanie korelacji między przyczynami uszkodzeń. W niniejszym artykule zastosowano kopuły Archimedesa jako alternatywny sposób rozwiązania problemu modelowania zależności wysoko wymiarowych. Charakterystyki prawdopodobieństwa dla przyczyn uszkodzeń opisano przy pomocy metody zaburzeń stochastycznych, zaś wskaźnik niezawodności oszacowano metodą standaryzacji momentu czwartego rzędu. Biorąc pod uwagę, że liczba potencjalnych przyczyn uszkodzeń systemów konstrukcyjnych jest stosunkowo duża, wykorzystano technikę oceny z zastosowaniem sieci probabilistycznych, która pozwala na zmniejszenie złożoności obliczeniowej. Następnie przeprowadzono analizę czułości przy użyciu metody macierzy równań różniczkowych. Przykłady liczbowe pokazują, że zastosowana procedura pozwala na skuteczną ocenę różnych przyczyn uszkodzeń systemów konstrukcyjnych w ramach oceny probabilistycznej oraz analizy czułości.

Słowa kluczowe: *niezawodność; czułość niezawodnościowa; analiza korelacji; kopuła.*

1. Introduction

Generally, structural system is composed of multiple components, the state of the structural system (failure or safe) depends on that of each component. The reliability of the structural system is then determined by the component reliability. Comparing with the reliability analysis of single structure element, the system reliability analysis becomes more difficult especially when the failure of the components is correlated.

The reliability analysis methods for structural system, such as Monte Carlo simulation method, bound method, and surrogate model method, has provided as efficient approaches for system reliability analysis. However, the methods have their own limitations. The Monte Carlo simulation method demanded enormous computational cost for assessing the low probability events [16]. The bound method have been widely used for computing reliability interval on the probabilities of series and parallel system, but cannot give a determined value [5, 19]. The first-order system reliability method transforms system reliability problems into multi-normal calculations based on the results of component reliability [8,10], which is applicable to series and parallel system reliability problems. The surrogate model method is very useful and effective dealing with implicit limit state function problems [1]. Zhao proposed a moment-based method for structural system reliability assessment which is applicable to both series and non-series systems [23]. Kang proposed a matrix-based system reliability (MSR) method to estimate the probabilities of complex system events by simple matrix calculations [9].

The existing system reliability methods are not flexible in incorporating various types and amount of available information on components and their statistical dependence. The Pearson correlation coefficient is frequently used to describe the linear correlation between failure modes, whereas the correlation of failure modes in structural systems are generally nonlinear. As a tool to establish a joint distribution function from its marginal distributions, copula functions are often adopted to solve the correlation problems [6,21]. Copula functions are useful tools for modeling dependence among the components. They provide a way of specifying joint distributions if only the marginal distributions are known. In terms of system reliability of multiple failure modes, the multivariate distribution could be built using the marginal distributions of each failure mode and the copula function.

Reliability-based sensitivity refers to the partial derivative of the reliability with respect to basic random variables [13, 24]. It ranks the design variables and guides the reliability design [25]. Reliability sensitivity analysis has been used to obtain the change rate of a structure response due to the random inputs [11, 12]. In terms of system reliability sensitivity problem, the independent assumption of multiple failure modes may lead to incorrect result. Thus, it is important to develop an efficient method for the reliability-based sensitivity estimation with dependent failure modes.

A novel method is proposed here to deal with the system reliability and reliability-based sensitivity problem of the structural systems. The stochastic perturbation technique is adopted to obtain the first few moments of the limit state function of failure mode. The fourth-moment standardization method is then used to calculate the reliability of each failure mode. The correlation between failure modes are estimated with the copula-based cumulated distribution function. The reliability-based sensitivity with respect to the random variables is then obtained by the matrix differential technology.

Section 2 provides an introduction to copulas. Section 3 firstly describes the reliability modeling procedure of the component reliability and then develops the method into the system level. Section 4 proposes the reliability-based sensitivity modeling procedure based on the system reliability model. Section 5 applies the newly derived method to the structural system problems, comparing its accuracy to sampling methods. Section 6 provides some conclusions on the proposed method.

2. Copulas

The copula of a multivariate distribution describes not only the correlations of the random variables, but also the dependence structure. It is uncoupled from the marginal distributions which can be modeled as empirical distributions or fitted standard distributions as usual [17]. After modeling the marginal distributions, then the estimation of the corresponding copula function could be carried out. A compact definition of copula function is given in [21]. The use of copula is common in finance and insurance. In this paper, we propose to use copula for the analysis of correlated failure modes in structural systems.

According to the Sklar theory [20], let $F_i\left(g_i(\boldsymbol{X})\right)$ and $F_j\left(g_j(\boldsymbol{X})\right)$ denote the marginal distribution functions of the failure modes $g_i(\boldsymbol{X})$ and $g_j(\boldsymbol{X})$, respectively. The joint distribution function $F_{ij}\left(g_i, g_j\right)$ can be expressed as:

$$F_{ij}\left(g_i, g_j\right) = C\left[F_i\left(g_i(x)\right), F_j\left(g_j(x)\right)\right] \quad (1)$$

where $C(u,v)$ is the copula function.

In the case of n marginal distribution functions, the joint distribution function of n failure modes could be similarly modeled as:

$$F\left(g_i, g_j, \cdots, g_n\right) = C\left[F_i\left(g_i(x)\right), F_j\left(g_j(x)\right), \cdots, F_n\left(g_n(x)\right)\right] \quad (2)$$

The Sklar theory provides an efficient way to model the dependence structure of random variables with the copula functions. However, the using of high-dimensional copula function makes it inevitably encounter the problem of parameter estimation, which is generally difficult to obtain. To overcome this problem, the Archimedean copulas are used as an alternative to solve the high-dimensional dependence modeling problem. The family of Archimedean copulas has been studied extensively by a number of authors including [2, 4, 7, 22]. Well known representatives of the Archimedean family are Gumbel-Hougaard, Frank and Clayton copula. The generator and parameter range of these Archimedean copulas are shown in Table 1, for more details, the reader is referred to [17]. Due to the characteristics of the Archimedean copula functions, any N-dimension Archimedes copula function could be deduced from a bivariant one [18]. Thus, the reliability problem with multiple failure modes could be transformed into the bivariant form:

$$\begin{aligned} &C\left(u_1,u_2,u_3\right) = C\left(C\left(u_1,u_2\right),u_3\right) \\ &C\left(u_1,u_2,u_3,u_4\right) = C\left(C\left(u_1,u_2,u_3\right),u_4\right) \\ &C\left(u_1,u_2,\cdots,u_{N-1},u_N\right) = C\left(C\left(u_1,u_2,\cdots,u_{N-1}\right),u_N\right) \end{aligned} \quad (3)$$

Thus, the first derivation of the copula-based CDF with respecet to the random parameter ζ (*i.e.* the mean, variance, et al.) can be obtained straightforwardly,

$$\begin{aligned} \frac{\partial C\left(P_1,P_2,\cdots,P_m\right)}{\partial \zeta} = &\frac{\partial C\left(P_1,P_2,\cdots,P_m\right)}{\partial C\left(P_1,P_2,\cdots,P_{m-1}\right)}\left(\frac{\partial C\left(C\left(P_1,P_2,P_{m-2}\right),P_{m-1}\right)}{\partial C\left(P_1,P_2,P_{m-2}\right)}\cdots\right. \\ &\left(\frac{\partial C\left(C\left(P_1,P_2\right),P_3\right)}{\partial C\left(P_1,P_2\right)}\left(\frac{\partial C\left(P_1,P_2\right)}{\partial P_1}\frac{\partial P_1}{\partial \zeta} + \frac{\partial C\left(P_1,P_2\right)}{\partial P_2}\frac{\partial P_2}{\partial \zeta}\right) + \right. \\ &\left.\frac{\partial C\left(C\left(P_1,P_2\right),P_3\right)}{\partial P_3}\frac{\partial P_3}{\partial \zeta}\right) + \cdots + \left.\frac{\partial C\left(C\left(P_1,P_2,P_3\right),P_{m-1}\right)}{\partial P_{m-1}}\frac{\partial P_{m-1}}{\partial \zeta}\right) + \\ &\frac{\partial C\left(C\left(P_1,P_2,\cdots,P_{m-1}\right),P_m\right)}{\partial P_m}\frac{\partial P_m}{\partial \zeta} \end{aligned} \quad (4)$$

Table 1. The generator and parameter range of commonly used Archimedean copula functions

Archimedean Copula	Generator	Parameter range
Clayton	$\varphi_\theta(x) = (1+\theta x)_+^{-1/\theta}$	$\theta \neq 0, \alpha_+ = \max\{\alpha, 0\}$
Gumbel-Hougaard	$\varphi_\theta(x) = \exp\left(-x^{1/\theta}\right)$	$\theta \geq 1$
Frank copula	$\varphi_\theta(x) = -\frac{1}{\theta}\ln\left(\frac{\exp(x)+\exp(-\theta)-1}{\exp(x)}\right)$	$\theta \neq 0$
Ali-Mikhail-Haq	$\varphi_\theta(x) = \frac{1-\theta}{\exp(x)-\theta}$	$\theta \in [-1,1]$

In this paper, authors applied a useful application of the Gumbel-Hougaard copula in the reliability analysis of structural systems . The distribution function of the Gumbel-Hougaard copula is as follows:

$$C_G(u,v;\theta) = \exp\left(-\left[(-\ln u)^{\frac{1}{\theta}} + (-\ln v)^{\frac{1}{\theta}}\right]^\theta\right) \; \theta \in (0,1] \quad (5)$$

The expression of the first derivative of the Gumbel-Hougaard copula with respect to variable (u and v) could be obtained as:

$$\frac{\partial C_G(\mu,v)}{\partial u} = -\frac{\left((-\ln(u))^{\frac{1}{\theta}} + (-\ln(v))^{\frac{1}{\theta}}\right)^\theta (-\ln(u))^{\frac{1}{\theta}} \mathrm{e}^{-\left((-\ln(u))^{\frac{1}{\theta}}+(-\ln(v))^{\frac{1}{\theta}}\right)^\theta}}{u\ln(u)\left((-\ln(u))^{\frac{1}{\theta}} + (-\ln(v))^{\frac{1}{\theta}}\right)} \quad (6)$$

$$\frac{\partial C_G(\mu,v)}{\partial v} = -\frac{\left(\left(-\ln(u)\right)^{\frac{1}{\theta}} + \left(-\ln(v)\right)^{\frac{1}{\theta}}\right)^{\theta} \left(-\ln(v)\right)^{\frac{1}{\theta}} e^{-\left(\left(-\ln(u)\right)^{\frac{1}{\theta}} + \left(-\ln(v)\right)^{\frac{1}{\theta}}\right)^{\theta}}}{v\ln(v)\left(\left(-\ln(u)\right)^{\frac{1}{\theta}} + \left(-\ln(v)\right)^{\frac{1}{\theta}}\right)} \tag{7}$$

3. Reliability estimation of structural systems

Structural systems normally have a variety of potential failure modes, which results in that the probabilistic analysis of the structural system is thus becomes a system reliability problem. Moreover, the correlation between failure modes can have a profound effect on their practical reliability and the neglect of such correlation may lead to excessive errors or even wrong conclusion.

Each failure mode caused by the failure of a group of structure components could be seemed as a parallel system, and the system failure could then be considered as a series failure of these failure modes. Consequently, the system reliability estimation of the structural system is to calculate the reliability of the series-parallel system. Generally, a parallel system formed from a failure path is seemed as a failure mode and the corresponding limit state function can be obtained in mechanics. A structural system could therefore be simplified into a series system of multiple failure modes.

The reliability problem of structural systems with multiple failure modes can be expressed as:

$$R = P(G > 0) = \int_0^{\infty} f_G(G)\mathrm{d}G \tag{8}$$

$$G(\boldsymbol{X}) = \left(g_1(\boldsymbol{X}), g_2(\boldsymbol{X}), \cdots, g_n(\boldsymbol{X})\right)^{\mathrm{T}} \tag{9}$$

where $\boldsymbol{X} = \{X_i\}_{i=1}^{n}$ denotes the random variable vector and $G(X)$ defines the limit state functions of multiple failure modes.

The first four moment of the random variable $\boldsymbol{X}$ can be deduced as follows according to the perturbation theory:

$$\mathrm{E}(\boldsymbol{X}) = \bar{\boldsymbol{X}} = \mathrm{E}(\boldsymbol{X}_{\mathrm{d}}) + \varepsilon \mathrm{E}(\boldsymbol{X}_{\mathrm{p}}) = \boldsymbol{X}_{\mathrm{d}} \tag{10}$$

$$\mathrm{Var}(\boldsymbol{X}) = \mathrm{E}\left\{\left[\boldsymbol{X} - \mathrm{E}(\boldsymbol{X})\right]^{[2]}\right\} = \varepsilon^2 \left[\boldsymbol{X}_{\mathrm{p}}^{[2]}\right] \tag{11}$$

$$\mu_3(\boldsymbol{X}) = \mathrm{E}\left\{\left[\boldsymbol{X} - \mathrm{E}(\boldsymbol{X})\right]^{[3]}\right\} = \varepsilon^3 \left[\boldsymbol{X}_{\mathrm{p}}^{[3]}\right] \tag{12}$$

$$\mu_4(\boldsymbol{X}) = \mathrm{E}\left\{\left[\boldsymbol{X} - \mathrm{E}(\boldsymbol{X})\right]^{[4]}\right\} = \varepsilon^4 \left[\boldsymbol{X}_{\mathrm{p}}^{[4]}\right] \tag{13}$$

where $(\bullet)^{[k]}$ represents the Kronecker product, *i.e.*,
$(\bullet)^{[k]}=(\bullet)\otimes(\bullet)\otimes\cdots\otimes(\bullet)$, $(A)_{p\times q}\otimes(B)_{s\times t}=[a_{ij}B]_{ps\times qt}$.

Due to that the complete statistical information of random variables cannot be fully accessed in most practical cases, the statistical moments higher than the fourth order are difficult to obtain. Thus, the moments of each failure mode are considered here according to the engineering reality, the corresponding expression in matrix form could be obtained according to the perturbation theory

$$\mathrm{Var}\left[g(\boldsymbol{X})\right] = \left(\frac{\partial g_{\mathrm{d}}(\boldsymbol{X})}{\partial \boldsymbol{X}^T}\right)^{[2]} \mathrm{Var}(\boldsymbol{X}) \tag{14}$$

$$\theta_{gi} = \left(\frac{\partial g_{\mathrm{d}}(\boldsymbol{X})}{\partial \boldsymbol{X}^T}\right)^{[3]} \mu_3(\boldsymbol{X}) \tag{15}$$

$$\eta_{gi} = \left(\frac{\partial g_{\mathrm{d}}(\boldsymbol{X})}{\partial \boldsymbol{X}^T}\right)^{[4]} \mu_4(\boldsymbol{X}) \tag{16}$$

According to the reliability theory, for a given limit state function $z_i = g_i(\boldsymbol{X})$, the reliability index and reliability could be defined as:

$$\beta_{Si} = \frac{\mathrm{E}\left[g_i(\boldsymbol{X})\right]}{\sqrt{\mathrm{Var}\left[g_i(\boldsymbol{X})\right]}} \tag{17}$$

Equation (17) use only the first two moments, *i.e.* the mean and the variance of the limit state function, which is suitable for the case that the basic random variables are normally distributed. As a matter of fact, the distribution types of the random variables are unknown on most occasions, the complete probabilistic information needed is unable to obtain. To overcome this problem, the fourth-moment reliability index is adopted here [23], and the reliability index of each failure mode could be expressed as the following equation according to the theory,

$$\beta_{Fi} = \frac{3(\alpha_{4gi} - 1)\beta_{Si} + \alpha_{3gi}(\beta_{Si}^2 - 1)}{\sqrt{(9\alpha_{4gi} - 5\alpha_{3gi}^2 - 9)(\alpha_{4gi} - 1)}} \tag{18}$$

where $\alpha_{3gi} = \theta_{gi}/\sigma_{gi}^3$, $\alpha_{4gi} = \eta_{gi}/\sigma_{gi}^4$ represent the coefficients of skewness and kurtosis of the ith failure mode, respectively. θ_{gi} and η_{gi} are the third and the fourth central moment of the ith failure mode.

Each failure mode can be represented as a limit state function $g_i(\boldsymbol{X})$, and the system reliability could then be expressed as:

$$\begin{aligned} R &= P\{g_1(\boldsymbol{X}) > 0 \cap g_2(\boldsymbol{X}) > 0 \cap \cdots g_n(\boldsymbol{X}) > 0\} \\ &= \int_0^{\infty} \cdots \int_0^{\infty} f_G(g_1, g_2, \cdots g_n)\mathrm{d}g_1 g_1 \cdots \mathrm{d}g_n \end{aligned} \tag{19}$$

where $f_G(g_1, g_2, \cdots g_n)$ is the joint probability density function of the potential failure modes.

Comparing to mechanical components, the failure of a structural system is usually accompanied with much more failure modes, which results in that the reliability analysis becomes much more complex. In order to overcome this problem, the probabilistic network evaluation technique (PNET) is adopted in this paper to identify the representative failure modes in structural system and reduce the complexity of the analysis procedure [15]. According to the PNET, failure modes of which the correlation coefficient $\square\rho_{ij}\square>\rho_0$ are considered as highly correlated modes, and the one with a less reliability index is selected as the representative failure mode. By repeating the procedure, all the representative failure modes can be selected. By using PNET, the system reliability problem of the structural system is simplified and only the representative failure modes is taken into account. In this case, according to the probabilistic theory and the copula-based cumulative distribution functions, the failure probability of the structural system with respect to m representative failure modes could then be expressed as:

$$P=P\left(\bigcup_{j=1}^{m} g_j\left(X_1,X_2,\cdots,X_n\right)\leq 0\right)=\sum_{j=1}^{m}P_j-\sum_{1\leq k<l\leq m}C\left(P_k,P_l\right)+\sum_{1\leq k<l<s\leq m}C\left(C\left(P_k,P_l\right),P_s\right)-\cdots+\left(-1\right)^{m-1}C\left(C\left(P_1,P_2,\cdots,P_{m-1}\right),P_m\right) \tag{20}$$

where P_j denotes the failure probability of the jth representative failure mode.

4. Copula-based reliability sensitivity analysis

Based on the scheme of the reliability analysis of structural system, the structural sensitivity analysis could then be performed. Reliability-based sensitivity involves studying the dependence of the failure probability on design parameters and refers to the partial derivative of the reliability with respect to design parameters $\boldsymbol{\zeta}$, such as the mean and the variance [14, 24].

Based on the matrix differential technology and copula-based joint probability distribution function, the reliability-based sensitivity with respect to random parameters of random variables (the mean $\boldsymbol{\zeta}_1$ and the variance $\boldsymbol{\zeta}_2$) considering correlated failure modes could be expressed as follows:

$$\frac{\partial P}{\partial\zeta}=\sum_{j=1}^{m}\frac{\partial P_j}{\partial\zeta}-\sum_{1\leq k\leq l\leq m}\frac{\partial C\left(P_k,P_l\right)}{\partial\zeta}+\sum_{1\leq k\leq l\leq s\leq m}\frac{\partial C\left(P_k,P_l,P_s\right)}{\partial\zeta}-\cdots+\left(-1\right)^{m-1}\frac{\partial C\left(P_1,P_2,\cdots P_m\right)}{\partial\zeta} \tag{21}$$

where:

$$\frac{\partial P_j}{\partial\zeta_1}=\frac{\partial P_j\left(\beta_{\mathrm{Fi}}\right)}{\partial\beta_{Fi}}\left\{\frac{\partial\beta_{\mathrm{Fi}}}{\partial\beta_{Si}}\left[\frac{\partial\beta_{Si}}{\partial\mu_{gi}}\frac{\partial\mu_{gi}}{\partial\zeta_1}+\frac{\partial\beta_{Si}}{\partial\sigma_{gi}}\frac{\partial\sigma_{gi}}{\partial\zeta_1}\right]+\frac{\partial\beta_{Fi}}{\partial\sigma_{gi}}\frac{\partial\sigma_{gi}}{\partial\zeta_1}\right\} \tag{22}$$

$$\frac{\partial P_j\left(\beta_{Fi}\right)}{\partial\beta_{Fi}}=-\varphi\left(-\beta_{Fi}\right) \tag{23}$$

$$\frac{\partial\beta_{Fi}}{\partial\beta_{Si}}=\frac{3\left(\alpha_{4gi}-1\right)+2\alpha_{3gi}\beta_{Si}}{\sqrt{\left(5\alpha_{3gi}^2-9\alpha_{4gi}+9\right)\left(1-\alpha_{4gi}\right)}} \tag{24}$$

$$\frac{\partial\beta_{Si}}{\partial\mu_{gi}}=\frac{1}{\sigma_{gi}} \tag{25}$$

$$\frac{\partial\mu_{gi}}{\partial\zeta_1}=\left[\frac{\partial g_i}{\partial\zeta_{11}},\cdots,\frac{\partial g_i}{\partial\zeta_{1n}}\right] \tag{26}$$

$$\frac{\partial\beta_{Si}}{\partial\sigma_{gi}}=-\frac{\mu_{gi}}{\sigma_{gi}^2} \tag{27}$$

$$\frac{\partial\beta_{Fi}}{\partial\sigma_{gi}}=\frac{\left(\alpha_{3gi}\left(3-5\beta_{Si}^2\right)-15\alpha_{4gi}\beta_{Si}+3\beta_{Si}\right)\Big/\sigma_{gi}}{\sqrt{\left(9\alpha_{4gi}-5\alpha_{3gi}^2-9\right)\left(\alpha_{4gi}-1\right)}}-\frac{1}{2}\frac{\left[3\beta_{\mathrm{Si}}\left(\alpha_{4gi}-1\right)+\alpha_{3gi}\left(\beta_{Si}^2-1\right)\right]}{\sqrt{\left(9\alpha_{4gi}-5\alpha_{3gi}^2-9\right)^3\left(\alpha_{4gi}-1\right)^3}}\left(50\alpha_{3gi}^2\alpha_{4gi}-30\alpha_{3gi}^2-72\alpha_{4gi}^2+72\alpha_{4gi}\right)\Big/\sigma_{gi} \tag{28}$$

$$\frac{\partial\sigma_{gi}}{\partial\zeta_1}=\frac{1}{2\sigma_{gi}}\left[\frac{\partial^2 g_i}{\partial{\zeta_1}^2}\otimes\frac{\partial g_i}{\partial\zeta_1}+\left(\frac{\partial^2 g_i}{\partial{\zeta_1}^2}\otimes\frac{\partial g_i}{\partial\zeta_1}\right)\left(\boldsymbol{I}_n\otimes\boldsymbol{U}_{n^2\times n^2}\right)\right]\left(\boldsymbol{I}_n\otimes\mathrm{Var}\left(\boldsymbol{X}\right)\right) \tag{29}$$

$$\frac{\partial P_i}{\partial\zeta_2}=\frac{\partial P_i\left(\beta_{Fi}\right)}{\partial\beta_{Fi}}\left(\frac{\partial\beta_{Fi}}{\partial\beta_{Si}}\frac{\partial\beta_{Si}}{\partial\sigma_{gi}}+\frac{\partial\beta_{Fi}}{\partial\sigma_{gi}}\right)\frac{\partial\sigma_{gi}}{\partial\zeta_2} \tag{30}$$

$$\frac{\partial\sigma_{gi}}{\partial\zeta_2}=\frac{1}{2\sigma_{gi}}\left[\frac{\partial\overline{g}_i}{\partial\boldsymbol{X}}\otimes\frac{\partial\overline{g}_i}{\partial\boldsymbol{X}}\right] \tag{31}$$

According to the known probabilistic information of the random variables, the reliability sensitivity of the structure system with m correlated representative failure modes could be obtained based on the above equations.

5. Numerical examples

5.1. The beam-cable structural system

A simple beam-cable structural system is shown in Figure 1. The length of the beam is $2l$=12m, the length of cables is L=3m. The cross section of the beam is a $b\times h$ rectangle. The cross sectional area of the cable is A_i (i=1,2). The plastic limit bending moment of the beam is M. The yield limit stress of the cable and the beam are σ_1 and σ_2, respectively. q is the uniformly distributed load. The random variables (b, h, A_1, A_2, σ_1, σ_2 and q) with known first four moments are assumed to be independent, and the probabilistic properties are listed in Table 2.

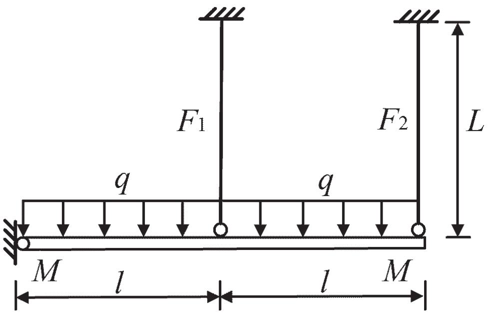

Fig. 1. Beam-cable structural system

There are four failure modes of the beam-cable structural system [23], the corresponding limit state functions are listed in Table 3. ($M=Wf_y$, $W=bh^2/6$ is the section modulus of bending of the beam, with the coefficient f_y=0.134).

According to the PNET method, the failure modes with the correlation coefficients higher than ρ_0=0.8 are selected as the representative failure modes, which are g_2 and g_1. Then, the system failure probability of the beam-cable system could be expressed as the following form according to equation (20).

$$P=P\left(g_1\left(\boldsymbol{X}\right)\leq 0\right)+P\left(g_2\left(\boldsymbol{X}\right)\leq 0\right)-P\left(g_1\left(\boldsymbol{X}\right)\leq 0\cap g_2\left(\boldsymbol{X}\right)\leq 0\right)$$
$$=P_1+P_2-C\left(P_1,P_2\right)$$

Table 2. The first four moments of random variables

Random variables	Mean	Standard deviation	The third moment	The fourth moment
b(mm)	152	0.76	1.4223e-1	1.1723
h(mm)	200	1	3.2400e-1	3.5140
A_1(cm^2)	6.45	0.032	1.0617e-5	3.6847e-6
A_2(cm^2)	3.32	0.017	1.5918e-6	2.9349e-7
σ_1(MPa)	413.6	41.36	2.2924e4	1.0283e7
σ_2(MPa)	300	30	8.7480e3	2.8463e6
q(kN/m)	29	5.84	6.4434e1	4.0791e3

Table 3. The limit state functions of the potential failure modes in example 5.1

$g_1 = 6M - ql^2/2$	$g_3 = M + A_2\sigma_2 l - ql^2/2$
$g_2 = A_1\sigma_1 l + 2A_2\sigma_2 l - 2ql^2$	$g_4 = 2M + A_1\sigma_1 l - ql^2$

The failure probability of each failure mode and the joint failure probability could be calculated with equation (19-21) and equation (4), respectively:

$$P_1{=}0.0057\ ,\ P_2 = \ 0.0052\ ,\ C\left(P_1,P_2\right){=}\ 3.5\text{e-}04$$

Thereout, the system failure probability and system reliability could be obtained as:

$$P{=}P_1 + P_2 - C\left(P_1,P_2\right) = 0.0574\ ,\ R = 1 - P = 0.9426$$

To validate the result, a Monte Carlo simulation is carried out with 10^6 samples and gives R_{MCS}=0.9819, the relative error is ρ_P=|R-R_{MCS}|/R_{MCS}=4%.

Based on the reliability analysis results, the reliability-based sensitivity could then be obtained according to equation (21).

$$\frac{\partial P}{\partial \bar{\boldsymbol{X}}^{\mathrm{T}}} = \begin{bmatrix} \partial P/\partial b \\ \partial P/\partial h \\ \partial P/\partial A_1 \\ \partial P/\partial A_2 \\ \partial P/\partial \sigma_1 \\ \partial P/\partial \sigma_2 \\ \partial P/\partial q \end{bmatrix} = \begin{bmatrix} \text{-6.0246E-4} \\ \text{-9.1574E-4} \\ \text{-5.3980E2} \\ \text{-7.8308E2} \\ \text{-8.4181E-10} \\ \text{-8.6661E-10} \\ \text{1.7685E-5} \end{bmatrix} \quad \frac{\partial P}{\partial \mathrm{Var}(\boldsymbol{X})} = \begin{bmatrix} \partial P/\partial \mathrm{Var}(b) \\ \partial P/\partial \mathrm{Var}(h) \\ \partial P/\partial \mathrm{Var}(A_1) \\ \partial P/\partial \mathrm{Var}(A_2) \\ \partial P/\partial \mathrm{Var}(\sigma_1) \\ \partial P/\partial \mathrm{Var}(\sigma_2) \\ \partial P/\partial \mathrm{Var}(q) \end{bmatrix} = \begin{bmatrix} \text{1.0203E-4} \\ \text{2.3574E-4} \\ \text{5.7931E6} \\ \text{1.2191E7} \\ \text{1.4089E-17} \\ \text{1.4931E-17} \\ \text{6.0273E-9} \end{bmatrix}$$

The results display that the failure probability of the beam-cable structural system descends as the dimension parameter b, h, A_i and yield stress σ_i increase, but increases as the load q rises. Among all the random variables considered, the failure probability has a high dependency on A_i.

5.2. The six-bar truss structural system

As shown in Figure 2 is a six-bar truss structural system with five applied concentrated load F_i(i=1,2,…,5). All the bars are made of the same material with the yield limit σ. The cross section of each bar is A_i(i=1,2,…,6). The limit state functions of the potential failure modes of the structural system are listed in Table 4 [3]. The random variables (A_i, F_i, and σ) are independent with each other, and the probabilistic properties with known first four moments are listed in Table 5.

According to the PNET method, the representative failure modes of the six-bar truss structural system is determined, which are g_{15}, g_1 and g_6. The failure probability of each failure modes could be obtained as,

$$P_{15}{=}0.0657\ ,\ P_1{=}1.1102\text{e-}16\ ,\ P_6{=}0$$

$$C\left(P_{15},P_1\right){=}1.1102\text{e-}16\ ,\ C\left(P_{15},P_6\right){=}0\ ,$$

$$C\left(P_1,P_6\right){=}0\ ,\ C\left(P_{15},P_1,P_6\right){=}0$$

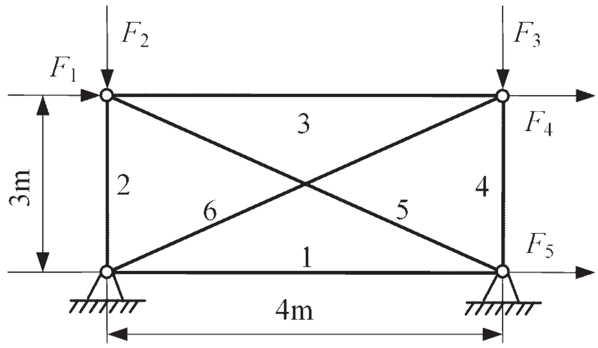

Fig. 2. Six-bar truss structural system

Table 4. The limit state functions of the potential failure modes in example 5.2

g_1=3$A_1\sigma$+4$A_2\sigma$-4F_2-3F_5	g_9=20$A_2\sigma$+12$A_6\sigma$-15F_1+20F_2-15F_4
g_2=$A_1\sigma$+$A_3\sigma$-F_1-F_5	g_{10}=3$A_3\sigma$+4$A_4\sigma$-4F_3-3F_4
g_3=3$A_1\sigma$+4$A_4\sigma$-3F_1-4F_3-3F_5	g_{11}=5$A_3\sigma$+4$A_5\sigma$-5F_1
g_4 = 5$A_1\sigma$ + 4$A_5\sigma$ - 5F_5	g_{12}=5$A_3\sigma$+4$A_6\sigma$-5F_4
g_5=5$A_1\sigma$+4$A_6\sigma$-4F_1-4F_4-4F_5	g_{13}=20$A_4\sigma$+12$A_5\sigma$-15F_1-20F_3-15F_4
g_6=4$A_1\sigma$+3$A_3\sigma$-3F_1+4F_2	g_{14}=5$A_4\sigma$+3$A_6\sigma$-5F_3
g_7=4$A_2\sigma$+4$A_4\sigma$-3F_1+4F_2-4F_3-3F_4	g_{15}=4$A_5\sigma$+4$A_6\sigma$-5F_1-5F_4
g_8=5$A_2\sigma$+3$A_5\sigma$-5F_2	

Thus, the system failure probability and the system reliability could be obtained as:

$$P = P_{15} + P_1 + P_6 - C\left(P_{15},P_1\right) - C\left(P_{15},P_6\right) - C\left(P_1,P_6\right) + C\left(P_{15},P_1,P_6\right) = 0.0657$$

$$R{=}1 - P{=}0.9343$$

To validate the result, a Monte Carlo simulation is carried out with 10^6 samples and gives R_{MCS}=0.9668, compare the result with that of the proposed method, the relative error is ε_R=|R-R_{MCS}|/R_{MCS}=3.36%.

Based on the above results, the reliability-based sensitivity of the structural system could then be obtained according to equation (21).

Table 5. Probabilistic properties of random variables

Random variables	Mean	Standard deviation	The third moment	The fourth moment
A_1(mm^2)	250	1.25	6.3281e-1	8.5791
A_2(mm^2)	100	0.5	4.0500e-2	2.1963e-1
A_3(mm^2)	100	0.5	4.0500e-2	2.1963e-1
A_4(mm^2)	250	1.25	6.3281e-1	8.5791
A_5(mm^2)	250	1.25	6.3281e-1	8.5791
A_6(mm^2)	150	0.75	1.3669e-1	1.1119
F_1(kN)	50	2.5	5.0625	1.3727e2
F_2(kN)	30	1.5	1.0935	1.7790e1
F_3(kN)	30	1.5	1.0935	1.7790e1
F_4(kN)	20	1.0	0.324	3.514
F_5(kN)	20	1.0	0.324	3.514
σ(MPa)	240	12	5.5987e2	7.2866e4

$$\frac{\partial P}{\partial \mathrm{Var}(\boldsymbol{X})}=\begin{bmatrix}\partial P/\partial \mathrm{Var}(A_1)\\ \partial P/\partial \mathrm{Var}(A_2)\\ \partial P/\partial \mathrm{Var}(A_3)\\ \partial P/\partial \mathrm{Var}(A_4)\\ \partial P/\partial \mathrm{Var}(A_5)\\ \partial P/\partial \mathrm{Var}(A_6)\\ \partial P/\partial \mathrm{Var}(F_1)\\ \partial P/\partial \mathrm{Var}(F_2)\\ \partial P/\partial \mathrm{Var}(F_3)\\ \partial P/\partial \mathrm{Var}(F_4)\\ \partial P/\partial \mathrm{Var}(F_5)\\ \partial P/\partial \mathrm{Var}(\sigma)\end{bmatrix}=\begin{bmatrix}1.4539\text{E-}29\\ 2.5848\text{E-}29\\ -1.0408\text{E-}56\\ 0\\ 3.1994\text{E-}4\\ 3.1994\text{E-}4\\ 8.6789\text{E-}9\\ 4.4874\text{E-}34\\ 0\\ 8.6789\text{E-}9\\ 2.5242\text{E-}34\\ 8.8872\text{E-}4\end{bmatrix}\quad \frac{\partial P}{\partial \bar{\boldsymbol{X}}^{\mathrm{T}}}=\begin{bmatrix}\partial P/\partial A_1\\ \partial P/\partial A_2\\ \partial P/\partial A_3\\ \partial P/\partial A_4\\ \partial P/\partial A_5\\ \partial P/\partial A_6\\ \partial P/\partial F_1\\ \partial P/\partial F_2\\ \partial P/\partial F_3\\ \partial P/\partial F_4\\ \partial P/\partial F_5\\ \partial P/\partial \sigma\end{bmatrix}=\begin{bmatrix}-8.0203\text{E-}29\\ -1.0694\text{E-}28\\ -8.7822\text{E-}56\\ 0\\ -5.9940\text{E-}3\\ -5.9940\text{E-}3\\ 3.1219\text{E-}5\\ 4.4557\text{E-}31\\ 0\\ 3.1219\text{E-}5\\ 3.3418\text{E-}31\\ -9.99\text{E-}3\end{bmatrix}$$

The results show that the failure probability of the six-bar truss structural system descends as the cross section of each bar A_i and the yield stress σ increase, but increases as the load F_i rises. It is necessary to mention that the system reliability sensitivity with respect to the variables A_4 and F_3 are 0 because of the two variables are not involved in the representative failure modes. Besides, in terms of the degree of influences, the system reliability is very sensitive to cross section A_5, A_6 and yield limit σ.

6. Conclusions

This paper presents a system reliability and parameter sensitivity analysis method of structural systems with correlated failure modes. The reliability of the component failure is estimated with the perturbation theory and the moment method. The system reliability of the structural system is firstly simplified by adopting the probabilistic network evaluation technique , and then is analysed with consideration of the correlation between each component failure. The Archimedean copula function is served as the modelling tool to establish the copula-based joint distribution function. The parameter sensitivity analysis is realized by matrix differential technology. The results of the numerical examples serve as testimony to the effectiveness of the proposed method and should be useful when considering the reliability problem of structural systems with correlated failure modes.

Acknowledgement

The work is supported by National Natural Science Foundation of China (51405490), A Project Funded by the Priority Academic Program Development of Jiangsu Higher Education Institutions (PAPD) and the Fundamental Research Funds for the Central Universities (2013QNA23).

References

1. Bichon B J, McFarland, J M, Mahadevan S. Efficient surrogate models for reliability analysis of systems with multiple failure modes. Reliability Engineering & System Safety 2011; 96(10): 1386-1395, http://dx.doi.org/10.1016/j.ress.2011.05.008.
2. Bücher A, Dette H, Volgushev S. A test for Archimedeanity in bivariate copula models. Journal of Multivariate Analysis 2012; 110(9): 121-132, http://dx.doi.org/10.1016/j.jmva.2012.01.026.
3. Cardoso J B, de Almeida J R, Dias J M, et al. Structural reliability analysis using Monte Carlo simulation and neural networks. Advances in Engineering Software 2008; 39(6): 505-513, http://dx.doi.org/10.1016/j.advengsoft.2007.03.015.
4. Corbella S, Stretch D D. Simulating a multivariate sea storm using Archimedean copulas. Coastal Engineering 2013:76(6): 68-78, http://dx.doi.org/10.1016/j.coastaleng.2013.01.011.
5. Chang Y, Mori Y. A study on the relaxed linear programming bounds method for system reliability. Structural Safety 2013; 41(2): 64-72, http://dx.doi.org/10.1016/j.strusafe.2012.11.002.
6. Eryilmaz S. Estimation in coherent reliability systems through copulas. Reliability Engineering & System Safety 2011; 96(5): 564-568, http://dx.doi.org/10.1016/j.ress.2010.12.024.
7. Hofert M. Sampling Archimedean copulas. Computational Statistics & Data Analysis 2008; 52(12): 5163-5174, http://dx.doi.org/10.1016/j.csda.2008.05.019.
8. Hohenbichler M, Rackwitz R. First-order concepts in system reliability. Structural Safety 1983; 1(3):177-88, http://dx.doi.org/10.1016/0167-4730(82)90024-8.
9. Kang W H, Song J, Gardoni P. Matrix-based system reliability method and applications to bridge networks. Reliability Engineering & System Safety 2008; 93(11):1584-1593, http://dx.doi.org/10.1016/j.ress.2008.02.011.
10. Katsuya M, Shinji N, Kazuhiro I, Masataka Y, Nozomu K. Reliability-based structural optimization of frame structures for multiple failure criteria using topology optimization techniques. Structural and Multidisciplinary Optimization 2006; 32(4): 299-311, http://dx.doi.org/10.1007/s00158-006-0039-5.

11. Li C, Zhang Y, Wang Y. Gradual reliability and its sensitivity analysis approach of cutting tool in invariant machining condition and periodical compensation. Jixie Gongcheng Xuebao(Chinese Journal of Mechanical Engineering), 2012; 48(12): 162-168, http://dx.doi.org/10.3901/JME.2012.12.162.
12. Lemaître P, Sergienko E, Arnaud A, et al. Density modification-based reliability sensitivity analysis[J]. Journal of Statistical Computation and Simulation, 2015; 85(6): 1200-1223, http://dx.doi.org/10.1080/00949655.2013.873039.
13. Lu H, He Y H, Zhang Y M. Reliability-Based robust design of Mechanical Components with Correlated Failure Modes Based on Moment Method. Advances in Mechanical Engineering 2014; 2014(6): 1-17.
14. Lu H, Zhang Y M. Reliability-Based Robust Design for Structural System with Multiple Failure Modes. Mechanics Based Design of Structures and Machines 2011; 39(4): 420-440 ,http://dx.doi.org/10.1080/15397734.2011.560541.
15. Ma H F, Ang A H S. Reliability Analysis of Redundant Ductile Structural Systems. Urbana Champaign: University of Illinois, 1981.
16. Naess A, Leira B J, Batsevychc O. System reliability analysis by enhanced Monte Carlo simulation. Structural Safety 2009; 31(5): 349-355, http://dx.doi.org/10.1016/j.strusafe.2009.02.004.
17. Nelsen R B. An introduction to copulas. Springer Verlag, 2006.
18. Pfeifer D, Nešlehová J. Modeling dependence in finance and insurance: the copula approach. Blätter der DGVFM, 2003; 26(2): 177-191, http://dx.doi.org/10.1007/BF02808371.
19. Song J H, Kiureghian A D. Bounds on system reliability by linear programming. Journal of Engineering Mechanics 2003; 129(6): 627-636, http://dx.doi.org/10.1061/(ASCE)0733-9399(2003)129:6(627).
20. Sklar A. Fonctions de répartition à n dimensions et leurs marges. Publications de l'Institut de Statistique de l'Université de Paris, 1959; 8: 229-231.
21. Sklar A. Random variables, joint distribution functions, and copulas. Kybernetika 1973; 9: 449-460.
22. Tang X S, Li D Q, Zhou C B, Phoon K K, Zhang L M. Impact of copulas for modeling bivariate distributions on system reliability. Structural Safety 2013; 44(9):80-90, http://dx.doi.org/10.1016/j.strusafe.2013.06.004.
23. Zhao Y G, Ang A H S. System reliability assessment by method of moments. Journal of Structural Engineering 2003; 129(10): 1341-1349, http://dx.doi.org/10.1061/(ASCE)0733-9445(2003)129:10(1341).
24. Zhang Y M, Yang Z. Reliability-based sensitivity analysis of vehicle components with non-normal distribution parameters. International Journal of Automotive Technology 2009; 10(2): 181-194, http://dx.doi.org/10.1007/s12239-009-0022-4.
25. Zhang F, Lu Z Z, Cui L J, Song S F. Reliability Sensitivity Algorithm Based on Stratified Importance Sampling Method for Multiple Failure Modes Systems. Chinese Journal of Aeronautics 2010; 23(6): 660-669, http://dx.doi.org/10.1016/S1000-9361(09)60268-5.

Lu HAO
College of Mechanical and Electrical Engineering
China University of Mining and Technology (Nanhu Campus), No.1 Daxue Road, Xuzhou, China. Postcode: 221116

Jiangsu Key Laboratory of Mine Mechanical and Electrical Equipment
China University of Mining & Technology
Xuzhou, China. Postcode: 221116

Zhu ZHENCAI
College of Mechanical and Electrical Engineering
China University of Mining and Technology (Nanhu Campus), No.1 Daxue Road, Xuzhou, China. Postcode: 221116

E-mail: haolucumt@163.com; zhulscumt@163.com

Article citation info:
WOCH M, KURDELSKI M, MATYJEWSKI M. Reliability at the checkpoints of an aircraft supporting structure. Eksploatacja i Niezawodnosc – Maintenance and Reliability 2015; 17 (3): 457–462, http://dx.doi.org/10.17531/ein.2015.3.18.

Marta WOCH
Marcin KURDELSKI
Marek MATYJEWSKI

RELIABILITY AT THE CHECKPOINTS OF AN AIRCRAFT SUPPORTING STRUCTURE

NIEZAWODNOŚĆ W PUNKTACH STRUKTURY NOŚNEJ STATKÓW POWIETRZNYCH*

For complex systems, such as the structure of an aircraft, the implementation of prognostic and health management techniques can effectively improve system performance. This paper presents some recent results of research on risk assessment for aircraft structures and intends to show the procedures of reliability calculation for a point of aircraft structure as an object under investigation. In this paper, the ways to determine failure rate and failure probability at the location of interest have been presented based on the example of the PZL-130 TC II ORLIK aircraft structure. The results can be applied to optimize the process of aircraft flight authorization, while ensuring safety during operations.

***Keywords**: aircraft structure, reliability testing, crack propagation.*

W przypadku złożonych systemów, jakim jest struktura samolotu wdrożenie technik prognostycznych oraz zarządzania czasem zdatności do eksploatacji może skutecznie poprawić wydajność systemu. Celem publikacji jest przedstawienie metody oceny niezawodności konstrukcji lotniczych oraz odpowiedniej procedury obliczeń wraz z ostatnimi wynikami badań. W niniejszej pracy określono chwilową intensywność uszkodzeń oraz prawdopodobieństwo awarii w wybranych miejscach struktury samolotu PZL-130 TC II ORLIK. Uzyskane wyniki mogą być zastosowane do optymalizacji procesu dopuszczenia statków powietrznych do lotów, przy jednoczesnym zapewnieniu bezpieczeństwa ich eksploatacji.

***Słowa kluczowe**: struktura nośna samolotu, badania niezawodnościowe, propagacja pęknięć.*

1. Introduction

This contribution presents a reliability prediction as well as sustainability methods for selected areas of the airframe in terms of fatigue processes and the aging process. Supporting structure may be classified as an element with a high correlation between the airworthiness parameter values and adequate fatigue life of the aircraft [27].

One of the most important issues associated with aircraft maintenance is analysing durability of their structure components [10, 20]. The previous experience in operation confirms that exhaustion of aircraft service life cannot be unambiguously identified with its unserviceability for further, reliable flights. Not always does the service life exhaustion result in the loss of aircraft technical condition and in the reliability parameters exceedance. The inadequacies of the traditional (service life) approach to aircraft maintenance used were the reason for developing new methods for assessing the durability of the aircraft structure, which are presented in the new study [21, 22].

The presented mathematical model is implemented with the use of specialized software known as PRobability Of Fracture (PROF) [13] and is commonly used by United States Air Force [4, 6]. National Research Council Canada [12, 24] uses a similar mathematical approach for reliability analysis of aircraft structure in its ProDTA (PRObabilistic Damage Tolerance Anylisis) software.

The presented method and the research results make it possible to extend aircraft service life. Discussed procedures are not performed for aircraft owned by Polish Air Force, particularly for PZL-130 TC II ORLIK aircrafts. The exceptions are the F-16, for which such analyses are performed by Lockheed Martin.

2. The reliability prediction method of support structure points

Failure rate function [5, 9] is defined as the limit, if it exists, of the ratio of the conditional probability that the instant of time, T, of a failure of an item falls within a given time interval $t+\Delta t$ and the length of this interval, Δt, when Δt leads to zero, given that the item is in an up state at the beginning of the time interval, which can be described as:

$$\lambda(t) = \lim_{\Delta t \to 0^+} \frac{P\{t < T \le t + \Delta t \mid T > t\}}{\Delta t} \tag{1}$$

where T is a continuous positive random variable of device operation time.

If T has a density f(t) and the distribution F(t) equation (1) will take the form [1÷3]:

$$\lambda(t) = \frac{f(t)}{1 - F(t)} \tag{2}$$

where $F(t) = \int_0^t f(u)du = P\{T \le t\} = 1 - P\{T > t\}$.

Given the failure rate *λ(t)* the life distribution can be calculated by the equation:

(*) Tekst artykułu w polskiej wersji językowej dostępny w elektronicznym wydaniu kwartalnika na stronie ***www.ein.org.pl***

$$F(t) = 1 - e^{-\int_0^t \lambda(x)dx} \tag{3}$$

In the aircraft reliability analysis to determine the probability of failure two independent events are taken into consideration. The failure can be recognized as a state in which:

- crack length exceeds a pre-defined size a_{cr},
- stress cycle at a crack size smaller than a_{cr} that produces a stress intensity factor K which exceeds the fracture toughness K_c is encountered.

Failure rate at the critical airframe location is calculated using the equation:

$$\lambda(t) = \lambda_1(t) + \lambda_2(t) \tag{4}$$

where: $\lambda_1(t)$ – failure rate resulting from exceeding the allowable crack length a_{cr},

$\lambda_2(t)$ – failure rate resulting from exceeding the allowable stress in flight.

Based on the knowledge of the failure rate *λ(t)* failure function can be calculated using the equation (3) for a single location.

Function *g* which defines the relation between stress intensity factor, stress, and crack size can be expressed as:

$$K / \sigma = \sqrt{\pi a}\beta(a) = g(a) \tag{5}$$

where: σ – stress,

β(a) –geometry correction factor specified for a cracks length *a*.

For the material under consideration and a specific location in the aircraft supporting structure, the critical crack size a_{cr} is a value corresponding to a mean value of the fracture toughness $\overline{K_c}$ and the mode parameter of the stresses occurring in flight for the place under consideration, which can be mathematically represented as:

$$a_{cr} = g^{-1}\left(\frac{\overline{K_c}}{\tilde{\sigma}}\right) \tag{6}$$

where g^{-1} is the inversion of function (5).

The probability of component failure during a time period $(0,t)$ caused by exceeding the allowable crack length can be described as:

$$F_1(t) = 1 - F_A(a^*(t_{cr} - t)) \tag{7}$$

where: F_A – the distribution function of crack length at the start of the interval,

$a^*(t)$ – the crack growth function corresponding to the time of failure $t_f = t_{cr} - t$,

t_{cr} – the time, when crack size will reach the predefined size a_{cr}.

Failure rate associated with cracks growing to a_{cr} is then given by (2):

$$\lambda_1(t) = \frac{f_1(t)}{1 - F_1(t)} \tag{8}$$

The probability that a peak load will cause a failure during a flight at time *t* for cracks that are less than a_{cr} can be calculated as:

$$POF(t) = \int_0^\infty \int_0^{a_{cr}} \hat{H}(\sigma_{cr}(a,k_c)) f_A(a)da \cdot f_{K_c}(k_c)dk_c \tag{9}$$

where: $\hat{H} = 1 - H = P\{\sigma > \sigma_{cr} = K_c / \beta(a)\sqrt{\pi a}\}$ is the exceedance probability for the peak load per flight,

$f_A(a)$ is the density of the flaw size distribution at time interval *t*,

$f_{K_c}(k_c)$ is the density for fracture toughness,

POF(*t*) is the probability that a peak load will cause a failure during a flight at time *t*.

Failure rate due to a large stress can then be approximated by:

$$\lambda_2(t) = \frac{POF(t)}{\overline{t}} \tag{10}$$

where $\overline{t}$ is the average fight length.

3. Reliability analysis - input data

Reliability analysis has been performed for a possible crack in the area of a wing in the flange of the main spar, between ribs No. 5 and 6 [11, 18]. The defect was classified as HTC (Hole Through Thickness Crack) [6] (shown in Fig. 1).The finite element method (FEM) model study area is shown in Fig. 1.

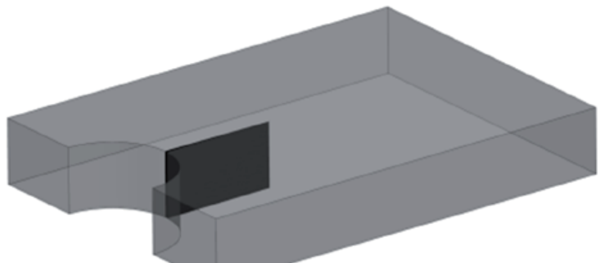

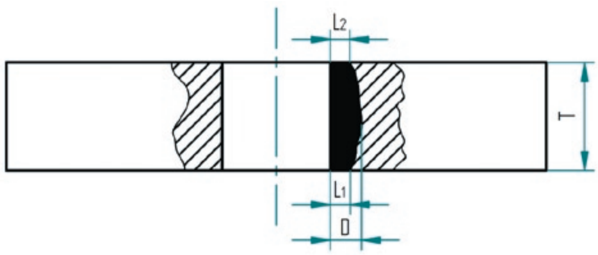

Fig. 1. HTC (Hole Through Thickness Crack) type damage on the graphic scheme

The parameter values which determine the normal distribution of K_{Ic} parameter which defines the fracture toughness for compact samples made of alloy 2024-T351 RCT type notched across the grain (L-T reference directions) are as follows:

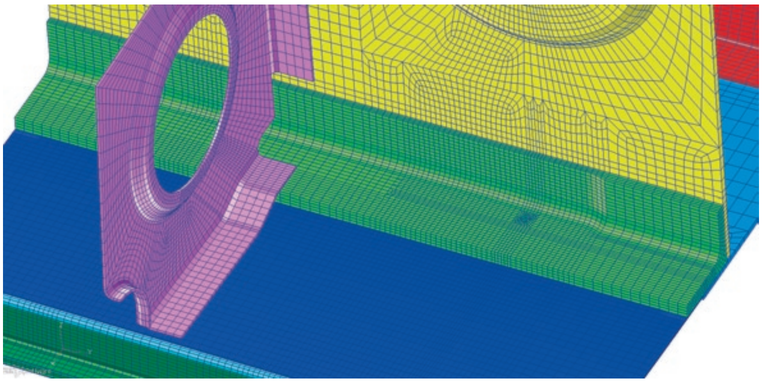

Fig. 2. FE model of the probable crack location [15]

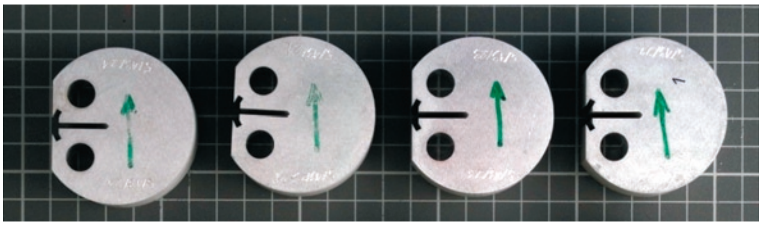

Fig. 3. RCT samples before testing [16]

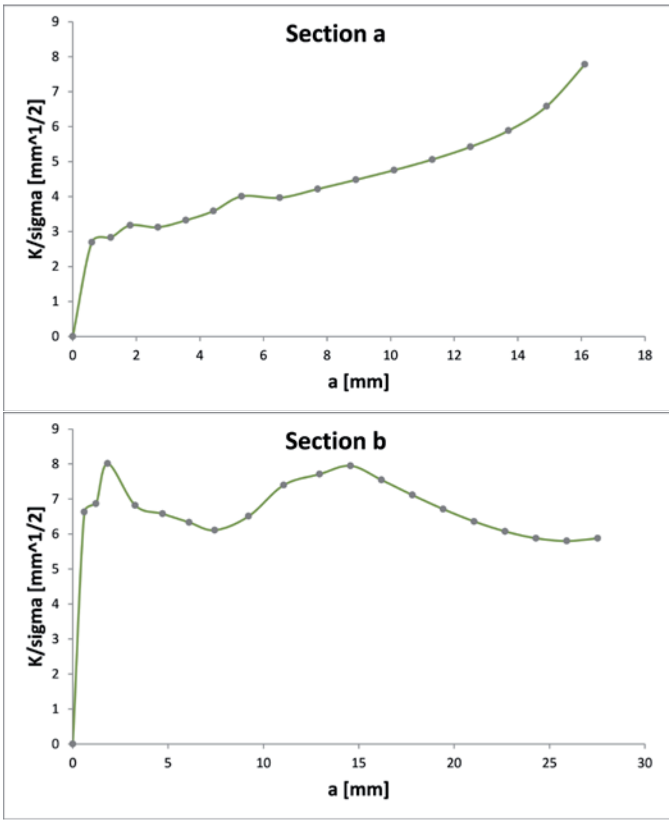

Fig. 4. K/σ versus a curve

- mean value – 36.75 $MPa\sqrt{m}$,
- standard deviation – 0.247 $MPa\sqrt{m}$ [16].

The static tensile tests were conducted in the Air Force Institute of Technology (AFIT) Laboratory for Materials Strength Testing [7, 16] with the use of material testing system MTS 810.23. The scope of the research included: a static tensile testing, the study of fatigue crack growth rate, material's resistance to fracture, low-cycle and high-cycle fatigue testing (HCF & LCF). The scope of the research allowed to complete and verify material information used in the Orlik airframe in the extent regarded by the service life assessment program (SEWST).

FEM analysis was performed with the use of MSC Software [15]. Based on the FEM analysis results the relation between stress intensity factor, stress *(K/σ)*, and crack size *a* has been established.

The crack has been divided into two sections due to the fact that calculation of the crack propagation in the AFGROW software can only be performed for a geometry that contains no holes. Figure 2 shows crack propagation sections and directions.

Based on flight data records covering the period from the beginning of the service of Orlik aircraft in the Polish Air Force, the average length of the flight has been determined to be 43 minutes.

Based on the AFGROW software analysis results the obtained shape of the crack propagation curve *a(t)* is shown in black on Fig. 5. Green colour indicates an adequate fit to the equation (11). Red curves indicate extrapolation with the use the exponential function:

$$a(t) = a_0 e^{bt} \tag{11}$$

In the calculation a simple *through crack* propagating from one side of the model was used. The relation between *β(a)* and crack size as well as the load spectrum based on strain gauge measurements were used. Material properties actual for 2024-T351 aluminum alloy such as Young's modulus (*E*) and K_{IC} were established based on tests carried out in the laboratory [16]. Model data used in calculations are presented in the Table 1.

Table 1. Data used in crack propagation calculations [15]

Parameter	Section ***a***	Section ***b***
Length	0,01731 [m]	0,02915 [m]
Thickness	0,005 [m]	0,0025 [m]
Initial crack length	0,0006 [m]	0,00061 [m]
K_{IC}	36,75 [MPa√m]	36,75 [MPa√m]
E	72 000 [MPa]	72 000 [MPa]
Stress Multiplication Factor	0,072 [-]	0,072 [-]

The distribution of maximum stress peak in a flight is modelled in terms of a Gumbel distribution of extreme values and is based on flight research results:

$$H(\sigma) = \exp\left[-\exp\left(-\frac{\sigma - B}{A}\right)\right] \tag{12}$$

where: *σ* – stress,
A – Gumbel distribution parameter determining the slope of the cumulative distribution,
B – Gumbel distribution parameter determining the 37th percentile of maximum stress on flights.

In order to obtain the *A* and *B* parameters of Gumbel distribution, correlation between maximum values of vertical load factor n_z and stress measured by strain gauge was verified. Data from 285 research flights with measuring-recording equipment KAM 500 were analysed. The next step of the calculation was to obtain a transfer func-

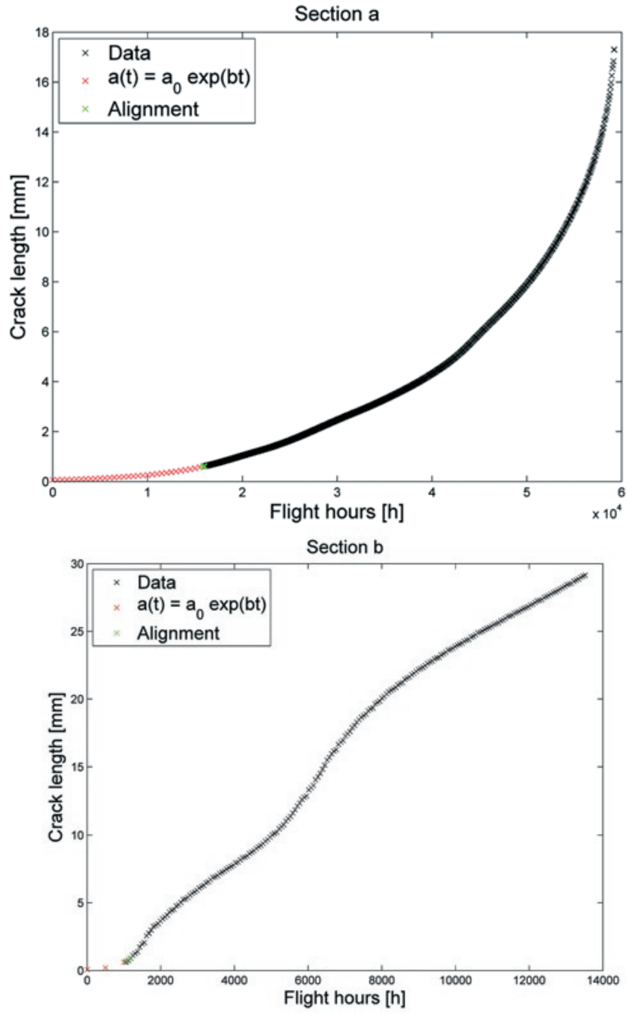

Fig. 5. Crack propagation curve

tion between vertical load factor n_z and stress. The algorithm of linear approximation that applies the method of least squares or non-linear Levenberg-Marquardt regression algorithm were used for calculation. Stress resulting from the global FE model calculations for n_z=1 in the region of interest was extracted. Coefficients of the transfer function and maximum overload of vertical load factor n_z were obtained from on-board flight recorders mounted on PZL-Orlik TC-I and TC-II aircrafts from the beginning of operation in 2010 were used for calculation. At that time more than 40 000 flights were performed. Stress values have been approximated to the Gumbel distribution with coefficients:

A = 8.6 [MPa],

B = 71.9 [MPa],

using a fitting for flight, in which vertical load factor n_z>4.6.

The initial crack size distribution was adopted pursuant to the article [7] (fig. 6).

Data from literature have been approximated using a Weibull distribution:

$$F_A(a) = 1 - e^{-(a/\lambda)^k} \tag{13}$$

where: λ – scale parameter,

k – shape parameter.

The initial crack size distribution shape is close to the Weibull distribution function, which was justified by Yang and Manning [19, 26].

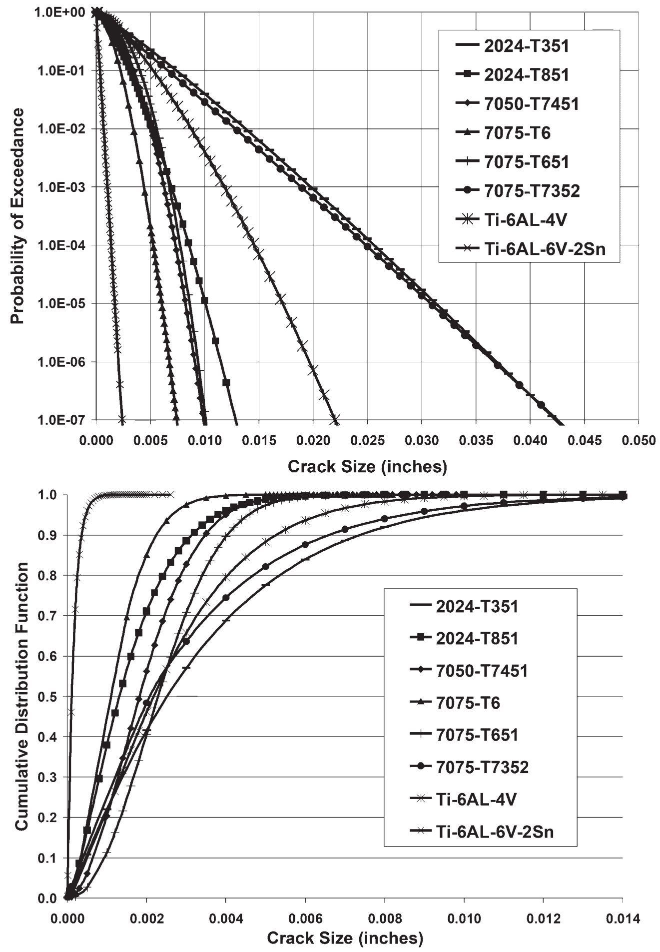

Fig. 6. Inverse cumulative distribution and cumulative distribution function for equivalent initial flaw sizes (EIFS) [7]

Following parameters were assumed for calculations: λ = 0.0891 mm, k = 1.1204.

4. Reliability analysis – result

For the crack section b, it is assumed that the beginning of crack propagation will be a time instant in which a section is damaged. For the military aircraft it is recommended to determine the event as unlikely (improbable). For the airframe it can be assumed that defect occurrence may not be experienced in the life of an item, if the failure rate is lower than 10^{-6} during aircraft service life. Events unlikely, but possible to occur in the life of a component during service life of the aircraft have failure (probability of occurrence) less than 10^{-3} but greater than or equal to 10^{-6} (Table 2). Another important criterion for events qualification is the failure probability. If the value of *F(t)* exceeds 10^{-3} admission to the further exploitation without schedule necessary inspections should be taken under consideration[23, 25]. Appropriate probability levels have been specified in the figure 7 of

Table 2. Probability levels [14]

Description	Level	Individual Aircraft	Fleet
Remote	D	Unlikely, but possible to occur in the life of an item during service life of the aircraft. Probability of occurrence less than 10^{-3} but greater than or equal to 10^{-6}	Unlikely but can reasonably be expected to occur
Improbable	E	So unlikely, it can be assumed that the occurrence will not be experienced in the life of an item. Probability of occurrence less than 10^{-6}	Unlikely to occur, but possible

failure rate. The figures 7 i 8 present charts of failure rate and failure probability of the area in aircraft PZL-130 TC II Orlik supporting structure.

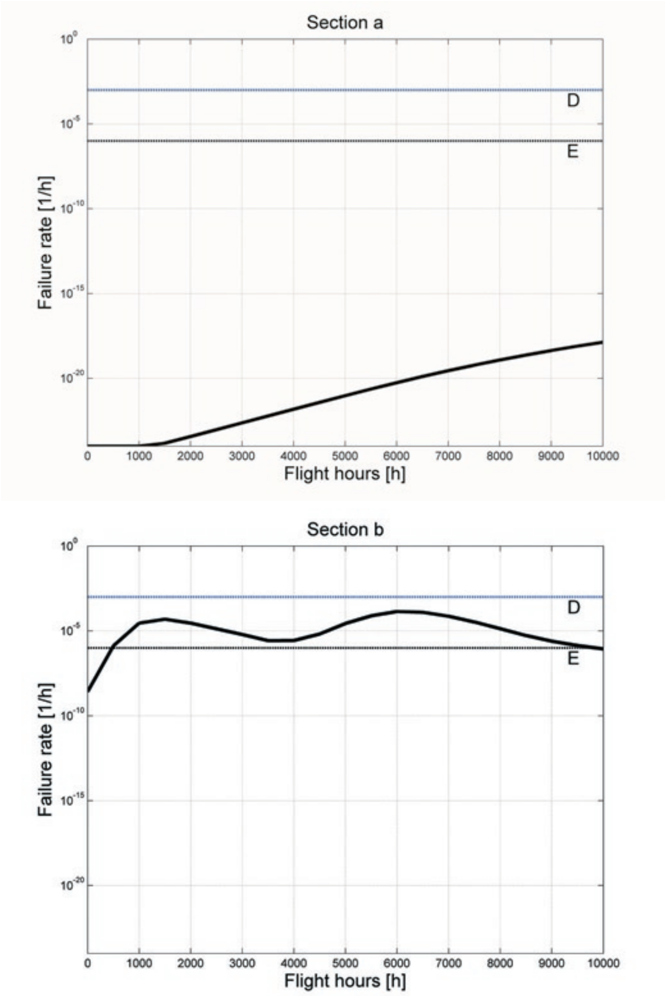

Fig. 7. Failure rate

5. Discussion of the results

The obtained simulation results indicate that a crack occurrence in the flange of main spar, between ribs No. 5 and 6 for 10 000 hours of service life can be described as improbable, since the probability of fracture, provided that the damage did not occur previously is less than 10^{-6} during the aircraft service life period. The shape of the obtained curve shown in Fig. 7a is due to a moderate increase of the crack propagation curve in the initial periods of aircraft service life and a relatively low stress value at the considered checkpoint with respect to the K/σ versus *a* curve. On the assumption that the section located above the hole will start to propagate at a time when the previous section, located under the hole fails, the probability of failure in the next flight hour significantly increases. The most important factor influencing the failure rate of section b is the crack propagation rate. This damage can be described as unlikely (remote), since the probability of occurrence is less than 10^{-3} but greater than or equal to 10^{-6}.

For section b graphical comparison of relation between stress intensity factor, stress *(K/σ)*, and crack size *a* (Fig. 4) together with a failure probability (Fig. 8*b*) demonstrated a strong influence of geometry correction factor (*β(a)*) on the reliability analysis. The fact that (*K/σ*) curve for crack length of ~ 5 mm (Fig. 4*b*) is not monotonic suggests a failure rate decrease in about 3 000 flight hours. Decrease

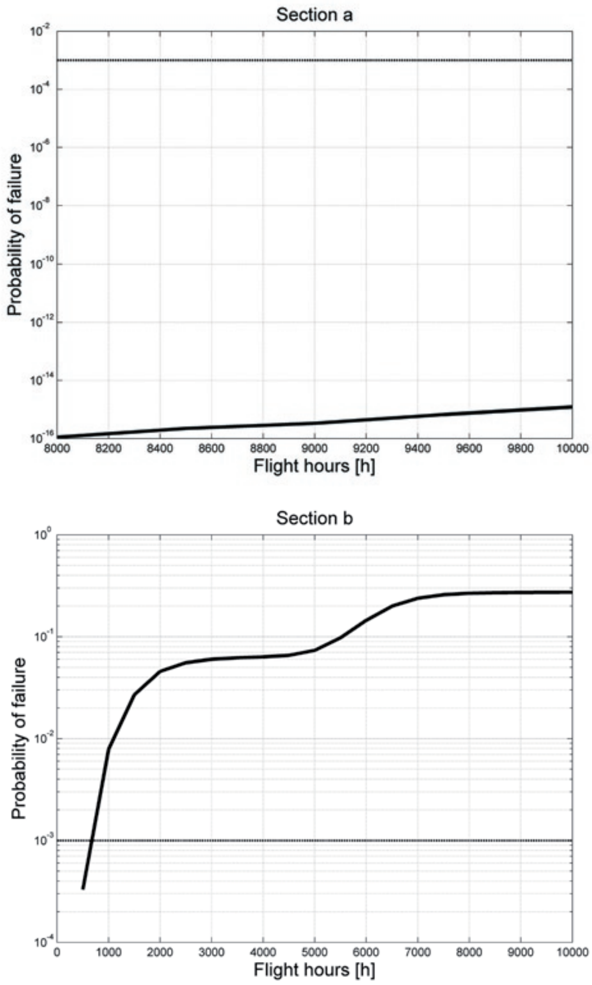

Fig. 8. Failure probability

in *λ(t)* function contributes to the slower failure probability increment within the period of 2 000 ÷ 5 000 flight hours.

6. Conclusions

The presented analyses have confirmed that it is possible and also advisable to determine the reliability at the points of the selected critical airframe locations. Approach of this kind while monitoring failures allows to make optimal decisions on flight approval, while ensuring the safety of an aircraft during operation. In addition, it was possible to specify the most important input parameters that have the greatest impact on the final assessment of the reliability at the checkpoints of airframe critical locations.

Performed research suggests that in the case of supporting structure components , essential for reliability are the parameters that define the crack propagation rate and structural determinants expressed by the dimensionless geometry correction factor (independent of the applied load) which specifies the state of stress in the crack tip and takes into account the shape of the tested element.

In the future an in-depth numerical methods study for reliability assessment is planned and implementation of the presented methodology on in-house software. Such an approach will enable time-saving and will provide accuracy of results through the use of effective optimization algorithms together with implementation in low-level languages.

References

1. Babiarz B. An introduction to the assessment of reliability of the heat supply systems. International Journal of Pressure Vessels and Piping 2006; 4(83): 230-235, http://dx.doi.org/10.1016/j.ijpvp.2006.02.002.
2. Babiarz B. Chudy-Laskowska K. Forecasting of failures in district heating systems. Engineering Failure Analysis 2015; In Press, Corrected Proof, http://dx.doi.org/10.1016/j.engfailanal.2014.12.017.
3. Babiarz B. Risk assessment in heat supply system. Safety and reliability: Methodology and Applications 2014; 513-520.
4. Babish C. Application of risk & reliability analysis for fatigue cracking in F-16 aircraft structure. Technical report, 2010 F-16 ASIP.
5. Bedford T. Cooke R. Probabilistic Risk Analysis Foundations and Methods. Cambridge: Cambridge University Pressn, 2001, http://dx.doi.org/10.1017/CBO9780511813597.
6. Dixon B. Molent L. Ex-Service F/A-18 Centre Barrel Fatigue Flaw Identification Test Plan. Melbourne: DSTO Platforms Sciences Laboratory, 2003.
7. Gallagher J. Babish C. Malas J. Damage Tolerant Risk Analysis Techniques for Evaluating the Structural Integrity of Aircraft Structures. 11th International Conference on Fracture 2005; 1: 71-76.
8. Jankowski K. Reymer P. Simulating crack propagation of the selected PZL-130 ORLIK TC-II aircraft structural component. Fatigue of Aircraft Structures 2015, In Press.
9. Koucky M. Valis D. Reliability of sequential systems with a restricted number of renewals. Proceedings and Monographs in Engineering, Water and Earth Sciences 2007; 1845-1849.
10. Leski A. An Algorithm of Selecting a Representative Load Sequence for a Trainer. 2nd International Conference on Engineering Optimization 2010; CD: 1-8.
11. Leski A. Reymer P. Kurdelski M. Development of Load Spectrum for Full Scale Fatigue Test of a Trainer Aircraft. ICAF 2011 Structural Integrity: Influence of Efficiency and Green Imperatives 2011: 573-584.
12. Liao M. Bombardier Y. Renaud G. Bellinger N. Cheung T. Development of advanced risk assessment methodologies for aircraft structures containing MSD/MED. ICAF 2009 Bridging the Gap between Theory and Operational Practice 2009: 811-837.
13. Miedlar P. Berens A. Hovey P. Boehnlein T. Loomis J. PRoF v3 PRobability Of Fracture Aging Aircraft Risk Analysis Update. Dayton: University of Dayton Research Institute, 2005.
14. MIL-STD-882E, Department of Defense, Standard Practice For System Safety 2012.
15. Podskarbi S. Leski A. Reymer P. Jankowski K. Kurdelski M. Stefaniuk M. Obliczenia stanu naprężenia oraz obliczenia szybkości wzrostu pęknięć dla CP z wykorzystaniem rzeczywistych widm obciążeń eksploatacyjnych. Sprawozdanie nr SP-58/31/2014. Warsaw: Air Force Institute of Technology, 2014.
16. Raport z badań nr 5/13. Raport z badania odporności materiału na pękanie. Warsaw: Air Force Institute of Technology, 2013.
17. Reymer P. Jankowski K. Kłysz S. Lisiecki J. Leski A. Crack propagation of the selected PZL-130 Orlik TC-II aircraft structural component based on laboratory test results. Proceedings of the Fourth Asian Conference on Mechanics of Functional Materials and Structures 2014, 181-184.
18. Reymer P. Leski A. Flight Loads Acquisition for PZL-130 ORLIK TCII Full Scale Fatigue Test. Fatigue of Aircraft Structures 2011; 3: 78-85, http://dx.doi.org/10.2478/v10164-010-0041-7.
19. Rudd J. Yang J. Manning S. Garver W. Durability Design Requirements and Analysis for Metallic Airframes. Design of Fatigue and Fracture Resistant Structures, ASTM STP 761, American Society for Testing and Materials l982; 133-151.
20. Tomaszek H. Jasztal M. Zieja M. A simplified method to assess fatigue life of selected structural components of an aircraft for a variable load spectrum. Eksploatacja i Niezawodnosc - Maintenance and Reliability 2011; 4: 29-34.
21. Tomaszek H. Jasztal M. Zieja M. Application of the Paris formula with m=2 and the variable load spectrum to a simplified method for evaluation of reliability and fatigue life demonstrated by aircraft components. Eksploatacja i Niezawodnosc – Maintenance and Reliability 2013; 4: 297-303.
22. Valis D. Koucky M. Zak L. On approaches for non-direct determination of system deterioration. Eksploatacja i Niezawodnosc - Maintenance and Reliability 2012; 1: 33-41.
23. Valis D. Vintr Z. Dependability of mechatronics systems in military vehicle design. Proceedings and Monographs in Engineering, Water and Earth Sciences 2006; 1703-1707.
24. Valis D. Vintr Z. Koucky, M. Contribution to highly reliable items' reliability assessment. Reliability, Risk and Safety: Theory and Applications 2010; 1-3: 1321-1326.
25. White P. Molent L. Barter S. Interpreting fatigue test results using a probabilistic fracture approach. International Journal of Fatigue 2005; 27: 752-767, http://dx.doi.org/10.1016/j.ijfatigue.2005.01.006.
26. Zieja M. Wazny M. A model for service life control of selected device systems. Polish Maritime Research 2014; 2(21): 45-49.
27. Żurek J. Models of team actions within the national rescue system. Journal of Konbin 2011; 4(20): 185-200.

Marta WOCH
Marcin KURDELSKI
Airworthiness Division
Air Force Institute of Technology
ul. Księcia Bolesława 6, 01-494 Warsaw, Poland
E-mail: marta.woch@itwl.pl, marcin.kurdelski@itwl.pl

Marek MATYJEWSKI
Division of Fundamentals of Machine Design
Warsaw University of Technology
ul. Nowowiejska 24, 00-665 Warsaw, Poland
E-mail: mmatyjew@meil.pw.edu.pl

Article citation info:
KILIKEVIČIENĖ K, SKEIVALAS J, KILIKEVIČIUS A, PEČELIŪNAS R, BUREIKA G. The analysis of bus air spring condition influence upon the vibration signals at bus frame. Eksploatacja i Niezawodnosc – Maintenance and Reliability 2015; 17 (3): 463–469, http://dx.doi.org/10.17531/ein.2015.3.19.

Kristina KILIKEVIČIENĖ
Jonas SKEIVALAS
Artūras KILIKEVIČIUS
Robertas PEČELIŪNAS
Gintautas BUREIKA

THE ANALYSIS OF BUS AIR SPRING CONDITION INFLUENCE UPON THE VIBRATION SIGNALS AT BUS FRAME

ANALIZA WPŁYWU STANU TECHNICZNEGO RESORA PNEUMATYCZNEGO AUTOBUSU NA SYGNAŁY DRGAŃ W RAMIE AUTOBUSU

The paper analyses the spread of vibration intensity through the bus frame mechanical structure. The research has been completed upon application of the theory of covariance functions. Results of measuring the intensity of vibrations at fixed bus framepoints were recorded on the time scale in the form of data arrays (matrixes). The authors have completed the estimation of covariance functions by measuring the intensity of vibrations between the arrays of digital results and auto-covariance functions of single arrays upon changing the quantization interval on the time scale. The research results enable to define if the solidity of bus frame is disordered and to assess the technical condition of pneumatic suspension considering the vibration of frame points. Dangerous zones of bus suspension and reliability level of bus exploitation can be determined by application of these results.

Keywords: *pneumatic suspension, covariance function, cross-covariance, quantization interval.*

W pracy przeprowadzono analizę rozkładu intensywności drgań w mechanicznej konstrukcji ramy autobusu. Badania prowadzono z zastosowaniem teorii funkcji kowariancji. Wyniki pomiaru intensywności drgań w ustalonych punktach ramy autobusu rejestrowano na skali czasu, w postaci tablic danych (matryc). Funkcje kowariancji obliczano porównując natężenie drgań pomiędzy tablicami wyników cyfrowych, zaś funkcje auto-kowariancji pojedynczych tablic obliczano po zmianie przedziału kwantyzacji w skali czasowej. Wyniki badań pozwalają na określenie, czy zaburzona została stabilność struktury ramy autobusowej oraz umożliwiają ocenę stanu technicznego zawieszenia pneumatycznego na podstawie drgań w określonych punktach ramy. Wyniki te można wykorzystać do określenia niebezpiecznych stref zawieszenia autobusowego oraz poziomu niezawodności pracy autobusu.

Słowa kluczowe: *zawieszenie pneumatyczne, funkcja kowariancji, kowariancja wzajemna, przedział kwantyzacji.*

1. Introduction

Pneumatic suspension, especially air springs, are widely used in the automotive industry as the main components in suspension systems for buses, because they possess advantages such as a consistent structure, adjustable resilient, continuous controlling of the body bottom level from the ground, reasonable guiding effects and convenience in maintenance. Nevertheless, bus exploitation specialists keep searching for new innovative methods and actions to simplify the technical inspection of bus air spring and body frame solidity. The aim of these investigations is to ensure the reliability and the passenger comfort of transportation by a bus. Reducing the time and cost of the bus entire maintenance is possible by applying a non-destructive testing.

The temporal dependence structure of a stationary stochastic process is characterised by the auto-covariance function, or equivalently by its Fourier transform, the spectral density function. Data reconciliation, first introduced by Kuehn and Davidson [10], is a model based filtering method that applies simple process models to improve the reliability and precision of measured variables. Under favourable observation conditions, data reconciliation also allow the estimation of unmeasured process variables. These abilities are valuable for process industries since in many practical cases strategic variables are only measured with limited precision or simply not measured because of technical or economic constraints. Data reconciliation has been applied to a large number of processes as summarized by Mah [11], Narasimhan and Jordache [12]. Other topics are related to data reconciliation, such as sampling error and reconciliation criterion weighing factor evaluation [15], reconciled value accuracy evaluation [6], use of reconciled values to calculate and display plant performance indices, such as concentrate grade and recovery.

The reconciliation of process measurements subject to linear constraints involves finding the minimum weighted sum of squares of adjustments to the measurements. Linear data reconciliation by maximizing the information entropy to obtain probability distributions of the data with the minimum incorporation of prior knowledge was reformulated in the paper [3]. Two cases are presented, first with only the bounds on the data being specified and second with the variance-covariance matrix of the data being specified additionally. The first case provides a means of performing data reconciliation in the absence of information on the variance-covariance matrix of the data. In the second case, reconciliation using maximum likelihood is formally identical to the conventional least-squares solution. The least-prejudiced probability distribution is a truncated normal distribution, which for reasonably precise data essentially coincides with the multivariate normal distribution.

Different data reconciliation techniques have been proposed on the basis of various assumptions concerned with the process dynamics and depending on the subsequent application of the reconciled data. Steady-state data reconciliation is largely used to estimate the underlying average regime of a plant in applications such as reduction accounting, on process audit, or survey analysis. On the other hand, advanced process control, fault detection algorithms, and real-time optimization require the estimation of true dynamic states of a process, and are generally coupled to dynamic data reconciliation. Different approaches could be taken for dynamic data reconciliation. The filtering algorithm complexity depends on the selected process model. It could range from a simple mass conservation constraint sub-model to a complete causal dynamic model. The selection of the most appropriate algorithm results in a compromise between modelling efforts, required to develop and adapt the observer and improvement of estimate precision.

Researchers Puigjaner and Heyen have discussed the properties of steady-state observers and related problems such as steady-state detection, observation and redundancy analysis, as well as gross error detection [13].Researchers Poulin, Hodouin, and Lachance have studied steady-state data reconciliation applied on a real-time basis [14]. They have concluded that, despite the attractive simplicity of this solution, the estimate precision could be less than measurement precision itself depending on plant dynamics, which is not acceptable from practical point of view. Authors Vasebi, Poulin and Hodouin have proposed a modified stationary observer that takes advantage of the correlation of node imbalances to improve estimation performances [19].

Wavelet analysis has recently been recognized as a tool for important applications in time series, function estimation and image analysis. According to the development of recent wavelet methods, the fundamentals are not yet widely understood, and the guidance on their practical application is hard to find. Wavelets are an increasingly and widely used tool in many applications of signal and image processing. Applications in remote sensing include the combination of images of different resolutions, image compression, and the provision of edge detection methods. Researcher Horgan has reviewed the basic ideas of wavelets in order to represent the information in signals such as time series and images and described how the wavelet shrinkage is applied to smooth these signals [7]. This was illustrated by the application to a synthetic aperture radar image.

Researchers Ekstrom and McEwen have developed adaptive box-filtering algorithms to remove random bit errors (pixel values with no relation to the image scene) and smooth noisy data (pixels related to the image scene but with an additive or multiplicative noise component[5]. For both procedures they used the standard deviation of those pixels within a local box surrounding each pixel, hence they are adaptive filters. This technique effectively reduced speckle in radar images without eliminating fine details.

Cartographic compilation requires precision mensuration. The calibration of mensuration processes is based on the specific fiducial. External fiducial, around the exterior frame of the image, should be precisely measured to establish the overall sensor geometry [8]. Pre-marked ground points should be provided within the image ofa precise location of panels. Both types of registration marks must be known within the pixel space of a digitized image in order to be accurate with the feature extraction process with regards to delineated features. Classical mensuration of these targets requires that a photogrammetric view the image on a display and use pointing devices, such as a mouse, to pick exact points

Researchers Buchacz et al have decided to solve damping of vibration problems using piezo-electric sensors [2]. Siljak and Subasi investigated Fourier spectrum related properties of vibration signals in accelerated motor aging applicable for age determination[15]. Scientist Kosobudzki applied models to describe the way of loading in frequency domain, he proposed a new model for tracking loading of an element within the under-frame of high mobility wheeled vehicle [9].

The paper analyses the bus frame vibration digital signal estimates carried out upon application of random function theory.

2. A covariance model of vibration signal parameters

The theoretical model is based on the conception of a stationary random function while taking into account that errors of measuring the vibration parameters are random and of the same accuracy, i. e. the average error, the dispersion and covariance function of digital signals depends on difference between the arguments, i. e. on the quantization interval on the time scale.

For a theoretical model, we assumed that errors in measuring the intensity of digital signals of vibration field are random. In each column of the array of measuring the intensity of the vibration field, the trend of the measuring data of the column is eliminated. The interval of electromagnetic spread is used as one of the parameters.

We considered the random function (formed according to the arrays of measuring the intensity of the vibration field) as a stationary function (in a broad sense), i.e. its average value $M\{\phi(t)\} \to \text{const}$, and covariance function depend only on the difference of arguments – $K_\phi(\tau)$. The auto-covariance function of a single data array, or the cross-covariance function of two data arrays $K_\phi(\tau)$ is given below[17]:

$$K_\phi(\tau) = \frac{1}{T-\tau}\int_0^{T-\tau} \delta\phi_1(u)\delta\phi_2(u+\tau)\,du; \tag{1}$$

where, $\delta\phi_1(u), \delta\phi_1(u+\tau)$ – the centred values of vibration intensity measurements, u – vibration parameter, $\tau = k\cdot\Delta$– variable quantization interval, k– the number of measurement units, Δ – the value of a unit of measurement, T – time.

According to the available data on measurements of vibration parameters, the estimate $K'_\phi(\tau)$ of covariance function is calculated as follows:

$$K'_\phi(\tau) = K'_\phi(k) = \frac{1}{n-k}\sum_{i=1}^{n-k} \delta\phi_1(u_i)\delta\phi_2(u_{i+k}), \tag{2}$$

where n – total number of discrete intervals.

Formula (2) may be applied in theform of an auto-covariance function or a cross-covariance function. When the function is an auto-covariance one, the arrays $\phi_1(u)$ and $\phi_2(u+\tau)$ are parts of single arrays,whilethey are two different arrays in case the function is a cross-covariance one.

The estimate of a normed covariance function is given below:

$$R'_\phi(k) = \frac{K'_\phi(k)}{K'_\phi(0)} = \frac{K'_\phi(k)}{\sigma'^2_\phi}; \tag{3}$$

where σ'_ϕ – the estimate of the standard deviation of a random function.

For elimination of the trends of columns in the i-th digital array of measurements, the following formulas are applied:

$$\delta\phi_i = \phi_i - e\cdot\bar{\phi}_i^{\,T} = (\delta\phi_{i1},\ldots,\delta\phi_{im}); \tag{4}$$

where $\delta\phi_i$ – the i-th digital array of reduced values where a trend of column is eliminated; ϕ_i – the i-th array of the vibration intensity, e – a unit vector of the size ($n\times 1$); n – the number of lines in the i-th array, $\bar{\phi}_i$ – the vector of average values of columns in the i-th array, $\delta\phi_{ij}$ – the j-th column (vector) of the reduced values in the i-th array.

The vector of average values of columns in the i-th array is calculated according to the following formula:

$$\bar{\phi}_i^T = \frac{1}{n} e^T \cdot \phi_i = \frac{1}{n} \phi_i^T \cdot e. \tag{5}$$

A realization of the random function of the j-th column of the i-th array of vibration intensity in form of vectors is expressed as follows

$$\delta\phi_{ij} = \left(\delta\phi_{ij,1}, \ldots, \delta\phi_{ij,m}\right). \tag{6}$$

The estimation of the covariance matrix of the i-th array of wavelet intensity is expressed as follows:

$$K'\left(\delta\phi_i\right) = \frac{1}{n-1} \delta\phi_i^T \delta\phi_i. \tag{7}$$

The estimation of covariance matrix of two arrays of vibration intensity is written as follows:

$$K'\left(\delta\phi_i, \delta\phi_j\right) = \frac{1}{n-1} \delta\phi_i^T \delta\phi_j; \tag{8}$$

where the sizes of $\delta\phi_i, \delta\phi_j$ arrays should be the same.

The estimates $K'\left(\delta\phi_i\right)$ and $K'\left(\delta\phi_i, \delta\phi_j\right)$ of covariance matrixes are reduced into estimates of matrixes of correlation coefficients $R'\left(\delta\phi_i\right)$ and $R'\left(\delta\phi_i, \delta\phi_j\right)$ [18]:

$$R'\left(\delta\phi_i\right) = D_i^{-1/2} K'\left(\delta\phi_i\right) D_i^{-1/2}, \tag{9}$$

$$R'\left(\delta\phi_i, \delta\phi_j\right) = D_{ij}^{-1/2} K'\left(\delta\phi_i, \delta\phi_j\right) D_{ij}^{-1/2}, \tag{10}$$

where D_i, D_{ij} – the diagonal matrixes of members of principal diagonals in the estimates of covariance matrixes $K'\left(\delta\phi_i\right)$ and $K'\left(\delta\phi_i, \delta\phi_j\right)$, respectively.

The accuracy of the calculated coefficients of correlation is defined by the standard deviation σ_r, and the value of the latter is assessed according to the following formula:

$$\sigma_r = \frac{1}{\sqrt{n}}\left(1 - r^2\right). \tag{11}$$

where $n = 8000$,r – coefficient of correlation. The maximum value of the standard deviation is obtained when the value of r is close to zero and in this case $\sigma'_r \approx 0.01$; when $r \approx 0.5$ we obtain $\sigma'_r \approx 0.008$.

Estimates of the covariance functions of digital arrays of two vibration signals or the covariance functions of a single array are calculated upon transformation of ~~the~~ digital arrays into vectors. For processing the digital signals, discrete Fourier transform and the theory of wavelet functions were applied.

3. Results of the experiment and research

The data arrays of measuring the relevant parameters of vibration signals were formed in measuring vibrations of a bus body at certain points upon using vibration measuring and data processing „Bruel and Kjear“equipment (Fig. 1, side a) and seismic accelerometers 8344(Fig. 1, side b).

Fig. 1. The measuring equipment of vibration parameters: a) portable measurement data: processing, storage and control equipment „3660-D“ with DELL computer; b) accelerometer 8344.

Vectors of vibration signals were measured at the fixed points of the bus body and measurement data arrays of 4 vectors were obtained for each of two states. The signals were fixed in the interval τ_Δ=2,44140630$\cdot 10^{-4}$s for 4.0 s. Each vector of an array included n=16386 values of vibration signals.

Vibrations were measured at certain points of the bus body frame and suspension air springs (shown in Fig. 2) in quiescent state (i.e.

when the bus was not affected by external excitation), on starting the engine and upon shock excitation. The measurements were carried out in avertical position. The views of the measurement points are provided in Fig. 3. The measurement results are presented in Fig. 4, Fig. 5 and Fig. 6.

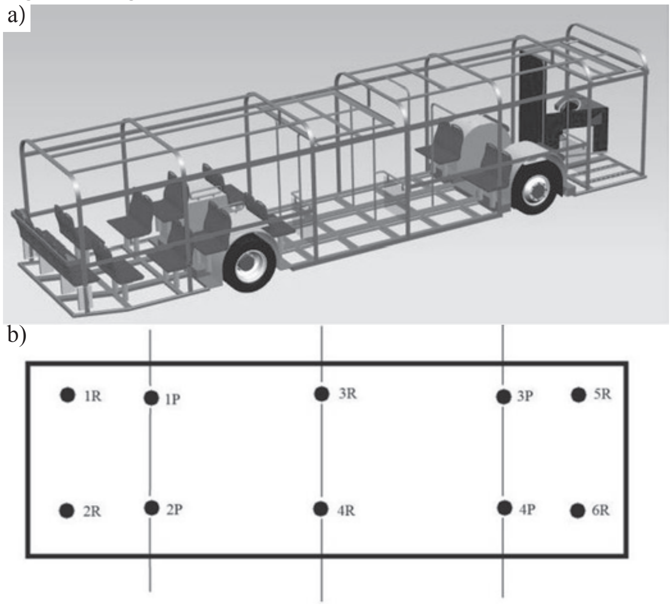

Fig. 2. The scheme of bus frame and pneumatic suspension vibration measurement points: a) the view of the body frame; b) the bottom view

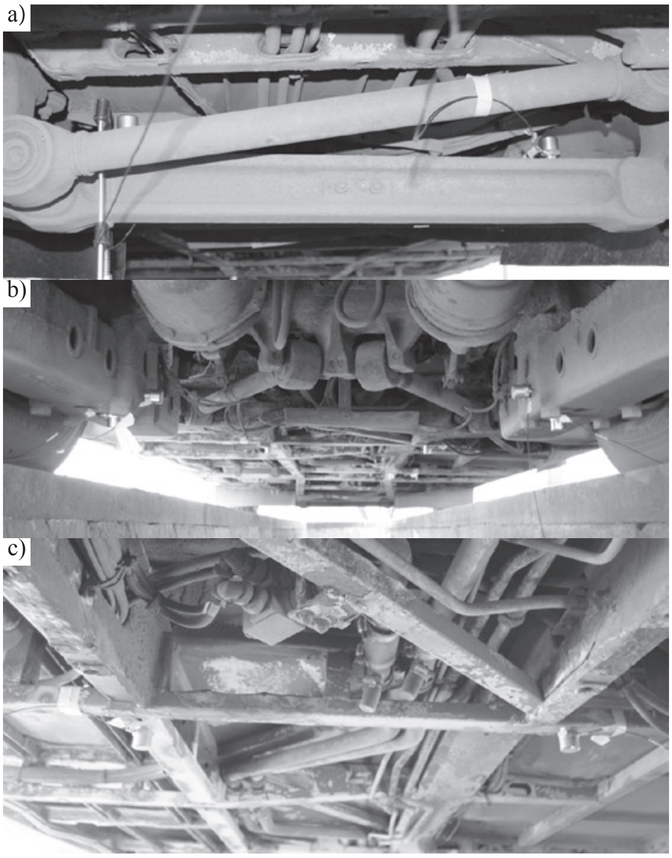

Fig. 3. The bus body frame and pneumatic suspension vibration measurement points: a) the points of the front suspension of the bus (Fig. 2, 1P and 2P); b) the points of the frame in the middle of the bus (Fig. 2, 3R and 4R); c) the points of the rear suspension of the bus (Fig. 2, 3P and 4P)

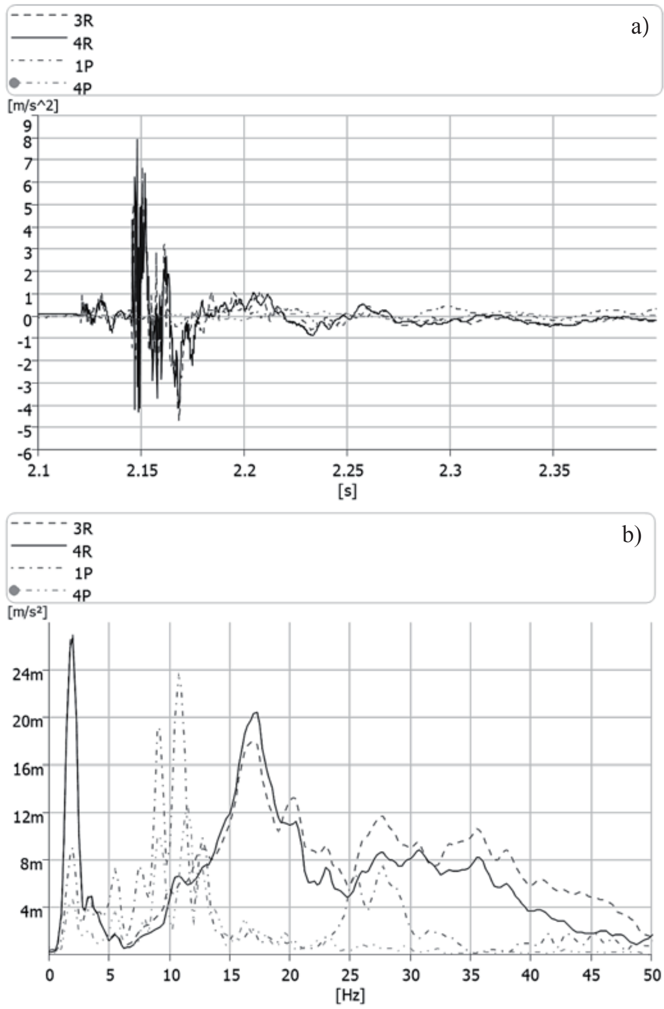

Fig. 4. The diagrams of time signal of absolute vibration vertical acceleration amplitude in the middle points of the frame (a) (Fig. 2 above, the points 3R and 4R) and the pneumatic suspension (b) (Fig. 2 above, the points 1P and 4P) upon shock excitation of the bus body centre(air pressure of 6.5 MPa).

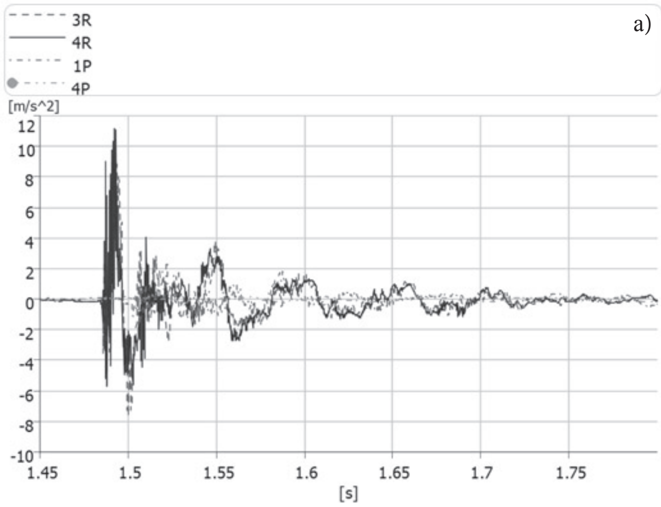

Fig. 5a.

The obtained results (Fig. 4 and Fig. 5 above) show that the air pressure increased by 1.5 MPa in the air springs causes reduction of the values of frequencies that correspond to the dominating amplitudes of acceleration on the frequency diagram from 2; 3.5; 5.5; 7.5;

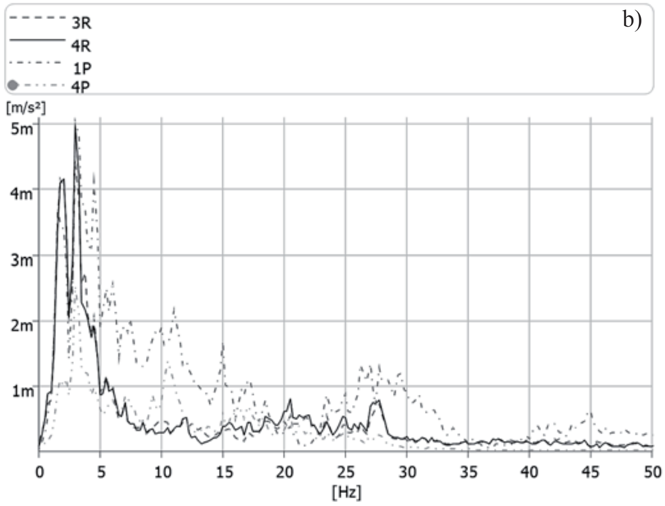

Fig. 5b. The diagrams of time signal of absolute vibration vertical acceleration amplitude in the middle points of the frame (a) (Fig. 2 above, the points 3R and 4R) and the pneumatic suspension (b) (Fig. 2 above, the points 1P and 4P) upon shock excitation of the bus body centre(air pressure of 6.5 MPa).

9.0; 10.75; 11.5; 12.75 and 17 Hz (at air pressure of 6.5 MPa) to 1.75; 3.0; 4.5; 5.5; 6.0; 9.25; 10.5; 11 and 15 Hz (at air pressure of 8 MPa).

A shock excitation have been applied for the measurements of vibration of the mechanical construction of the bus with air springs. Upon the first condition, the air pressure in the air springs was 6.5 MPa. Upon the second condition, the air pressure in the air springs was 8.0 MPa. For each condition, the measurements were carried out at four points of the bus frame (3R, 4R, 1P, 4P) and a vector of the measurement results was obtained for each point. Thus, four measurement vectors were obtained for each condition. In order to simplify numbering of these vectors the sequence numeration (1, 2, 3, 4) was applied in the calculation. The vectors of both conditions were integrated into one system and vectors were numbered (1, 2, 3, 4; 5, 6, 7, 8).

The arrays of the measuring data were processed according to the developed software upon applying operators of Matlab 7 program package.

The values of quantization intervals of the normed covariance functions vary from 1 to n/2, were – the number of lines (values) of the wavelet signal vector in an array. An array of measuring wavelet signals consists of 4 vectors (columns), were each point of the bridge surface corresponds to one vector of measuring results. For each vector, the estimate $K'_{\varphi}(\tau)$ of the normed covariance function $K_{\varphi}(\tau)$

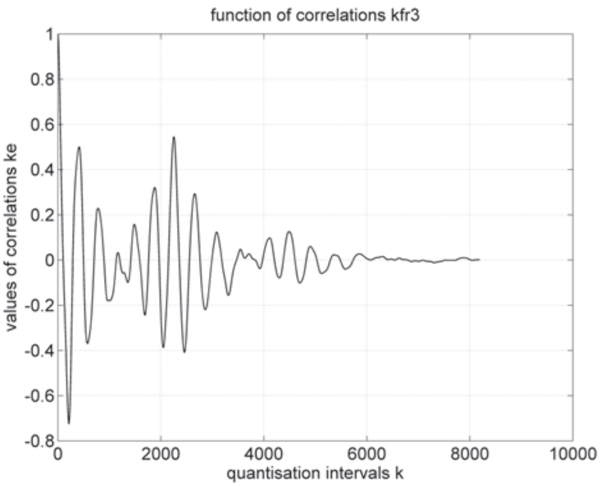

Fig. 6. The normed auto-covariance function of the vibration signals at the point 1P when the bus engine is off

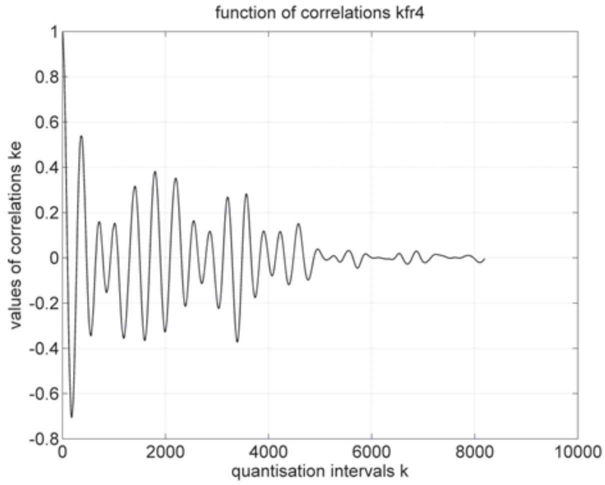

Fig. 7. The normed auto-covariance function of the vibration signals at the point 4P when the bus engine is off

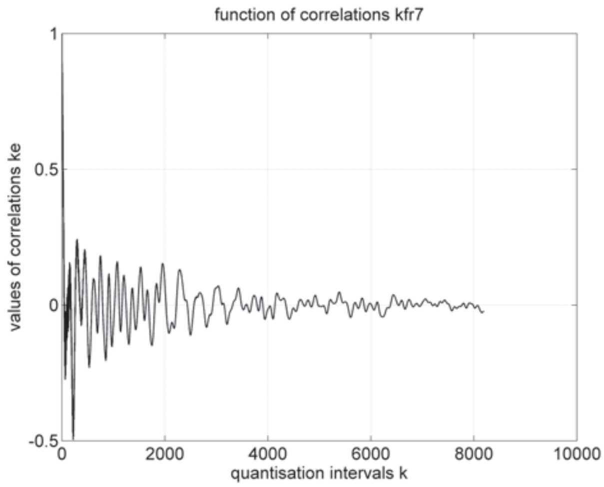

Fig. 8. The normed auto-covariance function of the vibration signals at the point 1P when the engine is in operating mode

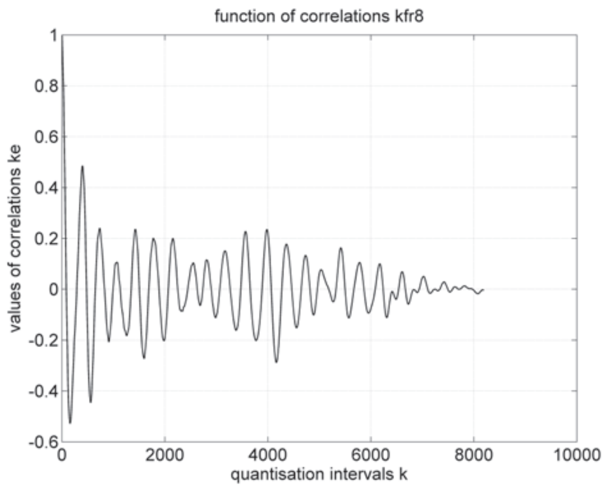

Fig. 9. The normed auto-covariance function of the vibration signals at the point 4P when the engine is in operating mode

was calculated and 6 graphical expressions of the normed covariance functions were obtained. In addition, the estimate of the normed cross-covariance functions $K'_{\varphi}(\tau)$ according to the vectors of all 4 points and 6 graphical expressions was obtained.

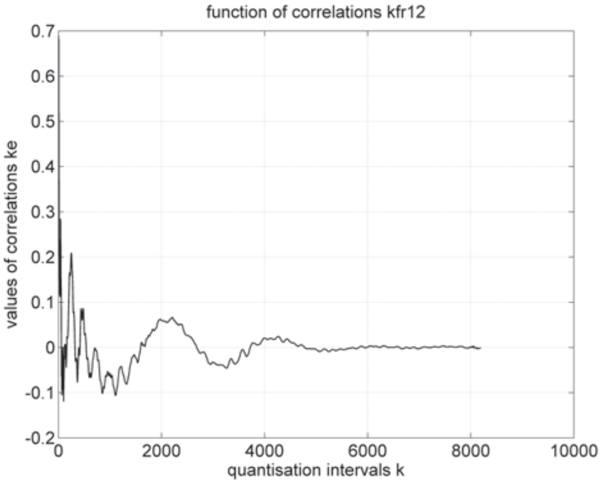

Fig. 10. The normed cross-covariance function of the vibration signals at the points 3R and 4R when the bus engine is off

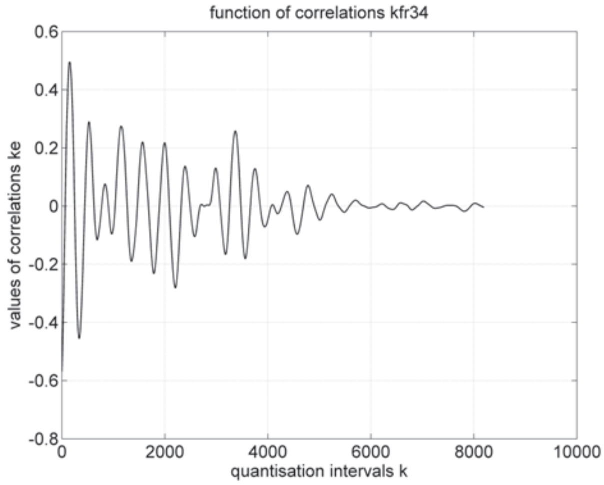

Fig. 11. The normed cross-covariance function of the vibration signals at the points 3P and 4P when bus engine is off

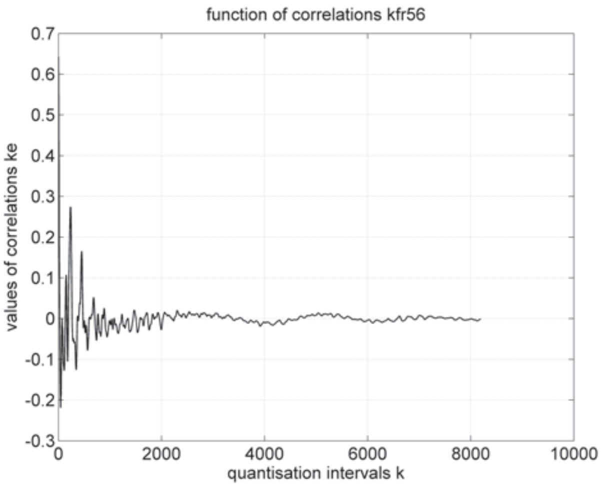

Fig. 12. The normed cross-covariance function of the vibration signals at the points 3R and 4R when engine is in operating mode

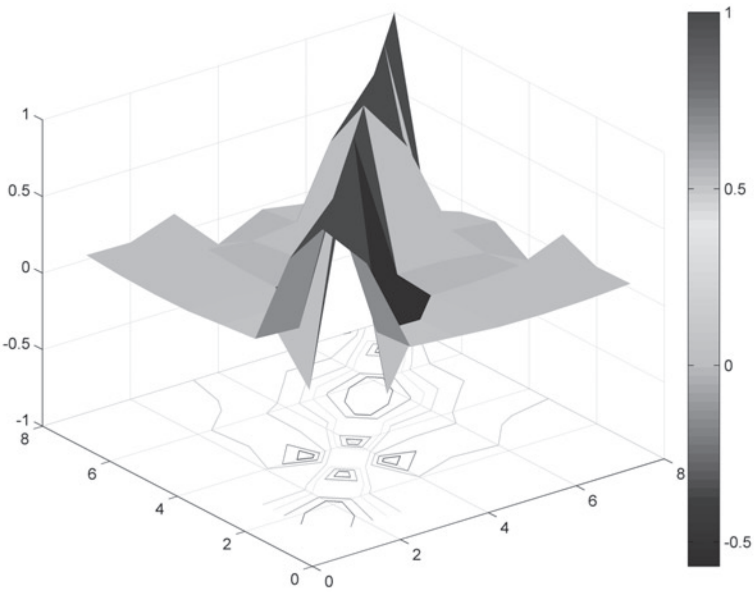

Fig. 13. The graphical expression of the generalized (spatial) correlation matrix of the array of 8 vectors of digital bus body vibration signals

The most important graphical expressions of normed auto-covariance and cross-covariance functions are provided in Fig. 6–12 below.

The graphical view of the generalized correlation matrix of 8-vector array for 4 points of the bus upon two states is presented in Fig. 13. The expression of the correlation matrix turns into a block of 8 pyramids where the values of correlation coefficients are shown as colours of the spectrum. The chromatic projection of the pyramids is shown in the horizontal plane.

The estimates of normed auto-covariance functions and cross-covariance functions are of “damping” character from and they become equal to 0 $k \to 0$ when the number of quantization intervals $k \to 4000$ or the time intervals $\tau_k = k \cdot \tau_\Delta = 0.98\text{s}$

The slower decrease of the estimates of the auto-covariance functions is caused by the vectors 1P and 4P upon the both states when $|r| \to 0.4-0.5$ at $k \to 4000(\tau_k \to 0.98\,s) - k \to 7000(\tau_k \to 1.7\,s)$ and they further decrease down to the value close to zero. This shows that “damping” of covariance of vibration signals is slower in the vectors 1P and 4P upon the both states.

The estimates of normed cross-covariance functions are close to zero when for all vectors and for all quantization intervals upon the both states, except of vectors with low values of the correlation coefficients between them. They include:

- 3R and 4R (for the state 1), when
- 1P and 4P (for the state 1), when
- 1P (for the state 1) and 4P (for the state 2), when
- 4P (for the state 1) and 4P (for the state 2), when
- 3R (for the state 2) and 4P (for the state 2), when
- 3R (for the state 2) and 4P (for the state 2), when
- 4R (for the state 2) and 4P (for the state 2), when

It must be stated that the pressure in the bus air spring practically makes no influence on the vibration intensity and correlation.

4. Conclusions

1. The normed auto-covariance and cross-covariance functions of vibration signals at the preselected points of the bus body mechanical structure enable to establish the changes of correlation between the data vectors according to the quantization interval on the time scale. The estimates of normed auto-covariance functions “damp” rather quickly when the quantization interval is from 0 to 4000 upon both the states under measurement. Slower “damping” of covariance of vi-

bration signals takes place in the vectors 1P and 4P within both the states.

2. The estimates of the normed cross-covariance functions are close to zero, when $|r| \to 0$ for all vectors of vibration signals andfor all quantization intervals in upon both states under measurement. The values of several cross-covariance functions are higher and vary in the range $|r| \to 0.2-0.5$. It must be stated that bus air spring pressure variation from 6.5 MPa up to 8.0 MPa practically makes no influence on the vibration intensity and correlation of the bus body.

References

1. Antoine JP. Wavelet analysis of signals and images. A grand tour, Revista Ciencias Matematicas (La Habana) 2000; 18: 113–143.
2. Buchacz A, Płaczek M, Wróbel A. Modelling of passive vibration damping using piezoelectric transducers – the mathematical model. Eksploatacja i Niezawodnosc – Maintenance and Reliability 2014; 16 (2): 301–306.
3. Crowe CM. Formulation of linear data reconciliation using information theory. Chemical Engineering Science 1996; 51: 3359–3366, http://dx.doi.org/10.1016/0009-2509(95)00369-X.
4. Dutkay DE, Jorgensen PET. Wavelets on fractals. Rev. Mat. Iberoamericana 2004; 22: 131–180.
5. Ekstrom M, McEwen A. Adaptive box filters for removal of random noise from digital images, Photogrammetric Engineering and Remote Sensing 1990; 56(4): 453-458.
7. Horgan G. Wavelets for SAR image smoothing, Photogrammetric Engineering and Remote Sensing 1998; 64(12): 1171-1177.
8. Hunt B, Ryan TW, Gifford FA. Hough transform extraction of cartographic calibration marks from aerial photography, Photogrammetric Engineering and Remote Sensing 1993; 59(7): 1161-1167.
9. Kosobudzki M. The use of acceleration signal in modeling proces of loading an element of underframe of high mobility wheeled vehicle. Eksploatacja i Niezawodnosc – Maintenance and Reliability 2014; 16 (4): 595–599.
10. Kuehn DR., Davidson H. Computer control II: Mathematics of control. Chemical Engineering Progress 1961; 57: 44–47.
11. Mah RSH. Process data reconciliation and rectification. In Chemical process structures and information flows. Butterworth-Heinemann 1990; 385–466, http://dx.doi.org/10.1016/B978-0-409-90175-7.50014-1.
12. Narasimhan S, Jordache C. Data reconciliation and gross error detection: An intelligent use of process data. Huston: Gulf Publishing Company, 2000.
13. Puigjaner L, Heyen G. Computer aided process and product engineering. Weinheim: Wiley-VCH, 2006, http://dx.doi.org/10.1002/9783527619856.
14. Poulin É, Hodouin D, Lachance L. Impact of plant dynamics on the performance of steady-state data reconciliation. Computers and Chemical Engineering 2010; 34: 354–360, http://dx.doi.org/10.1016/j.compchemeng.2009.11.018.
15. Romagnoli JA., Sanchez MC. Data processing and reconciliation for chemical process operations. San Diego: Academic Press, 2000.
16. Siljak H, Subasi A. Fourier spectrum related properties of vibration signals in accelerated motor aging applicable for age determination. Eksploatacja i Niezawodnosc – Maintenance and Reliability 2014; 16 (4): 616–621.
17. Skeivalas J. Theory and practice of GPS networks. Vilnius: Technika, 2008. [In Lithuanian].
18. Skeivalas J, Aleknienė E, Gečytė S. Analysis of identifying the digital images of the earth's surface. Geodesy and Cartography 2010; 36(4): 146–150. [In Lithuanian], http://dx.doi.org/10.3846/gc.2010.23.
19. Vasebi A, Poulin É, Hodouin, D. Observers for mass and energy balance calculation in metallurgical plants. The 18th IFAC World Congress Milano 28.08.2011-02.09.2011

Kristina KILIKEVIČIENĖ
Robertas PEČELIŪNAS
Department of Automobile Transport
Vilnius Gediminas Technical University
J. Basanavičiaus str. 28, LT-03224 Vilnius, Lithuania

Jonas SKEIVALAS
Dept of Geodesy and Cadastre
Vilnius Gediminas Technical University
Saulėtekio al. 11, LT-10223 Vilnius, Lithuania

Artūras KILIKEVIČIUS
Department of Mechanical Engineering
Vilnius Gediminas Technical University
J. Basanavičiaus str. 28, LT-03224 Vilnius, Lithuania

Gintautas BUREIKA
Department of Railway Transport
Vilnius Gediminas Technical University
J. Basanavičiaus str. 28, LT-03224 Vilnius, Lithuania

E-mail: kristina.kilikeviciene@vgtu.lt; robertas.peceliunas@vgtu.lt
jonas.skeivalas@vgtu.lt, arturas.kilikevicius@vgtu.lt
gintautas.bureika@vgtu.lt

Article citation info:
JAŚKOWSKI P. Methodology for enhancing reliability of predictive project schedules in construction. Eksploatacja i Niezawodnosc – Maintenance and Reliability 2015; 17 (3): 470–479, http://dx.doi.org/10.17531/ein.2015.3.20.

Piotr JAŚKOWSKI

METHODOLOGY FOR ENHANCING RELIABILITY OF PREDICTIVE PROJECT SCHEDULES IN CONSTRUCTION

METODYKA ZWIĘKSZENIA NIEZAWODNOŚCI PREDYKTYWNYCH HARMONOGRAMÓW REALIZACJI PRZEDSIĘWZIĘĆ BUDOWLANYCH*

Construction projects consist in providing new built facilities as well as in maintaining the existing building stock. Reliability engineering in construction encompasses all stages of the structure's life cycle from the earliest concept of the project to decommissioning. The project planning and design stages are aimed at selecting or creating technical and organisational solutions to assure that the built facility meets the sponsor's and the user's requirements; these requirements regulate also the construction process. The result of planning the construction process should be a reliable schedule – immune to disruptive effects of random occurrences, so assuring high probability of the actual processes meeting their predefined deadlines. A practical method of scheduling construction projects should enable the planner to generate schedules resistant to random occurrences, making them reliable so that the users can meet deadlines. The paper presents a proactive methodology for generating construction schedules of enhanced reliability. The methodology covers two fundamental stages. The first stage is a construction duration risk assessment based on a multi-attribute evaluation of operating conditions. The second stage is the allocation of time buffers. An original methodology supporting decisions at each stage is put forward, namely a methodology for evaluating process duration risk level, defining significance of operating conditions, estimating dispersion of process durations, and defining criticality of processes in the schedule. The author proposes a set of measures of schedule robustness to serve as surrogate criteria in the schedule instability cost minimization problem and buffer sizing. The proposed way of allowing for risk and uncertainty in creating reliable schedules is argued to be efficient in protecting the project completion date, as well as stage or even process start dates, against disruptions.

Keywords: *project programme reliability, construction project scheduling, construction and maintenance of built facilities, robustness, duration risk analysis and assessment, time buffer allocation*

Przedsięwzięcia budowlane obejmują swym zakresem procesy związane z wznoszeniem nowych obiektów, jak i utrzymaniem istniejących zasobów. Inżynieria niezawodności w budownictwie obejmuje wszystkie fazy cyklu życia obiektu budowlanego, od przygotowania koncepcyjnego po jego likwidację. Na etapie planowania i projektowania jest dokonywany dobór rozwiązań technicznych i organizacyjnych, które zapewnią spełnienie wymagań stawianych przez inwestora i użytkownika, w tym również w odniesieniu do fazy realizacji obiektu. Rezultatem projektowania przebiegu realizacji przedsięwzięcia powinien być niezawodny harmonogram o wysokim prawdopodobieństwie dotrzymania zaplanowanych terminów i małej wrażliwości na wpływ zjawisk losowych. W artykule zaprezentowano proaktywne podejście metodyczne do projektowania predyktywnych harmonogramów realizacji przedsięwzięć budowlanych, w celu zwiększenia ich niezawodności. Obejmuje ono dwa zasadnicze etapy: ocenę ryzyka czasu realizacji procesów budowlanych w oparciu o wieloatrybutową ocenę warunków realizacyjnych oraz alokację buforów czasu w harmonogramie. Opracowano oryginalną metodykę wspomagającą podejmowanie decyzji na każdym etapie tej procedury, tj. metodykę oceny poziomu ryzyka czasu realizacji procesów, określania istotności warunków realizacyjnych, dyspersji czasu realizacji procesów budowlanych i krytyczności procesów w harmonogramowaniu predyktywnym. Zaproponowano zestaw mierników odporności harmonogramu, stanowiących zastępcze kryteria w problemie minimalizacji kosztu niestabilności i określania wielkości buforów czasu. Proponowane ujęcie uwzględnienia warunków ryzyka w harmonogramach predyktywnych zwiększa ich niezawodność i zapobiega dezaktualizacji terminu końcowego oraz terminów realizacji poszczególnych procesów lub etapów przedsięwzięcia.

Słowa kluczowe: *niezawodność projektu realizacji, harmonogramowanie przedsięwzięć budowlanych, realizacja i eksploatacja obiektów, odporność na zakłócenia realizacyjne, analiza i ocena ryzyka czasu, alokacja buforów czasu*

1. Introduction

Problems of scheduling construction projects, that involve new construction, modernization as well as maintenance-related activities, stays the object of interest of many research centres [1, 3–5, 7, 10, 14, 16–18, 20, 22, 24, 26, 28-30]. Over the last decades, one can observe advance of scheduling methods that allow the user to precisely model real-life conditions, mainly resource availability restrictions and effects of random occurrences.

Projects are affected by risk that affect completion dates [8, 11, 14, 16–18, 21, 24, 26–27]. Striving for reducing impact of random occurrences provides rationale for rapid development of robust methods in statistics and operations research [2], and explains growing popularity of their application in many sectors of economy. An example of these trends in the field of project management are predictive sched-

(*) Tekst artykułu w polskiej wersji językowej dostępny w elektronicznym wydaniu kwartalnika na stronie ***www.ein.org.pl***

uling techniques with proactive approach [29] aimed at generating schedules resistant to interferences, called robust schedules. They are considered superior to the traditional reactive re-scheduling as disturbances make the initial plans expire.

Schedule robustness is defined as the schedule's ability to stay valid despite minor changes in duration of processes (activities) – these changes being due to risk [1]. Two optimization strategies of different focuses are in use [28], namely:

- improving quality robustness aimed at assuring stability of makespan (meeting the predefined completion date),
- improving solution robustness aimed at conducting processes according to the plan; in anticipation of disruptions, the planner strives for minimizing the difference between actual and scheduled activity start dates.

Both of these strategies are intended to improve schedule reliability. The reliability can be defined as the probability of the schedule's meeting expectations towards trustworthiness of planned dates: the project completion date and completion dates of particular processes.

The majority of current construction scheduling practices that assume process durations to be random values focus more on determining the project completion date with a predetermined probability [14, 20] rather than on building schedules with predefined process start dates. An analysis of network models in the function of time provides probabilistic output, which is of little practical use when it comes to contracting works and deliveries. Another difficulty is determination of the process duration probability distribution type and parameters.

Most methods in use: PERT (Program Evaluation and Review Technique), PNET (Probabilistic Network Evaluation Technique), NRB (Narrow Reliability Bounds method) assume that the random variables of process durations are independent, which is a far going simplification. Dawood [6] proposed a simulation-based method to model correlation of process durations as random variables and to improve precision of project duration estimates. Defining duration risk factors as well as assessing their impact on process times are experience based, which requires access to expert knowledge and historical records. Simulations enable the planner to determine the project duration's probability density function and density functions of process durations. It is thus possible to estimate the effect of particular risk factors on project progress. Practicability of Dawood's method is limited by the fact that the planner needs to have (or have access to) considerable experience and knowledge on probability distribution type and parameters of each particular risk factor. Subjectivity, errors in risk evaluation and basing on incomplete risk records would also negatively affect the output of analyses conducted by means of this method.

Nasir et al. [19] put forward a method to facilitate estimating pessimistic and optimistic durations of processes. The method is based on belief networks. Pessimistic and optimistic duration estimates can be than used in PERT analysis or Monte Carlo simulation. The procedure of developing a belief network comprises four steps to be supported by expert opinions: identifying risk factors, identifying risk factor relationships, developing network structure, and calculating conditional probabilities of risk occurrence. However, the authors report that collecting input and defining the network structure for a particular project case took six weeks. From the point of practice, this is a drawback.

Skorupka [26] presented an integrated method of risk identification with qualitative and quantitative risk assessment designed for construction projects (MOCRA). The method facilitates the assessment of risk reduction strategies and enables the planner to distribute residual risk throughout the project plan. The risk related with particular factors is calculated as a product of probability of occurrence and impact. The impact is expressed as duration increase in percent. The idea of risk allocation in MOCRA is based on the assumption that the defined and quantified risk factors that may affect a particular process by increasing its duration can be totalled and directly related to the pessimistic duration estimate. An increase in the pessimistic duration results in the change of the expected duration. If the interference persists, the mode of duration probability distribution can also be shifted. The assumption that risk effects are additive may be difficult to accept in some cases, but the MOCRA's ease of application may be considered an asset by the potential users.

Schatteman et al. [25] described their construction project risk management approach as integrated with proactive scheduling. The results of risk factors identification, analysis and quantification of occurrence frequency and impact on process durations are used in the heuristic procedure of buffer allocation to create schedules that are immune to interruptions (which means they have the lowest instability cost). Reliability of results obtained by the authors depends strongly on the reliability of expert's opinions, as the experience-based data are needed as input. The number of input parameters is considerable, which may result in cumulation of error. However, limiting the number of risk factors to these considered "most important" may reduce reliability of results by ignoring cumulated effect of minor factors.

In general, the attempts to utilize results of risk analysis in scheduling are aimed at improving the planning reliability. Efforts made towards making construction schedules immune to random disturbances are justified by following facts:

1. To employ subcontractors, one needs to provide them with clearly defined conditions of contract – including the date of their starting the job; the dates need to be established well ahead to allow for prior consent of the client.
2. The contractor needs a reasonable resource management basis. Resource employment plans, material procurement or component production plans require deterministic dates.
3. Failing to deliver a project of work package on time (with deadlines defined in a deterministic way) is related with serious contractual penalties.

The above observations inspired the author to develop an original approach to construction scheduling that allows for duration risks.

2. Proposed methodology of predictive scheduling

The proposed methodology for predictive scheduling of construction projects is an implementation of risk management concept. The rich literature on the subject of risk provides a variety of risk definitions [23]. The author adopts the approach by Williams and Heins [31] with risk consisting in variability of results and being described by probability distribution of results.

No construction project is risk-free. Risk can and should be managed – minimized, shared, transferred or accepted, but it should not be ignored [27]. There are many guidelines on dividing the process of risk management into steps. However, most approaches indicate that apart from identifying, analyzing and quantifying, the manager needs to develop and implement measures to actively reduce the scale of impact and probability of unfavourable occurrences. A proactive risk management strategy prompts that risk response planning needs to be incorporated into the scheduling process. It may take a form of time buffer allocation.

The proposed construction scheduling methodology comprises two coupled stages:

- duration risk assessment of the processes,
- allocation of time buffers.

The procedure is presented in Figure 1. Each process shown in the figure was provided with specific decision support methodology.

The objective of duration risk assessment is defining the risk profile by describing it explicitly by a duration probability density function for each process. The first stage of the methodology is crucial as it determines any consecutive action and outlays on risk protection.

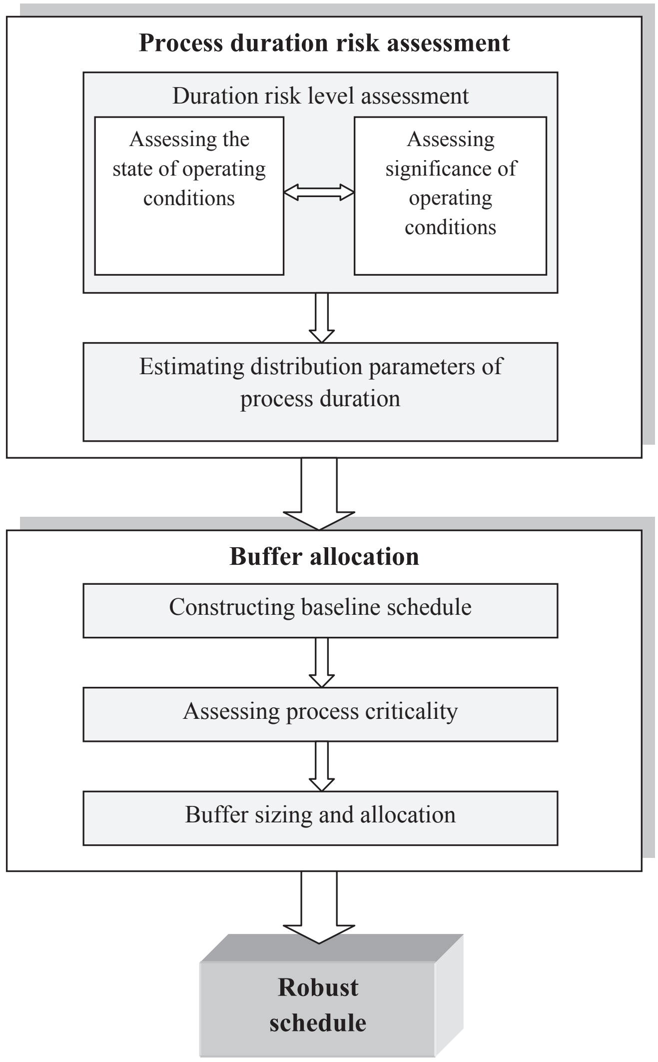

Fig. 1. Stages of predictive scheduling (proposed methodology)

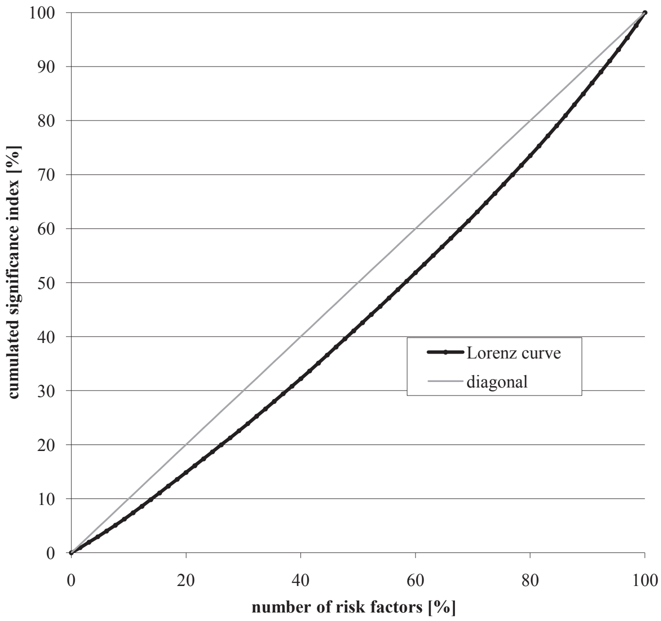

Fig. 2. Lorenz curve for mean risk factor's significance ratios (results of survey) [13]

In the classic approach to risk management, the basis of risk assessment is identification of risk sources, called risk factors. Information on actual probability distributions of the risk factors' impact on duration of particular processes is usually difficult to find. Thus, one needs to refer to subjective assessment based on personal experience, intuition or expert opinions.

To identify the set of most significant risk factors affecting duration and start dates of processes, the author conducted a survey among Polish construction practitioners [13].

A literature review and interviews with numerous construction project participants provided the author with a list of 63 potentially significant risk factors to construct a survey questionnaire. The target group for the survey were engineers employed by contractors active in Lublin region, Poland. They were asked to assess frequency of occurrence and impact of the risk factors from the list using a five-point scale (1-5). In the course of the survey, 91 complete questionnaires were returned; the sample size was enough to consider it statistically representative: the minimum sample size was 83 (with 3% relative error and at 90% confidence interval).

A significance index (a product of assessment of their impact and frequency of occurrence) was then calculated for each risk factor. As results from the survey, ten most significant risk factors are: winter weather (average significance index of 11.89), precipitation (11.29), delay of preceding works (10.91), shortage of skilled labour (10.33), mistakes and discrepancies in design documents (10.20), client's low speed of decision-making (10.13), variations of works scope and quantity due to design changes (10.01), demotivating remuneration system (9.91), client's change of requirements (9.89), difficulty with finding subcontractors (9.49). The risk factors were ordered according to their significance index from the least to the most significant. Figure 2 presents a graph of cumulated significance for this order (Lorenz curve) [13].

A relatively small deviation of the Lorenz curve from its diagonal indicates that concentration of risk factor's significance is low (Gini coefficient of 0.116). Therefore, there exists no small group of risk factors of particularly high impact on project duration. The conclusion is that the assessment of project duration risk cannot be limited to analyzing some set of "most important" factors and ignoring the remaining ones.

The statistical analysis of survey results indicated that experiences of respondents differ (low values of W-Kendall coefficient: 0.238 for the impact and 0.236 for frequency of occurrence indicate that the interviewees' answers are not consistent). Therefore, there is no justification for assuming the same significance of risk factors (so impact and probability of occurrence) for all projects and processes.

The above findings point to serious limitations of the traditional approach to risk factor identification. Because of that, the author proposes a different approach: a multi-attribute assessment of particular project operating conditions.

3. Methodology of assessing construction duration risk

The methodology of assessing duration risk of construction processes comprises the assessment of operating conditions, the assessment of significance of these conditions, the estimation of duration risk, and the estimation of distribution parameters of construction processes' durations.

3.1. Assessment of operating conditions and process duration risk level

The impact of particular risk factors is the object of analysis of many researchers [6, 25, 26]. Certainly, it is project-specific. It depends on actual conditions and particularities of decision situation [14].

Operating conditions, described by the set of qualities, phenomena, states and processes that determine the project or particular process progress, result from the state of the external and internal environment of the project organisation.

Changing even a small part of these conditions may significantly affect project development [17]. For instance, conducting some works during an unfavourable time of the year, may result in stoppage or serious productivity drop due to bad weather (low temperatures, heavy rain/snow). Another instance is the quality of plant and machinery – if poor, failures are more likely, and delays are to be expected.

Appreciating the fact that the frequency of occurrence and severity of impact of risk factors differs from case to case, the author attempted at developing a method for assessing duration risk with respect to particular conditions [11, 13].

Table 1 lists identified conditions related with duration risk – according to research presented in the literature and according to surveyed experts.

Table 1. Operating conditions affecting the process duration risk level [11, 13]

No.	Conditions
1	Time of the year
2	Experience and availability of resources
3	Quality of design and specification, quality of construction plans
4	Quality of project and construction management systems
5	Quality of remuneration and working conditions
6	Financial standing of the client and the contractor, project funding
7	Quality of the supply system
8	Location and space constraints of the construction site
9	External conditions (state of the economy, political climate, legal conditions, geographic location, availability of suppliers and cooperating organizations)
10	Quality and availability of plant and equipment

The proposed methodology assumes that the analysis and assessment of operating conditions is the basis for the duration risk assessment.

The author decided to rate the state of each condition in a five-point scale (0; 0,25; 0.5; 0.75; 1). 0 means most desirable state (positive effect on project progress, reduction of process times), 0.5 represents average state (meeting standard productivity rates), 1 stands for an unfavourable state (the condition increases the process duration). The remaining marks are to be used for intermediate states.

The assessment of a condition's state and significance can be conducted for groups of processes of similar susceptibility to this condition. It should be as objective as possible. The author recommends resorting to opinions of a number of experts, and using methods supporting group decision making processes, e.g. Delphi.

As the number of conditions to be considered with each process group is considerable, an aggregated rating of project operating conditions, PC, was proposed. It is expressed by a following formula::

$$PC = \sum_{i=1}^{n} pc_i \cdot w_i \ , \tag{1}$$

where: PC – aggregated rating of project operating conditions,
pc_i – rating of a state of project condition i,
w_i – weight of project condition i,
n – number of project conditions (n=10).

The aggregated rating is a measure of the process duration risk level. The estimates made this way allow for the overall operating conditions and for significant cumulation of the impact of secondary conditions.

3.2. Assessment of operating conditions significance

The significance of a particular operating condition in the process of assessing duration risk level is proposed to be expressed in the form of condition weights.

The weights for the whole set of operating conditions can be determined by means of Analytic Hierarchy Process (AHP). As the method cannot directly account for risks of incomplete information, subjectivity of assessment, and discordant opinions of experts, the author put forward a fuzzy extension of AHP [9].

This fuzzy AHP assumes that the number of experts involved in the decision process is K. Each expert provides $m = n(n-1)/2$ pairwise comparisons of operating conditions' significance, using the usual AHP scale of 1/9,1/7, 1/5, 1/3, 1, 3, 5, 7, 9; optionally, the scale can be extended by intermediate scores of 1/8, 1/6, 1/4, 1/2, 2, 4, 6, 8. A result of the pairwise comparison is a set of K matrices $\mathbf{A}_k = \{a_{ijk}\}, i = 1,2,...,n-1, j = 2,3,...,n, j > i, k = 1,2,...,K$, where a_{ijk} represents a preference of condition i over condition j (so a quotient of weights of condition i and j) according to expert k, expressed by means of the above mentioned scale.

This is done to define the vector of crisp weights for particular conditions, $\mathrm{w} = [w_1, w_2, ..., w_n]^T$ on the basis of the expert's pairwise judgments.

Relative preferences on conditions, aggregated on the basis of each expert's judgments, are expressed as fuzzy numbers $\tilde{a}_{ij}$. Their membership functions are $\mu_{\tilde{a}_{ij}}(x) \in [0,1]$, with characteristic points defined according to the following formulas [9]:

$$l_{ij} = \min_{k=1,2,...,K} \{a_{ijk}\} \tag{2}$$

$$m_{ij} = \left(\prod_{k=1}^{K} a_{ijk} \right)^{1/K} \tag{3}$$

$$u_{ij} = \max_{k=1,2,...,K} \{a_{ijk}\}. \tag{4}$$

The membership functions are constructed to model non-uniform distribution of the expert's opinions. Figure 3 presents an example of such a membership function.

The vector of condition weights for a finite number of α -cuts of the membership function is determined in a way that assures meeting the following condition (in the fuzzy sense):

$$l_{ij}(\alpha) \tilde{\leq} \frac{w_i}{w_j} \tilde{\leq} u_{ij}(\alpha), \quad i = 1, 2, ..., n-1, \ j = 2, 3, ..., n, \ j > i \ . \tag{5}$$

Thus, for each expert, $w_i / w_j \tilde{=} a_{ijk}$, the consistency of an expert's opinion with the opinions of the group is improved.

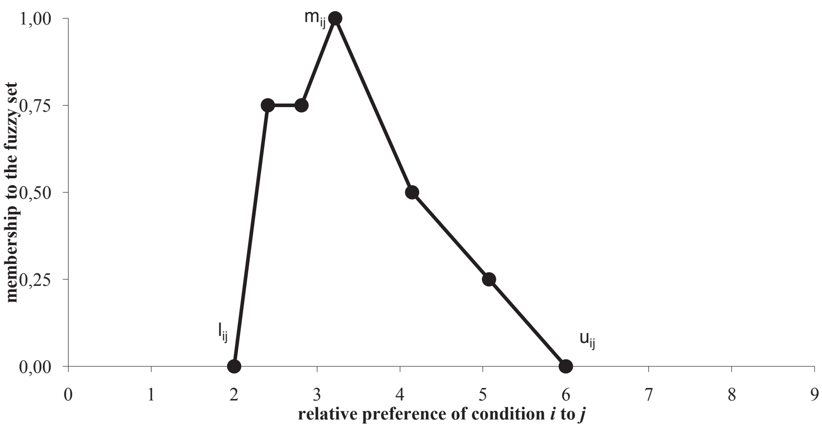

Fig. 3. Membership function for aggregated opinion $\tilde{a}_{ij}$ (example)

It was assumed that duration of a process j that lacks historical input for statistical analysis can be described by a triangular distribution. Its parameters are $a_j^{PC}, m_j^{PC}, b_j^{PC}$, meaning consecutively: the minimum, the mode, and the maximum of duration at a particular aggregated assessment of project conditions state that equals PC.

To define the probability density function parameters of a process's duration, $f_j^{PC}(x)$, at any state of project operating conditions ($PC \neq 0{,}5$) calculated according to Formula 1, the author used the least squares method and took the following assumptions [11]:

– The risk of defining the process duration to be t_j is directly proportional to the assessment of project operating conditions state PC, and in most favourable (perfect) conditions it equals 0. Therefore:

$$r^{PC}\left(t_j\right) = r^{0,5}\left(t_j\right) \cdot \frac{PC}{0,5}, \quad \forall t_j \in \left[a_j^{PC}, b_j^{PC}\right]. \tag{7}$$

– If PC>0,5, then the minimum duration a_j^{PC} and the mode of duration m_j^{PC} may be greater than these at PC=0,5.

– If PC<0,5, then the maximum duration b_j^{PC} and the mode of duration m_j^{PC} may be lower than at PC=0,5.

A set of graphs was developed to enable the user to define parameters of random variables of standardised triangular distribution at different aggregated assessment of project operating conditions state. The parameters can be defined for any assessment of the minimum, the mode and the maximum at average conditions. These parameters are necessary input for Monte Carlo simulations and calculating a measure of process criticality. An example of such graphs is given in Figure 4.

3.3. Assessing dispersion of construction process duration

To create construction schedules one needs to assume crisp values of process durations. However, durations are not deterministic and can be modelled as random variables of unique distributions. To determine actual distribution type and parameters of a construction process duration, one could conduct series of time-consuming and costly measurements on site. With these being usually unavailable, the researchers base on simplifying assumptions [6, 19, 25, 26].

For instance, authors of PERT assumed that process durations are random variables of beta-PERT distribution with parameters defined on the basis of pessimistic, optimistic and most probable estimates provided by experts. Johnson [15] argues that, without much loss on reliability, beta-PERT can be replaced by an even simpler triangular distribution, described by simple analytical relationships more understandable for scheduling practitioners. To explicitly define a triangular distribution, one needs to estimate the minimum duration, a_j, the most probable duration (the mode m_j), and maximum duration b_j.

The proposed approach assumes that minimum and maximum durations can be derived from historical records gathered by a contractor. The mode (with assumption of average operating conditions) can be calculated on the basis of standard productivity rates (median). The assessment of a construction process duration risk is aimed at defining the scale of possible increase of duration and estimating the probability of such occurrences. The risk, as defined by Williams and Heins [31], can be described by means of a delay's probability density function.

The author assumed that scheduling a particular process j to last $t_{j,}$ (so taking a particular crisp value of process duration) is related with risk; the risk's measure is the expected value of the process's extension [11]:

$$r^{PC}\left(t_j\right) = \int_{t_j}^{b_j^{PC}} \left(x - t_j\right) \cdot f_j^{PC}\left(x\right) dx, \tag{6}$$

where: $r^{PC}\left(t_j\right)$ – measure of risk related with scheduling a process j to take t_j units of time at the aggregated assessment of the state of project operating conditions being PC, calculated according to Formula 1;

$f_j^{PC}\left(x\right)$ – probability density function for duration of process j at the aggregated assessment state of project operating conditions of PC.

4. Methodology of allocating time buffers

The stage of buffer allocation comprises: creating the baseline schedule, assessing criticality of processes in the schedule, buffer sizing, and allocating buffers in the robust schedule.

4.1. Creating baseline schedule

To create a robust schedule of a project, one needs to start with presenting the project in the form of a network model. Precedence relations between activities are modeled by a direcded, acyclis unigraph $G = \langle V, E \rangle$, with no loops, with single initial and single final node. $V = \{1, 2, \ldots, n\}$ is a set of the graph nodes (representing construction processes). $E \subset V \times V$ is a relationship defining process sequence; it results from technological and organisational constraints and is a set of the graph's arches. Network techniques are used in construction to model projects of various character: complex of operations type, composed of one-off discrete processes, as well as projects with repetitive operations. Planning the latter is often based on methods that come in many variations and under many names (e.g. time couplings method) and are aimed at harmonization of work. For

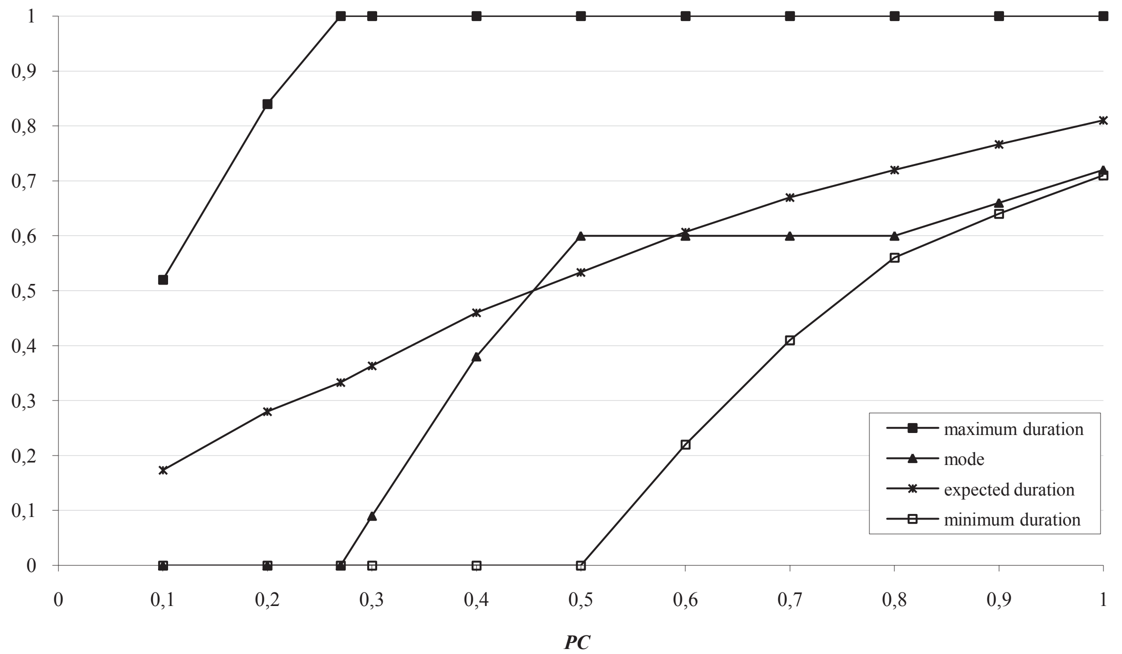

Fig. 4. Relationships between the aggregated assessment of project operating conditions state PC and the parameters of a standardised triangular distribution of the duration of process j conducted in these conditions (for $a_j^{0,5} = 0,\ m_j^{0,5} = 0,6,\ b_j^{0,5} = 1$)

such repetitive projects, identification of organizational relationships between processes should account for resource flows from operation to operation and from location to location. The processes are to be assigned durations corresponding to the expected values d_j ($\forall j \in V$) of random variables whose parameters are to be defined according to the method presented in chapter 3.3. Figure 5 presents a network model of a project to serve as illustration of the approach. The analysis of the network model in the function of time leads to calculating the shortest possible duration of the project, $T_{\min}$, the processes' early starts, and the processes' floats. These can be used for creating a baseline schedule with processes' starts s_j^0 ($\forall j \in V$) staying within total float limits. In the example, the baseline schedule uses early starts for all activities, and the shortest project duration is 277 days.

4.2. Assessing criticality of processes

The proposed methodology defines the process criticality as the susceptibility of a process's start to being delayed causing a change to the schedule. The magnitude of criticality is related with the scale of likely delays. Thus, critical processes need to be scheduled in a way that protects their start dates from being affected by disturbance. Criticality of a process is determined by the structure of the network model and by variability of durations of processes located in network paths that meet before the process starts. To allow for the impact of the predecessor's duration variability on the successors' start dates, the author used the *Monte Carlo* simulation. Simulation enabled modelling cases with some processes not being allowed to start before dates stated in the baseline schedule (*railway policy*).

The procedure of assessing a process's criticality consists in simulating the project's development according to the network model with an assumption that process durations are random variables of predetermined parameters (for particular state of project operating conditions), and that processes are allowed to start according to a predefined policy at times stated in the baseline schedule. Simulations provide the scheduler with estimates of expected values of start delays:

$$\Delta s_j = s_j^1 - s_j^0, \tag{8}$$

where: s_j^1 – mean start of process j determined in the course of simulation experiments,

s_j^0 – start of process j as stated in the baseline schedule.

The measure of a process start's susceptibility to delay (so the measure of the process's criticality) is defined as follows:

$$k_j = \Delta s_j + 3\sigma_j. \tag{9}$$

where: σ_j – standard deviation of start of process j, $j = 1, 2, ..., n$.

The value of multiplier by the standard deviation, 3, follows from the one-sided Chebyshev inequality with an assumption that the probability of the process's j start being delayed by more than k_j is lower than 0.1 regardless of the process start's s_j distribution type and parameters.

4.3. Buffer sizing

To improve the schedule's resistance to random occurrences, one can use the redundancy technique: introduce time buffers (idle time) before processes. The proposed approach to buffer sizing assumes that processes $j = 1, 2, ..., n$ are assigned a unit cost, c_j, of delaying their start beyond the date defined in the schedule. The processes of $c_j > 0$ need calculating their criticality values k_j. These processes are to be started according to the *railway policy*. The aim is to provide a robust schedule of a predetermined, contractually set completion date T_d, whose instability cost is minimal:

$$C = \sum_{j=1}^{n} c_j E\left(\mathrm{s}_j - s_j\right) \tag{10}$$

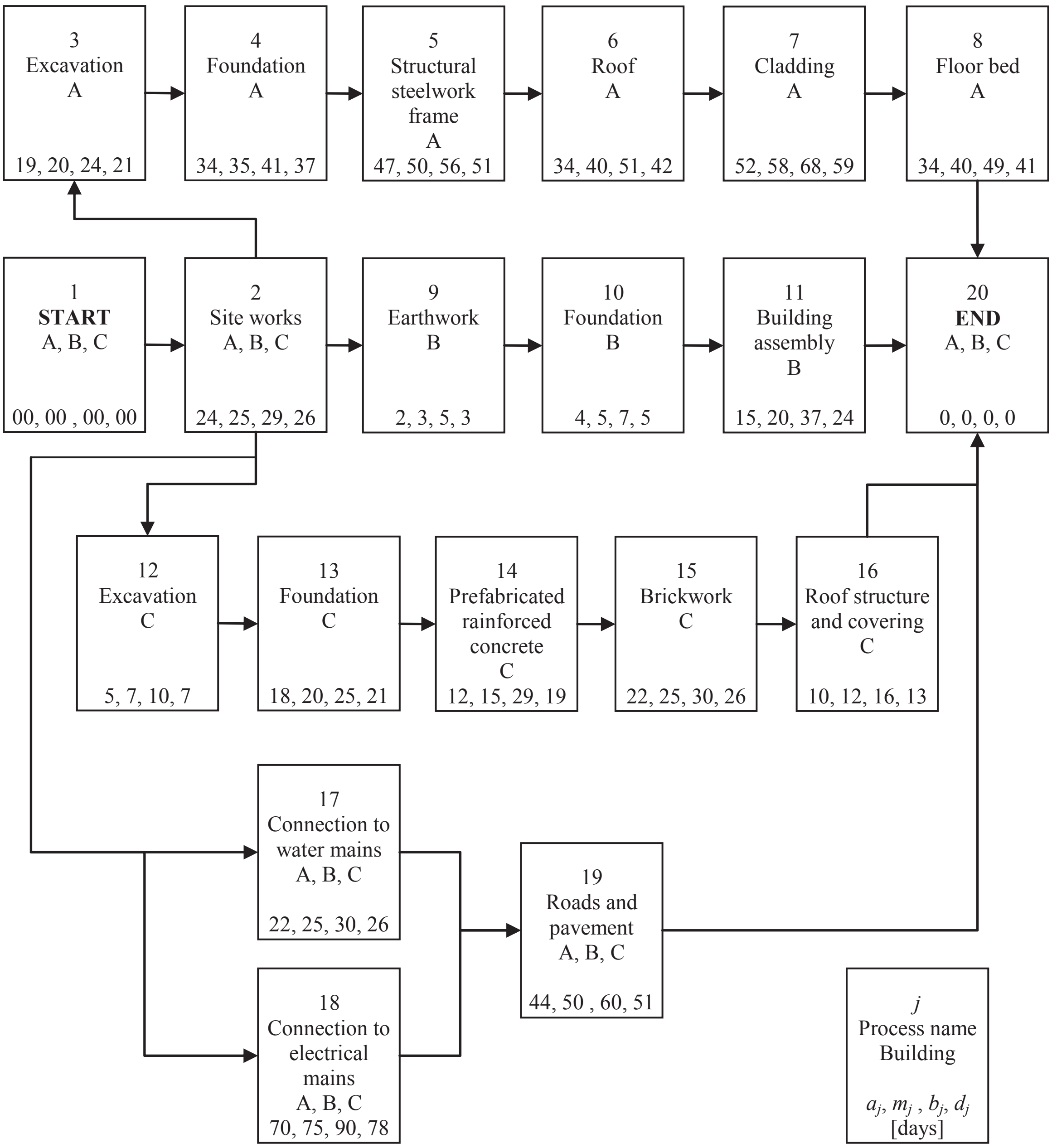

Fig. 5. Project network in the example

where: $\mathbf{s}_j$ – a random variable representing the start of process j,
s_j – the process's j start defined in the robust schedule,
c_j – unit cost of delaying the start of process j beyond the date stated in the robust schedule.

Considering the form of the objective function (minimizing the expected value of the process delay cost), the decision problem can be solved by means of stochastic programming methods. The complexity of the problem is considerable. Therefore, the author tested a number of substitute measures of robustness aimed at reducing computational effort and providing efficient scheduling algorithms, using these proposed by the literature on the subject, and compared them with measures of his own invention.

Size of buffers δ_j , $j = 1, 2, ..., n$ is determined in the following procedure [10]:

1. Calculate total float zc_j^0 of processes $j = 1, 2, ..., n$ according to the baseline schedule. Total floats of processes $j = 1, 2, ..., n$ for a predefined contractual duration T_d are $zc_j = zc_j^0 + T_d - T_{\min}$. The existing total float of paths in the baseline schedule should be redistributed, in the form of buffers, among the processes according to the process weights calculated as follows:

$$w_j = c_j \cdot k_j \tag{11}$$

2. Calculate buffer sizes – to do so, find solution of the following model:

$$\max z: \; z = \min_{j \in H} \left\{ \frac{\delta_j}{zc_j \cdot w_j} \right\} \tag{12}$$

$$s_1 = 0 \tag{13}$$

$$s_j - \delta_j \geq s_i + d_i,\ \forall (i,j) \in E \tag{14}$$

$$s_n + d_n \leq T_d \tag{15}$$

$$s_j \geq 0,\ \forall j \in V \tag{16}$$

$$\delta_j \geq 0,\ \forall j \in V \tag{17}$$

$$\delta_j = 0,\ \forall j \in V \setminus H \tag{18}$$

$$\delta_j \in \text{int},\ \forall j \in H, \tag{19}$$

where: $H = \{j : w_j > 0\}$ – a set of processes to be assigned buffers,

s_j – the start date of a process j, $j = 1, 2, ..., n$, in a buffered robust schedule.

The objective function (12) maximizes the value of the proposed surrogate measure of robustness. Conditions (13) and (14) enable the planner to calculate process starts in the buffered schedule. Project completion time cannot be exceeded (15).

The objective function as above provides solutions superior to solutions obtainable by means of methods presented in the literature – this was confirmed by verification tests presented in [10].

Additionally, the presented approach puts forward two alternative surrogate measures of schedule robustness:

$$\min_{j \in H} \left\{ \frac{\delta_j \cdot p_j}{zc_j \cdot w_j} \right\}, \tag{20}$$

$$\min_{j \in H} \left\{ \frac{\delta_j}{zc_j \cdot c_j} \right\}. \tag{21}$$

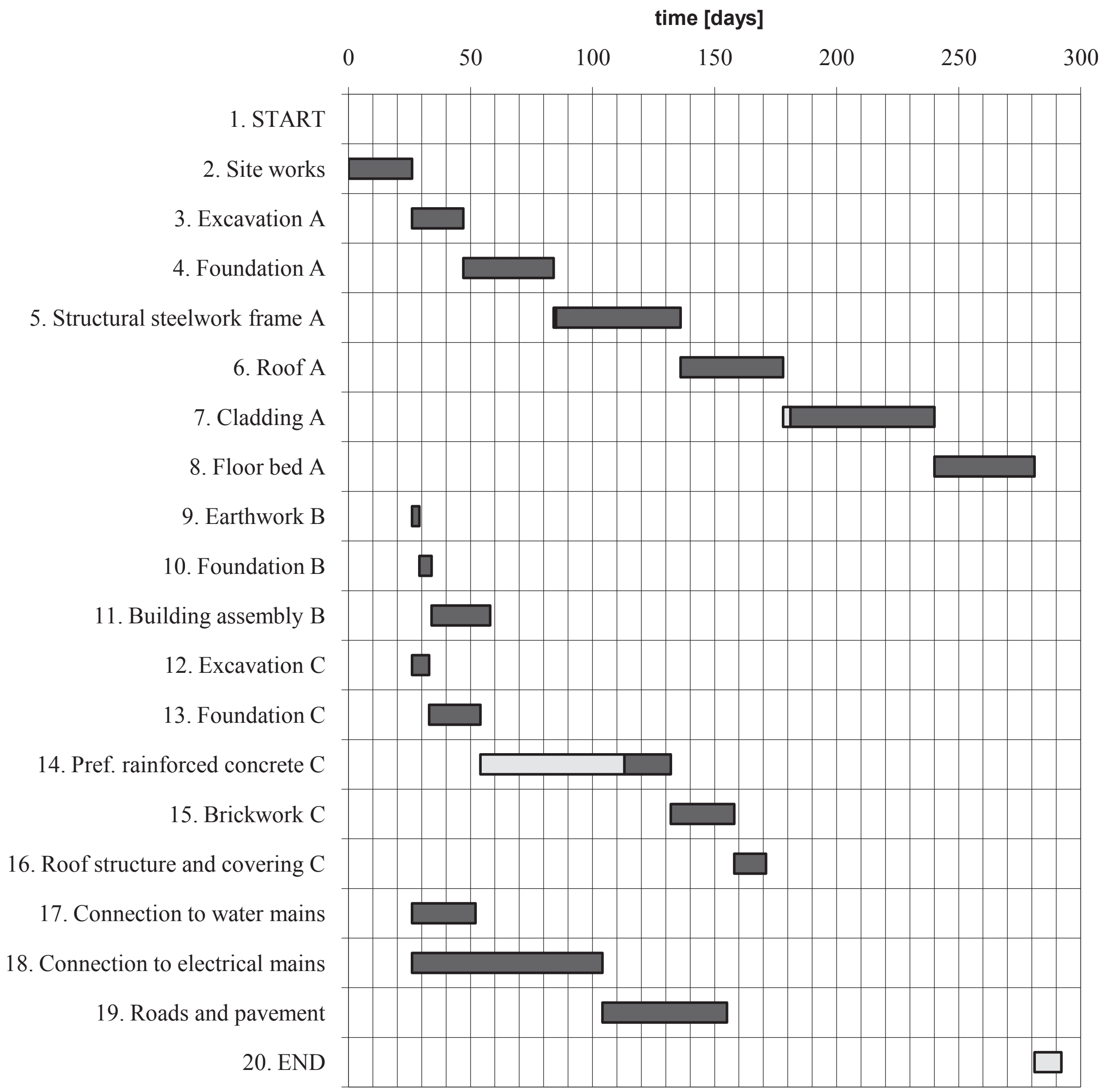

Fig. 6. Robust schedule with time buffers for the example; gray bars represent buffers located before the start of processes.

where: p_j – number of process j in the sequence of processes of total float zc_j, whose $c_j > 0$, and that belong to the same path.

Formula (20) allows for the location of a process on a path, and thus it allows for reduction of a process's criticality by preceding buffers that compensate for some part of disturbance.

The quality of the proposed surrogate measures of robustness was checked for a series of contractual project durations assumed for the same case. The network model of this case is shown in Figure 5. The tests were conducted for five sets of unit costs of process delays (results obtained for one of these sets were presented in [12]).

Figure 6 presents the outcome for this case – a robust schedule created on the following assumptions: unit costs of process start delays are $c_5 = 1$, $c_7 = 3$, $c_{14} = 5$, $c_{20} = 10$, unit costs of process start delays for the remaining processes equal 0, the contractually agreed project duration is $T_d = 292$. Buffer sizes, calculated as previously described, are as follows: $\delta_5 = 1$, $\delta_7 = 3$, $\delta_{14} = 59$, $\delta_{20} = 11$. The total instability cost of the schedule is $C = 2.69$. This solution (with lowest instability cost) was obtained for the surrogate measure of robustness described by Formula 20.

The results gave grounds for the following conclusions:

1. The scale of schedule instability cost is strongly affected by the allowed time for completion; the longer the contractual duration and process floats, the more robust the schedule.
2. Increasing the project buffer placed in the network before the project completion date, and reducing buffers that protect intermediate dates implicates increased schedule instability cost.
3. Lowest schedule instability costs were obtained in schedules of relatively high unit costs of process start delay for intermediate dates. Thus, there are grounds to claim that buffers placed before intermediate dates are of higher schedule protecting potential and may efficiently reduce propagation of disturbance.
4. Measures of schedule robustness (12), (20) and (21) are of the same family of functions of the following general form:

$$\min_{j \in H} \left\{ \alpha\left(p_j\right) \cdot \frac{\delta_j}{zc_j \cdot w_j} \right\}, \tag{22}$$

where $\alpha\left(p_j\right)$ – a parameter whose value depends on the process's position in the path of a network model.

Application of the set of measures (12), (20) and (21) enables the user – in the case that the solutions do not satisfy the decision maker – to reduce the extend of values of this parameter in the search for more robust schedules.

5. Conclusions

In the practice of construction management, there is a demand for scheduling methods integrated with risk management procedures [25, 26]. In particular, support for quantitative analyses for risk management (typically with lack of objective input but expected to offer reliable basis for decisions) would be most welcome by the industry. Improving schedule reliability is especially important in the case of unique, unrepeatable projects such as modernisation and refurbishment of facilities that stay operational during construction works.

The paper presented the methodology for creating robust construction schedules based on the idea of buffering – allocating a block of time along network paths to protect due dates. A robust schedule of a predefined completion date minimizes instability cost (i.e. expected value of delaying process starts) and offers higher probability of meeting deadlines (i.e. reliability).

The main results of research on developing and refining the methodology are:

1) Implementing the robust scheduling concept to construction scheduling, in particular:
   - providing practical measures of schedule robustness and a scheduling algorithm of low computational complexity,
   - defining process criticality in risky environment,
   - providing decision support for any stage of risk management process (integrated character of methodology).
2) Developing a methodology for risk level assessment that is based on an analysis of overall project operating conditions.
3) Developing a methodology for defining distribution parameters for process durations at various operating conditions; the method was applied to simulation research and to assessing quality of schedule improvement options.
4) Developing a fuzzy extension to AHP to support group decision making process, applicable in many fields of construction. The method improves objectivity of judgment, and can be used even if expert opinions are seriously discordant.

As the schedule instability cost is dependent upon the scale of the float of a sequence of processes distributed in the form of buffers, the author argues for developing scheduling methods aimed at minimizing project duration by means of soft logic [30], multi-skilling [5, 7], enabling changes of the sequence of the crew's migrating from location to location [4], and process duration crashing [22]. Applying them in combination with the proposed methodology will considerably improve construction schedules reliability.

***Acknowledgments**:*

The paper is financially supported by Ministry of Science and Higher Education S/63/2015.

References

1. Al-Fawzan M. A., M. Haouari M. A bi-objective model for robust resource-constrained project scheduling. International Journal of Production Economics 2005; 96(2): 175-187, http://dx.doi.org/10.1016/j.ijpe.2004.04.002.
2. Bertsimas D., Sim M. The Price of Robustness. Operations Research 2004; 52(1): 35-53, http://dx.doi.org/10.1287/opre.1030.0065.
3. Bożejko W., Hejducki Z., Wodecki M. Applying metaheuristic strategies in construction projects management. Journal of Civil Engineering and Management 2012; 18(5): 621-630, http://dx.doi.org/10.3846/13923730.2012.719837.
4. Bożejko W., Hejducki Z., Uchroński M., Wodecki M. Solving resource-constrained construction scheduling problems with overlaps by metaheuristic. Journal of Civil Engineering and Management 2014; 20(5): 649-659, http://dx.doi.org/10.3846/13923730.2014.906496.
5. Burleson R. C., Hass C. T., Tucker R. L., Stanley A. Multiskilled labor utilization strategies in construction. Journal of Construction Engineering and Management 1998; 124(6): 480-489, http://dx.doi.org/10.1061/(ASCE)0733-9364(1998)124:6(480).

6. Dawood N. Estimating project and activity duration: a risk management approach using network analysis. Construction Management and Economics 1998; 16(1): 41-48, http://dx.doi.org/10.1080/014461998372574.
7. Hegazy T., Shabeeb A. K., Elbeltagi E., Cheema T. Algorithm for scheduling with multiskilled constrained resources. Journal of Construction Engineering and Management 2000; 126(6): 414-421, http://dx.doi.org/10.1061/(ASCE)0733-9364(2000)126:6(414).
8. Hoła B., Schabowicz K. Estimation of earthworks execution time cost by means of artificial neural networks. Automation in Construction 2010; 19(5): 570-579, http://dx.doi.org/10.1016/j.autcon.2010.02.004.
9. Jaśkowski P., Biruk S., Bucoń R. Assessing contractor selection criteria weights with fuzzy AHP method application in group decision environment. Automation in Construction 2010; 19(2): 120-126, http://dx.doi.org/10.1016/j.autcon.2009.12.014.
10. Jaśkowski P., Biruk S. The method for improving stability of construction project schedules through buffer allocation. Technological and Economic Development of Economy 2011; 17(3): 429-444, http://dx.doi.org/10.3846/20294913.2011.580587.
11. Jaśkowski P., Biruk S. The conceptual framework for construction project risk assessment. Reliability: Theory & Applications 2011; 2(3): 27-35.
12. Jaśkowski P., Biruk S., Kowalski T. Trade-off between robustness of a construction schedule and project completion time. International Journal of Arts & Sciences 2011; 20(4): 205-215.
13. Jaśkowski P., Biruk S., Painting N. Using of fuzzy AHP for assessing risk of construction projects. International Journal of Arts & Sciences 2011; 19(4): 257-268.
14. Jaworski K. M. Metodologia projektowania realizacji budowy (Methodology of planning construction works). Warsaw: Wydawnictwo Naukowe PWN, 1999.
15. Johnson D. The triangular distribution as a proxy for beta distribution in risk analysis. The Statistician 1997; 46(3): 387-398, http://dx.doi.org/10.1111/1467-9884.00091.
16. Kapliński O. Planning instruments in construction management. Technological and Economic Development of Economy 2008; 14(4): 449-451, http://dx.doi.org/10.3846/1392-8619.2008.14.449-451.
17. Kasprowicz T. Inżynieria przedsięwzięć budowlanych (Construction project engineering). Radom–Warsaw: Wydawnictwo i Zakład Poligrafii Instytutu Technologii Eksploatacji, 2002.
18. Marcinkowski R. Metody rozdziału zasobów realizatora w działalności inżynieryjno-budowlanej (Contractor's resource assignment in construction and civil engineering). Warsaw: Military University of Technology, 2002.
19. Nasir D., McCabe B., Hartono L. Evaluating risk in construction–schedule model (ERIC–S): construction schedule risk model. Journal of Construction Engineering and Management 2003; 129(5): 518-527, http://dx.doi.org/10.1061/(ASCE)0733-9364(2003)129:5(518).
20. Połoński M., Pruszyński K. Impact of baseline terms on the course of critical paths and time buffers in the modified Goldratt's method. Archives of Civil Engineering 2013; 59(3): 313-320, http://dx.doi.org/10.2478/ace-2013-0017.
21. Rybka I., Bondar-Nowakowska E., Połoński M. The influence of stoppages on productivity during construction of water supply and sewage systems. Technical Transactions 2014; 2-B(6): 309-315.
22. Sakellaropoulos S., Chassiakos A. P. Project time-cost analysis under generalised precedence relations. Advances in Engineering Software 2004; 35(10-11): 715-724, http://dx.doi.org/10.1016/j.advengsoft.2004.03.017.
23. Samson S., Reneke J. A., Wiecek M. M. A review of different perspectives on uncertainty and risk and alternative modelling paradigm. Reliability Engineering and System Safety 2009; 94(2): 558-567, http://dx.doi.org/10.1016/j.ress.2008.06.004.
24. Schabowicz K., Hoła B. Application of artificial neural networks in predicting earthmoving machinery effectiveness ratios. Archives of Civil and Mechanical Engineering 2008; 8(4): 73-84, http://dx.doi.org/10.1016/S1644-9665(12)60123-X.
25. Schatteman D., Herroelen W., Van de Vonder S., Boone A. Methodology for integrated risk management and proactive scheduling of construction projects. Journal of Construction Engineering and Management 2008; 134(11): 885-893, http://dx.doi.org/10.1061/(ASCE)0733-9364(2008)134:11(885).
26. Skorupka D. Identification and initial risk assessment of construction projects in Poland. Journal of Management in Engineering 2008; 24(3): 120-127, http://dx.doi.org/10.1061/(ASCE)0742-597X(2008)24:3(120).
27. Taroun A., Yang J. B., Lowe D. Construction risk modeling and assessment: insights from a literature review. Journal of the Built & Human Environment 2011; 4(1): 87-97.
28. Van de Vonder S., Demeulemeester E., Leus R., Herroelen W. The use of buffers in project management: The trade–off between stability and makespan. International Journal of Production Economics 2005; 97(2): 227-240, http://dx.doi.org/10.1016/j.ijpe.2004.08.004.
29. Van de Vonder S., Demeulemeester E., Herroelen W. Proactive heuristic procedures for robust project scheduling: an experimental analysis. European Journal of Operational Research 2008; 189(3): 723-733, http://dx.doi.org/10.1016/j.ejor.2006.10.061.
30. Wang W. – Ch. Impact of soft logic on the probabilistic duration of construction projects. International Journal of Project Management 2005; 23(8): 600-610, http://dx.doi.org/10.1016/j.ijproman.2005.05.008.
31. Williams C. A., Heins R. M. Risk management and insurance. New York: McGraw-Hill Book Co., 1971.

Piotr JAŚKOWSKI
Faculty of Civil Engineering and Architecture
Lublin University of Technology
ul. Nadbystrzycka 40, 20-816 Lublin, Poland
E-mail: p.jaskowski@pollub.pl

INFORMATION FOR AUTHORS

Eksploatacja i Niezawodnosc – Maintenance and Reliability – the journal of the Polish Maintenance Society, under the scientific supervision of the Polish Academy of Sciences (Branch in Lublin), published four times a year.

The scope of the Quarterly

The quarterly *Eksploatacja i Niezawodnosc – Maintenance and Reliability* publishes articles containing original results of experimental research on the durability and reliability of technical objects. We also accept papers presenting theoretical analyses supported by physical interpretation of causes or ones that have been verified empirically. *Eksploatacja i Niezawodność – Maintenance and Reliability* also publishes articles on innovative modeling approaches and research methods regarding the durability and reliability of objects.

The following research areas are particularly relevant to the journal:

1. degradation processes of mechanical and biomechanical systems,
2. diagnosis and prognosis of operational malfunctions and failures.
3. analysis of failure risk/wear,
4. reliability-and-environmental-safety engineering in the design, manufacturing and maintenance of objects,
5. management and rationalization of object maintenance,
6. risk management in the processes of operation and maintenance,
7. the human factor and human reliability in operation and maintenance systems.

Terms and Conditions of Publication

The quarterly *Eksploatacja i Niezawodnosc – Maintenance and Reliability* publishes only original papers written in English or in Polish with an English translation. Translation into English is done by the Authors after they have received information from the Editorial Office about the outcome of the review process and have introduced the necessary modifications in accordance with the suggestions of the referees! Acceptance of papers for publication is based on two independent reviews commissioned by the Editor.

The quarterly *Eksploatacja i Niezawodnosc – Maintenance and Reliability* proceeds entirely online at submission.ein.org.pl

Technical requirements

- After receiving positive reviews and after acceptance of the paper for publication, the text must be submitted in a Microsoft Word document format.
- Drawings and photos should be additionally submitted in the form of high resolution separate graphical files in the TIFF, SVG, AI or JPG formats.
- A manuscript should include: names of authors, title, abstract, and key words that should complement the title and abstract (in Polish and in English), the text in Polish and in English with a clear division into sections (please, do not divide words in the text); tables, drawings, graphs, and photos included in the text should have descriptive two-language captions, if this can be avoided, no formulae and symbols should be inserted into text paragraphs by means of a formula editor; references (written in accordance with the required reference format); author data – first names and surnames along with scientific titles, affiliation, address, phone number, fax, and e-mail address.

The Editor reserves the right to abridge and adjust the manuscripts. All submissions should be accompanied by a submission form.

Detailed instructions to Authors, including evaluation criteria can be found on the journal's website: www.ein.org.pl

Editor contact info

Editorial Office of „Eksploatacja i Niezawodnosc - Maintenance and Reliability"
Nadbystrzycka 36, 20-618 Lublin, Poland
e-mail: office@ein.org.pl

INFORMATION FOR SUBSCRIBERS

Fees

Yearly subscription fee (four issues) is 100 zloty and includes delivery costs. Subscribers receive any additional special issues published during their year of subscription free of charge.

Orders

Subscription orders along with authorization to issue a VAT invoice without receiver's signature should be sent to the Editor's address.

Note

In accordance with the requirements of citation databases, proper citation of publications appearing in our Quarterly should include the full name of the journal in Polish and English without Polish diacritical marks, i.e.,

Eksploatacja i Niezawodnosc – Maintenance and Reliability.

Wydawca:
Polskie Naukowo Techniczne
Towarzystwo Eksploatacyjne
Warszawa

Publisher:
Polish Maintenance Society
Warsaw

Członek:
Europejskiej Federacji
Narodowych Towarzystw
Eksploatacyjnych

Member of:
European Federation of National
Maintenance Societies

Patronat naukowy:
Polska Akademia Nauk
Oddział Lublin

Scientific Supervision:
Polish Academy of Sciences
Branch in Lublin